Stavros Karathanasis

Linear Fresnel Reflector Systems for Solar Radiation Concentration

Theoretical Analysis, Mathematical Formulation and Parameters' Computation using MATLAB

EXTRAS ONLINE

Springer

Linear Fresnel Reflector Systems for Solar Radiation Concentration

Stavros Karathanasis

Linear Fresnel Reflector Systems for Solar Radiation Concentration

Theoretical Analysis, Mathematical Formulation and Parameters' Computation using MATLAB

With about 270 Figures and Illustrations

Springer

Stavros Karathanasis
Department of Environment and Spatial
Planning of Central Macedonia
Decentralized Administration of Macedonia
and Thrace
Thessaloniki, Greece

ISBN 978-3-030-05278-2 ISBN 978-3-030-05279-9 (eBook)
https://doi.org/10.1007/978-3-030-05279-9

Library of Congress Control Number: 2018963291

This Springer imprint is published by the registered company Springer Nature Switzerland AG
The registered company address is: Gewerbestrasse 11, 6330 Cham, Switzerland

I would like to dedicate this book
to my beloved Prof. Ioannis Ziomas
who left this world too soon.
He never had stopped believing in me
and always supported all my efforts.

Preface

Energy production, and in particular electric power production, is one of the greatest challenges our world has to deal with. Since we have been proved unable to handle energy consumption by reducing energy waste and energy losses, we must, at least, use environmentally friendly energy resources.

Solar radiation is abandoned and could solve many energy problems the human society faces today. Nevertheless, harvesting it is not an easy task. Solar radiation has to be concentrated if we would like to use it efficiently in power production. One of the recently applied technologies serving this goal is solar radiation concentration using Linear Fresnel Reflector Systems. These Systems are more economical and easier to be constructed than other technologies.

This book deals with the theoretical analysis and mathematical formulation of the above Systems aiming to help all interested parties involved in the development (design), construction and implementation of them. It presents a concise and comprehensive aspect of the theory governing these Systems, and at the same time, it provides useful and efficient calculation procedures that can facilitate their designing and development. To accomplish this goal, this book contains a considerable large number of mathematical formulas, illustrations, graphs and, to a lesser extent, tables. As all presented information are gathered from the international scientific bibliography, it is well tested and widely accepted. No new technology approaches are presented here. It is not the aim of this book. Its most important feature is that it constitutes a complete guide of designing Linear Fresnel Reflector Systems for solar radiation concentration, providing all necessary theoretical and computational tools available in one piece of work.

Linear Fresnel Reflector Systems, despite their construction advantages, have inherent design difficulties and drawbacks. These must be tackled if we would like to overcome their lower efficiency in comparison to other more efficient Solar Radiation Concentrating Systems, like Parabolic Troughs and parabolic dishes.

This book aspires to accomplish this goal. It contains all relevant information necessary for the conceptual understanding of these Systems. However, apart from the extended mathematical formulation provided, the physical background is extensively explained, using a lot of figures and drawings. In addition, methods of solving the complex mathematical equations are given, along with the necessary computational code developed in MATLAB® (incorporated in the text and stored in electronic form in the supplementary CD). Moreover, two small-scale Fresnel Reflector Systems (one linear and one concentric, or more correctly conical) are completely analysed and developed, as a general case study that implements the theory and methodology presented in this book.

Subsequently, this book is a useful tool for both students, who study these Systems for their first time, and engineers and scientist, who apply their already acquired knowledge, helping them to develop more energy-efficient Linear Fresnel Reflector Systems.

The book consists of ten (10) Chapters. In Chap. 1, a general introduction to the energy problem and its possible solution with Concentrated Solar Radiation Power Systems (alternative energy sources) is given. After that, Chap. 2 deals with the characteristics of solar radiation reaching the Earth's surface, and the phenomena affecting it, as well as the parameters required to calculate it. Geometrical optics is essential to calculate the solar radiation received from a device, an absorber, after being concentrated by an appropriate reflective surface. This is dealt with in Chap. 3, whereas Chap. 4 is a comprehensive description of the geometrical characteristic of a typical Linear Fresnel Reflector System and the phenomena affecting its optical performance. Appropriate mathematical formalism is introduced so that in Chap. 5 analytical mathematical equations for the calculation of the optical losses of these Systems to be developed. They are based on the equations describing Sun's and the reflective elements' position, presented in Chap. 4, and take into account the effect the reflectors width, the spacing between adjacent reflectors, the receiver height, the reflectors configuration, the System orientation angle and the site latitude may have on Systems optical efficiency. While the primary reflectors' field is studied in Chap. 5, Chap. 6 deals with the optical performance and efficiency of different types of secondary reflectors. Chapter 7 focuses on the derivation of the mathematical relationships needed to calculate the design parameters of a Linear Fresnel Reflector System: the width, the position and the inclination of the primary reflective elements. These formulas are used in Chap. 8 to study a simple but interesting implementation of Fresnel Reflector Systems: Fresnel Reflector Solar Cookers. The required construction parameters have been calculated by developing appropriate computational code in MATLAB®. Since MATLAB® can be used to solve all mathematical equation associated with Concentrated Solar Radiation Power Systems that use Linear Fresnel Reflector System to concentrate the solar radiation, Chap. 9 provides a brief but concise introduction to MATLAB®. Finally, Chap. 10 provides some computational applications of the previous chapters and the corresponding MATLAB® code. Among them, the MATLAB® code developed for calculating the construction parameters of the cases studies presented in Chap. 8 is also included.

The developed code is contained in the supplementary CD that accompanies this book. Apart from the above applications, the MATLAB® code for two extra case studies, not included in Chap. 10, is also contained in the supplementary CD. There, all MATLAB® M-files are extensively described and documented, so that even a novice in programming to be able to understand them. This way, anyone interested in applying the methodology presented in this book will have all source code at hand, and with minimum additional effort, they will be able to expand it in other design configurations by introducing appropriate modifications.

However, before completing this short introduction to the book, I would like to give you some information about my area of work and career, as I reckon that it can highlight the usefulness of the book. My core job duty is the assessment of environmental impact statements (EISs) for a large variety of activities. Among them, power production from renewable energy sources constitutes a considerable large part. As I have to assess EISs in order to be able to approve (or not approve) them and decide on proposing the issuing of an Environmental Permit, I have studied this matter in depth. My experience all these years (more than 15 years in this post) has taught me that it is not an easy task to adequately explain the technology used and the design parameters chosen for the development of a project. Experts who conduct the environmental impact assessment (EIA) find it difficult to describe accurately and comprehensibly the production process, let alone some technical features, of the intended project. Despite the fact that Linear Fresnel Reflector Systems are a state of the art, and an important new technology, they do not constitute an exception. So, my effort to understand this matter lead me to extensive studies and, consequently, to have gathered a lot of related information.

The aforementioned, combined with the fact that from 2003 until 2017 I was teaching in the Postgraduate Study Program (Master Program) "Environmental Physics", offered by Aristotle University of Thessaloniki, Greece (School of Physics), impelled me to write this book, making use of my experience and knowledge acquired all these years. My key aim is to help students, engineers and scientist to cope with the conceptual understanding, the development and the appropriate presentation of this particular kind of technology. Since this knowledge and experience was proven helpful to me and facilitated my effort to cope with the difficult task of understanding someone else's work, I reckon that it will be proven useful to anyone dealing with this technology, too.

Finally, as this book deals with only one kind of Solar Radiation Concentrating Systems, Linear Fresnel Reflector Systems, it ends up to be a comprehensive study of their critical construction parameters. It provides a detailed methodological analysis of their physical and optical characteristic, which can be used to produce optimal designs with the maximum performance. In addition, the methodology presented can also be applied in configurations other than those analysed in this book, with equal effectiveness. This enhances even more the usefulness of the book.

However, despite a great deal of effort I put into the writing of this book, I realise that it is inevitable to eliminate all possible errors or mistakes. Any time I edit or proofread the manuscript, I always encounter some points that could be

improved. Therefore, I would appreciate any comment send in the following email: Karathanasis.Stav@gmail.com improving or correcting the information providing in this book.

Thessaloniki, Greece

Dr. Stavros Karathanasis
Physicist
Ph.D. in Physics
M.Sc. in Environmental Physics

Acknowledgements

I would like to express my gratitude to Dr. Konstantinos Evangelidis, Associate Professor at Department of Civil, Surveying and Geoinformatics Engineering, Faculty of Applied Technology, Technological Educational Institute of Central Macedonia, in the discipline "Web-centric Information Systems and Geospatial Databases". Konstantinos is an old classmate and a friend of mine, and if it was not for his encouragement, I would never have written this book.

I would also like to thank The MathWorks, Inc. (http://www.mathwork.com) for providing the most recent versions of the MATLAB® software [MATLAB Version: 9.5.0.944444 (R2018b)] to develop the solution codes of the problems included in this book.

For MATLAB and Simulink product information, please contact:

The MathWorks, Inc.
3 Apple Hill Drive
Natick, MA, 01760-2098 USA
Tel: 508-647-7000
Fax: 508-647-7001
Email: info@mathworks.com
Web: https://www.mathworks.com
How to buy: https://www.mathworks.com/store
Find your local office: https://www.mathworks.com/company/worldwide

Contents

1 Concentration of Solar Radiation 1
1.1 The Need for Concentrated Solar Energy 1
1.2 Utilization of the Concentrated Solar Energy 2
1.3 Concentrated Solar Radiation Power Systems 3
1.3.1 Solar Tower or Central Tower Power Systems 4
1.3.2 Parabolic Dish Power Systems 5
1.3.3 Parabolic Trough Power Systems 6
1.3.4 Linear Fresnel Reflector Power Systems 7
1.4 Advantages and Disadvantages of Linear Fresnel Reflector Systems 9
1.4.1 Advantages 9
1.4.2 Disadvantages 10
References 11

2 Solar Radiation 13
2.1 Fundamentals of Solar Radiation 13
2.1.1 Key Definitions of Radiation 14
2.1.2 Radiation's Laws 15
2.2 Solar Radiation on the Edge of Earth's Atmosphere 18
2.2.1 The Solar Radiation Spectrum 18
2.2.2 Solar Radiation at the Top of the Atmosphere (Extraterrestrial Radiation)—Solar Constant 19
2.2.3 Energy Emitted by Sun 19
2.3 Solar Radiation on Earth's Surface—Radiation Extinction Processes in the Atmosphere 20
2.3.1 Scattering of Solar Radiation in the Atmosphere 20
2.3.2 Absorption of Solar Radiation in the Atmosphere 21
2.3.3 Solar Radiation Extinction Coefficient 22
2.3.4 The Atmospheric Optical Depth 23

2.3.5 The Air Mass . . . 26
2.3.6 Direct Solar Radiation Striking a Flat Horizontal and a Tilted Surface . . . 30
2.4 Geometrical Aspects of Direct Solar Radiation . . . 32
2.4.1 The Sun–Earth Distance . . . 33
2.4.2 Coordinate Systems . . . 35
2.5 Direct Solar Radiation on an Arbitrary Surface . . . 41
2.6 Sun's Coordinates . . . 49
2.6.1 Solar Declination . . . 49
2.6.2 Solar Hour Angle, Official Time and Solar Time . . . 50
2.6.3 Solar Altitude Angle and Solar Azimuth . . . 54
2.7 Direct Solar Radiation Models . . . 55
2.7.1 Empirical Models . . . 56
2.7.2 Parametric Models . . . 63
References . . . 70

3 Geometric Optics . . . 73
3.1 The Ray Aspect of Light . . . 73
3.2 Wave Fronts and Rays . . . 74
3.3 Fermat's Principle . . . 75
3.4 The Law of Reflection . . . 77
3.5 Light Ray Redirection and Light Concentration . . . 82
3.5.1 Plane Mirrors . . . 82
3.5.2 Spherical Mirrors . . . 83
3.5.3 Parabolic Mirrors . . . 88
3.5.4 Linear Fresnel Mirrors . . . 94

4 Linear Fresnel Reflector Systems Design Parameters . . . 97
4.1 Linear Fresnel Reflector . . . 98
4.2 Geometrical Parameters of Linear Fresnel Reflector . . . 103
4.3 Sun Tracking . . . 105
4.3.1 The Orientation of the Reflective Elements . . . 107
4.3.2 The Tracking Angle . . . 109
4.3.3 Sun's Path Across the Sky and System Orientation . . . 115
4.4 The Effect of Sun's Finite Size . . . 119
4.5 Aperture Area, Concentration Ratio and Total Concentrated Solar Power . . . 120
4.5.1 Aperture Area . . . 120
4.5.2 Concentration Ratio . . . 120
4.5.3 Total Concentrated Solar Power . . . 122
4.6 The Receiver . . . 122
4.6.1 Multiple Tube Receivers . . . 123
4.6.2 One Tube Receivers . . . 124

4.7 Optical Efficiency . . . 127
4.7.1 Optical Efficiency Parameterization . . . 127
4.7.2 Optical Efficiency Modelling and Ray Tracing . . . 129
4.7.3 Solar Field Energy Losses . . . 130
4.7.4 Receiver Losses . . . 134
References . . . 135

5 Geometric Optical Losses . . . 137
5.1 Introduction . . . 138
5.2 Shading and Blocking Effects . . . 142
5.2.1 Shading Effect . . . 144
5.2.2 Blocking Effect . . . 159
5.2.3 Effect of Sun's Finite Size on Shading and Blocking . . . 160
5.2.4 Shading and Blocking Effects Evaluation . . . 161
5.3 End Losses . . . 162
5.4 Cosine Effect . . . 169
5.5 Receiver Shading . . . 172
5.6 Time Averaged Losses . . . 181
References . . . 184

6 Receiver Secondary Reflector . . . 185
6.1 Introduction . . . 185
6.2 Methodology . . . 187
6.2.1 Secondary Reflector Shape and Aperture Width . . . 191
6.2.2 Primarily Reflected Solar Radiation to Be Concentrated . . . 193
6.3 Secondary Reflector's Profiles . . . 206
6.3.1 Horizontally Arranged Multiple Narrow Tubes Absorber and Trapezoidal Cavity . . . 207
6.3.2 Single Circular Tube Absorber . . . 213
References . . . 221

7 Design Parameters . . . 223
7.1 Introduction . . . 223
7.2 Methodology . . . 227
7.2.1 Distance Between Consecutive Reflective Elements . . . 229
7.2.2 Reflective Elements' Tilt Angle . . . 237
7.2.3 A Different Approach . . . 249
7.2.4 Reflective Elements' Width . . . 252
7.3 Sun's Angular Size Effect . . . 257
7.4 South–North-Oriented Linear Fresnel Reflector Systems . . . 269
7.5 Design Parameters' Computation . . . 270
References . . . 275

8 Case Study—Fresnel Reflector Solar Cookers . . . 277
8.1 Introduction . . . 277
8.2 The Fresnel Reflector Solar Cookers . . . 281
8.3 Design Parameters' Computation . . . 287
8.4 The Solar Cookers' Construction . . . 298
8.4.1 The Linear Fresnel Reflector Solar Cooker . . . 299
8.4.2 The Conical Fresnel Reflector Solar Cooker . . . 300
References . . . 302

9 Short Introduction to MATLAB® . . . 305
9.1 Introduction . . . 305
9.2 Programming with MATLAB®—Script Files . . . 306
9.2.1 Structuring Script M-Files . . . 308
9.2.2 Creating and Saving Script Files . . . 309
9.2.3 Interpreting Script Files . . . 309
9.3 Variables . . . 310
9.3.1 Statements . . . 312
9.3.2 Scalars, Vector and Matrices . . . 312
9.3.3 Creating Vector and Matrices . . . 314
9.4 Array and Matrix Operations . . . 315
9.4.1 Array Operations or Element-by-Element Operations . . . 315
9.4.2 Matrix Operations . . . 316
9.5 Decision-Making Structures . . . 319
9.5.1 The IF Statement . . . 320
9.5.2 The IF-Else Statement . . . 320
9.5.3 Nested IF-Else Statements . . . 321
9.5.4 IF-Else Statements . . . 321
9.5.5 The Switch Statement . . . 322
9.6 Relational and Logical Operators . . . 323
9.7 Statements' Iteration or Statements' Loops . . . 324
9.7.1 FOR Loops . . . 325
9.7.2 WHILE Loops . . . 326
9.8 Displaying and Saving Results . . . 326
9.9 Plotting Results . . . 330
9.9.1 Customizing and Formatting Graphics and Plots Using Commands . . . 330
9.9.2 Multiple Graphs in the Same Plot—on the Same Axes . . . 333
9.10 Saving Graphs and Plots . . . 334
References . . . 334

10 Applications . . . 337

Index . . . 349

Chapter 1
Concentration of Solar Radiation

Solar radiation, the energy emitted by the Sun and reaches the Earth, is the driving factor of live on Earth. However, despite the fact that it is actually true, how easy is to exploit it? Is its harvesting a simple and easy task? Or do we need special equipments or sophisticated arrangements? This chapter deals with the possibility of electric energy production using solar radiation. The different technologies developed to serve this purpose are briefly introduced, and the main advantages and disadvantages of Linear Fresnel Reflector Systems, the topic of the Book, are presented. However, this chapter does not constitute an exhausted analysis of the matter; it is rather a short and comprehensive introduction.

1.1 The Need for Concentrated Solar Energy

Energy production, and in particular electric power production, is one of the most crucial problems our world has to solve. However, it may have adverse environmental and social consequences if not be dealt with properly (Bellos et al. 2016). Since we have been proved unable to handle energy consumption by reducing energy waste and energy losses, we must, at least, use environmentally friendly energy sources. On account of this, and despite the fact that there are some serious concerns about their implementation, e.g. capital costs, and intermittent nature, the use of renewable energy sources seems to be a potential solution to this problem. Moreover, from all available renewable energy sources, solar energy, the energy radiated from Sun in the form of heat and light, is the most abundant, plentiful, unlimited and the most spatially available. In fact, Sun provides Earth with more energy in 1 h than it is consumed on the planet in a year (Zhang et al. 2013).

Keeping in mind the environmental benefits from limited fossil fuel use, it is not surprising why solar energy has won people and scientists' interest: it is ubiquitous, inexhaustible and pollution-free. As a result, in the recent years a great deal of research has been put into the solar radiation harvesting for power production. By

S. Karathanasis, *Linear Fresnel Reflector Systems for Solar Radiation Concentration*, https://doi.org/10.1007/978-3-030-05279-9_1

using proper installations, solar energy can be converted into thermal and electric energy. However, solar energy is variable, both within the day (day–night, clouds) and within the year (winter–summer) and, as it has a low density per unit area (typically ranging from 0.5 to 1 kW/m^2), it requires large collectors to harvest it (Kesari et al. 2015). Therefore, if we would like to use solar energy as a durable and widespread primary energy source, we should capture, store and use it in a cost-effective manner (Zhang et al. 2013).

Stationary solar energy collectors are devices that capture solar energy and convert it into heat (Bellos et al. 2016). The simpler of them include solar air, water and space heating Systems, crop driers and water desalination Systems (Mahdi and Bellel 2014). Most of these solar collectors have been applied for domestic use reaching temperature lower than 80 °C. However, these temperatures are very low and insufficient for industrial processes or power production. The latter requires temperatures over 100 °C. In other words, solar energy is not very useful since it has very low power density unless it is used in some other way that multiplies its power. Hence, to reach the required temperatures for electricity production, it is necessary to somehow concentrate the solar radiation (Gharbi et al. 2011).

Form this brief analysis, it is obvious that although solar radiation is abandon and widely distributed, and could potentially solve many energy problems the human society faces today, harvesting it is not a very easy task, as it is dispersed and available only at low rates. For this reason, we must develop appropriate Solar Radiation Concentrating Systems and subsequently Concentrated Solar Radiation Power Systems. They are the only technology that can really make use of solar energy in an effective manner achieving the required temperature levels for electricity production (Beltagy et al. 2017).

1.2 Utilization of the Concentrated Solar Energy

Concentrated Solar Radiation Power Systems produce electricity by first concentrating solar radiation on an absorbing surface and then heating a material (liquid or solid) that is used in a downstream process for electricity generation. Electricity production via Concentrated Solar Radiation Power Stations does not differ substantially from a traditional Thermal Power Station. In fact, Concentrated Solar Radiation is an alternative heat source. In other words, instead of using coal or natural gas as fuel, we use solar energy in the form of radiation which is converted into heat. It has the advantage of being a clean, safe and inexhaustible (in our timescale) source. Hence, what distinguishes Concentrated Solar Radiation Power Systems from a Thermal Power Plant is how thermal energy is produced and exploited (Fig. 1.1).

Notwithstanding the obvious benefits of Concentrated Solar Radiation Power Systems, the time-varying nature of solar radiation remains the main problem for all technologies of this kind. They face short-term variations of solar radiation on cloudy days and cannot produce electric energy during night hours, unless they have incorporated excess thermal energy storage units (Zhang et al. 2013). In

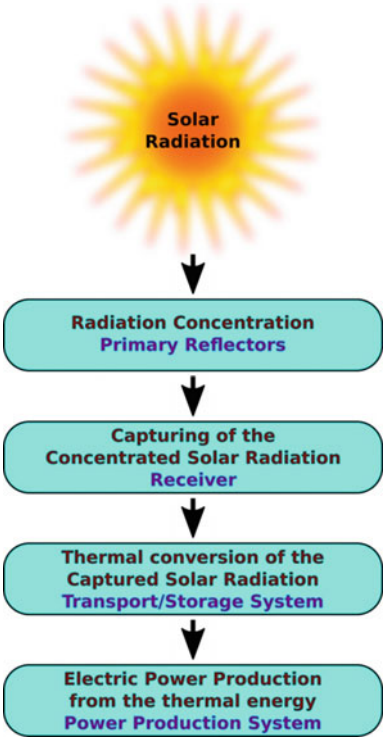

Fig. 1.1 Concentrated Solar Radiation Power Systems are based on a very simple general scheme: using reflectors, sunlight is redirected, focused and collected as heat by a number of proper receivers. Next, the concentrated solar radiation is used to heat up a fluid (e.g. water) producing saturated or superheated steam. Then it is introduced into a thermodynamic cycle driving a turbine coupled with a generator. As the produced steam goes through the turbine, its thermal energy is converted into mechanical energy of the rotated turbine, which drives a generator joined with it producing electricity. Therefore, such a plant consists, in general, of solar concentrators, steam generators, turbines and electricity generators

addition, as they only utilize the direct component of solar radiation, these Systems are suitable only in areas with high solar irradiance. Moreover, they can operate successfully only when equipped with a Sun-tracking System to keep solar radiation concentrated on the receiver (Pavlović et al. 2012).

1.3 Concentrated Solar Radiation Power Systems

Solar radiation can be concentrated on a point or on a line. Subsequently, different concentration ratios can be achieved, and as a result, each type of Concentrated Solar Radiation Power Systems operates at different temperature ranges. This affects their electric power production efficiency, as it depends on the operation

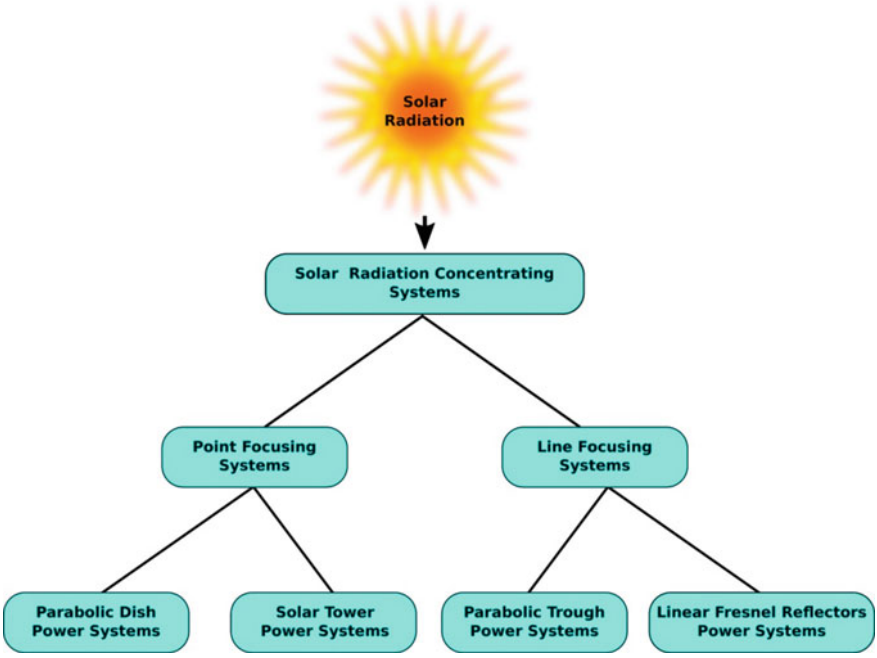

Fig. 1.2 Concentrating Solar Radiation Technologies categorized by their focusing type

temperature. Linearly focusing Systems produce high solar radiation density on a linear receiver and can achieve concentration ratios of some tens. Cylindrical parabolic concentrators (or Parabolic Troughs) are a typical example of this type of Solar Radiation Concentrating Systems. On the other hand, point focusing systems generally produce much higher radiation density in an area that can be deemed as a point. Paraboloid reflectors are a representative example of point focusing concentrators (Mahdi and Bellel 2014).

In general, there are four main types of Systems that use concentrated solar radiation to produce electric power (Concentrated Solar Radiation Power Systems) (Fig. 1.2). They are (e.g. Kesari et al. 2015; Mahdi and Bellel 2014; Gharbi et al. 2011):

- Solar Tower or Central Tower Systems
- Parabolic Dish Power Systems
- Parabolic Trough (Cylindrical) Systems and
- Linear Fresnel Reflector Systems.

1.3.1 Solar Tower or Central Tower Power Systems

A Solar Tower Power System is composed of a large number of flat mirrors (reflectors/heliostats/heliostats' field) distributed around a central receiver mounted

on the top of a tower (Barlev et al. 2011). Receivers are made of ceramics or metals that are stable at high temperatures (have very high melting point). A fluid circulating in a closed-loop System passes through the receiver and absorbs thermal energy for power production and/or storage. Working fluid can be water, molten salt, liquid sodium or some other material, such as mineral oils. Solar Tower Power Stations are equipped with steam generators, turbines and electricity generators (Barlev et al. 2011). Steam's thermal energy is converted into mechanical energy and next into electric energy. The steam after passing through the turbine is condensed in a condenser and pumped into a boiler where it again receives heat from the receiver, and the cycle is repeated (Pavlović et al. 2012).

The efficiency of Solar Tower Power Systems is influenced by the optical and geometrical characteristics of the heliostats, the cleanliness of the mirrors, the precision of the tracking System, by shading and blocking effects, and by the atmospheric attenuation of the reflected solar radiation (Pavlović et al. 2012; Barlev et al. 2011). Therefore, planning the layout of a heliostats field is a very important task.

Heliostats are composed of several flat mirrors that reflect solar radiation onto the receiver. They usually have a surface area ranging from 50 to 150 m^2. Using slightly concave mirrors on heliostats, the concentration ratio of the reflected solar radiation can be increased. However, this elevates manufacturing costs (Barlev et al. 2011). Each heliostat has its own mechanism for Sun tracking. They can move along two axes and are individually oriented to reflect the incident sunlight directly onto the receiver. Mounting the receiver on a tall tower decreases the required distance between adjacent heliostats so that shading and blocking effects to be avoided. Typically, solar towers' heights are about 75–150 m (Barlev et al. 2011).

Solar Tower Power Systems are typically large units (10 MW and above). However, in order to be cost efficient and profitable, their power has to be higher than 50 MW (Pavlović et al. 2012). This is necessary, if we would like to overcome the high costs associated with this technology (Barlev et al. 2011). Since the solar flux concentrated on the receiver yields very high concentration ratios (300×–1500×), Solar Tower Power Systems can operate at very high temperatures (over 1500 °C) enhancing their power conversion efficiency (Barlev et al. 2011). This is an advantage of these Systems as the large amount of solar radiation concentrated on a relatively small area minimizes heat losses and simplifies heat transport and storage requirements, allowing the use of high-energy thermodynamic cycles (Barlev et al. 2011).

Lastly, compared to other Concentrated Solar Radiation Power technologies, Solar Tower Power Systems require the biggest area per unit of generated electric energy and large quantity of water (Pavlović et al. 2012).

1.3.2 Parabolic Dish Power Systems

A Parabolic Dish Power System is composed of a paraboloid reflector, in the form of a shallow dish, a Stirling engine, placed on the focus of the dish, and a generator

of electric energy. In the Stirling engine, the heat produced by the concentrated solar radiation is converted into mechanical energy. Next, a generator of electric energy connected to the Stirling engine produces electric power (Pavlović et al. 2012).

During the day, the parabolic dishes are automatically directed towards the Sun by a two-axes tracking Systems so that they always reflect solar radiation towards the Stirling engine. Parabolic dishes have diameter of 5–10 m and a surface of about 40–120 m^2. This way they can achieve concentration ratios of about 2000× and working fluids temperature in the order of 700–1000 °C (Pavlović et al. 2012). Furthermore, the produced electric power of an individual Parabolic Dish Power System ranges between 5 and 50 kW (Pavlović et al. 2012).

1.3.3 Parabolic Trough Power Systems

Parabolic Trough Power Systems are composed of large number of interconnected linear parabolic reflector troughs, concentrated solar radiation receivers (or absorbers), steam generators, turbines and electric energy generators (Pavlović et al. 2012).

The reflectors are composed of sheets of reflective materials, which are curved along their longer dimension forming a Parabolic Trough. Many sheets are put together in series forming long troughs (up to several hundred metres). These modules have a linear focus (focal line) along which a receiver is mounted (Barlev et al. 2011). The entire set of the reflectors is called the solar field (Zhang et al. 2013). The Parabolic Trough reflectors feature relatively high efficiency, reaching concentration ratios of the incoming solar radiation in the order of 80–100× (Barlev et al. 2011).

However, the accurate receiver configuration is of crucial importance for efficient solar radiation collection, heat transfer to the working fluid, as well as reduction of heat losses. The receiver is generally a metal pipe. As radiant heat losses from receiver play an important role in the overall System's performance, the receiver's surface is often covered with a selective coating that features high absorbance of solar radiation and low thermal emittance. On the other hand, because thermal losses due to temperature gradients between the receiver and the environment also have a significant impact on system's efficiency, the receiver is encased in a glass pipe to limit heat losses by convection. This glass tube is typically coated with antireflective coating to enhance transmissivity and avoid energy losses due to reflexion on it. In addition, to minimize thermal losses vacuum can be applied in the space between the protecting glass and the metal receiver (Barlev et al. 2011).

The reflectors and the receiver move together following Sun's motion (Zhang et al. 2013). For this reason, they are mounted on a single-axis sun-tracking System that can keep incident solar light rays parallel to the plane of symmetry of the Parabolic Trough. This way, the reflected solar radiation can be focused on the

receiver throughout the day. Furthermore, as these Systems feature a linear symmetry, their orientation in relation to Sun's position plays an even crucial role. From all possible orientation East–West and North–South are implemented most frequently, if not exclusively. They provide different annual efficiency, with the former type collecting more solar radiation annually, and the latter collecting more solar radiation in the summer months when energy requirements are generally the highest (Barlev et al. 2011).

The tracking mechanism must rotate the Parabolic Trough and receiver System around a rotation axis continuously so that they can follow Sun's position very accurately. Only this way can be accomplished the desired heating level of the receiver tube. However, trough reflectors are large constructions and generally face wind drag. Therefore, they must be robust enough to account for wind loads and prevent deviations from normal radiation incidence, fact that causes a series of serious problems (e.g. increased investments costs) and put important constrains.

The exploitation of the concentrated solar radiation is accomplished via a working fluid (usually a mineral oil) that fills the absorber tube and is heated up to about 400 °C. This fluid, in turn, heats up another fluid, usually water, to generate steam for electricity generation in a Rankine cycle: the heated working fluid is transferred by pumps from the solar radiation absorber into the heat exchanger. There the collected heat is used to produce overheated steam which is sent to a turbine to produce mechanical energy and subsequently electricity (Pavlović et al. 2012).

1.3.4 Linear Fresnel Reflector Power Systems

Linear Fresnel Reflector Systems are linearly focusing Solar Radiation Concentrating Systems suitable for power production (Heimsath et al. 2014). They approximate the parabolic shape of Parabolic Troughs Concentrating Systems by using long rows of flat or slightly curved mirrors (Zhang et al. 2013). The first who applied this principle was Giorgio Francia (Francia 1968). He developed a Linear and two-axis tracking Fresnel Reflector Systems at Genoa, Italy, in the 1960s (Kesari et al. 2015). Linear Fresnel Reflectors reflect and concentrate solar radiation on a linear receiver. There the concentrated solar energy can be directly absorbed by the receiver or it can be concentrated a second time using a small reflector. This secondary reflector is attached on the top of the receiver (Ahmed and Amin 2016; Poullikkas et al. 2012).

The receiver is a fixed structure mounted above and along the linear reflectors (Zhang et al. 2013). On account of this, in order to focus sunlight onto the absorber all day long, the reflectors have to be able to change their orientation. This is achieved by rotating them around their longer axis (Kesari et al. 2015). In fact, all Linear Fresnel Reflectors are automatically and continuously reoriented during the day (Pavlović et al. 2012). Apart from linear reflectors and receivers, Concentrated Solar Radiation Power Systems with Linear Fresnel Reflectors are composed of

secondary reflectors, steam generators, turbines and electric energy generators (Pavlović et al. 2012).

Linear Fresnel Reflector Systems is a relatively new technological application for Concentrated Solar Radiation Power production when compared to Parabolic Troughs, Solar Towers and Parabolic Dish Systems. They are one of the most promising technologies for electric energy production from concentrated solar radiation with a remarkable potential to reduce construction and maintenance costs (Abbas et al. 2017; Boito and Grena 2016). Despite the widespread installation and operation of Concentrated Solar Radiation Power Plant with Parabolic Trough Reflectors, there are many reasons for the use of Linear Fresnel Reflectors as Solar Radiation Concentrating Systems. They have many construction advantages. In addition, innovations in receivers and reflectors design have made these Systems relatively economical (Barlev et al. 2011). Their considerable economic advantages are principally originated from their constructive simplicity. They rely on an array of linear reflective elements that concentrate the sunlight onto a fixed receiver. So, the flat mirrors are easier and cheaper to manufacture, their supporting structures are lighter, wind effects are not important compared to other technologies, there is no need for rotating joints, as is the case in Parabolic Trough Systems, and the land requirement is lower (Abbas et al. 2017).

Linear Fresnel Reflector Systems are capable of concentrating solar energy to approximately 30 times its normal intensity. When developed for large-scale power production, they can provide electric power in the order of many tens of MW. On the other hand, when scaled down, they meet medium temperature ranges (100–250 °C) suitable for generation of industrial process heat. Small-scale Fresnel Reflector Systems could be suitable for medium temperature applications (in the range of 70–250 °C), such as cleaning, drying, evaporation, distillation, pasteurization, sterilization, cooking, as well as applications with low temperature demand as domestic hot water, space heating and swimming pool heating, heat-driven refrigeration and cooling.

Due to their lower concentration ratios, Linear Fresnel Reflector Systems achieve lower operating temperatures of the working fluid, resulting in lower power production efficiency. However, their constructive simplicity offers advantages which balance their low efficiency (Pauletta 2016).

To recapitulate:

- In **Parabolic Trough Reflector Systems**, long rows of Parabolic Through reflectors concentrate solar radiation onto a heat collecting element mounted along the reflector's focal line. The troughs track Sun's position by being rotated around one axis parallel to their longer dimension.
- **Linear Fresnel Reflector Systems** use large arrays of long flat or nearly flat mirrors (slightly curved), positioned closer to the ground reducing construction and maintenance costs. The advantage of Linear Fresnel Reflectors is that the installation costs can be lower than those for Parabolic Trough Systems. However, their disadvantage is that their annual optical performance is lower.

- On the other hand, **Solar Power Towers** are able to generate much higher temperatures than Parabolic Troughs and Linear Fresnel Reflectors, although they require a two-axis tracking System. They use an array of mirrors (heliostats) which track Sun individually in order to reflect its radiation onto the fixed receiver at the top of the tower. In this way, temperatures higher than 1000 °C can be reached, while in linearly focusing Systems the maximum temperature is about 400 °C. This higher temperature is a benefit, because the thermodynamic cycles that can be used for generating electricity are more efficient.
- Lastly, a **Parabolic Dish Power System** uses a paraboloid reflecting surface to concentrate solar radiation onto a receiver mounted at its focal point. In these Systems, the receiver moves with the dish. They are suitable for applications requiring high temperatures (about 900 °C).

1.4 Advantages and Disadvantages of Linear Fresnel Reflector Systems

As with any kind of technology, there are some advantages and disadvantages associated with Solar Radiation Concentrating Systems that use Linear Fresnel Reflectors. However, in order to be able to assess the usefulness of these systems we compare them to their counterpart, the Parabolic Trough Systems. So, Linear Fresnel Reflector Systems have some advantages, as well as disadvantages, compared to Parabolic Troughs (Bellos et al. 2016). They may have lower efficiency than Parabolic Troughs, but in general they have lower, very attractive, construction's, maintenance's and operation's costs. These may well compensate their main disadvantages, providing a cost-effective solution for Concentrated Solar Radiation Power production.

1.4.1 Advantages

The most important advantages of Linear Fresnel Reflector Systems are mainly related to their construction's characteristics. In more details:

- The greatest advantage of these Systems is that they use flat or slightly curved reflectors whose construction is simpler and cheaper compared to parabolic curved reflectors which are typically more expensive. In addition, they offer lower construction and operational costs.
- Another advantage of Linear Fresnel Reflector Systems is the absence of moving junctions that suffer thermal dilation, problems typically related with Parabolic Trough Systems. In Linear Fresnel Systems, the receiver is fixed. It is not connected to the moving parts of the reflectors and does not follow the

tracking movements of the mirrors. Therefore, Linear Fresnel Reflector Power Plants do not need movable high pressure joints between the absorber tubes (which are a constructive challenge in Parabolic Trough Power Plants), providing a less vulnerable heat transfer System. This leads to even lower construction costs.

- The arrangement of the reflective elements close to the ground and almost in one plane has the advantage that wind loads are lower, making these structures less susceptible to wind damages than Parabolic Troughs and minimizing structural requirements.
- Because of the reflectors light weight, the limiting factor for their size (width and length) is their optical accuracy and not the mechanical load.
- Linear Fresnel Reflectors can provide a larger collection area for each receiver which leads to reduced cost for receivers and at the same time simplifies the handling of the working fluid circulation.
- As each mirror is far smaller than the mirrors of a Parabolic Trough System, they require relatively small parts for their construction, contributing to even lower construction and maintenance costs.
- As shading and blocking of the reflected solar radiation between adjacent reflectors are lower in Linear Fresnel Reflector Systems than in Parabolic Trough Systems (where a considerable distance between adjacent Parabolic-Trough rows is required), Linear Fresnel Reflectors field can be more densely packed leading to higher and more efficient land use.
- Lastly, cleaning is simpler for Linear Fresnel mirrors than for Parabolic Troughs.

1.4.2 Disadvantages

The main Linear Fresnel Reflector Systems disadvantage, in comparison to Parabolic Troughs, arises from their higher optical losses. As Fresnel Reflectors cannot be adjusted to follow the motion of the Sun in the sky as Parabolic Troughs can, there are more optical losses. These losses do not exist at all or in the same degree at Parabolic Troughs. In general, Linear Fresnel Reflector Systems:

- Have lower concentration factors (10–40) compared to Parabolic Troughs (30–100).
- Change their optical efficiency along the day in a significant degree.
- Have lower efficiency than Parabolic Trough Systems with the same active area.
- Have lower optical efficiency, especially when Sun is near sunrise or sunset.
- Have larger sensitivity to optical and tracking errors, due to the larger distances between mirrors and receiver, and due to the fixed receiver configuration.
- Suffer from shading losses, as reflectors may shade each other, especially at high solar zenith angles (low Sun elevation angles).

- Suffer from blocking losses, as reflectors may block part of the reflected solar radiation at high solar zenith angles (low Sun elevation angles).
- Display transversal cosine losses, whereas Parabolic Troughs, on the contrary, have only longitudinal cosine losses as they track Sun by moving the complete trough. This is the most important additional optical loss at Linear Fresnel Reflectors in comparison to Parabolic Troughs.

Although Linear Fresnel Reflector Systems may have lower efficiency than Parabolic Troughs, the likely reduced cost may well compensate this, providing a cost-effective solution for solar energy collection on a large scale (Benyakhlef et al. 2016). Moreover, their efficiency can be further improved with careful optical designs (inter-reflector distance, reflectors' shape, width and orientation) , development of alternative configurations (e.g. Compact Linear Fresnel Reflector, inclination of reflectors) and enhanced thermal performance.

Shading and blocking effects between adjacent reflectors is a significant drawback of Linear Fresnel Reflector Systems. However, to solve this issue with the easy way, it requires either increased spacing between reflectors, which takes up more land and increases the investment cost, or increased receiver height, which also increases the cost. For this reason, a great deal of effort has been made by scientists to develop improved configuration trying to tackle these problems. A solution to the shading and blocking problem is proposed by Mills and Morrison (2000). They designed a Compact Linear Fresnel Reflector (CLFR) Scheme where a number of adjacent reflectors are oriented towards different receivers. The use of multiple receivers allows a more compact reflector distribution avoiding shading and blocking effects and utilizing a portion of solar flux that otherwise would be lost. Reflectors near the base of a receiver are always oriented towards it, whereas, when reflectors' place reaches a nearly equidistant point between the two receivers, some minors reverse their orientation. This allows us to place the reflectors closer to each other without shading or blocking effects. For commercial power production (greater than 1 MW scale), and especially in areas where land is limited, it is very reasonable to have multiple receivers (Barlev et al. 2011). Another new geometry of Reflector Fields for limiting blocking end shading effects and maximizing the concentrated solar radiation density has been studied by Chaves and Collares-Pereira (2010). They proposed a reformation of the platform on which reflectors are mounted into a wave-shaped configuration.

References

Abbas, R., M. Valdés, M.J. Montes, and J.M. Martínez-Val. 2017. Design of an innovative linear Fresnel collector by means of optical performance optimization: A comparison with parabolic trough collectors for different latitudes. *Solar Energy* 153: 459–470.

Ahmed, Mohamed H., and Amr M.A. Amin. 2016. Thermal Analysis of the Performance of Linear Fresnel Solar Concentrator. *Journal of Clean Energy Technologies* 4 (5): 316–320.

Barlev, David, Ruxandra Vidu, and Pieter Stroeve. 2011. Innovation in concentrated solar power. *Solar Energy Materials and Solar Cells* 95: 2703–2725.

Bellos, E., E. Mathioulakis, C. Tzivanidis, V. Belessiotis, and K.A. Antonopoulos. 2016. Experimental and numerical investigation of a linear Fresnel solar collector with flat plate receiver. *Energy Conversion and Management* 2016 (130): 44–59.

Beltagy, Hani, Djaffar Semmar, Christophe Lehaut, and Noureddine Said. 2017. Theoretical and experimental performance analysis of a Fresnel type solar concentrator. *Renewable Energy* 101: 782–793.

Benyakhlef, S., A. Al Mers, O. Merroun, A. Bouatem, N. Boutammachte, S. El Alj, H. Ajdad, Z. Erregueragui, and E. Zemmouri. 2016. Impact of heliostat curvature on optical performance of Linear Fresnel solar concentrators. *Renewable Energy* 89, 463–474.

Boito, Paola, and Roberto Grena. 2016. Optimization of the geometry of Fresnel linear collectors. *Solar Energy* 135: 479–486.

Chaves, J., and M. Collares-Pereira. 2010. Etendue-matched two-stage concentrators with multiple receivers. *Solar Energy* 84 (2): 196–207.

Francia, G. 1968. Pilot plants of solar steam generation systems. *Solar Energy* 12: 51–64.

Gharbi, Najla El, Halima Derbal, Sofiane Bouaichaoui, and Noureddine Said. 2011. A comparative study between parabolic trough collector and linear Fresnel reflector technologies. *Energy Procedia* 6 (2011): 565–572.

Heimsath, A., F. Cuevas, A. Hofer, P. Nitz, and W.J. Platzer. 2014. Linear Fresnel collector receiver: Heat loss and temperatures. *Energy Procedia* 49, 386–397.

Kesari, J.P., Mohit Gupta, Aadish Jain, and A.K. Ojha. 2015. Review of the Concentrated Solar Thermal Technologies: Challenges and Opportunities in India, IJRSI, Volume II, Issue I, January 2015, pp 105–111, ISSN 2321–2705.

Mahdi, Khaled, and Nadir Bellel. 2014. Development of a Spherical Solar Collector with a cylindrical Receiver. *Energy Procedia* 52: 438–448.

Mills, D.R., and G.L. Morrison. 2000. Compact linear Fresnel reflector solar thermal power plants. *Solar Energy* 68 (3): 263–283.

Pavlović, Tomislav M., Ivana S. Radonjić, Dragana D. Milosavljević, and Lana S. Pantić. 2012. A review of concentrating solar power plants in the world and their potential use in Serbia. *Renewable and Sustainable Energy Reviews*, 16 (6), 3891–3902.

Poullikkas, Andreas, Constantinos Rouvas, Ioannis Hadjipaschalis, and George Kourtis. 2012. Optimum sizing of steam turbines for concentrated solar power plants. *International Journal of Energy and Environment* 3(1): 9–18, ISSN: 2076-2895 (Print), ISSN: 2076-2909 (Online).

Stefano, Pauletta. 2016. A solar Fresnel collector based on an evacuated flat receiver. *Energy Procedia* 101: 480–487.

Zhang, H.L., J. Baeyens, J. Degreve, and G. Caceres. 2013. Concentrated solar power plants: Review and design methodology. *Renewable and Sustainable Energy Reviews* 22: 466–481.

Chapter 2
Solar Radiation

Solar energy is virtually inexhaustible and potentially available to be used everywhere. However, Solar Radiation Concentrating Systems exclusively depend on direct solar radiation. As a consequence, to plan and design them effectively, we need proper calculation and computation tools that allow us to estimate the amount of direct solar radiation falling on System's collectors. For this reason, it would be beneficial to study the nature of solar radiation, as well as the geometrical parameters affecting its amount on the edge of Earth's atmosphere. In addition, radiation–matter interaction's processes further modify solar radiation reaching Earth's surface. These phenomena must be taken into consideration when choosing or developing the most appropriate direct solar radiation model. Moreover, Sun's position in the sky and collectors' set-up are another two important factors. All these issues affect the design, the development and the efficiency of Solar Radiation Concentrating Systems and are dealt within this chapter.

2.1 Fundamentals of Solar Radiation

The main energy source of Earth is Sun. Solar energy is produced in the core of Sun due to fusion processes in the form of an extremely large number of high-energy particles and photons. They leave Sun's core and travel to its surface transporting energy. A part of this energy is released as radiation of matter, namely energetic elementary particles, composing the solar wind. However, the bigger part of solar energy is in the form of electromagnetic radiation, photons.

S. Karathanasis, *Linear Fresnel Reflector Systems for Solar Radiation Concentration*, https://doi.org/10.1007/978-3-030-05279-9_2

2.1.1 Key Definitions of Radiation

Although they are basic concepts of radiation physics, radiation, radiant energy, radiant power, radiant flux, irradiation and irradiance are terms that are easily mistaken. Therefore, before we proceed with the study of solar radiation, it would be helpful to clarify their meaning:

Radiation: This term is used in a very general way, neither indicating a specific physical quantity nor having any dimension. Radiation indicates a specific way of energy transport. In this process, energy is propagated through a medium or the empty space via energetic particles or photon. In this book, only, electromagnetic radiation (energy transport via electromagnetic waves) is considered.

Radiant Energy: It is the energy of electromagnetic waves (unit: joule [J]).

Radiant Power: It is the radiant energy per unit time (unit: watt [W], joule per second [J s^{-1}]).

Irradiance: This is the main term used throughout this book and indicates the incident radiant energy per unit area per unit time, or in other word the incident radiant power per unit area (unit: watt per square metre [W m^{-2}]). It is also called **radiant flux**.

Irradiation: This term describes the amount of incident radiant energy per unit area falling on a surface exposed to radiation for a specific time span (unit: joule per square metre [J m^{-2}]). It is computed by integration of irradiance over a specific time, usually an hour or a day.

Insolation: This term stands for the incoming solar radiation.

Extraterrestrial

Radiation: It is the solar radiation falling on a surface at the top of Earth's atmosphere perpendicular to the direction of radiation's propagation.

Direct Solar

Radiation: It is the solar radiation received directly from Sun, or else the solar energy falling on a surface without taking into account the radiation been scattered by the atmosphere and hitting the surface.

Solar constant: It is the solar radiant flux (irradiance) received on a surface of unit area perpendicular to the direction of solar radiation's propagation at the average Sun–Earth distance, outside Earth's atmosphere.

Normal Solar

Radiation: It is the solar radiant flux (irradiance) received on a surface of unit area being perpendicular to the direction of the solar radiation's propagation.

2.1.2 Radiation's Laws

The energy spectrum of electromagnetic radiation emitted from Sun resembles the thermal radiation emitted from a hot body at a certain temperature. Therefore, in order to understand solar radiation's characteristics, it is important to study and understand the concept of black body and its thermal radiation characteristics.

2.1.2.1 Black and Grey Bodies

If we sufficiently heat up a body, it starts to glow; that is, it begins to emit light, electromagnetic radiation. A common example is a metal that is heated. At first, it glows in dim reddish light. At around 700 °C, it becomes red. If we continue to heat it up, it will glow more intensely and the colour of the emitted light will change. The hotter it gets, the shorter the wavelength of the emitted light, and the initial red glow gradually turns to orange, yellow, white and even blue. At higher temperatures, even more radiation is emitted.

In radiation physics, the concept of the ideal absorber and emitter is used. This is a body that neither reflects any incident electromagnetic radiation nor lets it pass through. As it absorbs all radiation falling on it, it looks black. Such a body is called a black body (or blackbody). At equilibrium, radiation absorbed must equal radiation emitted. Therefore, although all hot bodies emit radiation, black bodies emit the maximum amount of radiation at a given temperature (at thermal equilibrium). Black bodies do not exist in reality. They are just useful theoretical concepts that help us to describe the radiation behaviour of real hot bodies.

However, although the emission behaviour of a hot object depends on its temperature, its material and surface properties play an even important role, resulting in lower amount of total radiation emitted, or absorbed, than an ideal black body does (they are called grey bodies).

2.1.2.2 Planck's Formula

The electromagnetic radiation emitted from a black body, the thermal radiation, has a continuous spectrum. The energy density of the emitted radiation as a function of its frequency was studied in the late nineteenth century by Lord Rayleigh and by Sir James Jeans using classical statistical physics. Although the Rayleigh–Jeans distribution fits the low-frequency behaviour of the experimental energy density spectrum very well, at high frequencies it failed to describe its form. According to their formula, as the frequency increases, the spectral irradiance increases and the total emitted radiation energy becomes infinite. This, however, contradicts the experimental fact that the total black body radiation is finite, and the spectral density has a maximum. As classical physics was proven unable to describe the wavelength distribution of electromagnetic radiation emitted from heated object,

Max Planck proposed, at the beginning of the twentieth century, a new mathematical expression describing this distribution. This formula was derived from experimental black body radiation data.

Plank formulated the law of black body radiation by assuming that the energy of radiation can only take discrete values. More specifically, he assumed that the energy, ε, of radiation with frequency v can only take integer multiples of a basic value $h{\cdot}v$, the so-called energy quantum, namely

$$\varepsilon = 0, hv, 2hv, 3hv, \ldots \tag{2.1}$$

Since by that time the underlying physics of Plank's assumption was not understood, he believed that this quantization of energy was only a mathematical trick, which was necessary in order his empirically obtained formula to be consistent with the knowledge of physics known at that time. Planck's law for the spectral power density, $E(\lambda, T)$, of the radiation emitted by a black body at temperature T (namely, its power emitted per unit area in the wavelength range from λ to $\lambda + \mathrm{d}\lambda$), is given by the formula

$$E(\lambda, T) = \frac{2\pi hc^2}{\lambda^5\left(\mathrm{e}^{\frac{hc}{\lambda kT}} - 1\right)} \tag{2.2a}$$

If it is expressed in terms of frequency, v, instead of wavelength, λ, it takes the form:

$$E(\lambda, T) = \frac{2\pi v^2}{c^2} \cdot \frac{hv}{\mathrm{e}^{\frac{hv}{kT}} - 1} \tag{2.2b}$$

In this formula, $k = 1.381 \times 10^{-23}$ W s K^{-1} (or J K^{-1}) is Boltzmann's constant, $h = 6.626 \times 10^{-34}$ W s^2 (or J s) is Planck's constant, and $c = 2.998 \times 10^8$ m s^{-1} is the velocity of light in vacuum.

A few years later, the profound significance of the quantization of radiation and the meaning of Planck's constant were discovered and published by Albert Einstein in his work on quanta and the interpretation of the photoelectric effect.

2.1.2.3 Stefan–Boltzmann Law

The total radiant power emitted by a black body, summed up over all wavelengths, or frequencies, depends on temperature, although not linearly. Higher temperatures are related to higher total radiant power. The corresponding relation was experimentally discovered by Jozef Stefan and backed by Ludwig Boltzmann using thermodynamics, before Planck's formula was formulated.

Stefan–Boltzmann law states that the total power radiated by a black body (the flux of radiation emitted by the body per unit area) is directly proportional to the fourth power of its absolute temperature:

$$P = \sigma \cdot T^4 \tag{2.3}$$

where $\sigma = 5.67 \times 10^{-8}$ W m^{-2} K^{-4} is the Stefan–Boltzmann constant.

Since the total radiation power is proportional to the fourth power of absolute temperature, it increases very rapidly with temperature.

Stefan–Boltzmann law can also be derived by the integration of Eqs. 2.2a and 2.2b over all possible wavelengths, or frequencies, from zero to infinity. Thus, by integrating the spectral irradiance over frequency, the total emitted power per unit area is

$$\begin{aligned} U(T) &= \int_0^\infty \frac{2\pi h\nu^3}{c^2} \cdot \frac{\mathrm{d}\nu}{\mathrm{e}^{\frac{h\nu}{kT}} - 1} \\ &= \frac{2\pi h}{c^2} \cdot \left(\frac{kT}{h}\right)^4 \cdot \int_0^\infty \frac{x^3 \mathrm{d}x}{\mathrm{e}^x - 1} \\ &= \frac{2}{15} \cdot \frac{\pi^5 k^4}{c^2 h^3} \cdot T^4 \end{aligned} \tag{2.4}$$

where the mathematical identity

$$\int_0^\infty \frac{x^3 \mathrm{d}x}{\mathrm{e}^x - 1} = \frac{\pi^4}{15} \tag{2.5}$$

was applied.

In this equation, the quantity

$$\sigma \equiv \frac{2}{15} \cdot \frac{\pi^5 k^4}{c^2 h^3} = 5.67 \times 10^{-8} \frac{\mathrm{W}}{\mathrm{m}^2 \cdot \mathrm{K}^4} \tag{2.6}$$

is Stefan–Boltzmann's constant.

2.1.2.4 Wien's Displacement Law

Although a black body emits radiation over a range of wavelengths, λ, there is a maximum of radiation power at a certain wavelength. In addition, the wavelength where the maximum appears varies with temperature in an inversely proportional way to the temperature: the higher the temperature, the smaller is the wavelength at

the maximum power of the radiation. The quantitative relation between the maximum wavelength and the corresponding temperature was derived experimentally by Wien and is known as Wien's displacement law. It states that the wavelength at the point of maximum spectral radiant power is inversely proportional to the temperature:

$$\lambda_{\max} = \frac{b}{T} \tag{2.7}$$

where $\lambda_{\max}$ is the wavelength at peak intensity (in metres, m), b is a constant ($=2.898\times10^{-3}$ m K), and T is the absolute temperature (in Kelvin, K).

This relation allows us to derive the temperature of a body from the radiation spectrum it emits.

Despite an experimental result, Wien's displacement law can also be derived mathematically by the differentiation of Planck's formula with respect to the wavelength. [Stefan–Boltzmann law results from the integration of Plank law, over the whole range of wavelengths, or frequencies, whereas Wien's displacement law results from the differentiation of Planck's law.]

These three, in fact interconnected, laws, Planck's radiation law, Wien's displacement law and the Stefan–Boltzmann law, represent an important physical background to understand solar radiation and its possible use by developing appropriate exploitation Systems.

2.2 Solar Radiation on the Edge of Earth's Atmosphere

2.2.1 The Solar Radiation Spectrum

Sun is a hot sphere of gas heated by nuclear fusion reactions at its centre. The intense radiation produced in its interior is initially absorbed by the overlying layers of hydrogen ions. Thus, energy is transferred in Sun's interior by convection and then reradiated from its outer surface, the photosphere, to the space. Since there are no black bodies in reality, as they are only an idealization, neither Sun is one. Nevertheless, its radiation spectrum and radiation power resemble approximately the spectrum and the intensity of the radiation of a black body emitter at around 5780 K. Its electromagnetic spectrum contains an enormous range of wavelengths, or frequencies, of radiation, from gamma and X-rays to ultraviolet (UV), visible, infrared (IR) and radio waves. However, Earth's atmosphere allows only solar radiation from the UV wavelengths to the near- and midinfrared wavelengths to reach the ground.

However, Sun's radiation spectrum and black body emitter's spectrum at 5780 K are not identical. The reason is that Sun is not exactly a black body, as it does not have uniform surface temperature. In fact, there are areas on its surface as

well as under surface layers with different temperatures. Furthermore, solar spectrum is interrupted by dark lines due to absorption processes in Sun's atmosphere.

The biggest part of solar energy (a bit less than half of it) comes in the form of radiation in the visible part of the electromagnetic spectrum (the lower wavelength limit is taken to be between 360 and 400 nm and the upper limit between 760 and 830 nm). The remaining part is mainly in the near infrared (above 800 nm) with a smaller contribution from the ultraviolet part of the spectrum (from about 250 to about 400 nm). Using Wien's displacement law, the effective Sun temperature is estimated to be about 6300 K. However, if we use the total emitted power and the Stefan–Boltzmann law, Sun is a black body radiator at about 5780 K.

2.2.2 *Solar Radiation at the Top of the Atmosphere (Extraterrestrial Radiation)—Solar Constant*

The power of solar radiation per unit area (the solar irradiance) at the outer border of Earth's atmosphere (consequently, not the irradiance on Earth's surface) is essentially unvarying and nearly constant. Its mean value is referred to as the solar constant. If we assume that Sun's temperature and radius (more precisely its photosphere's temperature and radius, which emits the major part of the radiation that leaves Sun) are constant, solar constant depends basically only on the distance between Sun and Earth.

Because Sun–Earth distance is not constant, the supposition that solar constant is constant is not true. Actually, there are regular variations during the year, as well as long-term variations. The actual value of solar constant fluctuates about 6.9% during a year due to Earth's varying distance from Sun (Paulescu et al. 2013). Therefore, solar constant can be deemed only as an average value over a certain time period. On account of this, several experiments have been made, using high altitude aircraft, balloons and satellite measurements, trying to determine solar constant's characteristics (value and variation). Eventually, the World Meteorological Organization fixed in 1982 the value of 1367 W/m^2 as the solar constant.

2.2.3 *Energy Emitted by Sun*

Sun emits radiation into space isotropically. As no radiation can get lost, due to the energy conservation principle, the total radiant flux through Sun's surface equals the flux through any spherical surface concentric to Sun. So, if we consider a sphere around Sun, located on Earth's orbit, all radiant energies leaving Sun arrive at this sphere. This means that if we know the irradiance at this sphere we can calculate the total solar radiation power by multiplying the irradiance at this point by the area of

the sphere. As this sphere has a radius equal to the mean Sun–Earth distance, $r_{SE} = 1.496 \times 10^{11}$ m, the total radiation power emitted by Sun is:

$$P_S = \varepsilon_0 \cdot 4\pi \cdot r_{SE}^2 \Rightarrow$$
$$P_S = 1.367\,\mathrm{W\ m^{-2}} \cdot 4 \cdot 3.14 \cdot \left(1.496 \times 10^{11}\right)^2 \mathrm{m^2} \Rightarrow$$
$$P_S = 3.85 \times 10^{26}\,\mathrm{W}$$

2.3 Solar Radiation on Earth's Surface—Radiation Extinction Processes in the Atmosphere

As presented in the previous paragraph, solar constant is the radiant power per square metre incident on a surface on the top of the atmosphere normal to the direction of the radiation's propagation. However, the irradiance on Earth's surface will be different, less than this value, as not all solar radiations falling on Earth's atmosphere reach the ground. When solar radiation crosses the atmosphere, several radiation-attenuating effects occur that reduce it by about 30% by the time it reaches Earth's surface (Iqbal 1983).

Earth's atmosphere is composed of nitrogen (N_2), oxygen (O_2), carbon dioxide (CO_2), water vapour (H_2O) and a number of other minor constituents. Most of them are well mixed, resulting in virtually constant ratios throughout the atmosphere. However, water vapour (H_2O) is an exception, as its concentration is extremely variable in space and time and, depending on atmosphere's temperature, they can condense, forming clouds. The clouds reduce the solar radiation reaching Earth's surface, due to reflection, absorption and scattering.

2.3.1 Scattering of Solar Radiation in the Atmosphere

Scattering occurs when a part of the radiation is forced to deviate from its initial direction of propagation due to non-uniformities found in its way (molecules, dust particles, etc.). It happens when particles or large gas molecules present in the atmosphere interact with solar electromagnetic radiation and force it to be re-emitted into other directions, different from its initial propagation path. The amount of radiation scattered depends on several factors including the wavelength of the radiation, the abundance of particles or gases, and the distance the radiation travels through the atmosphere. In the case of solar radiation, there are three (3) types of scattering processes, Rayleigh, Mie and non-selective scattering. Which of these happens depends on the size of the non-uniformities in relation to the wavelength of the passing radiation. Because of scattering processes, solar radiation reaches Earth's surface partially as diffuse radiation and partially as direct radiation.

Rayleigh scattering occurs when particles' size is very small compared to the wavelength of the radiation (nitrogen and oxygen molecules) and, therefore, it is the dominant mechanism in the upper atmosphere. As sunlight passes through the upper atmosphere, the shorter wavelengths of the spectrum are scattered more than the longer wavelengths. It is more obvious at sunrise and sunset when solar radiation has to travel longer distances through the atmosphere than at midday, and the scattering of the shorter wavelengths is more intense. This fact explains why sky appears blue during the day and red at sunrise and sunset, as the longer wavelengths penetrate the atmosphere in greater proportion.

On the other hand, Mie scattering occurs when the size of the particles is just about the same size as the wavelength of the radiation. Hence, dust, pollen, smoke and small water droplets are common causes of Mie scattering. They affect longer wavelengths than those affected by Rayleigh scattering. Since larger particles are more abundant in the lower part of the atmosphere, Mie scattering occurs mostly in troposphere.

Except from the above-mentioned mechanisms, particles larger than the wavelength of the radiation (large water droplets and large dust particles) can also scatter solar radiation. This type of scattering is called non-selective scattering. It gets its name from the fact that there is not any preferred wavelength to be scattered; instead, all wavelengths are scattered about the same. This is the reason why fog and clouds appeared white.

Scattering does not convert radiation into other forms of energy. Nevertheless, it reduces direct solar radiation. Considering Concentrated Solar Radiation Power Systems, which use only direct solar radiation, scattering constitutes a loss of useable radiation.

2.3.2 *Absorption of Solar Radiation in the Atmosphere*

Absorption is the other main mechanism which attenuates electromagnetic solar radiation as it passes through the atmosphere. In contrast to scattering, where a portion of solar radiation is dispersed in many directions, absorption is caused by molecules in the atmosphere that absorb energy at specific wavelengths. This process reduces the available solar radiation at Earth's surface considerably.

Ozone (O_3), water vapour (H_2O) and carbon dioxide (CO_2) absorb radiation of a certain spectral range. They are the three main atmospheric constituents that alter solar radiation reaching Earth's surface by absorbing electromagnetic energy in different, but very specific, regions of the spectrum. Ozone (O_3) in the upper atmosphere absorbs almost completely the ultraviolet radiation (shortwave radiation) emitted from Sun at wavelengths below 290 nm. This radiation is harmful to most living beings. Above 290 nm, ozone (O_3) absorption decreases, until at 350 nm, where there is almost no absorption. Another weak ozone (O_3) absorption

band is near 600 nm. Stratospheric ozone (O_3) depletion allows more of this short wavelength radiation to reach Earth, with consequent harmful effects on biological systems.

On the other hand, carbon dioxide (CO_2) absorbs radiation strongly in the far infrared portion of the spectrum leading to the so-called greenhouse effect. Water vapour (H_2O) and methane (CH_4) are the main greenhouse gasses. Water vapour (H_2O) in the atmosphere absorbs strongly in the longwave infrared part and the shortwave microwave regions of the solar radiation spectrum, with absorption bands at 1, 1.4 and 1.8 μm. However, their presence in the lower atmosphere varies greatly from location to location and from time to time during the year, complicating the solar energy spectrum that reaches Earth's surface. Due to carbon dioxide (CO_2) and water vapour (H_2O) absorbance, the radiation transmission through the atmosphere is very low at wavelengths above 2.5 μm. Lastly, oxygen (O_2) and nitrogen (N_2) absorb radiation over a large wavelength range.

2.3.3 Solar Radiation Extinction Coefficient

The above-presented effects affect solar radiation reaching Earth's surface considerably. Therefore, we have to take them all into account when designing Concentrated Solar Radiation Power Systems. Solar radiation at ground level has two components: direct radiation and diffuse radiation. However, Concentrated Solar Radiation Power Systems can utilize only direct solar radiation, since this is the sole component of solar radiation that can be concentrated. Therefore, in order to be able to develop these Systems effectively, we must be able to calculate this particular component of solar radiation at Earth's surface.

As it has been already mentioned, solar radiation attenuates as it passes through the atmosphere by absorption and scattering. Their combined effect is called extinction or attenuation. We can define a linear extinction coefficient α by applying the following approach: let the intensity of solar radiation at a level z in the atmosphere be I. At another level in the atmosphere, $z - \mathrm{d}z$, situated lower by a distance $\mathrm{d}z$, the intensity of solar radiation has dropped, as a result of absorption and scattering, to $I - \mathrm{d}I$, where $\mathrm{d}I$ is the change in intensity across $\mathrm{d}z$. The linear extinction coefficient $\alpha(z)$ is defined as the fractional decrease in solar radiation intensity over the distance $\mathrm{d}z$ and is given by the equation

$$-\frac{\mathrm{d}I}{I} = \alpha(z) \cdot \mathrm{d}z \tag{2.8}$$

In general, α depends on the composition of the atmosphere at the level z and the frequency, v, or the wavelength, λ, of the radiation. For a particular wavelength, λ, this equation can be written as

$$-\frac{\mathrm{d}I_\lambda}{I_\lambda} = \alpha_\lambda(z) \cdot \mathrm{d}z \tag{2.9}$$

If we integrate both sides of Eq. 2.9 from the upper limit of the atmosphere, z_{atm}, to the Earth's surface, $z = 0$, the intensity of the passing solar radiation, I_λ, at Earth's surface is

$$\begin{gathered}\int_{I_\lambda^0}^{I_\lambda} \frac{\mathrm{d}I'_\lambda}{I'_\lambda} = -\int_{z_{\mathrm{atm}}}^{0} \alpha_\lambda(z) \cdot \mathrm{d}z \Rightarrow \\ \ln(I_\lambda) - \ln\left(I_\lambda^0\right) = \ln\left(\frac{I_\lambda}{I_\lambda^0}\right) = -\int_{z_{\mathrm{atm}}}^{0} \alpha_\lambda(z) \cdot \mathrm{d}z \Rightarrow \\ I_\lambda = I_\lambda^0 \cdot \mathrm{e}^{-\int_{z_{\mathrm{atm}}}^{0} \alpha_\lambda(z) \cdot \mathrm{d}z}\end{gathered} \tag{2.10}$$

If α is uniform and not a function of z, $\alpha(z) = \alpha$, and for the case where Sun is at the local zenith, Eq. 2.10 becomes

$$I_\lambda = I_\lambda^0 \cdot \mathrm{e}^{-a \cdot h_{\mathrm{atm}}} \tag{2.11}$$

where h_{atm} is the height of the atmosphere.

This equation is the Beer–Lambert–Bouguer law and describes quantitatively the reduction (attenuation) of the radiation intensity, I_λ, when it passes through a medium with extinction coefficient α (α_λ at wavelength λ). It is frequently used in atmospheric physics (Sportisse 2010).

2.3.4 The Atmospheric Optical Depth

Another useful concept in radiation attenuation processes is the so-called optical depth τ_λ (unitless), which for a monochromatic radiation is defined by the equation

$$\mathrm{d}\tau_\lambda = \alpha_\lambda(z) \cdot \mathrm{d}z \tag{2.12}$$

where $\mathrm{d}z$ is the length of the radiation propagation path through the medium. If we integrate both sides of Eq. 2.12, the atmospheric optical depth in the case of Sun being at the local zenith becomes

$$\begin{aligned}
\int_0^{\tau_\lambda^0} \mathrm{d}\tau'_\lambda &= \int_{z_{\mathrm{atm}}}^{0} \alpha_\lambda(z) \cdot \mathrm{d}z \Rightarrow \\
\tau_\lambda^0 &= \int_{h_{\mathrm{atm}}}^{0} \alpha_\lambda(z) \cdot \mathrm{d}z \Rightarrow \\
\tau_\lambda^0 &= \alpha_\lambda \cdot h_{\mathrm{atm}}
\end{aligned} \tag{2.13}$$

Substituting Eq. 2.13 into Eq. 2.11, it becomes

$$I_\lambda = I_\lambda^0 \cdot \mathrm{e}^{-\tau_\lambda^0} \tag{1.14}$$

Integrating this equation over all wavelengths, we obtain the equation that describes solar radiation attenuation as it passes through Earth's atmosphere, in its most frequently used form in atmospheric physics:

$$I = I^0 \cdot \mathrm{e}^{-\tau^0} \tag{2.15}$$

where I^0 is the solar irradiance at the top of Earth's atmosphere, or the solar constant, I is the solar irradiance at Earth's surface, and τ^0 is the total optical depth of the atmosphere due to all attenuation effects when Sun is at the local zenith (Sun's zenith angle, $\theta_z = 0°$). [The solar zenith angle, θ_z, is the angle between Sun's position and the point directly overhead, the local zenith (Fig. 2.1).]

If Sun is not at the local zenith, but on a zenith angle, $\theta_z = \theta > 0°$, then the solar radiation passes through a larger part of the atmosphere and its length path is longer. As it can be seen from Fig. 2.1, if we consider that the atmosphere is horizontally homogeneous, the total (for all wavelengths) attenuation coefficient, $\alpha(z)$, at a level z above the surface is nearly constant for a layer of thickness $\mathrm{d}z$. In this case, the total optical depth, $\mathrm{d}\tau'$, along the elementary radiation path, $\mathrm{d}s$, is

$$\begin{aligned}
\mathrm{d}\tau' &= \alpha(z) \cdot \mathrm{d}s \Rightarrow \\
\mathrm{d}\tau' &= \alpha(z) \cdot (\mathrm{d}z/\cos\theta_z) \Rightarrow \\
\mathrm{d}\tau' &= \frac{\alpha(z) \cdot \mathrm{d}z}{\cos\theta_z} \Rightarrow \\
\mathrm{d}\tau' &= \alpha(z) \cdot \mathrm{d}z \cdot \frac{1}{\cos\theta_z} \Rightarrow \\
\mathrm{d}\tau' &= \mathrm{d}\tau^0 \cdot \frac{1}{\cos\theta_z}
\end{aligned} \tag{2.16}$$

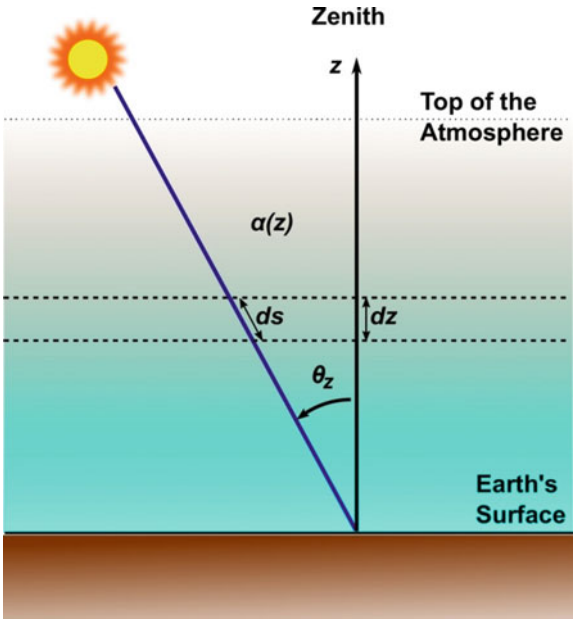

Fig. 2.1 The solar zenith angle, θ_z, is the angle between Sun's position and the point directly overhead, the local zenith. If Sun is not at the local zenith, its zenith angle, θ_z, is greater than 0°, and solar radiation passes through a larger part of the atmosphere. Consequently, the length path ds is longer than the length path dz. However, if we consider that the atmosphere is horizontally homogeneous, the total (for all wavelengths) attenuation coefficient, $\alpha(z)$, at a level z above the surface is nearly constant for a layer of thickness dz

If we integrate Eq. 2.16 for the whole extent of the atmosphere, we come to the following formula

$$\begin{aligned}
&\int_0^{h_{\text{atm}}} \mathrm{d}\tau' = \int_0^{h_{\text{atm}}} \mathrm{d}\tau^0 \cdot \frac{1}{\cos\theta_z} \Rightarrow \\
&\int_0^{h_{\text{atm}}} \mathrm{d}\tau' = \frac{1}{\cos\theta_z} \cdot \int_0^{h_{\text{atm}}} \mathrm{d}\tau^0 \Rightarrow \\
&\tau' = \tau^0 \cdot \frac{1}{\cos\theta_z} \\
&\tau' = \tau^0 \cdot m
\end{aligned} \tag{2.17}$$

where τ' is the total optical depth of the atmosphere when Sun is at zenith angle $\theta_z \neq 0$, τ^0 is the total optical depth of the atmosphere for vertical position of Sun, and $m = 1/\cos\theta_z$ is the so-called air mass.

Taking all these into account, we can easily conclude that the relative magnitude of direct solar radiation is a function of Sun's zenith angle, θ_z, and consequently, of the path length through the atmosphere. Consequently, solar irradiance changes throughout a day as Sun's zenith angle, θ_z, varies. For example, when Sun is close to the horizon, its radiation is lower than if it is close to zenith.

2.3.5 The Air Mass

In atmospheric optics, solar radiation path length through the atmosphere is parameterized by the above-mentioned term of air mass (or airmass). This term indicates the relative atmospheric air mass and is the ratio of the actual radiation path length to that at zenith and at sea level. By definition, sea-level air mass at zenith equals 1 ($m0 = 1$). Air mass increases as Sun's zenith angle, θ_z, increases. Thus, for example, for $\theta_z = 60°$, $m = 1/\cos\ (60°) = 1/0.5 = 2.0$, as shown in Fig. 2.2. However, it can also be less than 1 at elevations higher than sea level, as it will be discussed later.

In Concentrated Solar Radiation Power Systems, the air mass is indicated by the acronym AM, and its value is often given by appending it to AM, so that AM1 indicates an air mass of 1 ($m = 1$), AM2 indicates an air mass of 2 ($m = 2$), and so on. Subsequently, the region above Earth's atmosphere, where no atmospheric attenuation of solar radiation due to radiation—matter interaction occurs, is considered to have zero air mass (AM0).

Hence, in order to estimate the influence of atmospheric attenuation processes on the amount of solar radiation reaching Earth's surface we have to calculate the corresponding air mass (AM), which, in combination with the total optical depth, τ^0, represents the amount of the atmosphere through which solar radiation must pass. When the sky is clear, the maximum radiation reaching Earth's surface occurs when Sun is directly overhead, and solar radiation has the shortest path length

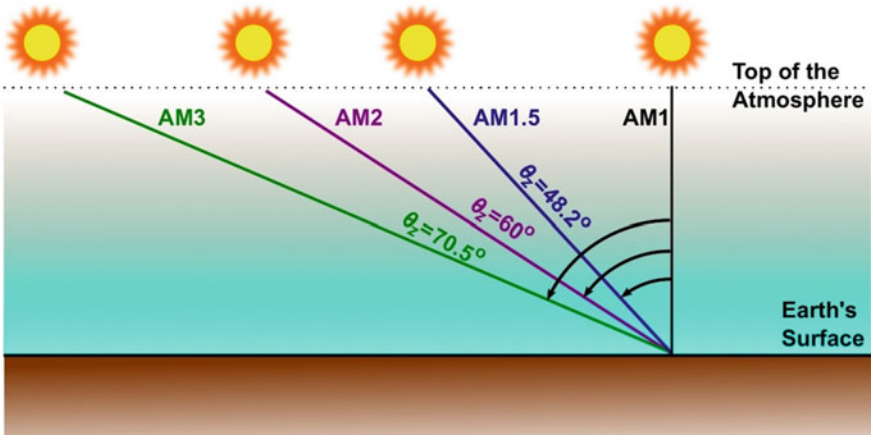

Fig. 2.2 Air mass increases as Sun's zenith angle, θ_z, increases. For $\theta_z = 48.2°$, $m = 1/\cos(48.2°) = 1/0.666 = 1.5$ (=AM1.5), for $\theta_z = 60°$, $m = 1/\cos(60°) = 1/0.5 = 2.0$ (=AM2.0), for $\theta_z = 70.5°$, $m = 1/\cos(70.5°) = 1/0.333 = 3.0$ (=AM3.0)

through the atmosphere. In any other case, the radiation path length can be approximated using the already mentioned expression of air mass

$$\mathrm{AM} = m = \frac{1}{\cos\theta_z} \tag{2.18}$$

However, not only solar zenith angle, θ_z, determines air mass, but also the altitude (or height), H, of a given place, since the actual thickness of the atmosphere above a site depends on the place's altitude above sea level. Therefore, the air mass estimated by Eq. 2.18 has to be corrected with respect to the site elevation above sea level.

The local atmospheric pressure, P_l, is directly related to the site altitude and the thickness of the atmosphere above it. In the absence of measured pressure data, a good approximation of P_l is given by the expression (Myers 2013)

$$P_l = P_0 \cdot \mathrm{e}^{-0.000832 \cdot H} \tag{2.19a}$$

where H is the site's altitude in kilometres and P_0 is the mean atmospheric pressure at sea level, taken equal to 101.325 hectopascals (hPa) or 1013.25 millibar (mb).

Iqbal (1983) presents this formula slightly differently:

$$P_l = P_0 \cdot \mathrm{e}^{-0.0001184 \cdot H} \tag{2.19b}$$

Thus, the pressure-corrected air mass m_p, representing the actual path length at a height $z = H$ above sea level in relation to the air mass, m_0, at sea level, $z = 0$, when Sun is at the local zenith is

$$\begin{aligned} m_p &= m_0 \cdot \frac{P_l}{P_0} \Rightarrow \\ m_p &= m_0 \cdot \mathrm{e}^{-0.000832 \cdot H} \end{aligned} \tag{2.20}$$

A similar treatment of the above issue is presented by Wong and Chow (2001). This formula for solar radiation evaluation is simple, nevertheless, widely used by engineers (Wong and Chow 2001).

So, the direct normal solar irradiance, I (in W m^{-2}), may be given by the equation

$$I = C_n \cdot I^0 \cdot \mathrm{e}^{-\frac{B}{\cos\theta_z} \cdot \frac{P}{P_0}} = C_n \cdot I^0 \cdot \mathrm{e}^{-B \cdot \left(\frac{P}{P_0}\right) \cdot \sec\theta_z} \tag{2.21}$$

where I^0 is the extraterrestrial irradiance, and C_n is the atmosphere's clearness, a dimensionless parameter. The dimensionless parameter B represents an overall broadband value of the atmospheric attenuation coefficient for the basic

atmosphere, P (in mbar) is the actual local air pressure, and P_0 is the standard air pressure equal to 1013.25 mbar.

The above equations are only an approximation of the reality as they are based on the assumption of homogeneous and non-refractive atmosphere. However, this introduces an error when Sun is close to the horizon because the atmosphere has a nonzero curvature. In reality, Earth's atmosphere is a spherical shell surrounding the planet. In addition, the refraction index of the atmosphere (~ 1.0002772) is slightly, but meaningfully, different from the corresponding for space (1.0). These two facts mean that the propagation path of solar radiation is bent as it is inserted from space into the atmosphere (Fig. 2.3).

Nevertheless, since the radius of curvature of the atmosphere is large, the approximation of horizontal stratification of the atmosphere is reasonable for solar zenith angles, θ_z, less than about 70°. On the other hand, at larger zenith angles, near sunrise or sunset, the effect of refraction is large. Consequently, the actual air mass, m_r, is larger than the air mass, m, calculated solely from geometry, using Eqs. 2.20 or 2.18, and needs to be corrected. There have been conducted many studies addressing the problem of the computation of the true air mass at high zenith angles. Thus, a more accurate calculation of the actual air mass, taking into account the refraction effect of the atmosphere on solar radiation propagation, is obtained by using the following empirically identified formulas:

$$\mathrm{AM}_r = m_r = \frac{1}{\cos\theta_z + 0.51 \cdot (93.885 - \theta_z)^{-1.253}} \tag{2.22a}$$

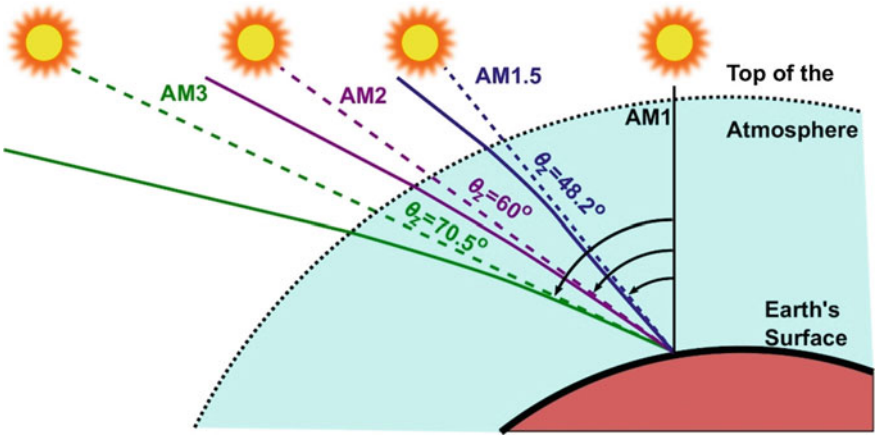

Fig. 2.3 Earth's atmosphere is a spherical shell surrounding the planet with a refraction index different from that for empty space. As a result, solar radiation's propagation path is bent at the air–space interface. This refraction effect of the atmosphere introduces an error on the estimation of the air mass when Sun is close to the horizon

$$\mathrm{AM}_r = m_r = \frac{1}{\cos\theta_z + 0.50572 \cdot (96.07995 - \theta_z)^{-1.6354}} \tag{2.22b}$$

$$\mathrm{AM}_r = m_r = \frac{1 - 0.012 \cdot (\sec^2\theta_z - 1)}{\cos\theta_z} \tag{2.22c}$$

$$\mathrm{AM}_r = m_r = \frac{35}{\sqrt{1224 \cdot \cos^2\theta_z + 1}} \tag{2.22d}$$

$$\mathrm{AM}_r = m_r = \frac{1.002432 \cdot \cos^2\theta_z + 0.148386 \cdot \cos\theta_z + 0.0096467}{\cos^3\theta_z + 0.149864 \cdot \cos^2\theta_z + 0.0102963 \cdot \cos\theta_z + 0.000303978} \tag{2.22e}$$

$$\mathrm{AM}_r = m_r = \frac{1}{\cos\theta_z + 0.00176759 \cdot \theta_z \cdot (94.37515 - \theta_z)^{-1.21563}} \tag{2.22f}$$

Equation 2.22a is presented by Iqbal (1983), Eq. (2.22b) by Kasten and Young (1989) (as cited by Myers 2013 and Reno et al. 2012) and Eqs. 2.22c, 2.22d, 2.22e and 2.22f by Reno et al. (2012).

Taking into account the altitude effect, described by Eq. 2.20, the actual air mass, m, for any solar zenith angle at any place on Earth with altitude, H, above sea level is given by the following expression (if we use only Eqs. 2.22a and 2.22b):

$$\mathrm{AM} = m = \frac{\mathrm{e}^{-0.000832 \cdot H}}{\cos\theta_z + 0.51 \cdot (93.885 - \theta_z)^{-1.253}} \tag{2.23a}$$

$$\mathrm{AM} = m = \frac{\mathrm{e}^{-0.000832 \cdot H}}{\cos\theta_z + 0.50572 \cdot (96.07995 - \theta_z)^{-1.6354}} \tag{2.23b}$$

Combining, now, Eqs. 2.15 and 2.17 with Eqs. 2.23a and 2.23b, solar irradiance, I', on a surface perpendicular to the direction of the solar radiation's propagation, at a place on Earth located at altitude H above sea level, and for any solar zenith angle, θ_z, is given by the equation:

$$I' = I^0 \cdot \mathrm{e}^{-\tau^0 \cdot m} \Rightarrow$$

$$I' = I^0 \cdot \mathrm{e}^{-\tau^0 \cdot \frac{\mathrm{e}^{-0.000832 \cdot H}}{\cos\theta_z + 0.51 \cdot (93.885 - \theta_z)^{-1.253}}} \tag{2.24a}$$

or

$$I' = I^0 \cdot \mathrm{e}^{-\tau^0 \cdot \frac{\mathrm{e}^{-0.000832 \cdot H}}{\cos\theta_z + 0.50572 \cdot (96.07995 - \theta_z)^{-1.6364}}} \tag{2.24b}$$

2.3.6 *Direct Solar Radiation Striking a Flat Horizontal and a Tilted Surface*

Equations 2.24a and 2.24b provide the irradiance of direct solar radiation on planes that are perpendicular to the direction of solar radiation's propagation, i.e. the direct normal irradiance (DNI). However, for designing Concentrated Solar Radiation Power Systems and performing calculations, it is necessary to calculate the irradiance on horizontal or tilted surfaces, which is different from the direct normal irradiance. The corresponding mathematical relationships can be derived by applying simple trigonometric formulas.

The incidence angle, θ, defined as the angle between the direction of the radiation's propagation and the normal on the irradiated plane, is, in general, nonzero, $\theta \geq 0$, whereas in planes perpendicular to the radiation direction the incidence angle is equal to 0° (Fig. 2.4). In the general case, the irradiance, I_t (the received irradiated power per square metre), on a surface inclined with respect to solar rays is inversely proportional to the illuminated area. Subsequently, the amount of energy per square metre received by the surface is lower. This is because solar power, I_n,

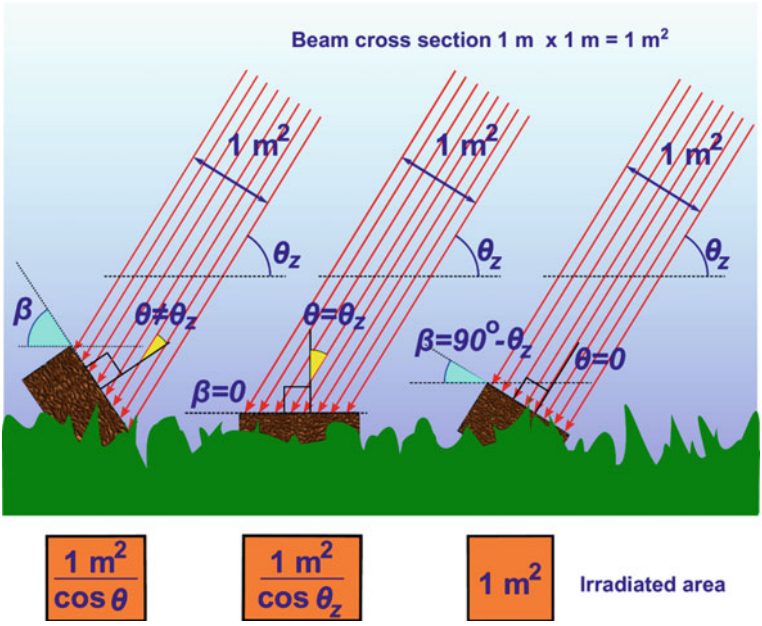

Fig. 2.4 The incidence angle, θ, the angle between the direction of the radiation's propagation and the normal on the irradiated plane, is, in general, nonzero, $\theta \geq 0$. In the case of a plane perpendicular to the direction of the radiation propagation, the incidence angle is 0°. The irradiated area is equal to the solar beam cross section, and the irradiance, I, (the received power per square metre) is maximum. In any other case, the amount of energy per square metre received by the surface is lower, as solar radiation is now spread on a larger area inversely proportional to cos θ_z

received by the plane is now distributed across a larger surface, S_t, which depends on the incidence angle, θ (Fig. 2.4). As it can be seen from Fig. 2.4, a solar radiation beam that strikes a surface at a vertical angle covers less area than in the case striking it at an oblique angle. In the first case, it provided more energy per surface unit. According to Fig. 2.4, and using the energy conservation principle, the total power received by the normal surface, S_n, and the inclined surface, S_t, remains constant:

$$I_n \cdot S_n = I_t \cdot S_t = \text{ constant} \tag{2.25}$$

However, the area of the tilt surface, S_t, is connected with the area of the surface, S_n, which is perpendicular to the direction of the radiation's propagation (the cross section of the solar radiation beam), and the incident angle, θ, through the following simple trigonometric relationship:

$$S_t = S_n \cdot \cos\theta \tag{2.26}$$

Therefore, if the direct normal irradiance is I_n, then the irradiance, I_t, on a tilted plane is given by the formula

$$I_t = I_n \cdot \cos\theta \tag{2.27}$$

where θ is the incidence angle.

The reduction of the direct solar irradiance due to non-normal orientation of the irradiated surface in relation to the direction of the radiation's propagation is called the cosine effect.

In the special case of a horizontal plane, the incidence angle, θ, is always equal to the solar zenith angle, θ_z, and the direct horizontal irradiance I_h is

$$I_h = I_n \cdot \cos\theta_z \tag{2.28}$$

However, in the general case the computation of the incidence angle of a tilted surface is complex. The surface tilt angle, β (the angle between the horizontal surface and the plane of the surface), the azimuth angle, γ, of the plane (the angle between south and the projection of the normal to the surface on a horizontal plane), and the azimuth angle, A, of the solar disc must be known. In other words, the angle of incidence, θ, for a given surface depends upon (i) the location on Earth, (ii) the time of the day and (iii) the day of the year. Taking all these into account, we can conclude that the irradiance at a site on Earth's surface is fully determined by Sun's position in the sky and the slope and orientation of the irradiated surface.

2.4 Geometrical Aspects of Direct Solar Radiation

The intensity of solar radiation received by a surface on Earth varies from place to place and throughout the year. There are two general kinds of variation in the received solar radiation that must be taken into account. The first is a variation in the extraterrestrial radiation, and the second is a variation due to the varying Sun's position in the sky. Moreover, the radiation emitted by Sun fluctuates with variability smaller than ±1.5% (Duffie and Beckman 1994, 2013). However, taking into account the uncertainties and variability of atmospheric transmission, the energy emitted by Sun can be considered to be constant for engineering purposes.

Earth moves around Sun once a year in an elliptical orbit with a small ellipticity or eccentricity. In this motion, Sun is situated in one of the two focuses of the ellipses. This means that sometimes Earth is closer to Sun than other times. The Sun–Earth distance is smaller when Earth is at perihelion (first week in January) and larger when Earth is at aphelion (first week in July) (the actual day is not fixed due to long-term variation in Earth's orbit). Due to the elliptical orbit, the Earth–Sun distance increases and decreases during a year by about ±1.7% in relation to the mean distance. As a consequence, since solar irradiance depends on the inverse power of the distance from Sun: $\sim 1/R^2$, it varies on top of Earth's atmosphere by about ±3.3% relative to its mean value of 1367 W/m^2 (Myers 2013).

Moreover, as clouds prevent more solar radiation from reaching Earth's surface than clear sky does, their irregular and unpredictable global distribution cause a significant spatial variation. Nevertheless, they only affect total insolation to a minor extent over long periods of time. Another reason accounting for the geographical distribution of solar radiation is Earth's spherical surface. At a specific time of the year, only some locations on Earth, lying on the same line of latitude, can receive radiation at right angles, while the rest receive solar radiation at varying oblique (sharp) angles (Fig. 2.5). As it has been also noted, Sun's position in the sky directly affects the intensity of solar irradiance, I_h, received on a surface lying horizontally on Earth.

If for a moment the highly variable attenuation of solar radiation by atmosphere is set aside, the main causes of solar radiation variations are due to Earth's rotation on its axis and its revolution around Sun. As Earth rotates once every 23 h 56 min (with respect to the distant stars—a sidereal day) around its axis, which is titled at an angle of 23.5° with respect to the plane of its orbit around Sun, Sun is not always at the same position in the sky. It depends on the time of the day and the day of the year and on the location on Earth. To put it differently, the tilted rotation axis produces seasonal and daily changes in the path of Sun on the sky dome, the points on the horizon where Sun rises and sets, and the period of daylight.

Therefore, as the irradiance on a plane normal to Sun's rays is exactly described by the extraterrestrial irradiance and Sun's position in the sky, these quantities have to be calculated. Because the accurate theory may be overwhelmingly complicated,

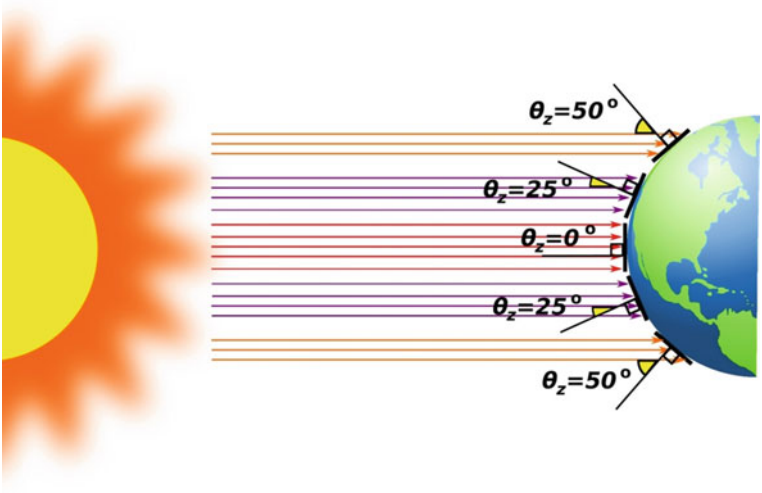

Fig. 2.5 Sun's position in the sky directly affects the intensity of solar irradiance, I_h, received of a surface lying horizontally on Earth. As a result, at any specific time of the year, only some locations on Earth, lying on the same line of latitude, can receive radiation at right angles, while the rest receive solar radiation at varying oblique (sharp) angles

in the following paragraphs simple models with analytic formulas will be presented. They are accurate enough and easily programmable, facilitating calculation on a computer.

2.4.1 The Sun–Earth Distance

According to Kepler's first law, Earth's trajectory around Sun is an ellipse with Sun at one focus. If the major axis of Earth's orbit equals to $2{\cdot}a$ and its minor axis equals to $2{\cdot}b$, then the shape of the ellipse is characterized by its eccentricity (ecc), defined by:

$$\text{ecc} = \frac{\sqrt{(a^2 + b^2)}}{a} \tag{2.29}$$

Although the geometrical parameters of Earth's orbit vary with time, at present its eccentricity is equal to 0.0167, very small. This means that Earth's orbit is very close to a circle, which corresponds to an eccentricity equal to zero.

According to Kepler's second law, as Earth moves on its orbit, its radius, the line from Sun to Earth, sweeps out equal areas in equal times. This leads to time-varying orbital speed and consequently to complex time-varying Earth–Sun distance.

The mean Earth–Sun distance, r_m, can be defined by

$$r_m = \sqrt{a \cdot b} = a\sqrt{1 - \text{ecc}^2} \tag{2.30}$$

Due to the energy conservation principle, the total power, P_S, emitted by Sun is equal to the irradiance, I_r, at a distance r from Sun multiplied by the surface, S_r, of the sphere with radius r:

$$\begin{aligned} P_S &= I_r \cdot S_r \Rightarrow \\ P_S &= I_r \cdot 4\pi \cdot r^2 \end{aligned} \tag{2.31}$$

Consequently, the total solar power, P_r, at a distance r will be equal to the total solar power, P_{r_m}, at a distance r_m, the mean Sun–Earth distance, where solar constant, I^0, is defined:

$$P_r = P_{r_m}$$

which results in

$$\begin{aligned} I_r \cdot 4\pi \cdot r^2 &= I^0 \cdot 4\pi \cdot r_m^2 \Rightarrow \\ I_r &= I^0 \cdot \frac{r_m^2}{r^2} = I^0 \cdot \left(\frac{r_m}{r}\right)^2 = I^0 \cdot R_c \end{aligned} \tag{2.32}$$

where R_c is the solar constant correction term, or the eccentricity correction factor, due to the elliptical motion of Earth around Sun and the varying Earth–Sun radius.

There are two popular equations for calculating solar constant correction term, R_c (Radosavljević and Đorđević 2001; Sung et al. 2015; Basunia et al. 2012; Bouzid et al. 2015; Myers 2013; Duffie and Beckman 1994, 2013; Iqbal 1983; Reno et al. 2012):

$$\begin{aligned} R_c = \left(\frac{r_m}{r}\right)^2 &= 1.000110 + 0.034221 \cdot \cos(d) + 0.001280 \cdot \sin(d) \\ &+ 0.000719 \cdot \cos(2d) + 0.000077 \cdot \sin(2d) \end{aligned} \tag{2.33a}$$

and

$$R_c = \left(\frac{r_m}{r}\right)^2 = 1 + 0.033 \cdot \cos\left(\frac{2\pi(\text{or } 360^\circ) \cdot d_n}{365}\right) \tag{2.33b}$$

where r_m is the mean distance, r is the actual distance, d_n is the number of the days in the year, with Jan 1 = 1, and d is computed from

$$d = \frac{2\pi \cdot (d_n - 1)}{365} \tag{2.34}$$

Thus, the solar constant, I^0, modified by the term R_c provides the extraterrestrial radiation incident on a plane normal to the direction of the radiation's propagation on the d_nth day of the year:

$$I^{0\prime} = I^0 \cdot R_c \tag{2.35}$$

2.4.2 Coordinate Systems

In order to be able to describe Sun's position in the sky and, consequently, direct solar radiation's direction, we need an appropriate coordinate system. From the point of view of an observer on Earth, Sun seems to be located on a concentric to Earth sphere of very large radius, the celestial sphere. As Sun is very far away from Earth, we are not interested in the Earth–Sun distance but only in the direction of Sun in relation to Earth or in relation to someplace on Earth. Hence, Sun's position can be described by using only two angles on the celestial sphere, without any distance coordinate.

There are two common coordinate systems for describing Sun's position in the sky in relation to Earth or to someplace on Earth, (a) the equatorial coordinate system and (b) the horizontal coordinate system. For designing Concentrated Solar Radiation Power Systems, it is most convenient to use the horizontal coordinate system, where the horizon of the observer constitutes the fundamental plane. Except from these, we need another coordinate system to describe the location of the place of interest on Earth. This is the common geographic coordinate system.

2.4.2.1 Terrestrial Coordinate System—The Geographic Coordinate System

Earth rotates around its axis which crosses its surface at two points: the North Pole and the South Pole. The great circle perpendicular to this axis is the equator. Any location on Earth can be determined by two coordinates, the latitude, φ, and the longitude, λ. The latitude, φ, of a point on Earth's surface is the angle between the equatorial plane and the straight line that passes through that point and the centre of Earth. Its values range from +90° at North Pole to −90° at South Pole. The equator is at zero degree latitude ($\varphi = 0°$). The line that joins all points on Earth having the same latitude forms a circle on Earth's surface called parallel, as it is parallel to the equator. Obviously, all parallels are parallel to the equator and to each other. On the other hand, the half circle passes through the North Pole and the South Pole and the place of interest is the local meridian. The longitude, λ, of this place is the angle

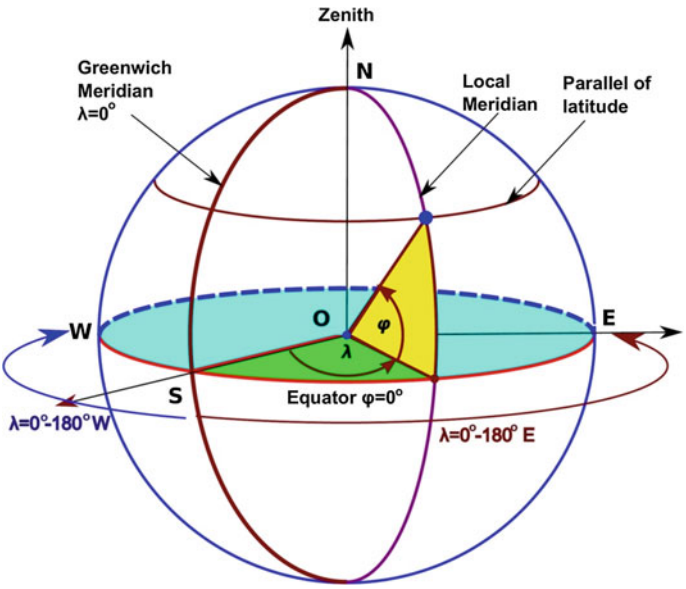

Fig. 2.6 In the geographic coordinate system, any location on Earth is determined by two coordinates, the latitude, φ, and the longitude, λ

formed by the plane of the local meridian with the plane of another reference meridian, the meridian of the British Royal Observatory in Greenwich, located in south-east London, England. This is the international prime meridian, but often simply called the Greenwich meridian. Longitude values range from −180° west the prime meridian to +180° east the prime meridian. To summarize, this coordinate system uses two fundamental planes, containing the equator and the prime meridian, and describes any point on Earth providing its angular deviations from these planes (Fig. 2.6).

2.4.2.2 Celestial Coordinate System

Sun's position on the celestial sphere is determined by using two fundamental planes that contain two great circles of the celestial sphere. Sun's coordinates are the values of two angles in these planes. The choice of the planes, as well as the choice of the starting points of the angles' measuring, determines the different coordinate systems.

The Horizontal Coordinate System

The horizontal coordinate system uses as fundamental planes: (a) the observer's horizontal plane and (b) the plane containing the local zenith, the north celestial pole and the observer's point on Earth. The intersection of the observer's horizontal plane with the celestial sphere defines a great circle, the horizon, where one of the coordinates is measured. The zenith is the point on the celestial sphere that is exactly above the observer. The line connecting the observer and the zenith is perpendicular to the plane of the horizon. The north celestial pole is the point where the northern extension of Earth's axis subtends the celestial sphere. The great circle connecting the Zenith with the celestial North Pole is called the meridian. It intersects horizon at point **S**, the south point of the horizon, which is the reference point for measuring one coordinate of the point of interest, in our case, Sun.

The two coordinates that are used in the horizontal coordinate system are the altitude angle, or height angle, or elevation angle, h, which is the angle between the horizontal plane and the line to the Sun, and the azimuth angle A, which indicates the angular displacement from south of the projection on the horizontal plane of the line connecting Sun with the observer. Displacements to the east are negative and to the west positive. Very often, instead of solar height angle, h, we also use solar zenith angle $\theta_z = 90° - h$, which indicates the angle between the vertical (pointing to the local zenith) and the line to Sun. Obviously, the height angle, h, of the celestial North Pole equals the geographical latitude of the observer, φ. The azimuth, A, is taken to be positive westwards, ranging from 0° to 360°. On the other hand, height angle, h, ranges from −90° below the horizon to +90° above it, towards zenith (Fig. 2.7).

The Equatorial Coordinate System

The equatorial coordinate system uses as fundamental planes those containing the celestial equator and the local meridian. The celestial equator is the projection of the terrestrial equator to the celestial sphere. Obviously, the two corresponding fundamental planes in the geographic and the equatorial coordinate system coincide. The other fundamental plane, containing the local meridian, the great circle containing the local zenith and the celestial North Pole, forms with its equivalent reference point in geographic coordinate system, the Greenwich meridian, an angle which is equal to the longitude, λ, of the place of interest. In addition, it intersects the equator at point **S**, which is the starting point for measuring one of the coordinates.

The position of any object on the celestial sphere, as is Sun in our case, is determined by the two coordinates: the declination, δ, and the hour angle, ω. According to all these mentioned above, in the equatorial coordinate system, the declination, δ, of an object on the celestial sphere is equivalent to the latitude, φ, of a place on Earth in the geographic coordinate system, and the hour angle, ω, is equivalent to the longitude, λ, of the same place. Sun's declination, δ, is the angle

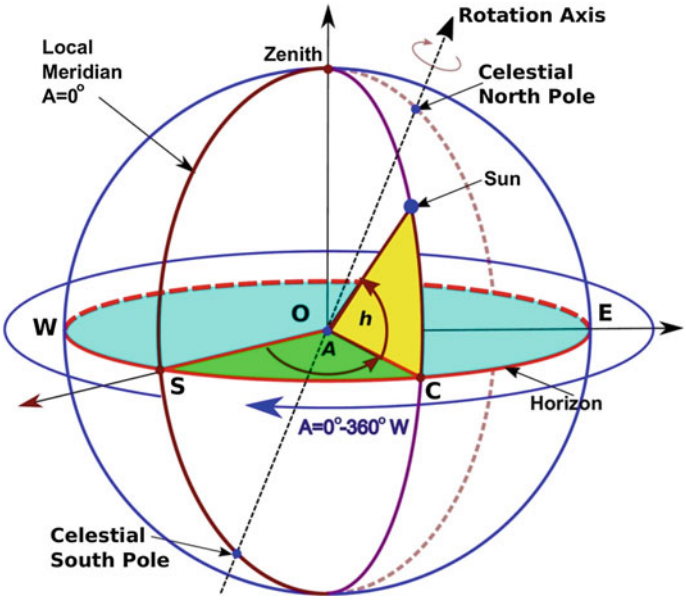

Fig. 2.7 The horizontal coordinate system uses as fundamental planes: **a** the observer's horizontal plane and **b** the plane containing the local zenith, the north celestial pole and the observer's point on Earth. The two coordinates that determine any object in the sky are the altitude angle, or height angle, or elevation angle, h, and the azimuth angle A

between the equatorial plane (containing the celestial equator) and the line to Sun. Its values are positive to the north of the celestial equator and negative to the south of it, ranging from −90° to +90°. On the equator, Sun's declination equals 0, $\delta = 0°$. On the other hand, the great circle connecting the celestial pole and Sun, which is called the solar hour circle, intersects the equator at point B. The angle $\widehat{SB}$ is the solar hour angle, ω (Fig. 2.8).

The solar hour angle, ω, defines the local solar time, t_{lst}, and its use facilitates many calculations. It indicates the time since Sun was at the local meridian, or the time it needs to be at the local meridian, due to Earth's rotation around its axis. Thus, solar hour angle, ω, is zero at local solar noon. The convention is the hour angle, ω, to be positive westwards of the local meridian. It is generally measured in radians or in hours (or h) (2π rad = 24 h). One hour (1 h) corresponds to an angle of 15° (=360°/24 h). To summarize, the morning hours are negative, the afternoon hours are positive, and at local solar noon the solar hour angle, ω, equals 0°.

The Celestial Equatorial Coordinate System

In the horizontal coordinate system, we describe Sun's position as perceived by an observer on a place on Earth's surface. This may be desirable and convenient when

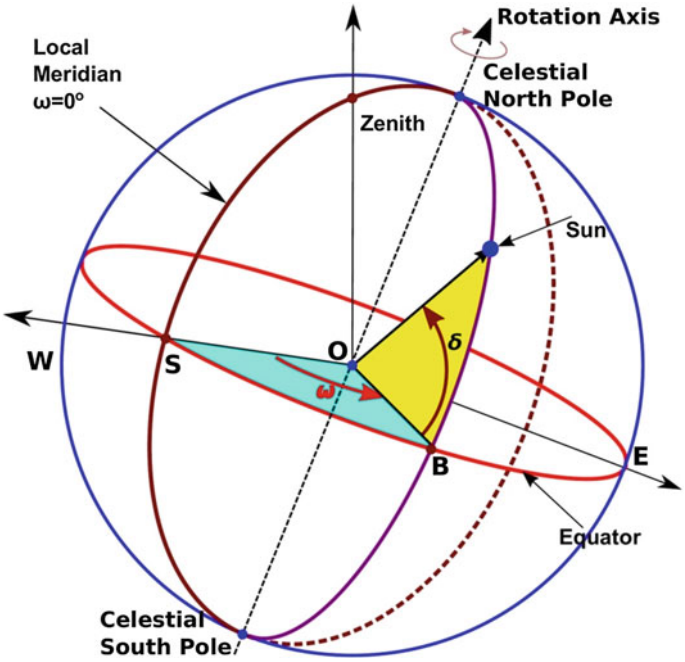

Fig. 2.8 In the equatorial coordinate system, the position of any object on the celestial sphere is determined by the declination, δ, and the hour angle, ω

studying Concentrated Solar Radiation Power Systems, but, because Earth is round and rotates around its axis, these coordinates depend on the location of the observer and vary over time in a complex manner. On the other hand, in the equatorial coordinate system, Sun's position is relatively independent of observer's location, depending only on the observer's longitude. Therefore, we need another coordinate system where Sun's motion can be described independently from observer's place on Earth. This is the Celestial Equatorial Coordinate System which is similar to the equatorial coordinate system with the only difference that the hour angle, ω, is replaced by the right ascension, α. The latter is measured eastwards along the celestial equator from the point (the zero reference point) where the celestial equator intersects the ecliptic, the vernal equinox point. It is measured in hours, ranging from 0 to 24 h (=360°, 1 h = 15° right ascension) (Fig. 2.9).

Ecliptic Coordinate System

As Earth revolves around Sun, its orbital plane, the ecliptic, does not coincide with the equator. In fact, it forms an angle, called the obliquity angle, ε, with the plane of the celestial equator. It varies over time, on a timescale of centuries, but for timescales related to human lifespan it is constant and currently $\varepsilon = 23.44°$. From

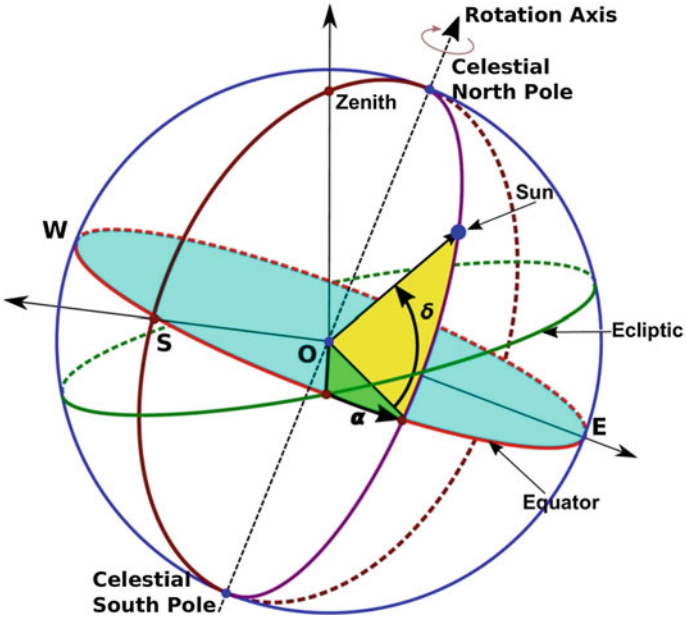

Fig. 2.9 The Celestial Equatorial Coordinate System is similar to the equatorial coordinate system with the only difference that the hour angle, ω, is replaced by the right ascension, α, measured eastwards along the celestial equator from the vernal equinox point

the point of view of an observer on Earth, Sun is moving on the ecliptic plane. In relation to the motion of Sun over a calendar year, there are four cardinal points of particular importance: the vernal equinox, where the trajectory of Sun intersects with the celestial equator when heading north, the summer solstice, where the trajectory of Sun reaches its most northern point above the celestial equator, equals 23.44° (or 23° 27′), and the autumnal equinox, where the trajectory of Sun intersects with the celestial equator when heading south, and the winter solstice, where the trajectory of Sun reaches its lowest point below the celestial equator, equals 23.44° (or 23° 27′) (Fig. 2.10). The dates and times of these four cardinal points vary year by year.

In a coordinate system having as fundamental plane that contains the ecliptic, Sun's motion is simple and can be described by only one coordinate. This system is the ecliptic coordinate system, and the coordinate is the ecliptic longitude, l. As a reference point for the ecliptic longitude, l, we use the vernal equinox (Fig. 2.10). Its values range from 0° to 360°, measured anticlockwise, along the ecliptic. The other coordinate is the ecliptic latitude, β, which measures the angular distance of an object from the ecliptic towards the north (positive) or south (negative) ecliptic pole (ranging from 0° to ± 90°). The ecliptic latitude of Sun is nearly 0, $\beta = 0°$.

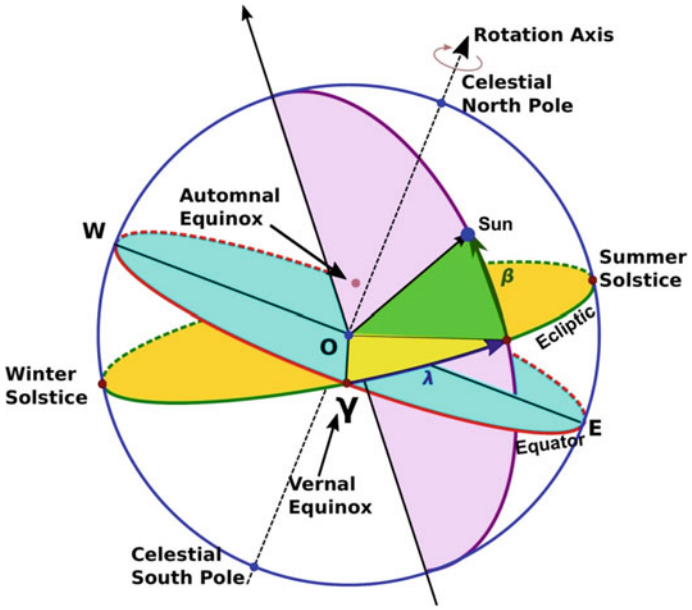

Fig. 2.10 The ecliptic coordinate system uses the ecliptic longitude, l, and the ecliptic latitude, β, to determine the position of any object in the sky, projected on the celestial sphere. Sun's ecliptic latitude is nearly 0, $\beta = 0°$

Right ascension, α, in the equatorial coordinate system, and ecliptic longitude, l, in ecliptic coordinate system have the same reference point, the vernal equinox, the point where the celestial equator intersects with the ecliptic.

2.5 Direct Solar Radiation on an Arbitrary Surface

Let us consider a tilted plane at a given geographical location and try to determine the incidence angle, θ, of the direct solar radiation on it. This is the angle formed between the direction of solar radiation and the normal to the irradiated surface. This angle depends on Sun's position in the sky and the tilt and orientation of the irradiated surface. More specifically, it depends on the geographical position (latitude and longitude) of the place the plane is located on, on the local solar time (the day of the year as well as the time of the day) that determines Sun's position and on the plane's position (tilt angle and azimuth angle). In other words, in order to be able to perform any calculation of the solar irradiance in a tilt surface on Earth, we have to know the *where*, *when* and *how*.

The parameters that define Sun's position in the horizontal coordinate system are solar azimuth, A, and solar altitude angle, h, or its complement, the solar zenith angle, θ_z. However, these parameters are a function of the place latitude, φ, and

longitude, λ, the solar hour angle, ω, and the solar declination, δ. Consequently, each of them is a function of the time of the day and the day of the year. The tilt angle, β, and the azimuth angle, γ, of the plane can be defined in the following way: we take a horizontal surface and incline it to the south (in positive direction) or to the north (in negative direction) by β, and then we rotate it to the west (in positive direction) or to the east (in negative direction) by γ.

To calculate the incident angle, θ, of solar radiation on a surface, we have to express the unit vector, $\widehat{\mathbf{S}}$, pointing from surface's centre to Sun, and the unit vector normal to the surface, $\widehat{\mathbf{N}}$, in the local horizontal coordinate system. Then, taking the dot (or scalar) product of these unit vectors, $\widehat{\mathbf{S}} \cdot \widehat{\mathbf{N}}$, we can find the cosine of the incident angle, θ:

$$\cos\theta = \frac{\widehat{\mathbf{S}} \cdot \widehat{\mathbf{N}}}{\left\|\widehat{\mathbf{S}}\right\| \cdot \left\|\widehat{\mathbf{N}}\right\|} = \frac{\widehat{\mathbf{S}} \cdot \widehat{\mathbf{N}}}{1 \cdot 1} = \widehat{\mathbf{S}} \cdot \widehat{\mathbf{N}} = s_1 \cdot n_1 + s_2 \cdot n_2 + s_3 \cdot n_3 \tag{2.36}$$

where s_1, s_2, s_1, n_1, n_2 and n_3, are the $\boldsymbol{i}$,$\boldsymbol{j}$ and $\boldsymbol{k}$ components, of $\widehat{\mathbf{S}}$ and $\widehat{\mathbf{N}}$, and $\hat{\mathbf{i}}$, $\hat{\mathbf{j}}$ and $\hat{\mathbf{k}}$, are the unit vector ($\left\|\hat{\mathbf{i}}\right\| = \left\|\hat{\mathbf{j}}\right\| = \left\|\hat{\mathbf{k}}\right\| = 1$) in the Cartesian coordinate system associated with the horizontal coordinate system (Fig. 2.11). As Sun moves from east to west, the direction to the south determines the x-axis, the direction to the east determines the y-axis, and the direction towards the zenith determines the z-axis. The unit vector pointing to Sun in the horizontal coordinate system is determined by the azimuth angle, A, and the height angle, h. As shown in Fig. 2.11.a, using the three unit vectors, $\hat{\mathbf{i}}$, $\hat{\mathbf{j}}$ and $\hat{\mathbf{k}}$, pointing to x, y and z, respectively, the unit vector, $\widehat{\mathbf{S}}$, pointing to Sun is given by

$$\begin{aligned}
&\widehat{\mathbf{S}} = s_1 \cdot \hat{\mathbf{i}} - s_2 \cdot \hat{\mathbf{j}} + s_3 \cdot \hat{\mathbf{k}} \Rightarrow \\
&\widehat{\mathbf{S}} = \cos A \cdot s_{1,2} \cdot \hat{\mathbf{i}} - \sin A \cdot s_{1,2} \cdot \hat{\mathbf{j}} + \sin h \cdot \hat{\mathbf{k}} \Rightarrow \\
&\widehat{\mathbf{S}} = \cos A \cdot \cos h \cdot \hat{\mathbf{i}} - \sin A \cdot \cos h \cdot \hat{\mathbf{j}} + \sin h \cdot \hat{\mathbf{k}}
\end{aligned} \tag{2.37}$$

The azimuth angle is taken positive towards west. However, in the horizontal Cartesian coordinate system the x-, y- and z-axes are defined to satisfy the rule of the right hand: the positive values of x-axis are towards south, and the positive values of y-axis are towards east. Therefore, the j component of Sun's position vector, $\widehat{\mathbf{S}}$, has a minus sing, as it corresponds in afternoon time.

Similarly, for a surface with altitude angle β, and azimuth angle γ, (Fig. 2.11b) the unit vector of its norm, $\widehat{\mathbf{N}}$, is given by

$$\begin{aligned}
&\widehat{\mathbf{N}} = n_1.\hat{\mathbf{i}} + n_2.\hat{\mathbf{j}} + n_3 \cdot \hat{\mathbf{k}} \Rightarrow \\
&\widehat{\mathbf{N}} = \cos\gamma \cdot \cos(90^\circ - \beta) \cdot \hat{\mathbf{i}} - \sin\gamma \cdot \cos(90^\circ - \beta) \cdot \hat{\mathbf{j}} + \sin(90^\circ - \beta) \cdot \hat{\mathbf{k}} \\
&\widehat{\mathbf{N}} = \cos\gamma \cdot \sin\beta \cdot \hat{\mathbf{i}} - \sin\gamma \cdot \sin\beta \cdot \hat{\mathbf{j}} + \cos\beta \cdot \hat{\mathbf{k}}
\end{aligned} \tag{2.38}$$

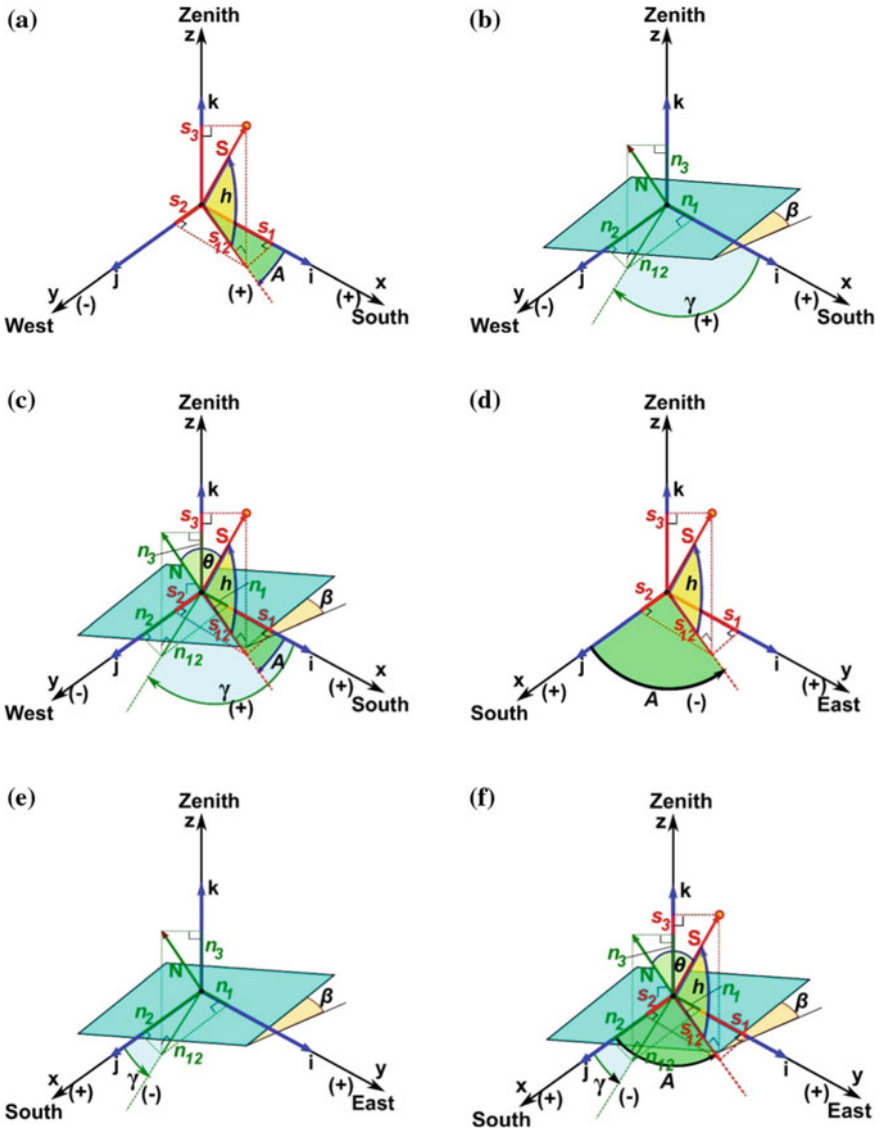

Fig. 2.11 **a** Cartesian coordinates for the horizontal coordinate system: the direction to the south determines the x-axis, the direction to the east determines the y-axis, and the direction towards the zenith determines the z-axis. The position of Sun is determined by two angles, height, h, and azimuth angle, A (being positive towards west). **b** The tilt angle, β, and the azimuth angle, γ, of the inclined irradiated surface. **c** The components of the vector pointing to Sun and the vector normal to the surface. **d–f** show the equivalent case for a negative value of Sun's azimuth angle, A, and surface azimuth angle, γ

So, using Formulas (2.36), (2.37) and (2.38), we can calculate the incidence angle, θ, according to the following:

$$\begin{aligned}\cos\theta &= \widehat{\mathbf{S}} \cdot \widehat{\mathbf{N}} \Rightarrow \\ \cos\theta &= \cos A \cdot \cos h \cdot \cos\gamma \cdot \sin\beta \\ &\quad + \sin \mathrm{A} \cdot \cos h \cdot \sin\gamma \cdot \sin\beta \\ &\quad + \sin h \cdot \cos\beta\end{aligned} \tag{2.39}$$

The horizontal coordinate system has the advantage to be more descriptive, because we observe Sun in a horizontal system. Nevertheless, it is less convenient for calculations related to the motion of Sun. The equatorial, or even the celestial equatorial, and the Ecliptic coordinate system provide more ease of calculation. The coordinates of Sun in the horizontal system can be obtained from the equatorial system using a coordinate transformation. The coordinate transformation from one spherical coordinate system to another can be performed by using spherical trigonometry. However, using Cartesian coordinates first, associated with each spherical coordinate system, and then transforming the corresponding Cartesian coordinates from one system to the other, is easier.

According to the methodology presented above, the unit vector, $\widehat{\mathbf{S}}$, pointing to Sun in the Cartesian coordinate system connected to the horizontal coordinate system is given by

$$\widehat{\mathbf{S}} = \cos A \cdot \cos h \cdot \hat{\mathbf{i}} - \sin A \cdot \cos h \cdot \hat{\mathbf{j}} + \sin h \cdot \hat{\mathbf{k}} \tag{2.37}$$

The Cartesian coordinates for the equatorial coordinate system and its relation to the horizontal coordinate system are shown in Fig. 2.12. The y'-axis is identical to that in the horizontal coordinate system. The z'-axis points to the North Pole, forming an angle equal to the geographical latitude, φ, of the place, and the x'-axis is perpendicular to both. The unit vectors in the equatorial coordinate system pointing to the x'-, y- and z'-axes are $\widehat{\mathbf{i}'}$, $\widehat{\mathbf{j}'}$ and $\widehat{\mathbf{k}'}$, respectively. In this system, the unit vector pointing to Sun, $\widehat{\mathbf{S}}$, is determined by the declination, δ, and the hour angle, ω. Using the same methodology as above, the unit vector $\widehat{\mathbf{S}}$ expressed in terms of $\widehat{\mathbf{i}'}$, $\widehat{\mathbf{j}'}$ and $\widehat{\mathbf{k}'}$ is given as

$$\widehat{\mathbf{S}} = \cos\omega \cdot \cos\delta \cdot \widehat{\mathbf{i}'} - \sin\omega \cdot \cos\delta \cdot \widehat{\mathbf{j}'} + \sin\delta \cdot \widehat{\mathbf{k}'} \tag{2.40}$$

From Fig. 2.12, we can easily derive the transformations between the two sets of unit vectors, $\hat{\mathbf{i}}$, $\hat{\mathbf{j}}$ and $\hat{\mathbf{k}}$, and $\widehat{\mathbf{i}'}$, $\widehat{\mathbf{j}'}$ and $\widehat{\mathbf{k}'}$. Each unit vector can be written as the sum of its corresponding components in relation to the unit vectors of the other coordinate system (Chen 2011):

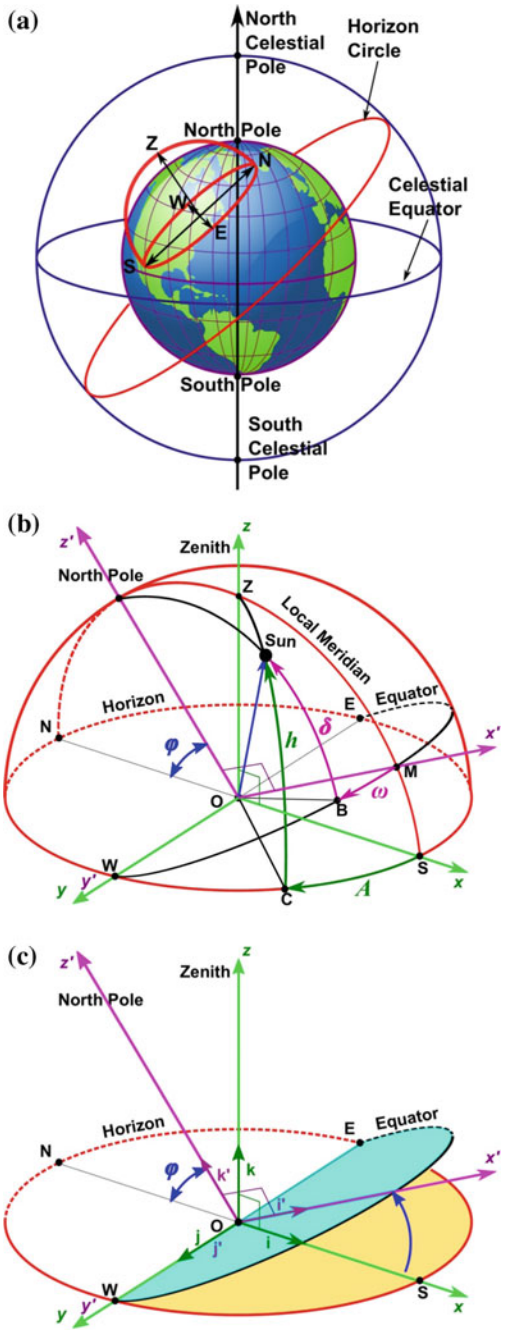

Fig. 2.12 Cartesian coordinates for the equatorial coordinate system and its relation to the corresponding for the horizontal coordinate system. The y'-axis is identical to that in the horizontal coordinate system. The z'-axis points to the North Pole, and the x-axis is perpendicular to both. The position of Sun is determined by the declination, δ, and the hour angle, ω

$$\widehat{\mathbf{i}'} = \sin\varphi \cdot \hat{\mathbf{i}} + \cos\varphi \cdot \hat{\mathbf{k}} \tag{2.41}$$

$$\widehat{\mathbf{j}'} = \hat{\mathbf{j}} \tag{2.42}$$

$$\widehat{\mathbf{k}'} = -\cos\varphi \cdot \hat{\mathbf{i}} + \sin\varphi \cdot \hat{\mathbf{k}} \tag{2.43}$$

and

$$\hat{\mathbf{i}} = \sin\varphi \cdot \widehat{\mathbf{i}'} - \cos\varphi \cdot \widehat{\mathbf{k}'} \tag{2.44}$$

$$\hat{\mathbf{j}} = \widehat{\mathbf{j}'} \tag{2.45}$$

$$\hat{\mathbf{k}} = \cos\varphi \cdot \widehat{\mathbf{i}'} + \sin\varphi \cdot \widehat{\mathbf{k}'} \tag{2.46}$$

By substituting Eqs. 2.41, 2.42, 2.43, 2.44, 2.45 and 2.46 into Eqs. 2.37 and 2.40 and performing the calculations, we obtain

$$\begin{aligned}\widehat{\mathbf{S}} = {} & \hat{\mathbf{i}} \cdot [\cos\delta \cdot \cos\omega \cdot \sin\varphi - \sin\delta \cdot \cos\varphi] \\ & + \hat{\mathbf{j}} \cdot [\cos\delta \cdot \sin\omega] \\ & + \hat{\mathbf{k}} \cdot [\cos\delta \cdot \cos\omega \cdot \cos\varphi + \sin\delta \cdot \sin\varphi]\end{aligned} \tag{2.47}$$

and

$$\begin{aligned}\widehat{\mathbf{S}} = {} & \widehat{\mathbf{i}'} \cdot [\cos h \cdot \cos A \cdot \sin\varphi + \sin h \cdot \cos\varphi] \\ & + \widehat{\mathbf{j}'} \cdot [\cos h \cdot \sin\omega] \\ & + \widehat{\mathbf{k}'} \cdot [-\cos h \cos A \cdot \cos\varphi + \sin h \cdot \sin\varphi]\end{aligned} \tag{2.48}$$

Now comparing Eqs. 2.37 and 2.40 with Eqs. 2.47 and 2.48, we can derive the transformation formulas for the two sets of angles (between the horizontal coordinate system and the equatorial coordinate system):

$$\cos A \cdot \cos h = \cos\delta \cdot \cos\omega \cdot \sin\varphi - \sin\delta \cdot \cos\varphi \tag{2.49}$$

$$\sin A \cos h = \cos\delta \cdot \sin\omega \tag{2.50}$$

$$\sin h = \cos\delta \cdot \cos\omega \cdot \cos\varphi + \sin\delta \cdot \sin\varphi \tag{2.51}$$

and

$$\cos\omega \cdot \cos\delta = \cos h \cdot \cos A \cdot \sin\varphi + \sin h \cdot \cos\varphi \tag{2.52}$$

$$\sin\omega \cdot \cos\delta = \cos h \cdot \sin\omega \tag{2.53}$$

$$\sin\delta = -\cos h \cdot \cos A \cdot \cos\varphi + \sin h \cdot \sin\varphi \tag{2.54}$$

In the case, the solar zenith angle, θ_z, is used instead of the solar altitude angle, h, sin h has to be replaced by cos θ_z, and cos h has to be replaced by sin θ_z.

Combining, now, Eq. 2.39 with Eqs. 2.49, 2.50 and 2.51, the cosine of the incident angle, θ, between the norm on the surface and the direction of solar radiation is

$$\begin{aligned}\cos\theta = \widehat{\mathbf{S}} \cdot \widehat{\mathbf{N}} &= \cos\gamma \cdot \sin\beta \cdot [\cos\delta \cdot \cos\omega \cdot \sin\varphi - \sin\delta \cdot \cos\varphi] \\ &+ \cos\delta \cdot \sin\omega \cdot \sin\gamma \cdot \sin\beta \\ &+ \cos\beta \cdot [\cos\delta \cdot \cos\omega \cdot \cos\varphi + \sin\delta \cdot \sin\varphi]\end{aligned} \tag{2.55}$$

or rearranging the terms

$$\begin{aligned}\cos\theta = &\sin\delta \cdot \sin\varphi \cdot \cos\beta \\ &- \sin\delta \cdot \cos\varphi \cdot \sin\beta \cdot \cos\gamma \\ &+ \cos\delta \cdot \cos\varphi \cdot \cos\beta \cdot \cos\omega \\ &+ \cos\delta \cdot \sin\varphi \cdot \sin\beta \cdot \cos\gamma \cdot \cos\omega \\ &+ \cos\delta \cdot \sin\beta \cdot \sin\gamma \cdot \sin\omega\end{aligned} \tag{2.56}$$

In some special cases, this formula has a simpler form:

A. If we consider horizontal surfaces (β = 0°), incidence angle becomes independent of the plane's azimuth angle, γ, as the terms that contain the azimuth angle, γ, disappear. In this case, the incidence angle, θ, is identical to the zenith angle, θ_z, and Eq. 2.56 takes the form

$$\cos\theta = \cos\theta_z = \cos\beta \cdot \cos\delta \cdot \cos\omega + \sin\varphi \cdot \sin\delta \tag{2.57}$$

B. For a surface facing south (γ = 0), Eq. 2.56 takes the form

$$\cos\theta = \sin(\varphi - \beta) \cdot \sin(\delta) + \cos(\varphi - \beta) \cdot \cos\delta \cdot \cos\omega \tag{2.58}$$

C. For inclined surfaces in the northern hemisphere facing towards the equator [towards south (γ = 0°)] with a tilt angle equal to the latitude angle ($\beta = \varphi$), Eq. 2.56 is simplified to:

$$\cos\theta = \cos\delta \cdot \cos\omega \tag{2.59}$$

D. For solar noon, where ω = 0°, Eq. 2.59 results in the form $\theta = |\delta|$. In this case, the surface gets the highest solar energy over the entire year, because cosδ is always greater than 0.93.

E. Equation 2.56 permits the calculation of the hour angles of sunrise and sunset ω_{ss}. As in this case plane's tilt is of no interest, we take a horizontal surface ($\beta = 0°$) and by setting $\theta = 90°$ we get the relatively simple relation:

$$0 = \cos\varphi \cdot \cos\delta \cdot \cos\omega_{ss} + \sin\varphi \cdot \sin\delta \tag{2.60}$$

and consequently

$$\cos\omega_{ss} = -\tan\delta \cdot \tan\varphi \tag{2.61}$$

F. For vertical surfaces ($\beta = 90°$) facing towards south ($\gamma = 0°$) in the northern hemisphere, Eq. 2.56 is transformed into:

$$\cos\theta = -\sin\delta \cdot \cos\varphi + \cos\delta \cdot \sin\varphi \cdot \cos\omega \tag{2.62}$$

while it takes the form

$$\cos\theta = \sin\delta \cdot \cos\varphi - \cos\delta \cdot \sin\varphi \cdot \cos\omega \tag{2.63}$$

for vertical surfaces ($\beta = 90°$) facing towards north ($\gamma = 0°$) in the southern hemisphere.

Summarizing, for the calculation of the incident angle, θ, of the direct solar radiation on a surface for a given site and time, in relation to the observers' horizontal system, we need to determine Sun's equatorial coordinates, declination, δ, and hour angle, ω. To calculate solar declination, δ, we only need the day of the year, to calculate solar hour angle, ω, we need the local solar time, t_{lso}, to calculate the local solar time, t_{lso}, and we need to know the location's longitude, λ, the day of the year and the local standard time, t_{std}. In addition, location's latitude, φ, must be known.

However, it must be noted that the above-presented formulas are derived based only on Sun's position in relation to Earth and the place of observation, without taking into account any deviation of light due to the curvature and the layered structure of the atmosphere, which slightly change Sun's apparent position. This effect may be important for Concentrated Solar Radiation Power Systems during sunrise and sunset as even small errors in tracking angles can lead to a loss in radiation collection efficiency. This is caused by the fact that part of the collected sunlight may not hit the absorbers any more. Nevertheless, although this error may be significant, solar radiation during sunrise or sunset is very small compared to the total daily irradiance and, consequently, can be omitted. In addition, the formulas describing these effects are complex and beyond the scope of this book.

2.6 Sun's Coordinates

2.6.1 Solar Declination

Sun's declination, δ, is a function exclusively of time and not of geographical position. It is the result of Earth's revolution around Sun and the obliquity of its orbital plane, the ecliptic, in relation to the celestial equator. Earth's revolution speed can be calculated by classical astronomical formulas. Afterwards, the rate of change of (the apparent) Sun's ecliptic longitude, l, can be derived relatively easily. Then by using similar methodology as in previous paragraphs (transformation from ecliptic coordinate system to celestial equatorial coordinate system), we can express Sun's declination, δ, in terms of its ecliptic longitude, l, and obtain an analytical formula describing its temporal variation.

However, the elliptic orbit of Earth around Sun and Kepler's second law cause Earth's revolution speed to be not constant. In addition, the equations describing how Sun's declination, δ, varies with time are significantly complex and beyond the scope of this book. Fortunately, there are some empirical approximations that in our case, the design and evaluation of Concentrated Solar Radiation Power Systems can be used successfully.

Taking into account that the variation of Sun's declination, δ, during the day is generally insignificant for practical purposes, as its maximum daily change is less than 0.5° (occurring at the equinoxes), it can be deemed constant for the whole day. Hence, Sun's declination, δ, can be approximated by a function of only one variable, the day of the year.

Some formulas for Sun's declination, δ, (in degrees) sufficient for engineering calculations, are (Emad and El-Nouby 2013; Benkaciali and Gairaa 2012; Duffie and Beckman 1994, 2013; Babatunde 2012; Radosavljević and Đorđević 2001; Myers 2013; Goosse et al. 2008–2010; Basunia et al. 2012; Chen 2011; Mohanty et al. 2015; Iqbal 1983; Maleki et al. 2017):

$$\delta = 23.45^\circ \cdot \sin\left(\frac{2 \cdot \pi(\text{or } 360^\circ) \cdot (284 + n)}{365}\right) \tag{2.64a}$$

$$\delta = 23.45^\circ \cdot \sin\left(\frac{2 \cdot \pi(\text{or } 360^\circ) \cdot (n - 80)}{365.2422}\right) \tag{2.64b}$$

$$\delta = \sin^{-1}\left\{0.39795 \cdot \cos\left[\frac{2 \cdot \pi(\text{or } 360^\circ) \cdot (\text{n} - 173)}{365}\right]\right\} \tag{2.64c}$$

$$\delta = \sin^{-1}\left\{0.4 \cdot \sin\left[\frac{2 \cdot \pi(\text{or } 360^\circ) \cdot (\text{n} - 82)}{365}\right]\right\} \tag{2.64d}$$

$$\begin{aligned}\delta = {} & 0.396372^\circ - 22.91327^\circ \cdot \cos d + 4.02543^\circ \cdot \sin d - 0.387205^\circ \\ & \cdot \cos(2 \cdot d) + 0.0519673^\circ \cdot \sin(2 \cdot \text{d})\end{aligned} \tag{2.64e}$$

$$\delta = 0.396372^\circ - 22.91327^\circ \cdot \cos d + 4.02543^\circ \cdot \sin d - 0.387205^\circ \cdot \cos(2 \cdot d) + 0.0519673^\circ \cdot \sin(2 \cdot d) - 0.1545267^\circ \cdot \cos(3 \cdot d) + 0.084798^\circ \cdot \sin(3 \cdot d) \tag{2.64f}$$

where

$$d = \frac{2 \cdot \pi \cdot (n - 1)}{365} \tag{2.65}$$

is the day angle in radians and n is the number of the day in the year, ranging from 1, for 1 January, to 365. It can be computed using the formula (Chen 2011)

$$n = \mathrm{INT}\left(\frac{275 \cdot M}{9}\right) - K \cdot \mathrm{INT}\left(\frac{M + 9}{12}\right) + D - 30 \tag{2.66}$$

where M is the month number, D is the day of the month, $K = 1$ for a leap year, and $K = 2$ for a common year. A leap year is defined as the year that is divisible by 4, but not by 100, except by 400. INT is a computer function and means taking the integer part of the number in parenthesis. The number 80 in Eq. 2.64b is the number of the day of the vernal equinox, 20 or 21 March. (The actual date varies from year to year and also differs between leap year and common year from $n = 79$ to $n = 81$. However, the most common number of the day of vernal equinox is $n = 80$).

Finally, it is worth noting that Sun's declination, δ, is a positive number during spring and summer of the northern hemisphere and a negative number during autumn and winter.

2.6.2 Solar Hour Angle, Official Time and Solar Time

The position of Sun in the sky in relation to an observer on Earth is a function of the geographical position of the observer and of time. Time enters the corresponding computational formulas in two different forms: in a rather coarse form, as the day of the year and, in a much more precise form, as the local solar time, t_{lso}.

The local solar time, t_{lso}, of a place on Earth is defined as Sun's hour angle, ω, increased by 12 h. This means that, at 12:00 h solar time, Sun is exactly in the south (in the northern hemisphere) or in the north (in the southern hemisphere) and its hour angle, ω, is 0 ($\omega = 0^\circ$). The time needed by Sun to pass the local meridian always exactly at noon two consecutive times is the true solar day. However, this time interval is not constant and not equal to Earth's rotation period, causing various problems as we will see later. There are many reasons accounting for this.

While Earth rotates around its axis, it also revolves around Sun in an elliptical orbit. However, as it has been noted, Earth's angular velocity is not constant. As a

result, the length of the true solar day is not constant either. This phenomenon produces a sinusoidal variation of time with amplitude equal to 7.66 min and a period of one year. Moreover, there is an additional variation of the solar day length. It is caused due to the tilt of the ecliptic plane with respect to the equatorial plane, which is about 23.45°. This causes an extra sinusoidal variation with amplitude equal to 9.87 min and a period of half a year.

For these reasons, the true solar time cannot be used in our everyday life, neither can be measured by clock mechanisms. Therefore, the concept of mean solar time, t_{mst}, had to be introduced. Sun is now replaced by the mean Sun which revolves around Earth in exactly 24 h. In addition, for practical reasons, Earth's surface is divided by 24 meridians into 24 regions, called time zones. In each time zone, the same constant time, the local standard time, t_{lst}, (the official time) is attributed. Each time zone has a local official time 1 h past or prior of its adjacent time zones.

As local solar time, t_{lso}, depends on the location of the observer (on their longitude), to define an official local time, a standard longitude must be selected. This task is similar to the determination of the longitude origin in the equatorial coordinate system. Thus, since the prime longitude located at Greenwich and the time starting at midnight at Greenwich have been selected as the standard longitude for the Universal Time, the latter is called Greenwich Mean Time (GMT) or, more often, Universal Time (UT). Next, each time zone has by definition a local standard, or official, time which differs mostly an integer number of hours from Greenwich Mean Time (GMT). The longitude, $\lambda\, s$, of the local standard meridian runs through the centre of each time zone ($\pm 7.5°$ from their boundaries, as each time zone is approximately 15° in width) . Time zones are numbered positive eastwards of Greenwich and negative westwards.

Taking into consideration what has been already mentioned about time, it is reasonable to note that there are three types of time in a place on Earth, (a) the local standard time, t_{lst}, (b) the local mean time, t_{lmt}, and (c) the local solar time, t_{lso}:

i. The local standard time, t_{lst}, is the official time in a given time zone (within the entire time zone).
ii. The local mean time, t_{lmt}, is the mean time of a location within a given time zone that has a fix difference to the local standard time, t_{lst}. This difference stems from the difference between the longitude, λ_s, of the time zone's standard meridian and the longitude, λ, of the location of interest. Therefore, the local mean time, t_{lmt}, is the same for all locations at the same longitude, λ. The difference between local standard time, t_{lst}, and local mean time, t_{lmt}, is given by the longitude correction.
iii. Local solar time, t_{lso}, is the timescale where Sun always crosses the local meridian exactly at noon. The difference between local mean time, t_{lmt}, and local solar time, t_{lso}, the so-called equation of time, is not constant, but varies annually.

As it has been shown, local standard time, t_{lst}, is so inexact that it is not useful for technical purposes, when used to give solar hour angle, ω. On the other hand, local solar time, t_{lso}, which is based on Sun's hour angle, ω, is the time used in all scientific calculations; however, it does not coincide with the local standard time, t_{lst}, the time our clocks measure. This difference can be more than 16 min. In order to be able to make a solar tracking System based on standard time, it is necessary to convert local standard time, t_{lst}, to local solar time, t_{lso}, and finally to a formula that gives Sun's hour angle, ω.

Local solar time, t_{lso}, is calculated from local standard time, t_{lst}, using the expression

$$t_{\text{lso}} = t_{\text{lst}} + \Delta \tag{2.67}$$

where Δ is their difference. This timescale conversion can be done by expressing the difference, Δ, in two corrections. First, there is a constant correction, Δ_λ, due to the difference in longitude, λ, between the observer's meridian (local longitude, λ_l) and the standard meridian (standard longitude, λ_S) , the longitude correction. In fact, this is the difference between the local mean time, t_{lmt}, and the local standard time, t_{lst}. Second, there is a difference between the local mean time, t_{lst}, and the local solar time, t_{lso}, the so-called equation of time, E_t. Consequently, $\Delta = \Delta_\lambda + E_t$.

2.6.2.1 The Longitude Correction

Earth rotates at a rate of 15° per 1 h, or equivalent, Sun needs 4 min to traverse an angle of 1° in the sky. Therefore, the longitude correction will be given by the expression

$$\begin{aligned} \Delta_\lambda &= (\lambda_S - \lambda_l) \cdot \frac{1\,h}{15^\circ} = (\lambda_S - \lambda_l) \cdot \frac{60\ \text{min}}{15^\circ} \\ \Delta_\lambda &= 4 \cdot (\lambda_S - \lambda_l) \cdot \frac{\text{min}}{1^\circ} \end{aligned} \tag{2.68}$$

where λ_S is the standard meridian for the local time zone and λ_l is the longitude of the location in question (longitude is in degrees, $-180^\circ < \lambda < +180^\circ$, west of Greenwich it is positive, and east of Greenwich it is negative).

In the case, the local standard time, t_{lst}, contains changes between summer time and normal time (daylight saving time), and an additional difference, Δ_{dst}, of one (1) hour (Δ_{dst} = 60 min) has to be taken into account, otherwise $\Delta_{\text{dst}} = 0$.

2.6.2.2 The Equation of Time

The difference between local solar time, t_{lso}, and local mean time, t_{lmt}, is described by the so-called equation of time, E_t, which is defined as

$$E_t = t_{\text{lso}} - t_{\text{lmt}} \tag{2.69}$$

It is the sum of the effects of the elliptic orbit of Earth around Sun and the axial tilt of the rotational axis of Earth with respect to the ecliptic. Its value varies from Sun being 14 min "slow" (crossing the local meridian afternoon standard time), in January, to 16 min "fast" (crossing the local meridian before noon standard time), in October.

The difference between local solar time, t_{lso}, and local mean time, t_{lmt}, can be expressed in minutes by the following empirical equations (Maleki et al. 2017; Reno et al. 2012; Chen 2011; Mohanty et al. 2015; Maleki et al. 2017; Iqbal 1983; Bouzid et al. 2015; Myers 2013; Duffie and Beckman 1994, 2013; Iqbal 1983; Becker 2001), which are sufficiently accurate to deal with problems in sunlight tracking:

$$E_t = 9.85 \cdot \sin(2 \cdot d_1) - 7.65 \cdot \sin(d_1) \tag{2.70a}$$

$$E_t = 9.87 \cdot \sin(2 \cdot d_2) - 7.35 \cdot \cos(d_2) - 1.5 \cdot \sin(d_2) \tag{2.70b}$$

$$E_t = -7.66 \cdot \sin(d_3) - 9.87 \cdot \sin[2 \cdot d_3 + 24.99^\circ + 3.83^\circ \cdot \sin(d_3)] \tag{2.70c}$$

$$E_t = 0.1236 \cdot \sin(d_3) - 0.0043 \cdot \cos(d_3) + 0.1538 \cdot \sin(2 \cdot d_3) + 0.0608 \cdot \cos(2 \cdot d_3) \tag{2.70d}$$

$$E_t = 0.017190 + 0.428146 \cdot \cos(d_3) - 7.352048 \cdot \sin(d_3) - 3.349758 \cdot \cos(2 \cdot d_3) - 9.362591 \cdot \sin(2 \cdot d_3) \tag{2.70e}$$

where d is the day angle in degrees or radians:

$$d_1 = \frac{2 \cdot \pi(\text{or } 360^\circ) \cdot (n - 80)}{365.2422} \tag{2.71a}$$

$$d_2 = \frac{2 \cdot \pi(\text{or } 360^\circ) \cdot (n - 81)}{365} \tag{2.71b}$$

$$d_3 = \frac{2 \cdot \pi(\text{or } 360^\circ) \cdot (n - 1)}{365(\text{or } 365.242)} \tag{2.71c}$$

and n is the number of the day in the year computed by Eq. 2.66.

Another more complex and precise formula for the computation of the equation of time, E_t, is presented by Mohanty et al. (2015):

Table 2.1 Coefficients for the computation of the equation of time, E_t, used in Eq. (2.70f)

k	$A_k \times 10^3$ (h)	$B_k \times 10^3$ (h)
0	0.2087	0.00000
1	9.2869	−122.29000
2	−52.2580	−156.98000
3	−1.3077	−5.16020
4	−2.1867	−2.98230
5	−1.5100	−0.23463

$$E_t = \sum_{k=0}^{5}\left[A_k \cdot \cos\left(\frac{2 \cdot \pi \cdot k \cdot n}{365.25}\right) + B_k \cdot \sin\left(\frac{2 \cdot \pi \cdot k \cdot n}{365.25}\right)\right] \tag{2.70f}$$

where n is the day in the 4-year cycle starting after the leap year. Values of the coefficients A_k and B_k are given in Table 2.1.

Combining the longitude correction and the equation of time, local solar time, t_{lso}, can be derived from local standard time, t_{lst}, and vice versa, using the equations:

$$t_{\text{lso}} = t_{\text{lst}} + 4 \cdot (\lambda_S - \lambda_l) \cdot \frac{\text{min}}{1^\circ} + E_t - \text{DST} \tag{2.72a}$$

$$t_{\text{lst}} = t_{\text{lso}} - 4 \cdot (\lambda_S - \lambda_l) \cdot \frac{\text{min}}{1^\circ} - E_t + \text{DST} \tag{2.72b}$$

where DST = 1 h during daylight saving time and DST = 0 otherwise.

Having computed the local solar time, t_{lso}, we can calculate Sun's hour angle, ω, using the definition of local solar time, t_{lso}:

$$t_{\text{lso}} = \omega + 12\,\text{h} \tag{2.73}$$

Consequently,

$$\begin{aligned} &\omega = f(t_{\text{lso}}) = 12\,\text{h} - t_{\text{lso}} \Rightarrow \\ &\omega = 12\,\text{h} - t_{\text{lst}} - 4 \cdot (\lambda_S - \lambda_l) \cdot \frac{\text{min}}{1^\circ} - E_t + \text{DST} \end{aligned} \tag{2.74}$$

2.6.3 Solar Altitude Angle and Solar Azimuth

After solar declination, δ, and solar hour angle, ω, have been calculated, the other two solar coordinates, solar height angle, h (or the solar zenith angle, θ_z) , and solar azimuth, A, can also be estimated by rearranging Eqs. 2.50 and 2.51:

$$\sin A = \frac{\cos \delta \cdot \sin \omega}{\cos h} \tag{2.75}$$

and

$$\cos \theta_z = \sin h = \cos \delta \cdot \cos \omega \cdot \cos \varphi + \sin \delta \cdot \sin \varphi \tag{2.76}$$

When Sun is at an altitude of 90°, Eq. 2.75 fails, because if Sun is directly overhead its azimuth angle, A, is undefined. This is important when developing computer program where we should include a check related to the values of cos h (the denominator) to prevent divide-by-zero errors when cos h = 0.

Using all above-presented equations, we can calculate Sun's position at any time and any geographical position and, consequently, determine the incident angle, θ, of direct solar radiation at any plane on Earth's surface.

2.7 Direct Solar Radiation Models

Having studied solar radiation variations due to Earth's motion around Sun, it is time to investigate the atmosphere's influence on solar direct irradiance at a plane on Earth's surface. Solar radiation at ground level is highly variable due to cloud cover variability, and atmospheric aerosol and key gas spatial distribution. This causes problems associated with the effectiveness of Concentrated Solar Radiation Power Systems. These Systems can operate properly only under cloudless conditions that allow direct solar radiation to reach Earth's surface. Therefore, since direct solar irradiance is an important factor in designing and evaluating any solar energy exploitation System, many researchers have tried to model it. As a result, there are many different solar radiation models available in the literature. By now, high-fidelity robust solar radiation models that work operationally for a wide variety of climatologic conditions are not available (Inman et al. 2013). Fortunately, a number of other satisfying approaches have been developed. Inman et al. (2013) present an overview of a considerable number of solar radiation forecasting methods, and a discussion on their effectiveness for operational use, while Gueymard (2003) investigated the performance of direct solar irradiance predictions of nineteen basic solar radiation models.

If analytical input parameters are not available, simple radiation models (like ESRA or Ineichen model) that require only a single input parameter can be used. On the other hand, if access to more sophisticated input parameters is not an issue, the Solis model would be an appropriate choice, as it gives the overall best results (Inman et al. 2013). In general, the input parameters—besides solar position parameters—needed in most radiation models are (Gueymard 2003):

- Air pressure, p (in mb or hPa)
- Precipitable water in the vertical column, w (in cm or g/cm^2)

- Reduced vertical ozone column amount, u_o (in atm-cm),
- Reduced vertical nitrogen dioxide (NO_2) column amount in the stratosphere, u_{ns} (in atm-cm)
- Reduced vertical nitrogen dioxide (NO_2) column amount in the troposphere, u_{nt} (in atm-cm)
- Ångström's spectral turbidity coefficient, β (unitless)
- Ångström's wavelength exponent, α (unitless)
- Unsworth–Monteith's broadband turbidity coefficient, τ_a (unitless) and
- Linke's turbidity factor, F_T.

The air mass, AM or m, which refers to the optical path length of the atmosphere through which radiation must propagate, in order to reach ground level, is not included as an input parameter as there exist many equations of it, as a function of solar zenith angle, θ_z, AM = $m = m(\theta_z)$. On the other hand, Linke's turbidity coefficient, T_L, which represents the number of clean and dry atmospheres that would be required to produce the observed irradiance at ground level, is usually expressed in relation to the optical thickness of a clear and dry atmosphere, τ_{cda}.

In this paragraph, commonly used direct solar radiation models, simple and easy to be converted into computer programs, are presented. However, they can be applied only when there are no clouds at all, only in clear sky with a total absence of clouds.

2.7.1 Empirical Models

Empirical models are based on correlations, or relations, derived through linear or multilinear regression analysis (curve fitting). They use ground-based observation of solar radiation conducted on different locations under clear sky conditions. These models are developed by assuming that measured solar radiation data can be described as a function of a number of other independently measured, or otherwise available, variables or parameters. One of the simplest approaches of this kind of models is to include all atmospheric effects of radiation attenuation in the parameter of air mass, m, attributing them only one attenuation factor.

1. A simple model for computing direct solar irradiance, I, at a surface perpendicular to the radiation's propagation direction on a clear day was presented by Meinel and Meinel (1976). This model estimates the direct solar irradiance, I, at sea level (Reno et al. 2012) by using only the extraterrestrial solar radiation, I_0, multiplied by the Earth–Sun distance correction factor, R_c, and the air mass, m:

$$I = R_c \cdot I_0 \cdot 0.7^{m^{0.678}} \tag{2.77}$$

2. This approach is very simple. To include the effects of location's altitude or atmosphere's state, additional terms are needed. For instance, an explicit model taking into account the altitude, H, of the location (in kilometres) as derived by Laue (Reno et al. 2012) is given by the formula:

$$I = R_c \cdot I_0 \left[(1.0 - 0.14 \cdot H) \cdot 0.7^{m^{0.678}} + 0.14 \cdot H \right] \tag{2.78}$$

These two extremely simple models provide only an approximate estimation of the normal direct solar irradiance under clear sky. It changes throughout the day as the air mass changes following Sun's position.

3. **Simple Solis Model**. Another simple model of the direct solar irradiance, based on the typical exponential extinction formula (the Beer–Lambert–Bouguer law), is Solis, presented by (Myers 2013):

$$I = R_c \cdot I_0 \cdot \mathrm{e}^{-\tau \cdot m} \tag{2.79}$$

where m is the air mass, τ the total optical depth of the atmosphere, I_0 the extraterrestrial irradiance, and R_c the Earth–Sun distance correction. However, in order to be able to account for the atmospheric attenuation of radiation in different wavelength bands, an exponent, b, was introduced modifying the air mass term, while τ was replaced by τ_b:

$$I = R_c \cdot I_0 \cdot \mathrm{e}^{-\tau_b \cdot m^b} \tag{2.80}$$

In addition, to address the possible high aerosol (or other additional) scattering phenomena, the extraterrestrial radiation was modified by being replaced by another value, I_0'. These modified equations were derived using regression techniques over a wide range of altitudes and atmospheric conditions in order to obtain the best fit, resulting in the values: $I_0' = 1.618\,\mathrm{W/m^2}$, $\tau_b = 0.606$, and $b = 0.491$ (Myers 2013).

4. **Extension of the Simple Solis Model**. To account for different atmospheric conditions, Ineichen (2008) introduced the following parameterization of the coefficients I_0, τ_b and b, of the above model:

   a. Enhanced extraterrestrial irradiance, I_0' :

$$I_0' = I_0 \cdot \left[0.071 + I_{0,0} + I_{0,1} \cdot \mathrm{aod}_{700} + I_{0,2} \cdot \mathrm{aod}_{700}^2 \right] \cdot \ln \frac{p}{p_0} \tag{2.81}$$

with

$$I_{0,0} = 1.08 \cdot w^{0.0051} \tag{2.82}$$

$$I_{0,1} = 097 \cdot w^{0.032} \tag{2.83}$$

$$I_{0,2} = 0.12 \cdot w^{0.56} \tag{2.84}$$

b. Optical depth of the atmosphere, τ:

$$\tau_b = \tau_{b0} + \tau_{b1} \cdot \text{aod}_{700} + \tau_{bp} \cdot \ln \frac{p}{p_0} \tag{2.85}$$

with

$$\tau_{b0} = 0.33 + 0.045 \cdot \ln(w) + 0.0096 \cdot \ln^2(w) \tag{2.86}$$

$$\tau_{b1} = 1.82 + 0.056 \cdot \ln(w) + 0.0071 \cdot \ln^2(w) \tag{2.87}$$

$$\tau_{0p} = 0.0089 \cdot w + 0.13 \tag{2.88}$$

c. Exponent, b, which was introduced to modify the air mass term:

$$b = b_1 \cdot \ln(w) + b_0 \tag{2.89}$$

with

$$b_0 = -0.0172 + 0.0148 \cdot \text{aod}_{700} + 0.0925 \cdot \text{aod}_{700}^2 \tag{2.90}$$

$$b_1 = +0.4557 + 0.5057 \cdot \text{aod}_{700} - 0.7565 \cdot \text{aod}_{700}^2 \tag{2.91}$$

where p_0 is the atmospheric pressure at sea level, p the atmospheric pressure at the considered altitude, w the water vapour column in cm, and aod_{700} the aerosol optical depth at 700 nm.

In this model, all parameterizations are related to the atmospheric optical depth at 700 nm, aod_{700}. However, if it is not known or available, we can use a linear combination of its optical depth at 500 and 380 nm, aod_{500} and aod_{380}, respectively, as presented by Myers (2013):

$$\text{aod}_{700} = 0.27583 \cdot \text{aod}_{380} + 0.35 \cdot \text{aod}_{500} \tag{2.92}$$

An alternative, however rough, estimation is made by using the following formula (Myers 2013):

$$\text{aod}_{700} = 0.85 \cdot \text{aod}_{500} \tag{2.93}$$

5. Hottel presented a method for estimating direct solar radiation transmitted through a clear atmosphere which takes into account Sun's zenith angle, θ_z, and the location's altitude, H, for a standard atmosphere and for four climate types (Al-Dabbas 2012; Khan and Ahmad 2012; Edeoja et al. 2013; Duffie and Beckman 1994, 2013):

$$I = I_0 \cdot \left[a_0 + a_1 \cdot \mathrm{e}^{-\frac{k}{\cos\theta_z}}\right] \tag{2.94}$$

where the constants a_0, a_1 and k, for a standard atmosphere with 23 km visibility, and for altitudes, H, of the observer (in kilometres) less than 2.5 km, are given by the equations:

$$a_0 = r_0 \cdot a_0^* \tag{2.95}$$

$$a_1 = r_1 \cdot a_1^* \tag{2.96}$$

$$k = r_k \cdot k^* \tag{2.97}$$

Moreover, a_0^*, a_1^* and k^* are given by the formulas

$$a_0^* = 0.4237 - 0.00821 \cdot (6 - H)^2 \tag{2.98}$$

$$a_1^* = 0.5055 - 0.00595 \cdot (6.5 - H)^2 \tag{2.99}$$

$$k^* = 0.2711 - 0.01858 \cdot (6.5 - H)^2 \tag{2.100}$$

where the correction factors, r_0, r_1 and r_k, for different climate types, are given in Table 2.2.

Table 2.2 Correction factors, r_0, r_1 and r_k, for different climate types, used in Hottel's formula

Climate type	r_0	r_1	r_k
Tropical	0.95	0.98	1.02
Midlatitude summer	0.97	0.99	10.2
Subartic summer	0.99	0.99	1.01
Midlatitude winter	1.03	1.01	1.00

6. Another popular method for estimating the attenuation of solar radiation due to the matter–radiation interaction in the atmosphere uses the Linke turbidity factor, T_L, proposed by Linke in 1922 (Reno et al. 2012).

The calculation of Linke's turbidity factor is based on the Beer–Bouguer–Lambert extinction law:

$$I = I_0 \cdot \mathrm{e}^{-\xi \cdot s} \tag{2.101}$$

where I_0 is the extraterrestrial solar irradiance, I is the intensity of solar radiation after extinction, ξ is the extinction coefficient, and s is the distance that light travels through the atmosphere.

The extinction coefficient, ξ, depends on the Rayleigh- and Mie-scattering factors and on the absorption's factors. The introduction of only one attenuation coefficient (known as transmission factor, turbidity factor or attenuation factor) that includes all atmospheric attenuation effects allows us to simplify the calculations. So, the transmitted direct solar irradiance is expressed by the formula:

$$I = I_0 \cdot \mathrm{e}^{-\tau \cdot T_L \cdot m} \tag{2.102}$$

Linke's turbidity factor, T_L, accounts for both absorption (by water vapour) and scattering (by aerosol particles) in the atmosphere by being based on the introduction of an optical depth, τ, of the clean (aerosol free) and dry (no water vapour) atmosphere (the so-called Rayleigh atmosphere including ozone absorption) which is given by different formulas (Myers 2013; Reno et al. 2012; Benkaciali and Gairaa 2012; Kasten 1996; Jäger et al. 2014):

$$\tau = 0.128 - 0.054 \cdot \log(m) \tag{2.103a}$$

$$\tau = \frac{1}{9.4 + 0.9 \cdot m} \tag{2.103b}$$

$$\tau = \frac{1}{6.6296 + 1.7513 \cdot m - 0.1202 \cdot m^2 + 0.0065 \cdot m^3 - 0.00013 \cdot m^4} \tag{2.103c}$$

$$\tau = \frac{1}{5.4729 + 3.0312 \cdot m - 0.6329 \cdot m^2 + 0.091 \cdot m^3 - 0.00512 \cdot m^4} \tag{2.103d}$$

Linke's turbidity factor, T_L, is a unitless number and typically takes values between 2 for very clear skies and 7 for heavily polluted skies.

To summarize, this factor incorporates the entire extinction of solar radiation in the atmosphere by using only one optical depth of a hazy and humid atmosphere expressing it by means of the number of pure and dry air masses, m, that would result in the same extinction as the examined real hazy and damp atmosphere.

7. The direct solar radiation, I, reaching Earth's surface, based on the above-presented Linke's approach, can be modified to include changes in the atmosphere due to different air pressures, p, on the surface, in relation to a reference air pressure, $p0$ = 1023.25 hPa, as follows (Becker 2001):

$$I = I_0 \cdot \mathrm{e}^{-\tau \cdot T_L \cdot m \cdot \frac{p}{p_0}} \tag{2.104}$$

The pressure correction, p/p_0, takes the following form, according to Becker (2001):

$$\frac{p}{p_0} = \frac{10 \cdot H}{18{,}400 \cdot (1 + 1.004 \cdot T_A)} \tag{2.105}$$

where T_A is the surface air temperature in °C and H is the height above sea level.

For a solar height angle $h > 10°$, we can use the following approximation to compute the air mass, m:

$$m = \frac{1}{\sin h} \tag{2.106}$$

In addition, according to Benkaciali and Gairaa (2012), Linke's turbidity factor, T_L, is given by the following expression:

$$T_L = T_1 + T_2 + T_3 \tag{2.107}$$

with

$$\begin{aligned} T_1 = {} & [2.4 + 0.9 \cdot \sin \varphi] + 0.1 \cdot [2 + \sin \varphi] \cdot A - 0.2 \cdot H \\ & - (1.22 + 0.14 \cdot A) \cdot [1 - \sin h] \end{aligned} \tag{2.108}$$

$$T_2 = 0.89^H \tag{2.109}$$

$$T_3 = (0.9 + 0.4 \cdot A) \cdot 0.63^H \tag{2.110}$$

$$A = \sin\left[\frac{360 \cdot (n - 121)}{365}\right] \tag{2.111}$$

where φ is the geographical altitude, H the site altitude, h the Sun's altitude angle, and n the number of the days in the year.

Moreover, Reno et al. (2012) present another formula for Linke's turbidity factor in terms of water vapour, w, and aerosol optical depth at 550 nm (aod_{550}). It also takes into account the altitude, H, of the site, for a fixed air mass value, m, equal to 2:

$$T_1 = 3.61 \cdot \text{aod}_{550} \text{e}^{\frac{p_0}{p}} + 0.376 \cdot \ln(w) + 2 + 0.54 \cdot \left(\frac{p_0}{p}\right) - 0.5 \cdot \left(\frac{p_0}{p}\right)^2 + 0.16 \cdot \left(\frac{p_0}{p}\right)^3 \tag{2.112}$$

8. A more accurate model of the direct solar irradiance for clear sky is given by the equation (Jäger et al. 2014)

$$I = I_0 \cdot R_c \cdot \text{e}^{-0.8662 \cdot T_L(\text{AM2}) \cdot m \cdot \tau} \tag{2.113}$$

where T_L(AM2) is Linke's turbidity factor taken at an air mass 2, m is the air mass, and τ is the Rayleigh optical thickness.

Since the relative optical path length decreases with increasing site's height above sea level, H, a correction is applied, which is equal to the ratio of the mean atmospheric pressure, p, at the site's height to the mean atmospheric pressure at sea level, p_0. This correction is particularly important in mountainous areas. Thus, the air mass, m, is approximated by the following function of solar height, h (Jäger et al. 2014):

$$m = \frac{\frac{p}{p_0}}{\sin h + 0.50572 \cdot (\text{h} - 6.07995)^{-1.6364}} \tag{2.114}$$

with the height correction being given by:

$$\frac{p}{p_0} = \text{e}^{-\frac{H}{H_0}} \tag{2.115}$$

where H_0 is the scale height of the Rayleigh atmosphere near Earth's surface, equal to 8434.5 m.

9. Rigollier et al. (2000) present a modification of the previously presented model by inserting a correction of solar height angle, h, due to the atmospheric refraction, given by the equation (as proposed by Kasten and Young 1989):

$$h^{\text{true}} = h + \Delta h \tag{2.116}$$

where Δh is

$$\Delta h = 0.061359 \cdot \left(\frac{180}{\pi}\right) \cdot \frac{0.1594 + 1.1230 \cdot \left(\frac{\pi}{180}\right) \cdot h + 0.065656 \cdot \left(\frac{\pi}{180}\right)^2 \cdot h^2}{1 + 28.9344 \cdot \left(\frac{\pi}{180}\right) \cdot h + 277.3971 \cdot \left(\frac{\pi}{180}\right)^2 \cdot h^2} \tag{2.117}$$

In addition, they used Eq. 2.103c if $m \leq 20$ (namely, $h \geq 1.9°$) and the following equation if $m > 20$ (namely, $h < 1.9°$) [proposed by Kasten (1996) and used by Rigollier et al. (2000)]

$$\tau = \frac{1}{10.4 + 0.718 \cdot m} \tag{2.118}$$

The difference between Eq. 2.103c and Eq. 1.118 at $m = 20$ is equal to 1.6×10^{-2}, which is negligible (Rigollier et al. 2000).

2.7.2 Parametric Models

Parametric or parameterization models for the estimation of clear sky direct solar radiation use a combination of correlation techniques and physical principles and, in general, are more accurate (Wong and Chow 2001). They require detailed information of atmospheric conditions and meteorological parameters as is the type, the amount and the distribution of clouds, the fractional sunshine or cloud cover, the atmospheric turbidity, the precipitable water content, ozone, etc.

Nitrogen (N_2), oxygen (O_2), carbon dioxide (CO_2), water vapour (H_2O), stratospheric ozone (O_3) and aerosols, or other small scattering centres suspended in the atmosphere, attenuate the incoming solar radiation in different degrees as it passes through the atmosphere. We can attribute a different transmittance, T, to each of these constituents defined as the ratio of the radiation reaching at the top of the atmosphere to its amount remaining at ground level. Thus, T_r is the transmittance due to Rayleigh scattering, T_a is the transmittance due to aerosol properties, T_g is the transmittance due to optical properties of gases, T_0 is the transmittance due to ozone (O_3) in the stratosphere, and T_w is the transmittance of water vapour. Each individual transmittance can be parameterized in terms of the air mass, m, and the concentration, or the amount, of the corresponding constituent in the atmosphere. Thus, the total transmittance of the atmosphere, T, can be written as the product of the above terms:

$$T = T_r \cdot T_a \cdot T_g \cdot T_o \cdot T_w \tag{2.119}$$

So, the direct normal irradiance I (W m^{-2}) can be given by the equation

$$I = I_0 \cdot T = I_0 \cdot T_r \cdot T_a \cdot T_g \cdot T_o \cdot T_w \tag{2.120}$$

where I_0 is the solar irradiance at the top of the atmosphere and I is the direct solar irradiance at a surface normal to the radiations' propagation direction.

Many models have been developed according to this approach. Some of them use a slightly modified version of this formula inserting a factor, C, because the spectral interval of solar radiation considered is from 0.3 to 3 mm:

$$I = C \cdot R_c \cdot I_0 \cdot T_r \cdot T_a \cdot T_g \cdot T_o \cdot T_w \tag{2.121}$$

R_c is the dimensionless eccentricity correction factor of the Earth's orbit.

1. **The Bird Model**. In Bird model, the parameter C equals 0.9662 (C = 0.9662) (Gueymard 2003). The transmittance equations derived by Bird and Hulstrom (1981) to compute the direct solar irradiance according to Eq. 2.121 are given by the formulas (as cited by Myers 2013):

$$T_r = \mathrm{e}^{-0.0903 \cdot m_p^{0.84} \cdot \left(1.0 + m_p - m_p^{1.01}\right)} \tag{2.122}$$

$$T_g = \mathrm{e}^{-0.0127 \cdot m_p^{0.26}} \tag{2.123}$$

$$T_o = 1 - 0.1611 \cdot \mathrm{O}_{3,m} \cdot \left(1.0 + 139.48 \cdot \mathrm{O}_{3,m}\right)^{-0.3035} - \frac{0.002715 \cdot \mathrm{O}_{3,m}}{1 + 0.044 \cdot \mathrm{O}_{3,m} + 0.0003 \cdot \mathrm{O}_{3,m}^2} \tag{2.124}$$

$$T_w = 1 - \frac{2.4959 \cdot w}{1 + 6.385 \cdot w + 79.034 \cdot w^{0.6828}} \tag{2.125}$$

$$T_a = \mathrm{e}^{-T_{au}^{0.873} \cdot \left(1 + T_{au} - T_{au}^{0.7088}\right) \cdot m^{0.9108}} \tag{2.126}$$

$$T_{au} = 0.2758 \cdot T_{a,3} + 0.35 \cdot T_{a,5} \tag{2.127}$$

where m_p is the air mass corrected for the local air pressure, P, with respect to sea-level atmospheric pressure P_0 = 1013.25 mB (Wong and Chow 2001)

$$m_p = m \cdot \frac{P}{1013.25} \tag{2.128}$$

$\mathrm{O}_{3,m} = \mathrm{O}_3 \cdot m$, O_3 is the total column ozone amount in cm, w = Pw·m, Pw is the precipitable water vapour amount in cm, $T_{a,3}$ is the aerosol optical depth at 380 nm, and $T_{a,5}$ is the aerosol optical depth at 380 nm.

Since spectral optical depths are generally not known, Gueymard (2003) modified Eq. 2.127 using the Ångström law:

$$T_{a,\lambda} = \beta \cdot \lambda^{-\alpha} \tag{2.129}$$

Moreover, as he considered a single value of the wavelength exponent a, $\alpha = 1.3$, Eq. 2.127 becomes:

$$T_{au} = 1.832 \cdot \beta \tag{2.130}$$

There are many methods for calculating absorption of solar radiation due to ozone (O_3). All of them need the amount of ozone in the optical path as an input parameter. However, since measurements are usually not available, appropriate ozone models have been developed. One of them is a simple mathematical model introduced by van Heuklon in 1979 (Karavana-Papadimou et al. 2013). To calculate the total ozone column with this model, we only need the day of the year, the latitude, φ, and longitude, λ, of the location of interest. This model assumes that the atmospheric amounts of ozone (O_3) (in Dobson units) for any day of the year and any location on Earth's northern hemisphere can be represented by the combination of three terms in relation to the equatorial annual average ozone content, J (Karavana-Papadimou et al. 2013):

$$O_3 = J + \{A + C \cdot \sin[D \cdot (n + F)] + G \cdot \sin[H \cdot (\lambda + I)]\} \cdot \sin^2(\beta \cdot \varphi) \tag{2.131}$$

where φ is the latitude (in degrees), λ is the longitude (in degrees), the parameter A is taken as constant and represents the part of ozone increase that can be attributed to latitude effects alone, β is a constant correction factor for the latitude of maximum ozone content, C is the half amplitude of the seasonal variation wave depending on the day of the year, n, D is a constant equal to 360/365.25 = 0.9856 which makes the number of days a fractional part of 360°, F is a correction parameter which transposes the days of maximum and minimum observations accordingly to the maximum and minimum of the variation wave (days 90 and 180, respectively), taken as constant, G is equivalent to the half amplitude of the maximum observed longitudinal variation, I is an empirical parameter added to modify the longitude, and H causes the repetition of the sine wave every 120° (Karavana-Papadimou et al. 2013).

For European area, Eq. 2.131 proposed by van Heuklon takes the form

$$O_3 = 235 + \{150 + 40 \cdot \sin[0.9865 \cdot (n - 30)] + 20 \cdot \sin[3 \cdot (\lambda + 20)]\} \cdot \sin^2(1.28 \cdot \varphi) \tag{2.132}$$

However, estimations based on van Heuklon's model (Eq. 2.132) are nowadays out of acceptable accuracy because average ozone levels declined during the 1980s and 1990s over Europe (Karavana-Papadimou et al. 2013). On account of this,

Karavana-Papadimou et al. (2013) recalculated all coefficients, based on the TOMS data, and presented a new adjusted form of van Heuklon Model for Europe:

$$O_3 = 260.0 + \{76.3 + 48.91 \cdot \sin[0.9865 \cdot (n - 17.85)] - 1.44 \cdot \sin[3 \cdot (\lambda + 51.2)]\} \cdot \sin^2(1.497 \cdot \varphi) \tag{2.133}$$

On the other hand, Myers (2013) proposed the use of the following formulas to estimate the total ozone column, O_3, for each day of the year, n (January 1 = 1), and for any latitude, φ, and longitude, λ (both in degrees) on Earth's surface:

For the northern hemisphere ($\phi > 0$), if $\lambda \geq 0$ (eastern hemisphere), then

$$O_3 = 235 + \left\{150 + 40 \cdot \sin\left[0.017218\left(=\frac{\pi}{365}\right) \cdot (n - 30)\right] + 20 \cdot \sin[0.05256 \cdot (\lambda + 20)]\right\} \cdot \sin^2(0.02234 \cdot \varphi) \tag{2.134}$$

(where all angles are in radians).

If $\lambda < 0$ (western hemisphere), then

$$O_3 = 235 + \{150 + 40 \cdot \sin[0.017218 \cdot (n - 30)] + 20 \cdot \sin[0.017218 \cdot n]\} \cdot \sin^2(0.02234 \cdot \varphi) \tag{2.135}$$

For the whole southern hemisphere ($\varphi \leq 0$ and $-180° \leq \lambda < 180°$, eastern and western hemisphere):

$$O_3 = 235 + \left\{ \begin{array}{l} 100 + 30 \cdot \sin[0.017218 \cdot (n + 152.625)] \\ \quad + 20 \cdot \sin[0.03491 \cdot (\lambda - 75)] \cdot \sin^2(0.02618 \cdot \varphi) \end{array} \right\} \tag{2.136}$$

The total precipitable water amount, Pw, the equivalent depth of water in millimetres if condensed out of the entire atmosphere above the location, can be estimated from the relative humidity, RH, using the following equations (Myers 2013):

$$\mathrm{Pw} = 1.5 + 1.45 \cdot E \tag{2.137}$$

$$E = \mathrm{RH} \cdot E_s \cdot \frac{P}{1013.25} \tag{2.138}$$

$$\log_{10} E_s = -0.842926609 - \frac{1827.17833}{T} - \frac{71,208.271}{T^2} \tag{2.139}$$

where E_s is the saturated water vapour pressure in millibar (mB), T is the air temperature in Kelvin (°K = °C + 271.73°), and E is the pressure-corrected water vapour pressure for relative humidity RH and air pressure P with respect to the sea-level atmospheric pressure of 1013.25 mB.

On the other hand, according to Iqbal's C model, presented, by Wong and Chow (2001), the precipitable water vapour thickness, Pw′ (in cm), reduced to standard pressure, P_0 = 1013.25 mbar, and temperature, T = 273 K, is calculated from the precipitable water vapour thickness, Pw, under the actual condition, by the formula

$$\mathrm{Pw}' = \mathrm{Pw} \cdot \left(\frac{p}{1013.25}\right)^{\frac{3}{4}} \cdot \left(\frac{273}{T}\right)^{\frac{1}{2}} \tag{2.140}$$

Iqbal also presents the following formulas for the computation of the precipitable water vapour thickness, Pw′ (in cm):

$$\mathrm{Pw}' = 0.125 \cdot \mathrm{e}^{0.295 \cdot p_v^{1/2} - 0.803} \tag{2.141}$$

where p_v is the vapour pressure at ground level (in millibars).

2. **Iqbal's C model**. Iqbal's C model is based on the original Bird model, using a slightly modified version of Eq. 2.121:

$$I = 0.9751 \cdot R_c \cdot I_0 \cdot T_r \cdot T_a \cdot T_g \cdot T_o \cdot T_w \tag{2.142}$$

Here, the factor C equals 0.9751 (Wong and Chow 2001; Gueymard 2003).

The transmittance equations used in Iqbal's C model are equivalent to *Bird* model, as presented by Myers (2013) and Wong and Chow (2001).

3. **Meteorological Radiation Model (MRM)**. In MRM, the transmittance equations are given by the formulas (Gueymard 2003):

$$T_r = 0.8325 + 0.0216 \cdot m' + 0.0174 \cdot m'^2 - 0.0007 \cdot m'^3 + 0.0002 \cdot m'^4 \tag{2.143}$$

$$T_g = \mathrm{e}^{-0.0123 \cdot m_p^{0.2538}} \tag{2.144}$$

$$T_o = 1 - 0.1611 \cdot \mathrm{O}_{3,m} \cdot \left(1.0 + 139.48 \cdot \mathrm{O}_{3,m}\right)^{-0.3035} - \frac{0.002715 \cdot \mathrm{O}_{3,m}}{1 + 0.044 \cdot \mathrm{O}_{3,m} + 0.0003 \cdot \mathrm{O}_{3,m}^2} \tag{2.145}$$

$$T_w = 1 - \frac{3.4462 \cdot w}{3.3584 \cdot w + (1 + 770.248 \cdot w)^{0.414}} \tag{2.146}$$

$$T_a = \mathrm{e}^{-T_{au}^{0.873} \cdot \left(1 + T_{au} - T_{au}^{0.7088}\right) \cdot m'^{0.9108}} \tag{2.147}$$

$$T_{au} = 0.394 \tag{2.148}$$

where $O_{3,m} = O_3 \cdot m$, O_3 is the total column ozone amount in cm, $w = \mathrm{Pw} \cdot m$, Pw is the precipitable water vapour amount in cm (as presented above), m and m' are used as defined in Kasten and Young (1989), and T_{au} is fixed at the constant value 0.394 rather than being a turbidity variable.

For solar zenith angle $\theta_z > 85°$, Eq. 2.121 is replaced by

$$I = 0.6531 \cdot I_0 \tag{2.149}$$

4. **Perrin de Brichambaut's model**. Perrin de Brichambaut and Vauge (internal reference of Gueymard 2003) devised a number of simple equations, which Gueymard (2003) combined to form a complete radiation model, resulting in the following formulas (Gueymard 2003):

$$I = I_0 \cdot T_r \cdot T_a \cdot \left(1 - \alpha_0 - \alpha_w - \alpha_g\right) \tag{2.150}$$

where

$$T_r = \mathrm{e}^{-0.031411 - 0.064331 \cdot m'} \tag{2.151}$$

$$T_a = \mathrm{e}^{-1.4327 \cdot m \cdot \beta} \tag{2.152}$$

$$\alpha_0 = 0.015 + 0.024 \cdot m \cdot O_3 \tag{2.153}$$

$$\alpha_w = 0.1 + 0.03 \cdot \ln(m \cdot \mathrm{Pw}) + 0.03 \cdot \ln^2(m \cdot \mathrm{Pw}) \tag{2.154}$$

$$\alpha_g = 0.013 - 0.015 \cdot \ln(m \cdot \mathrm{Pw}) \tag{2.155}$$

where Kasten's expression is used for m.

5. **Rodgers' model**. This radiation model predicts the incident direct solar radiation, I, using the aerosol transmittance T_a, the precipitable water vapour amount, Pw, in cm, and the relative air mass, m, without calculating separate atmospheric transmittances. It uses the following set of formulas (Gueymard 2003):

$$I = I_w \cdot T_a \tag{2.156}$$

where

$$I_w = \mathrm{e}^{b_0 + b_1 \cdot m' + b_2 \cdot m'^2 + b_3 \cdot m'^3} \tag{2.157}$$

and

$$m' = \frac{\frac{p}{1013.25}}{\cos\theta_z} \quad \text{if } \theta_z < 80^\circ \tag{2.158}$$

$$m' = \frac{p}{1013.25} \cdot \mathrm{e}\left[\begin{array}{c} 3.67985 - 24.4465 \cdot cos\theta_z + 154.017 \cdot \cos^2\theta_z - \\ 742.181 \cdot \cos^3\theta_z + 2263.36 \cdot \cos^4\theta_z \\ -3804.89 \cdot \cos^5\theta_z + 2661.05 \cdot \cos^6\theta_z \end{array}\right] \quad \text{if } \theta_z \geq 80^\circ \tag{2.159}$$

$$b_0 = -0.129641 + 0.0412828 \cdot w + 0.0112096 \cdot w^2 \tag{2.160}$$

$$b_1 = -0.0642111 - 0.0801046 \cdot w + 0.0153069 \cdot w^2 \tag{2.161}$$

$$b_2 = -0.0046883 + 0.0220414 \cdot w - 0.00429818 \cdot w^2 \tag{2.162}$$

$$b_3 = 0.000844097 - 0.00191442 \cdot w + 0.000374176 \cdot w^2 \tag{2.163}$$

The aerosol transmittance, T_a, is calculated by the Unsworth–Monteith turbidity coefficient, τ_a,

$$T_a = \mathrm{e}^{-m \cdot \tau_z} \tag{2.164}$$

where the relative air mass, m, in Eq. 2.164 is defined by the equation (Gueymard 2003)

$$m = \frac{35}{\sqrt{1 + 1224 \cdot \cos^2\theta_z}} \tag{2.165}$$

6. **Yangs' model**. The equations describing this model are (after some correction by Gueymard 2003):

$$I = I_0 \cdot \left(T_r \cdot T_a \cdot T_g \cdot T_o \cdot T_w - 0.013\right) \tag{2.166}$$

where

$$T_r = \mathrm{e}^{-\frac{0.008735 \cdot m'}{\left(0.5474 + 0.01424 \cdot m' - 0.0003834 \cdot m'^2 0.00000459 \cdot m'^3\right)^{4.08}}} \tag{2.167}$$

$$T_o = \mathrm{e}^{-0.0365 \cdot (m \cdot \mathrm{O}_3)^{0.7136}} \tag{2.168}$$

$$T_g = \mathrm{e}^{-0.0.117 \cdot m'^{0.3139}} \tag{2.169}$$

$$T_w = \mathrm{Min}[1.0, 0.909 - 0.036 \cdot \ln(m \cdot w)] \tag{2.170}$$

$$T_a = \mathrm{e}^{-m \cdot \beta \cdot \left[0.6777 + 0.1464 \cdot m \cdot \beta - 0.0.00626 \cdot (m \cdot \beta)^2\right]^{-1.3}} \tag{2.171}$$

and m' is the pressure-corrected air mass based on Kasten.

References

Al-Dabbas, Mohammed Awwad Ali. 2012. The analysis of the characteristics of the solar radiation climate of the daily global radiation and diffuse radiation in Amman, Jordan. *International Journal of Renewable Energy* 5(2) (2010).

Ahmed, Emad A., and M. El-Nouby Adam. 2013. Estimate of Global Solar Radiation by Using Artificial Neural Network in Qena, Upper Egypt. *Journal of Clean Energy Technologies* 1(2) (2013).

Babatunde, Elisha B. 2012. *Solar Radiation*. Publisher InTech, ISBN 978-953-51-0384-4, p 484.

Basunia, M.A., H. Yoshiob, and T. Abec. 2012. Simulation of Solar Radiation Incident on Horizontal and Inclined Surfaces. *TJER* 9 (2): 27–35.

Becker, Stefan. 2001. Calculation of Direct Solar and Diffuse Radiation in Israel. *International Journal of Climatology* 21: 1561–1576.

Benkaciali, S., and K. Gairaa. 2012. Comparative study of two models to estimate solar radiation on an inclined surface. *Revue des Energies Renouvelables* 15 (2): 219–228.

Bird, R.E., and R.L. Hulstrom. 1981. Review, evaluation, and improvement of direct irradiance models. *Transactions of the ASME, Journal of Solar Energy Engineering* 103: 182–192.

Bouzid, Zakaria, Nassera Ghellai, and Miloud Benmedjahed. 2015. Estimation of Solar Radiation, Management of Energy Flow and Development of a New Approach for the Optimization of the Sizing of Photovoltaic System. *Application to Algeria, International Journal of Renewable Energy Research* 5 (1): 317–324.

Duffie, J.A., and W.A. Beckman. 1994. *Solar Engineering of thermal Processes*, 2nd ed, 910. New York: Wiley.

Duffie, John A., and William A. Beckman. 2013. *Solar Engineering of Thermal Processes.* NewYork: Wiley (ISBN 978-0-470-87366-3).

Edeoja, Alex Okibe, and C. Andrew Eloka-Eboka. 2013. Experimental Validation of Hottel's Transmittance Model for Estimating Beam Radiation in Makurdi Location. *American Journal of Engineering Research (AJER)* 02(08): 51–57 (e-ISSN: 2320-0847 and p-ISSN : 2320-0936).

Goosse, H., P.Y. Barriat, W. Lefebvre, M.F. Loutre and V. Zunz. 2008-2010. Introduction to climate dynamics and climate modeling, Online textbook available at http://www.climate.be/textbook (The Energy balance, hydrological and carbon cycles, Chap 2).

Gueymard, Christian A. 2003. Direct solar transmittance and irradiance predictions with broadband models. *Part I: Detailed Theoretical Performance Assessment, Solar Energy* 74: 355–379.

Ineichen, Pierre. 2008. A broadband simplified version of the Solis clear sky model. *Solar Energy* 82: 758–762.

Inman, Rich H., Hugo T.C. Pedro, and Carlos F.M. Coimbra. 2013. Solar forecasting methods for renewable energy integration. *Progress in Energy and Combustion Science* 39: 535–576.

Iqbal, Muhammad. 1983. *An Introduction to Solar Radiation*, 408. London: Academic Press (ISBN: 978-0-12-373750-2) Available online at http://www.sciencedirect.com/science/book/9780123737502.

Jäger, Klaus, Olindo Isabella, Arno H.M. Smets, René A.C.M.M. van Swaaij, and Miro Zeman. 2014. *Solar Energy, Fundamentals, Technology, and Systems*. Delft University of Technology, Available online at https://courses.edx.org/c4x/DelftX/ET.3034TU/asset/solar_energy_v1.1.pdf.

Julian, Chen C. 2011. *Physics of Solar Energy*, 373. New York: Wiley (ISBN 978-0-470-64780-6).

Karavana-Papadimou, K., B.E. Psiloglou, S. Lykoudis, and H.D. Kambezidis. 2013. Model For Estimating Atmospheric Ozone Content Over Europe for Use in Solar Radiation Algorithms. *Global NEST Journal* 15 (2): 152–162.

Kasten, F., and A.T. Young. 1989. Revised optical air mass tables and approximation formula. *Applied Optics* 28 (22): 4735–4738.

Kasten, F. 1996. The Linke turbidity factor based on improved values of the integral Rayleigh optical thickness. *Solar Energy* 56: 239–244.

Maroof, Khan M., and M. Jamil Ahmad. 2012. Estimation of global solar radiation using clear sky radiation in Yemen. *Journal of Engineering Science and Technology Review* 5 (2): 12–19.

Mousavi, Maleki Seyed Abbas, H. Hizam, and Chandima Gomes. 2017. Estimation of Hourly, Daily and Monthly Global Solar Radiation on Inclined Surfaces: Models Re-Visited. *Energies* 2017 (10): 134.

Meinel, A.B., and M.P. Meinel. 1976. *Applied Solar Energy: An Introduction.* Reading, MA: Addison Wesley Publishing.

Mohanty, P., T. Muneer, and Kohle M. (eds.) 2015. *Solar Photovoltaic System Applications*, 184. New York: Springer International Publishing (IX ISBN 978-3-319-14662-1).

Myers, Daryl R. 2013. *Solar Radiation, Practical Modeling for Renewable Energy Applications*, 199. London: Taylor & Francis Group, LLC, CRC Press (ISBN-13: 978-1-4665-0327-4, eBook–PDF).

Paulescu, M., E. Paulescu, P. Gravila, and V. Badescu. 2013. *Weather Modeling and Forecasting of PV Systems Operation*, XVIII, 358. Berlin: Springer (ISBN 978-1-4471-4648-3).

Radosavljević, Jasmina, and Amelija Đorđević. 2001. Defining of the Intensity of Solar Radiation on Horizontal and Oblique Surfaces on Earth. *Working and Living Environmental Protection* 2 (1): 77–86.

Reno, Matthew J., Clifford W. Hansen, and Joshua S. Stein. 2012. Global Horizontal Irradiance Clear Sky Models: Implementation and Analysis, SANDIA REPORT, Sandia National Laboratories, New Mexico, California, SAND2012-2389, Unlimited Release, Printed March 2012. Available online at http://energy.sandia.gov/wp-content/gallery/uploads/SAND2012-2389_ClearSky_final.pdf.

Rigollier, Christelle, Olivier Bauer, and Lucien Wald. 2000. On the clear sky model of the ESRA - European Solar Radiation Atlas with respect to the Heliosat method. *Solar Energy* 68 (1): 33–48. (Elsevier).

Sportisse, B. 2010, *Fundamentals in Air Pollution, From Processes to Modelling*, 299. Berlin: Springer (ISBN 978-90-481-2969-0).

Sung, Taehong, Sang Youl Yoon, and Kyung Chun Kim. 2015. A Mathematical Model of Hourly Solar Radiation in Varying Weather Conditions for a Dynamic Simulation of the Solar Organic Rankine Cycle. *Energies* 8: 7058–7069.
Wong, L.T., and W.K. Chow. 2001. Solar radiation model. *Applied Energy* 69: 191–224.

Chapter 3
Geometric Optics

In recent years, considerable research has been carried out on renewable energy sources, and scientists and engineers have tried to design cheap but efficient devices to harvest solar power. Solar radiation has low power density. For this reason, we must use concentrating devices to increase the amount of solar radiation reaching the receiver to be able to obtain temperatures higher than 100 °C. However, mirrors' shape is of key importance to the efficiency of these Systems. Plane mirrors are the simplest and more economical devices, whereas parabolic mirrors provide a more efficient solution. In any case, when designing Solar Radiation Concentrating Systems, the optical features of the reflective elements must be analysed and taken into account along with other phenomena and requirements, such as Sun's finite size, aberrations at non-normal incidence, receiver placement and solar tracking.

In this chapter, we will discuss light redirection and concentration by mirrors using the concept of light rays. Knowing how light propagates is crucial to understand the efficiency of the aforementioned Systems. In our study, we shall consider only smooth surfaces that cause specular (geometric) reflections and ignore ragged, rough surfaces that diffuse the incident solar radiation.

3.1 The Ray Aspect of Light

When light interacts with an object that is several times larger than its wavelength, light observable behaviour is like that of a ray; it does not display any wave characteristics. On the other hand, when light interacts with smaller objects, it has very prominent wave characteristics, such as constructive and destructive interference. However, as the wavelength of light is less than a micron, so short compared to the size of most objects we are familiar with, almost all common optical phenomena can be explained by tracing light rays, and interference and diffraction effects can be considered negligible.

S. Karathanasis, *Linear Fresnel Reflector Systems for Solar Radiation Concentration*, https://doi.org/10.1007/978-3-030-05279-9_3

Since light moves in straight lines until a new interface, a surface between two materials, or media, is reached, where it interacts with these materials and changes direction, and light's propagation can be described by a set of well-defined geometrical rules and simple trigonometry. The part of optics where the ray aspect of light dominates is called geometric optics, even though it should be better called ray optics. This model assumes that light travels in straight-line paths called light rays. Strictly speaking, ray optics is the limit of wave optics when the wavelength, λ, of the light is infinitesimally small compared to the dimension, d, of the object it interacts with ($\lambda \ll d$).

A light ray is considered to trace the motion of a single hypothetical photon. However, the light ray is a concept that does not exist. Actually, it is an idealization, meant to represent an extremely narrow beam of light. An approach that avoids the difficulties arising from a physical definition is that of treating light rays as mathematical entities. So, mathematically, the light ray is defined as the path the light energy follows when propagating.

Ray optics is an approximate theory which deals with the location and direction of light rays. Nevertheless, it is very useful when studying mirrors, the way they redirect light and focus it on a single point or line. The basic laws for ray tracing are extremely simple. At a reflecting surface, we use the fact that the angle of reflection, θ_r, the angle of an outgoing light ray, equals the angle of incidence, θ_i, the angle of the corresponding incoming light ray: $\theta_r = \theta_i$. Actually, this chapter is entirely based on this simple rule.

To summarize, and as it will be shown in more detail in the following paragraph, light rays propagate in straight lines in homogeneous media and have curved paths in heterogeneous media. They have positions, directions, speed and carry energy, and power per area, approximated by ray density. Between any pair of points on a given ray, there is a geometrical path length and an optical path length, which are reversible. At smooth interfaces between optically different media, media with different refraction indices, light rays get refracted and reflected.

3.2 Wave Fronts and Rays

To describe light propagation, the concept of wave fronts is usually used. They are surfaces passing through points of the space where light has the same phase and amplitude. Figure 3.1 shows a wave emitted by a point light source. Light rays are another auxiliary concept used to describe the direction of light propagation, instead of pointing vector used in wave theory of light. They are vectors perpendicular to the wave front and represent the direction of light energy propagation. So, light rays corresponding to a plane wave are parallel straight arrows; for a spherical wave, light rays are diverging arrows emerging from the point light source. Figure 3.1 shows two representations of spherical wave fronts with their diverging light rays.

The curvature of a wave front decreases as it propagates further away from the point light source. If the waves were to propagate infinitely far away, then it would

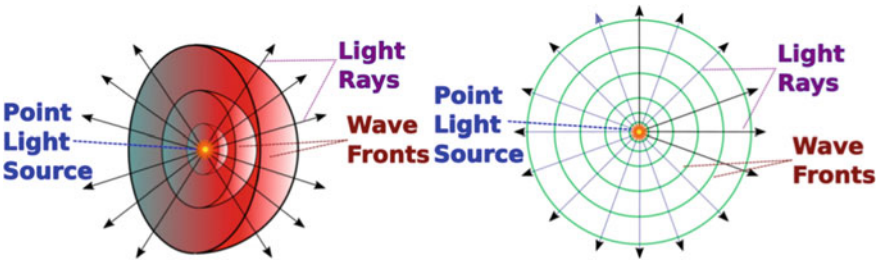

Fig. 3.1 The fundamental assumption in ray optics is that light travels in the form of rays. A single ray could represent a beam of light, but typically we need many rays to model light propagation (e.g. to model the performance of a Solar Radiation Concentrating System). If the light wave is emanating from a point light source, the wave fronts are spherical surfaces and the light rays are diverging vectors perpendicular to the wave fronts

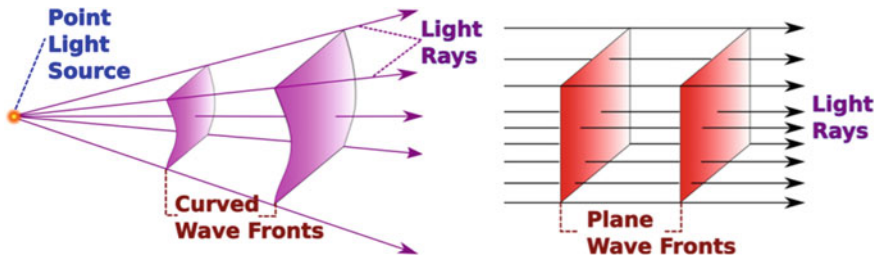

Fig. 3.2 At finite distance from a point light source, the light rays always diverge. At larger distances, the wave fronts become less and less curved and approach the limiting case of a plane wave. A plane wave has flat wave fronts, and the light rays are parallel to each other and parallel to the propagation direction

completely flatten as shown in Fig. 3.2. This results in parallel plane wave fronts. Light sources in the physical world cannot be so far away (even though Sun can fulfil this condition); however, plane wave fronts serve as both a useful approximation for distant light sources and an ideal way to describe mirrors' behaviour mathematically.

3.3 Fermat's Principle

A useful principle in optics is ***Fermat's principle***. It can help us understand light propagation course in a medium. According to it, each light ray passing through two points in the space follows the timely shortest path. Or, in other words, travelling between any two points in the space, light will always take that path requiring the least time. Fermat's principle can be used to derive the law of reflection (as we will see below), the rule governing light rays propagation when falling at the boundary of two optically different media.

Light rays propagate in optical media. To avoid unnecessary complication of the study, we can assume that these media are lossless, and therefore, they can be completely characterized by their index of refraction, n. In optics, the refractive index or index of refraction, n, of a material is a dimensionless number that describes how fast light propagates through that medium. It is defined as $n = c/\upsilon$, where c is the speed of light in vacuum ($c = 2.998 \times 10^8$ m/s) and υ is the speed of light in this medium. Usually, $n \geq 1$, with $n = 1$ corresponding to vacuum. Thus, the only effect the refractive index has is the change of light's speed.

Let us come back to the fundamental principle of ray optics, Fermat's principle, and consider a path s between two points A and B inside an optical medium, so that A corresponds to a position vector $\mathbf{r_A}$ and B corresponds to a position vector $\mathbf{r_B}$ (Fig. 3.3).

In an inhomogeneous medium, the refractive index, $n(\mathbf{r})$, is a function of the position $\mathbf{r} = (x, y, x)$. The optical path length, l, along a given path between two points A and B is equal to the length of the path, s, weighted by the local refractive index, $n(\mathbf{r})$:

$$l_{\mathbf{r_A} \to \mathbf{r_B}} = \int_{\mathbf{r_A}}^{\mathbf{r_B}} n(\mathbf{r}) \mathrm{d}s \tag{3.1}$$

where ds is the differential element of the length along the path.

The time, t, taken by light to travel from A to B is proportional to the optical path length, l ($t = l/c$), or equivalently, the optical path length, l, is proportional to the time, t, light needs to travel across the path s.

However, Fermat's principle states that optical rays travelling between two points, A and B, follow a path such that time, t, of travel (or the optical path length) between these two points is an extremum (in fact a minimum) relative to any other neighbouring path. This means that any optical rays' path has to satisfy the condition

$$\frac{\mathrm{d}l}{\mathrm{d}t} = \frac{\mathrm{d} \int_{r_A}^{r_B} n(r) \mathrm{d}s}{\mathrm{d}t} = 0 \tag{3.2}$$

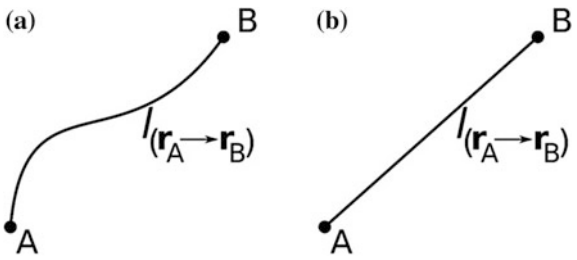

Fig. 3.3 According to Fermat's principle, or the principle of least time, a light ray follows the path that can be traversed in the least time. Light propagation **a** in a inhomogeneous medium and **b** in a homogeneous medium

However, in the common case of a homogeneous medium, where the refractive index, n, is everywhere constant, and so the speed of light in this medium, the optical path length is equal to the geometrical length, s, of the path multiplied by the constant value of the refractive index, n. Thus, the minimum optical path length, l, occurs for the path with the minimum geometrical length, s (the minimum distance), which is a straight line (Fig. 3.3b).

Therefore, in the case of homogenous media the optical path length is given by the equation

$$l_{r_A \to r_B} = n \int_{r_A}^{r_B} \mathrm{d}s = nd \tag{3.3}$$

where d is the length of the linear path connecting points A and B.

In general, when applying Fermat's principle, the idea is to specify the starting point as well as the endpoint (where the light originates from and where it ends up), and then ask what does it do in the meantime, by applying the condition $\mathrm{d}l/\mathrm{d}t = 0$, yielding to a minimum for l.

3.4 The Law of Reflection

When a narrow beam of light strikes the interface between two optically different media, at least one part of it changes its propagation direction keeping on travelling in the same medium. This phenomenon is called reflection, and the light ray is said to be reflected. The rest part of the ray can be either absorbed by the second medium or, if it is transparent, like glass or water, it can be transmitted through it (Fig. 3.4). In the case of transmission, the light ray travels through the material of the second medium and exits on the other side. For a transparent material, the transmitted light rays are slowed down and bent. For a material that is not transparent (a translucent material), the light rays scatter into various directions before exiting. In the case of absorption, energy is absorbed by the material and transformed into thermal energy, as the light becomes trapped. In the third case, reflection, the light is deflected from the surface. For a very smooth shiny object such as a silvered mirror, over 95% of the light can be reflected. Usually, all three phenomena, transmission, absorption and reflection, occur simultaneously. The amount of energy divided between them depends on many factors, such as the angle of approach, the wavelength and differences between the two adjacent materials.

We define the angle of incidence, θ_i, to be the angle an incident (or incoming) light ray makes with the normal (perpendicular) to the surface, and the angle of reflection, θ_r, to be the angle the reflected (or outgoing) light ray makes with the

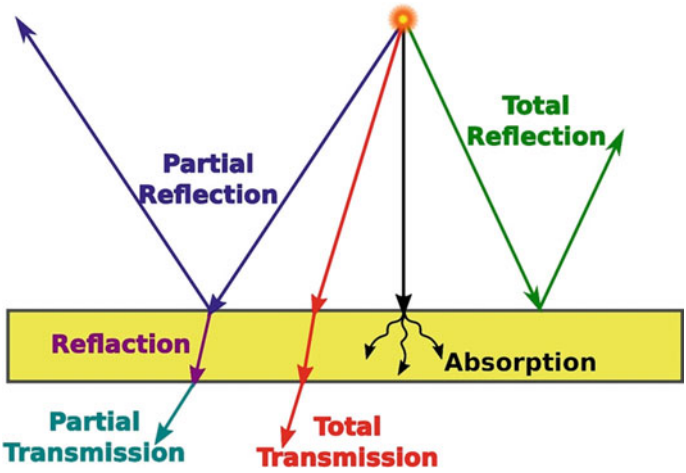

Fig. 3.4 As light hit the boundary of two optically different media, it can be transmitted through, absorbed or reflected

same normal (Fig. 3.5). It is found that the incident and reflected rays lie on the same plane with the normal to the surface and that the angle of reflection equals the angle of incidence

$$\theta_{\mathrm{i}} = \theta_{\mathrm{r}} \tag{3.4}$$

This is the law of reflection. It is illustrated in Fig. 3.5.

The law of reflection applies to all types of reflective surfaces. Therefore, it is applicable to plane surfaces, as ordinary mirrors in bedrooms and bathrooms are, as well as to spherical and parabolic surfaces, even to any other shape of curved surface. The simplest reflective surface is the plane mirror, whereas the most commonly used type of curved mirror is the spherical mirror, where the reflective surface is part of the surface of a sphere. For the case of curved reflective surfaces, the normal is drawn perpendicular to the plane that is tangent to the curved surface at the point of incidence (the point where the incident light ray hits the surface) (Fig. 3.6). The plane of incidence is the plane formed by the incident ray and the normal to the mirror at the point of incidence.

Any surface reflects at least part of the light falling on it, whereas a highly polished surface, such as mirrors, reflects most of the falling light. Mirrors are made of certain highly polished metallic surfaces, or metallic or dielectric films deposited on a substrate such as glass.

We expect to see reflections from smooth surfaces, but when light incidents a rough surface, even microscopically rough, such as a piece of paper, it is reflected in many directions, as illustrated in Fig. 3.7. This is called diffuse reflection. The law of reflection still applies to small sections of the surface. Because the light strikes different parts of the surface at different angles, it is reflected in many

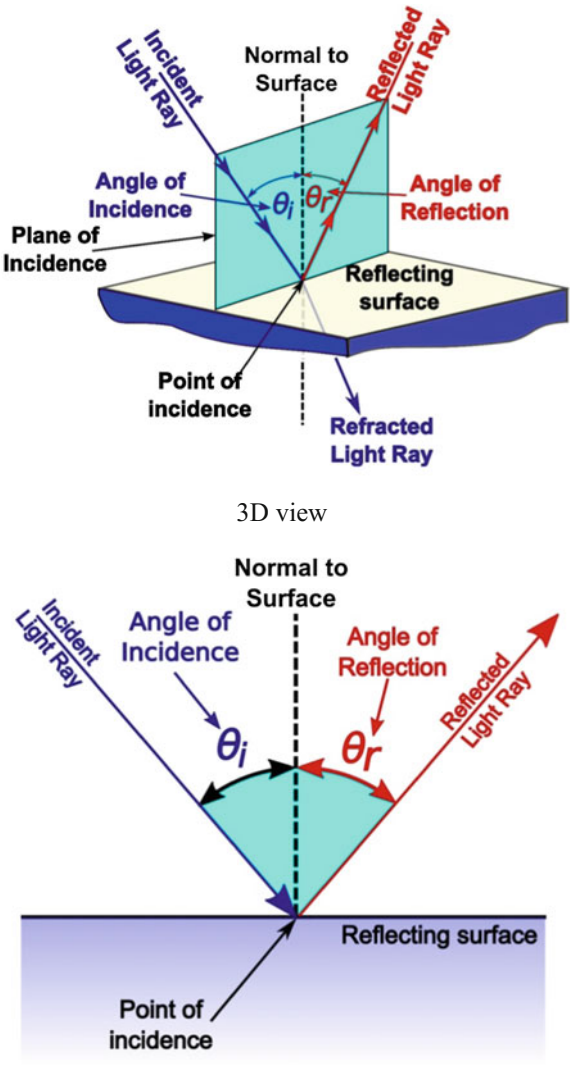

Fig. 3.5 Reflection of light rays at the interface between two optically different media. This diagram illustrates how a light ray is reflected by a flat mirror. The incoming light ray, called the incident ray, hits the mirror at the incidence point. At this point, a line perpendicular to the mirror, the normal, acts as the line of symmetry for the incident ray and the reflected ray. The angle between the reflected ray and the normal, the angle of reflection, and the angle between the incident ray and the normal, the angle of incidence, are always equal. The incident ray, the normal to the mirror at the point of incidence and the reflected ray, all lie on the same plane

different directions. The reflected light no longer maintains its spatial regularity, and it is said to undergo diffuse reflection (Fig. 3.7b). Although most objects have rough surfaces, a mirror has a smooth surface (compared with the wavelength of light) and reflects light at specific angles.

The law of reflection can be derived from Fermat's principle. After reflection, the outgoing light ray is on the same plane with the incoming ray and the normal at the point of incidence. Let A be the starting point and B the endpoint of the light ray (Fig. 3.8). We assume a homogeneous medium above the mirror with refractive

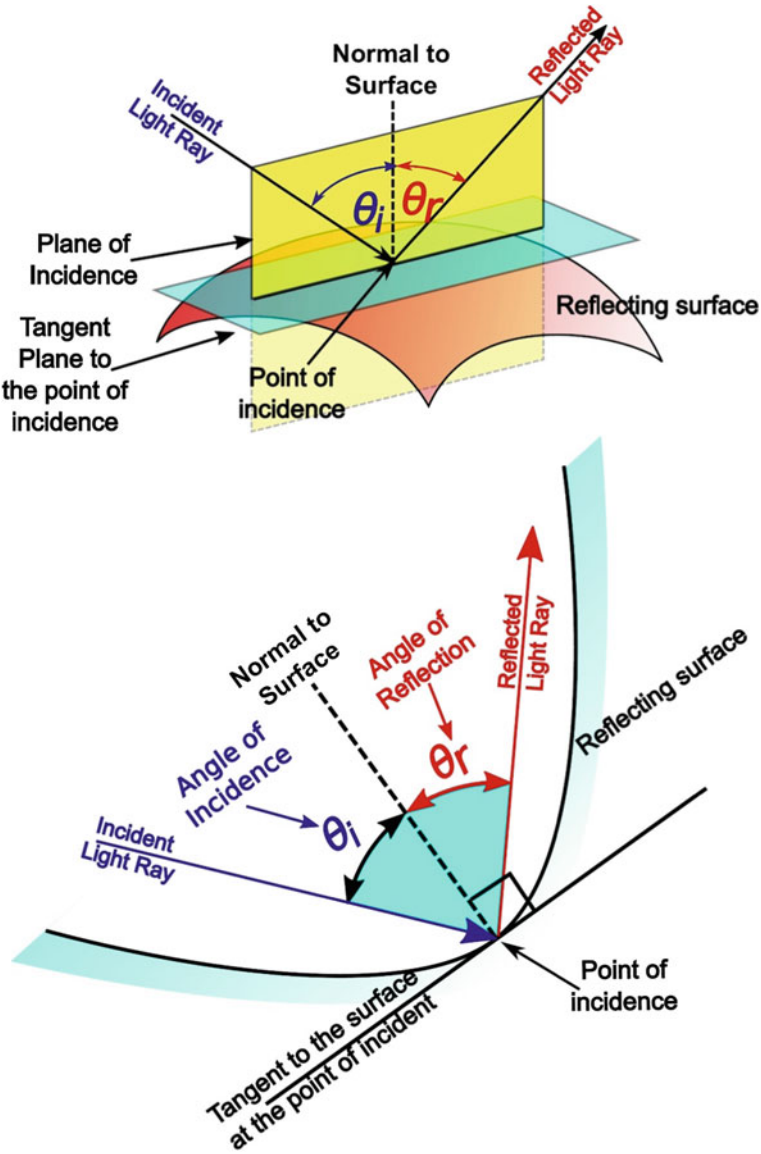

Fig. 3.6 Law of reflection for curved surfaces. The normal is perpendicular to the tangent plane at the incidence point

index n, and because light travels in straight lines within a uniform material, we can follow its path in this medium by tracing straight rays that are representative of the light beam. The Cartesian coordinates of points A and B in an arbitrary coordinate system are (x_A, y_A) and (x_A, y_A), respectively. As light travels between points A and

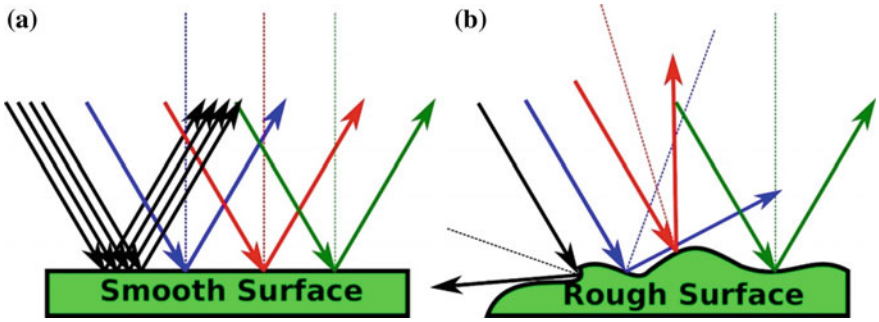

Fig. 3.7 **a** If the interface between two media is a smooth plane surface, an incident plane wave with parallel light rays will undergo specular reflection from the surface and the reflected light rays remaining parallel, **b** whereas in a, even microscopically, rough surface, each individual light ray is reflected in different directions. This phenomenon is called diffuse reflection

B in the shortest time, we want to find the point P for which the time, t, required for light to go from A to B, is the least, or, because the refraction index n of the medium is constant, and so the light speed, the path length, l, is the minimum. Without losing of any generality, we suppose the plane of the reflective surface to be taken perpendicular to y-axis. So, the Cartesian coordinates of point P are $(L, 0)$. The length, l, of the light path APB is (Fig. 3.8):

$$\begin{aligned} &l = AP + PB \Rightarrow \\ &l = \sqrt{(L - x_A)^2 + y_A^2} + \sqrt{(x_B - L)^2 + y_B^2} \end{aligned} \tag{3.5}$$

To minimize the path length, l, we differentiate it with respect to the x-coordinate of point P, L, $(\mathrm{d}l/\mathrm{d}L)$ and equate the resulting quantity with 0 $(\mathrm{d}l/\mathrm{d}L = 0)$. This way we can find the minimum path length, l, and subsequently the point P.

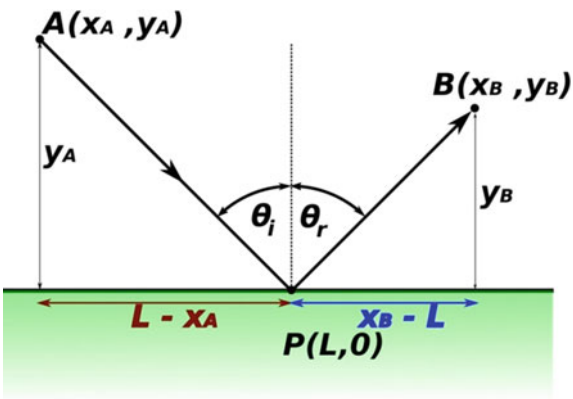

Fig. 3.8 The reflection of light follows Fermat's law requiring its path length to be the minimum. This results in the angle of incidence to be equal to the angle of reflection

$$\frac{\mathrm{d}l}{\mathrm{d}L} = +\frac{L - x_A}{\sqrt{(L - x_A)^2 + y_A^2}} - \frac{x_B - L}{\sqrt{(x_B - L)^2 + y_B^2}} = 0 \Rightarrow$$
$$\frac{L - x_A}{\sqrt{(L - x_A)^2 + y_A^2}} = \frac{x_B - L}{\sqrt{(x_B - L)^2 + y_B^2}} \tag{3.6}$$

Using the definitions of sin θ_i and sin θ_r, and the notation in Fig. 3.8, Eq. 3.6 becomes

$$\frac{L - x_A}{AP} = \frac{x_B - L}{PB} \Rightarrow$$
$$\sin\,\theta_\mathrm{i} = \sin\,\theta_\mathrm{r} \Rightarrow \tag{3.7}$$
$$\theta_\mathrm{i} = \theta_\mathrm{r}$$

This way we arrived at the law of reflection for light rays, where θ_i and θ_r are the angle of incidence and the angle of reflection, respectively.

3.5 Light Ray Redirection and Light Concentration

3.5.1 Plane Mirrors

We call mirror any smooth and glossy surface that reflects all lights falling on it. We will begin our study of reflective surfaces by considering the simplest possible mirror, the flat mirror. We distinguish two possible cases of reflection.

Reflection of a beam of parallel light rays. Let us consider that a light beam consisted of a group of parallel light rays strikes a plane reflective surface. Using the law of reflection—the angle of incidence, θ_i, equals the angle of reflection, θ_r—we can see that all light rays remain parallel after being reflected as all form the same angle with the normal to the surface (Fig. 3.9a).

Reflection of a beam of diverging light rays. Let us now consider a point source of light placed at a point S in a distance s in front of a flat mirror. The point light source emits diverging straight light rays to all directions. Let some of these light rays be reflected by the surface of a plane mirror. As the law of reflection applies to all light rays, we can determine for each light ray exiting the source and reaching the surface of the mirror the direction of the reflected ray. After being reflected, the light rays continue to diverge (spread apart). However, if we extrapolate these diverging rays, they appear to the viewer to come from a point I behind the mirror. Point I is called the image of the point light source at S (Fig. 3.9b).

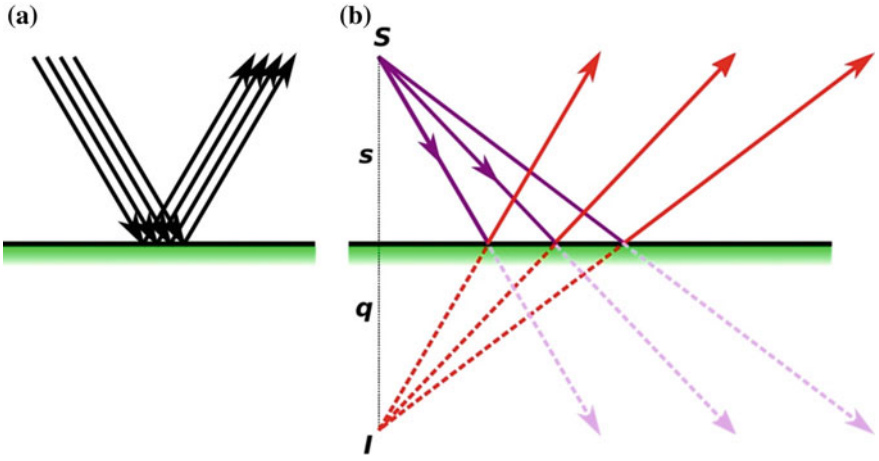

Fig. 3.9 Reflection from a flat mirror. **a** Parallel light rays remain parallel after being reflected by a plane mirror. This way a light beam is redirected, but light is not focused. **b** When a group of diverging light rays hit a plane mirror, each light ray is reflected following the law of reflection. This way they appear to emanate from a point behind the mirror. This point is called the image of the point light source. The source is located at *S*, at a distance *s* from the mirror, whereas the image location *I* is behind the mirror at a distance *q*. For a flat mirror, $s = q$. Solid lines indicate actual light rays, and dotted lines indicate "virtual" rays

3.5.2 Spherical Mirrors

As reflective surfaces can also be curved, we turn, now, our attention to the effects curved mirrors have on light rays. The most common type of curved mirror is the spherical mirror, which just sounds like: the reflective surface has the shape of an arc of a circle, or more correctly it is a section of a sphere. Spherical mirrors are typically made from a section of a spherical shell of a material that is polished and coated with a highly reflective metal coating. The centre, *C*, of this sphere is the centre of curvature of the spherical mirror, and its radius, *R*, is the radius of curvature of the mirror. There are two types of spherical mirrors, depending on which side of the spherical surface faces the light. A spherical mirror is called convex if the reflection takes place on the outer surface of the spherical shape, whereas a mirror is called concave if the reflecting surface is on the inner surface of the sphere (Fig. 3.10).

Spherical mirrors can be uniquely described by the radius, *R*, of the sphere making up them, whether they are concave or convex. The geometric centre of a curved mirror is called vertex (*V*) or pole (*P*), and the straight line passing through *V* and *C* is called principal (or optical) axis (Fig. 3.11). The reflective surface of a spherical mirror has usually a circular outline. The diameter of this circle is its aperture. Because ray diagrams are difficult to be drawn in three dimensions, curved mirrors are illustrated in two dimensions.

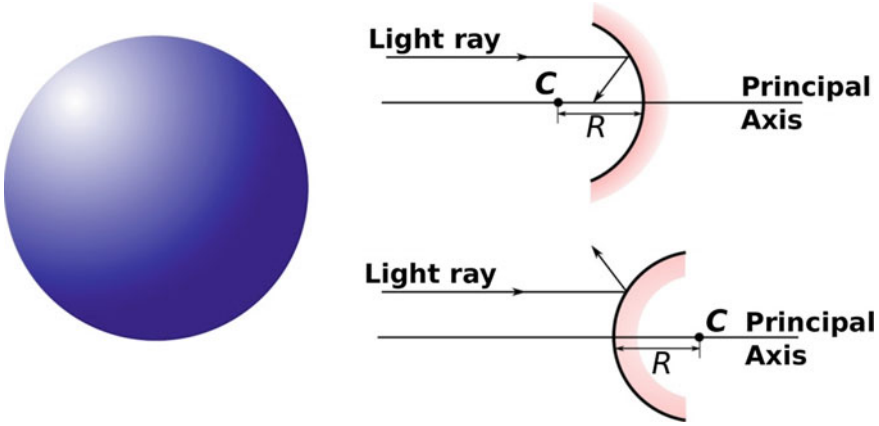

Fig. 3.10 Spherical mirrors come in two basic types: those that converge parallel incident light rays and those that diverge parallel light rays. These mirrors are not a complete sphere, but a sector taken from a large imaginary sphere

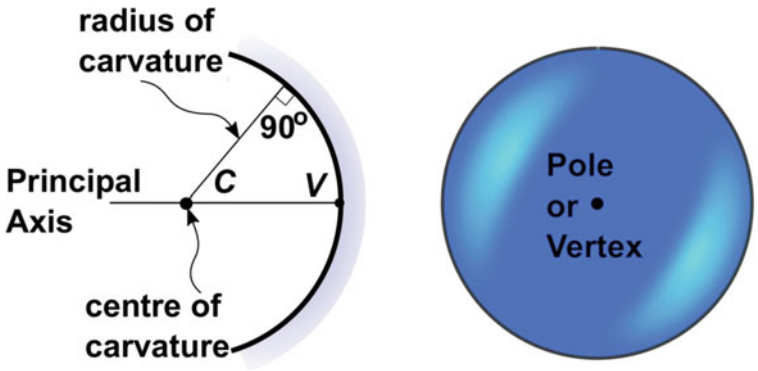

Fig. 3.11 The geometric centre of a curved mirror is called vertex (*V*) or pole (*P*), and the straight line passing through *V* and the centre, *C*, of the sphere is called principal (optical) axis. The reflective surface of a spherical mirror has usually a circular outline. The diameter of this circle is its aperture

Spherical mirrors redirect the light rays concentrating them on a point. They work in the same fundamental way plane mirrors do. The law of reflection applies just as it does for a plane mirror, and the angles of incidence and reflection are measured from the normal to the mirror surface at the point of incidence.

To see how spherical mirrors concentrate sunlight, let us consider a point light source that is very far away from a concave mirror. For a very distant light source (Fig. 3.12), the rays emanating from each point of it and striking the mirror will be nearly parallel. For a light source infinitely far away (Sun approaches this condition), the light rays would be precisely parallel.

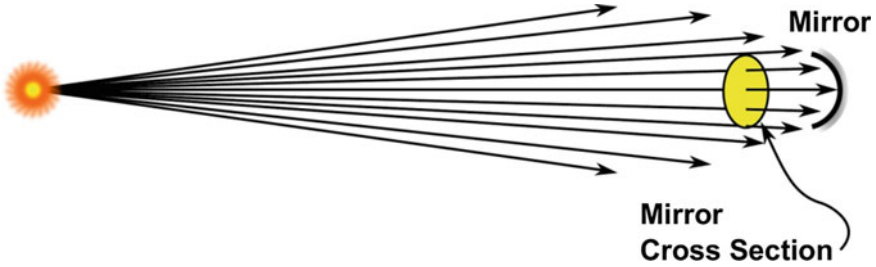

Fig. 3.12 For very distant point light sources, far enough from the mirror, compared to its curvature radius, *R*, the incident light rays are all nearly parallel to the principle axis. Any small angle away from the principle axis will result in the light rays diverging too far to hit the mirror. Only those light rays at tiny angles relative to the principle axis will hit the mirror

Now, let us consider a group of parallel light rays falling on a concave mirror as in Fig. 3.13. The law of reflection applies to each of these light rays at the point each strikes the mirror. However, they do not converge to a single point (Fig. 3.13a). Consequently, a spherical mirror cannot concentrate sunlight on a single point.

Nevertheless, as we will show below, if the mirror aperture is small compared to its radius of curvature, *R*, and the incident rays continue to be parallel to the principal axis forming only very small angles with the normal to the mirror surface (Fig. 3.13b), then the reflected light rays will cross each other at nearly the same point. The point where incident parallel rays come to a focus after reflection is called the focal point, *F* (or principal focus), of the mirror. The distance between the focal point, *F*, and the centre of the mirror, *P*, (its pole or vertex, *V*), the length *FP* along the principal axis, is called the focal length, *f*, of the mirror.

To determine the focal length, *f*, of a spherical mirror, we shall consider only those mirrors having aperture much smaller than their radius and those light rays that form a small angle with the principal axis; such rays are called paraxial rays (Fig. 3.13b). So, paraxial and parallel light rays are reflected from the concave mirror and converge at the focal point *F*. There is a relationship between the radius of curvature, *R*, and the focal length, *f*, of the spherical mirror: the radius of curvature, *R*, is found to be equal to twice the focal length, *f*:

$$R = 2f \tag{3.8}$$

Or else, the principal focus, *F*, of a spherical mirror is halfway between the pole, *P*, and centre of curvature, *C*:

$$f = \frac{R}{2} \tag{3.9}$$

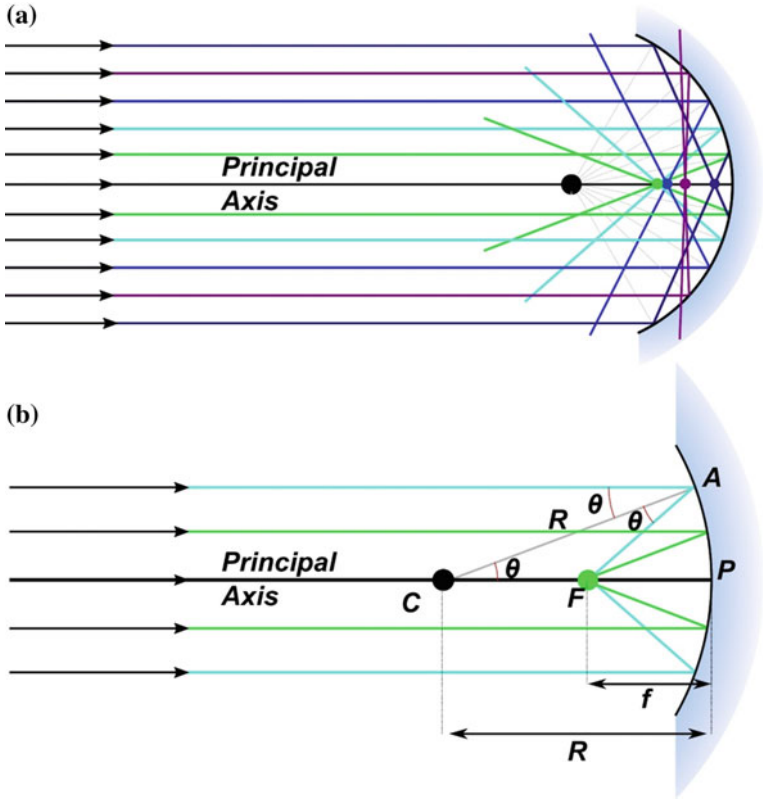

Fig. 3.13 **a** Parallel rays striking a concave spherical mirror do not focus on precisely a single point. This phenomenon is referred to as spherical aberration. **b** Rays parallel to the principal axis of a concave spherical mirror are converged to a point F, as long as the mirror width is small compared to its radius of curvature, R, so that the parallel rays form a small angle with the normal to the mirror surface

Let us prove Eq. 3.9. We consider a light ray that strikes the mirror at the point A, as it is illustrated in Fig. 3.14. The point C is the centre of the mirror curvature, hence, line CA is equal to R, the radius of curvature, and it is also the normal to the mirror surface at point A. The incoming light ray hitting the mirror at the point A forms an angle, θ, with this normal. Likewise, the reflected light ray, BF, also makes an angle equal to θ with the normal (law of reflection). The reflected light ray intersects the principal axis BC at the point F. In addition, the angle $\widehat{FCA}$ is also equal to θ, the angle of incidence, as the incident light ray is parallel to the principal axis and the two angles are alternate interior angles lying on opposite sides of the transversal line segment AC. Moreover, angle $\widehat{AFB}$ is equal to 2θ, as it is an exterior angle in the triangle ACF, and therefore it is equal to the sum of the two non-adjacent interior angles.

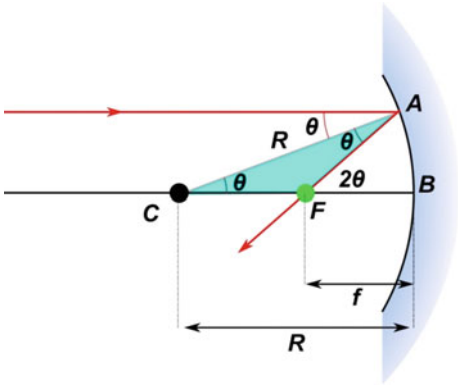

Fig. 3.14 Light rays parallel to the principal axis are reflected from a concave mirror according to the law of reflection and pass through the focal point *F*, where they converge

We will assume θ to be small enough, as the incoming light ray is parallel to and close to the principal axis. In addition, triangles *CAB* and *FAB* are approximately right triangles with the same side *AB*. From triangle *CAB*, we have:

$$\begin{aligned} \tan\theta &= \frac{AB}{CB} = \frac{AB}{R} \Rightarrow \\ AB &= R \cdot \tan\theta \end{aligned} \tag{3.10}$$

Similarly, from triangle *FAB* we have:

$$\begin{aligned} \tan 2\theta &= \frac{AB}{FB} = \frac{AB}{f} \Rightarrow \\ AB &= f \cdot \tan 2\theta \end{aligned} \tag{3.11}$$

Now, we apply the approximation $\tan\theta \approx \theta$ if $\theta \to 0$. Thus, Eqs. 3.10 and 3.11 take the form

$$AB = R \cdot \theta \tag{3.12}$$

$$AB = f \cdot 2\theta \tag{3.13}$$

By equating the second parts of Eqs. 3.12 and 3.13, we can find the relationship between the focal length, *f*, and the radius of curvature, *R*, of the spherical mirror:

$$\begin{aligned} R \cdot \theta &= f \cdot 2\theta \Rightarrow \\ R &= 2f \\ f &= \frac{R}{2} \end{aligned} \tag{3.14}$$

Since in this analysis we assumed only that the angle of incidence, θ, was small enough, without any other assumption about any specific ray, we can infer that this result applies to all incident paraxial rays. Therefore, after being reflected on the mirror surface, all paraxial rays pass through the same point F, the focal point. However, as it is only approximately true, the more curved the mirror, the worse this approximation. Nevertheless, if the mirror dimensions are small enough compared to the radius of curvature, then the assumption of convergence of the reflected light will be more reasonable and the light rays can be consider to converge to a single focal point. On the other hand, if the mirror is large, then the focal point is not a single point any more, but rather a line segment on the principal axis, due to the fact that light rays farther from the principal axis are focused on shorter focal lengths (Fig. 3.13a). This "defect" of spherical mirrors is called spherical aberration. It may occur in both large and small mirrors. As long as the mirror's aperture, A, is small compared with its focal length, f, the amount of spherical aberration is negligible.

However, if the incoming group of parallel light rays forms small but nonzero angle with the principal axis, then they are also reflected by the converging spherical mirror, but now they converge at a different point (Fig. 3.15). This point is also a focus. Obviously, different light beams forming different angles with the principal axis converge to different points. When all these foci, including the principal focus, are joined, they form a plane perpendicular to the principal axis, the focal plane. Thus, if a converging spherical mirror is lit by a distant, but extended light source, different groups of rays coming from different points of the source reach the mirror at slightly different angles. Consequently, they converge at different points on the focal plane.

3.5.3 Parabolic Mirrors

The fact that spherical mirrors focus a distant light source on a single point makes them potentially useful for, e.g., Solar Radiation Concentrating Systems. However, there is a more efficient shape of mirror that can focus all distant light rays on a single point, not just those close to the central axis: the parabola. In fact, it is the only curve where all incident light rays parallel to mirror's principal axis will be focused upon reflection on a single point, the focus of the parabola, as it is illustrated in Fig. 3.16. In other words, if the surface of the mirror were parabolic, rather than spherical, then the reflected light rays would truly be focused on the same focal point no matter how large the mirror is. However, because parabolic shapes are much harder to be made and therefore much more expensive, spherical mirrors are used for most purposes. Nevertheless, parabolic mirrors are used in a number of more critical applications, including solar collectors.

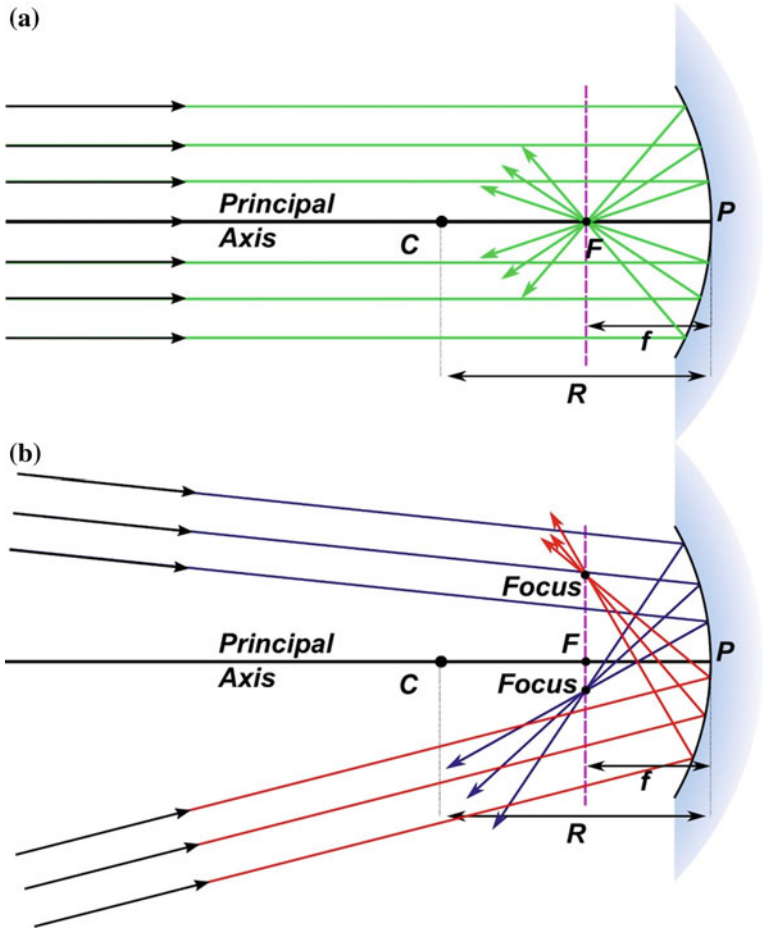

Fig. 3.15 **a** A group of light rays parallel to the principal axis of a converging spherical mirror converge to the same point located on the principal axis, the principal focus, F. **b** However, if the incoming group of parallel light rays forms a small but nonzero angle with the principal axis, then they converge at a different point, which is also a focus. All these points are located on the focal plane of the mirror. This plane is normal to the principal axis and passes through the principal focus of the spherical mirror

However, how does this work? Let us consider a curved mirror surface denoted by $y(x)$ in the x–y-plane, with the y-axis to be the symmetry axis; i.e. $y(-x) = y(x)$. Let us consider a light ray parallel to the y-axis. This ray strikes the curved mirror surface with an angle of incidence θ_i, with respect to the normal to the curve $y(x)$ at the point $P(x, y)$. At each point $P(x, y)$ of the curved surface, we can draw a tangent line, ε, and erect a normal from that point P on the surface. Using the law of reflection, the angle of reflection, θ_r, is equal to the angle of incidence, θ_i, namely $\theta_r = \theta_i = \theta$. The reflected ray intersects the y-axis at a point $F(0, f)$, as shown in Fig. 3.17.

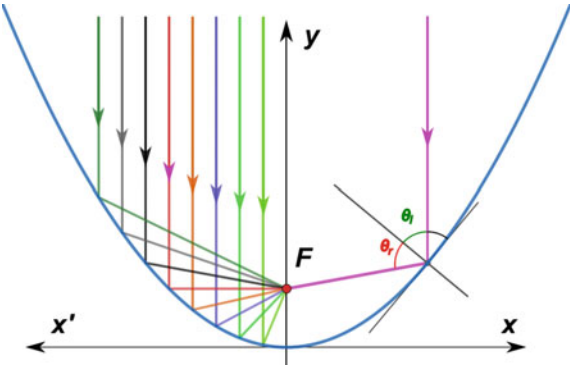

Fig. 3.16 Focusing on parallel light rays by a parabolic mirror. Light rays parallel to each other and parallel to the principal axis of the parabola will be focused on a single point, F

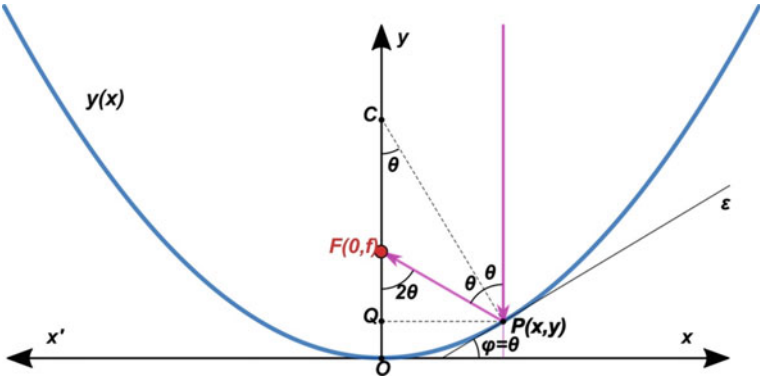

Fig. 3.17 Light reflection on an arbitrary curved reflective surface

Since the sides of angle, φ, are perpendicular to the sides of angle θ, angle φ is equal to θ. Hence,

$$\tan\,\varphi = \frac{\mathrm{d}y}{\mathrm{d}x} = \tan\,\theta \tag{3.15}$$

where the derivative of the curve $y(x)$ is evaluated at the point P.

In addition, angle $\widehat{FCP}$ is also equal to the angle of reflection, θ, as the incident light ray is parallel to y-axis and the two angles are alternate interior angles lying on opposite sides of the transversal line segment CP that intersects the two parallel lines, the y-axis and the direction of the incoming light ray. Moreover, angle QFP is equal to 2θ, as it is exterior angle in the triangle FCP and therefore it is equal to the sum of the two non-adjacent interior angles. Hence, the focal length f is given by the equation:

$$f = OF = OQ + FQ = y + \frac{x}{\tan 2\theta} \tag{3.16}$$

Using the trigonometric identity,

$$\tan 2\theta = \frac{2\tan\theta}{1 - \tan^2\theta} \tag{3.17}$$

Equation 3.16 becomes

$$f = y + \frac{x \cdot (1 - \tan^2\theta)}{2\tan\theta} \tag{3.18}$$

In addition, taken into account Eq. 3.15 and substituting it into Eq. 3.18, the latter takes the form

$$f = y + \frac{x}{2\frac{dy}{dx}} \cdot \left[1 - \left(\frac{dy}{dx}\right)^2\right] \tag{3.19}$$

However, since point P is an arbitrary point along the curved surface, we can always apply the above-presented methodology and find the direction of any reflected ray and the corresponding point, $F(0, f)$.

Let us determine the curve $y(x)$ that has the property that all incoming light rays parallel to the y-axis pass through the same point, the focal point F, after being reflected by the mirror. This means that the y-coordinate of the point F the reflected ray must pass through is independent of its x-coordinate. This is mathematically expressed by the condition: $df/dx = 0$. So, taking the derivative of Eq. 3.19 with respect to x and setting it equal to zero ($df/dx = 0$), it results in the following equation

$$\frac{dy}{dx} + \frac{1}{2\left(\frac{dy}{dx}\right)^2} \cdot \left\{\frac{dy}{dx}\left[1 - \left(\frac{dy}{dx}\right)^2 - 2x\frac{dy}{dx}\frac{d^2y}{dx^2}\right] - x\left[1 - \left(\frac{dy}{dx}\right)^2\right]\frac{d^2y}{dx^2}\right\} = 0 \tag{3.20}$$

Multiplying both sides of this equation by $-2\left(\frac{dy}{dx}\right)^2$ and performing the calculations, the resulting equation has the form

$$\begin{aligned} &x\frac{d^2y}{dx^2} - \frac{dy}{dx} + x\left(\frac{dy}{dx}\right)^2\frac{d^2y}{dx^2} - \left(\frac{dy}{dx}\right)^3 = 0 \Rightarrow \\ &\left[1 + \left(\frac{dy}{dx}\right)^2\right]\left(x\frac{d^2y}{dx^2} - \frac{dy}{dx}\right) = 0 \end{aligned} \tag{3.21}$$

The solutions to this equation are given by the solutions to the following two equations

$$1 + \left(\frac{dy}{dx}\right)^2 = 0 \tag{3.22a}$$

and

$$x\frac{d^2y}{dx^2} - \frac{dy}{dx} = 0 \tag{3.22b}$$

Because it is always true that

$$1 + \left(\frac{dy}{dx}\right)^2 > 1 > 0 \tag{3.23}$$

we end up solving only the very simple differential Eq. 3.22b.

The solution of this differential equation is given by the equation (the proof is out of the scope of this book)

$$y = Ax^2 + B \tag{3.24}$$

where A and C are arbitrary constants. Equation 3.24 is a parabola, whose symmetry axis coincides with the y-axis. Hence, the parabola is the unique curve that has the property all incoming on-axis parallel rays after being reflected on it to pass through the same point F.

To find the focal length, f, of a parabolic mirror, we can for simplicity, but without losing of generality, consider a parabola that is described by the equation

$$y = Ax^2 \tag{3.25}$$

Taking the derivative of y with respect to x ($dy/dx = 2Ax$) and substituting this result into Eq. 3.17, the focal length, f, is given by the following equation

$$\begin{aligned} f &= y + \frac{x}{2\frac{dy}{dx}} \cdot \left[1 - \left(\frac{dy}{dx}\right)^2\right] \\ &= Ax^2 + \frac{x}{2 \cdot 2Ax} \cdot \left[1 - (2Ax)^2\right] \\ &= Ax^2 + \frac{1}{4A} \cdot \left[1 - 4A^2x^2\right] \\ &= Ax^2 + \frac{1}{4A} - \frac{4A^2x^2}{4A} \\ &= Ax^2 + \frac{1}{4A} - Ax^2 \Rightarrow \\ f &= \frac{1}{4A} \end{aligned} \tag{3.26}$$

This means that the focal length f is independent of the point P where the incident light ray hits the parabolic mirror. So, all light rays parallel to the symmetry axis of the parabola, the y-axis, pass through the focal point F after being reflected by the mirror.

Although parabola's ability to reflect light on a single focus point is a very important and special property, it is only useful when light rays form a zero angle with the parabola's principal axis. In other words, the aforementioned requirement of light rays to be parallel to the symmetry axis of the parabola is crucial. If the incident light rays are parallel to each other but are not parallel to the symmetry axis of the parabola (called off-axis parallel rays), then the reflected rays are not focused on a unique focal point. In fact, the reflected rays completely miss the focal point at any other incoming angle. Consequently, despite the fact that the reflected on-axis light rays all converge onto a single point, the focal point, the reflected off-axis rays do not converge at all (Fig. 3.18). Nevertheless, because Solar Radiation Concentrating Systems are concentrating light on a surface (the receiver), rather than a single point, they can still function at incidence angles slightly greater than 0°.

Parabolic Trough reflectors. A Parabolic Trough reflector is a trough in which cross section has the shape of a parabola. They have a focal line instead of a focal point. This line consists of the focal points of each infinitesimal parabolic cross section. Sunlight that enters parallel to the optical plane (equivalent to the optical axis of the parabola) is focused on the focal line.

In order to describe a Parabolic Trough geometrically, the following four parameters are commonly used to characterize its form and size: the trough length, the focal length, the aperture width and the rim angle. The definition of the length of the trough is obvious. The focal length is the distance between the focal point and the vertex of the parabolic cross section. The aperture width is the distance between its two rims, and the rim angle is the angle between the optical axis and the line connecting the focal point and the mirror rim.

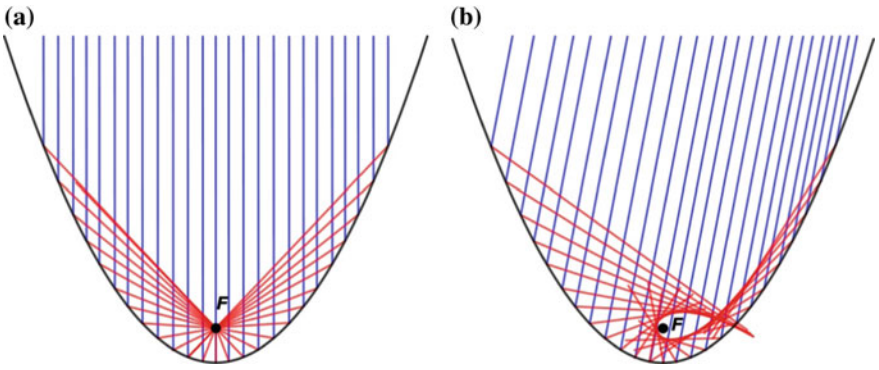

Fig. 3.18 The phenomenon of coma is a specific type of aberration of parabolic mirrors. The dot on the image is the focus on the parabola (the mirror). **a** Parallel rays coming in parallel to the axis of the parabola are focused on a point, **b** whereas rays coming in at a different nonzero angle do not focus at all

3.5.4 *Linear Fresnel Mirrors*

In order to make the diverging light rays emitted from a (point) light source parallel, we need a lens with short focal length, *f*. By placing it in front of the light source, with the light source been placed on the focus, *F*, of the lens, we produce a parallel light beam. Lenses with short focal length require very small curvature radius, *R*, or else, they need to be thick. However, this kind of lenses is too heavy. The solution would be thin, low-weight and low-volume lenses with short focal lengths. It has been given by Augustin-Jean Fresnel (1788–1828), a French physicist known, among others, for his invention of a special type of lenses, which had been used in lighthouses. They were used to concentrate light horizontally and make it visible over long distances, helping ships avoid crashing into the rocks at sea. The operation principle of Fresnel lenses is very simple. Given that the refractive function of a lens takes place at its surface, by removing as much of its material as possible, while still maintaining the surface curvature, we can still have the same result (Fig. 3.19).

The principle of dividing an optical element (in the previous case the surface of a lens) into segments that have all together the same, or a very similar, optical effect like the original element can also be applied to mirrors. In an analogous manner, a linear Fresnel mirror can be constructed by substituting a Parabolic Trough by linear segments that focus the radiation arriving on them on the focal line of the original Parabolic Trough (Fig. 3.20). Similarly, it is possible to divide a paraboloid mirror (parabolic dish) into annular segments forming a circular Fresnel mirror.

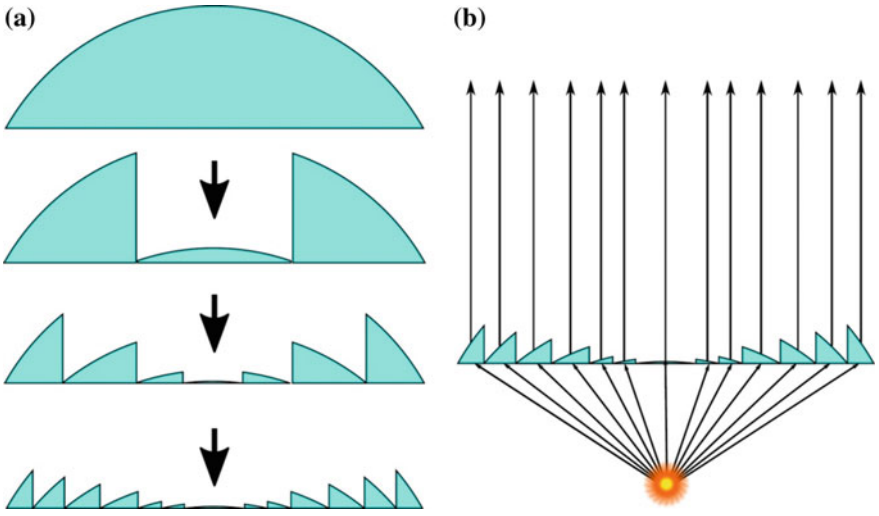

Fig. 3.19 An ordinary converging spherical lens is transformed into an equivalent Fresnel lens by collapsing its continuous surface. The idea behind the invention of Fresnel lenses was to reduce the quantity of material used in a conventional lens

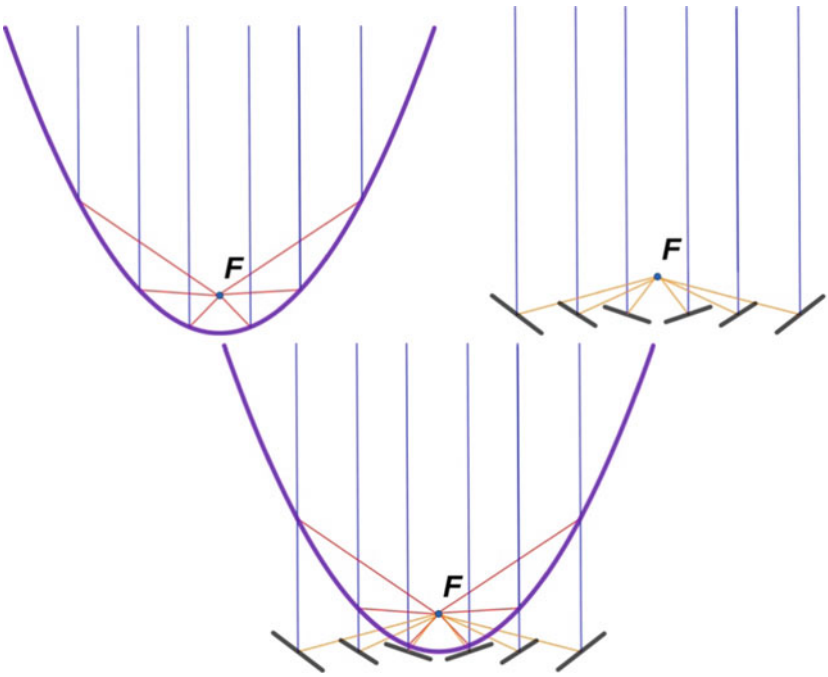

Fig. 3.20 Schematic presentation of the operating principle of a Linear Fresnel Reflector

This Fresnel mirror focuses the light that arrives parallel to its optical axis on the focal point of the original paraboloid mirror. In other words, the operation principle of Fresnel mirrors is the replacement of the continuous surface of the original mirror with a set of reflective surfaces that form a compound reflective surface. This allows a substantial reduction in the size (and thus weight and volume) of the mirror, at the expense of its imaging quality. Since Fresnel mirrors follow the operation principle of Fresnel lenses, they have got their name from Augustin-Jean Fresnel.

Concerning the concentration of solar radiation, a Linear Fresnel Reflector (LFR) System is made up of multiple narrow segments of mirrors arranged in such a way that they reflect and concentrate sunlight on an absorber above them, placed at the focal line, emulating the function of a Parabolic Trough (Fig. 3.21). The greatest advantage of these Systems is that they use flat or slightly curved reflectors which are cheaper compared to parabolic reflectors. Additionally, the reflective elements are mounted close to the ground minimizing the wind drag and thus structural requirements.

To recapitulate, in order to concentrate solar radiation on a (focal) line at a height, H, using Fresnel technology, the incident radiation is reflected by a set of linear mirrors. These mirrors are arranged symmetrically on both sides of the receiver and are characterized by their position, Q_j, the gap between two successive mirrors, S_j, their width, W_j, and their inclination angle, θ_j (Fig. 3.21). Each mirror

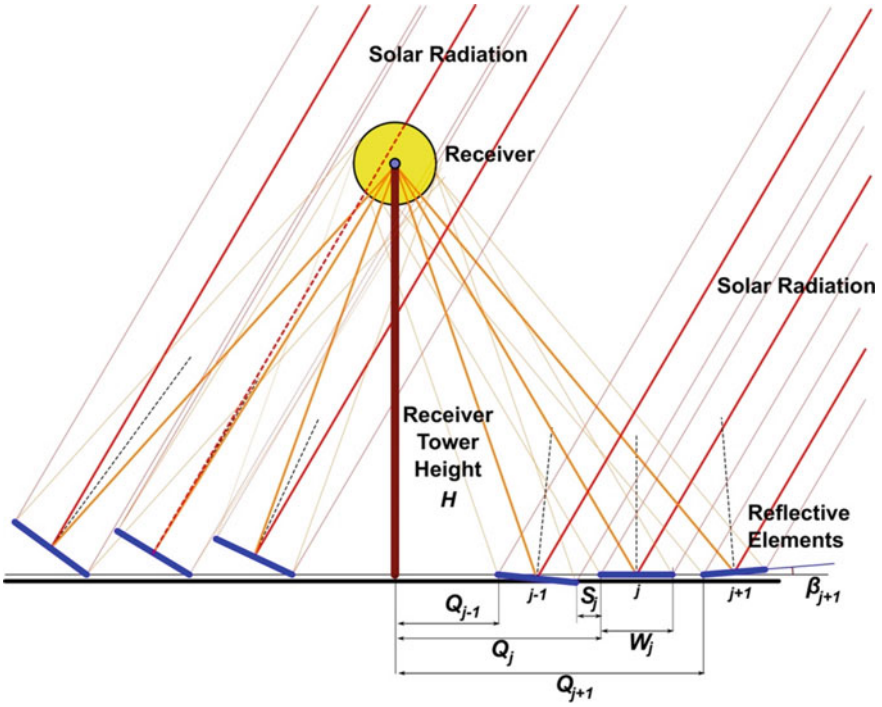

Fig. 3.21 A Linear Fresnel Reflector System has a similar effect to a corresponding Parabolic Trough. It is made up of a set of multiple narrow segments of mirrors arranged in such a way that they reflect and concentrate sunlight on a line above them, emulating the corresponding Parabolic Trough. The mirrors are arranged symmetrically on both sides of the receiver and are characterized by their position, Q_j, the gap between two successive (adjacent) mirrors, S_j, their width, W_j, and their inclination angle, θ_j

reflects solar radiation on the receiver individually and independently. Although there have been proposed mirrors having different shapes, like parabolic or spherical, plane mirrors are most usually used as they are more economical. For this reason, we will study the operation principle of a Linear Fresnel Reflector System with plane elements. In addition, because these Systems are symmetrical with respect to the vertical plane containing the receiver, it is adequate to study a typical cross section of them.

Chapter 4
Linear Fresnel Reflector Systems Design Parameters

Linear Fresnel Reflector Systems are characterized by simple design and low construction and maintenance costs. They typically use a set of long flat or slightly curved reflective elements of equal or varying width mounted on trackers. The reflectors are arranged so that they reflect the direct solar radiation concentrating it onto a stationary central linear receiver (absorber) located above them. When designing Linear Fresnel Reflector Systems, we realize that there is a large variety of possible configurations, because the geometrical characteristics of the reflectors and the receiver can be determined independently. However, although usually uniform configurations are implemented (e.g. all reflectors have the same width and are equally spaced, or not spaced at all), this is not at all mandatory. Actually, despite the fact that this kind of configuration is simpler in design and construction, it does not maximize System's efficiency. The main reason is that the performance of the System is influenced by a relatively large number of variables, e.g. the distance of the receiver from each reflector, the inclination of the reflectors, the shape of the reflected solar radiation, the shadowing and blocking effects between adjacent reflectors, as well as the shadowing from the receiver, to name only a few. Therefore, despite the obvious ease of uniform configurations, many other solutions with varying width or spacing among the reflectors have been proposed and implemented.

For these reasons, there is plenty of space for optimization through improved designing. However, at the same time, the large number of variables and the nonlinear behaviour of the Systems make parameters' optimization not at all an easy task. For example, more reflectors do not necessarily mean that the total reflecting surface is substantially increased and the total efficiency of the System has been enhanced (Abbas et al. 2017).

In this chapter, we will study the geometrical characteristic of a typical Linear Fresnel Reflector System, as well as the phenomena that affect its optical performance. The main goal is to develop the appropriate mathematical formalism so that to be able to calculate the key parameters of any Linear Fresnel Reflector System aiming to optimal design and improved performance.

S. Karathanasis, *Linear Fresnel Reflector Systems for Solar Radiation Concentration*, https://doi.org/10.1007/978-3-030-05279-9_4

4.1 Linear Fresnel Reflector

As it has been presented in the previous chapter, the Linear Fresnel Reflectors technology owes its name to the Fresnel lenses, which have been developed by the French physicist Augustin-Jean Fresnel. They are based on the principle that a continuous reflective surface can be replaced by a set of discontinuous surfaces that have the same (or a very similar) optical effect to the original optical element, at the expense of reducing optical quality. Thus, it is possible, for instance, to divide a paraboloid reflector (parabolic dish) into annular (ring-shaped) segments (forming a Circular or Coaxial Fresnel Reflector System), which focus the solar radiation arriving parallel to its optical axis onto the focal point of the paraboloid reflector. In an analogous way, a Linear Fresnel Reflector System can be constructed by substituting a Parabolic Trough with linear segments that reflect the solar radiation arriving in a plane parallel to the symmetry plane (its longitudinal plane) of the Parabolic Trough onto its focal line.

Typically, Solar Radiation Concentrating System with Linear Fresnel Reflectors consists of three main components (Fig. 4.1):

- The primary Fresnel Reflectors field, which is made of flat parallel reflector stripes. The most important design variables are the width and the number of the reflectors, the gap between two consecutive reflectors and their inclination angle.
- The receiver. Its main components are the absorber tube(s) and the secondary reflector.
- The Sun-tracking mechanism. Solar Radiation Concentrating System using Linear Fresnel Reflectors usually has a one-axis tracking System. The motion of the reflectors depends only on Sun's position in the sky and not on their position. Each reflector tracks Sun individually, having, however, the same angular velocity.

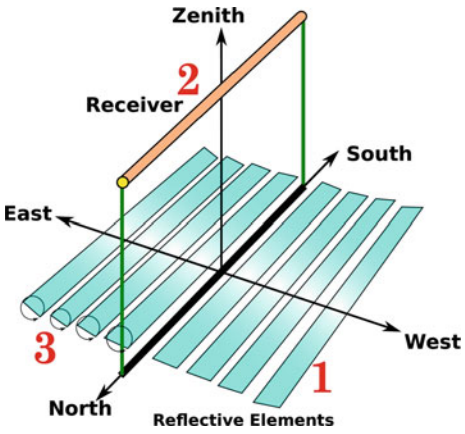

Fig. 4.1 Main component of a typical Solar Radiation Concentrating System with Linear Fresnel Reflectors: (1) the primary Fresnel Reflectors field, (2) the receiver and (3) the solar tracking mechanism

Based on the shape of the reflectors, there are two general types of Fresnel Reflector Systems. The first consists of concentric, or, more accurately, coaxial conical reflective rings (frustums) (Fig. 4.2a), and the second consists of a series of linear reflectors (Fig. 4.2b). In each case, the width of the reflective elements may be the same (constant) or different (varying) for each reflector. This changes the design's parameters, and consequently, the mathematical formulas and the involving calculation. Depending on the use, the receiver may be placed above (Fig. 4.2a, b), which is the most common case, or under (Fig. 4.2c, d) the reflective elements. In the latter arrangement, the reflectors are arranged so that they direct the solar radiation at the bottom of the assembly. Each approach has its own advantages and disadvantages both in construction and ease of use.

The shape of the receiver plays a major role on the reflectors' tilt and position. The receiver may be placed horizontally (Fig. 4.2e) or vertically (Fig. 4.2f). In addition, receiver's cross section further affects the configuration of the System. In Linear Fresnel Reflector Systems, the receiver is usually a rectangular parallelepiped (in this case, the receiver consists of many tubes) with its longer dimension being aligned with the longer dimension of the reflectors. In Concentric Fresnel Reflector Systems, it is a cylinder in which axis coincides with the symmetry axis of the whole construction. Apart from these cases, the receiver's cross section may be triangular (Fig. 4.2g), circular or semi-circular (Fig. 4.2h) affecting further the System configuration.

Sun's tracking System induces further construction modifications. In most cases, when constructing a Solar Radiation Concentrating System with Fresnel Reflectors we choose the whole construction to be stationary except the reflectors. They must change their inclination so that they always reflect and redirect the incoming solar radiation on the receiver, since Sun changes its position over the day (Fig. 4.3a, b). The inclination of the reflectors can be readjusted by rotating them around a constant point, or more precisely a constant axis, their rotation axis. The latter may go through the middle point of their narrower edge or coincide with one of their longer edge. In most cases, the rotation axes are on the same plane, although there have been proposed different configurations in the literature, e.g. a wave-shaped configuration (Chaves and Collares-Pereira 2010). On the contrary, in Concentric Fresnel Reflector Systems, the reflective elements are constant and the only possible readjustment of the structure so as to face Sun is by rotating the whole construction around its focal point (Fig. 4.3b).

Depending on the construction features, the geometry of each Solar Radiation Concentrating System with Fresnel Reflectors requires different mathematical approaches. In any case, each ring or linear reflector has to be tilted by an angle so that solar radiation falling on it to be reflected towards a central focal point or line. This angle needs to be precise is what makes the construction of a Fresnel Reflector System a bit challenging.

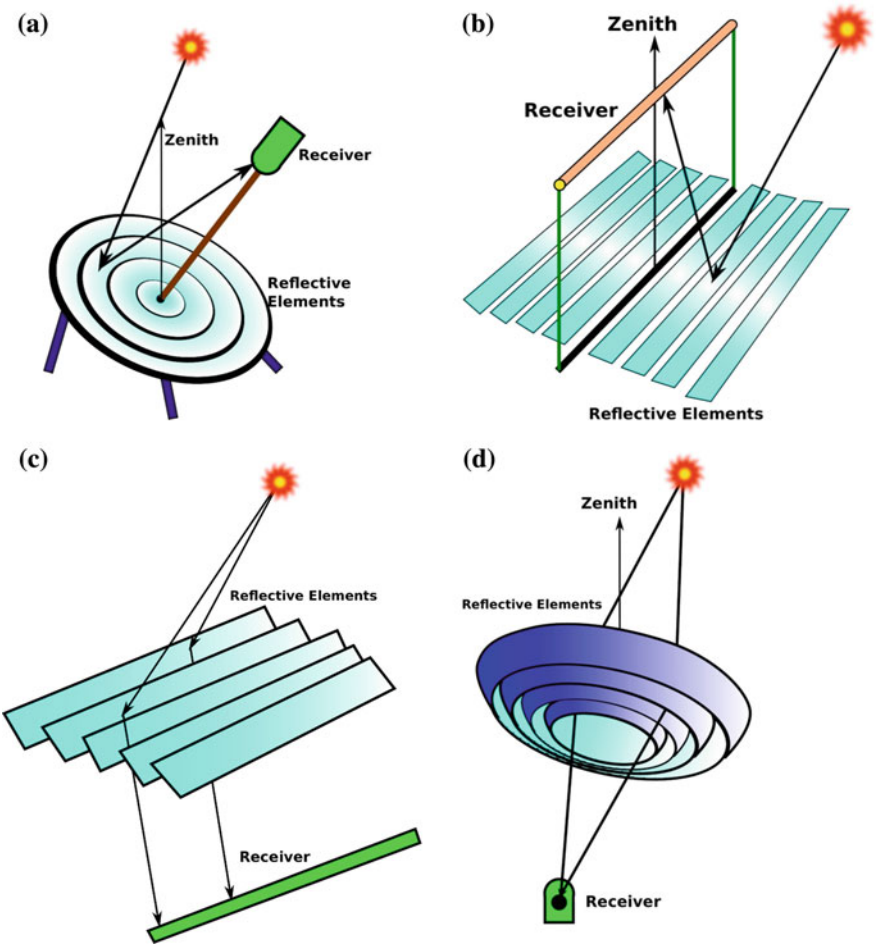

Fig. 4.2 Different Fresnel Reflector System depending on different design approaches: the reflectors have the form of coaxial conical rings (**a**), or the Sun rays fall on linear reflective strips and then they get focused on a linear receiver above the reflectors. In these cases, the receiver is placed above the reflective elements. Sometimes, it is desirable to put the receiver under the reflecting structure (**c**) and (**d**). Furthermore, the receiver may be horizontal (**e**) or vertical (**f**), or the receiver's vertical cross section may be triangular (**g**) or even circular or semi-circular (**h**)

Many parameters need to be considered for the design of a Linear Fresnel Reflector System:

- The number (N or n) of the reflective elements (the reflectors) on each side of receiver
- The shape of the reflective elements (flat, circular or parabolic), and, in the case of curved reflectors, their curvature
- The width (W_j) of the reflective elements (of the jth reflector)

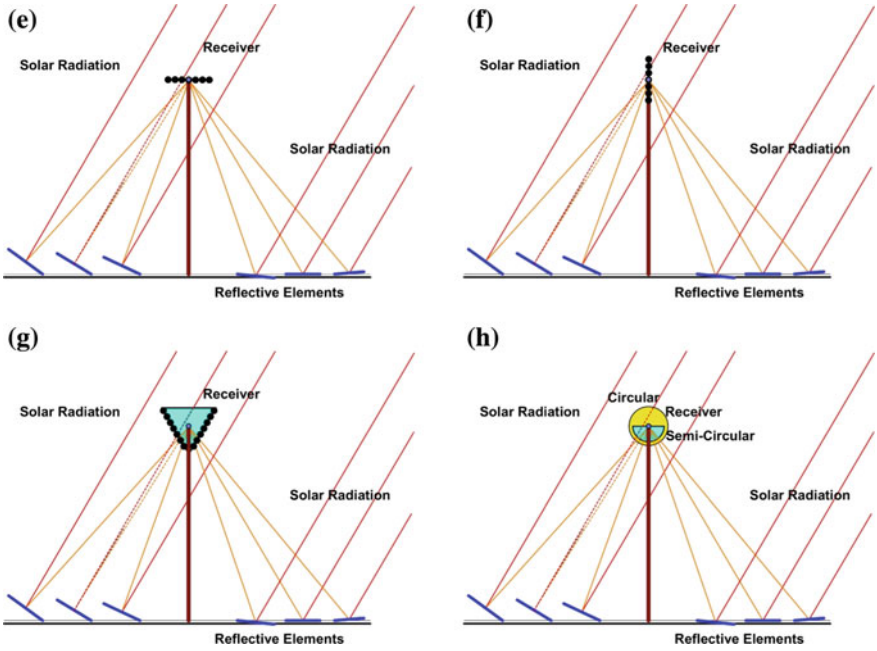

Fig. 4.2 (continued)

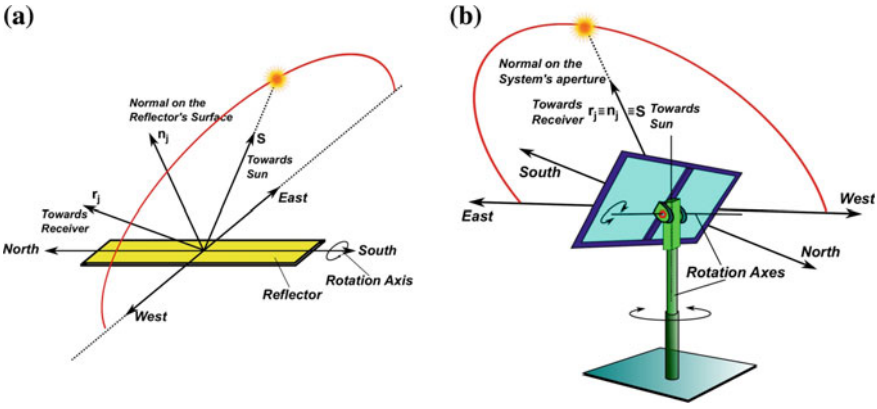

Fig. 4.3 Fresnel Reflector Systems use reflective elements that direct Sun's rays onto a receiver. As Sun's position in the sky changes over the day, the reflectors have to be readjusted so that the reflected solar radiation to be focused on the proper point (or line). This can be done by rotating only the reflective elements around one axis (**a**), or the whole construction around two perpendicular axes (**b**). In the first case, the rotation axis is parallel to the reflectors' longitudinal dimension and it may go through the middle point of their narrower edge (**c**) or it may coincide with one of their longer edge (**d**)

- The position (Q_j) of the reflective elements in relation to a reference point, which usually is the projection of the receiver centre on the plane of the reflectors (the horizontal plane)
- The space or gap (S_j) between the jth and the $(j-1)$th reflector, measured horizontally from the last point of the previous reflector to the first point of the next reflector
- The position of the reflectors' rotation axis, in the case of Linear Reflective Elements
- The tilt or inclination angle (β_j) of each reflector in relation to the aperture plane, measured anticlockwise from the horizontal plane
- The way and the rate the reflectors' tilt angle changes, or else the Sun's position tracking System
- The distance of the jth reflector from the receiver (L_j)
- The solar field filling factor (SF_{ff})
- The aperture diameter (D), or the horizontal dimensions (Length, L, and Width, W) of the System
- The total width of the reflectors (W_t)
- The solar field width (W_f)
- The shape or design of the receiver
- The width of the receiver (R_w), or the diameter (d) of the receiver tube
- The relative position of the receiver (above or under the reflective elements)
- The height of the receiver (H), or the focal distance (f), or else the distance between the central point of the receiver from the horizontal plane.

All these parameters directly affect the efficiency of the solar radiation concentration, as well as its absorption by the receiver. If they are not chosen properly, it will lead not only to a waste of material, but also to energy losses, reducing the efficiency of the System (Zhang et al. 2010; Ahmed and Amin 2016). However, in order to be able to calculate some of them, the rest parameters (or variables) have to be predefined. In other words, the construction of such a System requires the definition of a set of parameters and the calculation of the rest of them. However, some of these variables are connected via simple formulae, e.g.

$$W_t = \sum_{j=1}^{n} W_j = n \cdot W \tag{4.1}$$

$$SF_{ff} = \frac{W_t}{W_f} \tag{4.2}$$

Fortunately, whether it concerns a Concentric Fresnel Reflectors or a Linear Fresnel Reflector System the model geometry is the same, as the cross section of both types along their symmetry plane or axis is identical, making our life simpler.

4.2 Geometrical Parameters of Linear Fresnel Reflector

Linear Fresnel Reflector Systems are made out of flat reflector strips, although the truth is that they may not always be flat, even though they seem to be flat. A higher concentration factor could be achieved if reflectors were slightly bent. The perfect shape to focus the incident solar radiation onto a single focal line would be the parabola (a shallow Parabolic Trough). Nevertheless, manufacturing a high number of small parabolic reflectors with specific and different focal length is difficult and costly. In addition, there are differences between Parabolic Troughs and Linear Fresnel Collectors that do not suggest a parabolic shape for the reflective elements. In Parabolic Troughs, the receiver moves with the reflective surface and the reflector's aperture is always perpendicular to the incoming solar radiation, while in Linear Fresnel Reflectors the receiver is fixed, and therefore, when the reflectors rotate to track Sun, their aperture does not always stay perpendicular to the direction of the incoming solar radiation. This results in the reflected solar radiation to not being able to get focused exactly onto the receiver centreline, leading to aberrations. However, if the reflectors' width is relatively narrow, there is no need to use a parabolic shape; a cylindrical shape could be used instead, which would result in easier manufacturing, and thus in lower costs. However, as it has been already mentioned, although there have been proposed reflectors having different shapes, like parabolic or spherical, plane reflectors are more usually used, as they are more economical. For this reason, we will study the operation principle of a Linear Fresnel Reflector System with plane elements.

Let us consider an arbitrary reflective element, a plane reflector, of a Linear Fresnel Reflector System, as it is depicted in Fig. 4.4. Let it be the j reflector, located at a distance Q_j from the origin of the coordinate system, which coincides with the projection of the receiver centre on the horizontal plane. This reflector forms an angle β_j with the horizontal axis $x'x$. The incoming solar radiation forms an angle θ with the same axis. This angle, without losing of any generality, can be taken equal to Sun's height angle, h, at a first approximation (in fact, we assume that the whole construction is oriented perpendicular to Sun's direction. This is a special case which will be discussed in more details later). As Sun is too far away from Earth, we can consider solar light rays to be parallel. As a result, angle θ is the same for all reflective elements.

Taking into account the analysis of reflection for plane reflectors presented in the previous chapter, we can conclude that a solar light beam hitting the jth reflector remains parallel upon reflection and is directed towards the receiver only when the incidence angle, $\theta_{i,j}$, plus the reflection angle, $\theta_{r,j}$, equal the angle, ω_j, formed by the incident light beam and the line connecting the jth reflective element and the receiver (in fact their centres or another point properly defined). In order for this constraint to be satisfied, the reflective element must be inclined in such a way that the normal on its surface, the vector $\mathbf{n_j}$, to coincide with the bisector of angle ω_j (Fig. 4.4). In addition, when plane reflective elements are used, their width, W_j, has to be chosen in such a way that the cross section of the reflective solar light beam to

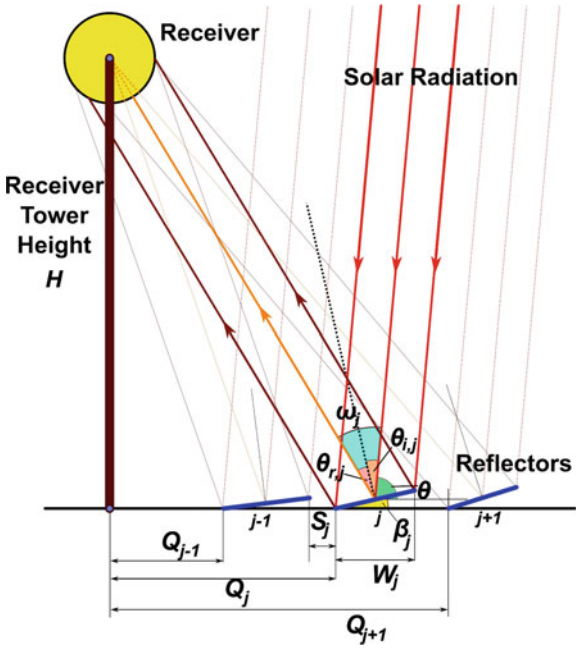

Fig. 4.4 Schematic presentation of the operating principle of a Linear Fresnel Reflector System

be equal to (or smaller than) the projection of the irradiated receiver surface on a plane perpendicular to the reflected light beam. Otherwise, a part of the reflective solar radiation misses the receiver, resulting in energy losses. However, as Sun's position in the sky changes continuously during the day, the radiation incidence angle, $\theta_{i,j}$, varies as well. For this reason, we have to choose the width, W_j, of the jth reflective element so that the maximum cross section of the reflected light beam to be equal to (or smaller than) the projection of the irradiated receiver surface on a plane perpendicular to the reflected light beam. This happens only when light strikes each reflective element perpendicular to its aperture and the reflection angle, $\theta_{r,j}$, and the incidence angle, $\theta_{i,j}$, are equal to zero, as the normal to the reflective element surface coincides with the direction of the incoming solar radiation. However, in this case the reflective element is overshadowed by the receiver. In any other case, the cross section of the reflected solar light beam is equal to the cross section of the incoming light beam multiplied by the cosine of the incidence angle ($\cos\ \theta_{i,j}$). This effect—the cosine effect—will be discussed in more details in the next chapter.

Obviously, in order for a Linear Fresnel Reflector System with plane elements to be able to concentrate solar radiation onto the receiver, the above-presented analysis must be performed for each reflective element. As each reflector is on a different position, the line connecting their centres with the central point of the receiver forms different angles with the horizontal plane. The direction of these

lines has to coincide with the direction of the reflected solar light rays from each reflector. Therefore, the width, W_j, and the inclination angle, β_j, of each reflective element, as well as the distance, S_j, between them, must be determined independently.

4.3 Sun Tracking

Like all Solar Radiation Concentrating Systems, Linear Fresnel Reflector Systems can use only direct solar radiation. Due to Earth's rotation around Sun, the position of Sun in the sky changes during the day and all over the seasons, resulting in significant variations and fluctuations in the incoming direct solar radiation. However, the solar radiation concentration depends not only on the angle of incidence of Sun's rays on the reflectors' aperture, but also on the reflectors' and the receiver's area, as well as the reflectors' inclination angle. Hence, if the reflectors were fixed, the solar radiation concentration would reach its maximum value at a very specific time of the day and would decline rapidly around this time. For this reason, all Linear Fresnel Reflector Systems have a mechanism to track Sun.

Sun tracking Systems modify the angle of incidence of solar radiation by aligning the reflectors in the optimal direction to maximize the amount of solar radiation reflected to and, consequently, absorbed by the receiver, and thus improve the System efficiency. The tracking mechanisms can be divided into two categories: one-axis and two-axis tracking Systems. In one-axis tracking mechanisms, the reflectors are oriented along a fixed direction, e.g. a North–South line, and Sun's position is tracked from East to West throughout the day. This kind of mechanism is mainly used by Parabolic Trough Systems, Cylindrical Trough Systems and Linear Fresnel Reflector Systems.

As a result, when studying Solar Radiation Concentrating Systems, and in particular Linear Fresnel Reflector Systems, sooner or later we will come up against the problem of calculating the right inclination angle, β_j, the reflective element must have so that they are able to redirect solar radiation to the receiver. However, since the positions of each reflective element, as well as the position of the receiver, are fixed, depending only on the construction design, the direction of the reflected solar radiation is known beforehand: it is the direction of the receiver in relation to each reflective element, j, denoted by the position unit vector $\mathbf{r_j}$ (Fig. 4.5). What is changing during the day is the direction of the incoming solar radiation, being characterized by the unit vector $\mathbf{S}$, which is independent of the reflective elements' position.

A standard Sun-tracking System consists of a tracking algorithm, a controller, a positioning System, a driving mechanism, sensors and switches. The tracking algorithm executed in the controlling unit orders the positioning System (the motors) to orient the reflective elements (reflectors) in the optimal angle, β_j, through actuators and gears. Generally, Sun-tracking Systems are distinguished in passive, or open-loop, and active, or closed-loop, trackers. Passive tracking Systems depend

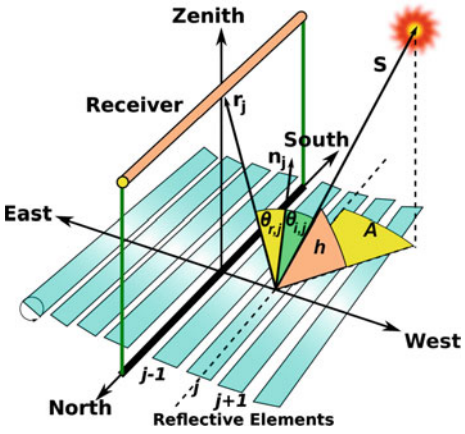

Fig. 4.5 In a Linear Fresnel Reflector System, the positions of each reflective element and the position of the receiver are fixed. In this case, the direction of the reflected solar radiation is known beforehand. It is the direction of the receiver in relation to each reflective element, *j*, denoted by the position unit vector $\mathbf{r_j}$. On the other hand, the direction of the incoming solar radiation, being characterized by the unit vector **S**, and hence the incidence angle, $\theta_{i,j}$, in relation to a horizontal surface, must be calculated any time

on an open-loop approach based on mathematical algorithms and formulas to control actuators and motors. On the other hand, active tracking Systems use electro-optical sensors that provide feedback. Passive Systems are cheaper with simple design, whereas active Systems are more efficient.

The control requirements of Linear Fresnel Reflector Systems differ from the equivalent of Parabolic Trough Systems, as in Linear Fresnel Reflector Systems, a large number of reflectors need to be driven. Actually, several, if not all, reflectors could be connected by a coupling mechanism and be operated by a single motor, as all reflectors turn with the same angular speed (as we will see later in this chapter). However, reflectors reorientation is commonly operated individually or in small groups of reflectors as this treatment leads to higher degree of accuracy and avoids a complete breakdown of the System.

Compared to Parabolic Trough collectors, the tracking System of Linear Fresnel Reflector Systems needs lower power to move the reflectors, as they are much smaller and lighter. In addition, their structure can be easily designed so that the reflectors centre of gravity to be on the rotational axis. On account of this, motors and gears are quite simpler.

As real-time Sun tracking is implemented by complex tracking mechanisms, its accuracy is critical in achieving high efficiency of Linear Fresnel Reflector Systems. Tracking errors can be caused due to reflectors' exocentric structure (the rotation axes do not coincide exactly with the symmetry axes), differences in reflectors orientation, the height of the absorber, reflectors' supporting structure

imperfections, the drivers' accuracy, the tracking software algorithm, the Sun's position algorithm, differences in geographic latitude and longitude among the modules of the System, if the installation occupies a large area, and structure errors.

4.3.1 The Orientation of the Reflective Elements

The real problem in Sun tracking is to find the appropriate orientation of the reflective elements. The normal on the reflective element surface, denoted by the unit vector $\mathbf{n_j}$, must intersect the angle being formed by the direction of the incident solar radiation (the vector **S**), and the line connecting the receiver (vector $\mathbf{r_j}$) with the j reflective element. This proceeds from the application of the law of reflection for each reflective element, j: the angle of incidence, $\theta_{i,j}$, must be equal to the angle of reflection, $\theta_{r,j}$. Despite the fact that the direction of the receiver, $\mathbf{r_j}$, in relation to each reflective element, j, is constant and a construction parameter, and the direction of the incident solar radiation (vector **S**) is the same for all reflective elements, j, the latter is not constant during the day. This means that the normal, $\mathbf{n_j}$, to the surface of each reflective element has to change constantly, so that the solar radiation be redirected correctly to the receiver after being reflected by the reflectors.

Having constant vectors $\mathbf{r_j}$, and being able to calculate vector **S** any time of the day using the equations describing Sun's position in the sky presented in the previous chapter, what we need is a way to calculate $\mathbf{n_j}$, the normal on each reflecting element, as a function of **S** and $\mathbf{r_j}$. Essentially, this problem is trying to find the direction of the bisector of the angle of two straight lines in vector calculus.

In the general case, to find the bisector vector of the angle between two straight lines in 3D space, we can, without losing of any generality, suppose that the point of intersection of these lines is the origin O of the Cartesian coordinate system (Fig. 4.6).

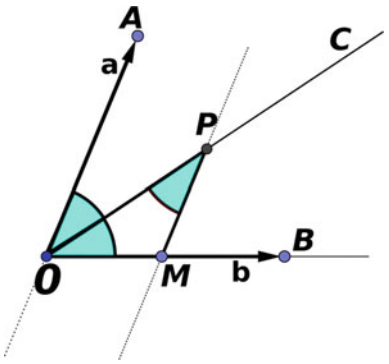

Fig. 4.6 Bisector of the angle formed by two lines can easily be determined using vector calculus

So, let **a** and **b** be the unit vectors along the directions of the two straight lines *OA* and *OB*, respectively. Now, let *OC* be the bisector of the angle $\widehat{AOB}$, *P* be any point on *OC* and *PM* be drawn parallel to *OA*. Then angle $\widehat{COA}$ is equal to the angle $\widehat{COB}\left(\equiv \widehat{MOP}\right)$, by definition, as *OC* is the bisector of angle $\widehat{AOB}$. Moreover, angle $\widehat{MPO}$ is equal to the angle $\widehat{AOP}$ as they are alternate interior angles lying on opposite sides of the transversal line segment *OC* that intersects the parallel lines *OA* and *PM*. Hence, since angles $\widehat{MOP}$ and $\widehat{MPO}$ are equal, we have $OM = MP$, or otherwise, the triangle *OPM* is isosceles. In addition, as vector **OM** is collinear with vector **b** and vector **MP** is collinear with vector **a**, we can take $\mathbf{OM} = t \cdot \mathbf{b}$ and $\mathbf{PM} = t \cdot \mathbf{a}$ (as *OM* = *MP*) for some scalar *t*.

Then, if $\mathbf{OP} = \mathbf{n}$, we have

$$\mathbf{n} = \mathbf{OP} = \mathbf{OM} + \mathbf{MP} = t \cdot (\mathbf{a} + \mathbf{b}) \tag{4.3}$$

Because every point, *P*, of the bisector *OC* corresponds to a vector **n** given by Eq. 4.3 for any real value of *t*, **n** is the position vector of the line *OC* and hence Eq. 4.3 gives the vector form of the bisector of the angle of the two straight lines corresponding to the unit vectors **a** and **b**.

If vectors **a** and **b** are not unit vectors, they can be transformed into unit vectors by getting normalized: $\mathbf{a} \equiv \mathbf{a}/|\mathbf{a}|$ and $\mathbf{b} \equiv \mathbf{b}/|\mathbf{b}|$. To make vector **n** a unit vector, $|\mathbf{n}| = 1$, we have to normalize it as well. According to Eq. 4.3, we have

$$\begin{aligned} &|\mathbf{n}| = |t \cdot (\mathbf{a} + \mathbf{b})| = |t| \cdot |\mathbf{a} + \mathbf{b}| = |t| \cdot \sqrt{|\mathbf{a}| + |\mathbf{b}| + 2 \cdot \mathbf{a} \cdot \mathbf{b}} = 1 \Rightarrow \\ &|t| = \frac{1}{\sqrt{|\mathbf{a}| + |\mathbf{b}| + 2 \cdot \mathbf{a} \cdot \mathbf{b}}} \end{aligned} \tag{4.4}$$

Hence, substituting Eq. 4.4 into 4.3 we have

$$\begin{aligned} \mathbf{n} &= \frac{\mathbf{a} + \mathbf{b}}{\sqrt{|\mathbf{a}| + |\mathbf{b}| + 2 \cdot \mathbf{a} \cdot \mathbf{b}}} \Rightarrow \\ \mathbf{n} &= \frac{\mathbf{a} + \mathbf{b}}{\sqrt{|\mathbf{a}| + |\mathbf{b}| + 2 \cdot |\mathbf{a}| \cdot |\mathbf{b}| \cdot \cos\,\omega}} \Rightarrow \\ \mathbf{n} &= \frac{\mathbf{a} + \mathbf{b}}{\sqrt{1 + 1 + 2 \cdot 1 \cdot 1 \cdot \cos\,\omega}} \Rightarrow \\ \mathbf{n} &= \frac{\mathbf{a} + \mathbf{b}}{\sqrt{2 + 2 \cdot \cos\,\omega}} \Rightarrow \\ \mathbf{n} &= \frac{\mathbf{a} + \mathbf{b}}{\sqrt{2(1 + \cos\,\omega)}} \end{aligned} \tag{4.5}$$

where ω is the angle between vectors **a** and **b**, while **a** and **b** are unit vectors, $|\mathbf{a}| = |\mathbf{b}| = 1$.

In the case where vectors **a** and **b** are not unit vectors, Eq. 4.5 has the general form

$$\mathbf{n} = \frac{\frac{\mathbf{a}}{|\mathbf{a}|} + \frac{\mathbf{b}}{|\mathbf{b}|}}{\sqrt{|\mathbf{a}| + |\mathbf{b}| + 2 \cdot \mathbf{a} \cdot \mathbf{b}}} \tag{4.6}$$

Now substituting vector **a** with vector **S** and vector **b** with vectors $\mathbf{r_j}$, Eqs. 4.5 and 4.6 become

$$\mathbf{n_j} = \frac{\mathbf{S} + \mathbf{r_j}}{\sqrt{2(1 + \cos\,\theta_j)}} \tag{4.7}$$

$$\mathbf{n_j} = \frac{\frac{\mathbf{S}}{|\mathbf{S}|} + \frac{\mathbf{r_j}}{|\mathbf{r_j}|}}{\sqrt{|\mathbf{S}| + |\mathbf{r_j}| + 2 \cdot \mathbf{S} \cdot \mathbf{r_j}}} \tag{4.8}$$

where ω_j is the angle between the direction of the incident solar radiation vector **S** and the direction of the reflected solar radiation from the *j*th reflective element, or else the position (or direction) vector of the receiver, $\mathbf{r_j}$, in respect to the *j*th reflective element, and last, $\mathbf{n_j}$ is the normal on the surface of the *j*th reflective element, and consequently its orientation.

By being able to calculate the orientation of each reflective element, we can successfully redirect solar radiation and concentrate it onto the receiver. What is left is to change the reflective elements' direction using an appropriate tracking System that turns them constantly. An expression for the rate of change can be found by taking the derivative of Eq. 4.7, or Eq. 4.8, with respect to time. However, this will be studied later in this chapter.

4.3.2 The Tracking Angle

The angle of incidence, $\theta_{i,j}$, of the direct solar radiation for an arbitrarily oriented surface can be described by Eq. 2.56 of Chap. 2 in terms of the orientation of the surface (in our case the reflectors' aperture) and Sun's position in the sky. Since the receiver is fixed above the reflectors, each reflector has a different inclination which depends on its horizontal and vertical distance from the receiver and on Sun's position in the sky. However, when designing Solar Radiation Concentrating Systems, it is of primary importance to be able to compute the tracking angle, the amount of rotation required to reorientate the reflective elements, as well as the rate at which this angle changes. The latter is not constant and depends on the location, the time of the day and the day of the year.

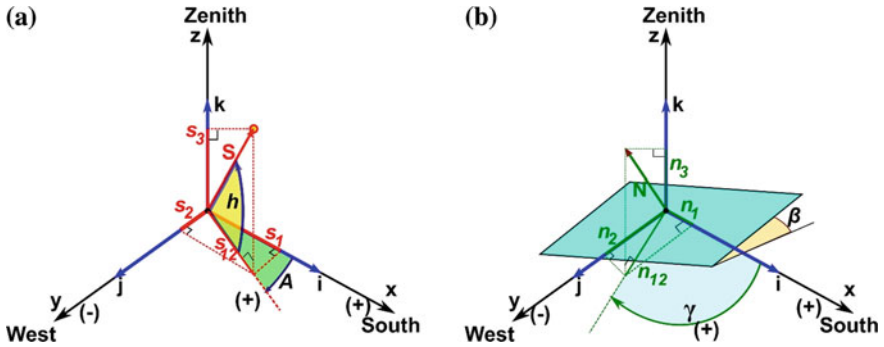

Fig. 4.7 **a** Cartesian coordinates for the horizontal coordinate system: the direction to the South determines the *x*-axis, the direction to the East determines the *y*-axis and the direction towards the zenith determines the *z*-axis. The position of Sun is determined by two angles, height h and azimuth angle A. **b** The tilt angle, β, and the azimuth angle, γ, of the reflective element determine its orientation

The position vector, $\mathbf{n_j}$, of the *j*th reflective element is characterized by its slope or tilt angle β_j and its azimuth angle γ_j. Using the notation developed in Chap. 2, vector $\mathbf{n_j}$ is expressed in the local Cartesian coordinate system by Eq. 2.38 of Chap. 2 (Fig. 4.7)

$$\begin{aligned}&\hat{\mathbf{N}} = n_1 \cdot \hat{\mathbf{i}} + n_2 \cdot \hat{\mathbf{j}} + n_3 \cdot \hat{\mathbf{k}} \Rightarrow \\ &\hat{\mathbf{n}}_\mathbf{j} = \cos\gamma_j \cdot \sin\beta_j \cdot \hat{\mathbf{i}} - \sin\gamma_j \cdot \sin\beta_j \cdot \hat{\mathbf{j}} + \cos\beta_j \cdot \hat{\mathbf{k}}\end{aligned} \tag{4.9}$$

where $\hat{\mathbf{i}}$, $\hat{\mathbf{j}}$ and $\hat{\mathbf{k}}$ are the three unit vectors pointing to *x*-, *y*- and *z*-axes, (towards South, East and zenith) respectively, and vector $\mathbf{n_j}$ is a unit vector, $\left|\hat{\mathbf{n}}_\mathbf{j}\right| = 1$. (For more details, refer back to Chap. 2, Sect. 2.5.)

Similarly, in the local Cartesian coordinate system, the vector, **S,** of the incident solar radiation is given by the following Equation (Fig. 4.7)

$$\begin{aligned}&\hat{\mathbf{S}} = s_1 \cdot \hat{\mathbf{i}} + s_2 \cdot \hat{\mathbf{j}} + s_3 \cdot \hat{\mathbf{k}} \Rightarrow \\ &\hat{\mathbf{S}} = \cos A \cdot \cos h \cdot \hat{\mathbf{i}} - \sin A \cdot \cos h \cdot \hat{\mathbf{j}} + \sin h \cdot \hat{\mathbf{k}}\end{aligned} \tag{4.10}$$

where $\hat{\mathbf{S}}$ is the unit vector pointing to Sun.

However, although Sun's position in the sky is typically denoted by its azimuth, A, and altitude angle, h, sometimes, when studying Linear Fresnel Reflector Systems, it is more convenient to be described by two other angles, which are related to the two characteristic planes of these Systems. These planes are the transversal plane, which is vertical and perpendicular to the receiver, and the longitudinal plane, which is also vertical but parallel to the receiver (Fig. 4.8).

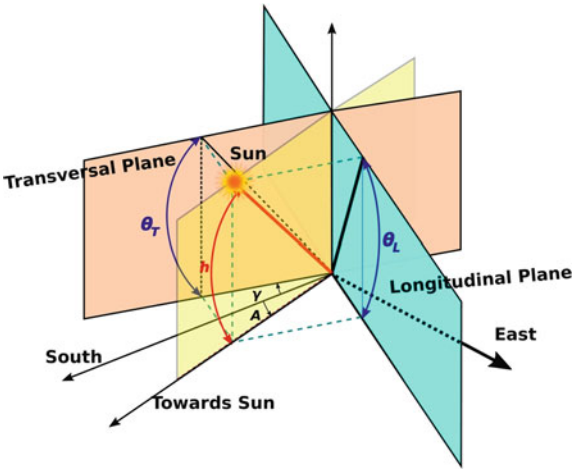

Fig. 4.8 Sun's position in the sky in relation to the two characteristic planes of any arbitrarily oriented Linear Fresnel Reflector System: Sun's transversal angle, θ_T, and Sun's longitudinal angle θ_L

The two angles of Sun's position in the sky in relation to the two characteristic planes of any arbitrarily oriented Linear Fresnel Reflector System, the Sun's transversal angle, θ_T, and the Sun's longitudinal angle θ_L, are defined as follows:

- Sun's transversal angle, θ_T: It is the angle between the horizontal plane and the projection of Sun's position onto the transversal plane of the Linear Fresnel Reflector System.
- Sun's longitudinal angle, θ_L: It is the angle between the horizontal plane and the projection of Sun's position onto the longitudinal plane of the Linear Fresnel Reflector System.

Figure 4.8 illustrates Sun's position in relation to the two characteristic planes of a Linear Fresnel Reflector System. (It must be noted that these angles are defined differently than it is done in the literature. In fact, these angles are the complements of those defined in the literature.)

The transversal angle, θ_T, of Sun can be determined by its altitude, h, and azimuth angle, A, and the azimuth angle, γ, of the Linear Fresnel Reflector System. From the geometry of Fig. 4.8 and using simple trigonometric formulas and the methodology used in Chap. 2, Sect. 2.5, we can derive the following formulas for Sun's transversal angle, θ_T, and Sun's longitudinal angle, θ_L (Hongn et al. 2015)

$$\tan\,\theta_T = \frac{\sin\,h}{\cos\,h \cdot \cos(\gamma - A)} = \frac{\tan\,h}{\cos(\gamma - A)} \tag{4.11}$$

$$\tan\,\theta_L = \frac{\sin\,h}{\cos\,h \cdot \sin(\gamma - A)} = \frac{\tan\,h}{\sin(\gamma - A)} \tag{4.12}$$

If we consider a North–South orientation of the System, the reflective elements are inclined towards East or West, and the systems orientation angle, γ,

equals ± 90° ($\gamma = -90°$ East and $\gamma = 90°$ West). Whereas for an East–West-oriented system, the reflective elements are inclined towards the equator (South of North), and the Systems orientation angle, γ, equals 0° or 180° ($\gamma = 0°$ South, and $\gamma = 180°$ North). Thus for

$\gamma = -90°$

$$\tan\,\theta_{\mathrm{T}} = \frac{\tan\,h}{\cos(-90^{\mathrm{o}} - \mathrm{A})} = -\frac{\tan\,h}{\sin\,A} \tag{4.11′}$$

$$\tan\,\theta_{\mathrm{L}} = \frac{\tan\,h}{\sin(-90^{\mathrm{o}} - \mathrm{A})} = -\frac{\tan\,h}{\cos\,A} \tag{4.12′}$$

and for $\gamma = 0°$

$$\tan\,\theta_{\mathrm{T}} = \frac{\tan\,h}{\cos(-\mathrm{A})} = \frac{\tan\,h}{\cos\,\mathrm{A}} \tag{4.11″}$$

$$\tan\,\theta_{L} = \frac{\tan h}{\sin(-\mathrm{A})} = -\frac{\tan h}{\sin \mathrm{A}} \tag{4.12″}$$

For reasons of simplicity, and in order to take advantage of the inherent symmetry of Linear Fresnel Reflector Systems, it would be desirable that their aperture to be always perpendicular to Sun's direction. However, this configuration would require a two-axis tracking System which is not feasible for large-scale constructions. Therefore, large-scale Linear Fresnel Reflector Systems are constructed having one of their characteristic planes perpendicular to Sun's direction at noon, the time of maximum solar irradiance. So, these Systems are oriented whether in the direction South–North or East–West, and using a one-axis tracking System, they modify the tilt angle β_j of each reflector (Fig. 4.9). In the case the receiver is oriented parallel to the North–South direction, we speak of a North–South orientation of the Linear Fresnel Reflector System. As a consequence, the longitudinal plane of the System is oriented North–South, whereas the transversal plane is oriented East–West. This does not only simplify the required calculus but also takes advantage of the symmetrical movement of Sun in the sky around noon. As a result, the operation period of a Linear Fresnel Reflector System can be divided into two parts: one part from sunrise until local noon, and a second part from local noon until sunset. The duration of these parts is equal. In addition, Sun's movement in the sky is identical for both of them, though in the reverse course. Therefore, it is sufficient to study only one of these subperiods, usually the first half of the day, and then to reduplicate the results to cover the other half of the day. Using this convention, the tracking angle can be easily computed.

For South–North orientation of a Linear Fresnel Reflector Systems, the tilt angle, β_j, of each reflector can be computed using the geometry of Fig. 4.10 (a and b) from the angle ξ_j, (it is the angle formed by the horizontal plane with the position vector of the receiver $\mathbf{r_j}$ in respect to the *j*th reflective element), which is determined by the

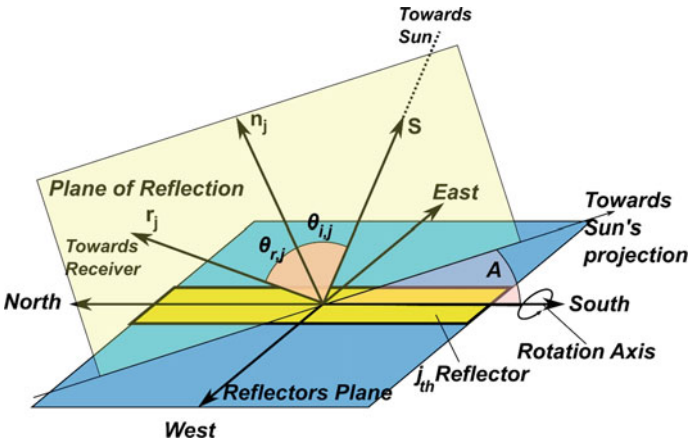

Fig. 4.9 Linear Fresnel Reflectors have a single axis tracking System and track Sun by being rotated around their main axis. As each reflector reflects solar radiation onto the receiver individually and independently, each one has to track Sun individually and independently as well. The change of the reflectors inclination must be performed with the most possible high accuracy to minimize energy losses

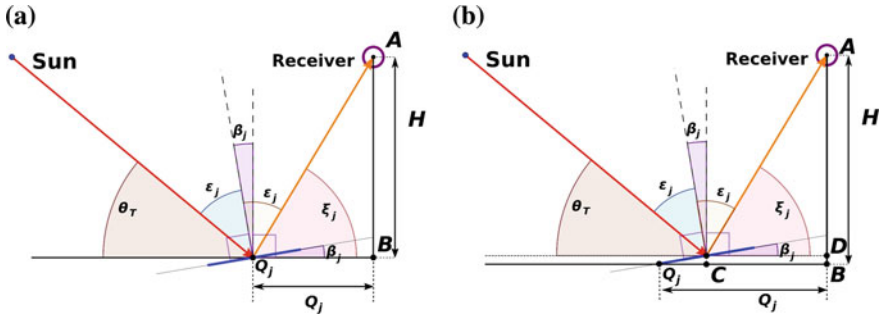

Fig. 4.10 Angles geometry of a Linear Fresnel Reflector Solar Radiation Concentrating System when the reflective elements are centrally pivoted (**a**) and when the rotation axis coincides with one of their longer edge (**b**)

distance, Q_j, of the reflective element from the origin of the local Cartesian coordinate system, the height, H, of the receiver and the transversal Sun angle, θ_T. As it can be seen from this figure, the geometry concerning the angles ξ_j, β_j and ε_j is the same (ε_j is the angle of reflection of the incoming solar radiation by the jth reflective element) for the two differently pivoted reflective elements [centrally (a) and site (b) pivoted]. So, the relationships connecting these three angles are:

$$\begin{aligned} &\varepsilon_j + \theta_T + \beta_j = 90^{\circ} \Rightarrow \\ &\varepsilon_j = 90^{\circ} - \theta_T - \beta_j \end{aligned} \tag{4.13}$$

and

$$\begin{aligned} &\xi_j + \varepsilon_j - \beta_j = 90^{\circ} \Rightarrow \\ &\xi_j = 90^{\circ} - \varepsilon_j + \beta_j \end{aligned} \tag{4.14}$$

Substituting Eq. 4.13 into Eq. 4.14, it becomes

$$\begin{aligned} \xi_j &= 90^{\circ} - \left(90^{\circ} - \theta_T - \beta_j\right) + \beta_j \Rightarrow \\ \xi_j &= 90^{\circ} - 90^{\circ} + \theta_T + \beta_j + \beta_j \Rightarrow \\ \xi_j &= \theta_T + 2 \cdot \beta_j \Rightarrow \\ 2 \cdot \beta_j &= \xi_j - \theta_T \Rightarrow \\ \beta_j &= \frac{\xi_j - \theta_T}{2} \end{aligned} \tag{4.15}$$

The mathematical expression connecting the sides BQ_j and AB and the angle ξ_j of the triangle ABQ_j in Fig. 4.10a is

$$\begin{aligned} \tan \xi_j &= \frac{AB}{BQ_j} \Rightarrow \\ \tan \xi_j &= \frac{H}{Q_j} \Rightarrow \\ \xi_j &= \tan^{-1}\left(\frac{H}{Q_j}\right) \end{aligned} \tag{4.16}$$

Substituting Eq. 4.16 into Eq. 4.15, it becomes

$$\beta_j = \frac{1}{2}\tan^{-1}\left(\frac{H}{Q_j}\right) - \frac{\theta_{\mathrm{T}}}{2} \tag{4.17}$$

As it has been also noted before, the knowledge of the rate at which the reflectors' inclination angle, β_j, must change is of primary interest to the designers of Sun tracking System. An expression for this rate can be found by taking the derivative of Eq. 4.17 with respect to time:

$$\begin{aligned} &\frac{\mathrm{d}\beta_j}{\mathrm{d}t} = \frac{\mathrm{d}}{\mathrm{d}t}\left[\frac{1}{2}\tan^{-1}\left(\frac{H}{Q_j}\right) - \frac{\theta_{\mathrm{T}}}{2}\right] \Rightarrow \\ &\frac{\mathrm{d}\beta_j}{\mathrm{d}t} = \frac{1}{2}\frac{\mathrm{d}\theta_{\mathrm{T}}}{\mathrm{d}t} \end{aligned} \tag{4.18}$$

From Eq. 4.18, it is obvious that the temporal variation of the angle β_j, i.e. $d\beta_j/dt$, depends only on the temporal variation of the angle θ_T, i.e. on Sun's apparent motion in the sky, not on the reflectors' position. The different reflectors have different angular positions, but they rotate at the same angular velocity. As it has been also mentioned in a previous paragraph, theoretically, this makes possible to connect all reflectors with a mechanical coupling and to drive them by a single motor. Nevertheless, individual reflector tracking has been found to be more accurate.

At this point, it must be pointed out that the accurate expression for the calculation of the rate the tilt angle, β_j, of the reflective elements must change can be derived from the differentiation of Eq. 4.7. This equation describes the position of each reflective element for the most general case, an arbitrarily oriented system. However, analysing Sun's position in the transversal and the longitudinal planes of the Linear Fresnel Reflector System, we take advantage of the System symmetry and simplify the calculus. Nevertheless, using only the transversal angle of Sun we do not take into account the fact that a part of the reflected solar radiation is getting lost due to its longitudinal component. However, this will be studied in the next chapter, which will deal with the optical losses of Linear Fresnel Reflector Systems (end losses).

4.3.3 Sun's Path Across the Sky and System Orientation

Sun moves along a circle on the celestial sphere every day, but it follows different paths at different days of the year. The most northern path appears at the June solstice and the most southern at the December solstice. At the equinoxes, exactly half of Sun's circular path lies above the horizon, while in June, considerably more than half of the circle is above the horizon, and in December, much less than half the circle is visible (Fig. 4.11). This accounts for why locations in the northern hemisphere have more hours of daylight in June (during summer) than in December (during winter).

At the two equinoxes (the spring equinox on March 21, and the fall equinox on September 21), Sun rises exactly at the East and sets exactly at the West. At solar noon, Sun's altitude angle, h_s, equals the local latitude, φ, minus 90°, and the length of the day is exactly 12 h everywhere on Earth. On the other hand, at the winter solstice (on December 21 on the northern hemisphere), the day has its shortest duration of the year (its accurate duration depends on the location on Earth), and Sun rises in the South of East and sets in the South of West. Sun's altitude angle, h_s, at solar noon is 23.5° less than its value at the equinox (the 23.5° is the tilt of Earth's rotation axis relative to the plane of Earth's orbit). This is the lowest value of Sun's altitude angle, h_s, at noon in the year. Similarly, at the summer solstice (on June 21 on the northern hemisphere), the day has its longest duration of the year, and Sun rises in the North of East and sets in the North of West. In addition, Sun's altitude angle, h_s, at noon is 23.5° more than its value at the equinox (Fig. 4.12).

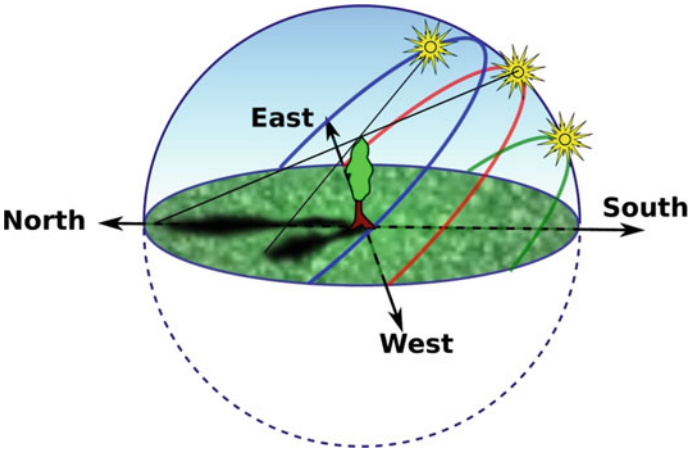

Fig. 4.11 Sun's paths in the sky depend on observer location on Earth (its latitude) and the day of the year

So, since Sun's daily path in the sky changes across the year, it is important to have studied it before designing a Solar Radiation Concentrating System. This way we can obtain useful information that may be proven crucial for the design and operation of these Systems. Sun Charts (Fig. 4.13) are diagrams that can serve this purpose. They show Sun's position in the sky for a number of characteristic days of the year for a specific location on Earth. Sun's position is denoted by the azimuth, A, and elevation angles, h, (Fig. 4.14), where the elevation angle, h, is the complement of Sun's zenith angle, θ_z. These charts can be created free of charge at a number of websites, like http://solardat.uoregon.edu/SunChartProgram.html, or https://www.suncalc.org/, or https://www.sunearthtools.com/dp/tools/pos_sun.php#top, or http://suncalc.net, or http://andrewmarsh.com/apps/releases/sunpath3d.html, or, alternatively, they can be created using the equations describing Sun's position in the sky presented in Chap. 2.

From these charts, we can see that there is a time span in the day where Sun's elevation angle, h, is almost constant or varies very slowly. This happens around noon. The duration of this time span is longer for summer than for winter (Fig. 4.13). This information, along with the fact that only the transversal component of Sun's position can be used to harvest solar energy, may lead in a different arrangement of the reflective elements than it could have been decided in a preliminary stage. (The longitudinal component of Sun's position leads to end losses, as we will study in a following chapter.) Depending on the location on Earth, we may decide to orient the Solar Radiation Concentrating System whether South–North or East–West. Near the equator, or in the summer, if System's operation efficiency is of more importance in this time period, when Sun is high in the sky, a South–North orientation of the receiver, and consequently of the entire System, may be more beneficial. On the other hand, on higher latitudes, or in the winter, an East–West orientation might be

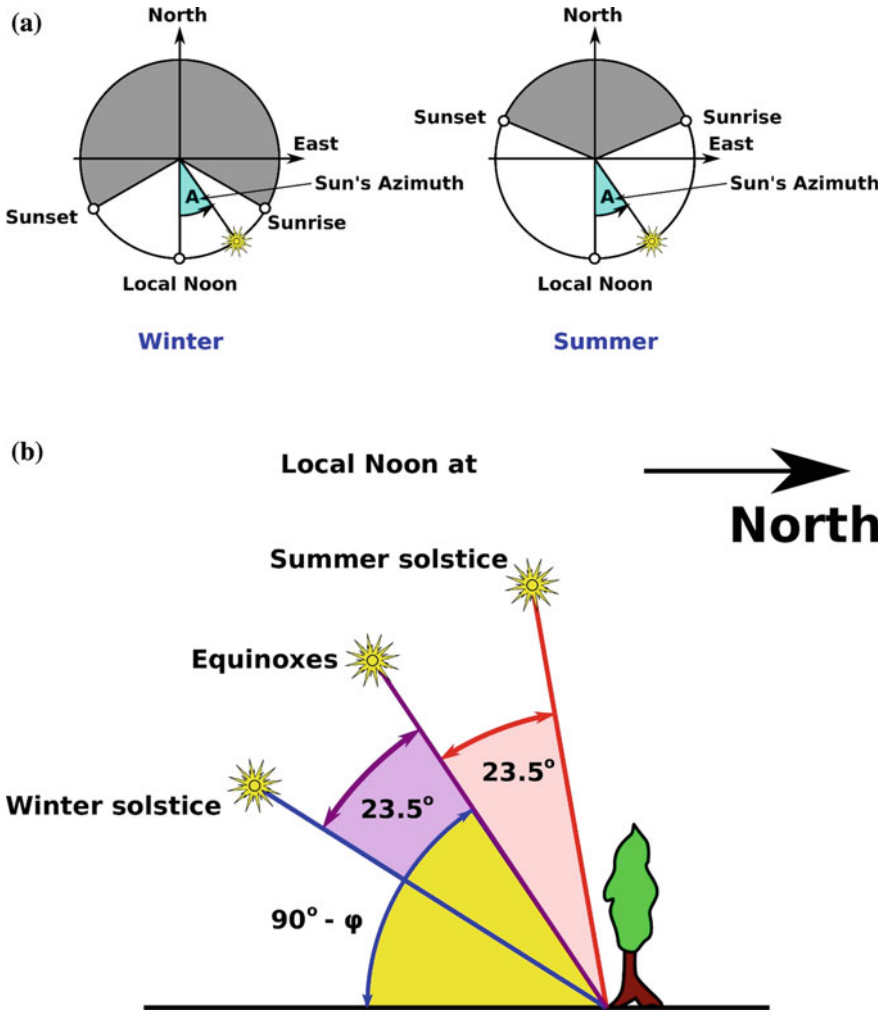

Fig. 4.12 **a** Sunrise and sunset positions for the summer and winter solstices, and **b** Sun's altitude angle at the solstices and equinoxes. Sun's path varies throughout the year. In the summer, Sun is high in the sky and rises and sets North of the East–West line on the northern hemisphere. It also rises much earlier and sets much later in summer than in winter. In the winter, Sun is low in the sky and rises and sets South of the East–West line on the northern hemisphere

preferable. However, the most critical case does not concern locations near equator or on higher latitudes, but rather locations on middle latitudes.

In addition, despite the fact that we may have developed a Solar Radiation Concentrating System with high optical efficiency, early in the morning or late in the evening, the low level of solar radiation at these periods of the day may not be adequate and the Concentrated Solar Radiation Power System may cannot operate

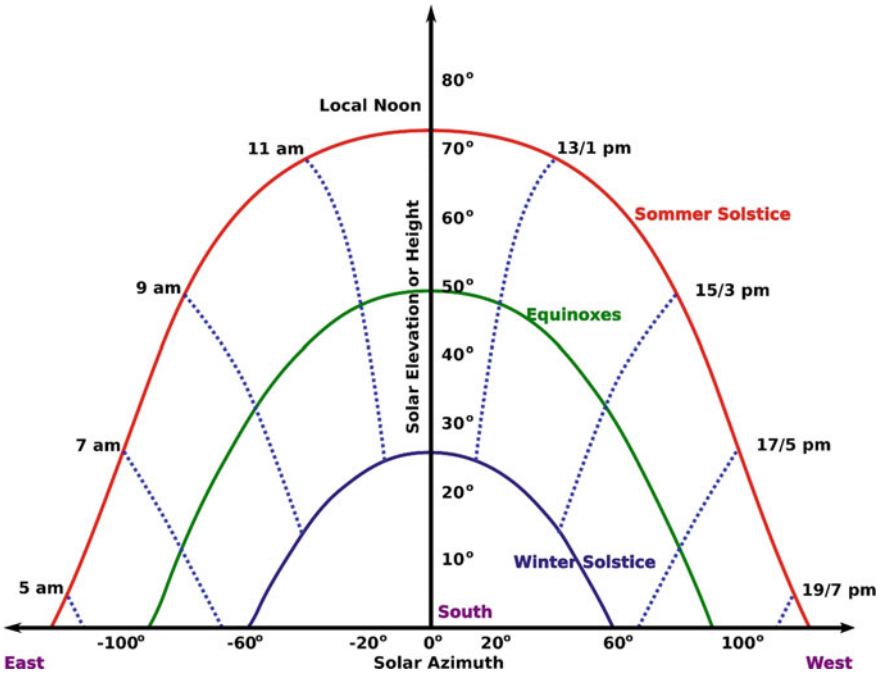

Fig. 4.13 Sun's paths over the celestial sphere through the course of the day for an observer in Thessaloniki, Greece, at 40.74°N latitude, and for four representative days of the year, winter solstice, summer solstice and equinoxes (March equinox or Northward equinox and September equinox or Southward equinox). The *y*-axis of the chart represents the solar elevation or altitude angle, *h*, measured from 0° degrees on the horizon to 90° directly overhead. The x-axis represents the solar azimuth angle, *A*. The centre of the chart is at 0° or due South. The intersections of Sun's paths with the horizontal axis show the azimuths from South where Sun rises and sets that day (adapted from http://solardat.uoregon.edu/SunChartProgram.html)

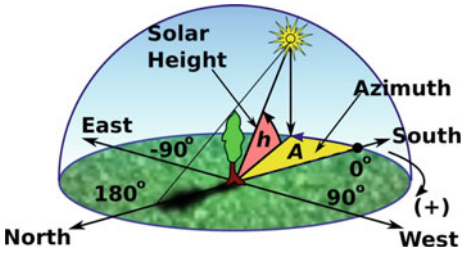

Fig. 4.14 Sun's position in the sky: azimuth, *A*, and altitude, *h*, angles. North is defined to have an azimuth angle of 180°, South an azimuth of 0°, East −90° (or 270°) and West 90°

properly, or, even, not at all. Incoming solar radiation levels mainly depend on Sun's position in the sky. For example, as can we see for Fig. 4.13, a location on Earth receives the maximum solar radiation between about 9.00 a.m. and about 3.00 p.m. (local time) when Sun is sufficiently high in the sky. Hence, to harness the possibly maximum energy on a given geographic location, the accurate time span,

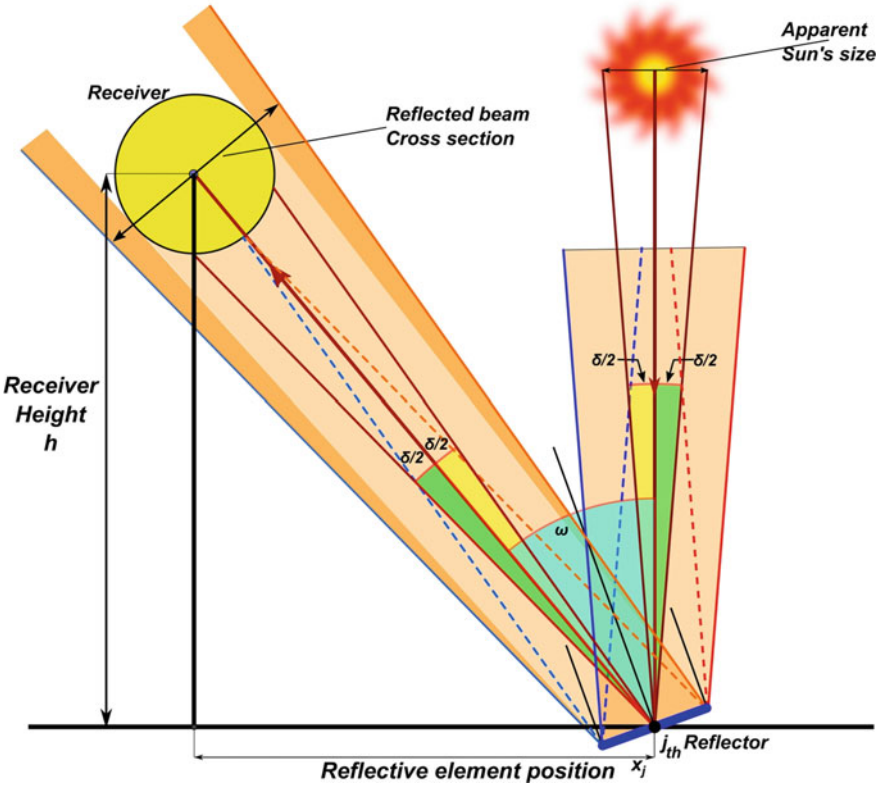

Fig. 4.15 Sun rays diverge upon their reflection by the reflective element (reflector) due to Sun's finite angular size ($\delta \approx 32'$). This may cause energy losses if the receiver size is smaller than the reflected beam cross section at the receiver position. It depends on the relative distance between the reflective element and the receiver

as well as the time points in the day when solar radiation takes values higher than a threshold, has to be determined. To highlight it one more time, this depends on Sun's azimuth, A, and elevation angles, h, and the orientation of the Solar Radiation Concentrating System.

4.4 The Effect of Sun's Finite Size

Linear Fresnel Reflector Systems concentrate solar light to a larger surface than Parabolic Trough Systems. For this reason, they are slightly more tolerant for marginal errors of alignment. However, when and how quickly begin the reflected rays to miss the target, and when and how quickly the tracking errors are no longer tolerant? Is there an optimal focal height, f, an optimal receiver height, H, or a target

size that will always be adequately tolerant of alignment or tracking errors? Or else, to what extent deviations from the desirable situation are tolerable?

Due to the finite size of Sun, solar light rays are not exactly parallel. However, the mean angular diameter of Sun is so small ($\delta = 31'59'' \approx 32'$) that the reflected rays do not diverge very much. Let us opt one point on each edge of the surface of a representative reflective element and draw three light rays hitting on them: the ray coming from Sun's centre, the central ray and two rays hitting the reflector with angles $+\delta/2(\approx 16')$ and $-\delta/2(\approx 16')$ with respect to the central ray (Fig. 4.15). These rays originate from the edges of solar disc. As we can see from Fig. 4.15, one of the two outer reflected light rays may miss the receiver after being reflected on the reflector. It depends on the cross section of the reflected light beam, the size of the receiver and the distance of the reflector from the receiver. This affects Sun's tracking accuracy, namely the rate the inclination angle, β_j, of each reflective element has to change so that the reflected solar radiation to be concentrated on the receiver. The proper and prompt reflector adjustment determines the amount of energy losses.

4.5 Aperture Area, Concentration Ratio and Total Concentrated Solar Power

4.5.1 Aperture Area

The aperture area of a reflected element is an important construction parameter of a Solar Radiation Concentrating System, as it determines the maximum solar radiation captured. The aperture area, A_j, of each reflective element, j, is calculated as the product of its aperture width, W_j, and its length, L_j:

$$A_j = W_j \cdot L_j \tag{4.19}$$

4.5.2 Concentration Ratio

The concentration ratio of a Solar Radiation Concentrating System is another important parameter which affects the construction's efficiency. It determines the operating temperatures of the System. The concentration ratio, C, is defined as the ratio of the solar radiation flux concentrated on the receiver, F_r, to the direct solar radiation flux incident on the aperture of the reflectors, F_m:

$$C = \frac{F_r}{F_m} \tag{4.20}$$

However, the concentration ratio, C, can be determined without any measurement. It is equivalent to the ratio of the reflectors' effective aperture area, A_m, to the receiver illuminated aperture area, A_r.

$$C = \frac{A_m}{A_r} \tag{4.21}$$

In many cases, the projected area of the absorber tube to a proper direction is chosen as the receiver aperture, A_r. In this case, the receiver aperture area, A_r, is a rectangle with area equal to $d \cdot L$, where d is the absorber tube diameter. Consequently, the concentration ratio, C, is given by the equation

$$C = \frac{A_m}{A_r} = \frac{\sum_j A_j}{d \cdot L} \tag{4.22}$$

Another possibility is to take the irradiated absorber surface area as the receiver aperture area.

However, since the reflective elements are not arranged perpendicular to the incoming solar radiation, their effective aperture surface is smaller and the collected solar radiation is lower. The effective aperture area, $A_{e,j}$, of the jth reflective elements as encountered by the approaching solar light rays in the transversal plane can be calculated by the formula,

$$A_{e,j} = W_j \cdot \cos\theta_j \cdot L_j \tag{4.23}$$

where θ_j is the solar radiation incidence angle on the jth reflector.

Let us assume that the solar radiation reflected from each reflector is distributed uniformly over the absorber's surface. The concentration ratio on the absorber is determined by summing up the contributions of all reflecting elements. For a Linear Fresnel Reflector System with reflective elements of width W_j, the contribution of the jth reflector on the absorber, C_j, is given by

$$C_j = \frac{A_{e,j}}{A_r} = \frac{W_j \cdot \cos\theta_j \cdot L_j}{A_r} \tag{4.24}$$

If we assume that the solar radiation reflected from different reflector is distributed differently over the absorber's surface, then the contribution, C_j, of the jth reflective element on the absorber is given by

$$C_j = \frac{A_j}{a_j} = \frac{W_j \cdot \cos\theta_j \cdot L_j}{a_j} \tag{4.25}$$

where a_j is the area of the receiver irradiated by the jth reflective element equal to $W_{r,j} \cdot L$, where W_r is the receiver's cross section width that is irradiated.

Finally, the total concentration ratio, *CR*, on the surface of the receiver, is calculated by summing up all the above-presented individual concentration ratios C_j:

$$\begin{aligned} C &= \sum_{j=1}^{N} C_j = \sum_{j=1}^{N} \frac{A_j}{A_r} = \sum_{j=1}^{N} \frac{W_j \cdot \cos\theta_j \cdot L_j}{a_j} \Rightarrow \\ C &= \left[\sum_{j=1}^{N} \frac{W_j \cdot \cos\theta_j}{a_j} \right] \cdot L \Rightarrow \\ CR &= \left[\sum_{n=1}^{N} \frac{W_j \cdot \cos\theta_j}{W_{r,j} \cdot L} \right] \cdot L \Rightarrow \\ CR &= \left[\frac{W_j \cdot \cos\theta_j}{W_{r,j}} \right] \end{aligned} \tag{4.26}$$

4.5.3 Total Concentrated Solar Power

The solar radiation, I_j, that reaches the receiver from the *j*th reflector is given by the equation

$$I_j = \rho_j \cdot I \cdot W_j \cdot \cos\theta_j \cdot L \tag{4.27}$$

where ρ_j is the reflectivity of the *j*th reflector, and *I* is the intensity of the direct solar radiation, which in a rough approximation can be assumed to be equal to 800 W/m^2. Thus, the total concentrated solar power, C_P, on the receiver due to the contribution of all reflective elements is calculated as the sum of the reflected flux from each individual reflector, and hence, it is given by the equation,

$$\begin{aligned} C_P &= \sum_{j=1}^{N} I_j = \sum_{j=1}^{N} \rho_j \cdot I \cdot W_j \cdot \cos\theta_j \cdot L \Rightarrow \\ C_P &= I \cdot L \cdot \sum_{j=1}^{N} \rho_j \cdot W_j \cdot \cos\theta_j \end{aligned} \tag{4.28}$$

4.6 The Receiver

The receiver is this part of a Linear Fresnel Reflector System that receives the concentrated solar radiation and transforms it into useful heat, as effectively as possible. However, once the absorber is heated, it losses energy by emitting long wavelength radiation to the surroundings and by convection (Heimsath et al. 2014).

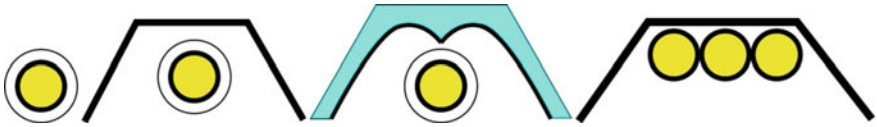

Fig. 4.16 Receiver of a Linear Fresnel Reflector System may be a single absorbing tube enclosed in a glass tube that can be either evacuated or non-evacuated, optionally equipped with a secondary reflector above it to enhance solar rays interception, or a bundle of small tubes placed inside a cavity. Evacuated absorbers are similar to those used for Parabolic Trough Systems, but usually they also have a secondary reflector. Non-evacuated absorber is usually used for low-to-medium working fluid temperatures and may be sealed inside the secondary reflector cavity (filled with air) to reduce thermal losses (convection)

On account of this, the ratio between the heat loss from the absorber and the available concentrated solar radiation must be kept minimum. For this reason, a number of different receiver configurations have been investigated and presented in the literature. However, the use of flat reflective elements, the inherent divergence of the reflected solar radiation due to the distribution of solar radiation across Sun's disc (especially from the furthest reflectors), and tracking and reflecting errors, entail the use of specific receiver configurations, wide receiver constructions or a kind of secondary concentration.

In general, two possible kinds of configuration for the receivers in Linear Fresnel Reflector System can be used (Fig. 4.16). The receiver construction may be either of the

- One tube type (encaged in an evacuated glass tube or not), equipped with an (optional) secondary reflectors, or
- Non-evacuated multiple tube type (an array of parallel and very close to each other tubes) inside a (convection suppression) cavity, of usually trapezoidal shape.

4.6.1 Multiple Tube Receivers

In Linear Fresnel Reflector Systems with multiple tube receivers, the enlargement of the receiver aperture is achieved by the use of small absorbing tubes placed very close to each other. In this case, the diameter of each tube is small compared to the width of the receiver (Fig. 4.17). Therefore, the whole receiver construction can be considered as a plane (or more correctly as a parallelogram), with its long symmetry axis at the focal line of the reflective elements. This way, the concentration efficiency of the reflective elements is independent of the number of tubes used in the receiver construction.

The most common multiple tube receiver configuration is the use of a trapezoidal cavity properly insulated (Fig. 4.17). A glass cover can be located at the

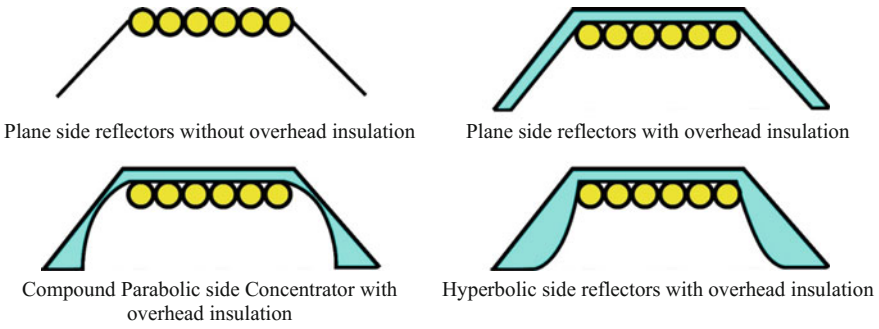

Fig. 4.17 Large aperture width of receivers composed of multiple tubes allows the capturing of all solar radiation reflected by the primary reflectors without the need for a secondary concentrator. However, this results in lower concentration ratios, adequate only when warm water is needed. In electric energy production, higher working fluid temperature is usually necessary. Therefore, secondary reflectors are used. The sides of the trapezoidal cavity are usually appropriately formed reflectors so that as much as possible radiation provided by the primary reflective elements to be captured by the absorber

opening of the cavity to protect the selective coating of the tubes, decreasing simultaneously the losses due to thermal emission by creating a greenhouse effect. This enhances the receiver's performance (Ahmed and Amin 2016). (The Selective Coating is applied to the surface of a solar radiation absorbing element to reduce thermal radiation losses and enhance solar radiation absorption.) Moreover, there is no direct radiation heat loss to the sky, as the tubes are facing to the ground. The drawback of this type of receivers is that due to the width of the (flat) glass cover the cavity cannot be evacuated, leading in a convection heat transfer from the tubes to the glass cover. In addition, the use of selective coating is not always possible as it is susceptible to reactions with the oxygen of the air, unless it uses nitrogen instead of air (Abbas et al. 2013).

4.6.2 One Tube Receivers

Another usual receiver configuration is the one tube receiver. It may be encased in an evacuated glass tube or not, to minimize heat losses. It is usually equipped with a secondary reflector that is placed above the absorbing tube providing an additional concentration of the reflected solar radiation (Fig. 4.18) (Heimsath et al. 2014). The exterior surface of the secondary reflector is usually insulated. The single tube absorber may be placed inside an evacuated glass cover to reduce the convective heat losses. A selective coating is applied on the exterior surface of the absorbing tube for higher absorption of the solar radiation and lower heat emission.

The effective aperture of the one tube absorber, without a secondary reflector, is this part of the absorbing tube circumference that is visible by the primary

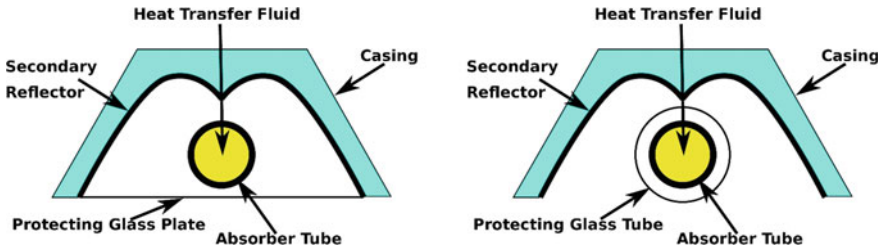

Fig. 4.18 In one tube receiver type, the absorbing tube is usually either protected with a glass tube or the bottom of the cavity is covered with a glass plate to reduce heat losses from the absorber. An absorber with glass tube is usually evacuated, a configuration originally developed for Parabolic Trough Systems. An additional possibility is to apply a non-evacuated glass tube around the absorber

reflectors' field. This corresponds to a little more than the half circumference of the tube. However, in order to improve the distribution of the concentrated solar radiation over the absorber and also to increase the concentration ratio, usually a secondary reflector is used. This second stage reflection maximizes the energy received by the absorber by reflecting the solar light rays that miss the absorber back to it. Using an appropriately formed secondary receiver, the reflected solar radiation reaching the receiver aperture within an acceptance angle, θ_A, is concentrated on the receiver. The acceptance angle, θ_A, is the angle formed by the lines connecting the edges of the primary reflectors' field with the receiver:

$$\theta_A = \tan^{-1} \frac{W_f}{H} \tag{4.29}$$

where W_f is the width of the reflectors field, and H is the height of the receiver.

Apart from additional concentration, the secondary reflector distributes the reflected solar radiation more uniformly around the surface of the absorber, enlarges the target area for the primary reflectors, facilitates the Sun tracking procedure, by being more tolerant to changes in reflector tilt angle, protects the absorber from convection losses and serves as a wind protection cover reducing further the convective losses. In this case, the element that is placed at the focal line of the primary reflectors is not the absorbing tube, but the aperture of the secondary reflector.

The secondary reflector has to be designed in such a way that the maximum amount of the primarily reflected solar radiation to be able to get reflected a second time and be concentrated onto the absorber's surface. At the same time, the concentrated solar radiation is as uniformly as possible distributed on the absorber's surface avoiding hot spots on it. As a consequence, a number of secondary concentrators have been developed and investigated (Fig. 4.19). The parabolic shape has been proved to be one of the best solutions with maximum optical efficiency, while the most used shape is the compound parabolic concentrator which further increases the optical efficiency of the System. Moreover, it is more flexible than the single parabolic surface allowing wider acceptance angles. Parabolic surfaces are

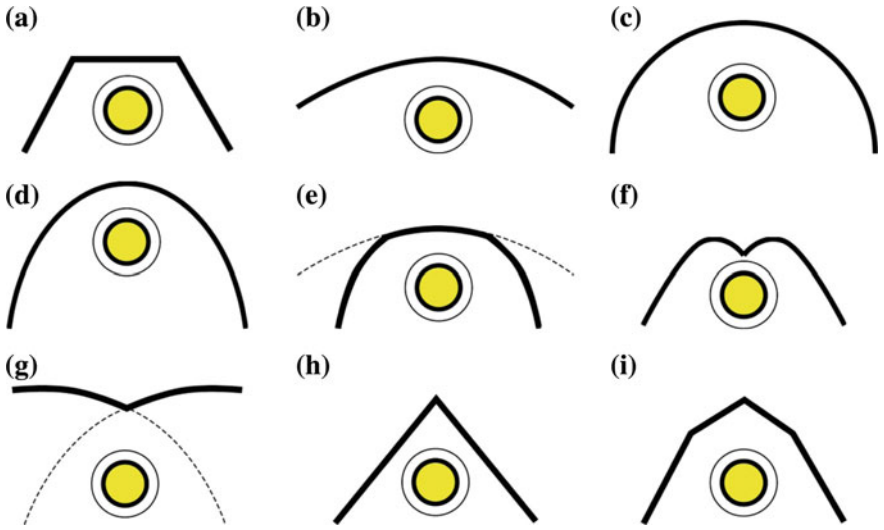

Fig. 4.19 Various shapes have been investigated as secondary concentrators attempting to increase the solar radiation captured by the absorber. A uniform solar radiation distribution around the absorber is obtained by optimizing the Linear Fresnel Reflector System's design parameters, like the tilt angle of the primary reflectors and the shape and the acceptance angle of the secondary reflector. This is necessary in order to protect the absorber from the occurrence of hot spots, since prolonged exposure to high heat flux at a particular area will eventually affect the life of the absorber. This figure shows different types of secondary reflectors: **a** trapezoidal cavity receiver, **b** arc-shaped and **c** semi-circular cavity receiver, **d** parabolic concentrator, **e** segmented parabolic concentrator, **f** compound parabolic concentrator, **g** parabolic wing-like structure, **h** V-shaped and **i** compound V-shaped

suitable when the incoming radiation is normal to their aperture. However, in Linear Fresnel Reflector Systems this is the case only for the reflective elements that are lying directly below the receiver. In other cases, as it is, for example, the reflected solar light rays coming from the outer edges of the primary reflectors field, the incoming solar radiation forms a large angle with the normal to the receiver aperture. In parabolic reflectors, this leads in severe aberrations, the phenomenon of coma, presented in Chap. 3. Nevertheless, compound parabolic concentrators allow the absorbing tube to be located in a place that is almost always irradiated by the secondarily reflected solar radiation lowering construction cost and raising the working fluid temperature.

To recapitulate, the two-stage concentration has been used in Solar Radiation Concentrating Systems that employ Linear Fresnel Reflectors, as it leads to more flexible structures and higher concentration ratios (Zhang et al. 2014). On the other hand, although the trapezoidal secondary concentrators with multiple tubes have simpler design and are easier to manufacture, they provide lower concentration ration resulting in lower working fluid temperatures.

4.7 Optical Efficiency

4.7.1 Optical Efficiency Parameterization

As the optical efficiency analysis of a Linear Fresnel Reflector System aims to facilitate potential improvements of the solar field, we can evaluate the performance of these Systems by studying and analysing the influence of the most important phenomena (shadowing by the receiver and adjacent reflectors, blocking by adjacent reflectors, reflectors' slope error, reflected solar radiation spillage on the receiver, Sun tracking errors, material characteristics, solar disc shape influence) and optimizing some or all of the corresponding parameters (Lee et al. 2015). As a consequence, the optical analysis plays a significant role in Linear Fresnel Reflector Systems design.

To model the optical efficiency of these Systems, only the direct solar radiation has to be considered, as well as the assumption that the primary solar field reflective elements are perfectly tracking the Sun. However, it is not necessary to employ a direct normal irradiance model. Instead, we can set it equal to a constant value, e.g. 1000 W/m^2. This stem from the fact that the direction of Sun rays and the considered phenomena (solar rays reflection and refraction) are independent of the solar radiation values, and the corresponding calculations are purely geometry dependent.

The Optical Efficiency, η, of a Linear Fresnel Reflector System is defined as the ratio of the solar radiation received by the absorber, E_{rec}, to the amount of the radiation incident on the System's primary reflectors field, E_{in}. Similarly, the optical efficiency of the secondary reflector is the ratio of the solar radiation received by the absorber, E_{rec}, after being rereflected from the secondary reflector, to the solar radiation reaching the secondary reflectors' aperture, E_{refl}. In general, the available radiation on the absorber, E_{rec}, (the energy emitted from Sun and reaching the receiver after being reflected by the reflectors) is equal to the incident solar radiation, E_{in}, multiplied by an efficiency factor η:

$$E_{\text{rec}} = \eta \cdot E_{\text{in}} \tag{4.30}$$

This efficiency factor, η, is a function of design parameters, chosen materials properties and environmental effects:

$$\eta = f(\text{design, material, environment}) \tag{4.31}$$

It can be mathematically expressed as the multiplication of the individual efficiencies of these factors:

$$\eta = \eta_{\text{design}} \cdot \eta_{\text{material}} \cdot \eta_{\text{environment}} \tag{4.32}$$

The efficiencies due to the material and environmental factors are not considered in this book. The design efficiency can be further divided into reflectors and receiver efficiencies:

$$\eta_{\text{design}} = \eta_{\text{reflectors}} \cdot \eta_{\text{receiver}} \tag{4.33}$$

Furthermore, the reflectors' optical efficiency, $\eta_{\text{reflectors}}$, is a function of the dimensions and the design parameters of the System, and can be calculated as follows (Schenk et al. 2014):

$$\eta_{\text{reflectors}} = \eta_{\text{shad}} \cdot \eta_{\text{block}} \cdot \eta_{\text{end}} \cdot \eta_{\text{clean}} \tag{4.34}$$

where

- η_{clean} describes the reduction of the optical efficiency due to soiling of the reflectors (it is considered to be equal to 1 as it is difficult to be parameterized and prescribed and depends on the reflectors cleaning System).
- η_{end} accounts for the energy losses due to the fact that when the incident angle of the solar radiation is different from the normal, a part of the reflected solar irradiation misses the receiver, while at the same time another part of the receiver does not receive any solar radiation at all.
- η_{shad} and η_{block} account for shading and blocking effects that occur when Sun's elevation angle, h, is low, or else, Sun is near the horizon.

The optical efficiency, $\eta_{\text{reflectors}}$, can also be described using the product of the maximum optical efficiency, η_0—the optical efficiency at normal incidence on perfectly clean reflectors which are not shaded and the reflected solar radiation is not blocked—and the Incidence Angle Modifier, IAM, which describes the relative reduction of the optical efficiency due to the incidence angle (Yang et al. 2015):

$$\eta_{\text{reflectors}} = \eta_0 \cdot \text{IAM} \tag{4.35}$$

In other words, the Incidence Angle Modifier, IAM, is defined as the ratio of the optical efficiency at a certain Sun position to the optical efficiency at normal incidence (Yang et al. 2015):

$$\text{IAM} = \frac{\eta_{\text{reflectors}}}{\eta_0} \tag{4.36}$$

For Linear Fresnel Reflector Systems, the Incidence Angle Modifier, IAM, is a complex function which can be described as the product of a transversal and a longitudinal component (Schenk et al. 2014):

$$\text{IAM}(A, h, \gamma) = \text{IAM}_{\text{T}}(\theta_{\text{T}}) \cdot \text{IAM}_{\text{L}}(\theta_{\text{L}}) \tag{4.37}$$

where

- A is Sun's azimuth angle.
- h is the Sun's elevation angle.
- γ is the azimuth angle of the Linear Fresnel Reflector System.
- θ_T is the transversal angle and θ_L the longitudinal angle of Sun's position in the sky in respect to the system's orientation.
- $IAM_T(\theta_T)$ is the Incidence Angle Modifier with respect to the transversal plane of the System.
- $IAM_L(\theta_L)$ is the Incidence Angle Modifier with respect to the longitudinal plane of the System.

4.7.2 *Optical Efficiency Modelling and Ray Tracing*

Modelling Linear Fresnel Reflector Systems to achieve the best possible optical efficiency is a challenging task, as there are several parameters and phenomena (such as the height of the receiver, H, the shape and the place of the receiver, the distance between adjacent reflectors, S_j, the reflectors width, W_j, shadow and blocking effects, end losses, primary solar field filling factor) that must be described by a set of equations, representing as accurately as possible the behaviour of the System. Therefore, when seeking to optimize the design of a Linear Fresnel Reflector System, one or more of these parameters are kept unchanging in order to optimize the rest of them. For example, the tube diameter or the shape of the receiver and the secondary concentrator is usually kept fixed.

Optimizing the optical efficiency of these Systems means minimizing the optical losses which lead to better utilization of the available land, making the implementation more cost-effective (Rungasamy et al. 2015). In fact, the function to be optimized is the amount of the solar radiation collected by the receiver. Since the most common variables considered in the optical efficiency optimization of a Linear Fresnel Reflector System are the position and the width (and focal lengths if they are curved and not plane reflectors) of the reflectors, there are four different levels of optimization that can be performed: The reflective elements of the solar field can be (Boito and Grena 2016)

- Uniformly spaced and of the same width
- Uniformly spaced and of variable width
- Non-uniformly spaced and of the same width
- Non-uniformly spaced and of variable width (full optimization).

Due to the complexity of the reflectors and receiver geometry and the number of the associated parameters, instead of using an analytical approach many researchers resort to ray-tracing software in order to calculate the influence of these parameters

on the performance of Linear Fresnel Reflector Systems. A well-known methodology used for this purpose is the probabilistic Monte Carlo ray-tracing method (or algorithm). It generates a large number of solar light rays (stochastic paths) and traces them as they interact with the various components of the System (primary reflective elements, secondary reflector and receiver) (Benyakhlef et al. 2016; Lee et al. 2015). Each ray carries the same amount of energy and has a specific direction determined by an appropriate probability density function based on a predefined Sun's shape. The interaction of each ray with the above surfaces depends on their optical characteristics (transmissivity, reflectance, absorbability), which are described by a set of statistical relationships (Craig et al. 2016).

In the literature, many ray-tracing software have been proposed and used, such as HFLCAL, HELIOS, MIRVAL, DELSOL, SOLTRACE, ENERTRACER, RCELL, SPRAY, SOLFAST, Tonatiuh, Tracer, Raytrace3D or TracePro (Heimsath et al. 2014; Benyakhlef et al. 2016; Bellos et al. 2016; Craig et al. 2016). However, ray-tracing software usually requires a large amount of computing time. This is a problem when many calculations have to be carried out for a single optimization. For this reason, in this book the analytical approach is preferred and a detailed algorithm is developed in the next chapter.

Besides the plant geometry and the optical properties, there is another important parameter that has to be taken into account, the minimum value of the collected solar radiation. This bottom limit (threshold) does not affect only the System's efficiency but also its operation possibility, as each System is designed to operate in a certain range of concentrated solar radiation intensities in order to be able to achieve the required operation temperature. This is also important for the optimization procedure, since without its estimation the optimal System could be totally unrealistic. For example, a System with a very low solar radiation concentration can easily have a high optical efficiency, but this is not a realistic solution (Boito and Grena 2016).

4.7.3 Solar Field Energy Losses

There are some energy losses in Linear Fresnel Reflector Systems that affect the overall System's energy collection efficiency. These losses, expressed in terms of efficiencies, can be allocated to either the solar field efficiency or the receiver efficiency. Some of them are originated from the specific geometry of this kind of Solar Radiation Concentrating Systems that, for example, prevents part of the reflected solar radiation from reaching the receiver. In Fresnel Reflector Systems, there are three most important phenomena that reduce the amount of the energy reaching the receiver: shading and blocking by adjacent reflectors and end losses. Cosine loss is another energy loss mechanism that is, however, an inherent negative feature of Linear Fresnel Reflector Systems (it is present in Solar Tower Power

Systems too). Apart from these, energy losses can also be caused due to the diverging reflected solar radiation beams, or narrow receivers, while a part of the reflected solar radiation misses the receiver (spillage losses). Imperfections in reflectors' surface or impurities in reflectors' glass can further reduce the ability of the solar field to collect the incoming solar radiation (specular and transmissivity losses, respectively). Nevertheless, since these kind of energy losses are difficult to be described and parameterized they are not taken into account in this book, and the corresponding efficiency factors are considered to be equal to 1 ($\eta_{spec} = \eta_{trans} = 1$). Solar radiation losses due to tracking errors, mechanical and manufacturing tolerances of the Systems tracking mechanism, are treated in the same way and are excluded from the System's efficiency optimization. Lastly, solar field energy losses caused by receiver shading (shading of reflectors by the receiver) are considered insignificant. (Despite this, they are studied in the next chapter.)

Usually at noon, when Sun's altitude, h, is maximum there is no blocking or shading losses for a well-designed solar field. However, blocking and shading effects do take place in the mornings and afternoons, especially in the winter, when Sun is low in the sky. In general, shading and blocking occur at Sun's elevation angles, h, lower than a specific value, the design Sun's elevation angle, h_{design}. This angle is used to calculate the reflectors' position so that no shading and blocking losses occur. It also affects the System's operation time. Shading and blocking reduce the available solar radiation on the receiver increasing the time needed for a Power Plant to start-up during the morning as well as limits the time the Power Plant can operate in the evening.

In more details, shading occurs at low Sun's angles when a reflector casts its shadow on an adjacent reflector which is located behind it, in relation to Sun's position. This reduces the incoming solar radiation on the shaded reflector. Consequently, not all incident solar radiation reaches the reflectors, and the area of the reflectors that really reflects the direct solar radiation is smaller than the nominal reflectors' aperture.

On the other hand, blocking losses involve the interruption of the solar radiation after being reflected by the reflectors. It also occurs at low Sun elevation angles, h, when a reflector in front of another blocks the reflected solar radiation and prevents it from reaching the receiver. This way, the area of the reflectors that is actually used for collecting direct solar radiation is reduced. Both phenomena, shading and blocking, are illustrated in Fig. 4.20.

The amount of shading and blocking in a particular solar field is a function of the reflectors' spacing and size, the receiver's height and Sun's position in the sky. While it is possible to design a Solar Radiation Concentrating System that avoids internal shading, as well as blocking, it could result in the use of too large land areas and too costly construction to be feasible. In practice, a balance between the implementation's cost, the size of the reflectors field and the efficiency of the Systems with some losses due to shading and blocking at low Sun elevation angles in the mornings and the evenings should be acceptable.

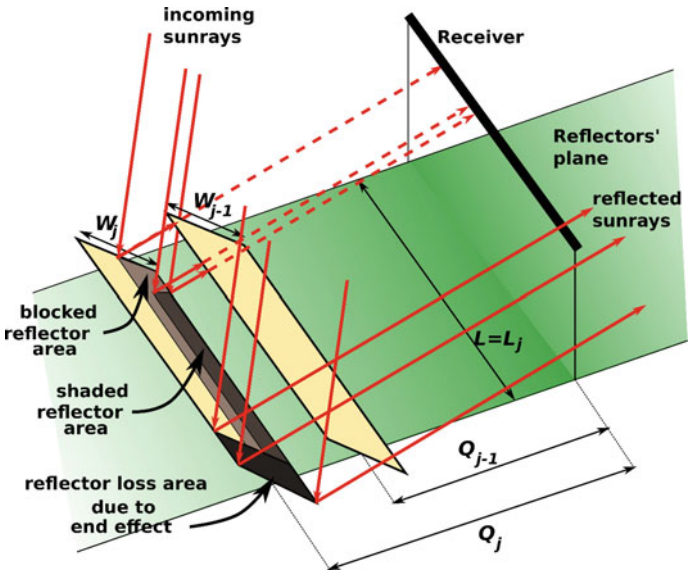

Fig. 4.20 Shading and blocking losses for a typical Linear Fresnel Reflector System

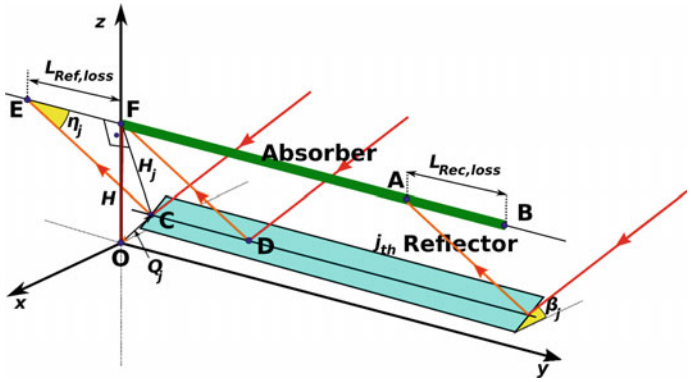

Fig. 4.21 Part of the solar radiation reflected by the reflectors misses the receiver because the solar radiation incident usually forms a nonzero angle with the longitudinal plane of the System, and the reflective elements and the receiver are not infinite

In Linear Fresnel Reflector Systems, the useful receiver length, the part of the receiver that really receives the concentrated solar radiation, is different from the receiver actual length. This is caused by the variable Sun's position in the sky and the fixed orientation of the System. This type of loss is called end loss and depends on the absorber length, L, and the height of the receiver, H (Fig. 4.21). It is noticeable that for small-scale application (small reflectors and absorbers) this type of energy loss can be very big.

Although low-absorption glass reflectors can be manufactured, having a reflectance of about 94%, age and dust soon reduce it to an average value of about 90%. In other words, every reflective element loses its optical efficiency due to soiling. Dust and other contaminants can be accumulated on the reflectors and absorb and scatter the solar radiation that otherwise would be directed to the receiver and be absorbed. These energy losses are highly variable and depend on the specific weather and climate conditions of the construction site (e.g. the local drought levels, the amount of dust, the frequency of precipitation which can clean the reflectors). Soiling losses can be avoided or eliminated by keeping the reflectors clean and in good condition. It is essential in order to maximize the annual energy collection. However, because of its highly variable and unpredictable nature and our capability to eliminate it by cleaning the reflectors, we consider that the reflectance losses can be kept near zero and the corresponding efficiency factor equals 1 ($\eta_{soil} = 1$).

Lastly, despite the fact that the energy losses associated with the reflectors' field include the presented phenomena, the biggest influence to the Systems' efficiency is due to the effect of the incident angle of the incoming solar radiation (cosine effect). As it has already mentioned above, this is an inherent drawback of the Linear Fresnel Reflector Systems and is not treated as a mechanism of energy loss. A reflector's ability to collect direct solar radiation by reflecting and redirecting it depends on the angle between Sun's rays and its aperture plane. The maximum direct solar radiation striking a reflector occurs when the reflector is oriented normal to Sun rays (perpendicular incident angle). At larger incident angles, the radiation striking the reflector's plane is reduced by the cosine of the incidence angle, θ (it has been studied in Chap. 2, Sect. 2.3.4), which has given the name to this phenomenon, cosine losses (Fig. 4.22).

All these losses have to be taken into account when calculating the solar radiation reaching the receiver and evaluating the System's efficiency. However, they

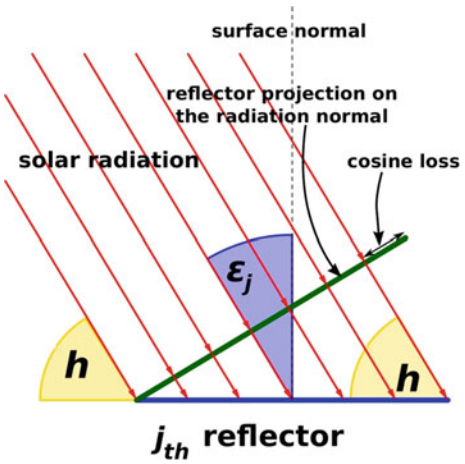

Fig. 4.22 Reduction of the concentrated solar radiation caused by the cosine of the angle between the solar radiation and the surface normal is called the cosine effect

are complex calculation, depending on the Systems (reflectors and receiver) geometry.

4.7.4 Receiver Losses

The various processes that lead to energy losses in the receiver are depicted in Fig. 4.23. Receiver efficiency can be defined as the product of efficiency factors of the individual loss mechanisms:

$$\eta_{\text{receiver}} = \eta_{\text{spill}} \cdot \eta_{\text{absorb}} \cdot \eta_{\text{rad}} \cdot \eta_{\text{conv}} \cdot \eta_{\text{cond}} \tag{4.38}$$

where η_{spill}, η_{absorb}, η_{rad}, η_{conv} and η_{cond} are the efficiency factors (i.e. 1 minus the fraction of energy lost in the process) due to reflected solar radiation spillage, receiver absorption, heat radiation, heat convection and heat conduction losses, respectively.

The most important receiver energy loss originates from convection and radiation heat transfer to the surroundings. Radiation and convection losses depend on the receiver design (its size, whether it is a cavity or an external receiver, its heated area, the orientation of the receiver, receiver absorbability, which depends on the coating of the absorbing surface—e.g. high-absorption paints), the wind velocity, the ambient temperature and the operation temperature of the System. Heat losses through the receiver supporting System are typically only a small fraction of the total receiver heat loss. It can be kept small by minimizing the number and the size of the receiver's attachment points as well as by using low thermal conductance materials in the construction.

Usually, the receiver is constructed large enough to intercept most of the solar radiation reflected by the primary reflective elements. However, its size is limited due to receiver radiation and convection heat losses that are directly proportional to the receiver area. As a result, spillage losses emerge, as part of the reflected solar radiation misses the absorbing area of the receiver. Reflected solar radiation spillage

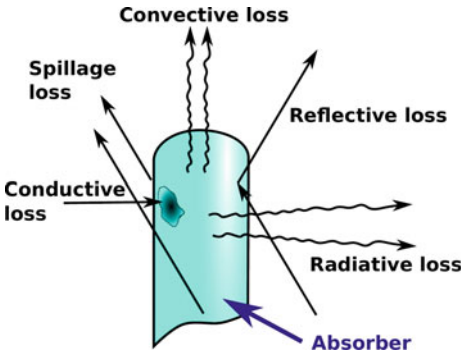

Fig. 4.23 Receiver energy loss processes

losses depend on the reflectors field (reflectance and Sun tracking accuracy, beam spread), the reflectors distance from the receiver and the receiver design (receiver's size, shape). However, this loss factor is arbitrarily included in the receiver efficiency rather than in the solar field efficiency. In Linear Fresnel Reflector Systems, this type of losses can be reduced by using a Secondary Reflector that reflects and redirects the reflected solar radiation that misses the receiver back on it.

Lastly, the rate of the receiver energy losses affects the operation threshold of the System. As a Concentrated Solar Radiation Power System can operate only when the reflected solar radiation is sufficient enough to overcome the receiver energy losses, this threshold corresponds to a specific solar radiation incident angle. Operation at incident angles lower than this value is also constrained due to the rapid increase of blocking and shading effect.

References

Abbas, R., J. Muñoz-Antón, M. Valdés, and J.M. Martínez-Val. 2013. High concentration linear Fresnel reflectors. *Energy Conversion and Management* 72: 60–68.

Abbas, R., M. Valdés, M.J. Montes, and J.M. Martínez-Val. 2017. Design of an innovative linear Fresnel collector by means of optical performance optimization: A comparison with parabolic trough collectors for different latitudes. *Solar Energy* 153: 459–470.

Ahmed, Mohamed H., and Amr M. A. Amin. 2016, September. Thermal analysis of the performance of Linear Fresnel Solar Concentrator. *Journal of Clean Energy Technologies* 4 (5): 316–320.

Bellos, E., E. Mathioulakis, C. Tzivanidis, V. Belessiotis, and K.A. Antonopoulos. 2016. Experimental and numerical investigation of a linear Fresnel solar collector with flat plate receiver. *Energy Conversion and Management* 130: 44–59.

Benyakhlef, S., A. Al Mers, O. Merroun, A. Bouatem, N. Boutammachte, S. El Alj, H. Ajdad, Z. Erregueragui, and E. Zemmouri. 2016. Impact of heliostat curvature on optical performance of Linear Fresnel solar concentrators. *Renewable Energy* 89: 463–474.

Boito, Paola, and Roberto Grena. 2016. Optimization of the geometry of Fresnel linear collectors. *Solar Energy* 135: 479–486.

Chaves, J., and M. Collares-Pereira. 2010. Etendue-matched two-stage concentrators with multiple receivers. *Solar Energy* 84 (2): 196–207.

Craig, K.J., M.A. Moghimi, A.E. Rungasamy, J. Marsberg, and J.P. Meyer. 2016. Finite-volume ray tracing using Computational Fluid Dynamics in linear focus CSP applications. *Applied Energy* 183: 241–256.

Heimsath, A., F. Cuevas, A. Hofer, P. Nitz, and W.J. Platzer. 2014. Linear Fresnel collector receiver: Heat loss and temperatures. *Energy Procedia* 49: 386–397.

Hongn, Marcos, Silvana Flores Larsen, Marcelo Gea, and Martin Altamirano. 2015. Least square based method for the estimation of the optical end loss of linear Fresnel concentrators. *Solar Energy* 111: 264–276.

Lee, H.-J., J.-K. Kim, S.-N. Lee, H.-K. Yoon, Y.-H. Kang, and M.-H. Park. 2015. Calculation of optical efficiency for the first central-receiver solar concentrator system in Korea. *Energy Procedia* 69: 126–131.

Rungasamy, A.E., K.J. Craig, and J.P. Meyer. 2015. 3-D CFD modeling of a slanted receiver in a compact linear Fresnel plant with etendue-matched mirror field. *Energy Procedia* 69: 188–197.

Schenk, Heiko, Tobias Hirsch, Jan Fabian Feldhoff, and Michael Wittmann. 2014, November. Energetic comparison of linear Fresnel and parabolic trough collector systems. *Journal of Solar Energy Engineering* 136, 041015, 1–11. (ASME).

Yang, F., D. Itskhokine, S. Benmarraze, M. Benmarraze, A. Hofer, F. Lecat, and A. Ferrière. 2015. Acceptance testing procedure for Linear Fresnel Reflector solar systems in utility-scale solar thermal power plants. *Energy Procedia* 69: 1479–1487.

Zhang, Hui, Li Zhu, Yiping Wang, and Yong Sun. 2010. Design and simulation of a linear flat mirror concentrator. In *Solar2010, The 48th AuSES Annual Conference*, 1–3 December 2010, Canberra, ACT, Australia.

Zhang, Yanmei, Gang Xiao, Zhongyang Luo, Mingjiang Ni, Tianfeng Yang, and Xu Weiping. 2014. Comparison of different types of secondary mirrors for solar application. *Optik* 125: 1106–1112.

Chapter 5
Geometric Optical Losses

Solar Radiation Concentrating technologies use large mirrors to concentrate sunlight onto a relatively small-aperture receiver. Solar Radiation Concentrating technologies use large mirrors to concentrate sunlight onto a relatively small-aperture receiver. Linear Fresnel Reflector Systems use long, narrow, flat or slightly curved mirrors that reflect Sun's rays onto a fixed linear receiver mounted above and along them. Even in small-scale, they usually adopt one axis tracking mechanisms. Therefore, as incident solar rays are generally oblique, it's inevitable for these Systems to not have optical losses: cosine effect, end losses, shading or blocking effects. Thus, although they have some advantages compared with other technologies (simplicity, robustness and low capital cost), they also have important drawbacks and limitations that significantly limit their efficiency.

There is a sufficient number of studies available in the literature for estimating the optical losses of these Systems. However, they generally use ray-tracing methods to account for shading and blocking effects, end losses and cosine effect. Nevertheless, despite the fact that ray tracing is the most used method to estimate optical losses, it is a very time-consuming procedure. For this reason, in this Chapter analytical mathematical equations are developed (an optical model), based on the equations describing Sun's and reflective elements' positions. So, the effect the reflectors width, the spacing between adjacent reflectors, the number of reflectors, the receiver height, the reflectors configuration, the system orientation angle and the site latitude may have on Systems optical efficiency can be estimated explicitly. This way, the best combinations of these parameters can easily be obtain, resulting in maximum efficiency, and consequently in minimum cost of electricity production. To give only a clue, in Linear Fresnel Reflector Systems, the receiver height affects the tilt of the reflectors and thus the energy losses due to cosine effect, shading and blocking.

S. Karathanasis, *Linear Fresnel Reflector Systems for Solar Radiation Concentration*, https://doi.org/10.1007/978-3-030-05279-9_5

5.1 Introduction

In a Linear Fresnel Reflector Systems, parallel rows of reflectors direct the incident solar radiation towards a linear receiver (Fig. 5.1a). However, in these Systems, the complete reflector aperture cannot be utilized, and a part of it remains unused, due to end effect (end losses), shading and blocking effects. End losses appear when a part of the reflected solar radiation does not hit the receiver, and it misses the receiver. Shading effects arise when a reflector prevents the incoming direct solar

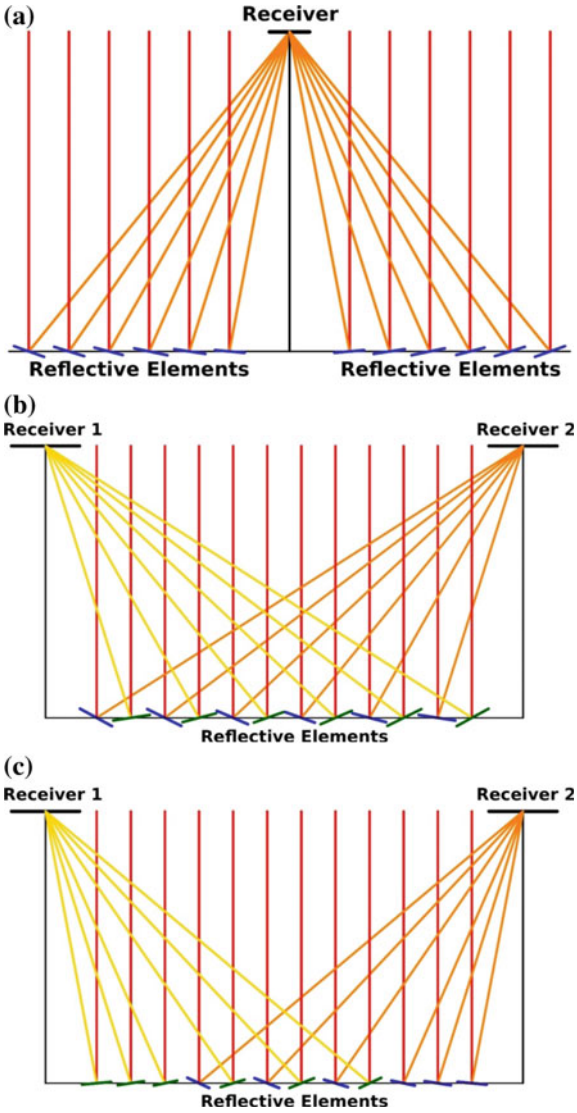

◂**Fig. 5.1** Schematic representation of **a** a Linear Fresnel Reflector Systems with one centrally positioned receiver (classical System) and two Compact Linear Fresnel Reflector Systems with different reflectors configurations (**b** and **c**). A classical Linear Fresnel Reflector System consists of N parallel reflectors, with length L and width W_j, and a fixed receiver. The System's aperture area is $N \cdot W \cdot L$, where W is its width, and the centre to centre distance between two adjacent reflectors is S_j. When N is even, $N/2$ reflectors are on either side of the receiver. In the case N is odd, $(N-1)/2$ reflectors are on either side of the receiver and the $[(N-1)/2 + 1]$th reflector is placed just underneath the receiver. The exterior reflector lying on the negative side of the horizontal axis is usually referred as the -nth reflector, while the exterior reflector lying on the positive side of the horizontal axis is the nth reflector, where $N = 2 \cdot n$ or $N = 2 \cdot n + 1$. A Compact Linear Fresnel Reflector System consists of two fixed linear receivers. It is assumed that 25% of the reflectors are on the West of the western receiver, 25% are on the East of the eastern receiver, and 50% of the reflectors are between the two receivers, for a North–South orientation. The intermediate reflectors may reflect the incoming solar radiation towards any of the two receivers. For s intermediate reflectors, this Subsystem can be configured in 2^s ways

radiation from falling onto the adjacent reflector, while blocking effects emerge when the reflected solar radiation is blocked from an adjacent reflector and cannot reach the receiver. In addition to these effects, cosine effect further contributes to energy losses. These effects depend on the length (L) and the width (W_j) of the reflector's aperture, the spacing between adjacent reflector (S_j), the number of reflectors ($N = 2 \cdot n$, or $N = 2 \cdot n + 1$), the receiver height (H), the reflectors configuration and the system orientation angle (γ).

The system orientation angle, γ, is the angle formed by the South direction and the tracking axes of the reflectors, or equivalently the receiver direction (measured clockwise), and plays a significant role in Systems performance. Systems with orientation angles γ and– γ have the same daily performance, but in the reverse time order. Therefore, the study of Linear Fresnel Reflector Systems can be limited in orientation angles between 0° and 90° (Sharma et al. 2015b). Apart from these, the latitude (φ) of the location, the reflectors arrangement or configuration, the day of the year, the time of the day, as well as material properties, also affect energy losses. By combining unused aperture area with radiation data, we can estimate the energy losses due to these phenomena. They influence the net energy collection ability of the System and hence the electricity generation efficiency and cost.

Increasing the spacing between reflectors, S_j, or the height of the receiver, H, we can reduce the influence of these effects, but more space is required. Furthermore, a well designed receiver can increase the Systems efficiency considerably. There exist several receiver designs that use simple tubes, plates, evacuated tubes and secondary concentrating devices. Typically, the horizontal type is favoured over a vertical or angled receiver (Nixon and Davies 2012). One particular design often used in Linear Fresnel Reflector Systems is the trapezoidal cavity receiver which is composed of a number of absorbing tubes, a secondary reflector, and a glass cover that forms a cavity minimizing heat losses (Nixon and Davies 2012).

In order to mitigate some of the aforementioned energy loss effects, the design, the width, the shape, the spacing and the number of the reflective elements have been modified and the resulting Systems have been studied by several researchers. Consequently, many alternative designs for various applications have been

proposed. In general, a Linear Fresnel Reflector System consists of a number of reflectors (that are placed parallel to each other) and a linear receiver. Mills and Morrison (2000) have proposed that, if the Linear Fresnel Reflector Subsystems were close enough, the reflectors of two Subsystems lying between two receivers would have an extra degree of freedom and could direct the incoming solar radiation towards any of the two receivers. The Linear Fresnel Reflector Systems having this flexibility are called Compact Linear Fresnel Reflector Systems (Fig. 5.1b).

In classical Linear Fresnel Reflector Systems, each Subsystem has only one receiver, and the reflective elements have no other choice but to direct the solar radiation onto this receiver. However, if there are many Subsystems, being installed close enough, then the reflectors may have the option to direct the reflected solar radiation onto two adjacent receivers. The n reflectors lying between the two receivers can be configured in 2^n different ways, and therefore, they can lead to a variety of different Systems (Fig. 5.2). By modifying the reflectors configuration, in Compact Linear Fresnel Reflector Systems, they can be placed more densely, avoiding at the same time shading and blocking effects.

Shading and blocking effects can also be reduced by using receivers in higher height. However, this increases the tracking accuracy requirements and consequently the implementation cost. On the other hand, by increasing the receiver's size (width), the reflective elements must have larger distances between them, and as a result, the ground utilization ratio is reduced. Therefore, the avoidance of larger reflectors' spacing and receiver height is important, as it reduces investment cost.

In general, two types of Linear Fresnel Reflector Systems have been developed and reported in the literature. In the first type, the reflectors are kept fixed and the whole reflector–receiver construction is moved tracking the apparent movement of Sun (Fig. 5.3a). In the second type, the receiver remains stationary and the reflectors are the System's elements that are rotated around an axis so as to follow the movement of Sun (Fig. 5.3b). The latter type is essentially those Systems that can be implemented on large scale. However, in contrast to the former type, in these Systems, end losses, shading and blocking effects are almost always present.

In order to simplify the mathematical description, and for ease of the calculations, without losing any generality, or introducing any error, the following assumptions are made:

- The Linear Fresnel Reflector Systems are deemed as ideal optical Systems.
- The Sun-tracking error is neglected, and receiver's misalignments are not accounted.
- The reflective elements and the receiver have the same length and the same orientation and are aligned to each other.
- The reflective elements are ideal specular surfaces; no reflection errors are considered.
- The surface of each reflector is assumed to be flat as for shading and blocking effects the mirrors' curvature has no effect on shading calculations and a very small effect on blocking (Sharma et al. 2015b).

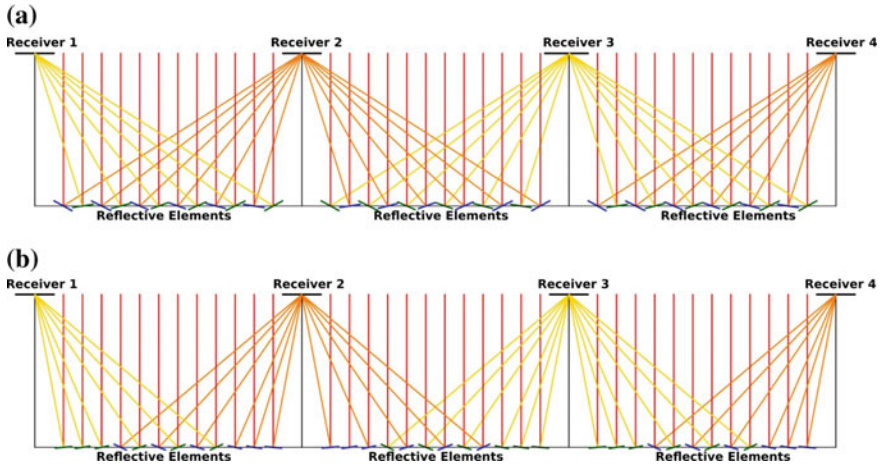

Fig. 5.2 Two of the 2^s possible different reflectors configurations for a Compact Linear Fresnel Reflector Systems with s reflectors lying between the two receivers

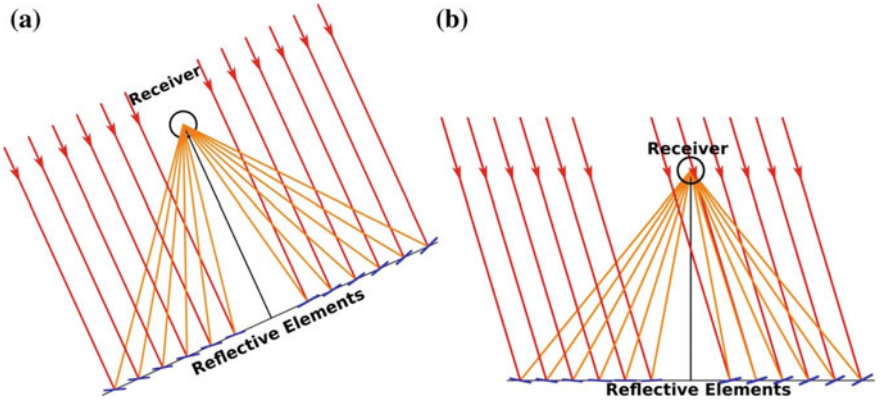

Fig. 5.3 Linear Fresnel Reflector Systems can be developed in two different Sun tracking approaches. **a** In small-scale Systems, the whole construction can be mounted on a board that can follow Sun's movement in the sky by a two-axis tracking mechanism. However, large-scale installations can be developed only using one-axis tracking mechanisms (**b**), where the reflective elements are rotated around an axis passing through their longer dimension

- Only direct solar radiation is considered, while diffuse radiation is neglected.
- Sun's position in the sky is accurately calculated using appropriate formulas and at a first approximation.
- The solar radiation reflection is calculated in the central axis of the reflectors.
- Receiver shadow on reflectors is neglected.
- Sun's rays are parallel, and the effect of Sun's shape is not considered.

5.2 Shading and Blocking Effects

The most common difficulty with Linear Fresnel Reflector Systems is to prevent the shading and blocking effects caused by adjacent reflectors early in the morning and late in the afternoon (Fig. 5.4). However, shading and blocking effects on a reflective element may occur at the same time, depending on the distance between adjacent reflective elements, as well as their inclinations angles (Fig. 5.5). This restricts the time the System can operate during the morning and the evening. However, if the incident angle of solar radiation on the reflective elements is known, as well as the geometry of the Systems, these losses can be easily calculated.

Reflectors shading and reflected solar radiation blocking are caused due to the non-normal incidence of the incoming solar radiation on System's aperture. However, instead of using Sun's elevation angle, h, and azimuth, A, that describe its position in the sky (the solar vector, $\mathbf{S}$), to estimate the influence of these effects, we use the transversal component of Sun's position, $\mathbf{S_T}$ (its transversal angle θ_T) as we did when we were calculating the reflectors' inclination angle, β_j, in Chap. 4, Sect. 4.3.2. However, this is used only for the calculation of the shaded or blocked width of the reflectors. To calculate their shaded or blocked length, we must use the actual position vector of Sun (the solar vector, $\mathbf{S}$), as it will be presented later.

The tilt (or inclination) angle β_j of each reflector can be computed using Eq. 4.17 presented in Chap. 4 (Fig. 5.6a):

$$\beta_j = \frac{\xi_j - \theta_T}{2} \Rightarrow \tag{5.1}$$

$$\beta_j = \frac{1}{2}\tan^{-1}\left(\frac{\mathrm{H}}{Q_j}\right) - \frac{\theta_T}{2} \tag{5.2}$$

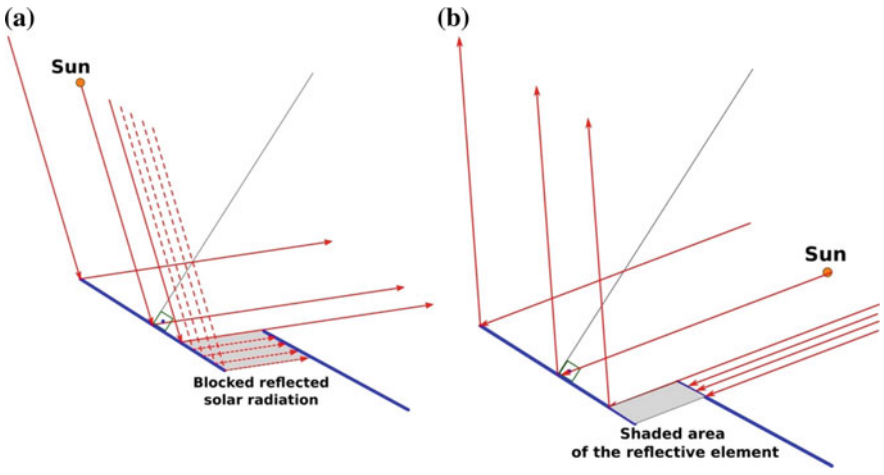

Fig. 5.4 Shading and blocking caused by adjacent reflectors in Fresnel Reflector Systems

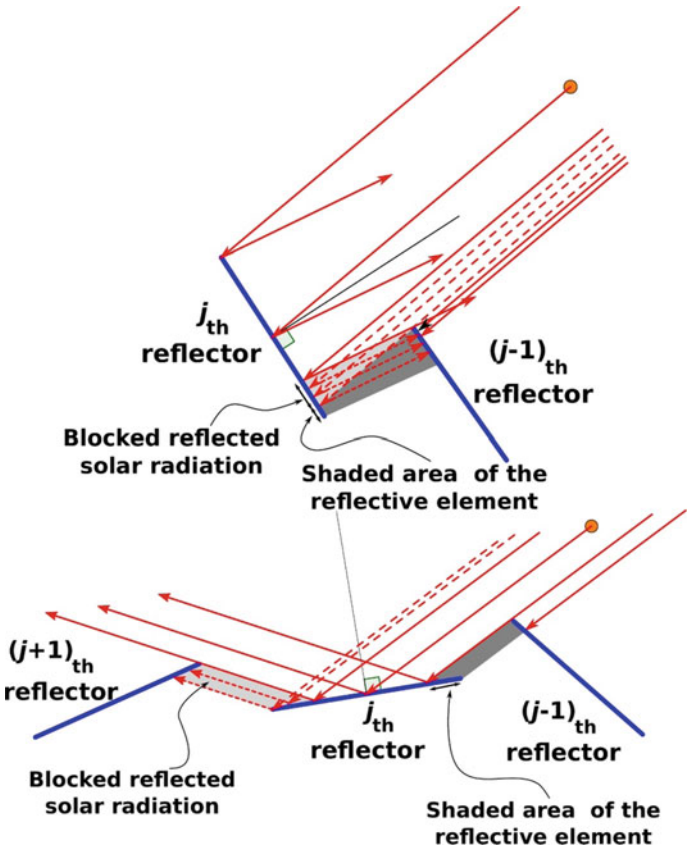

Fig. 5.5 Shading and blocking effects may both occur at the same time on a reflective element. This depends on the distances between adjacent reflective elements and their inclinations angles

where Q_j is the distance of the jth reflective element from the origin of the local Cartesian coordinate system, H is the height of the receiver (Fig. 5.6a), and θ_T is the transversal angle of Sun's position in the sky in relation to the orientation of the given Linear Fresnel Reflector System: The latter is given by Eq. 4.11 of Chap. 4:

$$\tan \theta_T = \frac{\tan h}{\cos(\gamma - \mathrm{A})} \tag{5.3}$$

where γ is the Systems orientation angle, different from the azimuth angles of the reflector, $\gamma \neq \gamma_j$. Systems' orientation angle, γ, is measured from the South direction being positive towards West (clockwise).

From Eq. 5.1, it can be concluded that when $\theta_T - \xi_j = 0°$, the jth's reflector aperture becomes horizontal. In any other case, their azimuth angle, γ_j, will be (Sharma et al. 2015a, b, c) (Fig. 5.7)

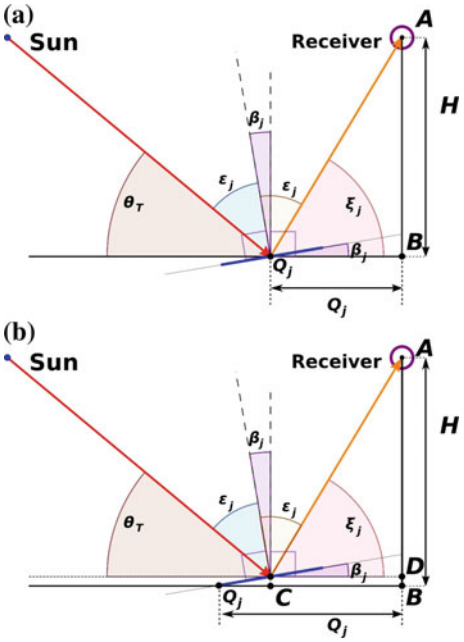

Fig. 5.6 Sun's position in the sky in relation to the transversal plane of a Linear Fresnel Reflector System in the case the reflective elements are centrally pivoted (**a**) and in the case their rotation axis coincides with one of their longer edges (**b**)

$$\gamma_j = \begin{cases} 90^\circ + \gamma, \text{ or } -90^\circ - |\gamma|, \text{if } \gamma < 0^\circ & \text{if } \theta_T > \xi_j \\ \text{or} & \\ \gamma, \text{ or } 90^\circ + |\gamma|, \text{ if } \gamma < 0^\circ & \text{if } \theta_T < \xi_j \end{cases} \tag{5.4}$$

It must be noted that the primary reflective elements are assumed to be always flat or else the radius of curvature is large enough (compared with their width), and all calculations concerning their inclination angle, β_j, are performed using their central point (or more correctly, their central longitudinal axis) (Pino et al. 2013).

5.2.1 Shading Effect

The total shadow that affects the overall reflective area of the System is the sum of two different components: (a) the shadow the receptor casts on the reflectors and (b) the shadows caused by one reflector on its adjacent reflector. The receptor's shadow is usually smaller in percentage than the reflectors' shadow, and it affects only a small number of the reflectors each time. The receiver shadow effect will be studied in the next paragraph of this chapter.

Until Sun's transversal angle, θ_T, reaches the design value, the value used to specify the reflectors spacing arrangement (see next chapter), a proportion of the reflective elements will be in shade (Nixon and Davies 2012). Shadowing between reflectors depends on their angular position, β_j, or in other words, on their rotation angle. Figure 5.8 illustrates a number of possible cases.

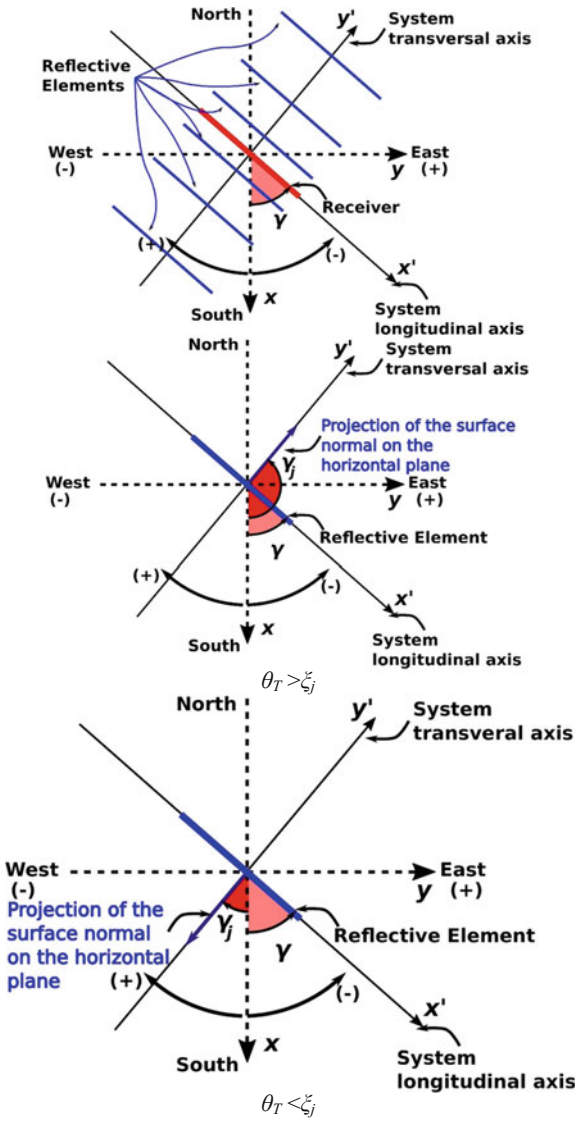

Fig. 5.7 Reflectors' azimuth angle, γ_j, and their relation to System's orientation, or azimuth, angle, γ

The aperture area, $A_{\text{shadLoss},j}$, of the jth reflector that remains unused due to shading effect is shown in Fig. 5.9. In fact, this area is trapezoidal. However, it can be assumed to be rectangular without loss of generality and without introducing significant error (Sharma et al. 2015a, b, c). Let $L_{\text{shadLoss},j}$ and $W_{\text{shadLoss},j}$ be the corresponding length and width of this area. Then, the aperture loss area of the jth reflector due to the shading effect, $A_{\text{shadLoss},j}$, can be written as

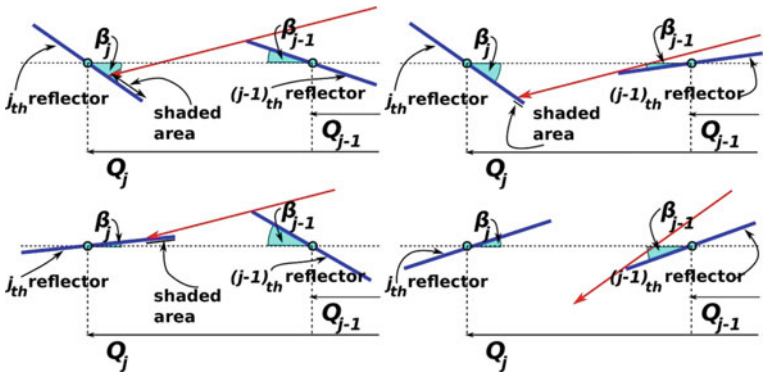

Fig. 5.8 Possible relative positions of adjacent reflective elements that affect the shading effect

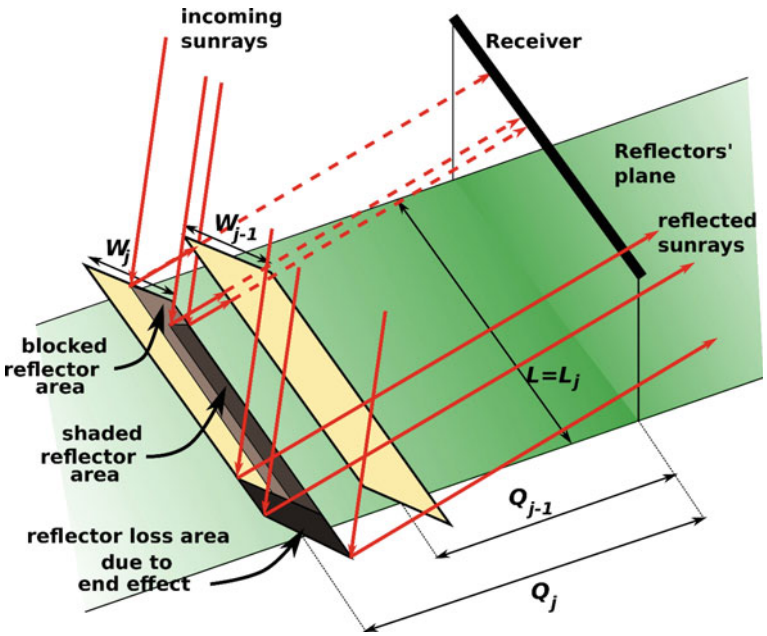

Fig. 5.9 Schematic representation of the shading, blocking, and end losses effects, and the corresponding reflectors unused areas

$$A_{\text{shadLoss},j} = L_{\text{shadLoss},j} \cdot W_{\text{shadLoss},j} \tag{5.4}$$

The shaded length, $L_{\text{shadLoss},j}$, and the shaded width, $W_{\text{shadLoss},j}$, of the jth reflector are calculated using different approaches, which will be presented in the next paragraphs. One difficulty in calculating the shaded area is that a part of it may also contribute to end losses and thus be admeasured twice. However, this problem will be dealt with in details in Sect. 5.2.1.3, where the shaded length, L_{shadLoss}, will be calculated.

5.2.1.1 Shaded Width

The shaded part, $W_{\text{shadLoss},j}$, of the width, W_j, of the jth reflective elements, and consequently the shade energy losses of the System, for a given time of the day, can be calculated from the geometry presented in Fig. 5.10. In this case, the reflectors' rotation axes are on the same horizontal plane and go through the middle point of the reflectors narrower edge (centrally pivoted). Figure 5.11 shows another case where reflectors' rotation axes are also on the same horizontal plane, but they coincide with the lower longitudinal edge of the reflectors (side pivoted). These two cases have different geometrical characteristics and need different mathematical approaches. However, in the second case, it is not easy to be implemented in practice, and therefore, the centrally pivoted reflective elements should be preferable.

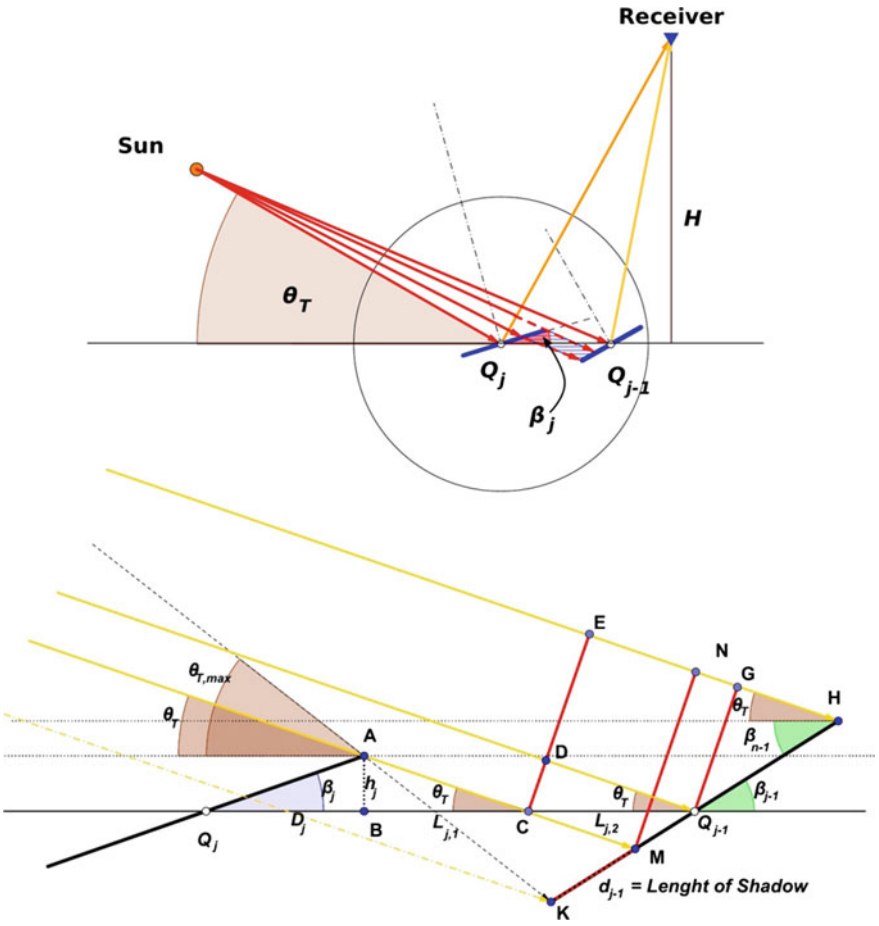

Fig. 5.10 Shading loss geometry when the reflectors' rotation axis are on the same horizontal plane and go through the middle point of their narrower edge. The reflective elements may shade each other when Sun's transversal angle is lower than the design value, $\theta_{T,\max}$

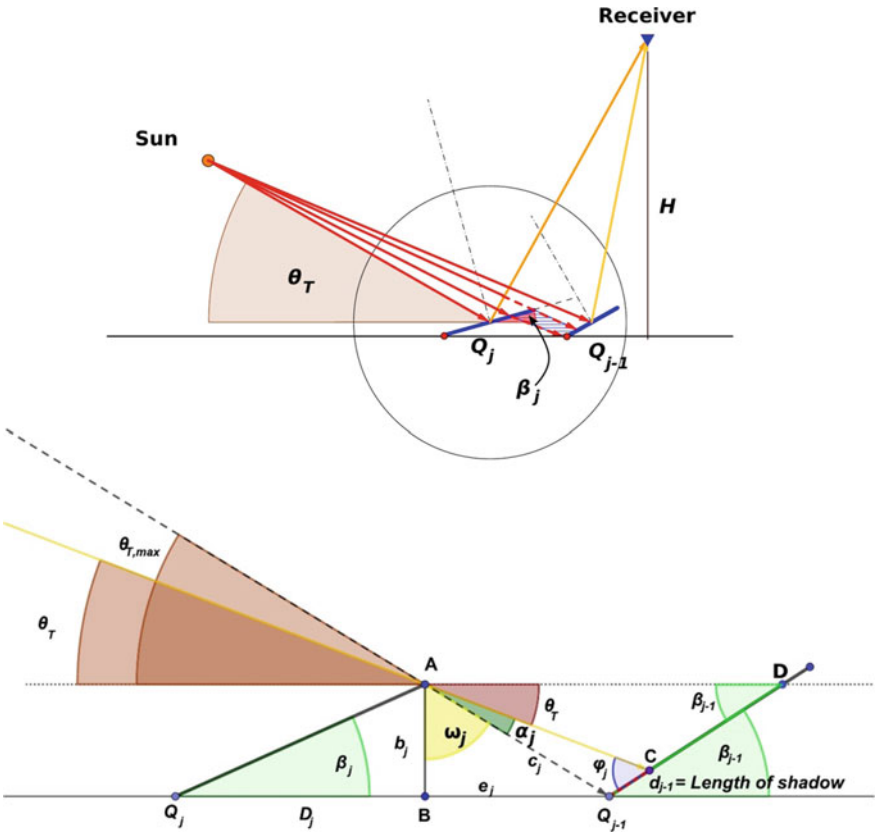

Fig. 5.11 Shading loss geometry when the reflectors' rotation axis is on the same horizontal plane and coincides with one of the reflectors' longer edge. The reflective elements may shade each other when Sun's transversal angle is lower than the design value, $\theta_{T,}$max

From the geometry of Fig. 5.10, we can deduce that the shading loss, the shaded width $W_{\text{shadLoss},j-1}$, of the (j–1)th reflector is equal to the line segment KM. However,

$$W_{\text{shadLoss},j-1} = KM = KH - MH = W_{j-1} - MH \tag{5.5}$$

The length of the line segment MH can be calculated from the geometry of the triangle MNH, as

$$\begin{aligned} \sin\left(\theta_T + \beta_{j-1}\right) &= \tfrac{MN}{MH} \Rightarrow \\ MH &= \tfrac{MN}{\sin\left(\theta_T + \beta_{j-1}\right)} \Rightarrow \end{aligned} \tag{5.6}$$

Next, the length of the line segment MN can be computed as the sum of the lengths of the two line segments CD and $Q_{j-1}G$:

$$\begin{gathered} MN = CE = CD + DE \Rightarrow \\ MN = \mathrm{CD} + Q_{j-1}G \end{gathered} \tag{5.7}$$

From the triangles CDQ_{j-1} and $GHQ_{j-1,}$ we have

$$MN = L_{j,2} \cdot \sin\theta_T + \frac{W_{j-1}}{2} \cdot \sin\left(\beta_{j-1} + \theta_T\right) \tag{5.8}$$

The length $L_{j,2}$ can be calculated using the positions of the reflectors' central points Q_j and Q_{j-1}:

$$\begin{gathered} L_{j,2} = Q_j - Q_{j-1} - L_{j,1} - Q_jB \Rightarrow \\ L_{j,2} = Q_j - Q_{j-1} - L_{j,1} - D_j \Rightarrow \\ L_{j,2} = Q_j - Q_{j-1} - L_{j,1} - \frac{W_j}{2} \cdot \cos\beta_j \end{gathered} \tag{5.9}$$

The length $L_{j,1}$ can be calculated using the geometry of triangle ABC:

$$\begin{gathered} L_{j,1} = h_j \cdot \tan\widehat{BAC} \Rightarrow \\ L_{j,1} = \frac{W_j}{2} \cdot \cos\beta_j \cdot \tan\widehat{BAC} \end{gathered} \tag{5.10}$$

But

$$\widehat{BAC} = 90^\circ - \theta_T \tag{5.11}$$

Substituting Eq. 5.11 into Eq. 5.10, then Eq. 5.10 into Eq. 5.9 and, finally, Eq. 5.9 into Eq. 5.8, it becomes:

$$\begin{aligned} MN = &\left[Q_j - Q_{j-1} - \frac{W_j}{2} \cdot \cos\beta_j \cdot \tan(90^\circ - \theta_T) - \frac{W_j}{2} \cdot \cos\beta_j\right] \cdot \sin\theta_T \\ &+ \frac{W_{j-1}}{2} \cdot \sin\left(\beta_{j-1} + \theta_T\right) \end{aligned} \tag{5.12}$$

Substituting, now, Eq. 5.12 into Eq. 5.6 and Eq. 5.6 into Eq. 5.5, the shaded width, $W_{\mathrm{shadLoss},j-1}$, of the $(j-1)$th reflector is equal to

$$\begin{aligned} W_{\mathrm{shadLoss},j-1} = &\frac{W_{j-1}}{2} \\ &- \left[Q_j - Q_{j-1} - \frac{W_j}{2} \cdot \cos\beta_j \cdot \tan(90^\circ - \theta_T) - \frac{W_j}{2} \cdot \cos\beta_j\right] \cdot \frac{\sin\theta_T}{\sin\left(\beta_{j-1} + \theta_T\right)} \end{aligned} \tag{5.13}$$

If $W_{\mathrm{shadLoss},j-1} = 0$ (or < 0), then no shading occurs, whereas if $W_{\mathrm{shadLoss},j-1} > 0$, shading losses are present. The total shaded surface is computed by multiplying the shaded width $W_{\mathrm{shadLoss},j-1}$ by the shaded length, $L_{\mathrm{shadLoss},j-1}$, of the reflector.

In the second case, where the reflectors' rotation axes coincide with the lower longitudinal edge of the reflectors (Fig. 5.11), the shaded Width, $W_{\text{shadLoss},j-1}$, of the (j–1)th reflector is more easily to be calculated. Using the geometry of Fig. 5.11 and simple trigonometry, the necessary equations can be derived.

Applying the sine law in triangle ACQ_{j-1}, we can derive the following equation for the shaded width, $W_{\text{shadLoss},j-1}$ of the $(j-1)$th reflector

$$\begin{gathered}\frac{\mathrm{d}_{j-1}}{\sin a_j} = \frac{c_j}{\sin \varphi_j} \Rightarrow \\ \mathrm{d}_{j-1} = \frac{c_j \cdot \sin a_j}{\sin \varphi_j} \Rightarrow \\ W_{\text{shadLoss},j-1} = \frac{c_j \cdot \sin a_j}{\sin \varphi_j}\end{gathered} \tag{5.14}$$

where $\varphi_j = \theta_T + \beta_{j-1}$, as external angle in the triangle ACD. Angles α_j, ω_j and θ_T satisfy the equation

$$\begin{gathered}a_j + \omega_j + \theta_T = 90^\circ \Rightarrow \\ a_j = 90^\circ - \omega_j - \theta_T\end{gathered} \tag{5.15}$$

Angle ω_j can be estimated from the triangle BAQ_{j-1} using the equations

$$\tan \omega_j = \frac{e_j}{b_j} \Rightarrow \omega_j = \tan^{-1}\left(\frac{e_j}{b_j}\right) \tag{5.16}$$

From triangle ABQ_j, we have

$$b_j = W_j \cdot \sin \beta_j \tag{5.17}$$

The three sides of triangle ABQ_{j-1} are connected with the Pythagorean theorem

$$c_j^2 = b_j^2 + e_j^2 \Rightarrow c_j = \sqrt{b_j^2 + e_j^2} \tag{5.18}$$

where e_j is determined by the equation

$$\begin{gathered}e_j = Q_j - Q_{j-1} - D_j \\ e_j = Q_j - Q_{j-1} - W_j \cdot \cos \beta_j\end{gathered} \tag{5.19}$$

Substituting Eqs. 5.19 and 5.17 into Eqs. 5.18, 5.19 and Eqs. 5.17 into Eqs. 5.16, 5.16 into Eq. 5.15 and, finally, Eqs. 5.15 and 5.18 into Eq. 5.14, the shaded width, $W_{\text{shadLoss},j-1}$, of the $(j-1)$th reflective element due to the shadow casted on it from the jth reflector becomes:

$$W_{\text{shadLoss},j-1} = \frac{\sqrt{\left(W_j \cdot \sin \beta_j\right)^2 + e_j^2} \cdot \sin\left(90^\circ - \tan^{-1}\left(\frac{e_j}{b_j}\right) - \theta_T\right)}{\sin\left(\theta_T + \beta_{j-1}\right)} \tag{5.20}$$

If $W_{\text{shadLoss},j-1} = 0$ (or < 0), then no shading occurs, else, if $W_{\text{shadLoss},j-1} > 0$, shading losses are present.

5.2.1.2 Shaded Width: General Calculation Approach

In the previous paragraph, the shaded width, $W_{\text{shadLoss},j-1}$, of the $(j-1)$th reflective element due to the shadow casted on it from the jth reflector is calculated for two typical cases of reflectors configuration, illustrated in Figs. 5.10 and 5.11, respectively. However, the number of the possible relative positions the adjacent reflective elements may have is considerably large, and, therefore, it is not sensible to develop separate equations for each different position combination. Instead, a more general approach should be followed and general equation be derived. For this reason, vector calculus in three dimensions (3D), vector geometry and analytic geometry are more suitable.

For this purpose, let us consider the typical case illustrated in Fig. 5.12. The jth reflective element casts its shadow on the $(j-1)$th reflective element [or the $(j+1)$ th reflector, depending on Sun's position in the sky and consequently on the time of the day], if at least one of the shadow vertices falls into the aperture area of the $(j-1)$th reflective element. The problem that arises is how to conclude whether these points are in or out the reflector aperture area. Well, let us follow the appropriate steps one by one and in the right order.

Each reflective element has four vertices which determine a plane. Considering that the origin of the local Cartesian coordinate system is underneath the midpoint of the receiver, then the direction to the South determines the x-axis, the direction to the East determines the y-axis, and the direction towards the zenith determines the z-axis. Hence, the four vertices, A_j, B_j, C_j and D_j, of the jth reflective element have the following coordinates:

$$A_j = \begin{pmatrix} A_{x,j} \\ A_{y,j} \\ A_{z,j} \end{pmatrix} = \begin{pmatrix} \frac{L}{2} \cdot \cos\gamma + \frac{W_j}{2} \cdot \cos\beta_j \cdot \sin\gamma + Q_j \cdot \sin\gamma \\ -\frac{L}{2} \cdot \sin\gamma + \frac{W_j}{2} \cdot \cos\beta_j \cdot \cos\gamma + Q_j \cdot \cos\gamma \\ z_j + \frac{W_j}{2} \cdot \sin\beta_j \end{pmatrix} \tag{5.21}$$

$$B_j = \begin{pmatrix} B_{x,j} \\ B_{y,j} \\ B_{z,j} \end{pmatrix} = \begin{pmatrix} \frac{L}{2} \cdot \cos\gamma - \frac{W_j}{2} \cdot \cos\beta_j \cdot \sin\gamma + Q_j \cdot \sin\gamma \\ -\frac{L}{2} \cdot \sin\gamma - \frac{W_j}{2} \cdot \cos\beta_j \cdot \cos\gamma + Q_j \cdot \cos\gamma \\ z_j + \frac{W_j}{2} \cdot \sin\beta_j \end{pmatrix} \tag{5.22}$$

$$C_j = \begin{pmatrix} C_{x,j} \\ C_{y,j} \\ C_{z,j} \end{pmatrix} = \begin{pmatrix} -\frac{L}{2} \cdot \cos\gamma - \frac{W_j}{2} \cdot \cos\beta_j \cdot \sin\gamma + Q_j \cdot \sin\gamma \\ \frac{L}{2} \cdot \sin\gamma - \frac{W_j}{2} \cdot \cos\beta_j \cdot \cos\gamma + Q_j \cdot \cos\gamma \\ z_j - \frac{W_j}{2} \cdot \sin\beta_j \end{pmatrix} \tag{5.23}$$

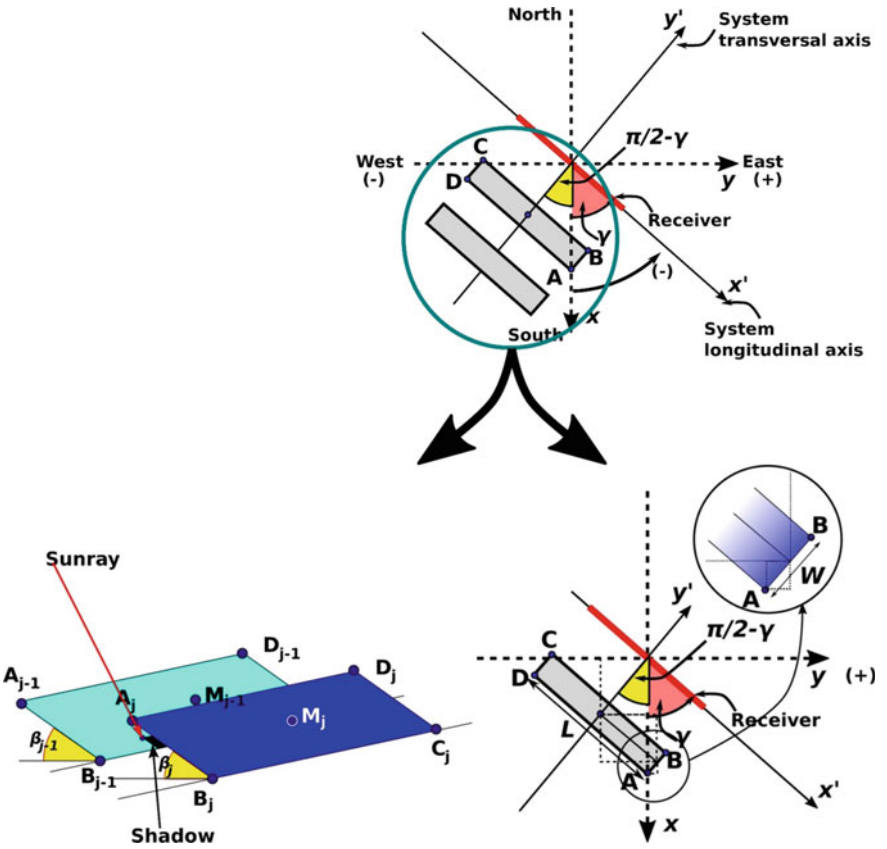

Fig. 5.12 This is a typical case of reflectors shading. The *j*th reflective element casts its shadow on the $(j-1)$th reflective element. However, the shadow may fall onto the aperture area of the $(j-1)$th reflective element if the reflective elements positions, Q_j, its inclination angle, β_j, as well as Sun's position in the sky satisfy well defined conditions

$$D_j = \begin{pmatrix} D_{x,j} \\ D_{y,j} \\ D_{z,j} \end{pmatrix} = \begin{pmatrix} -\frac{L}{2} \cdot \cos\gamma + \frac{W_j}{2} \cdot \cos\beta_j \cdot \sin\gamma + Q_j \cdot \sin\gamma \\ \frac{L}{2} \cdot \sin\gamma + \frac{W_j}{2} \cdot \cos\beta_j \cdot \cos\gamma + Q_j \cdot \cos\gamma \\ z_j - \frac{W_j}{2} \cdot \sin\beta_j \end{pmatrix} \tag{5.24}$$

where z_j is the vertical distance of the middle point of the *j*th reflective element from the *xy*-plane, if the reflective elements are not all on the same plane following a complex configuration (or else $z_j = z = 0$ for all *j*).

In addition, the coordinates of the middle point, M_j, of the jth reflective element are

$$M_j = (\, M_{x,j}, \quad M_{y,j}, \quad M_{z,j}\,) = (\, Q_j \cdot \sin\gamma, \quad Q_j \cdot \cos\gamma, \quad z_j\,) \tag{5.25}$$

In the most simple, and most frequently appeared case, the System has a North–South orientation, $\gamma = 0°$, and all reflective elements are on the same horizontal plane ($z_j = 0$, for all j). Then, Eqs. 5.21, 5.22, 5.23 and 5.24 become

$$A_j = (\, A_{x,j}, \quad A_{y,j}, \quad A_{z,j}\,) = \left(\tfrac{L}{2}, \quad \tfrac{W_j}{2}\cos\beta_j \cdot + Q_j, \quad \tfrac{W_j}{2} \cdot \sin\beta_j\right) \tag{5.26}$$

$$B_j = (\, B_{x,j}, \quad B_{y,j}, \quad B_{z,j}\,) = \left(\tfrac{L}{2}, \quad -\tfrac{W_j}{2}\cos\beta_j \cdot + Q_j, \quad + \tfrac{W_j}{2} \cdot \sin\beta_j\right) \tag{5.27}$$

$$C_j = (\, C_{x,j}, \quad C_{y,j}, \quad B_{z,j}\,) = \left(-\tfrac{L}{2}, \quad -\tfrac{W_j}{2}\cos\beta_j \cdot + Q_j, \quad -\tfrac{W_j}{2} \cdot \sin\beta_j\right) \tag{5.28}$$

$$D_j = (\, D_{x,j}, \quad D_{y,j}, \quad D_{z,j}\,) = \left(-\tfrac{L}{2}, \quad \tfrac{W_j}{2}\cos\beta_j \cdot + Q_j, \quad -\tfrac{W_j}{2} \cdot \sin\beta_j\right) \tag{5.29}$$

To be able to find the points the vertices A_j, B_j, C_j and D_j of the jth reflective element aperture cast their shadow on the $(j - 1)$th reflective element, we must first calculate the equation of the plane formed by the vertices A_{j-1}, B_{j-1}, C_{j-1} and D_{j-1}, of the $(j - 1)$th reflective element aperture, next the equations of the lines corresponding to the Sun's rays passing through the vertices A_j, B_j, C_j and D_j of the jth reflective element and, finally, we must find the intersection points of these lines with the above plane.

The formula describing a line, L, in the three dimensional (3D) space that passes through a point $A_0(x_0, y_0, z_0)$ and is travelling in the direction of the vector $\mathbf{a}(a, b, c) = a \cdot \widehat{\mathbf{i}} + b \cdot \widehat{\mathbf{j}} + c \cdot \widehat{\mathbf{k}}$ is

$$\mathbf{p}(t) = \mathbf{a}_0 + \mathbf{a} \cdot t \tag{5.30}$$

or

$$(x, y, z) = (x_0, y_0, z_0) + (a, b, c) \cdot t \tag{5.31}$$

in vector form,
or

$$x = x_0 + a \cdot t \tag{5.32}$$

$$y = y_0 + b \cdot t \tag{5.33}$$

$$z = z_0 + c \cdot t \tag{5.34}$$

in parametric form,

where t is a scalar parameter describing a particular point $P(x, y, z,)$, with pointing vector $\mathbf{p}$, on the line L, and $\mathbf{a_0}$ is the pointing vector of point A_0. Equations 5.32, 5.33 and 5.34 are basically the equations that results from the three components of the vector form, Eq. 5.31.

On the other hand, if $P_0(x_0', y_0', z_0')$ is a point on a plane which normal vector is $\mathbf{n}$ $(a', b', c') = a' \cdot \hat{\mathbf{i}} + b' \cdot \hat{\mathbf{j}} + c' \cdot \hat{\mathbf{k}}$, then any point $P(x, y, z)$ of the plane satisfies the vector equation of the plane

$$\begin{aligned} &\mathbf{n} \cdot \mathbf{p} = \mathbf{n} \cdot \mathbf{p}_0 \Rightarrow \\ &\mathbf{n} \cdot (\mathbf{p} - \mathbf{p}_0) = 0 \end{aligned} \tag{5.35}$$

where $\mathbf{p}$ and $\mathbf{p_0}$ are the pointing vectors of points P and P_0, respectively.

If we compute the dot product of vectors $\mathbf{n}$, $\mathbf{p}$ and $\mathbf{p_0}$, we get the scalar equation of the plane.

$$\begin{gathered} a' \cdot (x - x_0') + b' \cdot (y - y_0') + c' \cdot (z - z_0') = 0 \Rightarrow \\ a' \cdot x + b' \cdot y + c' \cdot z = a' \cdot x_0' + b' \cdot y_0' + c' \cdot z_0' \Rightarrow \\ a' \cdot x + b' \cdot y + c' \cdot z = d \end{gathered} \tag{5.36}$$

Now, the intersection point of a line and a plane in the three dimensional (3D) space can be found by substituting the parametric formulas for x, y and z of the equation of the line (Eqs. 5.32, 5.33 and 5.34) into the scalar equation of the plane (Eq. 5.36) and solving for t. Then, substituting t into the parametric equations of the line, we can compute the Cartesian coordinates of the point of intersection.

Applying the above-presented procedure to two consecutive reflective elements, j and $j - 1$ (or $j + 1$), we can find the points $A_j', B_j', C_j',$ and D_j', defining the four vertices of the shadow the jth reflective element cast on the plane defined by the $(j - 1)$th reflective element. The next problem is to define whether these points are in or out of the aperture area of the $(j - 1)$th reflective element. However, since the shape of the aperture area of the $(j - 1)$th reflective element is rectangular, which length equals L and its width equals W_{j-1}, we can narrow our study only in this type of shapes, simplifying the required calculations.

Thus, to check if a point $P(x, y, z)$ is inside a rectangle defined by the points A (x_1, y_1, z_1), $B(x_2, y_2, z_2)$, $C(x_3, y_3, z_3)$ and $D(x_4, y_4, z_4)$, we can calculate the perpendicular distances of point $P(x, y, z)$ from the four line segments AB, CD, AD and BC, forming the sides of the rectangle. To be inside the rectangle, the perpendicular distances from AB, P_{AB}, and from CD, P_{CD}, must be less than $|AD| = |BC| = L$, and the perpendicular distances from AD, P_{AD}, and from BC, P_{BC} must be less than $|CD| = |AB| = W$. If one of the perpendicular distances is greater than the respective length, W or L, then the point $P(x, y, z)$ is outside the rectangle. Else if, for example, $P_{AB} = 0$ and $P_{CD} = |AD|$, then the point $P(x, y, z)$ is on AB (Fig. 5.13).

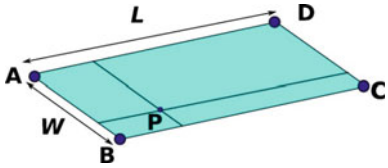

Fig. 5.13 A point $P(x, y, z)$ is inside a rectangle, defined by the points $A(x_1, y_1, z_1)$, $B(x_2, y_2, z_2)$, $C(x_3, y_3, z_3)$, $D(x_4, y_4, z_4)$, if the perpendicular distances of $P(x, y, z)$ from AB, P_{AB}, and from CD, P_{CD}, are less than $|AD| = |BC| = L$, and the perpendicular distances from AD, P_{AD}, and from BC, P_{BC} are less than $|CD| = |AB| = W$. The line segments AB, CD, AD and BC form the sides of the rectangle. If one of the perpendicular distances is greater than the respective length, W or L, then the point $P(x, y, z)$ is outside the rectangle. Else if, for example, $P_{AB} = 0$ and $P_{CD} = |AD|$, then the point $P(x, y, z)$ is on AB

However, the distance, $d_{P\text{-}AB}$, of a point $P(x, y, z)$ from a line passing through the points $A(x_1, y_1, z_1)$, $B(x_2, y_2, z_2)$ is given by the equation (in vector form)

$$d_{P-AB} = \frac{\|\mathbf{AP} \times \mathbf{AB}\|}{\|\mathbf{AB}\|} \tag{5.37}$$

where **AB** is the vector from point B to point A and **AP** is the vector from point P to point A:

$$\mathbf{AB} = (x_2 - x_1, \quad y_2 - y_1, \quad z_2 - z_1) \tag{5.38}$$

$$\mathbf{AP} = (x - x_1, \quad y - y_1, \quad z - z_1) \tag{5.39}$$

In most cases, only one of the points $A'_j, B'_j, C'_j,$ and D'_j defining the four vertices of the shadow the jth reflective element cast on the plane defined by the $(j - 1)$th reflective element falls inside the aperture area of the $(j - 1)$th reflective element, apart from the case where the jth reflective element is substantially narrower or wider than the $(j - 1)$th reflective element. In these cases, two or none shadow vertices fall within the aperture area of the $(j - 1)$th reflective element (Fig. 5.14).

Finally, the shaded width, $W_{\text{shadLoss},j-1}$, of the $(j - 1)$th reflective element, due to the shadow casted on it from the jth reflector, is equal to one of the perpendicular distances of the shadow vertex falling within the $(j - 1)$th reflective element from its two longer edges. Which one of these two distances corresponds to the shaded width, $W_{\text{shadLoss},j-1}$, depends on Sun's transversal angle, θ_T. If it is lower than 90°, then the shaded width, $W_{\text{shadLoss},j-1}$, corresponds to the perpendicular distance of the shadow vertex from the "eastern" edge of the $(j - 1)$th reflective element. On the other hand, if Sun's transversal angle, θ_T, is higher than 90°, then the shaded width, $W_{\text{shadLoss},j-1}$, corresponds to the perpendicular distance of the shadow vertex from the "western" edge of the $(j - 1)$th reflective element (Fig. 5.15).

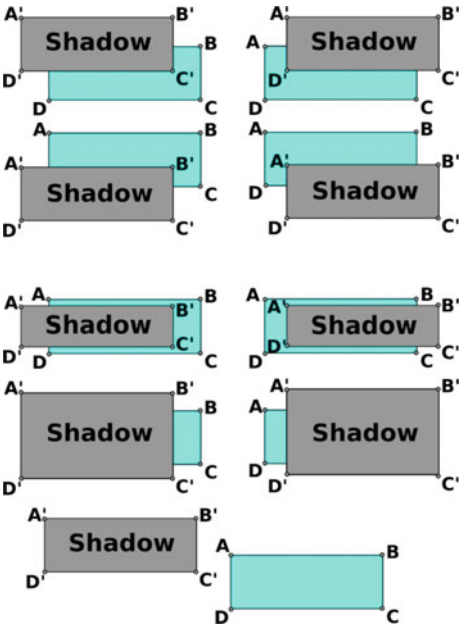

Fig. 5.14 In most cases, only one of the points $A'_j, B'_j, C'_j,$ and D'_j defining the four vertices of the shadow the jth reflective element cast on the plane defined by the $(j-1)$th reflective element falls inside the aperture area of the $(j-1)$th reflective element. However, if the jth reflective element is substantially narrower or wider than the $(j-1)$th reflective element, then two or none shadow vertices fall within the aperture area of the $(j-1)$th reflective element

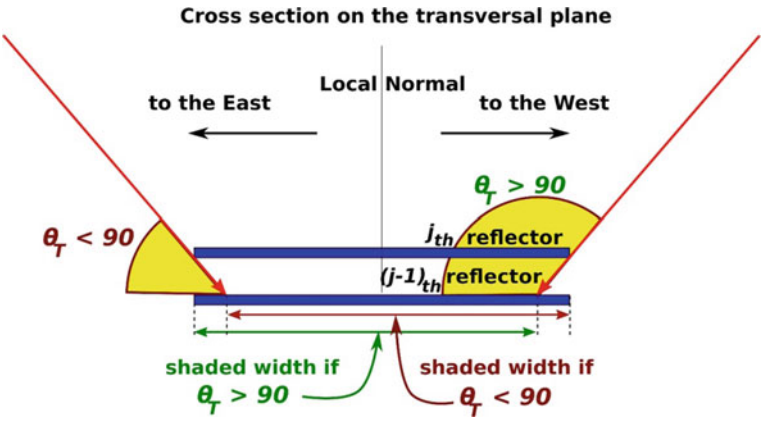

Fig. 5.15 Shaded width of the $(j-1)$th reflective element, due to the shadow casted on it from the jth reflector, depends on Sun's transversal angle, θ_T. (a) If it is lower than 90°, then the "eastern" part of the $(j-1)$th reflective element is shaded. On the other hand, (b) if Sun's transversal angle, θ_T, is higher than 90°, then its "western" part is shaded

5.2.1.3 Shaded Length

We can calculate the shaded length, $L_{\text{shadLoss},j-1}$, of the $(j-1)$th reflective element, applying the methodology used for the calculation of the shaded width, $W_{\text{shadLoss},j-1}$. However, in this case, there is a substantial difference. A part of the length of the reflective elements does not contribute to the solar radiation concentration due to the end loss effect, as it will be studied extensively in Sect. 5.3 and is illustrated in Fig. 5.9. This part of the length, $L_{\text{endLoss},j-1}$, of the $(j-1)$th reflective element will be partially shaded too. However, if we do not take into account the phenomenon of end loss, we will overestimate the shading losses of the System. Therefore, we have to exclude the end loss length, $L_{\text{endLoss},j-1}$, from the shaded length, $L_{\text{shadLoss},j-1}$, calculated with the methodology used for the calculation of the shaded width, $W_{\text{shadLoss},j-1}$, by introducing an effective shaded length, $L_{\text{ef,shadLoss},j-1}$:

$$L_{\text{ef,shadLoss},j-1} = L_{\text{shadLoss},j-1} - L_{\text{endLoss},j-1} \tag{5.40}$$

According to the above methodology, the shaded length, $L_{\text{shadLoss},j-1}$, of the $(j-1)$th reflective element, due to the shadow casted on it from the jth reflector, is equal to one of the perpendicular distances of the shadow vertex being inside the aperture area of the $(j-1)$th reflector from its two narrower edges. Which one of these two distances correspond to the shaded Length, $L_{\text{shadLoss},j-1}$, depends on Sun's longitudinal angle, θ_L. If it is lower than 90°, then the shaded length, $L_{\text{shadLoss},j-1}$, corresponds to the perpendicular distance of the shadow vertex from the "southern" edge of the $(j-1)$th reflective element. On the other hand, if Sun's longitudinal angle, θ_L, is higher than 90°, then the shaded length, $L_{\text{shadLoss},j-1}$, corresponds to the perpendicular distance of the shadow vertex from the "northern" edge of the $(j-1)$th reflective element (Fig. 5.16).

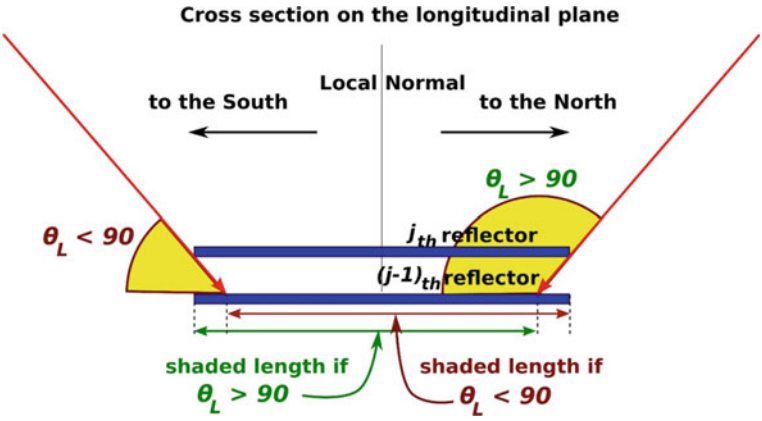

Fig. 5.16 Shaded length of the $(j-1)$th reflective element, due to the shadow casted on it from the jth reflector, depends on Sun's longitudinal angle, θ_L. (a) If it is lower than 90°, then the "southern" part of the $(j-1)$th reflective element is shaded. On the other hand, (b) if Sun's longitudinal angle, θ_L, is higher than 90°, then its "northern" part is shaded

5.2.1.4 Shading Loos Ratio and Shading Efficiency

The aperture area of the *j*th reflector that remains unused due to shading effect, the shaded area, $A_{\text{shadLoss},j}$, can be calculated as the product of the corresponding effective shaded length, $L_{\text{shadLoss},j}$, and the shaded width, $W_{\text{shadLoss},j}$,

$$A_{\text{shadLoss},j} = L_{\text{shadLoss},j} \cdot W_{\text{shadLoss},j} \tag{5.41}$$

The shading loss ratio, $fA_{\text{shadLoss},j}$, is equal to

$$fA_{\text{shadLoss},j} = \frac{A_{\text{shadLoss},j}}{A_j} \tag{5.42}$$

and its percentage value, the relative shaded area, is

$$pfA_{\text{shadLoss},j} = \frac{A_{\text{shadLoss},j}}{A_j} \cdot 100\% \tag{5.43}$$

where A_j is the aperture area of the *j*th reflector given by the equation

$$A_j = L_j \cdot W_j = L \cdot W_j \tag{5.44}$$

where L and W_j are the constructions (common) length and width of the reflective elements.

Finally, the total average relative shaded area loss, $\overline{fA}_{\text{shadLoss}}$, of the System is

$$\overline{fA}_{\text{shadLoss}} = \frac{1}{N} \cdot \sum_{j=1}^{N} fA_{\text{shadLoss},j-1} \tag{5.45}$$

or

$$\overline{fA}_{\text{shadLoss}} = \frac{1}{2 \cdot n} \cdot \sum_{j=-n(j\neq 0)}^{n} fA_{\text{shadLoss},j-1} \tag{5.46}$$

or

$$\overline{fA}_{\text{shadLoss}} = \frac{1}{2 \cdot n + 1} \cdot \sum_{j=-n}^{n} fA_{\text{shadLoss},j-1} \tag{5.47}$$

On the other hand, the shading efficiency, η_{shading}, of the System is defined as the aperture area of the reflectors which contributes to the solar radiation concentration

divided by the total aperture area of all reflectors. Alternatively, it can be calculated by the equations

$$\eta_{\text{shading},j} = 1 - fA_{\text{shadLoss},j} \tag{5.48}$$

$$\eta_{\text{shading}} = 1 - \overline{fA}_{\text{shadLoss}} \tag{5.49}$$

5.2.2 *Blocking Effect*

5.2.2.1 Reflectors Blocked Area

The aperture area, $A_{\text{blockLoss},j}$, of the jth reflector that remains unused due to blocking effect is also shown in Fig. 5.9. In fact, this area is trapezoidal, as in the case of the shading effect. However, it can be assumed to be rectangular without loss of generality and without introducing significant error (Sharma et al. 2015a, b, c). If we define $L_{\text{blockLoss},j}$ and $W_{\text{blockLoss},j}$ as the corresponding length and width of this area, then the aperture loss area of the jth reflector which remains unused due to the blocking effect, $A_{\text{blockLoss},j}$, can be written as

$$A_{\text{blockLoss},j} = L_{\text{blockLoss},j} \cdot W_{\text{blockLoss},j} \tag{5.50}$$

However, it must be noted that a part of the jth reflector that remains unused due to blocking effect may also contribute to end losses and thus be admeasured twice. This is the same problem as with shading effect and has already been dealt with in Sect. 5.2.1.3, where the shaded length, $L_{\text{shadLoss},j}$, is calculated. We can apply the same approach when calculating the blocked area.

In the previous paragraphs, we studied the shading effect by calculating the shaded width, $W_{\text{shadLoss},j-1}$, and the shaded length, $L_{\text{shadLoss},j-1}$, of the $(j-1)$th reflective element due to the shadow casted on it from the jth reflector. In general, we can use the same methodology to study the blocking effect the jth reflector may have on the reflected solar radiation of the $(j-1)$th reflective element. The principal difference is that in the first case we used the Sun's position vector, $\mathbf{S}$, while now we have to replace it with the vector determining the direction of the reflected solar radiation, the reflected Sun's rays vector, $\mathbf{R_j}$.

The direction of the solar radiation reflected by the jth reflector, vector $\mathbf{R_j}$, can be calculated using the vector form of the law of reflection. Thus, Sun's position vector, $\mathbf{S}$, coinciding with the incoming solar radiation, the normal unit vector on the jth reflective element, $\mathbf{n_j}$, and the vector $\mathbf{R_j}$ satisfy the equation:

$$\mathbf{R_j} = \mathbf{S} - 2 \cdot \left(\mathbf{S} \cdot \mathbf{n_j}\right) \cdot \mathbf{n_j} \tag{5.51}$$

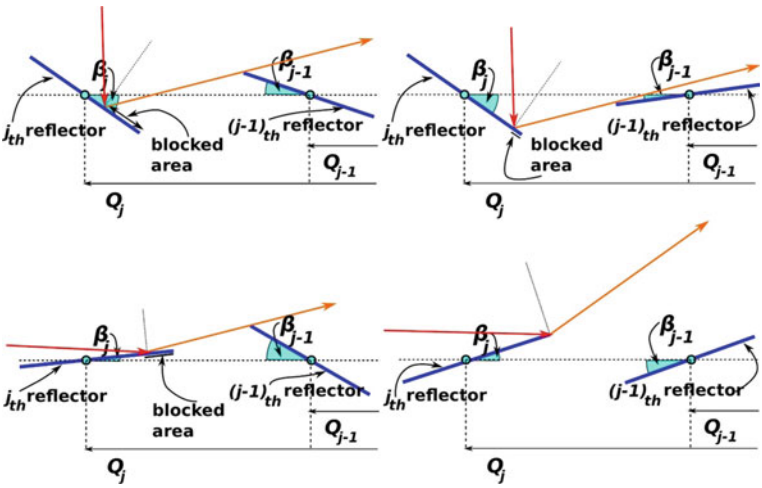

Fig. 5.17 Possible positions of adjacent reflective elements that affect the blocking effect

As in the case of shadowing between adjacent reflectors, blocking effect, apart from the distance between adjacent reflectors, also depends on reflectors angular position, β_j. Figure 5.17 illustrates a number of possible cases.

5.2.2.2 Blocking Loos Ratio and Blocking Efficiency

The definition and calculation of the aperture area of the jth reflector that remains unused due to blocking effect, the blocked area, $A_{\text{blockLoss},j}$, the relative blocked area, $fA_{\text{blockLoss},j}$, the blocking loss ratio and the blocking efficiency, η_{blocking}, of the System are similar to that presented in Sect. 5.2.1.4.

5.2.3 *Effect of Sun's Finite Size on Shading and Blocking*

In the previous paragraph, we assumed that Sun was a point source. However, Sun has a nonzero finite size, and despite its small angular diameter ($\delta = 31'59'' \approx 32'$), the reflected rays do diverge, although not very much. This may influence the reflectors shaded area (width and length), or the reflected solar radiation blocked area (width and length), depending on the distance between the adjacent reflectors. Figure 5.18 shows two different cases of reflectors area loss due to shading, when Sun is considered as a disc and not a point. In the first case, the diverging incoming solar radiation falls completely on the reflector aperture, while in the second case, one part of it falls outside the reflector. Due to the non-uniform distribution of solar radiation across Sun's cross section, in the first case, there is a partial energy gain

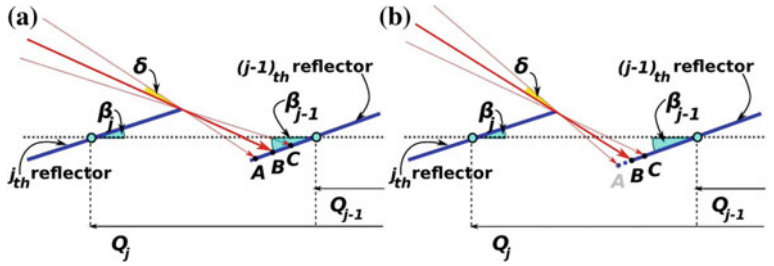

Fig. 5.18 Sun's finite size may influence the reflectors shaded width, or the reflected solar radiation blocked width, depending on the distance between the adjacent reflectors and their inclination angle

from the solar radiation falling on the line segment *AB* and a partial energy loss from the solar radiation falling on the line segment *BC*. However, since both energy gains and losses amounts are equal, the net effect is nullified. On the other hand, in the second case, the shading effect gets marginally affected, but this occurs for a very short time period. Consequently, the shading effect can accurately enough be estimated by considering only the central ray from Sun's disc. Similarly, blocking effect can also be estimated accurately enough by treating Sun as a point light source (Sharma et al. 2015c).

5.2.4 Shading and Blocking Effects Evaluation

According to Montes et al. (2014), shading is greater for denser mirror fields (higher filling factor) and higher receiver's height. In fact, the filling factor affects the shading losses more than the receiver height. On the other hand, blocking is comparatively less important than shading. Blocking effect increases as filling factor increases and receiver height decreases. In addition, the receiver height has a greater influence on the blocking than on shading effect.

However, if we define the optical efficiency of a Linear Fresnel Reflector System as the ratio between the solar radiation received by the receiver and the incoming solar radiation incident on the Systems aperture, the optical efficiency of a dense solar field, with high shading and blocking losses, is higher than that for a solar field with lower filling factor and, therefore, with lower shading and blocking losses. This is an inherent drawback of the optical efficiency definition, as Sun's rays falling on the gaps between two consecutive reflectors are considered as losses, while a shaded reflective element, or the blocked reflected radiation, is not, because the incoming solar radiation is directed towards the receiver by being reflected by the adjacent reflector, the reflector causing the shading of blocking effect. Nevertheless, this leads to material waste, increasing investments cost. Lastly, the lower the receiver height, the lower the end losses, as well as the solar radiation

dispersion due to Sun's finite size (as we will see in the next paragraph). Therefore, in order to obtain a maximum optical efficiency, we have to choose that receiver height, which leads in equilibrium among shading, blocking and end losses (Montes et al. 2014).

5.3 End Losses

Small-scale Solar Radiation Concentrating Systems based on Linear Fresnel Reflectors are suitable for heating or cooling of buildings, domestic water heating, steam generation for mining, hot water for food, textile and chemical industries, industrial heat processes, agriculture and timber uses (Hongn et al. 2015). In contrast to large-scale Systems, they are usually set up on rooftops, or areas surrounding industrial installations, and often their size is restricted by the available land or roof area, and therefore, they have to be accordingly adjusted. This leads to a variety of different receiver lengths. In addition, the orientation of the System may differ, more or less, from the optimum for maximal yield (North–South orientation). On the other hand, as they have a smaller size, they allow a higher degree of premanufacturing and ease of on-site installation, reducing potential optical error sources (e.g. shape and slope errors of the reflector, tracking errors or displacement of the receiver).

However, the optical efficiency of these Systems is affected by end losses, since a part of the receiver may not be illuminated by the solar radiation reflected by the primary reflectors, the solar field, due to the nonzero incidence angle of Sun's rays in the axial (or longitudinal) direction of the System. Due to Sun's move in the sky, the end losses, the non-illuminated length of the receiver, depend on the site's latitude, the System's size (small-/large-scale installation), the System's orientation (e.g. North–South orientation), the reflectors' arrangement, as well as the time (month, day and hour) when it is evaluated (Zhu et al. 2016).

End losses have significant influence (reduction) on the System's overall efficiency, when the end loss length, L_{recEnd}, constitutes an important part of the receiver length, and are higher in low solar altitude angles, h. This is more significant in regions with high latitude, φ. In addition, in small-scale Systems, like those installed on rooftops, the end losses ratio, f_{recEnd}, is more important than that in large-scale Systems. The solar radiation received by the absorber may be substantially lower than that reflected by the reflective elements (Li et al. 2015) due to the finite length of the receiver. Depending on construction's features, the phenomenon of end losses may cause the reflected solar radiation to completely miss the receiver early in the mornings and late in the afternoons. In winter days, these periods are longer (Hongn et al. 2015).

In small-scale Systems, end losses should always be considered and, if possible, be reduced or mitigated by appropriate measures, such as end mirrors, extended receiver length, increased length of the solar field (increased length of the reflectors), inclined aperture plane, or two-axis Sun-tracking mechanisms (Zhu et al.

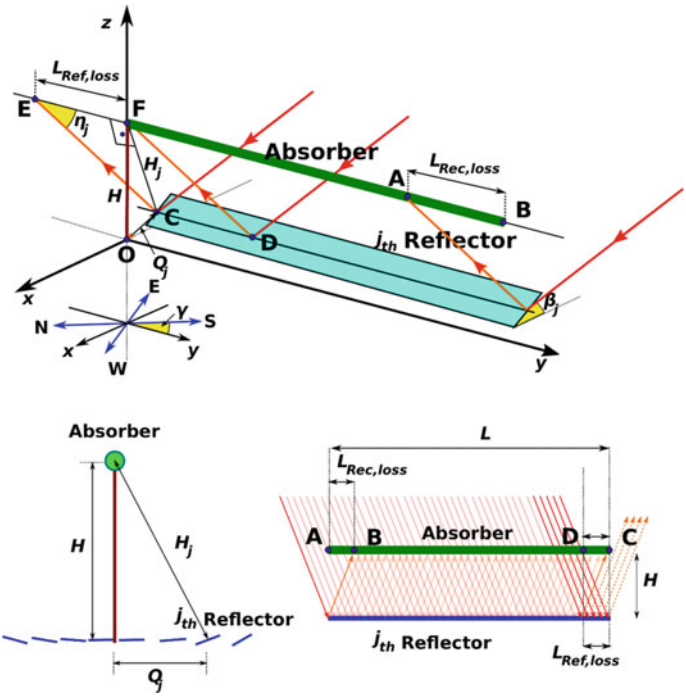

Fig. 5.19 Schematic representation of end losses of a Linear Fresnel Reflector System and the geometry governing the calculations

2016; Li et al. 2015). The first three methods solve the problem of end losses by adding more materials (larger receiver, or reflectors, or additional reflectors), while the last two methods change the mechanical structure of the System (inclined aperture plane or dual-axis tracking mechanism). In addition, a movable receiver has been proposed by Zhu et al. (2016) to reduce end losses. In the case of several Subsystems in a row, end losses can partially be counterbalanced because a part of the solar radiation reflected by the reflectors of one Subsystem hits the non-irradiated part of the receiver of the next Subsystem. Thus, a fraction of the end losses can be compensated by end gains (Eck et al. 2014).

In small-scale Solar Radiation Concentrating Systems, the shape and the orientation of the available land, or rooftop, do not always allow an ideal North–South orientation. As a consequence, we cannot take advantage of the System's symmetry, as well as Sun's symmetrical motion in the sky. Therefore, the analysis of end losses should cover a wide range of possible orientations or better to be conducted for an arbitrarily oriented system.

To estimate the end loss length, L_{recEnd}, the part of the receiver that is not irradiated and consequently does not contribute to heat production, and the corresponding end loss factor, f_{recEnd}, of a Linear Fresnel Reflector System, the receiver length, L, and the receiver height, H, the horizontal distance, Q_j, of the j reflector

from the projection of the centreline of the receiver on the reflectors plane and the site latitude, φ, are necessary.

The end loss length, $L_{\text{recEnd},j}$, of the receiver due to the jth reflector can be estimated using pure geometrical consideration (triangle ECF in Fig. 5.19). It is equal to (Eck et al. 2014; Bachelier and Stieglitz 2017; Zhu et al. 2016)

$$\begin{aligned} \tan\eta_j &= \frac{H_j}{L_{\text{recEnd},j}} \Rightarrow \\ L_{\text{recEnd},j} &= \frac{H_j}{\tan\eta_j} \Rightarrow \\ L_{\text{recEnd},j} &= \frac{\sqrt{Q_j^2 + H^2}}{\tan\eta_j} \end{aligned} \tag{5.52}$$

where H_j is the distance between the jth reflective element and the receiver, and η_j is the angle between the direction of the reflected solar radiation by the jth reflector (denoted by the vector $\mathbf{R}_j$) and the direction of the receiver, denote by the vector $\mathbf{l_{rec}}$, which is determined by its two edges (Fig. 5.19).

The end losses are caused due to the nonzero longitudinal component of the incoming solar radiation (of the solar vector, $\mathbf{S}$). Nevertheless, in this case, we cannot use Sun's longitudinal angle, θ_L, to calculate its effect on the reflected Sun's rays. We may have used the transversal component of Sun's position in the sky, $\mathbf{S_T}$ (its transversal angle, θ_T), when we were calculating the reflectors' inclination angle, β_j, in Chap. 4, Sect. 4.3.2, and the shading and blocking effects (shaded and blocked width), in previous paragraphs, but this was there feasible, as the transversal component of Sun's position vector in the sky, $\mathbf{S_T}$, the normal vector on reflectors' surface, $\mathbf{n_j}$, and the position (or direction) vector of the receiver $\mathbf{r_j}$ in respect to the jth reflective element are always on the same plane. This plane does not change its direction and is always perpendicular to the longitudinal axis of the Linear Fresnel Reflector System. In other words, it always coincides with the transversal plane of the System. Actually, despite the fact that the normal vector on reflectors' surface, $\mathbf{n_j}$, always changes its direction during the day, as the reflective elements are constantly rotated, the latter are arranged in such a way that the position (or direction) vectors of the receiver, $\mathbf{r_j}$, in respect to each of them to remain constant and to coincide with the direction of the transversal component of the reflected solar radiation, $\mathbf{R_{T,j}}$, $\mathbf{R_{T,j}} = \mathbf{r_j}$. As a result, according to the law of reflection, the three vectors $\mathbf{S_T}$, $\mathbf{n_j}$ and $\mathbf{R_{T,j}} = \mathbf{r_j}$ are always on the same plane, which in this case is constant.

However, on the other hand, the longitudinal component of Sun's position vector in the sky, $\mathbf{S_L}$, the normal vector on reflectors' surface, $\mathbf{n_j}$, and the position (or direction) vector of the receiver $\mathbf{r_j}$ in respect to each reflective element are principally not on the same plane. This means that the longitudinal component of the reflected solar radiation, $\mathbf{R_{L,j}}$, do not coincide with the position (or direction) vector of the receiver $\mathbf{r_j}$, $\mathbf{R_{L,j}} \neq \mathbf{r_j}$. Therefore, in order to be able to accurately calculate the end loss length, $L_{\text{recEnd},j}$, we cannot use simply Sun's longitudinal angle, θ_L, despite the fact that the end losses are caused due to the nonzero longitudinal component of the incoming solar radiation.

To calculate angle η_j, we must first calculate the direction of the vector corresponding to the reflected solar radiation. According to the vector form of the law of reflection, Sun's position vector, **S** (coinciding with the incoming solar radiation), the normal unit vector on the *j*th reflective element, $\mathbf{n_j}$, and the direction of the reflected solar radiation from the *j*th reflector, $\mathbf{R_j}$, are on the same plane and satisfy the equation:

$$\mathbf{R_j} = \mathbf{S} - 2 \cdot \left(\mathbf{S} \cdot \mathbf{n_j}\right) \cdot \mathbf{n_j} \tag{5.53}$$

Now, angle η_j can be computed by the dot (or scalar) product of vectors $\mathbf{R_j}$ and $\mathbf{l_{rec}}$, the direction vectors of the reflected solar radiation and the receiver:

$$\cos \eta_j = \frac{\mathbf{R_j} \cdot \mathbf{l_{rec}}}{\left\|\mathbf{R_j}\right\| \cdot \left\|\mathbf{l_{rec}}\right\|} \tag{5.54}$$

The unit vector pointing to Sun, **S**, in the horizontal coordinate system is determined by the azimuth angle, *A*, and the height, or altitude, angle, *h*, as it has been already presented in Chap. 2, Sect. 2.5, by the equation

$$\mathbf{S} = \cos A \cdot \cos h \cdot \hat{\mathbf{i}} - \sin A \cdot \cos h \cdot \hat{\mathbf{j}} + \sin h \cdot \hat{\mathbf{k}} \tag{5.55}$$

Similarly, for a reflective element with inclination angle β_j, and azimuth angle γ_j, its unit normal vector, $\mathbf{n_j}$, is given by

$$\mathbf{n_j} = \cos\gamma_j \cdot \sin\beta_j \cdot \hat{\mathbf{i}} - \sin\gamma_j \cdot \sin\beta_j \cdot \hat{\mathbf{j}} + \cos\beta_j \cdot \hat{\mathbf{k}} \tag{5.56}$$

(do not confuse the index *j*, denoting the reflective element, with the unit vector $\hat{\mathbf{j}}$, or the **j** component of a vector).

For an arbitrarily oriented Linear Fresnel Reflector System, with orientation angle equal to γ (γ = 0° due South), the two receiver edges, A_{rec} and B_{rec}, (being considered as a line segment) have the following coordinates (according to Figs. 5.7 and 5.12),

$$A_{\text{rec}} = \left(\tfrac{L}{2} \cdot \cos\gamma, \quad -\tfrac{L}{2} \cdot \sin\gamma, \quad \text{H}\right) \tag{5.57}$$

$$\text{B}_{\text{rec}} = \left(-\tfrac{L}{2} \cdot \cos\gamma, \quad \tfrac{L}{2} \cdot \sin\gamma, \quad \text{H}\right) \tag{5.58}$$

The corresponding receiver vector, $\mathbf{l_{rec}}$, is

$$\mathbf{l_{rec}} = \mathbf{B_{rec}A_{rec}} = \mathbf{r}_{\mathbf{A_{rec}}} - \mathbf{r}_{\mathbf{B_{rec}}} \tag{5.59}$$

where $\mathbf{r}_{\mathbf{A}_{\mathbf{rec}}}$ and $\mathbf{r}_{\mathbf{B}_{\mathbf{rec}}}$ are the pointing vectors

$$\mathbf{r}_{\mathbf{A}_{\mathbf{rec}}} = \frac{L}{2} \cdot \cos\gamma \cdot \hat{\mathbf{i}} - \frac{L}{2} \cdot \sin\gamma \cdot \hat{\mathbf{j}} + \mathrm{H} \cdot \hat{\mathbf{k}} \tag{5.60}$$

$$\mathbf{r}_{\mathbf{B}_{\mathbf{rec}}} = -\frac{L}{2} \cdot \cos\gamma \cdot \hat{\mathbf{i}} + \frac{L}{2} \cdot \sin\gamma \cdot \hat{\mathbf{j}} + \mathrm{H} \cdot \hat{\mathbf{k}} \tag{5.61}$$

of points A_{rec} and B_{rec}.

Substituting Eqs. 5.60 and Eq. 5.61 into Eq. 5.59, it gives

$$\mathbf{l}_{\mathbf{rec}} = L \cdot \cos\gamma \cdot \hat{\mathbf{i}} + L \cdot \sin\gamma \cdot \hat{\mathbf{j}} + 0 \cdot \hat{\mathbf{k}} \tag{5.62}$$

and

$$\begin{gathered} \|\mathbf{l}_{\mathbf{rec}}\| = \sqrt{(L \cdot \cos\gamma)^2 + (L \cdot \sin\gamma)^2} \Rightarrow \\ \|\mathbf{l}_{\mathbf{rec}}\| = \sqrt{L^2 \cdot \cos^2\gamma + L^2 \cdot \sin^2\gamma} \Rightarrow \\ \|\mathbf{l}_{\mathbf{rec}}\| = \sqrt{L^2 \cdot \left(\cos^2\gamma + \sin^2\gamma\right)} \Rightarrow \\ \|\mathbf{l}_{\mathbf{rec}}\| = L \end{gathered} \tag{5.63}$$

Substituting Eqs. 5.55 and 5.56 into Eq. 5.53, and then the result of Eqs. 5.53 and 5.62 into Eq. 5.54 and performing the calculus, we can calculate the cosine of angle η_j. Next, using the trigonometric identity

$$\begin{gathered} \cos^2\varphi = \frac{1}{1 + \tan^2\varphi} \Rightarrow \\ \tan\varphi = \pm\sqrt{\frac{1}{\cos^2\varphi} - 1} \end{gathered} \tag{5.64}$$

where φ is any angle different from 90° ($\varphi \neq 90° \Rightarrow \cos\varphi \neq 0$), we can compute the tangent of angle η_j.

Finally, substituting Eq. 5.64 into Eq. 5.52, we can compute the end loss length, $L_{\mathrm{recEnd},j}$, of the receiver length, L, related to the jth reflective element.

As it can be seen from Fig. 5.19, the reflective elements' and the receiver's longitudinal directions are parallel. In addition, Sun's rays remain parallel after being reflected by the reflectors. In other words, they form a parallelogram and consequently the line segments AB and CD are equal. Therefore, the length loss $L_{\mathrm{EndLoss},j}$, of the jth reflective elements is equal to the receiver end loss length, $L_{\mathrm{recEnd},j}$, due to the jth reflective elements:

$$L_{\mathrm{EndLoss},j} = L_{\mathrm{recEnd},j} \tag{5.65}$$

On the other hand, the width loss $W_{\text{EndLoss},j}$ of the jth reflective elements due to the end loss effect is considered equal to its width, W_j:

$$W_{\text{endLoss},j} = W_j \tag{5.66}$$

The aperture area, $A_{\text{endLoss},j}$, of jth reflector that remains unused due to end loss effect is shown in Fig. 5.9. This area is deemed rectangle. If we assume that $L_{\text{endLoss},j}$ and $W_{\text{endLoss},j}$ are its length and width, then the aperture loss area of the jth reflector due to the end loss effect, $A_{\text{endLoss},j}$, can be written as

$$A_{\text{endLoss},j} = L_{\text{endLoss},j} \cdot W_{\text{endLoss},j} = L_{\text{endLoss},j} \cdot W_j \tag{5.67}$$

The receiver end loss length, $L_{\text{recEnd},j}$, can take positive or negative values depending on whether the non-illuminated length is shifted towards North or South, for a North–South-oriented system (positive or negative values of the angle η_j), respectively. Its magnitude (absolute value), $|L_{\text{recEnd},j}|$, increases when the horizontal distance, Q_i, of the reflective element from the projection of the centreline of the receiver on the reflectors plane increases and is larger for higher latitudes. In addition, at locations on the northern hemisphere, this length is always shifted towards South ($L_{\text{recEnd},j} < 0$) in winter, while, in summer, it depends on the site latitude and the time of the day and the day of the year.

The receiver end losses factor, $f_{\text{recEnd},j}$, or end losses ratio due to the jth reflector is defined as the relative ratio of the non-illuminated fraction of the receiver length and is calculated from the following equation (Heimsath et al. 2014; Bachelier and Stieglitz 2017)

$$f_{\text{recEnd},j} = \frac{\left|L_{\text{recEnd},j}\right|}{L} \tag{5.68}$$

At this point, it must be noted that the end loss length, $L_{\text{recEnd},j}$, can take values higher than L, the receiver length. In this case, the end losses factor, $f_{\text{recEnd},j}$, is larger than unit. Therefore, as the end losses factor, $f_{\text{recEnd},j}$, can take values only between 0 and 1: $0 \leq f_{\text{recEnd},j} \leq 1$, Eq. 5.68 must be rewritten in the following form:

$$f_{\text{recEnd},j} = \begin{cases} \frac{\left|L_{\text{recEnd},j}\right|}{L}, & \text{if } 0 \leq \left|L_{\text{recEnd},j}\right| \leq L \\ 1, & \text{if } \left|L_{\text{recEnd},j}\right| > L \end{cases} \tag{5.69}$$

As it can be seen from Eqs. 5.52 and 5.69, the end loss length, $L_{\text{recEnd},j}$, does not depend on the receiver length L, whereas the end loss factor, $f_{\text{recEnd},j}$, do depend on it. In addition, as the end loss factor, $f_{\text{recEnd},j}$, depends on the inverse value of the receiver length, L, we can easily conclude that shorter receivers suffer higher end losses (Hongn et al. 2015).

Equations 5.52 and 5.69 provide the end loss length, $L_{\text{recEnd},j}$, and the end loss factor, $f_{\text{recEnd},j}$, due to the effect each individual reflective element has on the

System, at a particular time point of the day (instantaneous values). Hence, in order to compute the average instantaneous contribution of all reflected elements (the instantaneous average end loss length, $\overline{L}_{\text{recEnd}}$, and the instantaneous average end loss factor, $\overline{f}_{\text{recEnd}}$), Eqs. 5.52 and 5.69 have to be summed up over all individual values $f_{\text{recEnd},j}$, $f_{\text{recEnd},j}$, and then be divided by the total number of the reflective elements, N(=2 · n, or = 2 · n + *1*):

$$\overline{L}_{\text{recEnd}} = \frac{1}{N} \cdot \sum_{j=1}^{N} L_{\text{recEnd},j} \tag{5.70}$$

or

$$\overline{L}_{\text{recEnd}} = \frac{1}{2 \cdot n} \cdot \sum_{j=-n(j\neq 0)}^{n} L_{\text{recEnd},j} \tag{5.71}$$

or

$$\overline{L}_{recEnd} = \frac{1}{2 \cdot n + 1} \cdot \sum_{j=-n}^{n} L_{recEnd,j} \tag{5.72}$$

and

$$\bar{f}_{\text{recEnd}} = \frac{1}{N} \cdot \sum_{j=1}^{N} f_{\text{recEnd},j} \tag{5.73}$$

or

$$\overline{f}_{\text{recEnd}} = \frac{1}{2 \cdot n} \cdot \sum_{j=-n(j\neq 0)}^{n} f_{\text{recEnd},j} \tag{5.74}$$

or

$$\overline{f}_{\text{recEnd}} = \frac{1}{2 \cdot n + 1} \cdot \sum_{j=-n}^{n} f_{\text{recEnd},j} \tag{5.75}$$

Both parameters, the receiver end loss length, $L_{\text{recEnd},j}$, and the receiver end loss factor, $f_{\text{recEnd},j}$, are very useful in designing a (in particular small scale) Solar Radiation Concentrating System with Linear Fresnel Reflectors. For a given System geometry, they determine the absolute and the relative value of the non-illuminated length of the receiver, providing an estimation of the efficiency of the System. The receiver end loss efficiency, η_{end}, of the System (which is equal to the reflectors end

loss efficiency) is defined as the illuminated fraction of the receiver and alternatively can be calculated by the equations

$$\eta_{\text{end},j} = 1 - f_{\text{recEnd},j} \tag{5.76}$$

$$\eta_{\text{end}} = 1 - \overline{f}_{\text{recEnd}} \tag{5.77}$$

5.4 Cosine Effect

In order a Solar Radiation Concentrating System to be able to use the most possible direct solar radiation falling on it, it must have its aperture perpendicular to Sun's rays. In other words, its efficiency depends on the angle between Sun's rays and the normal on reflectors' aperture. As the incident angle deviates from the right angle, becoming smaller than this value, the reflected solar radiation is always lower than the maximum available for normal incidence (cosine effect losses).

Let us consider a reflector which surface faces Sun (its aperture is normal to Sun's rays). In this case, the direct solar radiation falling on it will be E_0, the maximum possible. However, if its surface is not normal to Sun's rays, the solar radiation falling on it will be reduced by the cosine of the angle between the surface normal and Sun's rays (it has been explicitly studied in Chap. 2, Sect. 2.3.3, Fig. 2.4). The energy, E_j, striking now the jth reflector is equal to the cosine of the incident angle, ε_j, times the potential maximum energy, E_0, if there were normal incidence on the reflector:

$$E_j = E_0 \cos \varepsilon_j \tag{5.78}$$

The cosine of the incident angle, ε_j, provides the name for this effect (Fig. 5.20).

The cosine effect is of high importance in optimizing the efficiency of Linear Fresnel Reflector Systems, as the latter depends on both Sun's position and the location of the individual reflective elements in relation to the receiver position. However, this is an inherent drawback of these Systems and we must try to mitigate it by proper designing of the solar field (reflective elements arrangement).

The solar radiation, E_j, reflected by the jth reflector depends on the solar irradiance, I_0, and the reflector aperture area, A_j:

$$E_j = I_0 \cdot A_j \cdot \cos \varepsilon_j \tag{5.79}$$

Instead of Sun's zenith angle, θ_z, or Sun's elevation angle, h, we can use its transversal angle, θ_T, and compute the angle of incidence, ε_j, on the transversal plane of the System. This is feasible as cosine effect is important only in the narrower dimension of the reflective elements, because the reflectors are arranged

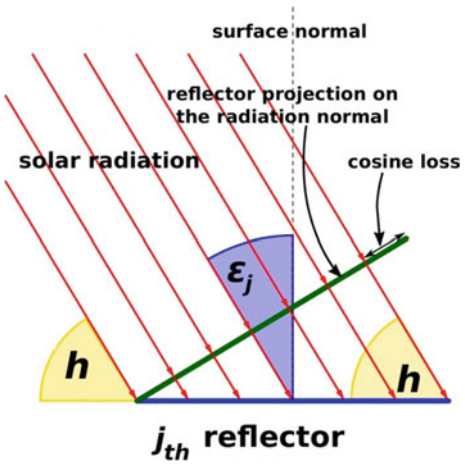

Fig. 5.20 Reduction of the available solar radiation due to not normal incidence is called the cosine effect. The solar energy falling on the reflector and on its projection on the normal on the propagation direction is the same. However, the area of the reflector is larger than its projection, making the solar energy per unit area and time unit falling on it lesser

so that their surface normal to bisect the angle between the transversal component of Sun's rays and the line drawn from each reflector to the receiver (being perpendicular to both of them). The longitudinal component of Sun's position contributes to the end loss effect and has been taken into account in the previous paragraphs when studying the corresponding loss effect.

Making advantage of the geometry presented in Fig. 5.6 and incorporating the appropriate receiver and reflector position coordinates, the following expression of this angle, ε_j, can be derived

$$\varepsilon_j = 90^{\circ} + \beta_j - \xi_j \tag{5.80}$$

where β_j is the inclination angle of the reflective elements and ξ_j is the angle the position vector of the receiver $\mathbf{r_j}$ in respect to the *j*th reflective element forms with the horizontal plane. Using Eq. 4.17 of Chap. 4 and substituting it in Eq. 5.80, it becomes

$$\varepsilon_j = 90^{\circ} - \frac{1}{2}\tan^{-1}\left(\frac{H}{Q_j}\right) - \frac{\theta_T}{2} \tag{5.81}$$

The cosine effect can be visualized by considering two reflectors at opposite positions in relation to the receiver and the transversal component of Sun's position in the sky (Fig. 5.21). Reflector A has a small cosine loss since its surface normal is almost pointing towards the receiver, while reflector B has a larger cosine loss. As it can be seen from Fig. 5.21, and from Eq. 5.81, the reflectors having the receiver between them and the Sun are the most efficient. This is the reason why most of the reflectors should be positioned North of the receiver in an East–West-oriented Linear Fresnel Reflector System.

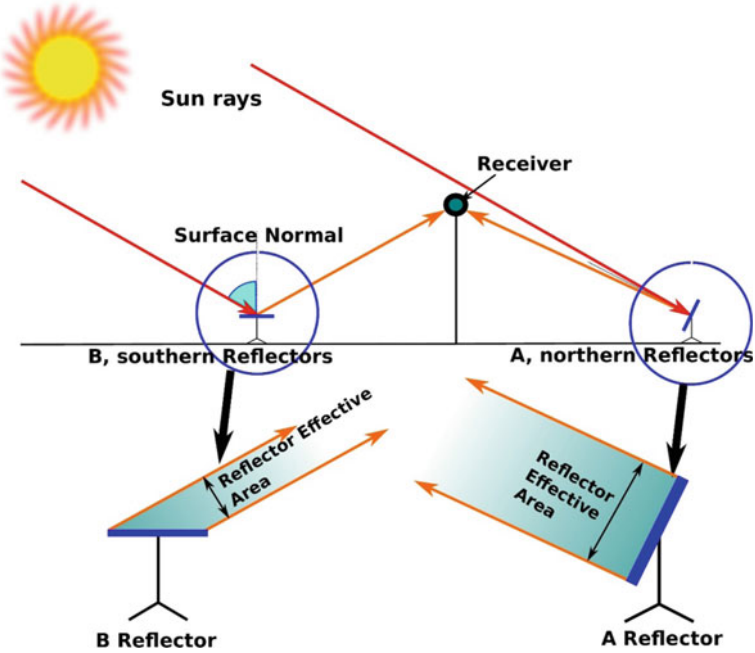

Fig. 5.21 Cosine effect for two reflective elements positioned in opposite side in relation to the receiver for a given Sun's position in the sky. In this case, Reflector *A* has much greater cosine efficiency (lower cosine losses, reflects more direct solar radiation) than reflector *B*

The energy loss factor due to cosine effect, $f_{\text{cosLoss},j}$, is given by the equation

$$f_{\text{cosLoss},j} = \frac{E_j}{E_0} = \frac{I_0 A_j \cos \varepsilon_j}{I_0 A_j} = \cos \varepsilon_j \tag{5.82}$$

The total averaged energy loss factor due to cosine effect, $\overline{f}_{\text{cosLoss}}$, can be computed by summing up the corresponding individual energy loss factors, $f_{\text{cosLoss},j}$, divided by the total number of the reflective elements, $N(=2 \cdot n$, or $= 2 \cdot n + 1)$:

$$\overline{f}_{\text{cosLoss}} = \frac{1}{N} \cdot \sum_{j=1}^{N} f_{\text{cosLoss},j} = \frac{1}{N} \cdot \sum_{j=1}^{N} \cos \varepsilon_j \tag{5.83}$$

or

$$\overline{f}_{\text{cosLoss}} = \frac{1}{2 \cdot n} \cdot \sum_{j=-n(j\neq 0)}^{n} f_{\text{cosLoss},j} = \frac{1}{2 \cdot n} \cdot \sum_{j=-n(j\neq 0)}^{n} \cos \varepsilon_j \tag{5.84}$$

or

$$\bar{f}_{\text{cosLoss}} = \frac{1}{2 \cdot n + 1} \cdot \sum_{j=-n}^{n} f_{\text{cosLoss},j} \frac{1}{2 \cdot n + 1} \cdot \sum_{j=-n}^{n} \cos \varepsilon_j \tag{5.85}$$

We can also compute the cosine efficiency, $\eta_{\cos}$, of the System using the following formula

$$\eta_{\cos,j} = 1 - f_{\cos,j} \tag{5.86}$$

$$\eta_{\cos} = 1 - \bar{f}_{\cos} \tag{5.87}$$

5.5 Receiver Shading

Lastly, an additional shading loss results from the shadow the receiver may cast on the reflective elements. The corresponding shading factor, f_{recLoss}, is defined as the ratio between the shaded reflectors aperture due to the receiver and the reflectors' aperture area without considering any other type of optical losses (end losses, shading or blocking effects) (Bachelier and Stieglitz 2017). Figure 5.22 schematically depicts the effect of receiver shading. The mathematical relationships describing the receiver shading effect can be derived using the transversal and the longitudinal component of Sun's position in the sky, since the relative positions of the receiver and the reflective elements remains constant. As the receiver shadow may be wider than the individual reflectors' aperture area, it may affect more than one reflector. In addition, this shadow may fall on reflectors of an adjacent Subsystem, whereas the first Subsystem may be affected by another Subsystem (Fig. 5.23).

The aperture area, A_{recLoss}, of reflectors that remains unused due to the receiver shading effect is shown in Fig. 5.22. In fact, this area is trapezoidal. However, it can be assumed to be rectangular without loss of generality and without introducing significant error. If we assume that L_{recLoss} and W_{recLoss} are the corresponding length and width of this area, then the aperture loss area of the reflectors field due to the receiver shading effect, A_{recLoss}, can be written as

$$A_{\text{recLoss}} = L_{\text{recLoss}} \cdot W_{\text{recLoss}} \tag{5.88}$$

To compute the length, L_{recLoss}, of this area is easier than to compute its width, W_{recLoss}. The problem arises from the gaps between reflectors. Hence, let us compute first the reflectors length, L_{recLoss}, which is affected by the receiver shadow.

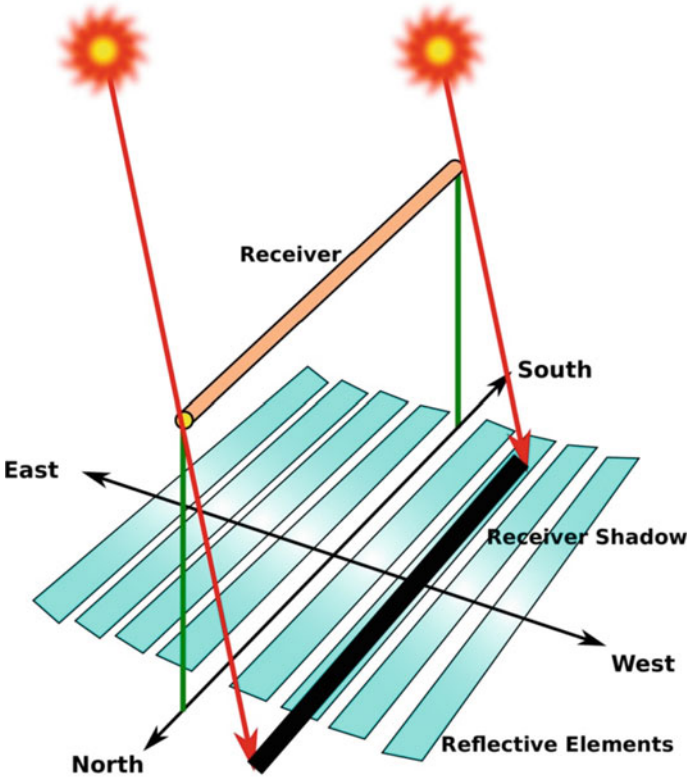

Fig. 5.22 Schematic illustration of the receiver shading effect

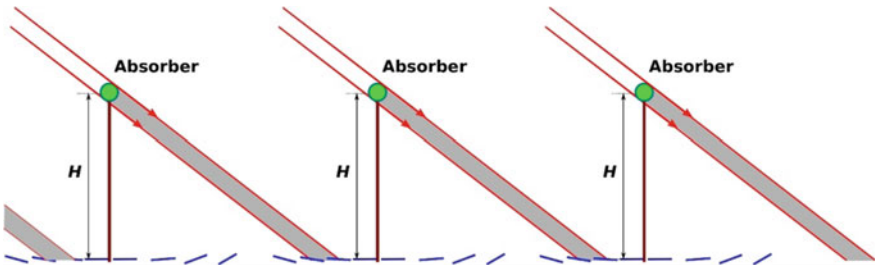

Fig. 5.23 Receiver shadow may fall on reflectors of an adjacent Subsystem, whereas the first Subsystem may be affected by another Subsystem

As it can be deduced from Fig. 5.24, this length equals the reflectors length, L, minus the length of their illuminated part, L_{illum}. To compute this length, we simply need to know the receiver height, H, and the longitudinal angle of Sun's rays, θ_L.

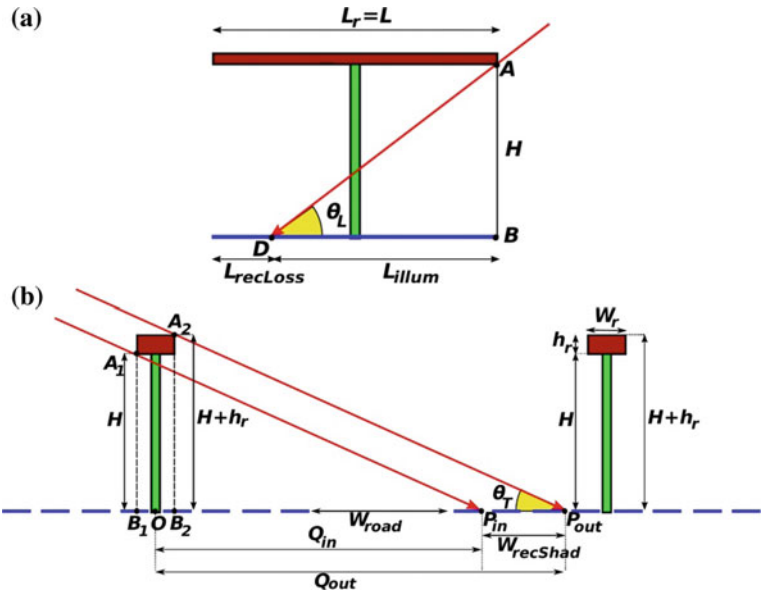

Fig. 5.24 Geometry of the receiver shadow calculations. **a** Receiver shadow length geometry and **b** receiver shadow width geometry

Both of them can be deemed as known parameters. Using the geometry of Fig. 5.24a and simple trigonometry, we get the following equation from triangle *ABD*

$$\begin{aligned} \tan\theta_L = \frac{AB}{DB} = \frac{H}{L_{\text{illum}}} \Rightarrow \\ L_{\text{illum}} = \frac{H}{\tan\theta_L} \end{aligned} \tag{5.89}$$

Therefore,

$$L_{\text{recLoss}} = L - L_{\text{illum}} = L - \frac{H}{\tan\theta_L} \tag{5.90}$$

According to Eq. 5.89, the length of the illuminated part of the reflectors, L_{illum}, can take positive or negative values depending on whether it is shifted towards North or South, for a North–South system orientation, due to the longitudinal angle of Sun's rays, θ_L, which can take positive or negative values. However, what matters is its magnitude, its absolute value, $|L_{\text{recEnd},j}|$, and not its sign denoting the shadow sifting. Therefore, Eq. 5.90 must be modified using absolute values

$$L_{\text{recLoss}} = L - L_{\text{illum}} = L - \left|\frac{H}{\tan\theta_L}\right| \tag{5.91}$$

In addition, if the illuminated part of the reflectors, L_{illum}, is longer than their length, L, $L_{\text{illum}} > L$, then the reflectors' length which is affected by the receiver shadow, L_{recLoss}, is not negative but zero. Hence, Eq. 5.91 gets its final form:

$$L_{\text{recLoss}} = \begin{cases} L - \left|\frac{H}{\tan\theta_L}\right| & \text{if} L_{\text{illum}} \leq L \\ 0 & \text{if} L_{\text{illum}} > L \end{cases} \tag{5.92}$$

Now, to compute the shaded width, W_{recLoss}, of the reflectors field, we have to use the transversal angle of Sun's position in the sky, θ_T, and the transversal cross section of the System, or more correctly of the Subsystem, as the receiver shading effect may be caused due to the shadow of the receiver of the adjacent Subsystem. In addition, the gaps between adjacent reflective elements change the effect the receiver shadow may have. Therefore, instead of the receiver shadow width, W_{recLoss}, as it is defined previously, we have to use the reflectors shaded width, $W_{\text{recLoss},k}$, where k is the reflector actually affected by the receiver shadow. Hence, the aperture loss area factor, f_{recLoss}, of the reflectors field due to the receiver shading effect can be calculated from the equation

$$\begin{aligned} f_{\text{recLoss}} &= \frac{1}{N} \cdot \sum_k f_{\text{recLoss},k} \Rightarrow \\ f_{\text{recLoss}} &= \frac{1}{N} \cdot \sum_{k=1}^{N} \frac{L_{\text{recLoss},k} \cdot W_{\text{recLoss},k}}{L_k \cdot W_k} \Rightarrow \\ f_{\text{recLoss}} &= \frac{1}{N} \cdot \sum_{k=1}^{N} \frac{L_{\text{recLoss}} \cdot W_{\text{recLoss},k}}{L \cdot W_k} \Rightarrow \\ f_{\text{recLoss}} &= \frac{L_{\text{recLoss}}}{N \cdot L} \cdot \sum_{k=1}^{N} \frac{W_{\text{recLoss},k}}{W_k} \end{aligned} \tag{5.93}$$

where k denotes the reflective element of the Linear Fresnel Reflector Subsystems that is affected by the receiver's shadow, and N is the total number of them.

The receiver shadow width, $W_{\text{recShad}} = W_{\text{recLoss}}$, casted on the reflective elements, can be calculated as the difference of the distances, Q_{in} and Q_{out}, of its two edges (P_{in} and P_{out}) from the origin, O, of the local Cartesian coordinate system of the current Linear Fresnel Reflector Subsystem, as they are depicted in Fig. 5.24b.

$$W_{\text{recShad}} = Q_{\text{out}} - Q_{\text{in}} \tag{5.94}$$

The two points, P_{in} and P_{out}, of the edges of the receiver shadow are defined in relation to Sun's transversal angle, θ_T. Point P_{in} is the point being always closer to Sun's direction.

The lengths Q_{in} and Q_{out} can be calculated from the triangles $A_1B_1P_{\text{in}}$ and $A_2B_2P_{\text{out}}$, of Fig. 5.24b:

$$\begin{aligned}\tan\theta_T = \frac{A_1B_1}{B_1P_{\text{in}}} = \frac{H}{\frac{W_{\text{rec}}}{2}+Q_{\text{in}}} \Rightarrow \\ \frac{W_{\text{rec}}}{2}+Q_{\text{in}} = \frac{H}{\tan\theta_T} \Rightarrow \\ Q_{\text{in}} = \frac{H}{\tan\theta_T} - \frac{W_{\text{rec}}}{2}\end{aligned} \tag{5.95}$$

and

$$\begin{aligned}\tan\theta_T = \frac{A_2B_2}{B_2P_{\text{out}}} = \frac{H+h_{\text{rec}}}{Q_{\text{out}}-\frac{W_{\text{rec}}}{2}} \Rightarrow \\ Q_{\text{out}} - \frac{W_{\text{rec}}}{2} = \frac{H+h_{\text{rec}}}{\tan\theta_T} \Rightarrow \\ Q_{\text{out}} = \frac{H+h_{\text{rec}}}{\tan\theta_T} + \frac{W_{\text{rec}}}{2}\end{aligned} \tag{5.96}$$

where W_{rec} is the receiver width, and h_{rec} is its height, while θ_T takes values between -90^{o} and $+90^{\text{o}}$.

Equation 5.96 is valid for rectangular receiver cross section. In the case the receiver has semicircular cross section (Fig. 5.25), this equation must be modified accordingly, getting the form:

$$\begin{aligned}\tan\theta_T = \frac{A_2B_2}{B_2P_{\text{out}}} = \frac{H+c}{Q_{\text{out}}-d} \Rightarrow \\ \tan\theta_T = \frac{A_2B_2}{B_2P_{\text{out}}} = \frac{H+\frac{W_{\text{rec}}}{2}\cdot\cos\theta_T}{Q_{\text{out}}-\frac{W_{\text{rec}}}{2}\cdot\sin\theta_T} \Rightarrow \\ Q_{\text{out}} - \frac{W_{\text{rec}}}{2}\cdot\sin\theta_T = \frac{H+\frac{W_{\text{rec}}}{2}\cdot\cos\theta_T}{\tan\theta_T} \Rightarrow \\ Q_{\text{out}} = \frac{H+\frac{W_{\text{rec}}}{2}\cdot\cos\theta_T}{\tan\theta_T} + \frac{W_{\text{rec}}}{2}\cdot\sin\theta_T\end{aligned} \tag{5.97}$$

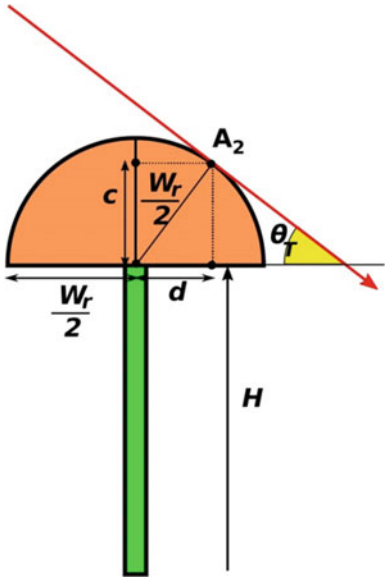

Fig. 5.25 Geometry of the receiver shadow width when the receiver has semicircular cross section

where W_{rec} is the diameter of the semicircular cross section of the receiver.

Substituting Eqs. 5.95 and 5.96 (or Eq. 5.97 for semicircular receiver cross section) into Eq. 5.94, the receiver shadow width, W_{recshad}, is

$$W_{\text{recShad}} = Q_{\text{out}} - Q_{\text{in}} \Rightarrow$$

$$W_{\text{recShad}} = \begin{cases} \frac{H + h_{\text{rec}}}{\tan\theta_T} + \frac{W_{\text{rec}}}{2} - \frac{H}{\tan\theta_T} - \frac{W_{\text{rec}}}{2} \\ \frac{H + \frac{W_{\text{rec}}}{2}\cdot\cos\theta_T}{\tan\theta_T} + \frac{W_{\text{rec}}}{2}\cdot\sin\theta_T - \frac{H}{\tan\theta_T} - \frac{W_{\text{rec}}}{2} \end{cases} \Rightarrow$$

$$W_{\text{recShad}} = \begin{cases} \frac{h_{\text{rec}}}{\tan\theta_T} \\ \frac{\frac{W_{\text{rec}}}{2}\cdot\cos\theta_T}{\tan\theta_T} + \frac{W_{\text{rec}}}{2}\cdot(\sin\theta_T - 1) \end{cases} \Rightarrow$$

$$W_{\text{recShad}} = \begin{cases} \frac{h_{\text{rec}}}{\tan\theta_T} & \text{rectangular} \\ \frac{W_{\text{rec}}\cdot\cos\theta_T}{2\cdot\tan\theta_T} + \frac{W_{\text{rec}}\cdot(\sin\theta_T - 1)}{2} & \text{semicircular} \end{cases} \tag{5.98}$$

Now, we have to find out the reflectors which are affected by the receiver shadow. In the first place, we have to examine whether the receiver shadow affects the reflectors of the current Linear Fresnel Reflector Subsystem, or the reflectors of its adjacent Subsystem, or none of the, if it falls on the gap between them. These cases are describes by the following conditions (Fig. 5.26):

Reflectors shading due to the receiver of the current Subsystem

$$If \quad Q_{\text{in}} < Q_n + \frac{W_n}{2\cdot\cos\beta_n} \tag{5.99}$$

The adjacent Subsystem is shaded due to the receiver of the current Subsystem

$$\text{If} \quad Q_{\text{out}} > Q_n + S_{\text{sub}} - \frac{W_{-n}}{2\cdot\cos\beta_{-n}} \tag{5.100}$$

No shading at all due to the receiver

$$\begin{gathered} Q_{\text{in}} \geq Q_n + \frac{W_n}{2\cdot\cos\beta_n} \\ \text{if} \quad \text{and} \\ Q_{\text{out}} \leq Q_n + S_{\text{sub}} - \frac{W_{-n}}{2\cdot\cos\beta_{-n}} \end{gathered} \tag{5.101}$$

where n is the outer reflective element of any Linear Fresnel Reflector Subsystem, W_n, Q_n and β_n are its width, its position and its inclination angle, respectively, and S_{sub} is the distance between two adjacent Subsystems.

Having determined whether there is a shading effect or not, the next step is to find out the reflectors which are actually affected. They are located within the receiver shadow. In other words, we have to find those reflectors, k, satisfying the condition (for $j = -n$ to n)

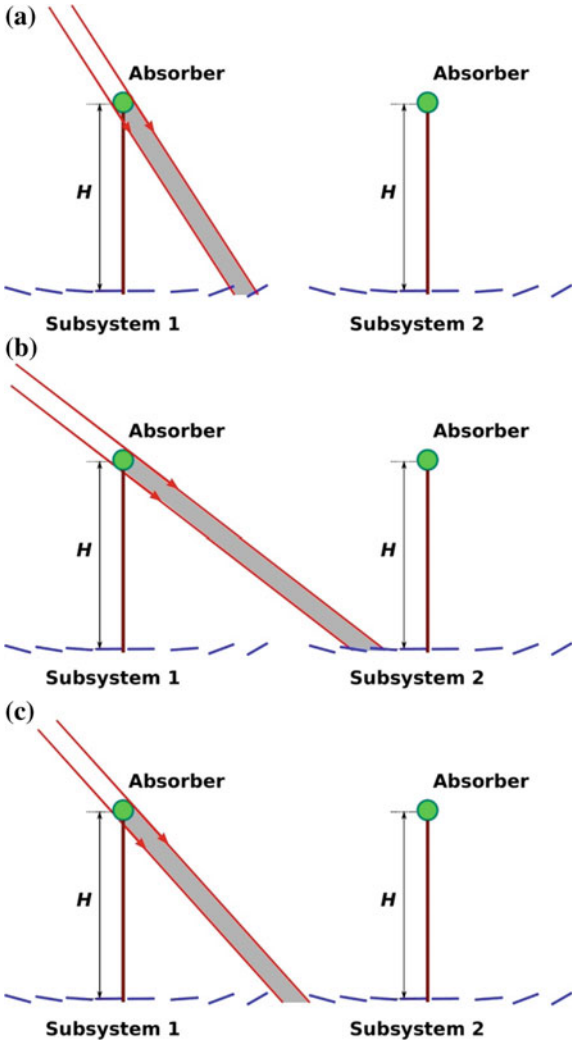

Fig. 5.26 Reflectors affected by the receiver shadow may **a** belong in the current Linear Fresnel Reflector Subsystem, or **b** in its adjacent Subsystem, or **c** the receiver shadow may fall on the gap between these two Subsystems

$$Q_{\text{in}} \leq Q_j - \frac{W_j}{2 \cdot \cos \beta_j} \tag{5.102a}$$

and

$$Q_j + \frac{W_j}{2 \cdot \cos \beta_j} \leq Q_{\text{out}} \tag{5.102b}$$

There are four (4) different cases of reflectors shading (always concerning the reflectors width). They are all depicted in Fig. 5.27. According to this figure, a

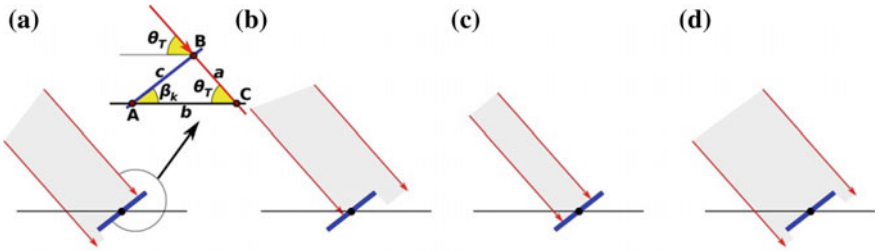

Fig. 5.27 Reflectors located within the receiver shadow may be partially (**a**, **b**, or **c**), or fully shaded (**d**). In the first case, the shaded part may be located on the lower part of the reflector (**a**), or the upper part of it (**b**), or somewhere between (**c**)

reflective element may be partially or fully shaded. In addition, if it is partially shaded, the shaded part may be located on the lower, or the upper part of it, or somewhere between. So, for each reflector satisfying the conditions of Eq. 5.101, we have to perform the following analysis:

A. Lower part shading. It occurs if

$$Q_{\text{in}} \le Q_k - \frac{W_k}{2 \cdot \cos \beta_k} \tag{5.103a}$$

and

$$Q_{\text{out}} < Q_k + \frac{W_k}{2 \cdot \cos \beta_k} \tag{5.103b}$$

In this case, the shaded width of the *j*th reflective element, $W_{\text{recLoss},k}$, is equal to

$$W_{\text{recLoss},k} = \frac{W_k}{2} + (Q_{\text{out}} - Q_k) \cdot \frac{\sin \theta_{\text{T}}}{\sin(\theta_{\text{T}} + |\beta_k|)} \tag{5.104}$$

It results from the law of sines in triangle *ABC* in Fig. 5.27

$$\begin{gathered} \frac{b}{\sin \widehat{\text{B}}} = \frac{c}{\sin \widehat{\text{C}}} \Rightarrow \\ \frac{Q_{\text{out}} - Q_k}{\sin(\theta_{\text{T}} + |\beta_k|)} = \frac{c}{\sin \theta_{\text{T}}} \Rightarrow \\ c = \left(Q_{\text{out}} - Q_{jk}\right) \cdot \frac{\sin \theta_{\text{T}}}{\sin(\theta_{\text{T}} + |\beta_k|)} \end{gathered} \tag{5.105}$$

B. Upper part shading. It occurs if

$$Q_{\text{in}} > Q_k - \frac{W_k}{2 \cdot \cos \beta_k} \tag{5.106a}$$

And

$$Q_{\text{out}} \geq Q_k + \frac{W_k}{2 \cdot \cos \beta_k} \tag{5.106b}$$

Similarly, in this case the shaded width of the jth reflective element, $W_{recLoss,k}$, is equal to

$$W_{\text{recLoss},k} = \frac{W_k}{2} - (Q_{in} - Q_k) \cdot \frac{\sin \theta_{\text{T}}}{\sin(\theta_{\text{T}} + |\beta_k|)} \tag{5.107}$$

C. Middle part shading. It occurs if

$$Q_{\text{in}} > Q_k - \frac{W_k}{2 \cdot \cos \beta_k} \tag{5.108a}$$

And

$$Q_{\text{out}} < Q_k + \frac{W_k}{2 \cdot \cos \beta_k} \tag{5.108b}$$

In this case, the calculation of the shaded width of the kth reflective element, $W_{\text{recsLoss},k}$, is a bit more complex. According to Fig. 5.27, the shaded width $W_{\text{recLoss},j}$ is given by the equation

$$W_{\text{recsLoss},k} = W_{\text{recsLoss},k,\text{in}} + W_{\text{recsLoss},k,\text{out}} \tag{5.109}$$

where

$$W_{\text{recLoss},k,\text{in}} = (Q_k - Q_{\text{in}}) \cdot \frac{\sin \theta_{\text{T}}}{\sin(\theta_{\text{T}} + |\beta_k|)} \tag{5.110}$$

$$W_{\text{recLoss},k,\text{out}} = (Q_{\text{out}} - Q_k) \cdot \frac{\sin \theta_{\text{T}}}{\sin(\theta_{\text{T}} + |\beta_k|)} \tag{5.111}$$

Substituting Eqs. 5.110 and 5.111 into Eq. 5.109, it becomes

$$W_{\text{recLoss},k} = (Q_{\text{out}} - Q_{\text{in}}) \cdot \frac{\sin \theta_{\text{T}}}{\sin(\theta_{\text{T}} + |\beta_k|)} \tag{5.112}$$

D. Total shading. It occurs if

$$Q_{\text{in}} \leq Q_k - \frac{W_k}{2 \cdot \cos \beta_k} \tag{5.113a}$$

and

$$Q_{\text{out}} \geq Q_k + \frac{W_k}{2 \cdot \cos \beta_k} \tag{5.113b}$$

In this case, the shaded width of the kth reflective element, $W_{\text{recLoss},k}$, equals the reflector's width, W_k,

$$W_{\text{recLoss},k} = W_k \tag{5.114}$$

Now, we can compute the aperture area loss factor, f_{recLoss}, of the reflectors field due to the receiver shading effect by substituting the shaded width of the kth reflective element, $W_{\text{recLoss},k}$, in Eq. 5.93. On the other hand, the receiver shading efficiency, $\eta_{\text{recshading}}$, of the System is defined as the aperture area of the reflectors which contribute to the solar radiation concentration and is not affected by the receiver shadow, divided by to the total aperture area of all reflectors. Alternatively, it can be calculated by the equation

$$\eta_{\text{recshading}} = 1 - f_{\text{recLoss}} \tag{5.115}$$

5.6 Time Averaged Losses

The relative shaded area, $fA_{\text{shadLoss},j}$, or shading loss ratio, the shading efficiency, η_{shading}, the relative blocked area, $fA_{\text{blockLoss},j}$, or blocking loss ratio, the blocking efficiency, η_{blocking}, the receiver end losses factor, $f_{\text{recEnd},j}$, or end losses ratio, the receiver end loss efficiency, η_{end}, the energy loss factor due to cosine effect, $f_{\text{cosLoss},j}$, the cosine efficiency, η_{cos}, as well as their averaged values, can timely be averaged on daily, monthly or annual basis (Hongn et al. 2015). Let us take, for example, the receiver end losses, the receiver end loss length, $L_{\text{recEnd},j}$, and the receiver end loss factor, $f_{\text{recEnd},j}$. As it has been already mentioned, the end loss length, $L_{\text{recEnd},j}$, can take positive or negative values depending on whether the non-illuminated length is shifted towards North or South, in a North–South system's orientation. However, in any case, what influences the end losses is the absolute value of the non-illuminated length and not its sign, denoting the shifting direction. Therefore, the averaged end loss length, $\overline{L}_{\text{end},j}$, (daily, monthly, or annually) and the averaged end loss factor, $f_{\text{end},j}$, results from the integration of Eqs. 5.52 and 5.69, over the desired averaging time period (T_{day}, T_{month}, T_{year}), using instead of $L_{\text{recEnd},j}$ its absolute value $|L_{\text{recEnd},j}|$:

$$\begin{aligned} \overline{L}_{\text{daily, recEnd},j} &= \frac{1}{T_{\text{day}}} \cdot \int_{\omega_{\min}}^{\omega_{\max}} \left|L_{\text{recEnd},j}\right| \cdot \mathrm{d}\omega \\ &= \frac{1}{\omega_{\max} - \omega_{\min}} \cdot \int_{\omega_{\min}}^{\omega_{\max}} \left|L_{\text{recEnd},j}\right| \cdot \mathrm{d}\omega \end{aligned} \tag{5.116}$$

$$\begin{aligned}\overline{L}_{\text{year,recEnd},j} &= \frac{1}{T_{\text{year}}} \cdot \int_{-\delta_{\max}}^{\delta_{\max}} \overline{L}_{\text{daily,recEnd},j} \cdot \mathrm{d}\delta \\ &= \frac{1}{2 \cdot \delta_{\max}} \cdot \int_{-\delta_{\max}}^{\delta_{\max}} \overline{L}_{\text{daily,recEnd},j} \cdot \mathrm{d}\delta\end{aligned} \tag{5.117}$$

and

$$\begin{aligned}\overline{f}_{\text{daily,recEnd},j} &= \frac{1}{T_{\text{day}}} \cdot \int_{\omega_{\min}}^{\omega_{\max}} f_{\text{recEnd},j} \cdot \mathrm{d}\omega \\ &= \frac{1}{\omega_{\max} - \omega_{\min}} \cdot \int_{\omega_{\min}}^{\omega_{\max}} f_{\text{recEnd},j} \cdot \mathrm{d}\omega\end{aligned} \tag{5.118}$$

$$\begin{aligned}\overline{f}_{\text{year,recEnd},j} &= \frac{1}{T_{\text{year}}} \cdot \int_{-\delta_{\max}}^{\delta_{\max}} \overline{f}_{\text{daily,recEnd},j} \cdot d\delta \\ &= \frac{1}{2 \cdot \delta_{\max}} \cdot \int_{-\delta_{\max}}^{\delta_{\max}} \overline{f}_{\text{daily,recEnd},j} \cdot d\delta\end{aligned} \tag{5.119}$$

Similarly, the total averaged values of the end loss length, ($\overline{L}_{\text{daily,end}}$, $\overline{L}_{\text{year,end}}$) and the end loss factor ($\overline{f}_{\text{daily,recEnd}}$, $\overline{f}_{\text{year,recEnd}}$) of the System can be computed by summing up the corresponding individual values $L_{\text{recEnd},j}$, $f_{\text{recEnd},j}$, of all reflective elements divided by the total number of them, N(= $2n$, or = $2n + 1$):

$$\overline{L}_{\text{daily,recEnd}} = \frac{1}{N} \cdot \sum_{j=1}^{N} \overline{L}_{\text{daily,recEnd},j} \tag{5.120}$$

or

$$\overline{L}_{\text{daily,recEnd}} = \frac{1}{2 \cdot n} \cdot \sum_{j=-n(j\neq 0)}^{n} \overline{L}_{\text{daily,recEnd},j} \tag{5.121}$$

or

$$\overline{L}_{\text{daily,recEnd}} = \frac{1}{2 \cdot n + 1} \cdot \sum_{j=-n}^{n} \overline{L}_{\text{daily,recEnd},j} \tag{5.122}$$

$$\overline{L}_{\text{year,recEnd}} = \frac{1}{N} \cdot \sum_{j=1}^{N} \overline{L}_{\text{year,recEnd},j} \tag{5.123}$$

or

$$\overline{L}_{\text{year,recEnd}} = \frac{1}{2 \cdot n} \cdot \sum_{j=-n(j\neq 0)}^{n} \overline{L}_{\text{year,recEnd},j} \tag{5.124}$$

or

$$\overline{L}_{\text{year,recEnd}} = \frac{1}{2 \cdot n + 1} \cdot \sum_{j=-n}^{n} \overline{L}_{\text{year,recEnd},j} \tag{5.125}$$

and

$$\overline{f}_{\text{daily,recEnd}} = \frac{1}{N} \cdot \sum_{j=1}^{N} \overline{f}_{\text{daily,recEnd},j} \tag{5.126}$$

or

$$\overline{f}_{\text{daily,recEnd}} = \frac{1}{2 \cdot n} \cdot \sum_{j=-n(j\neq 0)}^{n} \overline{f}_{\text{daily,recEnd},j} \tag{5.127}$$

or

$$\overline{f}_{\text{daily,recEnd}} = \frac{1}{2 \cdot n + 1} \cdot \sum_{j=-n}^{n} \overline{f}_{\text{daily,recEnd},j} \tag{5.128}$$

$$\overline{f}_{\text{year,recEnd}} = \frac{1}{N} \cdot \sum_{j=1}^{N} \overline{f}_{\text{year,recEnd},j} \tag{5.129}$$

or

$$\overline{f}_{\text{year,recEnd}} = \frac{1}{2 \cdot n} \cdot \sum_{j=-n(j\neq 0)}^{n} \overline{f}_{\text{year,recEnd},j} \tag{5.130}$$

or

$$\overline{f}_{\text{year,recEnd}} = \frac{1}{2 \cdot n + 1} \cdot \sum_{j=-n}^{n} \overline{f}_{\text{year,recEnd},j} \tag{5.131}$$

References

Bachelier Camille and Robert Stieglitz. 2017. Design and optimisation of linear Fresnel power plants based on the direct molten salt concept. *Solar Energy* 152: 171–192.

Eck, M., T. Hirsch, J.F. Feldhoff, D. Kretschmann, J. Dersch, A. Gavilan Morales, L. Gonzalez-Martinez, C. Bachelier, W. Platzer, K.-J. Riffelmann, and M. Wagner. 2014. Guidelines for CSP yield analysis—optical losses of line focusing systems; definitions, sensitivity analysis and modeling approaches. *Energy Procedia* 49: 1318–1327.

Guangdong, Zhu. 2013. Development of an analytical optical method for linear Fresnel collectors. *Solar Energy* 94: 240–252.

Heimsath, A., G. Bern, D. van Rooyen, and P. Nitz. 2014. Quantifying optical loss factors of small linear concentrating collectors for process heat application. *Energy Procedia* 48: 77–86.

Hongn, Marcos, Silvana Flores Larsen, Marcelo Gea, and Martin Altamirano. 2015. Least square based method for the estimation of the optical end loss of linear Fresnel concentrators. *Solar Energy* 111: 264–276.

Larbi, A.B., M. Godin, and J. Lucas 2000. Analysis of two models of (3D) fresnel collectors operating in the fixed-aperture mode with a tracking absorber. *Solar Energy* 69(1): 1–14.

Li, Ming, Chengmu Xu, Xu Ji, Peng Zhang, and Qiongfen Yu. 2015. A new study on the end loss effect for parabolic trough solar collectors. *Energy* 82: 382–394.

Marco, Binotti, Guangdong Zhu, Allison Gray, Giampaolo Manzolini, and Paolo Silva. 2013. Geometric analysis of three-dimensional effects of parabolic trough collectors. *Solar Energy* 88: 88–96.

Mills, David R., and Graham L. Morrison. 2000. Compact linear fresnel reflector solar thermal powerplants. *Solar Energy* 68 (3): 263–283.

Montes, María J., Carlo Rubbia, Ruben Abbas, and Jose M. Martínez-Val. 2014. A comparative analysis of configurations of linear Fresnel collectors for concentrating solar power. *Energy* 73: 192–203.

Nixon, J.D., and P.A. Davies. 2012. Cost-exergy optimisation of linear Fresnel reflectors. *Solar Energy* 86: 147–156.

Pino, F.J., R. Caro, F. Rosa, and J. Guerra. 2013. Experimental validation of an optical and thermal model of a linear Fresnel collector system. *Applied Thermal Engineering* 50: 1463–1471.

Qiu, Yu., Ya-Ling He, Ze-Dong Cheng, and Kun Wang. 2015. Study on optical and thermal performance of a linear Fresnel solar reflector using molten salt as HTF with MCRT and FVM methods. *Applied Energy* 146: 162–173.

Robledo Maria, Juan M. Escano, Amparo Nunez Carlos Bordons, and Eduardo F. Camacho 2011. Development and Experimental Validation of a Dynamic Model for a Fresnel Solar Collector. In *18th IFAC (International Federation of Automatic Control) World Congress Milano (Italy)* August 28–September 2, 2011.

Sharma, Vashi, Jayanta K. Nayak, and Shireesh B. Kedare. 2015a. Comparison of line focusing solar concentrator fields considering shading and blocking. *Solar Energy* 122: 924–939.

Sharma, Vashi, Jayanta K. Nayak, and Shireesh B. Kedare. 2015b. Effects of shading and blocking in linear Fresnel reflector field. *Solar Energy* 113: 114–138.

Sharma, Vashi, Sourav Khanna, Jayanta K. Nayak, and Shireesh B. Kedare. 2015c. Effects of shading and blocking in compact linear fresnel reflector field. *Energy* 94: 633–653.

Zheng, Jiantao, Junjie Yan, Jie Pei, and Guanjie Liu 2014. Solar tracking error analysis of fresnel reflector, hindawi publishing corporation. *The Scientific World Journal*, 2014, Article ID 834392, 6 pages.

Zhu, Yanqing, Shi Jifu, Li Yujian, Wang Leilei, Huang Qizhang, and Xu Gang 2016. Design and experimental investigation of a stretched parabolic linear Fresnel reflector collecting system. *Energy Conversion and Management* 126: 89–98.

Chapter 6
Receiver Secondary Reflector

Because Sun is not a point light source, in Linear Fresnel Reflector Systems the primarily reflected solar radiation beam is always diverging. In addition, if the reflective elements are not plane but curved the reflected beams' diverging nature is even more enhanced. As a result, its cross section is always larger than reflectors' effective area. Moreover, the fact that the radiation reflected from the furthest reflectors must travel long distances until impinging onto the receiver results in even larger beam cross sections. For this reason, Linear Fresnel Reflector Systems require wide absorbers, or, at least, receivers with wide openings and secondary concentrating devices. The latter are reflectors that have a specific shape allowing them to redirect the primarily reflected solar radiation that cannot hit the absorber back on it.

The aim of this chapter is to provide a method to study the optical performance and efficiency of different types of secondary reflectors. This method is based on an analytical approach of their optical behaviour, and not on graphical or statistical methods. Hence, it can easily be used for the identification of the most appropriate receiver design with the least computational effort and resources.

6.1 Introduction

Although Linear Fresnel Reflector Systems have been considered as a promising technology to exploit solar power, their effectiveness largely depends on the receiver efficiency to collect all the primarily concentrated solar radiation. Thus, apart from the primary reflectors field, an equally important component of a Linear Fresnel Reflector System is the receiver. In general, it consists of an absorbing surface (the absorber), a secondary concentrator, a glass plate or a glass tube that protects the absorber and the casing (Fig. 6.1).

The key components of a receiver construction are the secondary reflector and the single tube (with large diameter) or the multiple tube (many narrower tubes)

S. Karathanasis, *Linear Fresnel Reflector Systems for Solar Radiation Concentration*, https://doi.org/10.1007/978-3-030-05279-9_6

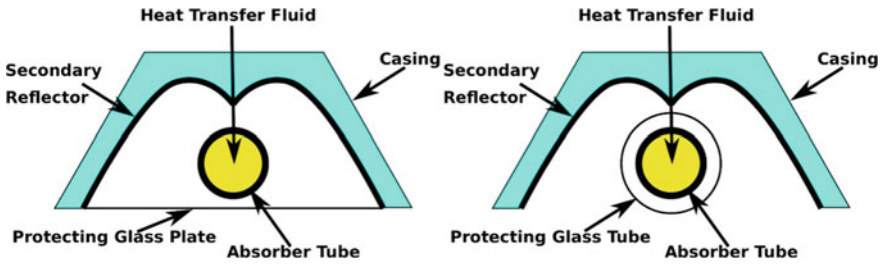

Fig. 6.1 Receiver construction of a Linear Fresnel Reflector System usually consists of an absorbing surface (the absorber), a secondary concentrator, a glass plate or a glass tube that protects the absorber and the casing

absorber. The tubes' number and their diameter play a fundamental role in the thermal efficiency of the absorber. They are affected by the cross section and the incidence angle of the primarily reflected solar radiation beam, as the objective of the absorber is to be able to capture as more as possible of it.

Since the cross section of the reflected solar radiation beam plays a significant role in the aperture width of the receiver, in order to narrow it the reflective elements' width, W_j, must be very small, as small as possible. However, this puts construction constraints. Fortunately, the use of a secondary concentrator allows us to overcome this problem by, essentially, enlarging the target area of the primary reflectors, while, at the same time, the formed cavity around the absorber provides extra protection that reduces convective heat losses. Moreover, in a Linear Fresnel Reflector System, the amount of solar energy concentrated on the upper half of the absorber is, in general, lower than that on the lower half. This non-uniform irradiation distribution can lead to large circumferential temperature difference, which in turn may cause significant deflection of the tube structure. However, this problem is also overcome by the use of secondary concentrators. This way the lower half of the absorber receives solar radiation reflected directly from the primary reflectors, whereas the upper half receives the solar radiation intercepted and reflected by the secondary concentrator (Chaitanya et al. 2017). Lastly, this way we increase the System tolerance on Sun tracking error, caused by the primary reflectors reorientations, as it cannot be continuous but stepwise.

Nevertheless, to choose, or even to design, the optimal shape a secondary reflector may have is an extremely challenging task as there is not available any well-established method (Zhu 2017). For this reason, a considerable number of authors have used and studied different types of receiver configurations, such as flat vertical, horizontal or triangular receivers, cavity receivers, trapezoidal cavity receivers, arc-shaped and semi-circular cavity receivers, V-shaped cavity receivers, parabolic concentrators, segmented parabolic concentrators, compound parabolic concentrators, parabolic involute concentrators, parabolic wing-like structures or combinations of them (e.g. Chaitanya et al. 2017; Lin et al. 2013). The aforementioned types are the most commonly used receiver configurations (Fig. 6.2). On the other hand, Zhu (2017) tried to reconstruct the ideal secondary reflector shape

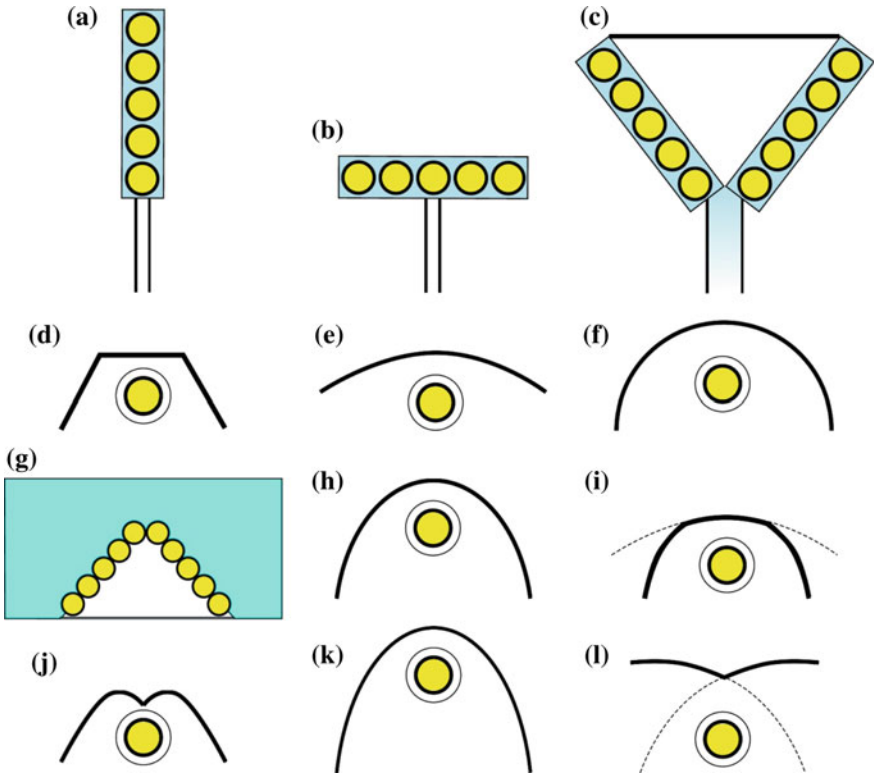

Fig. 6.2 Most common receiver configurations. Flat vertical (**a**), horizontal (**b**) or triangular (**c**) receiver, trapezoidal cavity receiver (**d**), arc-shaped (**e**) and semi-circular cavity receiver (**f**), V-shaped cavity receiver (**g**), parabolic concentrator (**h**), segmented parabolic concentrator (**i**), compound parabolic concentrator (**j**), parabolic involute concentrator (**k**) and parabolic wing-like structure (**l**)

using a graphical method and ray-tracing techniques. Similarly, all other researchers employed the ray-tracing technique to investigate the distribution of the solar radiation on the surface of the absorber after being reflected by the secondary reflector (e.g. Lin et al. 2013). However, in this chapter, we resort only on analytical approaches to investigate the secondary reflectors behaviour and efficiency.

6.2 Methodology

Although Sun's position in the sky varies with time, and as a result the direction of the incoming solar radiation also varies, it is possible to design, or at least to study, different profiles of secondary reflectors and choose the most suitable shape. This is feasible due to the fact that any Linear Fresnel Reflector System is designed so that

the primary reflective elements to redirect the solar radiation always onto the receiver. Hence, the direction of the reflected solar radiation is always constant and coincides with the direction of the line connecting each reflective element with the receiver (in fact, their central line with the receiver central line). What changes throughout the day is the cross section of each reflected solar radiation beam, as it depends on the reflectors' position and inclination angle and on the incidence angle of the incoming solar radiation on each reflective element, which in turn depends on Sun's position in the sky.

Therefore, since the direction of the primarily reflected solar radiation, the input of the receiver, remains unchanged, the optical behaviour of the secondary reflector can be studied independently from the rest of the System.

Now, let us study the behaviour of a secondary reflector having an arbitrary shape, by considering the reflected solar radiation beam originated by the *j*th reflective element. It forms an angle ζ_j with the receiver aperture and has a cross section equal to α_j. However, taking advantage of the inherent symmetry of Linear Fresnel Reflector Systems, we can simplify the problem by considering only the transversal component of the reflected solar radiation. In this case, the incident angle ζ_j corresponds to the angle, ξ_j, formed by the reflectors' plane and the line connecting the *j*th reflective element with the receiver, which is always constant (Fig. 6.3):

$$\zeta_j \equiv \xi_j = \tan^{-1} \frac{H}{Q_j} \tag{6.1}$$

In addition, the beam's cross section, α_j, can be replaced by the beam's width, d_j. In Eq. 6.1, Q_j is the distance of the *j*th reflective element from the origin of the local Cartesian coordinate System, and H is the height of the receiver place. This

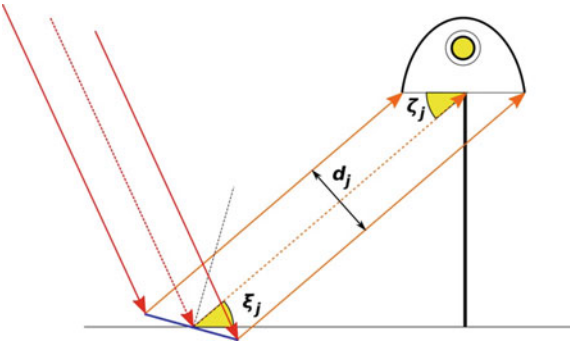

Fig. 6.3 Because of the inherent symmetry of Linear Fresnel Reflector Systems, we can simplify the study of the secondary reflector optical behaviour by considering only the transversal component of the reflected solar radiation. In this case, the incident angle ζ_j corresponds to the angle, ξ_j, formed by the reflectors plane and the line connecting the *j*th reflective element with the receiver, which is always constant

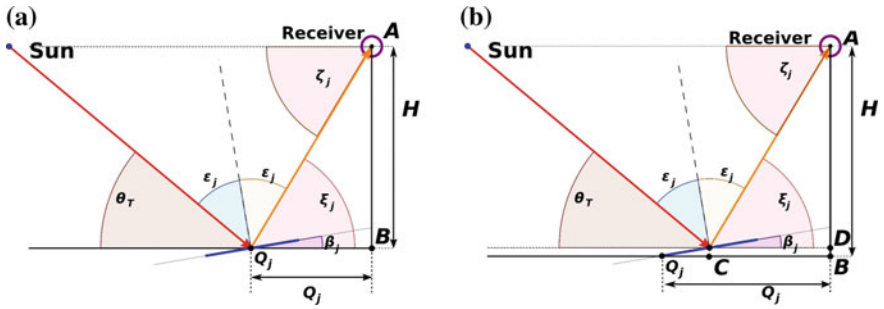

Fig. 6.4 Incidence angle of the primarily reflected solar radiation on the receiver in the case the reflective elements are centrally pivoted (**a**) and in the case, their rotation axis coincides with one of their longer edge (**b**)

equation corresponds to the case the reflective elements are centrally pivoted (Fig. 6.4a). In the case, the reflective elements' rotation axis coincides with one of their longer edges (Fig. 6.4b) the computations, as well as the construction and operational requirements are more complex and, therefore, this type of reflectors' reorientation method (Sun tracking mechanism) is not recommended. Equation 6.1 takes the following form for site pivoted reflective elements

$$\zeta_j \equiv \xi_j = \tan^{-1} \frac{H - \frac{W_j}{2} \cdot \sin \beta_j}{Q_j - \frac{W_j}{2} \cdot \cos \beta_j} \Rightarrow \tag{6.2}$$

Moreover, as it has been already mentioned, the width, d_j, of the reflected solar radiation beam depends on Sun's position in the sky, on the reflector's inclination angle, β_j (in fact on the angle θ_j, the solar radiation incidence angle on the jth reflector), and on the reflector's width, W_j. Using the geometry of Figs. 6.3 and 6.4a, the width, d_j, of the reflected solar radiation beam equals the width of the solar radiation beam falling on the reflector's surface and is given by the equation

$$d_j = W_j \cdot \left|\sin\left(\theta_T + \beta_j\right)\right| \tag{6.3}$$

where θ_T is Sun's transversal angle.

As the reflective elements are oriented so that the solar light ray hitting on their middle line to be directed on the middle line of the absorber (or the receiver, if it is a more complex construction), usually only a part of the reflected solar radiation beam is hitting the absorber, while the rest misses it. This depends on the reflected beam width, d_j, the absorber's width, W_a and the angle of incidence, ζ_j (=ξ_j), of the reflected solar radiation beam on the receiver (Fig. 6.5). According to the geometry

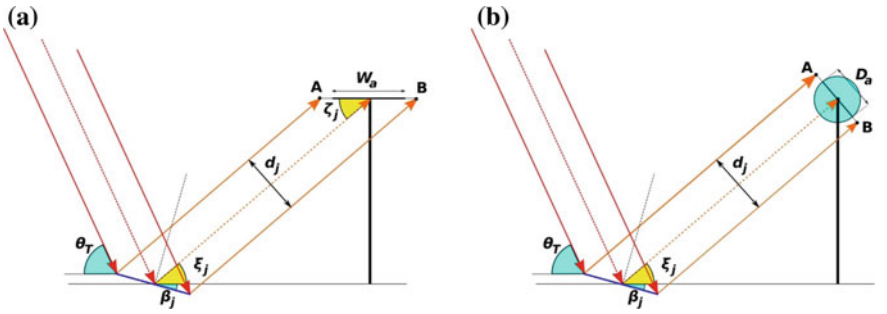

Fig. 6.5 Usually only a part of the primarily reflected solar radiation beam is hitting the absorber, while the rest misses it. This depends on the reflected beam width, d_j, the angle of incidence, ζ_j ($=\xi_j$), of the reflected solar radiation beam on the receiver, and the absorber size and shape. **a** The absorber is horizontal and flat, having short height (H_a), very large length (L_a), and width equal to W_a. In this case, it is a multiple tube receiver construction which consists of many narrow tubes positioned horizontally and close to each other. However, the absorber may also be composed of one wider tube with circular cross section (with or without a glass tube cover) (**b**)

of Fig. 6.5a, a part of the reflected solar radiation beam hitting the absorber misses it if the length of the line segment AB is larger than the absorber's width:

$$|AB| > W_a \tag{6.4}$$

The length of the line segment AB can be calculated from the geometry of Fig. 6.5a using the equation

$$\begin{gathered} |AB| = \frac{d_j}{\sin \xi_j} \Rightarrow \\ |AB| = \frac{W_j \cdot \left|\sin\left(\theta_T + \beta_j\right)\right|}{\sin \xi_j} \Rightarrow \\ |AB| = W_j \cdot \frac{\left|\sin\left(\theta_T + \beta_j\right)\right|}{\sin \xi_j} \end{gathered} \tag{6.5}$$

where the reflected beam width, d_j, has been replaced by Eq. 6.3.

Now, replacing Eq. 6.5 into Eq. 6.4, the reflected solar radiation loss condition (Eq. 6.4) becomes

$$W_j \cdot \frac{\left|\sin\left(\theta_T + \beta_j\right)\right|}{\sin \xi_j} > W_a \tag{6.6}$$

In the above-presented analysis, we assumed that the absorber is horizontal and flat, having short height (H_a), very large length (L_a) and width equal to W_a. In other words, it is a multiple tube receiver construction which consists of many narrow tubes positioned horizontally and close to each other. However, this is not the only possible case. Many times the absorber is composed of one wider tube with circular cross section (with or without a glass tube cover) (Fig. 6.5b). In this case, the

reflected solar radiation beam is always perpendicular to one diameter of the absorber cross section. As a result, the reflected solar radiation loss condition takes the simpler form

$$\begin{gathered} d_j > D_a \Rightarrow \\ W_j \cdot \left|\sin\left(\theta_T + \beta_j\right)\right| > D_a \end{gathered} \tag{6.7}$$

where $D_a = 2\ r_a$, is the absorber tube diameter, and r_a is its radius.

Having Eqs. 6.6 and 6.7 in mind, we can conclude that a secondary reflector is useful only if the reflected radiation beam width and the absorber dimensions satisfy these equations. Otherwise, the whole reflected solar radiation beam is hitting the absorber and potentially absorbed. On the other hand, it is obvious that these conditions may not be satisfied every time of the day as they depend not only on the reflector's width, W_j, but also on Sun's transversal angle, θ_T, which changes during the day, and on the reflector's inclination angle, β_j, which depends on their position, Q_j, and also on Sun's transversal angle, θ_T. Therefore, a secondary reflector is necessary, only if the part of the reflected solar radiation that misses the absorber is considerably high and, consequently, the energy losses affecting the System efficiency are significant. In addition, the secondary reflector aperture width, W_r, should be larger than a minimum value, so that the primarily reflected solar radiation can enter the receiver construction and not get lost. Therefore, the secondary reflector aperture width, W_r, should satisfy the following condition:

$$\begin{gathered} W_r \geq \cdot \frac{d_j}{\sin \xi_j} \Rightarrow \\ W_r \geq W_j \cdot \frac{\left|\sin\left(\theta_T + \beta_j\right)\right|}{\sin \xi_j} \end{gathered} \tag{6.8}$$

6.2.1 Secondary Reflector Shape and Aperture Width

Having defined the necessary condition that must be satisfied for the use of a secondary reflector, the next step would be the definition of the most appropriate shape the reflector should have. The problem raised is how to choose the proper shape so that the solar radiation reaching the secondary reflector to be concentrated on the absorber. However, the problem is more complex, as only one part of the initial beam has to be redirected and concentrated on the absorber, since the rest of the incoming solar radiation beam is already intercepted, and therefore absorbed, by the absorber. This part is determined by the beam width and the absorber dimensions. Moreover, once the ideal secondary reflector shape has been found, based on computation using one (even arbitrary) of the incoming solar radiation beams, we have to further investigate whether this shape can also concentrate the reflected solar radiation beams originated from the rest reflective elements.

The inherent difference among all primarily reflected solar radiation beams is their direction. The ideal secondary reflector should be able to concentrate all incoming solar radiation beams regardless of their angle of incidence, ζ_j ($=\xi_j$). However, this is not possible for most of the known and well-studied shapes of reflective surfaces. The key problem is that most reflectors (except for plane mirrors) are designed, studied and used for focusing electromagnetic radiation being parallel and near to their principal axis (their axis of symmetry). All these devices focus light on a point located on their principal axis, and they fail to do so when the direction of the incoming electromagnetic radiation forms large angles with this axis. A brief but comprehensive analysis of the optical behaviour of the most commonly used reflective surfaces has been presented in Chap. 3.

Fortunately, in Linear Fresnel Reflector System the desired focus is not an ideal (a mathematical) point but an extended line segment, or even a more complex shape (e.g. absorbers with circular cross section). Hence, what we have to do is only to study if the investigated reflector shape can reflect and redirect the primarily reflected solar radiation beams so that they are intercepted by the absorber surface. In the following paragraphs, we will present an analytical method suitable for this purpose.

So, let us consider, again, a solar radiation beam which is reflected by the jth reflective element and has an angle of incidence on the receiver equal to ζ_j ($=\xi_j$) and a width equal to d_j, and that the secondary reflector has arbitrary profile. First, let us define the proper receiver aperture width, W_r, that allows the total primarily reflected solar radiation enter the receiver and not get lost. In this case, the solar light ray hitting on the middle line of the reflective elements should be directed on the middle line of the receiver aperture and not on the absorber (Fig. 6.6). We could apply Eq. 6.8 to calculate the proper receiver aperture width, W_r. However, this equation provides different values of the receiver aperture width, W_r, for each primarily reflected solar radiation beam, as they have, in general, different width, d_j, and incidence angle ζ_j ($=\xi_j$). Their dependence on Sun's transversal angle, θ_T, and the reflective elements inclination angle, β_j, imply that the receiver aperture width,

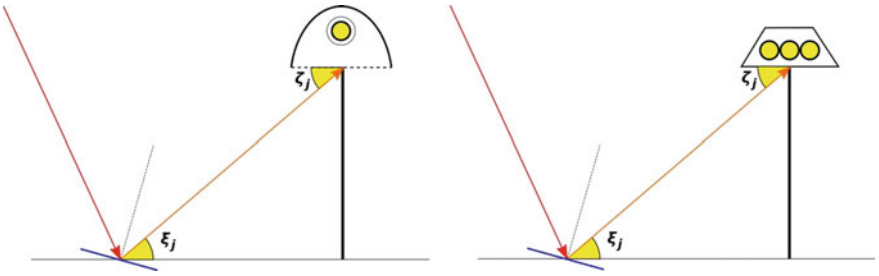

Fig. 6.6 When a secondary reflector is used along with the absorber, as a part of the receiver construction, the solar ray hitting on the middle line of the reflective elements should be directed on the middle line of the receiver aperture and not on the absorber's

W_r, should vary during the day. Therefore, a proper solution would be to take the maximum value of all receivers' aperture width, W_r, calculated by Eq. 6.8

$$W_r = \max_{j,t}\left(W_j \cdot \frac{\left|\sin\left(\theta_T + \beta_j\right)\right|}{\sin \xi_j}\right) \tag{6.9}$$

where the subscript t in Eq. 6.9 implies that we take the maximum value taking into account not only the reflective elements' width but also incorporating the effect the temporally changing reflective elements' inclination angle, β_j, and Sun's transversal angle, θ_T, may have.

However, these calculations may not be so easy to be conducted, as they are time-consuming. Furthermore, the benefit from an accurate computation of the receiver aperture width, W_r, may not be so beneficial, except for saving material, and a rough estimation would be sufficient. From Eq. 6.3, we can conclude that the width of the primarily reflected solar radiation beam takes its maximum value when the quantity $\left|\sin\left(\theta_T + \beta_j\right)\right|$ is maximum. However, since $\left|\sin\left(\theta_T + \beta_j\right)\right|$ cannot take values higher than 1, the possible maximum value of the primarily reflected beam width, $d_{j,\max}$, is equal to the width of the jth reflective element, $d_{j,\max} = W_j$. Moreover, the most inclined primarily reflected solar radiation beam striking the receiver aperture is that originated from the outer reflective element. Hence, Eq. 6.9 can be replaced by the expression

$$W_r = \max_{j}\left(\frac{W_j}{\sin \xi_j}\right) \tag{6.10}$$

An easier, but rougher, approximation of the receiver aperture width, W_r, could be given by the following simpler expression

$$W_r = \frac{\max\limits_{j} W_j}{\min\limits_{j}\left(\sin \xi_j\right)} \tag{6.11}$$

6.2.2 *Primarily Reflected Solar Radiation to Be Concentrated*

The next step in our analysis is to calculate the part of the primarily reflected solar radiation beam that misses the absorber and needs to be redirected back on it, while the rest part is directly absorbed by the absorber. For this reason, the receiver aperture width, W_r, the absorber dimensions and its position in the receiver construction are necessarily known. We assume of course that the primarily reflected solar radiation beam's width and incidence angle are known, or already calculated.

We begin by choosing the secondary reflector's vertex (V), or pole (P) (its geometric centre through which the straight line called principal (or optical) axis passes through and is perpendicular to its aperture), to coincide with the origin (O) of the Cartesian coordinate System, and its principal axis to coincide with the y-axis pointing towards the positive values of y (The secondary reflector is chosen to be symmetrical as there is not any obvious evidence for other choice) (Fig. 6.7). We, further, assume that the secondary reflector has an arbitrary random shape and the absorber is located somewhere inside the reflector but its centre of symmetry (C) is on the principal axis of the reflector. However, concerning the absorber shape, there are only two possible configurations that are worth: the horizontally arranged multiple narrow tubes absorber (Fig. 6.8a), and the single circular tube absorber (Fig. 6.8b). Certainly, there are many other absorber configurations possible, like vertically arranged multiple narrow tubes absorber (Fig. 6.8c) and V-shaped multiple narrow tubes absorber (Fig. 6.8d, f). However, they are rather used without a secondary reflector (vertically arranged multiple narrow tubes absorber and V-shaped multiple narrow tubes absorber) (Fig. 6.8c, d), or in a cavity (reversed V-shaped multiple narrow tubes absorber) (Fig. 6.8e). Consequently, we have two different cases which will be studied in the following paragraphs.

6.2.2.1 Horizontally Arranged Multiple Narrow Tubes Absorber

The receiver configuration comprising of a secondary reflector and a horizontally arranged multiple narrow tubes absorber is illustrated in Fig. 6.7a. We assume that the absorber construction is a three-dimensional (3D) shape, a parallelepiped, which has very short thickness (t_a) (virtually negligible, $t_a \to 0$), width equal to W_a, and very large length (L_a), and is oriented along the longer dimension of the secondary reflector. The absorber (its central point) is placed at a distance, or height, H_a from the origin (O) of the coordinate system ($H_a = |OC|$), and hence, the coordinates of its edges, L and M, are $(x_L, y_L) = (-W_a/2, H_a)$ and $(x_M, y_M) = (W_a/2, H_a)$, respectively. In addition, taking into account the fact that the receiver width is equal to W_r and its height (or depth) is equal to H_r, and the specific geometry of the problem, the coordinates of the points A and B, the edge points of the receiver aperture, are $(x_A, y_A) = (-W_r/2, H_r)$ and $(x_B, y_B) = (W_r/2, H_r)$, respectively.

From the geometry of Fig. 6.7a, we can calculate the part of the primarily reflected solar radiation beam that misses the absorber and needs to be redirected back on it. It consists of two parts. The first part (part I) is bordered by the outer light ray ε_A of the primarily reflected solar radiation beam and the light ray ε_L, passing through the edge L of the absorber, and the second part (part II) is bordered by the light ray ε_M, passing through the edge M of the absorber, and the outer light ray ε_B of the primarily reflected solar radiation beam. The equation describing these four lines, ε_A, ε_B, ε_L and ε_M, can be derived using the primarily reflected solar radiation beam incidence angle, ζ_j ($=\xi_j$), and the coordinates of the four points A, B, L and M.

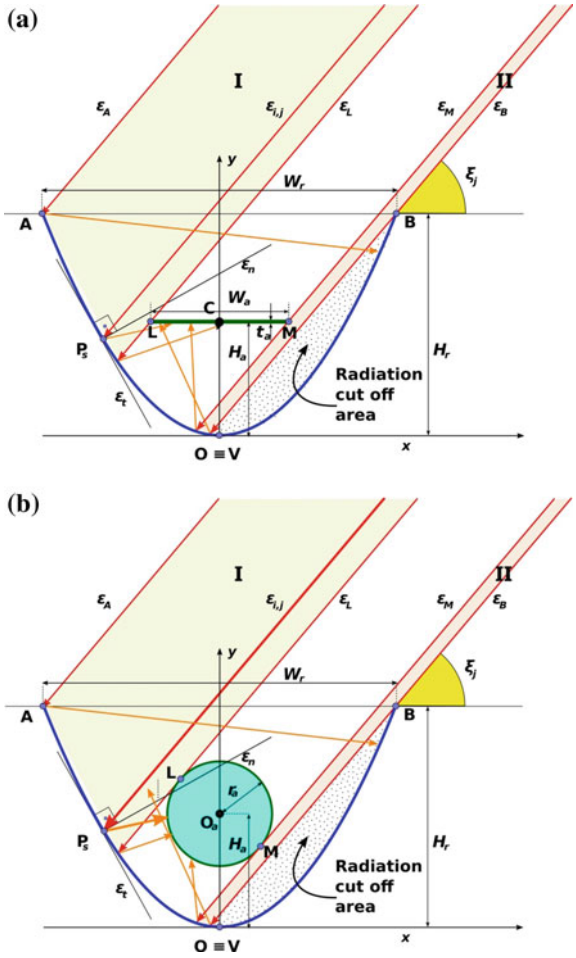

Fig. 6.7 Geometric centre of the secondary reflector, its vertex (V) or pole (P), through which the straight line called principal (or optical) axis passes through, perpendicular to its aperture, has been chosen to coincide with the origin (O) of the Cartesian coordinate system, whereas the principal axis to coincide with the y-axis pointing towards the positive values of y. Furthermore, the secondary reflector is chosen to be symmetrical as there is not any obvious evidence for other choice. **a** The receiver configuration consists of the secondary reflector and a horizontally arranged multiple narrow tubes absorber, which has very short thickness (t_a), width equal to W_a, very large length (L_a), and is oriented along the longer dimension of the secondary reflector. The absorber's central point is placed at a distance, H_a, from the origin (O) of the coordinate system. On the other hand, the absorber may be a single tube being surrounded by another glass tube for protection and thermal insulation (**b**)

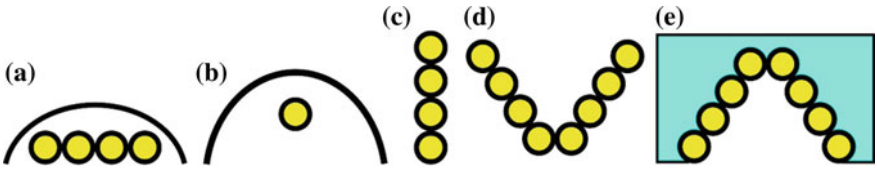

Fig. 6.8 Most important absorber shapes are **a** the horizontally arranged multiple narrow tubes and **b** the single circular tube. However, there has been used many other types, like the vertically arranged multiple narrow tubes (**c**) and V-shaped multiple narrow tubes (**d**, **f**). However, they are rather used in the free space without a secondary reflector (**c**, **d**), or in a cavity (**e**)

The algebraic equation describing a line, ε, on the xy-plane when we know the angle, ξ, it forms with the x-axis and the coordinates, (x_P, y_P), of a point, P, on this line is given by the formula

$$y - y_P = \tan\xi \cdot (x - x_P) \tag{6.12}$$

where $\tan\xi$ is the slope of the line.

Applying this formula to the four lines, ε_A, ε_B, ε_L and ε_M, we can find their algebraic equations:

$$y - H_r = \tan\xi_j \cdot \left(x + \frac{W_r}{2}\right), \quad \text{line } \varepsilon_A \tag{6.13}$$

$$y - H_r = \tan\xi_j \cdot \left(x - \frac{W_r}{2}\right), \quad \text{line } \varepsilon_B \tag{6.14}$$

$$y - H_a = \tan\xi_j \cdot \left(x + \frac{W_a}{2}\right), \quad \text{line } \varepsilon_L \tag{6.15}$$

$$y - H_a = \tan\xi_j \cdot \left(x - \frac{W_a}{2}\right), \quad \text{line } \varepsilon_M \tag{6.16}$$

In addition, any light ray of part I of the primarily reflected solar radiation beam hits the secondary reflector at a point P_s, with coordinates (x_s, y_s), where it is reflected following the law of reflection. To find out whether the reflected light ray is redirected back on the absorber, and potentially absorbed, or not, first we have to calculate the algebraic equation describing the line carrying this ray (its carrier), and second to investigate whether this line intersects the absorber surface or not. To do this, we have to follow a number of steps:

Step 1. ***Finding the normal vector of the reflecting surface at the point of incidence***

To find the normal vector, **n**, at the point of incidence, P_s, the algebraic equation (function) describing the reflecting surface has to be known. Until now, we have not made any assumption about the shape of the reflecting surface.

Let us suppose that its function is $y = f(x)$. The tangential vector, **t**, at any point, $P(x_s, y_s)$, of this surface has coordinates given by the formula

$$t = (x_t, y_t) = \left(1, \left.\frac{\mathrm{d}y}{\mathrm{d}x}\right|_{x=x_s}\right) = \left(1, \left.\frac{\mathrm{d}f(x)}{\mathrm{d}x}\right|_{x=x_s}\right) \tag{6.17}$$

where d/dx is the derivative of the curve at the point $P(x_s, y_s)$ with respect to x.

Now, to get the normal vector, **n**, at this point of the reflecting surface, we just have to turn the tangent vector, **t**, into a normal vector, by rotating it by 90°. For this purpose, we swap the two components (coordinates) of the tangent vector, **t**, and make one of them negative

$$\mathbf{n} = (x_n,\ y_n) = \left(-\left.\frac{\mathrm{d}y}{\mathrm{d}x}\right|_{x=x_s},\quad 1\right) = \left(-\left.\frac{\mathrm{d}f(x)}{\mathrm{d}x}\right|_{x=x_s},\quad 1\right) \tag{6.18a}$$

or

$$\mathbf{n} = (x_n,\ y_n) = \left(\left.\frac{\mathrm{d}y}{\mathrm{d}x}\right|_{x=x_s},\quad -1\right) = \left(\left.\frac{\mathrm{d}f(x)}{\mathrm{d}x}\right|_{x=x_s},\quad 1\right) \tag{6.18b}$$

If we compute the dot product of vectors **t** and **n,** we will find that it is equal to zero:

$$\begin{gathered}\mathbf{t}\cdot\mathbf{n} = x_t \cdot x_n + y_t \cdot y_n \Rightarrow \\ \mathbf{t}\cdot\mathbf{n} = -\left.\frac{\mathrm{d}y}{\mathrm{d}x}\right|_{x=x_s} + \left.\frac{\mathrm{d}y}{\mathrm{d}x}\right|_{x=x_s} = -\left.\frac{\mathrm{d}f(x)}{\mathrm{d}x}\right|_{x=x_s} + \left.\frac{\mathrm{d}f(x)}{\mathrm{d}x}\right|_{x=x_s} = 0\end{gathered} \tag{6.19}$$

which means that the two vectors are perpendicular.

However, how do we choose which component to make negative? If the reflective surface is on the positive part of x-axis and the light ray's incidence angle, ξ_j, is between 0 and $\pi/2$, we make the first component negative; otherwise, if it is between $\pi/2$ and π, we make the second component negative. Similarly, if the reflective surface is on the negative part of x-axis, and the light ray's incidence angle, ξ_j, is between 0 and $\pi/2$, we make the second component negative; otherwise, if it is between $\pi/2$ and π, we make the first component negative.

Finally, to make the normal vector, $\mathbf{n}$, a unit vector, we must divide it by its magnitude

$$|\mathbf{n}| = |x_n, y_n| = \sqrt{\left(\left.\frac{\mathrm{d}y}{\mathrm{d}x}\right|_{x=x_s}\right)^2 + 1} = \sqrt{\left(\left.\frac{\mathrm{d}f(x)}{\mathrm{d}x}\right|_{x=x_s}\right)^2 + 1} \tag{6.20}$$

Hence, the formula providing the coordinates of the unit normal vector, $\hat{\mathbf{n}}$, at any point of the reflecting surface has the form:

$$\begin{aligned}\hat{\mathbf{n}} = (x_n,\ y_n) &= \left(-\frac{\left.\frac{\mathrm{d}y}{\mathrm{d}x}\right|_{x=x_s}}{\sqrt{\left(\left.\frac{\mathrm{d}y}{\mathrm{d}x}\right|_{x=x_s}\right)^2 + 1}},\quad \frac{1}{\sqrt{\left(\left.\frac{\mathrm{d}y}{\mathrm{d}x}\right|_{x=x_s}\right)^2 + 1}} \right) \\ &= \left(-\frac{\left.\frac{\mathrm{d}f(x)}{\mathrm{d}x}\right|_{x=x_s}}{\sqrt{\left(\left.\frac{\mathrm{d}f(x)}{\mathrm{d}x}\right|_{x=x_s}\right)^2 + 1}},\quad \frac{1}{\sqrt{\left(\left.\frac{\mathrm{d}f(x)}{\mathrm{d}x}\right|_{x=x_s}\right)^2 + 1}} \right)\end{aligned} \tag{6.21a}$$

or

$$\begin{aligned}\hat{\mathbf{n}} = (x_n, y_n) &= \left(\frac{\left.\frac{\mathrm{d}y}{\mathrm{d}x}\right|_{x=x_0}}{\sqrt{\left(\left.\frac{\mathrm{d}y}{\mathrm{d}x}\right|_{x=x_0}\right)^2 + 1}},\quad -\frac{1}{\sqrt{\left(\left.\frac{\mathrm{d}y}{\mathrm{d}x}\right|_{x=x_0}\right)^2 + 1}} \right) \\ &= \left(\frac{\left.\frac{\mathrm{d}f(x)}{\mathrm{d}x}\right|_{x=x_s}}{\sqrt{\left(\left.\frac{\mathrm{d}f(x)}{\mathrm{d}x}\right|_{x=x_s}\right)^2 + 1}},\quad -\frac{1}{\sqrt{\left(\left.\frac{\mathrm{d}f(x)}{\mathrm{d}x}\right|_{x=x_s}\right)^2 + 1}} \right)\end{aligned} \tag{6.21b}$$

Step 2. ***Finding the vector of the incoming light rays***

The next step, before we are able to calculate the algebraic equation of the reflected light ray, by applying the vector form of the law of reflection, is to find the vector, $\mathbf{r}_{\mathbf{i},j}$. This vector describes the direction of the incoming light rays that hit the reflector's surface. The vector $\mathbf{r}_{\mathbf{i},j}$ is connected with the algebraic equation of the lines carrying the incoming light rays through their slope. However, all light rays reflected by the same, let us say the jth, primary reflective element have the same slope, the same angle of incidence on the receiver aperture, $\tan\xi_i$. Hence, the coordinates of vector $\mathbf{r}_{\mathbf{i},j}$ are given by the formula

$$\mathbf{r}_{\mathbf{i},j} = \left(x_{\mathbf{i},j}, y_{\mathbf{i},j}\right) = \left(-1, \quad -\tan\xi_j\right), \quad \text{if } 0 < \xi_j < \frac{\pi}{2} \tag{6.22a}$$

$$\mathbf{r}_{\mathbf{i},j} = \left(x_{\mathbf{i},j}, y_{\mathbf{i},j}\right) = \left(1, \quad \tan\xi_j\right), \quad \text{if } \frac{\pi}{2} < \xi_j < \pi \tag{6.22b}$$

To make the light ray vector, $\mathbf{r}_{\mathbf{i},j}$, a unit vector, we must divide it by its magnitude

$$\hat{\mathbf{r}}_{\mathbf{i},j} = \frac{\mathbf{r}_{\mathbf{i},j}}{\left|\mathbf{r}_{\mathbf{i},j}\right|} \tag{6.23}$$

which is given by the formula

$$\left|\mathbf{r}_{\mathbf{i},j}\right| = \left|x_{\mathbf{i},j}, \quad y_{\mathbf{i},j}\right| = \sqrt{\tan^2\xi_j + 1}, \tag{6.24}$$

Thus, the formula providing the coordinates of the unit vector, $\hat{\mathbf{r}}_{\mathbf{i},j}$, that describes the direction of the incoming light rays, has the form:

$$\hat{\mathbf{r}}_{\mathbf{i},j} = \left(x_{\mathbf{i},j}, \quad x_{\mathbf{i},j}\right) = \left(-\frac{1}{\sqrt{\tan^2\xi_j + 1}}, \quad -\frac{\tan\xi_j}{\sqrt{\tan^2\xi_j + 1}}\right) \tag{6.25a}$$

or

$$\hat{\mathbf{r}}_{\mathbf{i},j} = \left(x_{\mathbf{i},j}, \quad x_{\mathbf{i},j}\right) = \left(\frac{1}{\sqrt{\tan^2\xi_j + 1}}, \quad \frac{\tan\xi_j}{\sqrt{\tan^2\xi_j + 1}}\right) \tag{6.25a}$$

Step 3. ***Finding the vector of the reflected light rays***

Having calculated the normal vector, $\mathbf{n}$, at a point of the secondary reflector and the vector, $\mathbf{r}_{\mathbf{i},j}$, describing the direction of the incoming light rays, we can now compute the vector, $\mathbf{r}_{\mathbf{r},j}$, that describes the direction of the reflected light rays by the secondary reflector, by applying the vector form of the law of reflection

$$\mathbf{r}_{\mathbf{r}} = \mathbf{r}_{\mathbf{i}} - 2(\mathbf{r}_{\mathbf{i}} \cdot \mathbf{n})\mathbf{n} \tag{6.26}$$

where $\mathbf{r}_{\mathbf{i}} \cdot \mathbf{n}$ is the dot product of the vectors.

Replacing Eq. 6.22 (a or b) (or Eq. 6.25, a or b) and Eq. 6.18 (a or b) (or Eq. 6.21, a or b) into Eq. 6.26, we can find the coordinates of vector, $\mathbf{r}_{\mathbf{r},j}$, that describes the direction of the reflected light rays by the secondary reflector:

$$\begin{gathered} \mathbf{r}_{\mathbf{r},j} = \mathbf{r}_{\mathbf{i},j} - 2\left(\mathbf{r}_{\mathbf{i},j} \cdot \mathbf{n}\right)\mathbf{n} \Rightarrow \\ \left(x_{\mathbf{r}_{\mathbf{r},j}}, \quad y_{\mathbf{r}_{\mathbf{r},j}}\right) = \left(x_{\mathbf{i},j}, \quad y_{\mathbf{i},j}\right) - 2\left(x_{\mathbf{i},j} \cdot x_n + y_{\mathbf{i},j} \cdot y_n\right) \cdot \left(x_n, \quad y_n\right) \Rightarrow \\ \begin{pmatrix} x_{\mathbf{r},j} \\ y_{\mathbf{r},j} \end{pmatrix} = \begin{pmatrix} x_{\mathbf{i},j} - 2 \cdot x_{\mathbf{i},j} \cdot x_n \cdot x_n - 2 \cdot y_{\mathbf{i},j} \cdot y_n \cdot x_n \\ y_{\mathbf{i},j} - 2 \cdot x_{\mathbf{i},j} \cdot x_n \cdot y_n - 2 \cdot y_{\mathbf{i},j} \cdot y_n \cdot y_n \end{pmatrix} \end{gathered} \tag{6.27}$$

Step 4. ***Finding the algebraic equation of the reflected light rays***

The algebraic equation of a line passing through a point $P(x_P, y_P)$ and being parallel to a vector $\mathbf{a}(x_a, y_a)$ is given by the equation

$$\begin{gathered} \frac{x-x_P}{x_a} = \frac{y-y_P}{y_a} \Rightarrow \\ x - x_P = \frac{x_a}{y_a} \cdot (y - y_P) \end{gathered} \tag{6.28}$$

Applying this Equation to the case of a reflected light ray at the point $P_s(x_s, y_s)$ of the secondary reflectors surface, the algebraic equation of the line, $\varepsilon_{r,j}$, carrying this ray is given by the equation

$$x - x_s = \frac{x_{\mathbf{r},j}}{y_{\mathbf{r},j}} \cdot (y - y_s) \tag{6.29}$$

where $x_{i,j}$ and $y_{i,j}$ are the coordinates of vector $\mathbf{r}_{\mathbf{r},j}$ being parallel to the reflected light ray.

Step 5. ***Investigating whether the secondarily reflected solar radiation is concentrated on the receiver***

The above analysis and calculations have only one objective. To enable us to investigate whether the solar radiation reflected by the secondary reflector is, in the end, concentrated on the receiver. In order to take place such a phenomenon, the secondarily reflected light rays must be intersected by the absorber's surface. However, since in our case the receiver is considered as a line segment (in fact its cross section in the transversal plane), this hypothesis can easily be tested by solving the mathematical problem of two lines intersection. The first line is the carrier of the secondarily reflected light ray, $\varepsilon_{r,j}$, and the second line is the line formed by the two edges of the receiver, the points L and M (Fig. 6.7a). The algebraic equation describing the line passing through these points is given by the formula

$$y - y_L = \frac{y_M - y_L}{x_M - x_L}(x - x_L) \tag{6.30a}$$

or equivalently

$$y - y_M = \frac{y_L - y_M}{x_L - x_M}(x - x_M) \tag{6.30b}$$

where x_L, y_L, x_M and y_M are the coordinates of the points L and M.

Finally, the secondarily reflected light ray, $\varepsilon_{r,j}$, is focused on the receiver if Eqs. 6.29 and 6.30a, b are intersected at a point that belongs in the line segment LM, or else if these two equations (their common point) satisfy the condition

$$\begin{gathered} y = H_a \\ \text{and} \\ x_L \leq x \leq x_M \end{gathered} \tag{6.31}$$

In other words, we check if the following inequality is satisfied

$$x_L \leq x_s + \frac{x_{\mathbf{r},j}}{y_{\mathbf{r},j}} \cdot (H_a - y_s) \leq x_M \tag{6.32}$$

Lastly, to investigate if a part of the primarily reflected solar radiation beam that misses the receiver is not concentrated on the absorber and it is consequently lost, we must conduct the above analysis for all point, $P_s(x_s, y_s)$, of the secondary reflector being intersected by an incoming light ray belonging in the solar radiation beam that has been primarily reflected by the jth reflective element.

6.2.2.2 Single Circular Tube Absorber

In the previous paragraph, the absorber was a flat surface placed horizontally. However, it often consists of a single tube being surrounded by another glass tube for protection and thermal insulation. The procedure used to calculate the unabsorbed part of the primarily reflected solar radiation, and to investigate whether it is secondarily concentrated on the absorber or not is essentially the same as above, with some small differences. The first difference appears in the calculation of the unabsorbed part of the primarily reflected solar radiation. In this case, the reflected solar radiation beam is always perpendicular to a diameter of the absorber cross section let it be the LM (Fig. 6.7b). The part that misses the absorber and needs to be redirected back on it, it is also illustrated in Fig. 6.7b. It also consists of two parts. The first part (part I) is bordered by the outer light ray, ε_A, of the primarily reflected solar radiation beam and the light ray ε_L, being tangent to the circular absorber cross section at the point L (it is perpendicular to the diameter LM). The second part (part II) is bordered by the light ray ε_M being tangent to the circular absorber cross section at the point M, and the outer light ray ε_B of the primarily reflected solar radiation beam. The equation describing these four lines, ε_A, ε_B, ε_L and ε_M, can be derived by using the angle of incidence, ξ_j, of the jth primarily reflected solar radiation beam on the receiver aperture, and the coordinates of the four points A, B, L and M.

The algebraic equations of lines ε_A and ε_B are given by Eqs. 6.13 and 6.14, respectively. On the other hand, the algebraic equations of lines ε_L and ε_M are defined similarly to Eqs. 6.15 and 6.16 except that the points L and M are not fixed and depend on each primarily reflected solar radiation beam, in fact on each individual reflective element. Let us consider the jth reflective element. The slope, a_j, of the line carrying the diameter being perpendicular to the jth primarily reflected solar radiation beam is

$$a_j = -\frac{1}{\tan \xi_j} \tag{6.33}$$

Therefore, the algebraic equation of the line carrying the diameter being perpendicular to the *j*th primarily reflected solar radiation beam is given by the equation

$$\begin{gathered} y - y_a = a_j \cdot (x - x_a) \Rightarrow \\ y - y_a = -\frac{1}{\tan \xi_j} \cdot (x - x_a) \Rightarrow \\ y - H_a = -\frac{1}{\tan \xi_j} \cdot x \Rightarrow \end{gathered} \tag{6.34}$$

where $(x_a, y_a) = (0, H_a)$ are the coordinates of the centre, O_a, of the circular receiver, or more correctly, of its transversal cross section, since the receiver is a cylindrical tube.

The parametric equations for the coordinates x and y of any point $P(x, y)$ of a circle with centre at the point $O_c(x_c, y_c)$ and with a radius equal to r are

$$x = x_c + r \cdot \cos t \tag{6.35a}$$

$$y = y_c + r \cdot \sin t \tag{6.35b}$$

where the parameter t satisfies the condition $0 \leq t < 2\pi$.

If we move x_c and y_c in the first part of Eqs. 6.35a and b, square each part and then add these equations, we get the equation describing the circle in Cartesian coordinates

$$\begin{gathered} (x - x_c)^2 + (y - y_c)^2 = r^2 \cdot \sin^2 t + r^2 \cdot \cos^2 t \Rightarrow \\ (x - x_c)^2 + (y - y_c)^2 = r^2 \end{gathered} \tag{6.36}$$

In our case, the parametric equations describing the circumference of the one tube absorber, located (its centre) on the *y*-axis at a height H_a above the origin, $O(0, 0)$, of the local Cartesian coordinate system, e.g. at the point $O_a(0, H_a)$, which its radius is equal to r_a, are:

$$x = r_a \cdot \cos t \tag{6.37a}$$

$$y = H_a + r_a \cdot \sin t \tag{6.37b}$$

Subsequently, in order to find the points L and M, we just have to solve the system of Eqs. 6.37a, b and 6.34 and find the parameter t. So, replacing Eqs. 6.37a, b into Eq. 6.34 we get

$$\begin{aligned} H_a + r_a \cdot \sin t - H_a &= -\tfrac{1}{\tan \xi_j} \cdot r_a \cdot \cos t \Rightarrow \\ r_a \cdot \sin t &= -\tfrac{1}{\tan \xi_j} \cdot r_a \cdot \cos t \Rightarrow \\ \sin t &= -\tfrac{1}{\tan \xi_j} \cdot \cos t \Rightarrow \\ \tfrac{\sin t}{\cos t} &= -\tfrac{1}{\tan \xi_j} \Rightarrow \\ \tan t &= -\tfrac{1}{\tan \xi_j} \Rightarrow \\ t &= k \cdot \pi + \tan^{-1}\left(-\tfrac{1}{\tan \xi_j}\right) \Rightarrow \\ t &= k \cdot \pi - \tan^{-1}\left(\tfrac{1}{\tan \xi_j}\right) \end{aligned} \tag{6.38}$$

where k is an integer, and because t satisfies the condition $0 \leq t < 2 \cdot \pi$, k is equal to 1 or 2. Hence

$$t_L = \pi - \tan^{-1}\left(\frac{1}{\tan \xi_j}\right) \tag{6.39a}$$

and

$$t_M = 2 \cdot \pi - \tan^{-1}\left(\frac{1}{\tan \xi_j}\right) \tag{6.39b}$$

Replacing t (t_L and t_M) from Eqs. 6.39a, b into Eq. 6.37a, b, we can find the coordinates of the two points L and M.

Now, we can follow the same steps as in the first case of the horizontally arranged multiple narrow tubes absorber up to Step 5. However, in order to investigate whether the solar radiation reflected by the secondary reflector is, in the end, concentrated on the receiver or not (Step 5), we have to check if the carrier (the line) of the secondarily reflected light ray, $\varepsilon_{r,j}$, and the circumference of the absorber are intersected. Or, in other words, if the system of the following equation can be solved:

$$x - x_s = \frac{x_{\mathbf{r},j}}{y_{\mathbf{r},j}} \cdot (y - y_s) \tag{6.29}$$

$$x = r_a \cdot \cos t \tag{6.35a}$$

$$y = H_a + r_a \cdot \sin t \tag{6.35b}$$

where x_s, y_s are the coordinates of the point $P_s(x_s, y_s)$ of the secondary reflectors surface, where the jth incoming light ray is reflected, and $x_{\mathbf{r},j}$ and $y_{\mathbf{r},j}$, are the coordinates of the vector being parallel to the reflected light ray.

Similarly, just as in the previous case, in order to find out if a part of the primarily reflected solar radiation beam that misses the receiver is not concentrated on the absorber and it is consequently lost, we must conduct the above analysis for

all points, $P_s(x_s, y_s)$, of the secondary reflector being intersected by an incoming light ray belonging in the solar radiation beam primarily reflected by the jth reflective element.

For both cases, if the reflector's surface is composed by a well-defined curve described by an equation of the form $y = f(x)$, then we can easily carry out the above procedure for all x belonging in the intervals $[x_A, x_{L'}]$ and $[x_{M'}, x_B]$, where L' and M' are the points where lines ε_L and ε_M intersect the secondary reflectors surface, and $x_{L'}$ and $x_{M'}$ are their coordinates on the x-axis (or else for all $x_A \leq x_s \leq x_{L'}$ and $x_{M'} \leq x_s \leq x_B$).

Finally, all the above-presented calculations must be performed for each individual reflective element of the Linear Fresnel Reflector System and then all individual results must be added in order to compute, or evaluate, the whole effect the secondary reflector has on the Systems performance and efficiency.

6.2.2.3 Secondarily Absorbed Solar Radiation

The solar radiation concentrated on the absorber by the secondary reflector can be calculated from that part of the primarily reflected solar radiation beam that initially misses the absorber but in the end is redirected back on it by a second reflection on the secondary reflector. Its amount can be calculated if we take into account the fact that the solar radiation beam carries energy which is proportional to the area of its cross section, or, if we take advantage of the System's symmetry, to its width. However, there is present an extra loss mechanism that is difficult to be incorporated in the calculations.

In the horizontally arranged multiple narrow tubes absorber, a plane glass cover is used to prevent heat loss, while in the case of a single circular tube absorber the most frequently used protection mechanism is a glass tube that surrounds the absorbing tube, although a plane glass cover could also be used in the same manner as in the first case (Fig. 6.9). However, when light meets a glass surface, some of the light is reflected (depending on the angle of incidence and the refractive indices of the glass and the air) and the rest passes through. The fraction of the reflected and transmitted light energy can be determined using the Fresnel equations, which is, however, out of the scope of this book, as they are extremely complex and depend on many variables. In addition, although in the case of the plane glass cover, the

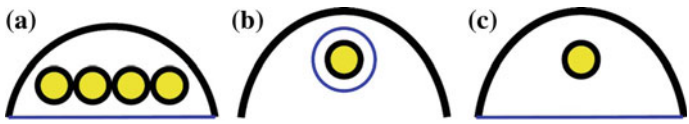

Fig. 6.9 In the horizontally arranged multiple narrow tubes absorber, a plane glass cover is used to prevent heat losses (**a**), whereas in the case of a single circular tube absorber the most frequently used protection mechanism is a glass tube that surrounds the absorbing tube (**b**), although a plane glass cover could also be used in the same manner as in the first case (**c**)

incidence angle on the cover is constant, in the case of the glass tube surrounding the absorber, the incidence angle of each secondarily reflected light ray is different, which makes the calculations even more difficult. Therefore, in the rest of the book, this type of energy loss is not taken into account.

Figure 6.10 illustrates a typical case of a secondary solar radiation concentrator. Usually not all light rays that initially miss the absorber can be redirected back on it. Let us consider the part of the primarily reflected solar radiation beam that misses the absorber denoted as Part A in Fig. 6.10. It is bordered by the two light rays ε_{I} and $\varepsilon_{\mathrm{II}}$. The shape of the secondary reflector is usually concave and has not any inflexion point (a point where the reflector's curve changes from being concave to being convex), and is symmetric around its principal axis. Hence, since the incoming light rays are parallel and, all are reflected according to the law of reflection, they are all redirected by being turned towards the same direction (clockwise or anticlockwise). What is different in each light ray is the extent of their turn. As a consequence, there is one light ray, ε_1, which is the first that is successfully redirected onto the absorber and another, ε_2, which is the last that falls on the absorber (Fig. 6.10). The rest light rays, before the first and after the last light ray, are getting lost. If we can determine these two light rays, their distance in the primarily reflected solar radiation beam is proportional to the solar energy that is secondarily concentrated on the absorber. For example, if these two light rays (in fact the lines carrying them) are at a distance $d_{s,A,j}$ in the primarily reflected solar radiation beam, and the beam's width is d_j, for the jth reflective element, then the corresponding secondary concentration factor, $C_{s,A,j}$, is given by the simple formula

$$C_{s,A,j} = \frac{d_{s,A,j}}{d_j} < 1 \tag{6.40}$$

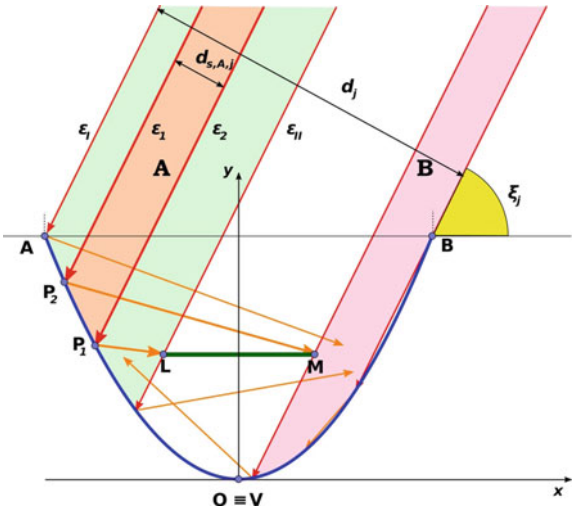

Fig. 6.10 Usually not all light rays that initially miss the absorber can be redirected back on it. As the secondary reflector is usually concave, there is one light ray, ε_1, that is, the first that is successfully redirected onto the absorber and another, ε_2, that is, the last that falls on the absorber. The rest light rays, before the first and after the last light ray, are getting lost

To compute the overall secondary concentration factor, C_s, we must add all the individual secondary concentration factors, $C_{s,A,j}$, for both parts A and B and for all reflective elements j (from $j = 1$ to N)

$$C_s = \sum_{\text{Part}=A}^{B} \sum_{j=1}^{N} C_{s,\text{Part},j} = \sum_{\text{Part}=A}^{B} \sum_{j=1}^{N} \frac{d_{s,\text{Part},j}}{d_j} \tag{6.41}$$

So, the last task to be done is to find the carrying lines of the two light rays ε_1 and ε_2. In general, they are described by Eq. 6.29.

$$x - x_s = \frac{x_{\mathbf{r},j}}{y_{\mathbf{r},j}} \cdot (y - y_s) \tag{6.29}$$

Hence, since the coordinates $x_{\mathbf{r},j}$ and $y_{\mathbf{r},j}$ of the vector of the reflected light ray are related to the point of reflection, $P_s(x_s, y_s)$, through Eqs. 6.18a, b and 6.27, we look for those points $P_1(x_1, y_1)$ and $P_2(x_2, y_2)$ of the secondary reflector that correspond to the two lines ε_1 and ε_2.

6.3 Secondary Reflector's Profiles

In the previous paragraphs, we did not consider any specific shape for the secondary reflector. We assumed that it is described by a one-dimensional function of the general form $y = f(x)$. The next step is to determine this function by an appropriate mathematic expression and to investigate the performance and the efficiency of the secondary reflector using the above-presented methodology.

A secondary reflector can be used only when the absorber is a single tube with a circular cross section, or when it consists of multiple narrow tubes which are arranged horizontally. In the second case, the receiver construction is a cavity, usually trapezoidal with plane reflectors or slightly bent, having the shape of a more complex curve, e.g. parabolic, and the absorbing tubes are placed on the top of the cavity, or, rarely, in a short distance below it (Fig. 6.11) (In this book, when a cavity construction is studied, it is placed in reverse manner than it is illustrated in Fig. 6.11, and the bottom is its top. For example, see Figs. 6.7 and 6.10, as well as

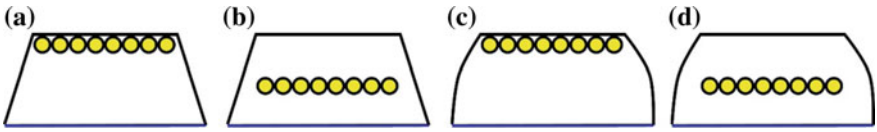

Fig. 6.11 When the absorber consists of multiple narrow tubes arranged horizontally, the receiver construction is a cavity, usually trapezoidal with plane reflectors (**a**, **b**) or slightly bent (**c**, **d**) having the shape of a more complex curve, e.g. parabolic. In any case, the absorbing tubes can be placed on the top of the cavity (**a**, **c**), or, rarely, in a short distance below it (**b**, **d**)

the next figures. This treatment simplifies the related calculations. So, if we would like to describe the receiver using this illustration the previous expression would be "*the absorbing tubes are place on the **bottom** of the cavity, or, rarely, in a short distance **above** it*"). On the other hand, in the first case, the secondary reflector may have more complex shapes that may either form a cavity or not. The most common secondary reflectors are arcs or semicircles, parabolic, parabolic wing-like, segmented parabolic, compound parabolic, parabolic involutes or combinations of them (Chaitanya et al. 2017; Lin et al. 2013). Hence, it is obvious that the performance of a secondary reflector is highly related to its shape and the relative place of the absorber.

6.3.1 Horizontally Arranged Multiple Narrow Tubes Absorber and Trapezoidal Cavity

In the case of trapezoidal, and trapezoidal-modified, cavities, the key geometric parameters of the receiver are the absorber width, W_a, the vertical distance of the absorber from the cavity bottom, H_a, and the dimensions and the shape of the cavity bottom and sides, as well as, the angles they form. The most commonly used configuration is all three sides of the cavity to be plane. In this case, the angles formed by the sides of the cavity with its bottom play a critical role. The next more complex stage is to replace the side plane reflectors with curved reflectors. This, however, complicates the construction requirements of the reflector's sides.

Let us, now, consider a trapezoidal cavity with plane sides. In addition, let its bottom's width be equal to b_r, the side reflectors' length equal to s_r, and the angles they form with the cavity bottom equal to φ_r (Fig. 6.12). Hence, the function, $y = f(x)$, describing the secondary reflector shape has the form

$$y = f(x) = \begin{cases} \tan\varphi_r \cdot \left(x + \frac{b_r}{2}\right) & -\left(\frac{b_r}{2} + s_r \cdot \cos(\pi - \varphi_r)\right) \le \mathbf{x} \le -\frac{b_r}{2} \\ 0, & -\frac{b_r}{2} \le \mathbf{x} \le \frac{b_r}{2} \\ \tan(\pi - \varphi_r) \cdot \left(x - \frac{b_r}{2}\right) & \frac{b_r}{2} \le \mathbf{x} \le \frac{b_r}{2} + s_r \cdot \cos(\pi - \varphi_r) \end{cases} \tag{6.42}$$

where $(-s_r \cdot \cos(\pi - \varphi_r) - b_r/2, s_r \cdot \sin\varphi_r)$, $(s_r \cdot \cos(\pi - \varphi_r) + b_r/2, s_r \cdot \sin\varphi_r)$, $(b_r/2, 0)$ and $(-b_r/2, 0)$, are the coordinates of the edges A, B, C and D of the secondary reflector cavity, respectively.

However, the trapezoidal cavity with plane bottom and sides can be studied with a lighter version of the previously presented methodology, due to the simpler geometry of the problem. The concentration efficiency of the secondary reflector can be studied for two characteristic primarily reflected solar radiation beams, the beam originated from the outer primary reflector and the beam coming from the reflector placed underneath the receiver. The first beam is the most oblique, the second may fall on the receiver aperture almost perpendicular and the rest

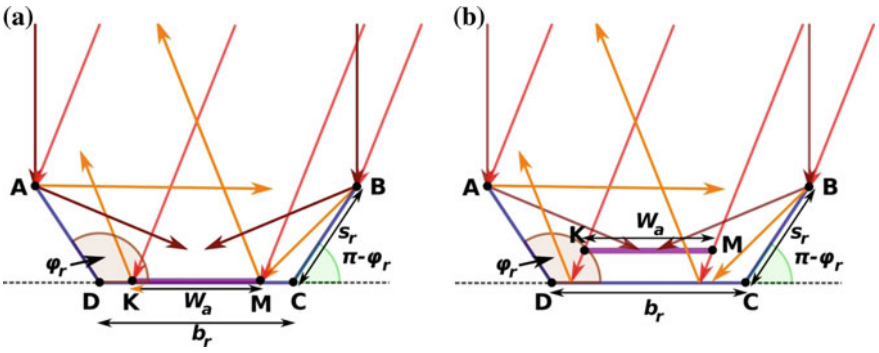

Fig. 6.12 In a trapezoidal cavity, the bottom's width, which is equal to b_r, the side reflectors' length, being equal to s_r, and the angles they form with the cavity's bottom, equal to φ_r, are the construction parameters that play a critical role in the receiver performance. In addition, the absorber width, W_a, when it is placed at a vertical distance equal to H_a from the cavity bottom, is another important factor. The secondary reflector efficiency can be studied using two characteristic primarily reflected solar radiation beams, the beam originated from the outer primary reflector, say the o beam, and the beam coming from the reflector placed underneath the receiver, the p beam. If the absorber is not placed on the receiver bottom (**a**), but is located at a distance H_a above it (**b**) the solar radiation concentration process is more complicated

beams hit the receiver having angles of incidence between these two extreme values. Let us assign the index o to the first beam, the most oblique, and the index p to the second beam, the almost perpendicular (Fig. 6.12). We can distinguish two main cases. In the first case, the absorber is placed on the receiver bottom, in fact, it forms the receiver' bottom (Fig. 6.12a), and in the second case the absorber is located at a distance H_a above the receiver bottom (Fig. 6.12b). In the first case, the receiver's bottom width, b_r, is equal to the absorber width, W_a, ($b_r = W_a$), whereas in the second case the absorber width, W_a, may be smaller than the receiver's bottom width, b_r, complicating the problem. Let us study each case separately.

6.3.1.1 Absorber on the Receiver's Bottom

This is the simpler case. The incoming solar radiation beam is split in two main parts. *Part A* is directly falling on the absorber and consequently absorbed, while the rest of the beam is divided in other two parts, part I and part II, falling each one outside of both edges of the absorber. Let part I be falling on the side where the oblique beam is coming (Fig. 6.13). Using the geometry of Fig. 6.13, the light rays $\varepsilon_{o\mathrm{I},1}$ and $\varepsilon_{o\mathrm{I},2}$ border part I of the primarily reflected solar radiation beam o are falling on the part CB of the secondary reflector and are reflected and redirected towards the absorber. Since the incoming light rays are parallel, they also remain parallel after their reflection by the side plane reflector (the part CB). Therefore, in order to be redirected part I of the primarily reflected solar radiation beam on the

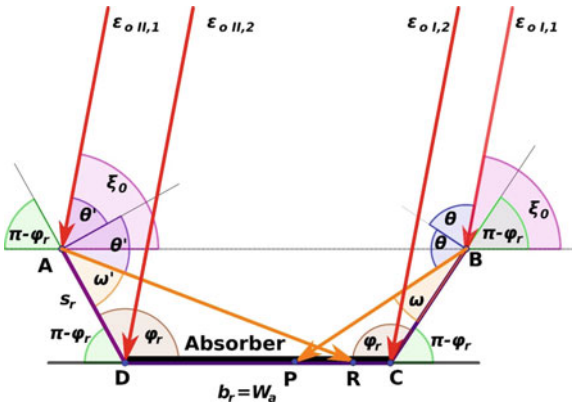

Fig. 6.13 Placing the absorber on the cavity's bottom is the simpler case. To study the solar radiation secondary concentration, we split the incoming solar radiation beam into three parts. *Part A* is directly falling on the absorber, while part I and part II are falling each one outside of both edges of the absorber. Part I is falling on the side where the oblique beam is coming and it is bordered by the light rays $\varepsilon_{o\mathrm{I},1}$ and $\varepsilon_{o\mathrm{I},2}$, which hit the secondary reflector at the points *C* and *B*, while light rays $\varepsilon_{o\mathrm{II},1}$ and $\varepsilon_{o\mathrm{II},2}$ are bordering part II. They hit the secondary reflector at the points *A* and *D*. Part I and part II are redirected on the absorber, if the light rays $\varepsilon_{o\mathrm{I},1}$ and $\varepsilon_{o\mathrm{II},1}$ hit the absorber at points *P* and *R*, respectively, located somewhere between the points *D* and *C*

absorber, the light ray $\varepsilon_{o\mathrm{I},1}$ must hit the absorber at a point *P* located somewhere between the points *D* and *C*. In other words, the following condition must be satisfied

$$|PC| \leq |DC| \tag{6.43}$$

The length $|PC|$ of the line segment *PC* can be easily calculated from Fig. 6.13 using the Law of sines. So,

$$\frac{|PC|}{\sin \widehat{PBC}} = \frac{|BC|}{\sin \widehat{BPC}} \tag{6.44}$$

Angle $\widehat{PBC}$ is given by the equation

$$\begin{aligned} \widehat{PBC} = \omega = \xi_o - (\pi - \varphi_r) \Rightarrow \\ \widehat{PBC} = \xi_o - \pi + \varphi_r \end{aligned} \tag{6.45}$$

where ξ_o is the angle of incidence of the beam *o*, and φ_r is the angle formed by the reflector's sides with its bottom.

On the other hand, angle $\widehat{BPC}$ is given by the equation

$$\begin{gathered}\widehat{BPC} = 2 \cdot \pi - \widehat{PBC} - \widehat{PCB} \Rightarrow \\ \widehat{BPC} = 2 \cdot \pi - (\xi_o - \pi + \varphi_r) - \varphi_r \Rightarrow \\ \widehat{BPC} = 2 \cdot \pi - \xi_o + \pi - \varphi_r - \varphi_r \Rightarrow \\ \widehat{BPC} = 3 \cdot \pi - \xi_o - 2 \cdot \varphi_r\end{gathered} \tag{6.46}$$

Now, substituting Eqs. 6.45 and 6.46 into Eq. 6.44 and then Eq. 6.44 into Eq. 6.43 it becomes

$$\begin{gathered}|BC| \cdot \frac{\sin(\xi_o - \pi + \varphi_r)}{\sin(3 \cdot \pi - \xi_o - 2 \cdot \varphi_r)} \leq |DC| \\ \frac{\sin(\xi_o - \pi + \varphi_r)}{\sin(3 \cdot \pi - \xi_o - 2 \cdot \varphi_r)} \leq \frac{|DC|}{|BC|}\end{gathered} \tag{6.47}$$

Since angle ξ_o is a construction parameter, depending on the receiver and the outer (the nth) reflective element position, given by the equation

$$\xi_o = \tan^{-1}\left(\frac{H}{Q_n}\right) \tag{6.48}$$

we must choose the appropriate value of angle φ_r, so that Eq. 6.47 to be satisfied. However, this is not the only condition that has to be satisfied in order that the whole energy of the primarily reflected solar radiation beam o to be concentrated on the absorber. A similar equation has to be derived for part II of the beam.

Let, now, $\varepsilon_{o\text{II},1}$ and $\varepsilon_{o\text{II},2}$ be the light rays bordering part II of the primarily reflected solar radiation beam o falling on the part AD of the secondary reflector. Part II is redirected on the absorber, if the light ray $\varepsilon_{o\text{II},1}$ must hit the absorber at a point R located somewhere between the points D and C. In other words, the following condition must be satisfied

$$|DR| \leq |DC| \tag{6.49}$$

The length $|DR|$ of the line segment DR can be easily calculated from Fig. 6.13 using the Law of sines. So,

$$\frac{|DR|}{\sin \widehat{DAR}} = \frac{|AD|}{\sin \widehat{ARD}} \tag{6.50}$$

Angle $\widehat{DAR}$ is given by the equation

$$\begin{gathered}\widehat{DAR} = \pi - \xi_o - (\pi - \varphi_r) \Rightarrow \\ \widehat{DAR} = \xi_o + \varphi_r\end{gathered} \tag{6.51}$$

On the other hand, angle $\widehat{ARD}$ is given by the equation

$$\begin{gathered}\widehat{ARD} = 2 \cdot \pi - \widehat{DAR} - \widehat{ADR} \Rightarrow \\ \widehat{ARD} = 2 \cdot \pi - (\xi_o + \varphi_r) - \varphi_r \Rightarrow \\ \widehat{ARD} = 2 \cdot \pi - \xi_o - \varphi_r - \varphi_r \Rightarrow \\ \widehat{ARD} = 2 \cdot \pi - \xi_o - 2 \cdot \varphi_r \end{gathered} \tag{6.52}$$

Now, substituting Eqs. 6.52 and 6.51 into Eq. 6.50 and then Eq. 6.50 into Eq. 6.49, it becomes

$$\begin{gathered}|DR| \cdot \frac{\sin(\xi_o + \varphi_r)}{\sin(2 \cdot \pi - \xi_o - 2 \cdot \varphi_r)} \leq |DC| \\ \frac{\sin(\xi_o + \varphi_r)}{\sin(2 \cdot \pi - \xi_o - 2 \cdot \varphi_r)} \leq \frac{|DR|}{|BC|}\end{gathered} \tag{6.53}$$

However, if the angle of incidence, ξ_o, is smaller than a critical angle, ψ,

$$\xi_o \leq \psi \tag{6.54}$$

then all reflected light rays of part II of the beam o are directed away from the absorber (Fig. 6.14).

From the geometry of Fig. 6.14, this angle is given by the equation

$$\begin{gathered}\psi = \pi - (\pi - \varphi_r) - \left(\frac{\pi}{2}\right) \Rightarrow \\ \psi = \pi - \pi + \varphi_r - \left(\frac{\pi}{2}\right) \Rightarrow \\ \psi = \varphi_r - \left(\frac{\pi}{2}\right)\end{gathered} \tag{6.55}$$

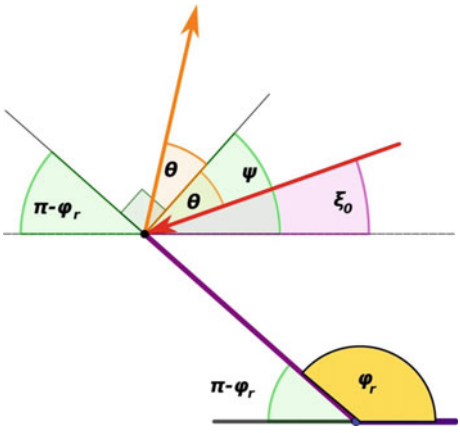

Fig. 6.14 If the angle of incidence, ξ_o, of a primarily reflected solar radiation beam is smaller than a critical angle, ψ, then all light rays of part II of the beam are reflected by the secondary reflector away from the absorber

Next, substituting Eq. 6.55 into Eq. 6.54 and solving the inequality for angle φ_r, we get the extra condition

$$\begin{aligned} \varphi_r - \left(\frac{\pi}{2}\right) &\leq \xi_o \\ \varphi_r &\leq \xi_o + \frac{\pi}{2} \end{aligned} \tag{6.56}$$

However, the above analysis must be carried out for all primarily reflected solar radiation beams, or at least for the most oblique solar radiation beam and that falling perpendicular on the receiver aperture. What is different is only the angle of incidence, ξ_j, which for the last case is equal to $\pi/2$.

Therefore, angle, φ_r, formed by the reflector's sides and its bottom has to satisfy all the following conditions:

$$\frac{\sin(\xi_o - \pi + \varphi_r)}{\sin(3 \cdot \pi - \xi_o - 2 \cdot \varphi_r)} \leq \frac{|DC|}{|BC|} \tag{6.47}$$

$$\frac{\sin(\xi_o + \varphi_r)}{\sin(2 \cdot \pi - \xi_o - 2 \cdot \varphi_r)} \leq \frac{|DR|}{|BC|} \tag{6.53}$$

$$\varphi_r \leq \xi_o + \frac{\pi}{2} \tag{6.56}$$

$$\frac{\sin\left(\varphi_r - \frac{\pi}{2}\right)}{\sin\left(\frac{5 \cdot \pi}{2} - 2 \cdot \varphi_r\right)} \leq \frac{|DC|}{|BC|} \tag{6.57}$$

$$\frac{\sin\left(\frac{\pi}{2} + \varphi_r\right)}{\sin\left(\frac{3 \cdot \pi}{2} - 2 \cdot \varphi_r\right)} \leq \frac{|DR|}{|BC|} \tag{6.58}$$

$$\varphi_r \leq \pi \tag{6.59}$$

6.3.1.2 Absorber Above the Receiver's Bottom

If the absorber is not placed on the receiver's bottom, but at a distance, H_a, above it, then the problem is a little more complicated. However, it is also dealt with the above-applied methodology with the key difference that part I is split into three parts, say α, β and γ, and part II is split also into three parts, say α', β' and γ' (Fig. 6.15) (it depends on the receiver geometry and the direction of the incoming solar radiation). The light rays of each subpart are reflected by different parts of the reflector and are directed onto different parts of the absorber. Therefore, the above methodology has to be applied separately in each subpart and the final conclusion about the proper value of angle φ_r has to take into account all individuals results.

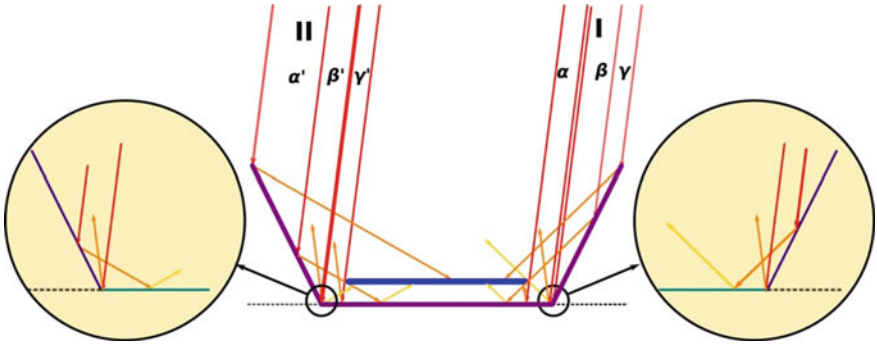

Fig. 6.15 If the absorber is placed at a distance, H_a, above the cavity's bottom, part I of the primarily reflected solar radiation beam is split in three parts, α, β and γ, while part II is split also in three parts, α', β' and γ'. The solar radiation of each subpart hits onto different parts of the absorber and therefore, it needs to be treated separately

6.3.2 Single Circular Tube Absorber

Obviously, the study of more complex secondary reflector shapes follows the same pattern as above with the important remark that the curved reflectors are concave and the secondary reflected light rays converge. As a consequence, the two border light rays, ε_1 and ε_2, or ε_3 and ε_4, of both parts of the primarily reflected solar radiation beam that miss the absorber are intersected at a point. This point may be beyond the absorber or somewhere between the absorber and the secondary reflector. Any other pair of light rays of both parts of the light beam leads to the same conclusion. However, despite the fact that all incoming light rays are parallel to each other the secondarily reflected are not. Therefore, the above procedure has to be applied stepwise, or even more correctly, by using a numerical integration method. In any case, the presentation of such analytical calculations is beyond the scope of this book, as they strongly depended on each particular reflector profile. This can easily be deduced from the above-presented treatment of the simple case of the trapezoidal cavity.

Nevertheless, the knowledge of the mathematical function describing the secondary reflector's shape (or profile) enables the implementation of this methodology any time it is required. Hence, in the following paragraphs, we will present the mathematical description of the most commonly used shapes of secondary reflectors.

6.3.2.1 V-Shaped Concentrator

The V-shaped concentrator may be deemed as a special case of the cavity receiver. In this case, the absorber consists of a single tube, encased in a glass tube or not. In the second case, the whole cavity is equipped with a protecting glass plate

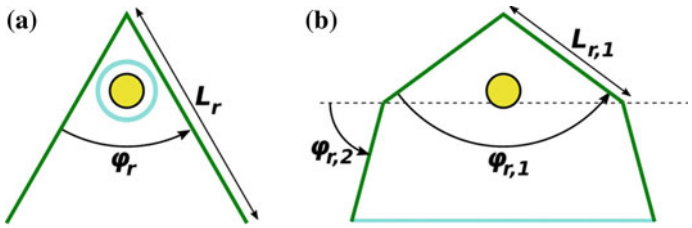

Fig. 6.16 V-shaped concentrator is a special case of cavity receivers. **a** The absorber consists of a single tube, encased in a glass tube or the whole cavity is equipped with a protecting glass plate. **b** A compound V-shaped concentrator can be more efficient if it consists of two slightly different parts. The first part is a classical V-shaped concentrator with a relatively large angle, $\varphi_{r,1}$, and the other part is a frustum V-shaped concentrator with a different, smaller, angle

(Fig. 6.16a). The characteristic parameters of this secondary reflector are the length, L_r, of its sides, and the angle, φ_r, they form. To be efficient this type of secondary reflectors, the angle, φ_r, has to be small enough and the absorber must be placed close to the vertex of the concentrator, at the point where its two sides are met.

On the other hand, a more efficient V-shaped concentrator could consist of two slightly different parts. The first part is a classical V-shaped concentrator with a relatively large angle, $\varphi_{r,1}$, and the other part is a frustum V-shaped concentrator with a different, smaller, angle. The two parts form a compound V-shaped concentrator (Fig. 6.16b). This secondary reflector is characterized by the length, $L_{r,1}$, of the sides of its first part, and the corresponding angle, $\varphi_{r,1}$, they form, the length, $L_{r,2}$, of the sides of its second part, and the angle, $\varphi_{r,2}$, each one forms with a line parallel to the x-axis. Moreover, the absorber tube with radius r_a is placed at a height H_a below the vertex of the concentrator which coincides with the origin of the local Cartesian coordinate system.

6.3.2.2 Arc-Shaped and Semi-circular Concentrator

The arc-shaped secondary reflector may be considered as a special case of a semi-circular concentrator. The vertex of the reflective surface coincides with the origin of the Cartesian coordinate system, O. If the radius of the corresponding circle is R_r, then the parametric algebraic equations describing the semi-circular secondary reflector are

$$x = R_r \cdot \cos t \tag{6.60}$$

$$y = R_r + R_r \cdot \sin t \tag{6.61}$$

where $\pi \leq t \leq 2 \cdot \pi$, as the centre Q of the circle is at the point $(0, R_r)$.

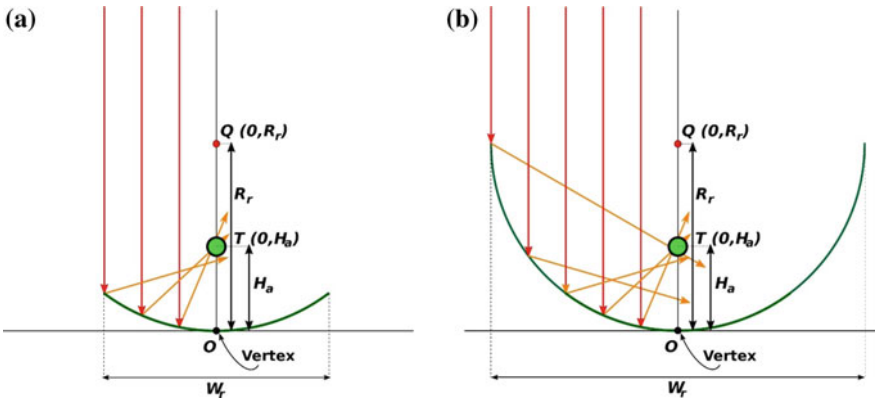

Fig. 6.17 Geometry of a typical arc-shaped (**a**), and a typical semi-circular secondary concentrator (**b**)

If the concentrator is not a full semicircle but only an arc of angle $\theta_r < \pi$, parameter t takes values in the closed interval

$$\left[\frac{3 \cdot \pi - \theta_r}{2}, \frac{3 \cdot \pi + \theta_r}{2}\right]$$

or else

$$\frac{3 \cdot \pi - \theta_r}{2} \leq t \leq \frac{3 \cdot \pi + \theta_r}{2}$$

In addition, the centre of the absorber is placed at the point $T(0, H_a)$, while its radius is equal to R_a. Figure 6.17 provides a typical example of an arc-shaped and a semi-circular concentrator. The problem related with this type of reflective surface is that parallel light rays do not converge at a single point but on a line (more correctly on a line segment) (Fig. 6.18). Moreover, parallel light ray that forms an angle with the principal axis of the mirror do not converge on the same line segment. In fact, each incident (primarily reflected) solar radiation beam converges on a different line segment (Fig. 6.18b, c). However, if the reflector is a small part of the circle (arc-shaped concentrator) with small aperture width, W_r, in relation to the circle radius, R_r, $W_r \ll R_r$, then the focus segment is very short (Fig. 6.19), and its angular deviation is also small.

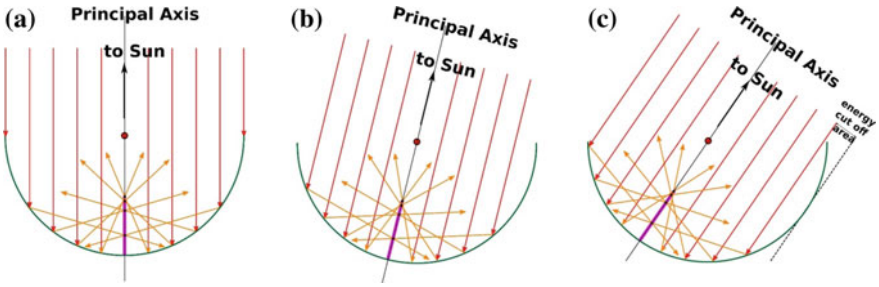

Fig. 6.18 Spherical, or cylindrical mirrors with circular cross section, suffer from spherical aberration. Parallel light rays does not converge at a single point but on a line (more correctly on a line segment) (**a**). Moreover, parallel light ray that forms an angle with the principal axis of the mirror do not converge on the same line segment. In fact, each incident (primarily reflected) solar radiation beam converges on a different line segment (**b**, **c**)

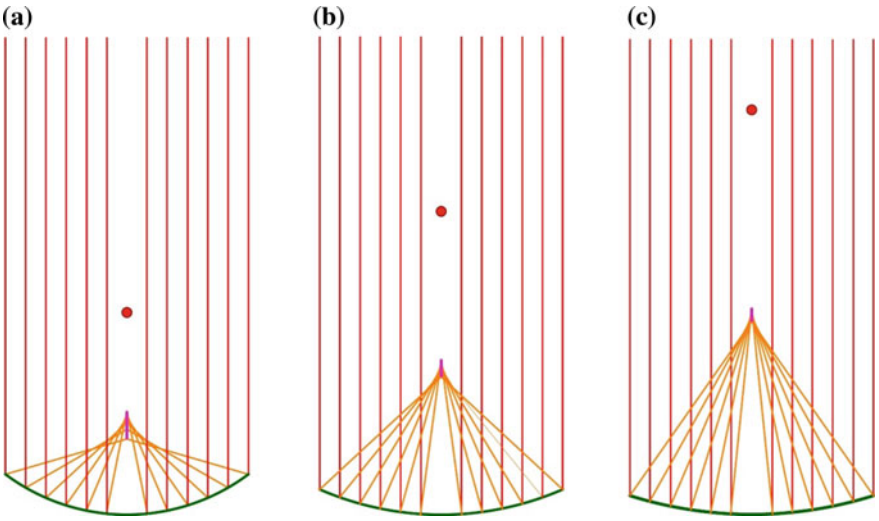

Fig. 6.19 Spherical, or cylindrical mirrors with circular cross section, may suffer from spherical aberration, but, if the reflector aperture width, W_r, is sufficiently small in relation to the circle radius, R_r, $W_r \ll R_r$, then the focus line segment is very short, simulating a point

6.3.2.3 Parabolic Concentrator

If the vertex of the parabolic reflective surface coincides with the origin of the Cartesian coordinate system, O, it is described by the following algebraic equation

$$y = \frac{1}{4 \cdot f} \cdot x^2 \tag{6.62}$$

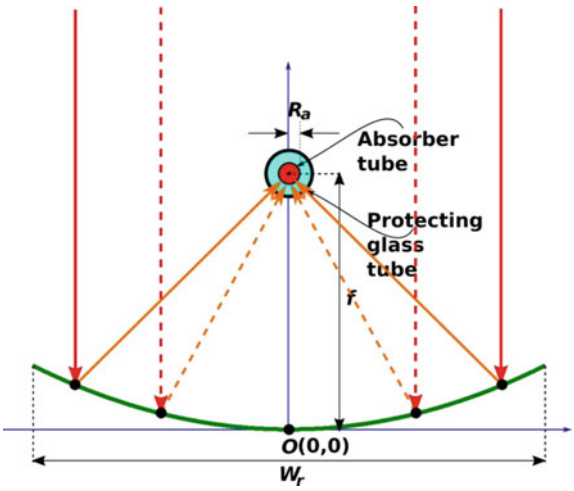

Fig. 6.20 Geometry of a typical parabolic secondary concentrator

where f is the focal length of the parabola, and x takes values in the closed interval

$$\left[-\frac{W_r}{2},\ +\frac{W_r}{2}\right]$$

or else

$$-\frac{W_r}{2} \leq x \leq +\frac{W_r}{2}$$

and W_r is the width of the receiver's aperture (Fig. 6.20).

Parabolic concentrator also suffers from aberration if the incident light rays are not falling perpendicular to the receiver aperture (it has been studied in Chap. 3, Sect. 3.5.3). The rest parameters, absorber place and size, are defined in the same way as in the previous paragraphs.

6.3.2.4 Compound Parabolic Concentrator

To overcome the problem of aberration, simple parabolic concentrators are modified and some parts of their surface are replaced by other shapes (Fig. 6.21). Each part of this compound concentrator is described by a different algebraic equation. In the case of the segmented parabolic concentrator illustrated in Fig. 6.21a, Part I is a simple parabola, while parts IIa and IIb are parabolic segments which principal axes have been turned towards the absorber by an angle φ. These parabolic segments

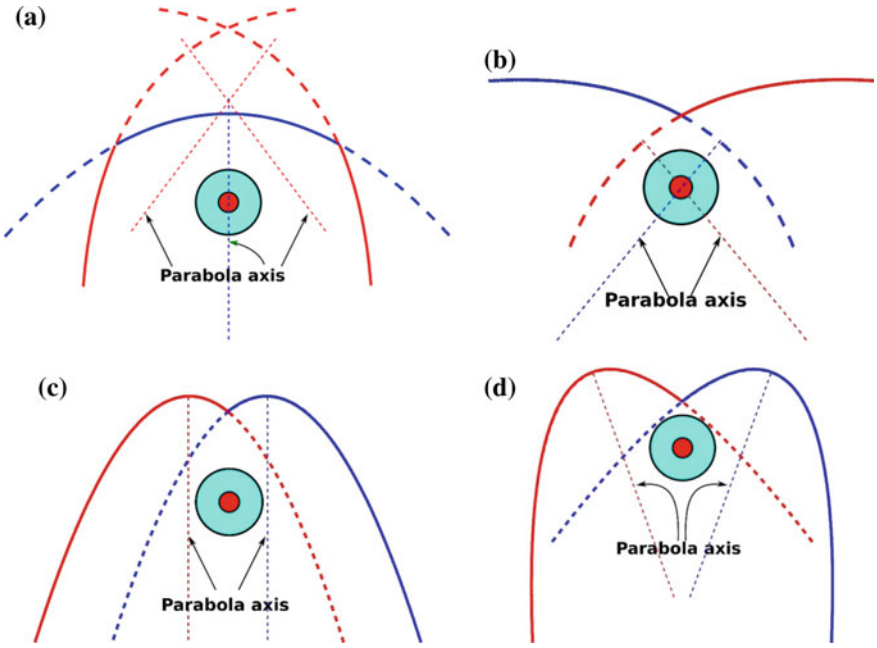

Fig. 6.21 Simple parabolic concentrators are modified and some parts of them are replaced by other shapes. The segmented parabolic concentrator consists of a simple parabola, and two parabolic segments which principal axes have been turned towards the absorber (**a**). The parabolic wing-like secondary reflector (**b**) is another special case of the segmented parabolic concentrator. It consists of the two parts of the parabolas not used in the segmented parabolic version. A more complex parabolic compound concentrator consists of two similar parabolas that are shifted towards both sides of the absorber by the same amount (**c**). The problem gets more complex when the two parabolas are turned towards the absorber (inwards, facing parabolas) (**d**). Properly designed compound parabolas can effectively focus solar radiation falling from different angles on the absorber surface

may also belong in parabolas having different focal lengths, $f_{\mathrm{II},a}$ and $f_{\mathrm{II},b}$, but usually it is $f_{\mathrm{II},a} = f_{\mathrm{II},b} = f_{\mathrm{II}}$. Hence, the algebraic equations describing the secondary reflector are more complex. Part I is described by the equation

$$y = \frac{1}{4 \cdot f_{\mathrm{I}}} \cdot x^2, \quad \text{for} \quad -\frac{W_{r,\mathrm{I}}}{2} \leq x \leq +\frac{W_{r,\mathrm{I}}}{2} \tag{6.63}$$

where f_{I} is the focal length of the parabola of this part, and $W_{r,\mathrm{I}}$, is its width.

Parts IIa and IIb correspond in parabolas which general equation is given by the formula

$$\frac{(ax + by + c)^2}{a^2 + b^2} = (x - f_x)^2 + (y - f_y)^2 \tag{6.64}$$

where f_x and f_y are the Cartesian coordinates of the parabola focus point F, $F(f_x, f_y)$, and a, b and c are the parameters of the parabola directrix ($ax + by + _c = 0$).

The parabolic wing-like secondary reflector (Fig. 6.21b) is a special case of the segmented parabolic concentrator. It consists of only two parts. As we can see from Fig. 6.21b, parabolic wing-like concentrators use the part of the parabola not used in the segmented parabolic version.

A more complex, but more easily mathematically described shape is the parabolic compound concentrator illustrated in Fig. 6.21c. It consists of two similar parabolas that are shifted towards both sides of the absorber by the same amount, say a_r. In this case, the reflective surface is described by the following system of equations

$$y = \frac{1}{4 \cdot f_1} \cdot (x + a_r)^2, \quad \text{for } -\frac{W_{r,1}}{2} \leq x \leq 0 \tag{6.65}$$

$$y = \frac{1}{4 \cdot f_1} \cdot (x - a_r)^2, \quad \text{for } 0 \leq x \leq \frac{W_{r,1}}{2} \tag{6.66}$$

The problem gets more complex when the two parabolas are turned towards the absorber (inwards), as it is the case illustrated in Fig. 6.21d. Then the algebraic equations describing the reflective surface are a little more complex. They can be derived by applying a coordinate rotation transformation. The new coordinates, x' and y' are given by the expressions

$$x' = x \cdot \cos\theta - y \cdot \sin\theta \tag{6.67}$$

$$y' = x \cdot \sin\theta + y \cdot \cos\theta \tag{6.68}$$

where θ is the rotation angle.

6.3.2.5 Involute Concentrators

The plane reflector, the circular reflector and the parabolic (simple or compound) reflector are the most usually used reflector types. However, there has been used another type of surface for the secondary reflector. This is the so-called involute curve, which is produced based on the shape of another known curve applying a proper technique. An involute is a curve obtained from another curve by attaching an imaginary taut string to this curve and tracing its free end as it is wound onto that given curve; or unwound (Fig. 6.22). Therefore, any involute curve is connected to another curve, e.g. a parabola. The last case is the most common, the parabola involute. In addition, even for a given well-defined initial curve there are more than one involute curves. And, as it is easily understood, the algebraic equations describing these surfaces are far from easy to be derived by a simple procedure and be described by a simple equation.

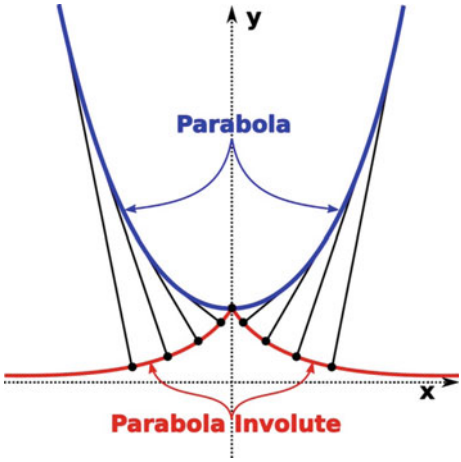

Fig. 6.22 Involute of a curve is not so easy to understand and visualize, except for simple cases as the parabolic curve. In general, an involute is a curve obtained from another curve by attaching an imaginary taut string to this curve and tracing its free end as it is wound onto that given curve; or unwound. However, even for the same parabola, there are more than one involute curves

6.3.2.6 General Compound Concentrators

Finally, as it is more than obvious, we can combine countless different shapes in an effort to construct the ideal secondary reflector (Fig. 6.23). However, this complicates, sometimes unnecessarily, both the computations required to study the efficiency of the new structure, and the construction requirements. As a consequence, they are not further studied in this book. Nevertheless, once defined the reflective surface, the above procedure can be applied, although pretty hard.

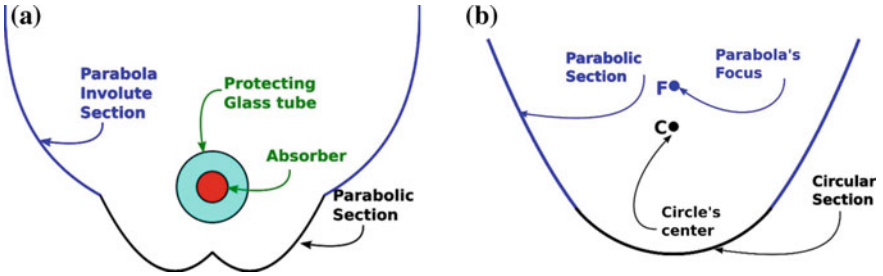

Fig. 6.23 Compound secondary reflectors consisting of **a** two parabolic and two parabolic involute parts and **b** one circular and two parabolic parts

References

Abbas, R., J. Muñoz, and J.M. Martínez-Val. 2012. Steady-state thermal analysis of an innovative receiver for linear Fresnel reflectors. *Applied Energy* 92: 503–515.

Balaji, Shanmugapriya, K.S. Reddy, and T. Sundararajan. 2016. Optical modelling and performance analysis of a solar LFR receiver system with parabolic and involute secondary reflectors. *Applied Energy* 179: 1138–1151.

Chaitanya Prasad, G.S., K.S. Reddy, and T. Sundararajan. 2017. Optimization of solar linear Fresnel reflector system with secondary concentrator for uniform flux distribution over absorber tube. *Solar Energy* 150: 1–12.

Grena, Roberto, and Pietro Tarquini. 2011. Solar linear Fresnel collector using molten nitrates as heat transfer fluid. *Energy* 36: 1048–1056.

Heimsath, A., F. Cuevas, A. Hofer, P. Nitz, and W.J. Platzer. 2014. Linear Fresnel collector receiver: Heat loss and temperatures, SolarPACES 2013. *Energy Procedia* 49: 386–397.

Lin, M., K. Sumathy, Y.J. Dai, R.Z. Wang, and Y. Chen. 2013. Experimental and theoretical analysis on a linear Fresnel reflector solar collector prototype with V-shaped cavity receiver. *Applied Thermal Engineering* 51: 963–972.

Mills, D., and G.L. Morrison. 2000. Compact linear Fresnel reflector solar thermal power plants. *Solar Energy* 68 (3): 263–283.

Singh, P.L., R.M. Sarviya, and J.L. Bhagoria. 2010. Thermal performance of linear Fresnel reflecting solar concentrator with trapezoidal cavity absorbers. *Applied Energy* 87: 541–550.

Zhang, Yanmei, Gang Xiao, Zhongyang Luo, Mingjiang Ni, Tianfeng Yang, and Weiping Xu. 2014. Comparison of different types of secondary mirrors for solar application. *Optik* 125: 1106–1112.

Zhu, Guangdong. 2017. New adaptive method to optimize the secondary reflector of linear Fresnel collectors. *Solar Energy* 144: 117–126.

Chapter 7
Design Parameters

When a Linear Fresnel Reflector System is designed, reflectors' width, curvature (flat, circular or parabolic) and location, as well as, the tracking System, the height and the type (multiple tubes or single tube) of the receiver, must all be taken into account. However, one of the most critical steps of the System design is the proper calculation of the reflective elements' characteristics as they determine its ability to operate according to the set standards. For example, the marginal reflected light rays must reach the receiver and not be intercepted by adjacent reflectors. This depends on the width, the location and the inclination of the reflective elements.

Thus, this chapter focuses on the derivation of the mathematical relationships needed to calculate the design parameters of a Linear Fresnel Reflector System: the width, the position and the inclination of the primary reflective elements. At the same time, the height, the length, the relative position and the configuration of the receiver are considered as predefined parameters, as they cannot be defined independently from the above-mentioned parameters. In addition, for the sake of simplicity, we assume throughout the whole chapter that the primary reflectors are flat and secondary reflectors are not taken into consideration. Nevertheless, it could be deemed that the treatment of a secondary reflector is incorporated in the study of the flat horizontal absorber. In this case, the absorber width can be replaced by the receiver aperture width that coincides with the secondary reflector aperture. Furthermore, primary reflective elements other than flat mirrors do not essentially affect the calculations and the conclusion of this chapter.

7.1 Introduction

In general, the performance of a Linear Fresnel Reflector Solar Radiation Concentrating System depends on the proper selection of the reflectors' number, N, width, W_j, position or location, Q_j, and tilt angle, β_j (Fig. 7.1). The tilt angle, β_j, of each reflective element has to be adjusted constantly so that the light ray falling on

S. Karathanasis, *Linear Fresnel Reflector Systems for Solar Radiation Concentration*, https://doi.org/10.1007/978-3-030-05279-9_7

its middle can strike the central point of the receiver after being reflected. In addition, in order for the whole solar radiation reflected by the jth mirror to reach the receiver and not be blocked by the previous reflector, the light ray being reflected by the lower edge of the reflector must touch at the most the upper edge of the previous, $(j - 1)$th, reflective element. So, an appropriate distance (called shift), S_j, must be kept between two consecutive reflectors so that they do not shade each other, or block the reflected solar radiation. As a consequence, each reflective element, j, can be characterized by three parameters: width, W_j, position or location, Q_j, and tilt angle, β_j. However, although the value of the shift, S_j, is included in the value of the location, Q_j, sometimes it is referred as an extra parameter.

The subscript j takes values from 1 to N, or from $-n$ to $+n$, where $N = 2 \cdot n$, or $N = 1 + 2 \cdot n$. In addition, the receiver, of appropriately predetermined size and shape, is placed at a height, H, above the reflectors plane, on the focal plane of the Linear Fresnel Reflector System. As a result, we can distinguish two possible configurations, according to the chosen design: (a) a central reflector ($j = 0$) is placed right under the receiver, and the subscripts of the reflectors to the left (to the East for a North–South-oriented System) take values in the closed interval $[-n, 1]$ (or $-n \leq j \leq 1$) and those to the right (to the West) take values in the closed interval $[1, n]$ (or $1 \leq j \leq n$), and (b) there is not a central reflector ($j \neq 0$) being

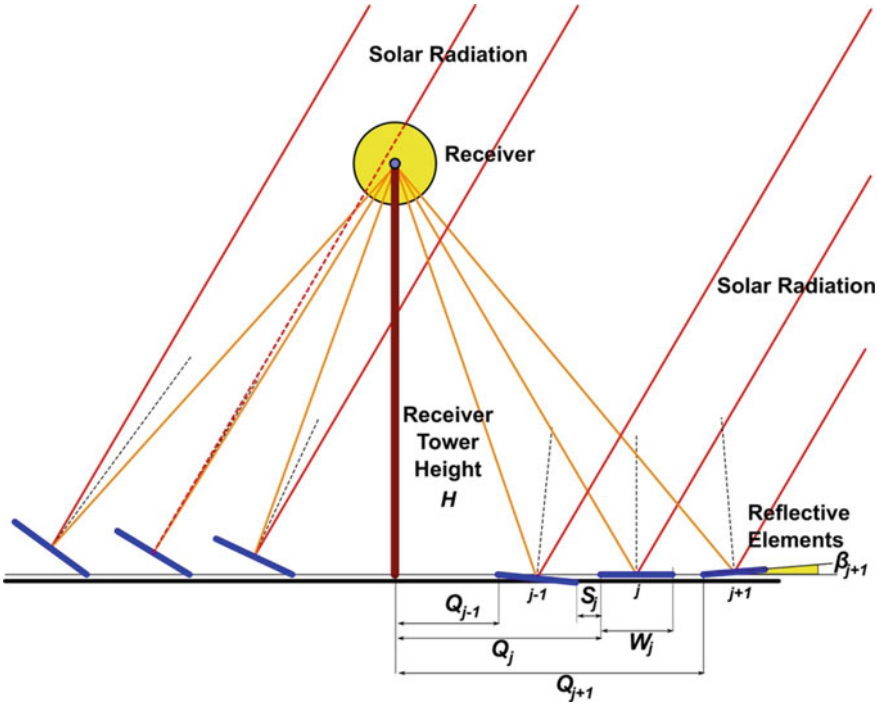

Fig. 7.1 A sketch of a typical Linear Fresnel Reflector System

placed right under the receiver. In this case, the subscripts of the reflectors to the left (to the East) take also values in the closed interval $[-n, 1]$ (or $-n \leq j \leq 1$) and those to the right (to the West) take also values in the closed interval $[1, n]$ (or $1 \leq j \leq n$), but there is not any reflector that is described by a subscript equal to zero (or $j \neq 0$). Moreover, in the first case the reflectors' number, N, satisfies the condition $N = 1 + 2 \cdot n$, whereas in the second case it satisfies the condition $N = 2 \cdot n$.

Apart from the above-presented parameters, the complete set of parameters characterizing a Linear Fresnel Reflector Solar Radiation Concentrating System, which must be calculated, or be known, consists of

- the width, W_j, of each reflective element
- the tilt, or inclination angle, β_j, of each reflective element
- the position, or location, Q_j, of each reflective element
- the distance, or shift, S_j, between two consecutive reflective elements
- the tilt, or inclination angle, θ, of the plane of the reflective elements
- the primary reflectors' field aperture width, D
- the primary reflectors' field aperture length, L, which coincides with the length, L_j, of each reflective element, $L = L_j$, for all j
- the receiver (or absorber if it is a simple construction) height, H, or the System's focal distance, f
- the receiver aperture width, W_r.

From these parameters, the width, W_j, the position or location, Q_j, the shift distance, S_j, and the tilt angle, β_j, along with the number, N, of the reflective elements can be characterized as the basic design parameters of a Linear Fresnel Reflector System. However, in order to be able to calculate these parameters we must resort to geometric optics, use some basic assumption, and take into account some fundamental facts:

- All reflective surfaces are treated as perfectly specular and free from deformations.
- Each reflector is pivoted on its longitudinal axis that (a) goes through the centre of its narrow side or (b) it coincides with one of their longer edges.
- The rotation axes of all reflectors are on the same plane.
- The reflective elements have equal lengths.
- The reflective elements do not shade each other or block the reflected solar radiation during the period of operation (or for a critical time interval of the day, e.g. for local solar time from 9:00 to 15:00, when the solar irradiance is maximum, or above a critical value).
- The Linear Fresnel Reflector System is horizontally arranged.
- In a first approximation, we assume that the incident light rays are parallel. Later on, we take into account the finite angular size of Sun's disc and generalize our study taking into account the fact that Sun's light rays reaching the reflectors, and consequently the absorber (or receiver), are non-parallel.

- Although all possible System orientations are applicable, we assume that the System is North–South oriented and, therefore, the absorber's direction is parallel to the local meridian. In this case, the System and Sun's trajectory in the sky have the same plane of symmetry. As a result, during the first part of the day the East part of the Systems behaves the same way the West part of the System behaves during the second part of the day, and vice versa. Therefore, we can study the System behaviour for only one half of the day (e.g. the first half of the day). This way we can reduce the required calculation and mathematical analysis by a factor equal to 2.
- Nevertheless, despite the fact that the former configuration has symmetry advantages that simplify the mathematical treatment of the System, in some cases, an East–West orientation is more preferable. Again, the symmetrical Sun movement in relation to the System's longitudinal axis allows us to study the System for only one half of the day (usually the first half) and reduce the required calculation and mathematical analysis by a factor equal to 2, too.
- In any case, only the transversal Sun angle, θ_T (on a plane being perpendicular to the absorber direction), is considered, as the longitudinal component of Sun's angle, θ_L, contributes only to energy losses. Nevertheless, since these losses are important in small-scale Systems, the study of the effect the longitudinal Sun angle, θ_L, may have on the performance of these System may lead to extra design improvements (e.g. introduction of a System inclination, or receiver displacement) (not considered in this chapter).
- In the North–South orientation of the System, the maximum value of the transversal component of Sun's angle, θ_T, is equal to $\pi/2$ ($\theta_{T,\max} = \pi/2$), while in the East–West orientation it is usually lower than $\pi/2$ ($\theta_{T,\max} \leq \pi/2$), depending on the sites latitude.

As the calculation of the proper value of the System's design parameters is a crucial step towards efficient operation of a Linear Fresnel Reflector System, it is not surprising that many researchers have worked on this matter, dealing with different aspects of the problem (e.g. Barbona et al. 2016; Mathur et al. 1991a, b; Singh et al. 2010; Nixon and Davies 2012; Negi et al. 1990; more information can be found in the *Reference and Further Reading* section of this chapter). For example, Mathur et al. (1991a, b) presented extended mathematical calculations for three different receiver geometries: flat horizontal, flat vertical and tubular receiver. In this chapter, detailed calculations of Fresnel Reflector Solar Radiation Concentrating Systems (a) with flat horizontal, flat vertical, triangular and circular absorber, (b) with reflectors of varying and constant width and (c) with centrally and side pivoted reflective elements are presented, extending the above-mentioned studies.

7.2 Methodology

In very low Sun angles, consecutive reflective elements may block the reflected radiation, or they may shade each other. As a consequence, a part of the incident solar radiation is lost. These losses can be reduced and limited by proper arrangement of the reflective elements, which involves the introduction of an ample distance between consecutive reflective elements, S_j. However, this leads to inherent constraints in the System design: the density of the reflective elements is limited, or in other words, the number, N, of the reflective elements for a given System area (or more accurately for a given System aperture width) has an upper threshold.

The calculation of the appropriate distance, S_j, of two consequent reflective elements, so that shading and blocking effects to be avoided, depends on Sun's angle, and in particular on its transversal component, θ_T. For Fresnel Reflector Systems that are constantly adjusted so that they always face Sun, Sun is always on their longitudinal plane and its transversal angle always equals 90° ($\theta_T = \pi/2$) (Fig. 7.2). In this case, it is obvious that we should calculate the reflectors' shift, S_j, for this particular angle of the incident solar radiation, aiming at eliminating the amount of shading. In any other case, that is for stationary Linear Fresnel Reflector Systems, the transversal component of Sun's angle equals 90° ($\theta_T = \pi/2$) only at one specific time of the day. It corresponds to the moment when Sun's and System's azimuth angles coincide. If the System is South–North oriented, it occurs at the local noon, while on the other hand, if the System is East–West oriented, it occurs only on two days of the year and only if the site's latitude, φ, is between ±23.5° (or $-23.5° \leq \varphi \leq +23.5°$, or $\varphi \in [-2.5°, +23.5°]$). In any other case, the transversal component of Sun's angle is lower than 90° ($\theta_T < \pi/2$) and reaches a maximum value at the local noon.

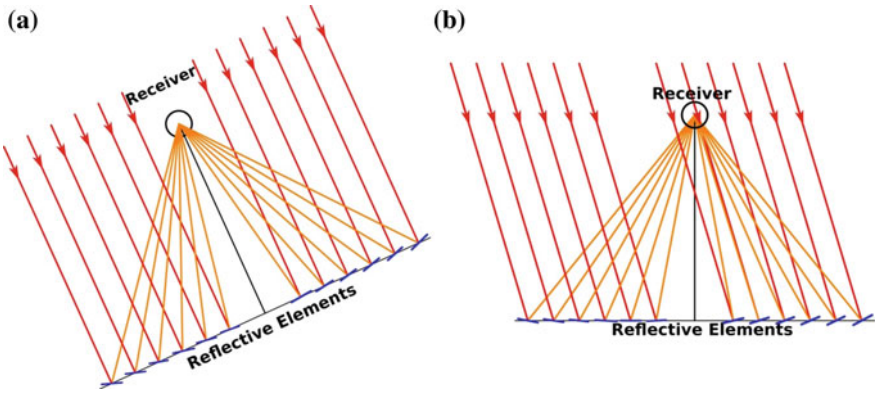

Fig. 7.2 If a Fresnel Reflector System can be constantly adjusted so that it always faces Sun, then the light rays fall always perpendicular to its aperture. However, in the case the whole System is stationery and only its reflective elements adjust their inclination, so that the incident solar radiation to be redirected and concentrated on the receiver, shading and blocking effects are almost always present

In addition, in all Linear Fresnel Reflector Systems what matters is their ability to concentrate the possible maximum amount of solar radiation any time of the day. However, this is not feasible, due to the design of these Systems. As a consequence, we are forced to choose only one period of the day in which the System can operate with its maximum performance. In other words, we can optimize the System's performance only for specific operation conditions. Since the local noon is the time with the maximum solar irradiance, we opt to design these Systems having their maximum performance at the local noon, at the maximum transversal component of Sun's angle, $\theta_{T,\max}$.

Shading and blocking effects depend on the location, Q_j, of a given reflector, its distance from its neighbouring reflectors, their tilt angles, β_j, as well as on Sun's position in the sky, determined by its altitude angle, h, and its azimuth, A, and in particular on its transversal component, θ_T. The latter is a function of the construction's site, the day of the year, the time of the day and System's orientation. For each reflector, shading effects are greater when Sun's transversal angle, θ_T, is lower, namely during early in the morning and late in the afternoon for a North–South-oriented System, and during winter if the System is East–West oriented (for a place on the northern hemisphere). In addition, during the morning, reflective elements placed in the western side of a North–South-oriented System suffer more from shading effects than those reflectors placed on the eastern side, while in the afternoon the situation is reversed. Similarly, southern reflectors are closer to the horizontal position, while northern reflective elements are closer to the vertical for an East–West-oriented System on the northern hemisphere. Therefore, due to their inclination, the reflective elements on the northern side of the System suffer from greater shadow effect than the reflective elements on the southern side. Lastly, in addition to the shadows between reflectors, the solar radiation reflected by a reflector may be intercepted by its neighbouring reflector on its way to the receiver. This effect, which is called blocking, is more important in reflectors far away from the receiver (Abbas and Martínez-Val 2015).

However, for each reflective element the maximum shading or blocking effects occurs at different time of the day. Therefore, in order to eliminate such losses across the primary reflectors field, the shift, S_j, or distance, between each pair of consecutive reflective elements should be calculated by considering different values of Sun's altitude, h, and azimuth angle, A, or, equivalently, different values of its transversal angle, θ_T, for each reflective element. But this is not feasible, because in this case we would be able to calculate the amount of shading or blocking beforehand, as it requires the knowledge of the reflectors' width, W_j, position, Q_j, and tilt angle, β_j. However, these quantities are determined simultaneously with the shift distance. For this reason, we have to choose a value of Sun's transversal angle, θ_T, common for all reflectors. This angle usually corresponds to the time of the maximum solar irradiance. As a result, we will apply the following analysis for the maximum value of the transversal component of Sun's angle, $\theta_{T,\max}$. This value equals to $\pi/2$ ($\theta_{T,\max} = \pi/2$) for a North–South-oriented System, whereas if the System's orientation is East–West it is usually lower than $\pi/2$ ($\theta_{T,\max} \leq \pi/2$), depending on the sites' latitude.

Nevertheless, since the mathematical formulas for a North–South-oriented System can straightforwardly be derived from the corresponding formulas for an East–West-oriented System, by setting the maximum value of Sun's transversal angle, $\theta_{T,\max}$, equal to $\pi/2$ ($\theta_{T,\max} = \pi/2$), we will study an typical East–West-oriented System and at the end we will proceed to the simpler case of a North–South-oriented System. Except for Sun's transversal angle, θ_T, the other core difference between the two types of Linear Fresnel Reflector Systems is that in East–West-oriented Systems the tilt angle, β_j, of the reflective elements changes its sign not below the receiver, but around the position where the angle, ξ_j, formed by the line connecting the reflectors midpoint with the receiver midpoint on the transversal plane, and the horizontal plane is equal to Sun's maximum transversal angle, $\theta_{T,\max}$ ($\xi_j = \theta_{T,\max}$). This reflector has subscript, j, equal to zero ($j = 0$). The subscripts of the rest reflectors take values in the closed interval $[-n_S, 1]$ (or $-n_S \leq j \leq 1$), if they are southern from the 0th reflector, and in the closed interval $[1, n_N]$ (or $1 \leq j \leq n_N$), if they are northern from it. In this case, the number, n_S, of the southern and the number, n_N, of the northern reflective elements satisfy the condition, $N = 1 + n_S + n_N$.

However, even if there is not a reflector being placed on the reference location where $\xi_0 = \theta_{T,\max}$ ($j \neq 0$), the rest reflectors continue to be described by the same subscripts presented above, but now they satisfy the condition $N = n_S + n_N$.

7.2.1 Distance Between Consecutive Reflective Elements

In the following paragraphs, a mathematical method for the calculation of the distance, S_j, between two adjacent reflective elements for the maximum Sun's transversal angle, $\theta_{T,\max}$, is presented. However, there are two discrete cases. In the first case, the reflectors' rotation axes go through the midpoint of their narrow side (Fig. 7.3a) (centrally pivoted) and in the second case, they coincide with one of their longer edge (Fig. 7.3b, c) (side pivoted). Depending on the position of the reflectors rotation axis, the distance, S_j, between each pair of them, so that shading or blocking effects to be avoided, can be calculated using the System's geometry shown in Figs. 7.3a–c, and 7.4a–c, respectively.

Furthermore, the reflectors placed southern from the reference location, where $j = 0$, are more possible to suffer from blocking effect, while the reflectors placed northern from it may suffer mainly from shading, although both effects may be present in all reflectors if they are not properly arranged. Therefore, for the East–West-oriented System, we will determine the proper shift, S_j, so that the reflected solar radiation not to be blocked from adjacent reflectors for the southern reflectors (with subscript ranging from $-n_S$ to -1), while the northern reflectors (with subscript ranging from 1 to n_N) must not be shaded from their adjacent reflectors. When proceeding to the North–South-oriented System, there is essentially no shading effect but only blocking problems, as the shadows the reflective element may cast are exactly below them, since the maximum Sun's transversal angle, $\theta_{T,\max}$, is equal

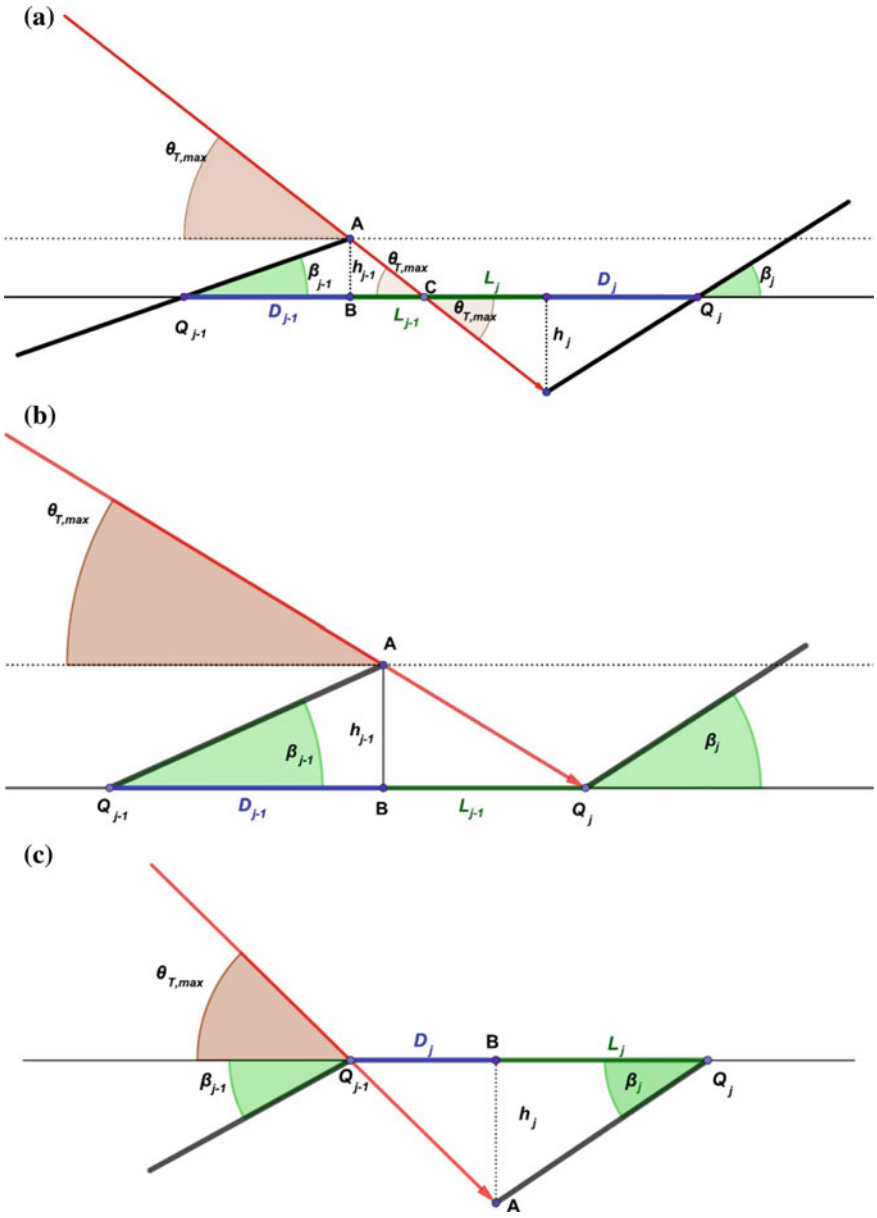

Fig. 7.3 Geometry used for the calculation of the distance, S_j, between two adjacent reflective elements placed in the northern part of a East–West-oriented Linear Fresnel Reflector System, in order to avoid shading effect for maximum Sun's transversal angle, $\theta_{T,\max}$. **a** In the first case, the reflective elements are pivoted on their longitudinal axis that goes through the midpoint of their narrow dimension (side). In the second and third cases, the rotation axis coincides with one of their longer edge, **b** with the southern and **c** with the northern edges, respectively

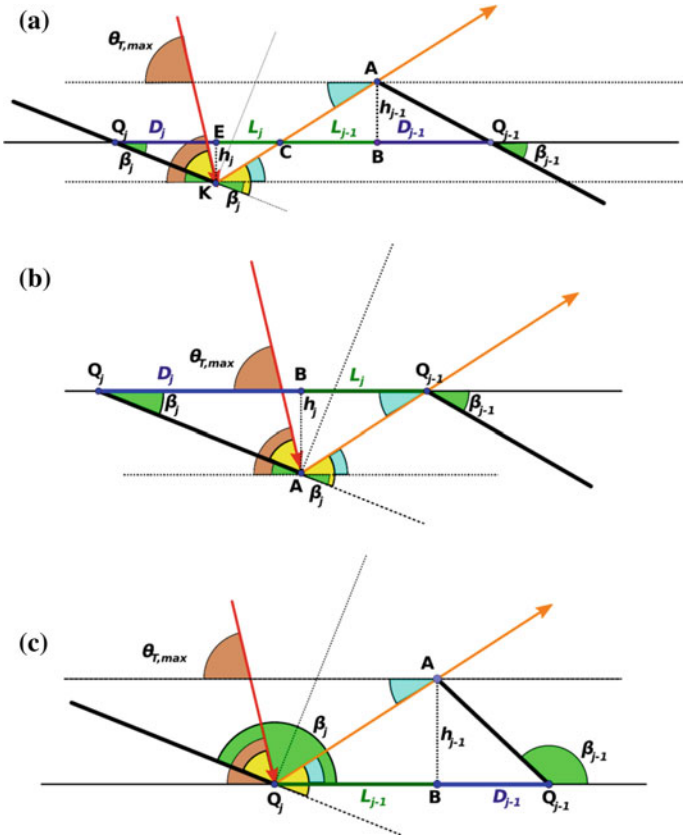

Fig. 7.4 Geometry used for the calculation of the distance, S_j, between two adjacent reflective elements placed in the southern part of a East–West-oriented Linear Fresnel Reflector System, in order to avoid blocking effect for maximum Sun's transversal angle, $\theta_{T,\max}$. **a** In the first case, the reflective elements are pivoted on their longitudinal axis that goes through the midpoint of their narrow dimension (side). In the second and third cases, the rotation axis coincides with one of their longer edge, **b** with the southern and **c** with the northern edges, respectively

to $\pi/2$(=90°) and Sun is considered overhead, and, therefore, only blocking effect may be present.

In any case, the distance S_j between two adjacent reflectors, the jth and the $(j-1)$th, is defined as the difference between their positions, Q_j and Q_{j-1}, as they are measured from the origin of the local Cartesian coordinate system:

$$S_j = Q_j - Q_{j-1} \tag{7.1}$$

Taken advantage of the System's geometry shown in Fig. 7.3a, the shift S_j, so that no shading occurs, can be calculated from the following equation:

$$S_j = D_{j-1} + L_{j-1} + D_j + L_j \tag{7.2}$$

where

$$D_{j-1} = \frac{W_{j-1}}{2} \cdot \cos \beta_{j-1} \tag{7.3}$$

and

$$D_j = \frac{W_j}{2} \cdot \cos \beta_j \tag{7.4}$$

while the length L_{j-1} can be calculated using the triangle ABC:

$$\begin{aligned} L_{j-1} &= h_{j-1} \cdot \tan \widehat{BAC} \Rightarrow \\ L_{j-1} &= \frac{W_{j-1}}{2} \cdot \sin \beta_{j-1} \cdot \tan \widehat{BAC} \end{aligned} \tag{7.5}$$

But

$$\begin{aligned} \widehat{BAC} &= 90^\circ - \widehat{ACB} \Rightarrow \\ \widehat{BAC} &= 90^\circ - \theta_{T,\max} \end{aligned} \tag{7.6}$$

Substituting Eq. 7.6 into Eq. 7.5, it becomes

$$L_{j-1} = \frac{W_{j-1}}{2} \cdot \sin \beta_{j-1} \cdot \tan\left(90^\circ - \theta_{T,\max}\right) \tag{7.7}$$

In a similar manner

$$L_j = \frac{W_j}{2} \cdot \sin \beta_j \cdot \tan\left(90^\circ - \theta_{T,\max}\right) \tag{7.8}$$

Thus, Eq. 7.2 takes the form

$$\begin{aligned} S_j = &\frac{W_j}{2} \cdot \cos \beta_j \\ &+ \frac{W_{j-1}}{2} \cdot \cos \beta_{j-1} \\ &+ \frac{W_j}{2} \cdot \sin \beta_j \cdot \tan\left(90^\circ - \theta_{T,\max}\right) \\ &+ \frac{W_{j-1}}{2} \cdot \sin \beta_{j-1} \cdot \tan\left(90^\circ - \theta_{T,\max}\right) \end{aligned} \tag{7.9}$$

In the case of side pivoted reflective elements, when the pivot axis coincides with the southern edge of the reflectors, we can take advantage of the System's

geometry shown in Fig. 7.3b, and in this case the proper shift distance, S_j, can be calculated from the following equation:

$$S_j = D_{j-1} + L_{j-1} \tag{7.10}$$

where

$$D_{j-1} = W_{j-1} \cdot \cos \beta_{j-1} \tag{7.11}$$

while the length L_{j-1} can be calculated using the triangle ABQ_j:

$$\begin{aligned} L_{j-1} &= h_{j-1} \cdot \tan \widehat{BAQ_J} \Rightarrow \\ L_{j-1} &= W_{j-1} \cdot \sin \beta \cdot \tan \widehat{BAQ_J} \end{aligned} \tag{7.12}$$

But

$$\begin{aligned} \widehat{BAQ_J} &= 90^\circ - \widehat{AQ_JB} \Rightarrow \\ \widehat{BAQ_J} &= 90^\circ - \theta_{T,\max} \end{aligned} \tag{7.13}$$

Substituting, now, Eq. 7.13 into Eq. 7.12, it becomes

$$L_{j-1} = W_{j-1} \cdot \sin \beta_{j-1} \cdot \tan\left(90^\circ - \theta_{T,\max}\right) \tag{7.14}$$

and, hence, Eq. 7.10 takes the form

$$S_j = W_{j-1} \cdot \cos \beta_{j-1} + W_{j-1} \cdot \sin \beta_{j-1} \cdot \tan\left(90^\circ - \theta_{T,\max}\right) \tag{7.15}$$

On the other hand, when the pivot axis coincides with the northern edge of the reflectors, we can calculate the proper shift distance, S_j, so that no shading occurs, by taking advantage of the System's geometry shown in Fig. 7.3c. In this case, the proper shift distance, S_j, can be calculated from the following equation:

$$S_j = D_j + L_j \tag{7.16}$$

where

$$L_j = W_j \cdot \cos \theta_j \tag{7.17}$$

while the length D_j can be calculated using the triangle ABQ_{j-1}:

$$\begin{aligned} D_j &= h_j \cdot \tan \widehat{BAQ_{J-1}} \Rightarrow \\ D_j &= W_j \cdot \sin \beta_j \cdot \tan \widehat{BAQ_{J-1}} \end{aligned} \tag{7.18}$$

But

$$\widehat{BAQ_{J-1}} = 90^\circ - \widehat{AQ_{J-1}} \Rightarrow$$
$$\widehat{BAQ_{J-1}} = 90^\circ - \theta_{T,\max} \tag{7.19}$$

Substituting, now, Eq. 7.19 into Eq. 7.18, it becomes

$$D_j = W_j \cdot \sin\beta_j \cdot \tan\left(90^\circ - \theta_{T,\max}\right) \tag{7.20}$$

and, hence, Eq. 7.16 takes the form

$$S_j = W_j \cdot \cos\beta_j + W_j \cdot \sin\beta_j \cdot \tan\left(90^\circ - \theta_{T,\max}\right) \tag{7.21}$$

From Eqs. 7.15 and 7.21, we can conclude that the reflectors' shift distance, S_j, may depend on the position of the reflective elements' pivot axis. If it is positioned on the southern edge of the reflective elements, the calculation of the distance between two consecutive reflectors, S_j, depends only on the width, W_{j-1}, and the tilt, β_{j-1}, of the previous reflector, the $(j-1)$th reflector (Eq. 7.15), which has been already calculated. On the contrary, if the pivot axis coincides with the northern edge of the reflective elements then the location, Q_j, of the jth reflector, depends on its own width, W_j, and tilt, β_j, which are not known and have to be calculated.

The above analysis concerns the calculation of the proper distance, S_j, between two reflective elements so that shading effects to be avoided. However, this is not the only effect that affects the System's performance. In the southern reflective elements, those been located southern from the reference location, where $j = 0$, the reflected solar radiation may be blocked by adjacent reflectors leading to additional energy losses. Therefore, the reflective elements must also be located sparsely enough, by introducing a proper distance, S_j, between them, so that blocking effects do not occur. This is illustrated in Fig. 7.4, which presents the geometry of the two discrete cases of the problem, centrally pivoted (Fig. 7.4a) and side pivoted (b and c) reflective elements.

As we did with the shading effect, in order to calculate the distance S_j between two adjacent reflectors, the jth and the $(j-1)$th, so that no blocking effects occur, we take advantage of the System's geometry shown in Fig. 7.4a and use the equation:

$$S_j = D_{j-1} + L_{j-1} + D_j + L_j \tag{7.22}$$

where

$$D_{j-1} = \frac{W_{j-1}}{2} \cdot \cos\beta_{j-1} \tag{7.23}$$

and

$$D_j = \frac{W_j}{2} \cdot \cos \beta_j \tag{7.24}$$

while the length L_{j-1} can be calculated using the triangle ABC:

$$\begin{aligned} L_{j-1} &= h_{j-1} \cdot \tan \widehat{BAC} \Rightarrow \\ L_{j-1} &= \frac{W_{j-1}}{2} \cdot \sin \beta_{j-1} \cdot \tan \widehat{BAC} \end{aligned} \tag{7.25}$$

But

$$\begin{aligned} \widehat{BAC} &= 90^\circ - \widehat{ACB} \Rightarrow \\ \widehat{BAC} &= 90^\circ - \left(\theta_{T,\max} - 2 \cdot \beta_j\right) \end{aligned} \tag{7.26}$$

Substituting, now, Eq. 7.26 into Eq. 7.25, it becomes

$$L_{j-1} = \frac{W_{j-1}}{2} \cdot \sin \beta_{j-1} \cdot \tan\left(90^\circ - \theta_{T,\max} + 2 \cdot \beta_j\right) \tag{7.27}$$

In a similar manner

$$L_j = \frac{W_j}{2} \cdot \sin \beta_j \cdot \tan\left(90^\circ - \theta_{T,\max} + 2 \cdot \beta_j\right) \tag{7.28}$$

Thus, Eq. 7.22 takes the form

$$\begin{aligned} S_j = &\frac{W_j}{2} \cdot \cos \beta_j \\ &+ \frac{W_{j-1}}{2} \cdot \cos \beta_{j-1} \\ &+ \frac{W_j}{2} \cdot \sin \beta_j \cdot \tan\left(90^\circ - \theta_{T,\max} + 2 \cdot \beta_j\right) \\ &+ \frac{W_{j-1}}{2} \cdot \sin \beta_{j-1} \cdot \tan\left(90^\circ - \theta_{T,\max} + 2 \cdot \beta_j\right) \end{aligned} \tag{7.29}$$

In the case of side pivoted reflective elements, when the pivot axis coincides with the southern edge of the reflectors, we can take advantage of the System's geometry shown in Fig. 7.4b, and, hence, the proper shift distance, S_j, can be calculated from the following equation:

$$S_j = D_j + L_j \tag{7.30}$$

where

$$D_j = W_j \cdot \cos \beta_j \tag{7.31}$$

while the length L_j can be calculated using the triangle ABQ_{j-1}:

$$\begin{aligned} L_j &= h_j \cdot \tan \widehat{BAQ_{J-1}} \Rightarrow \\ L_j &= W_j \cdot \sin \beta_j \cdot \tan \widehat{BAQ_{J-1}} \end{aligned} \tag{7.32}$$

But

$$\begin{aligned} \widehat{BAQ_{J-1}} &= 90^\circ - \widehat{AQ_{J-1}B} \Rightarrow \\ \widehat{BAQ_{J-1}} &= 90^\circ - \left(\theta_{T,\max} - 2 \cdot \beta_j\right) \end{aligned} \tag{7.33}$$

Substituting, now, Eq. 7.33 into Eq. 7.32, it becomes

$$L_j = W_j \cdot \sin \beta_j \cdot \tan\left(90^\circ - \theta_{T,\max} + 2 \cdot \beta_j\right) \tag{7.34}$$

and, hence, Eq. 7.30 takes the form

$$S_j = W_j \cdot \cos \beta_j + W_j \cdot \sin \beta_j \cdot \tan\left(90^\circ - \theta_{T,\max} + 2 \cdot \beta_j\right) \tag{7.35}$$

On the other hand, when the pivot axis coincides with the northern edge of the reflectors, we can calculate the proper shift distance, S_j, so that no blocking effects occur, by taking advantage of the System's geometry shown in Fig. 7.4c. Hence, the proper shift, S_j, can be calculated from the following equation:

$$S_j = D_{j-1} + L_{j-1} \tag{7.36}$$

where

$$D_{j-1} = W_{j-1} \cdot \cos \beta_{j-1} \tag{7.37}$$

while the length L_{j-1} can be calculated using the triangle ABQ_j:

$$\begin{aligned} L_{j-1} &= h_{j-1} \cdot \tan \widehat{BAQ_J} \Rightarrow \\ L_{j-1} &= W_{j-1} \cdot \sin \beta_{j-1} \cdot \tan \widehat{BAQ_J} \end{aligned} \tag{7.38}$$

But

$$\begin{aligned}\widehat{BAQ_J} &= 90^\circ - \widehat{AQ_JB} \Rightarrow \\ \widehat{BAQ_J} &= 90^\circ - \left(\theta_{T,\max} - 360^\circ + 2\cdot\beta_j\right) \Rightarrow \\ \widehat{BAQ_J} &= 90^\circ - \theta_{T,\max} + 2\cdot\beta_j \end{aligned} \tag{7.39}$$

Substituting, now, Eq. 7.39 into Eq. 7.38, it becomes

$$L_{j-1} = W_{j-1}\cdot\sin\beta_{j-1}\cdot\tan\left(90^\circ - \theta_{T,\max} - 2\cdot\beta_j\right) \tag{7.40}$$

and, hence, Eq. 7.36 takes the form

$$S_j = W_{j-1}\cdot\cos\beta_{j-1} + W_{j-1}\cdot\sin\beta_{j-1}\cdot\tan\left(90^\circ - \theta_{T,\max} - 2\cdot\beta_j\right) \tag{7.41}$$

Thus, the position, Q_j, of the jth reflective element can be calculated from the position Q_{j-1} of its previous (the $(j-1)$th) element by adding the proper shift distance, S_j, either from Eq. 7.9, or Eq. 7.15, or Eq. 7.21, or Eq. 7.29, or Eq. 7.35, or Eq. 7.41:

$$Q_j = Q_{j-1} + S_j \tag{7.42}$$

In all above cases, we use the absolute magnitude of angle β_j and the geometric feature of each case. This means that angle β_j is considered always positive regardless of its formation, clockwise or anticlockwise.

7.2.2 *Reflective Elements' Tilt Angle*

All Fresnel Reflector Systems are designed so that any light ray coming from the (centre of) Sun's disc and hitting the centre of the jth reflective element to be reflected to the centre of the receiver. In order for this condition to be accomplished, each reflective element has to be inclined, in relation to the horizontal plane, by an angle equal to β_j, its tilt angle. The calculation of this angle has already been presented in Chap. 4, Sect. 4.3.2. However, in order for the present chapter to be complete, we will present again the corresponding mathematical analysis in this paragraph, extending it in all possible cases.

In all Linear Fresnel Reflector Systems, the normal to their reflectors at their midpoint coincides with the bisector between the incoming light ray and the line that linking the reflector and the receiver in the transversal plane. This normal makes an angle δ_j with the horizontal axis which depends on Sun's transversal angle θ_T, and is directly connected with the reflectors' tilt angle, β_j. The tilt angle, β_j, of the jth reflector can be computed using the geometry of Fig. 7.5a–c, from the angle ξ_j (the angle formed by the horizontal plane with the line connecting the jth

reflectors' midpoint with the receiver's midpoint)—which is determined by the distance, Q_j, of the reflective element from the origin of the local Cartesian coordinate system, and the height, H, of the receiver—and the maximum Sun's transversal angle, $\theta_{T,\max}$. As it can be seen from this figure, the geometry concerning the angles ξ_j, β_j and ε_j (ε_j is the angle of reflection of the incoming solar radiation by the jth reflective element) for the two different pivoting options of the reflective elements [centrally (a) and site (b and c) pivoted] is the essentially the same. So, the relationships connecting these three angles are:

$$\begin{aligned} &\varepsilon_j + \theta_{T,\max} + \beta_j = 90^\circ \Rightarrow \\ &\varepsilon_j = 90^\circ - \theta_{T,\max} - \beta_j \end{aligned} \tag{7.43}$$

and

$$\begin{aligned} &\varepsilon_j - \beta_j + \xi_j = 90^\circ \Rightarrow \\ &\xi_j = 90^\circ - \varepsilon_j + \beta_j \end{aligned} \tag{7.44}$$

Substituting Eq. 7.43 into Eq. 7.44, it becomes

$$\begin{aligned} \xi_j &= 90^\circ - \left(90^\circ - \theta_{T,\max} - \beta_j\right) + \beta_j \Rightarrow \\ \xi_j &= 90^\circ - 90^\circ + \theta_{T,\max} + \beta_j + \beta_j \Rightarrow \\ \xi_j &= \theta_{T,\max} + 2 \cdot \beta_j \Rightarrow \\ 2 \cdot \beta_j &= \xi_j - \theta_{T,\max} \Rightarrow \\ \beta_j^{\mathrm{S}} \equiv \beta_j &= \frac{\xi_j - \theta_{T,\max}}{2} \end{aligned} \tag{7.45}$$

where β_j^S denotes the tilt angle of the southern reflective elements.

Equation 7.45 gives the tilt angle, β_j, of the jth reflective element so that the incoming solar radiation hitting its midpoint to be reflected and directed towards the receiver midpoint. It is derived based on the geometry of Fig. 7.5. This figure illustrates the case where the reflective element is placed southern from the receiver, but northern from the reference location $j = 0$ (Fig. 7.6c). In the reference location (Fig. 7.6b), the reflective element is horizontal, $\beta_0 = 0$, and Sun's transversal angle, θ_T, is essentially the complementary of the angle of incidence of the incoming solar radiation, which, due to the Law of reflection, equals to the angle of reflection, ε_0, and in addition, it coincides with the angle ξ_0, formed by the line linking the midpoint of the 0th reflector with the midpoint of the receiver, and the horizontal axis. Hence, in the reference location, we have the relationship

$$\theta_{T,\max} = \xi_0 \tag{7.46}$$

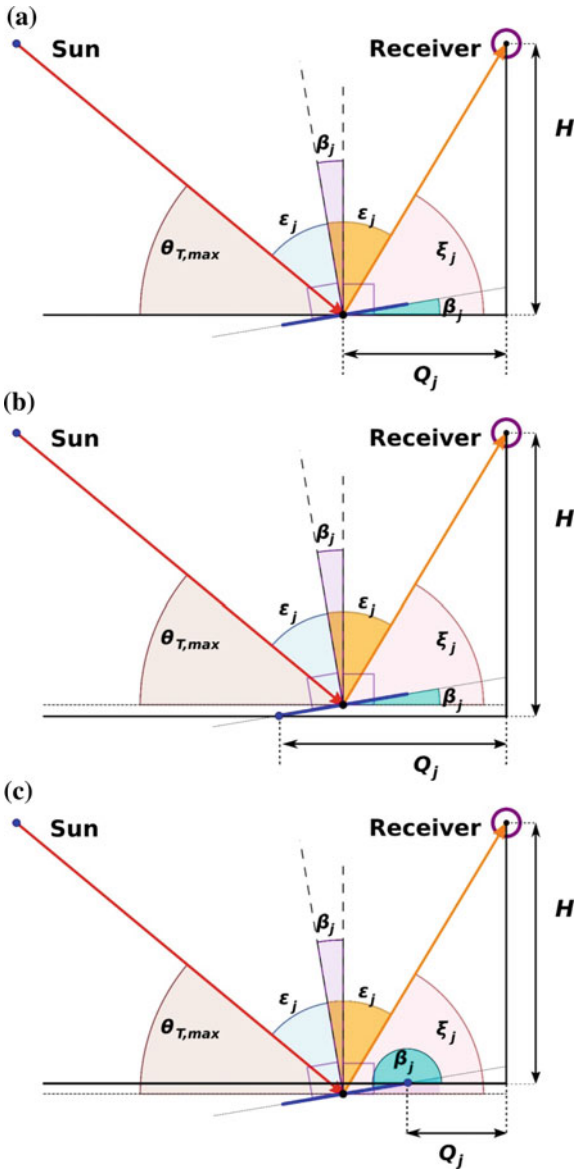

Fig. 7.5 Maximum Sun's transversal angle, $\theta_{T,\max}$, the reflectors tilt angle, β_j, the angle of reflection, ε_j, of the incoming solar radiation hitting the midpoint of the reflectors, and the angle, ξ_j, formed by the horizontal plane with the line connecting the reflectors' midpoint with the receiver midpoint, in a Linear Fresnel Reflector Solar Radiation Concentrating System where the reflective elements are **a** centrally pivoted, or their rotation axis coincides with **b** their southern, or **c** their northern longer edge, respectively. The reflector illustrated in this figure is placed northern from the reference location and southern from the receiver and correspond to the case (c) of Fig. 7.6

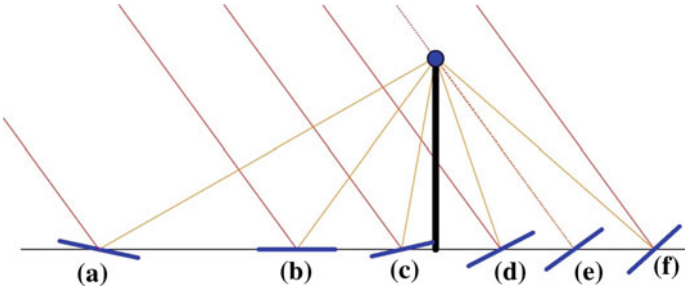

Fig. 7.6 In a Linear Fresnel Reflector Solar Radiation Concentrating System being oriented East–West, the reflective elements are placed either southern from the reference location and southern from the receiver (**a**) or northern from the reference location and southern from the receiver (namely between them) (**c**), or northern from the receiver (**d–f**), where with (**b**) is indicated the reference location where the reflector is horizontal

From Eq. 7.46, we can calculate the reference location, Q_0, by replacing the angle, ξ_0, with the corresponding expression form its definition formula, which is different for each different receiver configuration and reflectors pivoting option, as it will be presented later in this paragraph.

Except for the case illustrated in Fig. 7.6c, which has been analysed above, and the special case concerning the reference location, there are more possible locations for the reflective elements. Two of them are illustrated in Fig. 7.6a, d, which show a reflector placed southern from the reference point and another placed northern from the receiver, respectively. Figure 7.6f illustrates another possibility, where the reflective element is inclined more than that for normal incidence, as it is the case of Fig. 7.6e. However, if we make a little effort and apply the above analysis on these cases we will lead to the same conclusions, to Eq. 7.45. The difference is that now the angles β_j and ξ_j have not positive values, but negative. By convention, we consider as positive an angle formed anticlockwise and negative when it is formed clockwise.

Thus, using the geometry of Fig. 7.7a, the relationships connecting these three angles are:

$$\begin{aligned} &\varepsilon_j + \theta_{T,\max} - \left|\beta_j\right| = 90^\circ \Rightarrow \\ &\varepsilon_j = 90^\circ - \theta_{T,\max} + \left|\beta_j\right| \end{aligned} \tag{7.47}$$

and

$$\begin{aligned} &\varepsilon_j + \xi_j + \left|\beta_j\right| = 90^\circ \Rightarrow \\ &\xi_j = 90^\circ - \left|\beta_j\right| - \varepsilon_j \end{aligned} \tag{7.48}$$

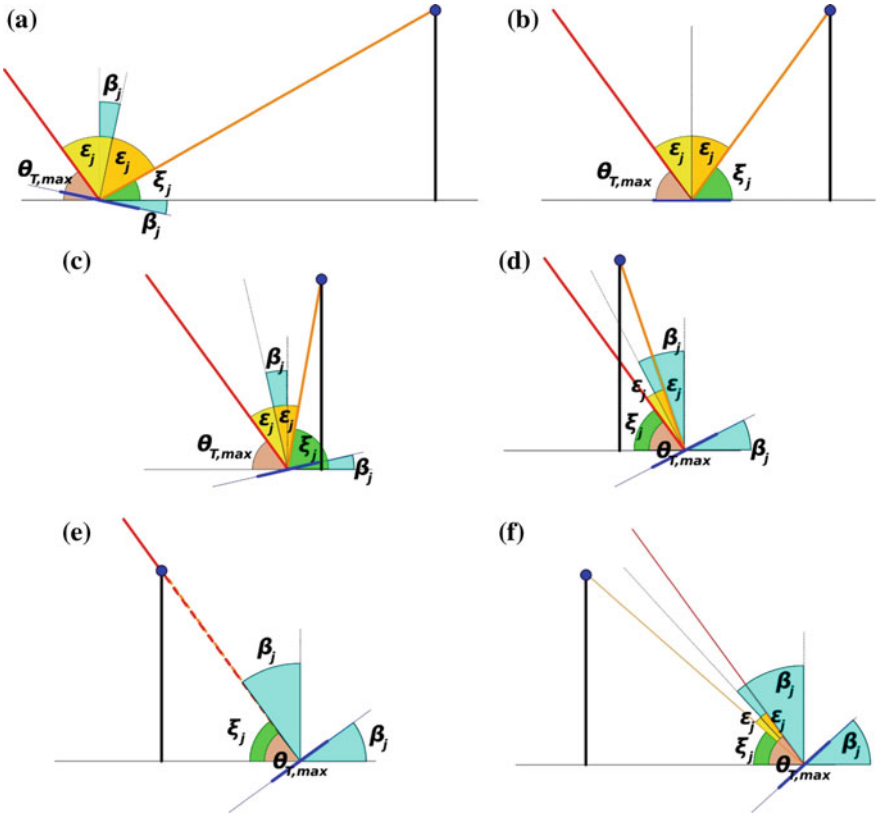

Fig. 7.7 Geometry of maximum Sun's transversal angle, $\theta_{T,\max}$, the reflectors tilt angle, β_j, the angle of reflection, ε_j, of the incoming solar radiation hitting the midpoint of the reflectors, and the angle, ξ_j, formed by the horizontal plane with the line connecting the reflectors' midpoint with the receiver midpoint, in a Linear Fresnel Reflector Solar Radiation Concentrating System-oriented East–West. The reflective elements are placed (**a**) southern from the reference location (**b**), between the reference location and the receiver (**c**) or (**d**–**f**) northern from the receiver, according to the Fig. 7.6

Substituting Eq. 7.47 into Eq. 7.48, it becomes

$$\begin{aligned} \xi_j &= 90^\circ - \left|\beta_j\right| - 90^\circ + \theta_{T,\max} - \left|\beta_j\right| \\ \xi_j &= \theta_{T,\max} - 2 \cdot \left|\beta_j\right| \Rightarrow \end{aligned} \tag{7.49}$$

$$\begin{aligned} 2 \cdot \left|\beta_j\right| &= \theta_{T,\max} - \xi_j \Rightarrow \\ \left|\beta_j\right| &= \frac{\theta_{T,\max} - \xi_j}{2} \end{aligned} \tag{7.50}$$

$$\begin{aligned} |\beta_j| &= \frac{\theta_{T,\max} - \xi_j}{2} \Rightarrow \\ -\beta_j &= -\frac{\theta_{T,\max} - \xi_j}{2} \Rightarrow \\ \beta_j^S \equiv \beta_j &= \frac{\xi_j - \theta_{T,\max}}{2} \end{aligned} \tag{7.51}$$

which is identical to Eq. 7.45.

Similarly, using the geometry of Fig. 7.7d, for the northern reflective elements, the relationships connecting these three angles are:

$$\begin{aligned} &\varepsilon_j + \theta_{T,\max} + \beta_j = 90^\circ \Rightarrow \\ &\varepsilon_j = 90^\circ - \theta_{T,\max} - \beta_j \end{aligned} \tag{7.52}$$

and

$$\begin{aligned} &|\xi_j| + \beta_j - \varepsilon_j = 90^\circ \Rightarrow \\ &|\xi_j| = 90^\circ - \beta_j + \varepsilon_j \end{aligned} \tag{7.53}$$

Substituting Eq. 7.52 into Eq. 7.53, it becomes

$$\begin{aligned} |\xi_j| &= 90^\circ - \beta_j + 90^\circ - \theta_{T,\max} - \beta_j \Rightarrow \\ |\xi_j| &= 180^\circ - \theta_{T,\max} - 2 \cdot \beta_j \Rightarrow \\ 2 \cdot \beta_j &= 180^\circ - \theta_{T,\max} - |\xi_j| \Rightarrow \\ \beta_j &= \frac{180^\circ - \theta_{T,\max} - |\xi_j|}{2} \\ \beta_j &= 90^\circ + \frac{\theta_{T,\max} + |\xi_j|}{2} \end{aligned} \tag{7.54}$$

However, taken into account that $\xi_j = -|\xi_j|$, Eq. 7.54 becomes

$$\begin{aligned} \beta_j &= 90^\circ + \frac{\theta_{T,\max} - \xi_j}{2} \Rightarrow \\ \beta_j^N \equiv \beta_j &= 90^\circ - \frac{\xi_j - \theta_{T,\max}}{2} \Rightarrow \end{aligned} \tag{7.55}$$

which is the complementary angle of Eq. 7.45, and β_j^N denotes the tilt angle of the northern reflective elements.

If we study the geometry of Fig. 7.7e which is similar to the case illustrated in Fig. 7.7f with the exception that the tilt angle β_j is above a critical value so that $\theta_{T,\max} > |\xi_j|$, the relationships connecting these three angles are:

$$\begin{aligned} &\theta_{T,\max} + \beta_j - \varepsilon_j = 90^\circ \Rightarrow \\ &\varepsilon_j = -90^\circ + \theta_{T,\max} + \beta_j \end{aligned} \tag{7.56}$$

and

$$\begin{aligned} &\left|\xi_j\right| + \beta_j + \varepsilon_j = 90^\circ \Rightarrow \\ &\left|\xi_j\right| = 90^\circ - \beta_j - \varepsilon_j \end{aligned} \tag{7.57}$$

Substituting Eq. 7.56 into Eq. 7.57, it becomes

$$\begin{aligned} \left|\xi_j\right| &= 90^\circ - \beta_j - \left(-90^\circ + \theta_{T,\max} + \beta_j\right) \Rightarrow \\ \left|\xi_j\right| &= 90^\circ - \beta_j + 90^\circ - \theta_{T,\max} - \beta_j \Rightarrow \\ \left|\xi_j\right| &= 180^\circ - \theta_{T,\max} - 2 \cdot \beta_j \Rightarrow \\ 2 \cdot \beta_j &= 180^\circ - \theta_{T,\max} - \left|\xi_j\right| \Rightarrow \\ \beta_j &= \frac{180^\circ - \theta_{T,\max} - \left|\xi_j\right|}{2} \\ \beta_j &= 90^\circ + \frac{\theta_{T,\max} + \left|\xi_j\right|}{2} \end{aligned} \tag{7.58}$$

However, taken into account that $\xi_j = -|\xi_j|$, Eq. 7.58 becomes

$$\begin{aligned} &\beta_j = 90^\circ + \frac{\theta_{T,\max} - \xi_j}{2} \Rightarrow \\ &\beta_j^N \equiv \beta_j = 90^\circ - \frac{\xi_j - \theta_{T,\max}}{2} \Rightarrow \end{aligned} \tag{7.59}$$

which is the complementary angle of Eq. 7.45 and identical with Eq. 7.55.

Equations 7.45 and 7.55 have a general form that describes all possible reflectors and receiver configuration. However, in order to be able to proceed to calculations, we must transform them into more useful forms taking into account the specific characteristics of each individual System configuration. The differences among the various Linear Fresnel Reflector Systems stem from the different reflectors' pivoting options and the different receiver configurations. There are three possible pivoting options (centrally pivoted and side pivoted reflectors with the pivot axis to coincide with the southern or the northern edge of the reflectors) and at least four

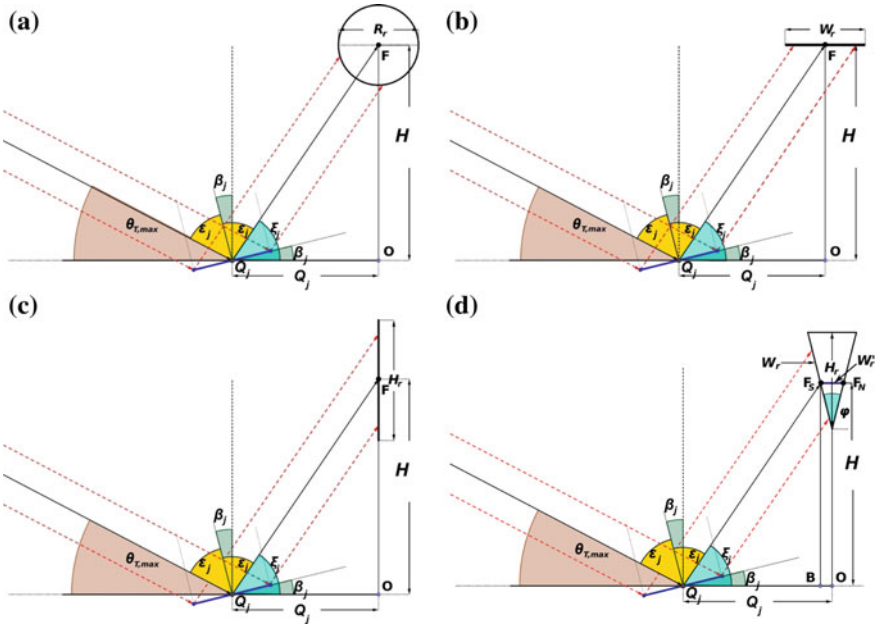

Fig. 7.8 Geometry used for the calculation of the reflectors tilt angle, β_j, of the cross section of a Linear Fresnel Reflector Solar Radiation Concentrating System with **a** circular receiver cross section (tubular absorber), **b** flat horizontal receiver aperture, **c** flat vertical receiver and **d** triangular receiver cross section, and rotation axis which goes through the midpoint of the narrow edge of the reflectors

general receiver configurations (flat horizontal, flat vertical, tubular and receiver with triangular cross section). The only possible modifications of Eqs. 7.45 and 7.55 concern the angle ξ_j, which is computed from different equation for each individual System configuration, depending on their special geometrical characteristics.

We will begin with the easier case, the centrally pivoted reflective elements (Fig. 7.8), and then we will proceed with the rest cases (the two differently side pivoted reflectors) (Figs. 7.9 and 7.10) introducing the proper modifications.

The tilt angle, β_j, of each reflective element is chosen so that the light ray falling on their midpoint to reach at the midpoint of the receiver aperture (the System's focal point, F), or at another appropriately chosen point. So, if the receiver is a single tube, a tubular absorber, the centre of its cross section coincides with the focal point, F, of the System (Fig. 7.8a), whereas, if the receiver has a flat horizontal aperture, its midpoint is what coincides with the focal point, F, of the System

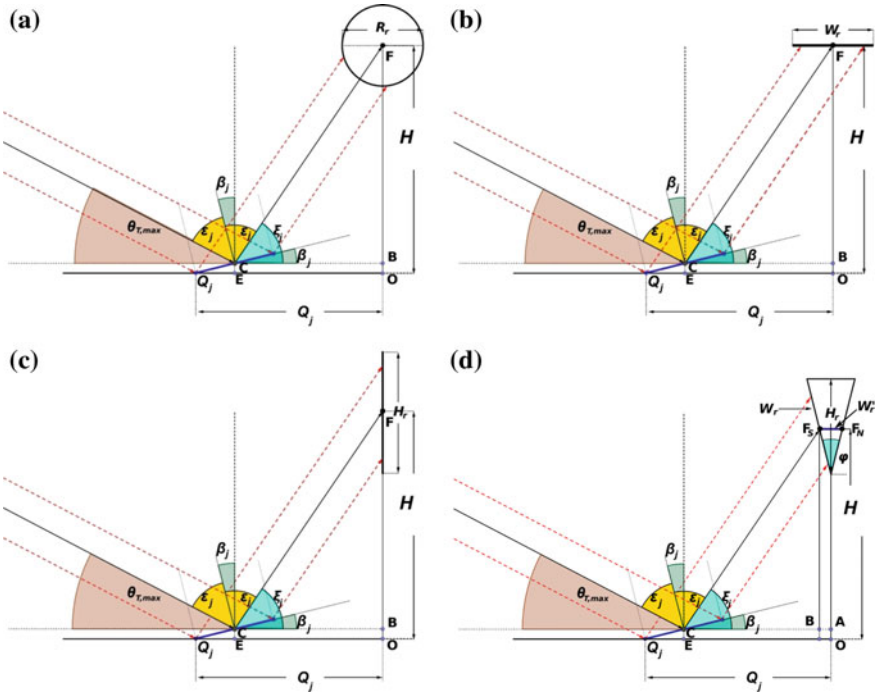

Fig. 7.9 Geometry used for the calculation of the reflectors tilt angle, β_j, of a Linear Fresnel Reflector Solar Radiation Concentrating System with **a** circular receiver cross section (tubular absorber), **b** flat horizontal receiver aperture, **c** flat vertical receiver and **d** triangular receiver cross section, and rotation axis which coincides with the southern edge of the reflectors

(Fig. 7.8b). On the other hand, if the Linear Fresnel Reflector Systems use flat vertical absorber, the reflected solar radiation is directed towards the midpoint of the receiver (absorber) aperture (Fig. 7.8c) and illuminates both surfaces of it. This means that the reflecting elements on the one half of the System, let us say the southern reflectors, illuminate the southern side of the absorber surface and the reflectors placed on the northern side of the System illuminate the surface on the northern side of the absorber. Lastly, if the receiver has a triangular cross section on the System's transversal plane, then the reflectors of each side of the System direct the incoming solar radiation towards the two different sides of the absorber. As in the case of the flat vertical absorber, the southern reflectors illuminate the southern side of the absorber surface and the northern reflectors illuminate its northern surface. However, as it can be deduced from the geometry of Fig. 7.8d, in this case there are two different focal points, F_S and F_N, one for each side of the absorber, that do not coincide. This affects, a little, the mathematical treatment of the problem. However, let us proceed with the first three cases that are identical.

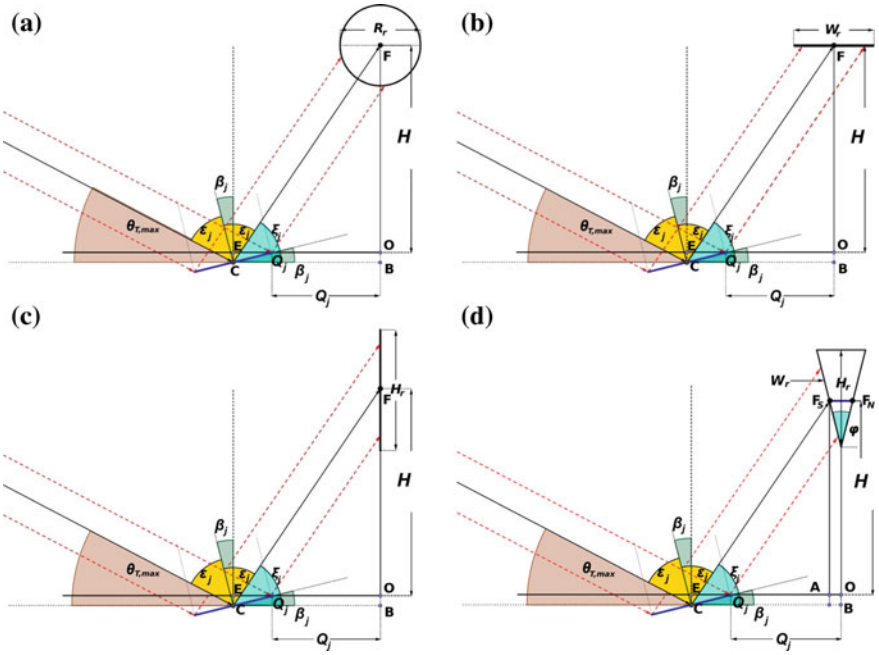

Fig. 7.10 Geometry used for the calculation of the reflectors tilt angle, β_j, of a Linear Fresnel Reflector Solar Radiation Concentrating System with **a** circular receiver cross section (tubular absorber), **b** flat horizontal receiver aperture, **c** flat vertical receiver and **d** triangular receiver cross section, and rotation axis which coincides with the northern edge of the reflectors

The mathematical expression connecting the sides OQ_j and FO and the angle ξ_j of the triangle FOQ_j in Fig. 7.8a–c is

$$\tan \xi_j = \frac{FO}{OQ_j} \Rightarrow$$
$$\tan \xi_j = \frac{H}{Q_j} \Rightarrow$$
$$\xi_j = \tan^{-1}\left(\frac{H}{Q_j}\right) \tag{7.60}$$

Substituting Eq. 7.60 into Eq. 7.45, it becomes

$$\beta_j^S = \frac{1}{2}\tan^{-1}\left(\frac{H}{Q_j}\right) - \frac{\theta_{T,\max}}{2} \tag{7.61}$$

and into Eq. 7.55 it becomes

$$\beta_j^N = 90^\circ - \frac{1}{2}\tan^{-1}\left(\frac{H}{Q_j}\right) + \frac{\theta_{T,\max}}{2} \tag{7.62}$$

In the case of the triangular receiver, Eqs. 7.61 and 7.62 take a little different form, as the length BQ_j does not coincides with the distance Q_j of the location of the jth reflective element form the origin, O, of the local Cartesian coordinates system, since both focal points, F_S and F_N, are not exactly above the origin O, but are displaced by a length BO (Fig. 7.8d). Using the geometry of Fig. 7.8d, the mathematical expression connecting the sides F_SB and BQ_j and the angle ξ_j of the triangle F_SBQ_j is

$$\begin{aligned}
\tan\xi_j &= \frac{F_SB}{BQ_j} \Rightarrow \\
\tan\xi_j &= \frac{F_SB}{Q_jO - BO} \Rightarrow \\
\tan\xi_j &= \frac{H}{Q_j - \frac{W_r'}{2}} \Rightarrow \\
\tan\xi_j &= \frac{H}{Q_j - \frac{H_r}{2}\cdot\tan\frac{\varphi}{2}} \Rightarrow \\
\xi_j &= \tan^{-1}\left(\frac{H}{Q_j - \frac{H_r}{2}\cdot\tan\frac{\varphi}{2}}\right)
\end{aligned} \tag{7.63}$$

where H_r is the receiver height and φ the angle formed by its two sides. The two foci are at the middle points of the receiver sides located at a distance equal to $H_r/2$ from its vertex.

Substituting, now, Eq. 7.63 into Eq. 7.45, it becomes

$$\beta_j^S = \frac{1}{2}\tan^{-1}\left(\frac{H}{Q_j - \frac{H_r}{2}\cdot\tan\frac{\varphi}{2}}\right) - \frac{\theta_{T,\max}}{2} \tag{7.64}$$

and into Eq. 7.55 it becomes

$$\beta_j^N = 90^\circ - \frac{1}{2}\tan^{-1}\left(\frac{H}{Q_j - \frac{H_r}{2}\cdot\tan\frac{\varphi}{2}}\right) + \frac{\theta_{T,\max}}{2} \tag{7.65}$$

Equations 7.61, 7.62, 7.64 and 7.65 are indissolubly connected with Eq. 7.42 through the shift distance, S_j, which also depends on the tilt angle, β_j, through Eqs. 7.9 and 7.29. Therefore, they cannot be solved analytically and the tilt angle, β_j, has to be computed using an iteration method, which will be presented in details later in this chapter.

Proceeding, now, with the Linear Fresnel Reflector System that use the other pivoting option, the side pivoted reflectors, we can notice from Fig. 7.9a–d that the first three cases—tubular absorber, flat horizontal receiver and flat vertical absorber—can again be treated identically, while the fourth receiver configuration, the triangular absorber, is again slightly different, as in the case of the centrally pivoted reflector. The difference between these two groups is again due to the location of the two focal points, F_S and F_N, of the triangular receiver, which are not exactly above the origin, O, of the local Cartesian coordinate system.

However, now, the angle ξ_j is not constant, as it is in the case of the centrally pivoted reflectors, since the midpoint of the reflective elements is not stationary, but it moves on a circle with centre on the reflectors rotation axis. What is stationary is the centre of rotation (or more correctly the edge which coincides with the rotation axis). Therefore, Eqs. 7.61, 7.62, 7.64, and 7.65 have to be properly modified.

For the first three cases—tubular absorber, flat horizontal receiver and flat vertical absorber—the angle ξ_j can be computed from the triangle FBC in Fig. 7.9a–c using the following mathematical expression (The angle β_j takes positive values anticlockwise and negative values clockwise, and $h_j = -\frac{W_j}{2} \cdot \sin\beta_j$).

$$\begin{aligned}
\tan\xi_j &= \frac{FB}{CB} \Rightarrow \\
\tan\xi_j &= \frac{FB}{EO} = \frac{FO - BO}{Q_jO - Q_jE} \Rightarrow \\
\tan\xi_j &= \frac{H - h_j}{Q_j - d_j} \Rightarrow \\
\tan\xi_j &= \frac{H + \frac{W_j}{2} \cdot \sin\beta_j}{Q_j - \frac{W_j}{2} \cdot \cos\beta_j} \Rightarrow \\
\xi_j &= \tan^{-1}\left(\frac{H + \frac{W_j}{2} \cdot \sin\beta_j}{Q_j - \frac{W_j}{2} \cdot \cos\beta_j}\right)
\end{aligned} \tag{7.66}$$

Substituting, now, Eq. 7.66 into Eq. 7.45, it becomes

$$\beta_j^S = \frac{1}{2}\tan^{-1}\left(\frac{H + \frac{W_j}{2} \cdot \sin\beta_j}{Q_j - \frac{W_j}{2} \cdot \cos\beta_j}\right) - \frac{\theta_{T,\max}}{2} \tag{7.67}$$

and into Eq. 7.55 it becomes

$$\beta_j^N = 90^\circ - \frac{1}{2}\tan^{-1}\left(\frac{H + \frac{W_j}{2} \cdot \sin\beta_j}{Q_j - \frac{W_j}{2} \cdot \cos\beta_j}\right) + \frac{\theta_{T,\max}}{2} \tag{7.68}$$

Following the same procedure as above, the tilt angles, β_j, of the reflectors in a Linear Fresnel Reflector System with triangular absorber and reflective elements pivoted around their southern edge are given by the formula

$$\beta_j^S = \frac{1}{2}\tan^{-1}\left(\frac{H + \frac{W_j}{2}\cdot\sin\beta_j}{Q_j - \frac{H_r}{2}\cdot\tan\frac{\varphi}{2} - \frac{W_j}{2}\cdot\cos\beta_j}\right) - \frac{\theta_{T,\max}}{2} \tag{7.69}$$

$$\beta_j^N = 90^\circ - \frac{1}{2}\tan^{-1}\left(\frac{H - \frac{W_j}{2}\cdot\sin\beta_j}{Q_j - \frac{H_r}{2}\cdot\tan\frac{\varphi}{2} - \frac{W_j}{2}\cdot\cos\beta_j}\right) + \frac{\theta_{T,\max}}{2} \tag{7.70}$$

In the case the reflective elements are pivoted around their northern edge (Fig. 7.10a–d), their tilt angle, β_j, is given by the following formulas

$$\beta_j^S = \frac{1}{2}\tan^{-1}\left(\frac{H + \frac{W_j}{2}\cdot\sin\beta_j}{Q_j + \frac{W_j}{2}\cdot\cos\beta_j}\right) - \frac{\theta_{T,\max}}{2} \tag{7.71}$$

$$\beta_j^N = 90^\circ - \frac{1}{2}\tan^{-1}\left(\frac{H + \frac{W_j}{2}\cdot\sin\beta_j}{Q_j + \frac{W_j}{2}\cdot\cos\beta_j}\right) + \frac{\theta_{T,\max}}{2} \tag{7.72}$$

if the Linear Fresnel Reflector System has tubular absorber, flat horizontal receiver and flat vertical absorber, and by the following formulas

$$\beta_j^S = \frac{1}{2}\tan^{-1}\left(\frac{H + \frac{W_j}{2}\cdot\sin\beta_j}{Q_j - \frac{H_r}{2}\cdot\tan\frac{\varphi}{2} + \frac{W_j}{2}\cdot\cos\beta_j}\right) - \frac{\theta_{T,\max}}{2} \tag{7.73}$$

$$\beta_j^N = 90^\circ - \frac{1}{2}\tan^{-1}\left(\frac{H + \frac{W_j}{2}\cdot\sin\beta_j}{Q_j - \frac{H_r}{2}\cdot\tan\frac{\varphi}{2} + \frac{W_j}{2}\cdot\cos\beta_j}\right) + \frac{\theta_{T,\max}}{2} \tag{7.74}$$

if the same System has a triangular absorber.

Caution We must note that in all above cases, the angle β_j takes positive values anticlockwise and negative values clockwise.

7.2.3 A Different Approach

The methodology presented above, and which will be followed in the rest of this chapter, differs from that presented in other studies published in the scientific bibliography. For example, Babu and Arasu (2015) use a slightly different approach to calculate the tilt angle, β_j, and the position, Q_j, of the reflective elements, as well as the shift distance, S_j, between two consecutive reflectors. They use the geometry of a Linear Fresnel Reflector System with a vertical absorber and side pivoted reflector as it is shown in Fig. 7.11.

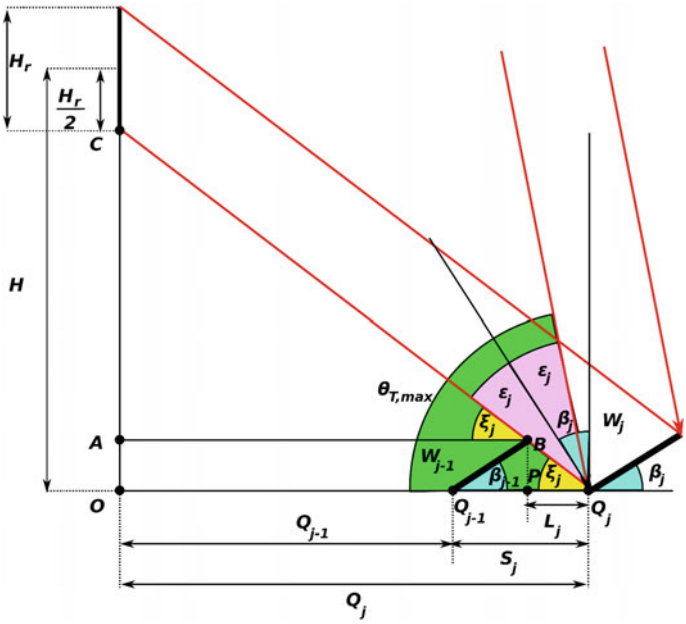

Fig. 7.11 Geometry of a Linear Fresnel Reflector Solar Radiation Concentrating System with flat vertical receiver and rotation axis which coincides with the southern edge of the reflectors used by Babu and Arasu (2015), as well as by other authors of related studies published in the scientific literature, for the calculation of the tilt angle, β_j, and the position, Q_j, of the reflective elements, as well as the shift distance, S_j, between two consecutive reflectors

According to their methodology, the light ray reflected by the bottom edge of the jth reflector should reach the absorber at a point being at height $H - H_r/2$ and the light ray reflected by the top edge of the same reflector should reach the absorber at a point being at height $H + H_r/2$, where H_r is the height (the vertical dimension) of the receiver and H is the height of its midpoint above the origin of the local Cartesian coordinate system. Furthermore, the light ray reflected by the bottom edge of the jth reflector should graze the top edge of the $(j - 1)$th reflector (Fig. 7.11).

Thus, the tilt angle, β_j, of the jth reflector, as a function of the maximum Sun's transversal angle, $\theta_{T,\max}$, and the angle ξ_j, as they are shown in Fig. 7.11, is given by the equation ($\theta_{T,\max} + \beta_j - \varepsilon_j = 90°$ and $\xi_j + \beta_j + \varepsilon_j = 90°$)

$$\beta_j = 90° - \frac{\xi_j - \theta_{T,\max}}{2} \tag{7.55}$$

However, using the geometry of the triangle OCQ_j in Fig. 7.11, the angle ξ_j is calculated by the following formula:

$$\begin{aligned} \tan\xi_j &= \frac{OC}{OQ_j} \Rightarrow \\ \tan\xi_j &= \frac{H - \frac{H_r}{2}}{Q_j} \Rightarrow \\ \xi_j &= \tan^{-1}\left(\frac{H - \frac{H_r}{2}}{Q_j}\right) \end{aligned} \tag{7.75}$$

Substituting Eq. 7.75 into Eq. 7.55, it becomes

$$\beta_j = 90^\circ - \frac{\theta_{T,\max}}{2} - \frac{1}{2}\cdot\tan^{-1}\left(\frac{H - \frac{H_r}{2}}{Q_j}\right) \tag{7.76}$$

On the other hand, the location, Q_j, of jth reflective element is still given by the relationship

$$Q_j = Q_{j-1} + S_j \tag{7.77}$$

where S_j is the appropriate shift distance of the jth reflective element from its adjacent $(j-1)$th reflector, located at a distance Q_{j-1}, so that no shading and blocking effect occur. However, using the geometry of Fig. 7.11, S_j is determined from the equation:

$$S_j = W_{j-1}\cdot\cos\theta_{j-1} + L_j \tag{7.78}$$

The length L_j can be calculated using the two similar triangles CAB and BPQ_j. By equating the base and the height ratios of these two triangles, we have

$$\begin{aligned} \frac{PQ_j}{PB} &= \frac{AB}{AC} \Rightarrow \\ \frac{L_j}{W_{j-1}\sin\theta_{j-1}} &= \frac{Q_{j-1} + W_{j-1}\cdot\cos\theta_{j-1}}{H - \frac{H_r}{2} - W_{j-1}\sin\theta_{j-1}} \Rightarrow \\ L_j &= \frac{\left(Q_{j-1} + W_{j-1}\cdot\cos\theta_{j-1}\right)\cdot W_{j-1}\sin\theta_{j-1}}{H - \frac{H_r}{2} - W_{j-1}\sin\theta_{j-1}} \end{aligned} \tag{7.79}$$

Substituting, now, Eq. 7.79 into Eq. 7.78 and the resulting equation into Eq. 7.77, the latter leads to the following expression for the location, Q_j, of jth reflective element:

$$Q_j = Q_{j-1} + W_{j-1} \cdot \cos\theta_{j-1} + \frac{\left(Q_{j-1} + W_{j-1} \cdot \cos\theta_{j-1}\right) \cdot W_{j-1} \sin\theta_{j-1}}{H - \frac{H_r}{2} - W_{j-1} \sin\theta_{j-1}} \tag{7.80}$$

which with Eq. 7.76

$$\beta_j = 90^\circ - \frac{\theta_{T,\max}}{2} - \frac{1}{2} \cdot \tan^{-1}\left(\frac{H - \frac{H_r}{2}}{Q_j}\right) \tag{7.76}$$

form the two equations that describe the design parameters (the tilt angle, β_j, and the position, Q_j) of all reflective elements of this particular Linear Fresnel Reflector System. They are a little different from the corresponding equations derived in the previous paragraph. However, they should lead to the same numerical results for the tilt angle, β_j, and the position, Q_j, when solved.

7.2.4 *Reflective Elements' Width*

Until now we have not made any assumption about the reflective elements' width. All above-presented equations are valid whether it is constant or not. In the case of constant width, the parameter W_j is replaced by the parameter W, the common reflectors' width. Its value can be calculated based, for example, on the requirement that the projection, P_r, of the absorber (or receiver) aperture width, W_r, on a line perpendicular to the direction of the solar radiation beam reflected by the most remote reflective element ($j = n$, or $j = n_S$, or $j = n_N$) must be equal to beam's cross section, CS_n.

On the other hand, in the case of varying reflectors' width, the above condition must be true for each reflector (always for a reference value of the transversal Sun's angle θ_T, e.g. $\theta_{T,\max}$). Thus, by taking advantage of the geometry of Fig. 7.12a–c, we can calculate the reflected solar radiation beam's cross section, CS_j, first in relation to the jth reflector's width, W_j, and then in relation to the absorber, or receiver, aperture width, W_r, and next to equate the two results. The resulting equation will define the width, W_j, of each reflector. However, in order to be able to compute these cross sections, CS_j, we must know the angle, xj, formed by the direction of the reflected solar radiation beam with the reflector's plane on the transversal plane of the System. Figure 7.12a–c illustrate the geometry of the three possible cases of the reflectors' position, namely reflectors being placed (a) southern from the reference location, (b) northern form the reference location and southern from the receiver, and (c) northern form the receiver. At a first glance, the geometry of these places seems to be different, but it results in the same general equation, as we will show soon.

Let us start with the case of Fig. 7.12a. The angle x_j is computed form the formula

$$\begin{aligned} x_j &= \xi_j + |\beta_j| \Rightarrow \\ x_j &= \xi_j - \beta_j \end{aligned} \tag{7.81}$$

since, $\beta_j = -|\beta_j|$, due to the angles' sign convention followed in this book (we consider an angle as positive if it is formed anticlockwise and as negative when it is formed clockwise).

Similarly, from Fig. 7.12b, the angle x_j is computed from the formula

$$x_j = \xi_j - \beta_j \tag{7.82}$$

In this case, both angles ξ_j and β_j are positive.

Finally, in the case of Fig. 7.12c (for the northern reflective elements), the angle x_j is computed from the formula

$$\begin{aligned} x_j + |\xi_j| + \beta_j &= 180^\circ \Rightarrow \\ x_j &= 180^\circ - |\xi_j| - \beta_j \Rightarrow \\ x_j &= 180^\circ + \xi_j - \beta_j \end{aligned} \tag{7.83}$$

since, now, it is $\xi_j = -|\xi_j|$, while the other two angles (x_j and β_j) are positive.

Equations 7.81 and 7.82 are identical for all cases and **independent from the reflectors pivoting option**. The same applies for Eq. 7.83, too. Therefore, the solar radiation beam's cross section, CS_j, after being reflected by the jth reflective element, can be calculated using the geometry of Fig. 7.12a–c by the formula

$$\begin{aligned} \sin x_j &= \frac{CS_j}{W_j} \Rightarrow \\ CS_j &= W_j \cdot \sin x_j \end{aligned} \tag{7.84}$$

Now, in order to derive the formulas that provide the projection, P_r, of the absorber (or receiver) aperture width, W_r, on a line perpendicular to the direction of the reflected solar radiation beam, we must treat each receiver configuration separately. The simpler case is the tubular receiver (one tube absorber) illustrated in Fig. 7.13a. In this case, the reflected solar radiation beam is always perpendicular to one diameter of the transversal cross section of the tubular absorber. Hence, in order the whole reflected solar radiation to be concentrated exactly on the absorber (not any part of it to get lost, while at the same time the most possibly larger area of the absorber to be illuminated), the two light rays bordering the reflected beam must touch the absorber's circumference. As a result, the cross section of the solar radiation beam reflected by the jth reflective element must be equal to the absorber diameter, $W_r = 2 \cdot R_r$:

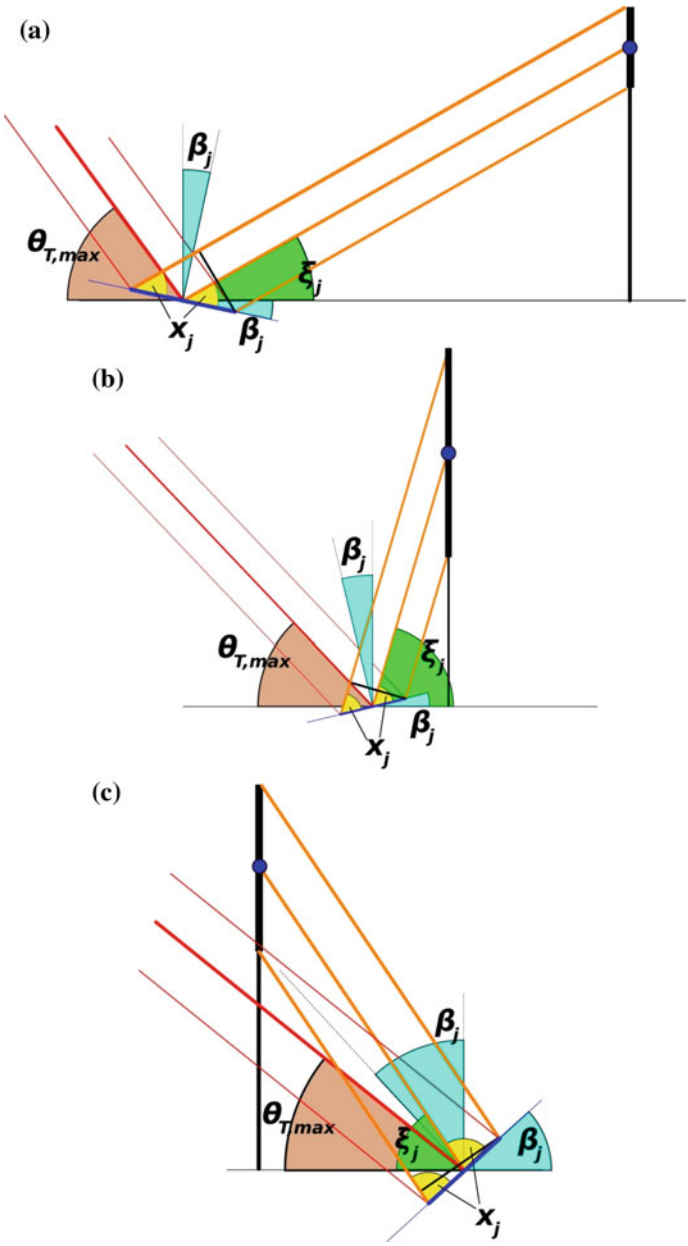

Fig. 7.12 In order to compute the appropriate reflectors' width, it is necessary to be able to calculate the cross section of the solar radiation beam being reflected by each reflective element. For this reason, the angle x_j formed by the direction of the reflected solar radiation with the reflector, on the transversal plane, is required. The geometry of the three possible locations of the reflectors—the reflective elements are placed **a** southern from the reference location, **b** northern from the reference location and southern from the receiver (namely between them), **c** northern from the receiver (see also Fig. 7.10)—seems different, but they lead to the same equation for the angle x_j in relation to the angles ξ_j and β_j

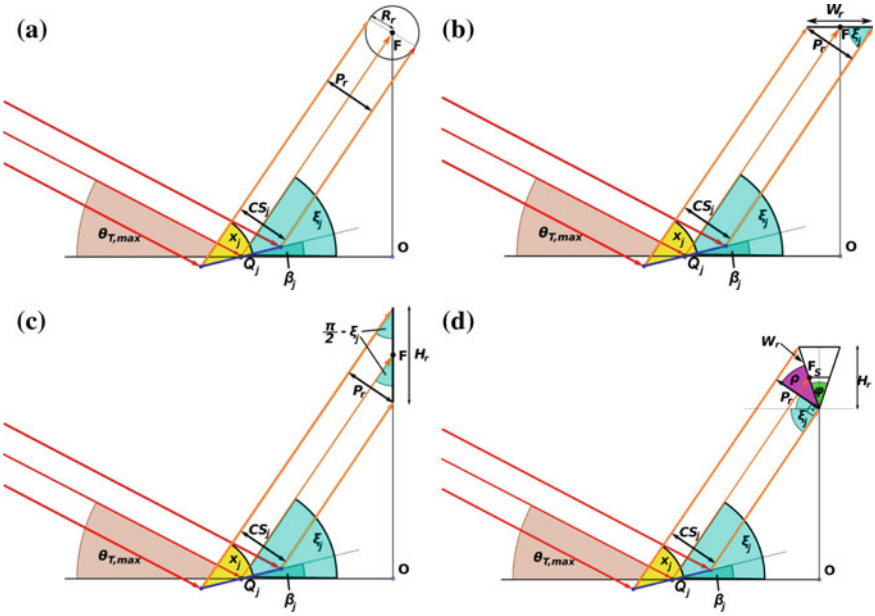

Fig. 7.13 Different receiver configurations, **a** circular receiver cross section (tubular absorber), **b** flat horizontal receiver aperture, **c** flat vertical receiver, **d** triangular receiver cross section, have also different influence on the way the reflected solar radiation is distributed on the absorber surface. For this reason, the reflected solar radiation beam cross sections, and consequently the reflectors' width, have to be different in each case. The corresponding geometry is not the same, and each case must be treated separately

$$\mathrm{CS}_j = W_r = 2 \cdot R_r \tag{7.85}$$

Equating, now, Eqs. 7.84 and 7.85, we have the following formula which gives the width, W_j, of each reflector for a tubular absorber

$$\begin{aligned} W_j \cdot \sin x_j &= W_r = 2 \cdot R_r \Rightarrow \\ W_j &= \frac{W_r}{\sin x_j} = \frac{2 \cdot R_r}{\sin x_j} \end{aligned} \tag{7.86}$$

Let us, now, proceed with the case of the flat horizontal receiver. From Fig. 7.13b, the projection, P_r, of the absorber (or receiver) aperture width, W_r, on a line perpendicular to the direction of the reflected solar radiation beam is given by the formula

$$\begin{aligned} \sin \xi_j &= \frac{P_r}{W_r} \Rightarrow \\ P_r &= W_r \cdot \sin \xi_j \end{aligned} \tag{7.87}$$

As in the previous case, the projection, P_r, of the absorber's aperture width must be equal to the cross section, CS_j, of the solar radiation beam after being reflected by the jth reflective element. Equating Eqs. 7.84 and 7.87, we obtain the following formula which gives the width, W_j, of each reflector for a flat horizontal absorber:

$$\begin{aligned} CS_j &= P_r \\ W_j \cdot \sin x_j &= W_r \cdot \sin \xi_j \\ W_j &= W_r \cdot \frac{\sin \xi_j}{\sin x_j} \end{aligned} \tag{7.88}$$

The case of the flat vertical absorber is similar. From Fig. 7.13c, the projection, P_r, of the absorber aperture width, W_r, on a line perpendicular to the direction of the reflected solar radiation beam is given by the formula

$$\begin{aligned} &\sin\left(\frac{\pi}{2} - \xi_j\right) = \frac{P_r}{W_r} \Rightarrow \\ &P_r = W_r \cdot \cos \xi_j \end{aligned} \tag{7.89}$$

Equating Eqs. 7.84 and 7.89, we obtain the following formula which gives the width, W_j, of each reflector for a flat vertical absorber:

$$\begin{aligned} CS_j &= P_r \\ W_j \cdot \sin x_j &= W_r \cdot \cos \xi_j \\ W_j &= W_r \cdot \frac{\cos \xi_j}{\sin x_j} \end{aligned} \tag{7.90}$$

The last case, the receiver with triangular cross section on the System's transversal plane, which has a height equal to H_r, while the angle formed by its two sides is equal to φ, is a little more complicated. It is illustrated in Fig. 7.13d. The angle ρ_j needed to compute the projection, P_r, of the aperture width, W_r, of both sides of the absorber on a line perpendicular to the direction of the solar radiation beam reflected by the jth reflective element is given by the following equation (Fig. 7.13d)

$$\begin{aligned} &\frac{\varphi}{2} + \rho_j + \frac{\pi}{2} - \xi_j = \frac{\pi}{2} \Rightarrow \\ &\rho_j = \xi_j - \frac{\varphi}{2} \end{aligned} \tag{7.91}$$

Consequently, according to the geometry of Fig. 7.13d the above projection, P_r, of the absorber aperture width, W_r, is given by the formula

$$\cos\rho_j = \frac{P_r}{W_r} \Rightarrow$$
$$\cos\rho_j = \frac{P_r}{\frac{H_r}{\cos\frac{\varphi}{2}}} \Rightarrow$$
$$P_r = H_r \cdot \frac{\cos\rho_j}{\cos\frac{\varphi}{2}} \tag{7.92}$$

Equating, now, Eqs. 7.84 and 7.92, we obtain the following formula which gives the width, W_j, of each reflector for a absorber with triangular cross section on the transversal plane of the System:

$$\begin{aligned} \mathrm{CS}_j &= P_r \\ W_j \cdot \sin x_j &= H_r \cdot \frac{\cos\rho_j}{\cos\frac{\varphi}{2}} \\ W_j &= H_r \cdot \frac{\cos\rho_j}{\cos\frac{\varphi}{2} \cdot \sin x_j} \\ W_j &= H_r \cdot \frac{\cos\left(\xi_j - \frac{\varphi}{2}\right)}{\cos\frac{\varphi}{2} \cdot \sin x_j} \end{aligned} \tag{7.93}$$

All above equations have been derived taking into account centrally pivoted reflective elements, but they are also applicable for site pivoted reflectors.

7.3 Sun's Angular Size Effect

The preceding analysis is based on the assumption that the incident light rays are parallel. However, this is not true, because Sun is not an ideal point light source. On the contrary, it has a finite angular size, $2 \cdot \delta_0$, which, for any observer on Earth's surface, is equal to 32′, $2 \cdot \delta_0 = 32'$. As a result, the light rays emanating from Sun's disc and reaching the receiver after reflection on the primary reflectors are not parallel, but diverging. This affects the width of the reflected solar radiation beams (its cross sections), CS_j, and consequently the secondary reflector's shape and aperture width. For the same reason, the angular dispersion of the reflected solar radiation affects the primary reflectors width, W_j, as well as the shift, S_j, between them, while their inclination angle, β_j, remains unaffected. Hence, to take into account the effect Sun's angular size, $2 \cdot \delta_0$, may have on the calculations of the design parameter of the System, we should properly modify the equations providing the reflective elements width, W_j, and location, Q_j.

Sun's angular size, $2 \cdot \delta_0$, affects only the size of the maximum value of Sun's transversal angle, $\theta_{T,\max}$. In fact, it increases its value by an amount equal to δ_0: $\theta'_{T,\max} = \theta_{T,\max} + \delta_0$. Hence, we can still use Eq. 7.9, or Eq. 7.15, or Eq. 7.21, or Eq. 7.29, or Eq. 7.35, or Eq. 7.41 to calculate the appropriate shift distance, S_j, between two consecutive reflective elements, but now we replace the maximum value of Sun's transversal angle, $\theta_{T,\max}$, with its new value

$$\theta'_{T,\max} = \theta_{T,\max} + \delta_0 \tag{7.94}$$

On the other hand, the effect Sun's angular size, $2 \cdot \delta_0$, may have on the reflective elements width, W_j, is more complex. The cross section, CS_j, of the reflected solar radiation's beam is not constant. Except for the part corresponding to parallel light rays, there are two additional parts that originate from the diverging nature of the solar light rays hitting the reflective elements at their edges (Fig. 7.14). However, despite the fact that this complicates the treatment of the problem, the main idea remains the same. We have to calculate the image of the reflected solar radiation beam on the receiver and connect it with the reflectors width. Figure 7.14a illustrates the case of centrally pivoted reflective elements and flat vertical absorber, while in Fig. 7.14b–d the absorber is flat horizontal (b), with circular cross section (tubular) (c) and with triangular cross section (d), respectively. In this paragraph, we will deal with the problem of the calculation of the varying width, W_j, of centrally pivoted reflective elements and flat vertical, flat horizontal and tubular absorber. The rest cases (triangular receiver and different pivoting options) can be treated similarly, but as the calculation procedure is extensive we limit the application of this methodology to these particular cases.

According to the Systems geometry illustrated in Fig. 7.14a, the length, L_j, of the illuminated part of the absorber aperture's width, W_r (or height, H_r, in this case), due to the contribution of the jth reflective element, may be considered to be equal to the sum of three individual lengths,

$$L_j = L_{j,0} + L_{j,T} + L_{j,B} \tag{7.95}$$

where the length $L_{j,0}$ corresponds to the parallel treatment of Sun's light rays, and the lengths $L_{j,T}$ and $L_{j,B}$ to the illuminated part of the absorber due to the diverging nature of Sun's light rays. The light ray T is reflected by the top and the light ray B by the bottom edge of the reflector, respectively. Apparently, it must be equal to the absorber aperture's width, W_r, $L_j = W_r$, so that solar radiation concentration on the absorber to be the maximum (maximum performance of the Systems).

The length $L_{j,0}$ can be calculated from Eq. 7.90 after being properly modified:

$$L_{j,0} = W_j \cdot \frac{\sin x_j}{\cos \xi_j} \tag{7.96}$$

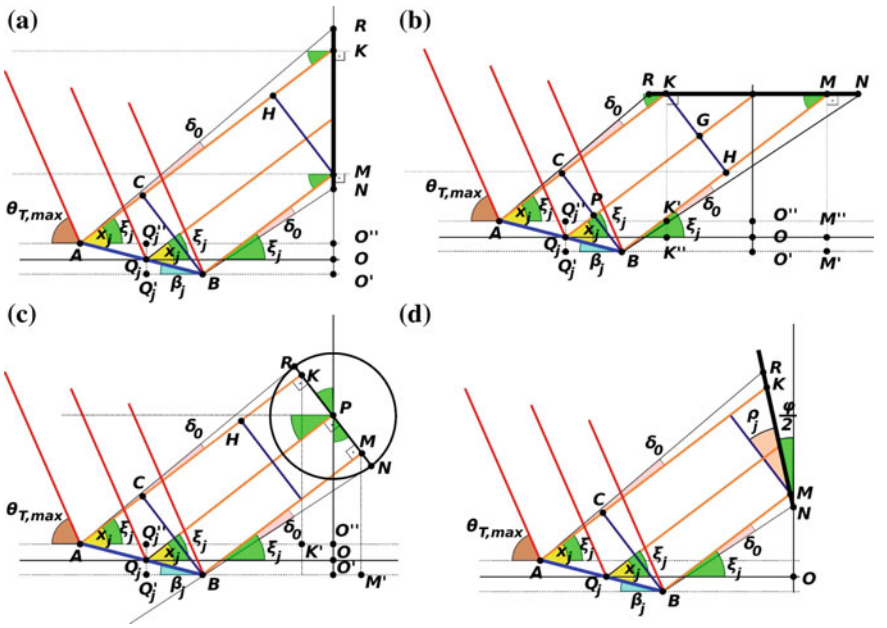

Fig. 7.14 Sun's angular size, $2 \cdot \delta_0$, affects the reflective elements width, W_j, due to the diverging nature of the reflected solar radiation's beam. Its cross section is not longer constant as it is travelling towards the receiver. If we accept that Sun has a nonzero but finite size, except for the part corresponding to parallel light rays, there are two additional parts of the reflected beam's cross section that originate from the diverging nature of the solar light rays hitting the reflective elements at their edges (points *A* and *B*). The resulting geometry is more complicated than in the case of parallel light rays, but the main concept of the problem treatment remains the same. The illuminated part, L_j, of the receiver aperture width, W_r, has to be equal to its width, W_r. The geometry of the problem is different for different receiver configurations and reflectors' pivoting option. Scheme (**a**) illustrates the case of centrally pivoted reflective elements and flat vertical absorber, while in (**b**–**d**) the absorber is flat horizontal (**b**), with circular cross section (tubular) (**c**) and with triangular transversal cross section (**d**), respectively

Next, the lengths $L_{j,T}$ and $L_{j,B}$ can be calculated using the geometry of Fig. 7.14a and the Law of Sines applied to the triangles *BMN* and *ARK*.

In triangle *BMN,* the angle $\widehat{MBN}$ is equal to δ_0, the angle $\widehat{MBN}$ is equal to $\pi/2 - \xi_j$, and the angle $\widehat{MNB}$ is equal to $\pi - (\pi/2 - \xi_j) - \delta_0 = \pi/2 + \xi_j - \delta_0$:

$$\widehat{MBN} = \delta_0 \tag{7.97a}$$

$$\widehat{BMN} = \frac{\pi}{2} - \xi_j \tag{7.97b}$$

$$\widehat{BNM} = \frac{\pi}{2} + \xi_j - \delta_0 \tag{7.97c}$$

In addition, the side BM, the side $O'B$ and the angle

$\widehat{O'MB}\left(=\widehat{BMN}=\frac{\pi}{2}-\xi_j\right)$ of the triangle $MO'B$ satisfy the equation

$$\sin\widehat{O'MB}=\frac{O'B}{BM}\Rightarrow$$
$$BM=\frac{O'B}{\sin\widehat{O'MB}} \tag{7.98}$$

However,

$$BO'=Q'_jO'-Q'_j\mathrm{B}\Rightarrow$$
$$BO'=Q_jO-\frac{W_j}{2}\cdot\cos\beta_j\Rightarrow$$
$$BO'=Q_j-\frac{W_j}{2}\cdot\cos\beta_j \tag{7.99}$$

Therefore, if we replace BO' from Eq. 7.99 in Eq. 7.98, we have

$$BM=\frac{Q_j-\frac{W_j}{2}\cdot\cos\beta_j}{\sin\left(\frac{\pi}{2}-\xi_j\right)} \tag{7.100}$$

$$BM=\frac{Q_j-\frac{W_j}{2}\cdot\cos\beta_j}{\cos\xi_j} \tag{7.101}$$

Applying now the Law of Sines in the triangle BMN, we have

$$\frac{MN}{\sin\widehat{MBN}}=\frac{BM}{\sin\widehat{BNM}}\Rightarrow$$
$$\frac{L_{j,B}}{\sin\delta_0}=\frac{\frac{Q_j-\frac{W_j}{2}\cdot\cos\beta_j}{\cos\xi_j}}{\sin\left(\frac{\pi}{2}+\xi_j-\delta_0\right)}\Rightarrow$$
$$\frac{L_{j,B}}{\sin\delta_0}=\frac{\frac{Q_j-\frac{W_j}{2}\cdot\cos\beta_j}{\cos\xi_j}}{-\sin\left(\xi_j-\delta_0\right)}\Rightarrow$$
$$L_{j,B}=\left(Q_j-\frac{W_j}{2}\cdot\cos\beta_j\right)\cdot\frac{-\sin\delta_0}{\cos\xi_j\cdot\sin\left(\xi_j+\delta_0\right)} \tag{7.102}$$

Applying the same procedure in triangle ARK, we can calculate the side AK and after that the length $L_{j,\mathrm{T}}$.

So, in triangle ARK the angle $\widehat{RAK}$ is equal to δ_0, the angle $\widehat{RKA}$ is equal to $\pi/2 + \xi_j$, and angle $\widehat{ARK}$ is equal to $\pi/2 - \xi_j - \delta_0$:

$$\widehat{RAK} = \delta_0 \tag{7.103a}$$

$$\widehat{RKA} = \frac{\pi}{2} + \xi_j \tag{7.103b}$$

$$\widehat{KRA} = \frac{\pi}{2} - \xi_j - \delta_0 \tag{7.103c}$$

In addition, the side AK, the side $O''A$, and the angle

$\widehat{AKO''}\left(=\frac{\pi}{2} - \xi_j\right)$ of triangle $KO''A$ satisfy the equation

$$\sin\widehat{AKO''} = \frac{O''A}{AK}$$

$$AK = \frac{O''A}{\sin\widehat{AKO''}} \tag{7.104}$$

However,

$$\begin{aligned} AO'' &= Q_j''O'' - Q_j''A \Rightarrow \\ AO'' &= Q_jO + \frac{W_j}{2}\cdot\cos\beta_j \Rightarrow \\ AO'' &= Q_j + \frac{W_j}{2}\cdot\cos\beta_j \end{aligned} \tag{7.105}$$

Therefore, if we replace AO'' from Eq. 7.105 in Eq. 7.104, we have

$$AK = \frac{Q_j + \frac{W_j}{2}\cdot\cos\beta_j}{\sin\left(\frac{\pi}{2} - \xi_j\right)}$$

$$AK = \frac{Q_j + \frac{W_j}{2}\cdot\cos\beta_j}{\cos\xi_j} \tag{7.106}$$

Applying now the Law of Sines to the triangle *ARK,* we have

$$\frac{RK}{\sin\widehat{RAK}} = \frac{AK}{\sin\widehat{KRK}} \Rightarrow$$

$$\frac{L_{j,T}}{\sin\delta_0} = \frac{\frac{Q_j + \frac{W_j}{2}\cdot\cos\beta_j}{\cos\xi_j}}{\sin\left(\frac{\pi}{2} - \xi_j - \delta_0\right)} \Rightarrow$$

$$\frac{L_{j,T}}{\sin\delta_0} = \frac{\frac{Q_j + \frac{W_j}{2}\cdot\cos\beta_j}{\cos\xi_j}}{\cos\left(\xi_j + \delta_0\right)} \Rightarrow$$

$$L_{j,T} = \left(Q_j + \frac{W_j}{2}\cdot\cos\beta_j\right)\cdot\frac{\sin\delta_0}{\cos\xi_j\cdot\cos\left(\xi_j + \delta_0\right)} \tag{7.107}$$

Now, combining Eqs. 7.95, 7.96, 7.102 and 7.107 and equating the illuminating length, L_j, of the receiver aperture with its width, W_r, we have

If we set $\delta_0 = 0$, then Eq. 7.108 takes the form of Eq. 7.90, as it should be.

The same procedure can be applied in the case of flat horizontal receiver with centrally pivoted reflective element, too (Fig. 7.14b). In the following, we will present the corresponding equations and calculation, which are almost similar to the previous case. We take advantage of the problem geometry illustrated in Fig. 7.14b and calculate the illuminated part, L_j, of the receiver aperture, W_r, due to the jth reflective elements, and finally we equate the two quantities. The illuminated length, L_j, continues to consist of three parts according to Eq. 7.95. The length $L_{j,0}$ can be calculated from Eq. 7.88 after being properly modified:

$$W_r = W_j\cdot\frac{\sin x_j}{\cos\xi_j} + \left(Q_j + \frac{0W_j}{2}\cdot\cos\beta_j\right)\cdot\frac{\sin\delta_0}{\cos\xi_j\cdot\cos\left(\xi_j + \delta_0\right)}$$
$$+ \left(Q_j - \frac{W_j}{2}\cdot\cos\beta_j\right)\cdot\frac{-\sin\delta_0}{\cos\xi_j\cdot\sin\left(\xi_j + \delta_0\right)} \Rightarrow$$

$$W_r = W_j\cdot\frac{\sin x_j}{\cos\xi_j} + Q_j\cdot\frac{\sin\delta_0}{\cos\xi_j\cdot\cos\left(\xi_j + \delta_0\right)} + \frac{W_j}{2}\cdot\cos\beta_j\cdot\frac{\sin\delta_0}{\cos\xi_j\cdot\cos\left(\xi_j + \delta_0\right)}$$
$$- Q_j\cdot\frac{\sin\delta_0}{\cos\xi_j\cdot\sin\left(\xi_j + \delta_0\right)} + \frac{W_j}{2}\cdot\cos\beta_j\cdot\frac{\sin\delta_0}{\cos\xi_j\cdot\sin\left(\xi_j + \delta_0\right)} \Rightarrow$$

$$
\begin{aligned}
W_r &= W_j \cdot \frac{\sin x_j}{\cos \xi_j} + Q_j \cdot \frac{\sin \delta_0}{\cos \xi_j} \cdot \left[\frac{1}{\cos(\xi_j + \delta_0)} - \frac{1}{\sin(\xi_j + \delta_0)} \right] \\
&\quad + \frac{W_j}{2} \cdot \frac{\cos \beta_j \cdot \sin \delta_0}{\cos \xi_j} \cdot \left[\frac{1}{\cos(\xi_j + \delta_0)} + \frac{1}{\sin(\xi_j + \delta_0)} \right] \Rightarrow \\
W_r &= W_j \cdot \frac{\sin x_j}{\cos \xi_j} + \frac{W_j}{2} \cdot \frac{\cos \beta_j \cdot \sin \delta_0}{\cos \xi_j} \cdot \frac{\sin(\xi_j + \delta_0) + \cos(\xi_j + \delta_0)}{\cos(\xi_j + \delta_0) \cdot \sin(\xi_j + \delta_0)} \\
&\quad + Q_j \cdot \frac{\sin \delta_0}{\cos \xi_j} \cdot \frac{\sin(\xi_j + \delta_0) - \cos(\xi_j + \delta_0)}{\cos(\xi_j + \delta_0) \cdot \sin(\xi_j + \delta_0)} \Rightarrow \\
&\quad W_r - Q_j \cdot \frac{\sin \delta_0}{\cos \xi_j} \cdot \frac{\sin(\xi_j + \delta_0) - \cos(\xi_j + \delta_0)}{\cos(\xi_j + \delta_0) \cdot \sin(\xi_j + \delta_0)} \\
&\quad = W_j \cdot \left[\frac{\sin x_j}{\cos \xi_j} + \frac{1}{2} \cdot \frac{\cos \beta_j \cdot \sin \delta_0}{\cos \xi_j} \cdot \frac{\sin(\xi_j + \delta_0) + \cos(\xi_j + \delta_0)}{\cos(\xi_j + \delta_0) \cdot \sin(\xi_j + \delta_0)} \right] \Rightarrow \\
&\quad \frac{W_r \cdot \cos \xi_j \cdot \cos(\xi_j + \delta_0) \cdot \sin(\xi_j + \delta_0) - Q_j \cdot \sin \delta_0 \cdot \left[\sin(\xi_j + \delta_0) - \cos(\xi_j + \delta_0) \right]}{\cos \xi_j \cdot \cos(\xi_j + \delta_0) \cdot \sin(\xi_j + \delta_0)} \\
&\quad = W_j \cdot \frac{2 \cdot \sin x_j \cdot \cos(\xi_j + \delta_0) \cdot \sin(\xi_j + \delta_0) + \cos \beta_j \cdot \sin \delta_0 \cdot \sin(\xi_j + \delta_0) + \cos(\xi_j + \delta_0)}{2 \cdot \cos \xi_j \cdot \cos(\xi_j + \delta_0) \cdot \sin(\xi_j + \delta_0)} \\
&\quad W_r \cdot \cos \xi_j \cdot \cos(\xi_j + \delta_0) \cdot \sin(\xi_j + \delta_0) \\
&\quad - Q_j \cdot \sin \delta_0 \cdot \left[\sin(\xi_j + \delta_0) - \cos(\xi_j + \delta_0) \right] \\
&\quad = W_j \cdot \frac{2 \cdot \sin x_j \cdot \cos(\xi_j + \delta_0) \cdot \sin(\xi_j + \delta_0) + \cos \beta_j \cdot \sin \delta_0 \cdot \sin(\xi_j + \delta_0) + \cos(\xi_j + \delta_0)}{2} \Rightarrow \\
W_j &= 2 \cdot \frac{W_r \cdot \cos \xi_j \cdot \cos(\xi_j + \delta_0) \cdot \sin(\xi_j + \delta_0) - Q_j \cdot \sin \delta_0 \cdot \left[\sin(\xi_j + \delta_0) - \cos(\xi_j + \delta_0) \right]}{2 \cdot \sin x_j \cdot \cos(\xi_j + \delta_0) \cdot \sin(\xi_j + \delta_0) + \cos \beta_j \cdot \sin \delta_0 \cdot \sin(\xi_j + \delta_0) + \cos(\xi_j + \delta_0)}
\end{aligned}
\tag{7.108}
$$

$$
L_{j,0} = W_j \cdot \frac{\sin x_j}{\sin \xi_j} \tag{7.109}
$$

Next, the lengths $L_{j,T}$ and $L_{j,B}$ can be calculated using the geometry of Fig. 7.14b and the Law of Sines applied to the triangles *ARK* and *BMN*.

In triangle *BMN*, the angle $\widehat{MBN}$ is equal to δ_0, the angle $\widehat{BMN}$ is equal to $\pi - \xi_j$, and the angle $\widehat{MNB}$ is equal to $\pi/2 - \xi_j - \delta_0$:

$$
\widehat{MBN} = \delta_0 \tag{7.110a}
$$

$$
\widehat{BMN} = \pi - \xi_j \tag{7.110b}
$$

$$
\widehat{MNB} = \xi_j - \delta_0 \tag{7.110c}
$$

In addition, the side *BM*, the side *MM′* and the angle

$\widehat{BMM'}\left(=\frac{\pi}{2}-\xi_j\right)$ of the triangle BMM' satisfy the equation

$$\cos\widehat{BMM'}=\frac{MM'}{BM}\Rightarrow$$
$$BM=\frac{MM'}{\cos\widehat{BMM'}} \tag{7.111}$$

However,

$$\begin{aligned} MM'&=MM''+M''M'\Rightarrow\\ MM'&=H+\tfrac{W_j}{2}\cdot\sin\beta_j \end{aligned} \tag{7.112}$$

Therefore, if we replace MM' from Eq. 7.112 in Eq. 7.111, we have

$$BM=\frac{H+\frac{W_j}{2}\cdot\sin\beta_j}{\cos\left(\frac{\pi}{2}-\xi_j\right)}$$
$$BM=\frac{H+\frac{W_j}{2}\cdot\sin\beta_j}{\sin\xi_j} \tag{7.113}$$

Applying now the Law of Sines in the triangle BMN, we have

$$\begin{aligned} \frac{MN}{\sin\widehat{MBN}}&=\frac{BM}{\sin\widehat{MNB}}\Rightarrow\\ \frac{L_{j,B}}{\sin\delta_0}&=\frac{\frac{H+\frac{W_j}{2}\cdot\sin\beta_j}{\sin\xi_j}}{\sin\left(\xi_j-\delta_0\right)}\Rightarrow\\ \frac{L_{j,B}}{\sin\delta_0}&=\frac{\frac{H+\frac{W_j}{2}\cdot\sin\beta_j}{\sin\xi_j}}{\sin\left(\xi_j-\delta_0\right)}\Rightarrow\\ L_{j,B}&=\left(H+\frac{W_j}{2}\cdot\sin\beta_j\right)\cdot\frac{\sin\delta_0}{\sin\xi_j\cdot\sin\left(\xi_j-\delta_0\right)} \end{aligned} \tag{7.114}$$

Applying the same procedure in triangle ARK, we can calculate the side AK and after that the length $L_{j,T}$.

In triangle ARK, the angle $\widehat{RAK}$ is equal to δ_0, the angle $\widehat{RKA}$ is equal to ξ_j, and angle $\widehat{RKA}$ $\widehat{KRA}$ is equal to $\pi-\xi_j-\delta_0$:

$$\widehat{RAK}=\delta_0 \tag{7.115a}$$

$$\widehat{RKA}=\xi_j \tag{7.115b}$$

$$\widehat{KRA} = \pi - \xi_j - \delta_0 \tag{7.115c}$$

In addition, the side AK, the side KK' and the angle

$\widehat{AKK'}\left(=\frac{\pi}{2}-\xi_j\right)$ of triangle AKK' satisfy the equation

$$\cos\widehat{AKK'} = \frac{KK'}{AK}$$

$$AK = \frac{KK'}{\cos\widehat{AKK'}} \tag{7.116}$$

However,

$$KK' = KK' - K'K'' \Rightarrow$$

$$KK' = H - \frac{W_j}{2}\cdot\sin\beta_j \tag{7.117}$$

Therefore, if we replace KK' from Eq. 7.117 in Eq. 7.116, we have

$$AK = \frac{H - \frac{W_j}{2}\cdot\sin\beta_j}{\cos\left(\frac{\pi}{2}-\xi_j\right)}$$

$$AK = \frac{H - \frac{W_j}{2}\cdot\sin\beta_j}{\sin\xi_j} \tag{7.118}$$

Applying now the Law of Sines to the triangle ARK, we have

$$\frac{RK}{\sin\widehat{RAK}} = \frac{AK}{\sin\widehat{KRA}} \Rightarrow$$

$$\frac{L_{j,T}}{\sin\delta_0} = \frac{\frac{H-\frac{W_j}{2}\cdot\sin\beta_j}{\sin\xi_j}}{\sin\left(\pi-\xi_j-\delta_0\right)} \Rightarrow$$

$$\frac{L_{j,T}}{\sin\delta_0} = \frac{\frac{H-\frac{W_j}{2}\cdot\sin\beta_j}{\sin\xi_j}}{\sin\left(\xi_j+\delta_0\right)} \Rightarrow$$

$$L_{j,T} = \left(H - \frac{W_j}{2}\cdot\sin\beta_j\right)\cdot\frac{\sin\delta_0}{\sin\xi_j\cdot\sin\left(\xi_j+\delta_0\right)} \tag{7.119}$$

Now, combining Eqs. 7.95, 7.109, 7.114 and 7.119 and equating the illuminating length, L_j, of the receiver aperture with its width, W_r, we have

$$
\begin{aligned}
&W_r = L_j = L_{j,0} + L_{j,T} + L_{j,B} \Rightarrow \\
&W_r = W_j \cdot \frac{\sin x_j}{\sin \xi_j} + \left(H - \frac{W_j}{2} \cdot \sin \beta_j\right) \cdot \frac{\sin \delta_0}{\sin \xi_j \cdot \sin\left(\xi_j + \delta_0\right)} \\
&\quad + \left(H + \frac{W_j}{2} \cdot \sin \beta_j\right) \cdot \frac{\sin \delta_0}{\sin \xi_j \cdot \sin\left(\xi_j - \delta_0\right)} \Rightarrow \\
&W_r = W_j \cdot \frac{\sin x_j}{\sin \xi_j} + H \cdot \frac{\sin \delta_0}{\sin \xi_j \cdot \sin\left(\xi_j + \delta_0\right)} - \frac{W_j}{2} \cdot \sin \beta_j \cdot \frac{\sin \delta_0}{\sin \xi_j \cdot \sin\left(\xi_j + \delta_0\right)} \\
&\quad + H \cdot \frac{\sin \delta_0}{\sin \xi_j \cdot \sin\left(\xi_j - \delta_0\right)} + \frac{W_j}{2} \cdot \sin \beta_j \cdot \frac{\sin \delta_0}{\sin \xi_j \cdot \sin\left(\xi_j - \delta_0\right)} \Rightarrow \\
&W_r = W_j \cdot \frac{1}{\sin \xi_j} \cdot \left[\sin x_j - \frac{1}{2} \cdot \sin \beta_j \cdot \frac{\sin \delta_0}{\sin\left(\xi_j + \delta_0\right)} + \frac{1}{2} \cdot \sin \beta_j \cdot \frac{\sin \delta_0}{\sin\left(\xi_j - \delta_0\right)}\right] \\
&\quad + H \cdot \frac{\sin \delta_0}{\sin \xi_j} \cdot \left[\frac{1}{\sin\left(\xi_j + \delta_0\right)} + \frac{1}{\sin\left(\xi_j - \delta_0\right)}\right] \Rightarrow \\
&W_r = W_j \cdot \frac{2 \cdot \sin x_j \cdot \sin\left(\xi_j + \delta_0\right) \cdot \sin\left(\xi_j - \delta_0\right) - \sin \delta_0 \cdot \sin \beta_j \cdot \left[\sin\left(\xi_j + \delta_0\right) - \sin\left(\xi_j - \delta_0\right)\right]}{2 \cdot \sin \xi_j \cdot \sin\left(\xi_j + \delta_0\right) \cdot \sin\left(\xi_j - \delta_0\right)} \\
&\quad + H \cdot \frac{\sin \delta_0}{\sin \xi_j} \cdot \frac{\sin\left(\xi_j + \delta_0\right) + \sin\left(\xi_j - \delta_0\right)}{\sin\left(\xi_j + \delta_0\right) \cdot \sin\left(\xi_j - \delta_0\right)} \Rightarrow \\
&\quad W_r - H \cdot \frac{\sin \delta_0}{\sin \xi_j} \cdot \frac{\sin\left(\xi_j + \delta_0\right) + \sin\left(\xi_j - \delta_0\right)}{\sin\left(\xi_j + \delta_0\right) \cdot \sin\left(\xi_j - \delta_0\right)} \\
&\quad = W_j \cdot \frac{2 \cdot \sin x_j \cdot \sin\left(\xi_j + \delta_0\right) \cdot \sin\left(\xi_j - \delta_0\right) - \sin \delta_0 \cdot \sin \beta_j \cdot \left[\sin\left(\xi_j + \delta_0\right) - \sin\left(\xi_j - \delta_0\right)\right]}{2 \cdot \sin \xi_j \cdot \sin\left(\xi_j + \delta_0\right) \cdot \sin\left(\xi_j - \delta_0\right)} \\
&\quad \frac{W_r \cdot \sin \xi_j \cdot \sin\left(\xi_j + \delta_0\right) \cdot \sin\left(\xi_j - \delta_0\right) - H \cdot \sin \delta_0 \cdot \left[\sin\left(\xi_j + \delta_0\right) + \sin\left(\xi_j - \delta_0\right)\right]}{\sin \xi_j \cdot \sin\left(\xi_j + \delta_0\right) \cdot \sin\left(\xi_j - \delta_0\right)} \\
&\quad = W_j \cdot \frac{2 \cdot \sin x_j \cdot \sin\left(\xi_j + \delta_0\right) \cdot \sin\left(\xi_j - \delta_0\right) - \sin \delta_0 \cdot \sin \beta_j \cdot \left[\sin\left(\xi_j + \delta_0\right) - \sin\left(\xi_j - \delta_0\right)\right]}{2 \cdot \sin \xi_j \cdot \sin\left(\xi_j + \delta_0\right) \cdot \sin\left(\xi_j - \delta_0\right)} \Rightarrow \\
&\quad W_r \cdot \sin \xi_j \cdot \sin\left(\xi_j + \delta_0\right) \cdot \sin\left(\xi_j - \delta_0\right) - H \cdot \sin \delta_0 \cdot \left[\sin\left(\xi_j + \delta_0\right) + \sin\left(\xi_j - \delta_0\right)\right] \\
&\quad = W_j \cdot \frac{2 \cdot \sin x_j \cdot \sin\left(\xi_j + \delta_0\right) \cdot \sin\left(\xi_j - \delta_0\right) - \sin \delta_0 \cdot \sin \beta_j \cdot \left[\sin\left(\xi_j + \delta_0\right) - \sin\left(\xi_j - \delta_0\right)\right]}{2} \Rightarrow \\
&W_j = \frac{2 \cdot W_r \cdot \sin \xi_j \cdot \sin\left(\xi_j + \delta_0\right) \cdot \sin\left(\xi_j - \delta_0\right) - 2 \cdot H \cdot \sin \delta_0 \cdot \left[\sin\left(\xi_j + \delta_0\right) + \sin\left(\xi_j - \delta_0\right)\right]}{2 \cdot \sin x_j \cdot in\left(\xi_j + \delta_0\right) \cdot \sin\left(\xi_j - \delta_0\right) - \sin \delta_0 \cdot \sin \beta_j \cdot \left[\sin\left(\xi_j + \delta_0\right) - \sin\left(\xi_j - \delta_0\right)\right]}
\end{aligned}
\tag{7.120}
$$

Again, as in the case of the vertical receiver, if we set $\delta_0 = 0$, Eq. 7.120 takes the form of Eq. 7.88, as it should be.

From the rest two receiver configurations, the tubular absorber and the receiver with triangular transversal cross section (Fig. 7.14c, d), the tubular absorber is simpler, while the triangular receiver is a little more complicated, or to be more correctly the calculations are more complicated. This receiver configuration may be deemed as the general form of both flat vertical and flat horizontal receivers. If the

angle, φ, formed by the two sides of the receiver is equal to π (or 180°), then the triangular receiver turns into flat horizontal receiver, while if it is equal to 0° then the triangular receiver turns into flat vertical receiver. For example, if we set $\varphi = 0^{o}$ in Eq. 7.93, it takes the form of Eq. 7.90, the equation providing the reflectors' width, W_j, of a Linear Fresnel Reflector Systems with flat vertical absorber.

In addition, apart from the centrally pivoted reflective elements, there is another option, the sided pivoted reflectors, with two possibilities. The rotation axis of the reflective element can coincide with their western or their eastern edge, for a South–North-oriented System. Furthermore, the possible combinations of the location of the pivoting axes and the receiver configuration are large enough to allow the description of all of them in a single chapter. For this reason, we will close their presentation with the tubular absorber and centrally pivoted reflectors (Fig. 7.14c). All other cases can be dealt with the same methodology, as it is applied above, and will be also applied in the case of the tubular absorber.

The illuminated length, L_j, consists of three parts according to Eq. 7.95. The length $L_{j,0}$ can be calculated from Eq. 7.76 after being properly modified:

$$L_{j,0} = W_j \cdot \sin x_j \tag{7.121}$$

However, using the geometry of the problem, as it is illustrated in Fig. 7.14c, and Thales Theorem, we can deduce that because the line segments AK, Q_jP and BM are parallel, and the line segments AQ_j and Q_jB are equal (the reflective elements are centrally pivoted and therefore Q_j is the midpoint of their edge AB), the line segment KM is bisected by the absorber centre P. Thus,

$$KP = PM = \frac{L_{j,0}}{2} = \frac{W_j}{2} \cdot \sin x_j \tag{7.122}$$

Next, the lengths $L_{j,T}$ and $L_{j,B}$ can be calculated from the geometry of Fig. 7.14c by the formulas:

$$\begin{aligned} \tan \widehat{RAK} &= \frac{RK}{AK} = \frac{L_{j,T}}{AK} \Rightarrow \\ L_{j,T} &= AK \cdot \tan \widehat{RAK} \Rightarrow \\ L_{j,T} &= AK \cdot \tan \delta_0 \end{aligned} \tag{7.123}$$

and

$$\begin{aligned} \tan \widehat{MBN} &= \frac{MN}{BM} = \frac{L_{j,B}}{BM} \Rightarrow \\ L_{j,B} &= BM \cdot \tan \widehat{MBN} \Rightarrow \\ L_{j,B} &= BM \cdot \tan \delta_0 \end{aligned} \tag{7.124}$$

The length of the line segments AK and BM can be calculated from triangle AKK' and BMM', respectively:

$$\begin{aligned}
\sin \widehat{AKK'} &= \frac{AK'}{AK} \Rightarrow \\
AK &= \frac{AK'}{\sin \widehat{AKK'}} \Rightarrow \\
AK &= \frac{Q_j + \frac{W_j}{2} \cdot \cos \beta_j - \frac{W_j}{2} \cdot \sin x_j \cdot \sin \xi_j}{\sin\left(\frac{\pi}{2} - \xi_j\right)} \Rightarrow \\
AK &= \frac{Q_j + \frac{W_j}{2} \cdot \cos \beta_j - \frac{W_j}{2} \cdot \sin x_j \cdot \sin \xi_j}{\cos \xi_j}
\end{aligned} \tag{7.125}$$

and

$$\begin{aligned}
\sin \widehat{BMM'} &= \frac{BM'}{BM} \Rightarrow \\
BM &= \frac{BM'}{\sin \widehat{BMM'}} \Rightarrow \\
BM &= \frac{Q_j - \frac{W_j}{2} \cdot \cos \beta_j + \frac{W_j}{2} \cdot \sin x_j \cdot \sin \xi_j}{\sin\left(\frac{\pi}{2} - \xi_j\right)} \Rightarrow \\
BM &= \frac{Q_j - \frac{W_j}{2} \cdot \cos \beta_j + \frac{W_j}{2} \cdot \sin x_j \cdot \sin \xi_j}{\cos \xi_j}
\end{aligned} \tag{7.126}$$

Replacing Eqs. 7.125 and 7.126 into Eqs. 7.123 and 7.124, respectively, the lengths $L_{j,T}$ and $L_{j,B}$ are given by the formulas

$$L_{j,T} = \frac{Q_j + \frac{W_j}{2} \cdot \cos \beta_j - \frac{W_j}{2} \cdot \sin x_j \cdot \sin \xi_j}{\cos \xi_j} \cdot \tan \delta_0 \tag{7.127}$$

$$L_{j,B} = \frac{Q_j - \frac{W_j}{2} \cdot \cos \beta_j + \frac{W_j}{2} \cdot \sin x_j \cdot \sin \xi_j}{\cos \xi_j} \cdot \tan \delta_0 \tag{7.128}$$

Now, combining Eqs. 7.95, 7.121, 7.127 and 7.128 and equating the illuminating length, L_j, of the receiver aperture with its diameter, $2 \cdot R_r$, we have

$$
\begin{aligned}
W_r = L_j &= L_{j,0} + L_{j,T} + L_{j,B} \Rightarrow \\
2 \cdot R_r &= W_j \cdot \sin x_j + \frac{Q_j + \frac{W_j}{2} \cdot \cos\beta_j - \frac{W_j}{2} \cdot \sin x_j \cdot \sin\xi_j}{\cos\xi_j} \cdot \tan\delta_0 \\
&\quad + \frac{Q_j - \frac{W_j}{2} \cdot \cos\beta_j + \frac{W_j}{2} \cdot \sin x_j \cdot \sin\xi_j}{\cos\xi_j} \cdot \tan\delta_0 \Rightarrow \\
2 \cdot R_r &= W_j \cdot \sin x_j \\
&\quad + Q_j \cdot \frac{\tan\delta_0}{\cos\xi_j} + \frac{W_j}{2} \cdot \frac{\cos\beta_j \cdot \tan\delta_0}{\cos\xi_j} - \frac{W_j}{2} \cdot \frac{\sin x_j \cdot \sin\xi_j \cdot \tan\delta_0}{\cos\xi_j} \\
&\quad + Q_j \cdot \frac{\tan\delta_0}{\cos\xi_j} - \frac{W_j}{2} \cdot \frac{\cos\beta_j \cdot \tan\delta_0}{\cos\xi_j} + \frac{W_j}{2} \cdot \frac{\sin x_j \cdot \sin\xi_j \cdot \tan\delta_0}{\cos\xi_j} \Rightarrow \\
2 \cdot R_r &= W_j \cdot \sin x_j + 2 \cdot Q_j \cdot \frac{\tan\delta_0}{\cos\xi_j} \Rightarrow \\
&\quad 2 \cdot R_r - 2 \cdot Q_j \cdot \frac{\tan\delta_0}{\cos\xi_j} = W_j \cdot \sin x_j \Rightarrow \\
&\quad \frac{2 \cdot R_r \cdot \cos\xi_j - 2 \cdot Q_j \cdot \tan\delta_0}{\cos\xi_j} = W_j \cdot \sin x_j \Rightarrow \\
W_j &= \frac{2 \cdot R_r \cdot \cos\xi_j - 2 \cdot Q_j \cdot \tan\delta_0}{\cos\xi_j \cdot \sin x_j}
\end{aligned}
\tag{7.129}
$$

Again, as in the two previous cases, if we set $\delta_0 = 0$, Eq. 7.129 take the form of Eq. 7.86, as it should be.

7.4 South–North-Oriented Linear Fresnel Reflector Systems

The previously presented analysis concerns East–West-oriented Systems, and not South–North oriented. However, as it has been already mentioned, the main difference between these two types of System is the fact that in East–West-oriented Systems, the maximum value of Sun's transversal angle, $\theta_{T,\max}$, is usually lower than 90°, whereas in contrast in South–North-oriented Systems, it is equal to 90°. This happens every day at the local noon, when the incoming solar radiation is also the maximum. For this reason, the equations providing the reflectors' width, W_j, position, Q_j, and tilt angle, β_j, of a South–North-oriented System can be derived from the corresponding equations of an East–West-oriented System, simply by replacing the maximum transversal component of Sun's angle, $\theta_{T,\max}$, with its value, namely 90°.

7.5 Design Parameters' Computation

In order to install the reflective elements of a Fresnel Reflector System on the right place and with the right inclination, the set of the corresponding equations have to be resolved and the basic design parameters—the width, W_j, the position or location, Q_j, and the tilt angle, β_j—of the N reflective elements have to be calculated. However, taking into account the form of all the previously presented equations, it is more than evident that it is not possible to derive an explicit expression for the calculation of these parameters. For this reason, the system of these nonlinear equations must be solved approximately using a numerical method.

Let us consider as an example the Linear Fresnel Reflector System illustrated in Fig. 7.15. It is a South–North-oriented Linear Fresnel Reflector System with tubular absorber and side pivoted reflective elements. Due to the Systems symmetry, the maximum Sun's transversal angle, $\theta_{T,\max}$, is equal to 90° and the eastern reflectors are pivoted on their western longer edge, while the western reflectors are pivoted on their eastern longer edge.

The location, Q_1, and the tilt angle, β_1, of the first reflector ($j = 1$) can be calculated using the following process. The absorber will cast a shadow on the plane of the reflective elements and, hence, no reflector should be placed underneath it. Therefore, the first reflecting element must be placed at an appropriate location, Q_1, so that it can contribute to the solar radiation concentration on the absorber surface. In other words, it must be outside the shadow the absorber casts on the horizontal plane and simultaneously it must have an appropriate tilt angle, β_1, in order to reflect the incoming direct solar radiation onto the receiver. So, the first reflector of this specific Linear Fresnel Reflector System must be placed at the distance (Fig. 7.16a)

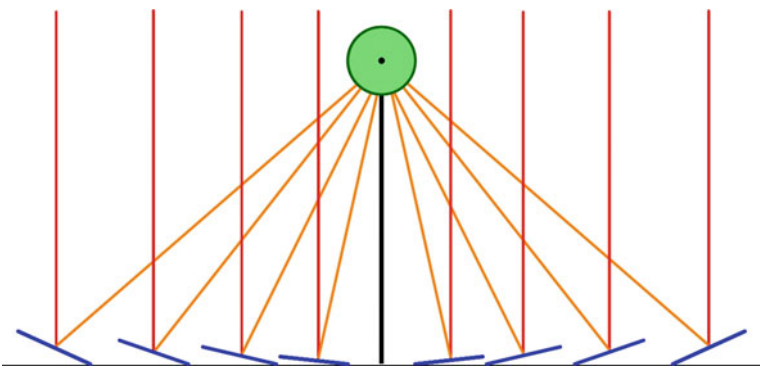

Fig. 7.15 In South–North-oriented Linear Fresnel Reflector System with tubular absorber and side pivoted reflective elements, the maximum Sun's transversal angle, $\theta_{T,\max}$, is equal to 90° and the eastern reflectors are pivoted on their western longer edge, while the western reflectors are pivoted on their eastern longer edge

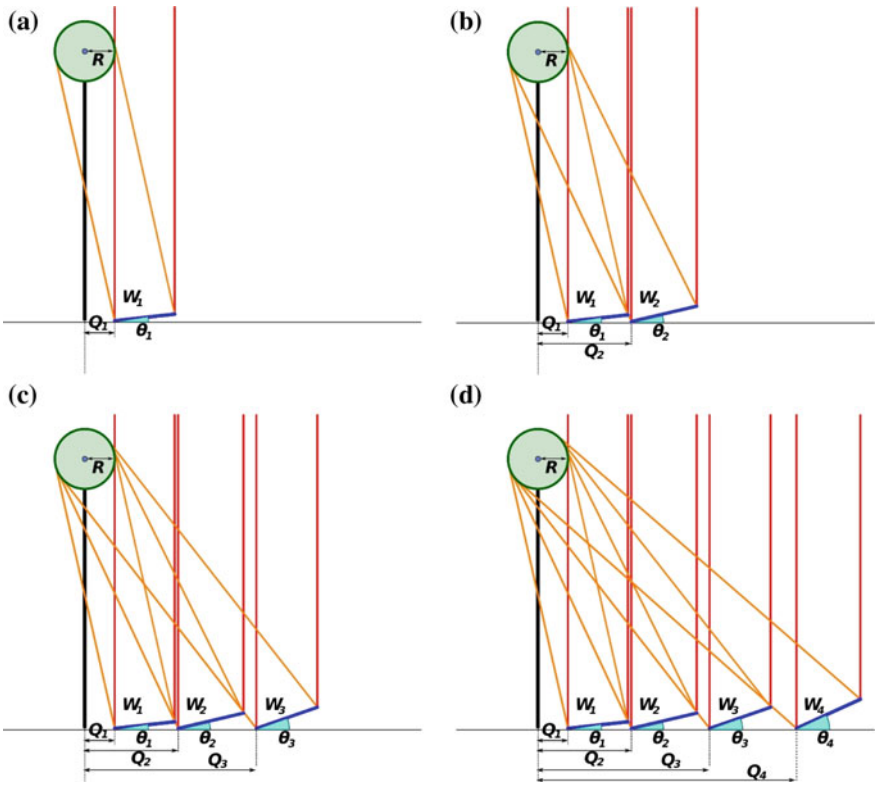

Fig. 7.16 Placement of the reflective elements in a Linear Fresnel Reflector System can be accomplished only stepwise. **a** First, we calculate the position, Q_1, and the tilt angle, β_1, of the first reflective element. **b** Next, we proceed to the calculation of the place, Q_2, and the inclination angle, β_2, of the second reflective element, taking into account the results of the previous step. **c**, **d** We keep on until the last reflective element is placed. However, due to the inherent symmetry of the System, the arrangement of the eastern reflective elements is a reflective image of the western elements with regard to the longitudinal plane of the System

$$Q_1 = R + H \cdot \tan \delta_0 \tag{7.130}$$

from the origin of the local Cartesian coordinate system, where R is the absorber's radius, H is the height of its centre from the reflectors' plane and $2 \cdot \delta_0$ is the angular size of Sun, if we would like to take into account its effect, otherwise, $\delta_0 = 0$ and $Q_1 = R$.

Moreover, the tilt angle, β_1, of the first reflective element in relation to the horizontal plane can be calculated from Eq. 7.72,

$$\beta_j^N = 90^\circ - \frac{1}{2}\tan^{-1}\left(\frac{H + \frac{W}{2}\cdot\sin\beta_j}{Q_j + \frac{W_j}{2}\cdot\cos\beta_j}\right) + \frac{\theta_{T,\max}}{2} \tag{7.72}$$

after the necessary modification:

$$\begin{aligned}
\beta_1 &= 90^\circ - \frac{1}{2}\tan^{-1}\left(\frac{H + \frac{W}{2}\cdot\sin\beta_1}{Q_1 + \frac{W}{2}\cdot\cos\beta_1}\right) + \frac{\theta_{T,\max}}{2} \\
\beta_1 &= 90^\circ - \frac{1}{2}\tan^{-1}\left(\frac{H + \frac{W}{2}\cdot\sin\beta_1}{Q_1 + \frac{W}{2}\cdot\cos\beta_1}\right) + \frac{90^\circ}{2} \\
\beta_1 &= 135^\circ - \frac{1}{2}\tan^{-1}\left(\frac{H + \frac{W}{2}\cdot\sin\beta_1}{Q_1 + \frac{W}{2}\cdot\cos\beta_1}\right)
\end{aligned} \tag{7.131}$$

where Q_1 is the location of the first reflective element as it is calculated from Eq. 7.130, and W is the common value of the reflectors' width (equal width). However, the above implicit equation cannot be solved analytically for β_1, but only approximately by using an iterative approach.

In any iterative method, we start from an arbitrary, but reasonable, initial value for the desired parameter and then we proceed stepwise until the new results to not differ substantially from the previously computed. The reasonable initial values for the location, Q_1, the tilt angle, β_1, and the shift distance, S_1, for the first reflector are $Q_1^0 = R + H\cdot\tan\delta_0$ (Eq. 7.130), $\beta_1^0 = 0$ and $S_1^0 = 0$, respectively. Essentially, only the tilt angle, β_1, has to be calculated approximately, since the location, Q_1, and the shift, S_1, are explicitly defined. In each step, i, of the approximate method the value of the tilt angle β_1^{i-1} calculated in the previous step $(i-1)$ is increased (or reduced) by a small amount, $\Delta\beta$, (a small angular increment) in the order of 1°:

$$\beta_1'^{\,i} = \beta_1^{i-1} + \Delta\beta \tag{7.132}$$

and the value of β_1 is recalculated using the expression

$$\beta_1^i = 135^\circ - \frac{1}{2}\tan^{-1}\left(\frac{H + \frac{W}{2}\cdot\sin\beta_1'^{\,i}}{Q_1 + \frac{W}{2}\cdot\cos\beta_1'^{\,i}}\right) \tag{7.133}$$

This iterative procedure is terminated when the new value differs from the previously calculated by a very small amount, a, the required precision, or else when the following condition is satisfied

$$\left|\beta_1^i - \beta_1^{i-1}\right| \le a \tag{7.134}$$

or

$$\frac{\left|\beta_1^i - \beta_1^{i-1}\right|}{\beta_1^i} \cdot 100 \le p\% \tag{7.135}$$

where i = 0, 1, 2, 3,…, is the step number of the iterative procedure, and p is the required level of accuracy.

The location, Q_2, and the tilt angle, β_2, of the second reflective element must be chosen so that the light ray emanating from the centre of the solar disc and striking the midpoint of the reflector to be reflected and directed towards the centre of the absorber, and the reflected solar radiation not to be blocked by the first reflective element (Fig. 7.16b). Hence, we have to introduce a space between the first and second reflectors, the shift distance S_2. It can be calculated using Eq. 7.41, after applying the required modifications (e.g. $\theta_{T,\max} = 90°$, $W_j = W$):

$$S_2 = W \cdot \cos\beta_1 + W \cdot \sin\beta_1 \cdot \tan(2 \cdot \beta_2) \tag{7.136}$$

So, the location Q_2 of the second reflective element and its tilt angle, β_2, with the horizontal plane are

$$\begin{aligned} &Q_2 = Q_1 + S_2 \Rightarrow \\ &Q_2 = Q_1 + W \cdot \cos\beta_1 + W \cdot \sin\beta_1 \cdot \tan(2 \cdot \beta_2) \end{aligned} \tag{7.137}$$

and

$$\beta_2 = 135° - \frac{1}{2}\tan^{-1}\left(\frac{H + \frac{W}{2} \cdot \sin\beta_2}{Q_2 + \frac{W}{2} \cdot \cos\beta_2}\right) \tag{7.138}$$

To compute the location, Q_2, and the tilt angle, β_2, of the second reflective element, we must solve approximately (numerically) the system of the two non-linear equations Eqs. 7.137 and 7.138 using the above-presented iterative procedure. The initial values for the second reflector are $Q_2^0 = Q_1 + W$ and $\beta_2^0 = 0$. Their approximate values, Q_2^i and β_2^i, at the i step of the iterative procedure are recalculated from the corresponding values in the previous step ($i - 1$), Q_2^{i-1} and β_2^{i-1}, by increasing (or reducing) the tilt angle β_2^{i-1} by a small amount, $\Delta\beta$ (a small angular increment), in the order of 1°

$$\beta_2'^i = \beta_2^{i-1} + \Delta\beta \tag{7.139}$$

using the expressions

$$Q_2^i = Q_1 + W \cdot \cos\beta_1 + W \cdot \sin\beta_1 \cdot \tan\left(2 \cdot \beta_2'^i\right) \tag{7.140}$$

$$\beta_2^i = 135^\circ - \frac{1}{2}\tan^{-1}\left(\frac{H + \frac{W}{2} \cdot \sin\beta_2'^i}{Q_2^i + \frac{W}{2} \cdot \cos\beta_2'^i}\right) \tag{7.141}$$

The iterations stop when the new values differ from the previously calculated by a very small amount, a and c, the required precisions, or else when the following conditions are satisfied

$$\left|\beta_2^i - \beta_2^{i-1}\right| \leq a \tag{7.142}$$

or

$$\frac{\left|\beta_2^i - \beta_2^{i-1}\right|}{\beta_2^i} \cdot 100 \leq p_a\% \tag{7.143}$$

and

$$\left|Q_2^i - Q_2^{i-1}\right| \leq c \tag{7.144}$$

or

$$\frac{\left|Q_2^i - Q_2^{i-1}\right|}{Q_2^i} \cdot 100 \leq p_c\% \tag{7.145}$$

where i = 0, 1, 2, 3,…, is the step number of the iterative procedure and p_a and p_c are the required levels of accuracy.

Similarly, the position, Q_j, and the tilt angle, β_j, of the jth reflective element, and consequently of all reflective elements, of the Linear Fresnel Reflector System illustrated in Fig. 7.15, can be calculated by applying this iterative method on the following equations

$$Q_j^i = Q_{j-1} + W \cdot \cos\beta_{j-1} + W \cdot \sin\beta_{j-1} \cdot \tan\left(2 \cdot \beta_j'^i\right) \tag{7.146}$$

$$\beta_j^i = 135^\circ - \frac{1}{2}\tan^{-1}\left(\frac{H + \frac{W}{2} \cdot \sin\beta_j'^i}{Q_j^i + \frac{W}{2} \cdot \cos\beta_j'^i}\right) \tag{7.147}$$

The initial values are $Q_j^0 = Q_{j-1} + W$ and $\beta_j^0 = 0$, and the termination conditions are described by the expressions

$$\left|\beta_j^i - \beta_j^{i-1}\right| \leq a \tag{7.148}$$

or

$$\frac{\left|\beta_j^i - \beta_j^{i-1}\right|}{\beta_j^i} \cdot 100 \leq p_a\% \tag{7.149}$$

and

$$\left|Q_j^i - Q_j^{i-1}\right| \leq c \tag{7.150}$$

or

$$\frac{\left|Q_j^i - Q_j^{i-1}\right|}{Q_j^i} \cdot 100 \leq p_c\% \tag{7.151}$$

where $i = 0, 1, 2, 3,\ldots$, is the step number of the iterative procedure and p_a and p_c are the required levels of accuracy, which usually are the same ($p_a = p_c$) for all reflective element and for both the position, Q_j, and tilt angle, β_j, or rarely, they are defined separately ($p_a \neq p_c$).

References

Abbas, R., and J.M. Martínez-Val. 2015. Analytic optical design of linear Fresnel collectors with variable widths and shifts of mirrors. *Renewable Energy* 75: 81–92.

Babu, M., and A. Valan Arasu. 2015. Theoretical performance analysis of linear fresnel reflector concentrating solar system with vertical absorber. *Australian Journal of Basic and Applied Sciences* 9 (20): 473–484.

Barbona, A., N. Barbon, L. Bayon, and J.A. Otero. 2016. Theoretical elements for the design of a small scale Linear Fresnel Reflector: Frontal and lateral views. *Solar Energy* 132: 188–202.

Mathur, S.S., T.C. Kandpal, and B.S. Negi. 1991a. Optical design and concentration characteristics of linear Fresnel reflector solar concentrators—I. Mirror elements of varying width. *Energy Conversion and Management* 31 (3): 205–219.

Mathur, S.S., T.C. Kandpal, and B.S. Negi. 1991b. Optical design and concentration characteristics of linear Fresnel reflector solar concentrators—II. Mirror elements of equal width. *Energy Conversion and Management* 31 (3): 221–232.

Negi, B., T. Kandpal, and S.S. Mathur. 1990. Designs and performance characteristics of a linear Fresnel reflector solar concentrator with a flat vertical absorber. *Solar and Wind Technology* 7: 379–392.

Nixon J.D., and P.A. Davies. 2012. Cost-exergy optimisation of linear Fresnel reflectors. *Solar Energy* 86: 147–156.

Singh, P.L., R.M. Sarviya, and J.L. Bhagoria. 2010. Thermal performance of linear Fresnel reflecting solar concentrator with trapezoidal cavity absorbers. *Applied Energy*, Elsevier 87 (2): 541–550.

Chapter 8
Case Study—Fresnel Reflector Solar Cookers

In areas where sunshine is plentiful, Solar Cookers can be used as a successful alternative way of preparing food. They are cheap, easy to use and require no fuel. However, for cooking food that requires temperature above 100 °C, Solar Cooker must be equipped with solar energy concentrating devices. They concentrate solar power onto a small area where a pot, or another cooking vessel, is placed. In general, Solar Cookers consist of a receiver, where the sunlight is absorbed and converted into the heat—the pot or the cooking vessel—and a concentrator—an optical device that reflects and concentrates the direct solar radiation onto the receiver. The receiver must have appropriate shape and surface (absorbing surface) so that to be able to (a) absorb the collected solar energy by transforming it into heat, (b) transfer the absorbed heat from the vessel's walls to the cooking load and finally (c) increase and retain the temperature of its content.

Because of their ease of fabrication and handling, Fresnel-type Reflective Systems can be used as concentrating devices in Solar Cookers. For this reason, the design, the parameter calculation, the development and the construction of two Fresnel Reflector Solar Radiation Concentrating Systems, that can be used for small-scale applications, like cooking, are presented in this chapter. They are a simple, but interesting, case studies of the theory presented in the previous chapters.

8.1 Introduction

Solar Cookers, or solar ovens, are an alternative environmentally friendly, convenient and affordable method for harnessing solar energy for cooking. These devices use solar energy (a renewable energy source) and convert it into heat to cook food, or alternatively for pasteurization and sterilization processes. Solar Cookers have been studied by scientists and researchers all over the world, as well as by manufacturers. For this reason, various types of Solar Cooker have been designed and developed. They have been used in many different places around the globe and for a

S. Karathanasis, *Linear Fresnel Reflector Systems for Solar Radiation Concentration*, https://doi.org/10.1007/978-3-030-05279-9_8

variety of purposes and circumstances, especially in developing countries. There, they are very popular, as cooking is one of the basic energy consumption reasons (Farooqui 2013).

The large variety of solar cooking designs makes their classification really difficult. Nevertheless, they can be broadly grouped into three main categories, based on the type of the collector used and the temperature range achieved: (a) Panel Solar Cookers, (b) Box Solar Cookers and (c) Parabolic Solar Cookers (Fig. 8.1) (Cuce and Cuce 2013; Farooqui 2013). Apart from these general types, there are many other types with substantial differences. For example, there have been developed Solar Cookers with a single vacuum tube, or with multiple vacuum tubes, Solar Cookers that allow the cooking to take place underneath a shade or inside a building, Solar Cookers with and without thermal storage, Solar Cookers with tracking or non-tracking Systems, direct-type Solar Cookers, which use solar radiation directly in the cooking process, and indirect Solar Cookers, which use a heat transfer fluid to transfer the heat from the receiver to the cooking unit and many more (Farooqui 2013; Yettou et al. 2014; Prasanna and Umanand 2011). A comprehensive presentation of the recent advances in research and development of solar cooking technology can be found in Yettou et al. (2014), Cuce and Cuce (2013), Stine and Geyer (2001), Yettou et al. (2014), Indora and Kandpal (2018), Herez et al. (2018), Muthusivagami et al. (2010), Panwara et al. (2012).

Panel-type Solar Cookers are the most easily constructed, more convenient and more affordable (low-cost) Solar Cooker, but they are not very efficient. Nevertheless, they are highly appreciated by many users because of their portability and ease of use. These Solar Cookers are usually made from flexible reflective materials (e.g. cardboard coated with aluminium foil) that direct sunlight onto a cooking vessel which is usually enclosed in a transparent plastic bag (Cuce and

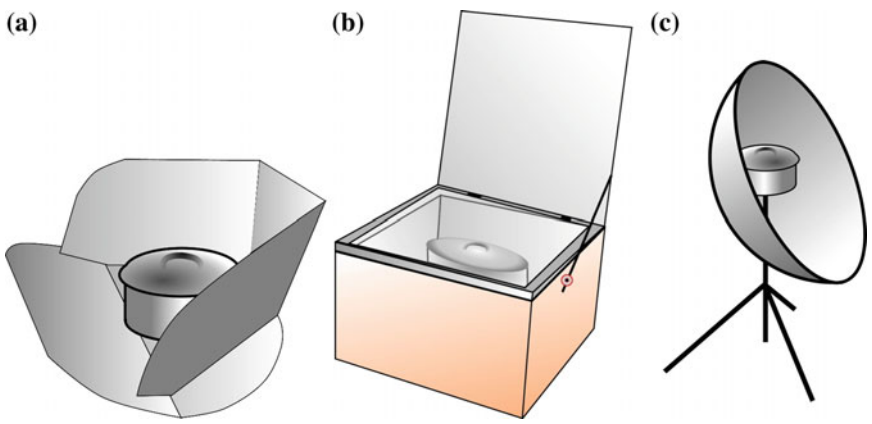

Fig. 8.1 Solar Cookers can be broadly classified in three main categories **a** Panel Solar Cookers, **b** Box Solar Cookers and **c** Parabolic Solar Cookers. The criterion used is the type of the collector and the temperature range achieved

Cuce 2013). In this type of Cookers, a temperature of around 100 °C can be achieved, which makes possible to cook food (Yettou et al. 2014).

On the other hand, Box-type Solar Cookers consist of an insulated wooden or plastic box with transparent glass cover and reflective surfaces that direct sunlight onto a specific area in the box. The area where the pot with the food is placed, or sometimes the whole inner part of the box, is painted black to maximize the sunlight absorption. For this reason, this part of the Solar Cooker is usually made from metal or other materials that absorb heat, but are heatproof. Furthermore, the cooking vessel may be placed either on the bottom surface inside the box, or at a specific height above it. The last case is applied when the inner side of the box is reflective and not absorbing. Sometimes, the cooking vessel is put under airtight conditions to increase the achieved temperature by preventing heat losses and enhancing the resulting greenhouse effect. Apart from the inner reflective surface, extra reflectors (commonly up to four) on the upper sides of the box are usually used to reflect more sunrays into the box (Farooqui 2013; Cuce and Cuce 2013) (Fig. 8.2).

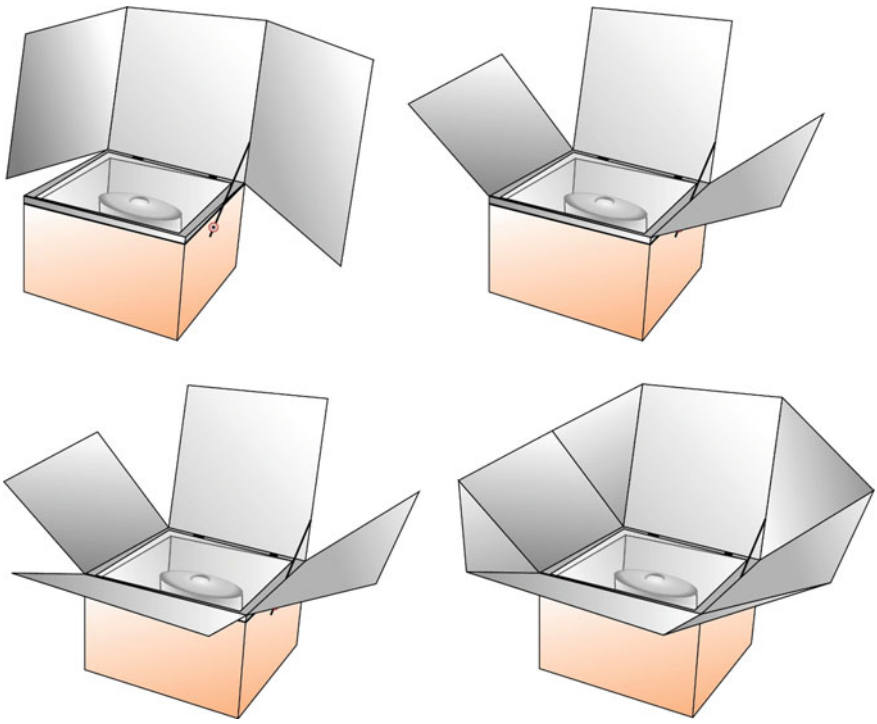

Fig. 8.2 Box-type Solar Cooker are relatively easy to be constructed because of their simple operation principle. Usually, they use up to four additional reflectors in different configurations to collect more solar energy

However, the most efficient design of concentrating-type Solar Cookers, that utilizes high-performance reflectors attains higher temperatures and is suitable for most types of food cooking, is the point focusing Paraboloid Solar Cooker (Fig. 8.3a) (Yettou et al. 2014). Another variation is the line-focusing Parabolic Solar Cooker (Fig. 8.3b). A Parabolic (or a Paraboloid) Solar Cooker consists of a parabolic (or paraboloid) reflector, a stand to support the System, and a Sun tracking mechanism (automatic or manual), while the cooking pot is located on the focus line (or point) of the parabola. This type of Solar Cookers attracts most people immediately due to their outstanding performance. They can reach extremely high temperatures in a very short time, and unlike the Panel or Box Solar Cookers, they do not need a special cooking vessel, except for the fact that it must be able to absorb the reflected solar radiation (be coated, or painted, black). However, there is always present the risk of burning the food if left unattended for a relatively length time span, because of the highly concentrated power, exactly as in the case of the conventional way of cooking (Cuce and Cuce 2013).

All above-presented types of Solar Cookers are concentrating types. They cannot work if there is not sufficient direct solar radiation, for example in no-sunshine conditions, or in the evening. In addition, most of them must be oriented frequently towards Sun in order to be able to work properly. Therefore, they are typically designed with a one- or two-axis tracking System allowing them to follow the course of Sun in the sky (Yettou et al. 2014).

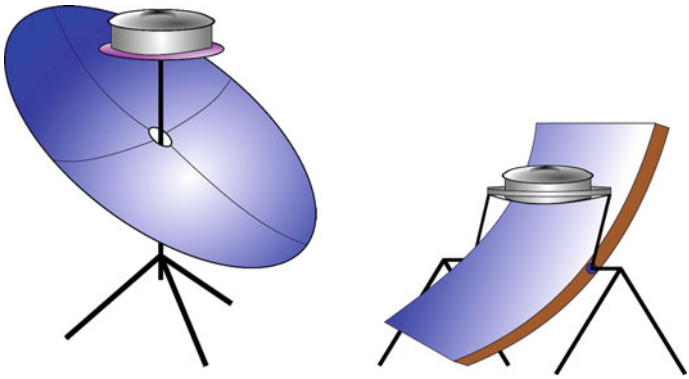

Fig. 8.3 Paraboloid and Parabolic Solar Cookers are the most efficient devices for preparing food using solar radiation. They are based on the same operation principle and take advantage of the parabola property to redirect the sunlight coming parallel to its principal axis onto a single point, its focal point

8.2 The Fresnel Reflector Solar Cookers

As Parabolic Solar Cooker are more efficient than other types, they can be used in more circumstances, and for preparing more food types. However, Fresnel Reflectors can reduce the construction costs of parabolic reflectors, as they are easier to be constructed and, therefore, cheaper. For this reason, the Solar Cookers developed in this chapter are based on the Fresnel concept. The choice of developing and presenting Solar Cookers in this book has been made because these Systems can be deemed as a simple, but interesting, application of the theory presented in the previous chapters.

Two different Fresnel Reflectors will be studied in this chapter, one linear and one circular, or more correctly Conical. The Linear Fresnel Reflector System will consist of long plane rectangular reflective strips, its reflective elements, fixed on an appropriate supporting surface, so that the whole construction to be able to rotate along a two-axis tracking System following Sun's movement in the sky. On the other hand, the Conical Fresnel Reflector System will consist of concentric frustum cones.

The receivers used in these Solar Cookers are simple and low cost, available in the market, and efficient enough, as they can be sealed airtight and watertight assisting the cooking process. The receiver of the Conical Fresnel Solar Cooker is a thin cylindrical tin pot of black colour (Fig. 8.4a). The receiver of the Linear Fresnel Solar Cooker is a cylindrical glass jar suitable for bakery painted black, also watertight. In contrast to the Conical Fresnel Solar Cooker, the receiver in the Linear Fresnel Solar Cooker is placed horizontally (Fig. 8.4b). Although the receiver in the Conical Fresnel Cooker is cylindrical, its cross vertical sections is a rectangle (Fig. 8.5). According to the cases studied in the previous chapter, its cross section could be deemed as the combination of flat horizontal and flat vertical receiver surfaces. However, it is more convenient to be considered as equivalent to the triangular receiver, taken, for example, as virtual target surfaces the two line segments *MB* and *MC* depicted in Fig. 8.5.

As these Fresnel Reflector Systems will be constantly oriented towards Sun, the incoming solar radiation will be always perpendicular to their apertures (Fig. 8.6).

Fig. 8.4 Receivers (cooking vessels) used in the Solar Cooker developed in this chapter. Both of them are cylinder, but the first **a** is placed horizontally, while the second **b** is placed vertically, and they are used in the Linear and the Conical Fresnel Reflector Solar Cooker, respectively

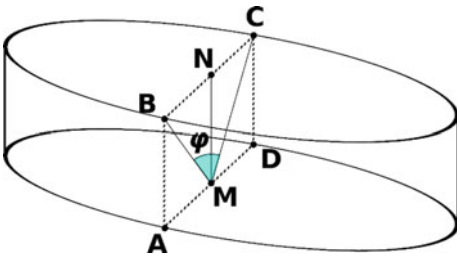

Fig. 8.5 Cross section of the cylindrical absorber on the transversal plane of the Systems is rectangle. According to the general cases studied in the previous chapter, it could be deemed as the combination of flat horizontal and flat vertical receiver surfaces. However, it is more convenient to be considered as equivalent to the triangular receiver, taken as virtual target surfaces the two line segments *BM* and *CM*

In order to take advantage of the Systems' symmetry the southern reflective elements of the Linear Fresnel Reflector Solar Cooker are inclined on their northern longer edge, and the northern reflective elements on their southern longer edge, since the System will be East–West oriented at the local noon. Thus, the System is composed of two seemingly different Subsystems. However, each of them is a reflective image of the other in relation to the longitudinal plane of the System. This way we reduce the mathematical calculations needed. At the same time, the cross section of the Linear Fresnel Reflector System, in respect to its transversal plane, is identical with the corresponding cross section of the Conical Fresnel Reflector Solar Cooker. Lastly, the design parameters of the Conical Fresnel Reflector Solar Cooker are calculated from the equations corresponding to the triangular absorber, while the design parameters of the Linear Fresnel Reflector Solar Cooker from the equations corresponding to the absorber with circular cross section.

According to the analysis presented in Chap. 7, the calculation of the appropriate distance, S_j, of two consequent reflective elements, so that shading and blocking effects to be avoided, depends on Sun's angle, and in particular on its transversal component, θ_T. However, for this particular types of Fresnel Reflector Systems, that are constantly adjusted so that they always face Sun, Sun's transversal angle is always equal to 90° ($\theta_T = \pi/2$) (Fig. 8.6). Therefore, it is obvious that we should calculate the reflectors shift distance, S_j, for normal incidence angle of the incoming solar radiation. The mathematical formulas for Sun-oriented Systems can straightforwardly be derived from the corresponding formulas for stationary East–West-oriented System, by setting the maximum value of Sun's transversal angle, $\theta_{T,max}$, equal to $\pi/2$ ($\theta_{T,max} = \pi/2$). Thus, the proper shift distance, S_j, between two consecutive reflective elements, so that no shading and blocking effects occur, for both Systems, can be calculated from the following equation (Eq. 7.41):

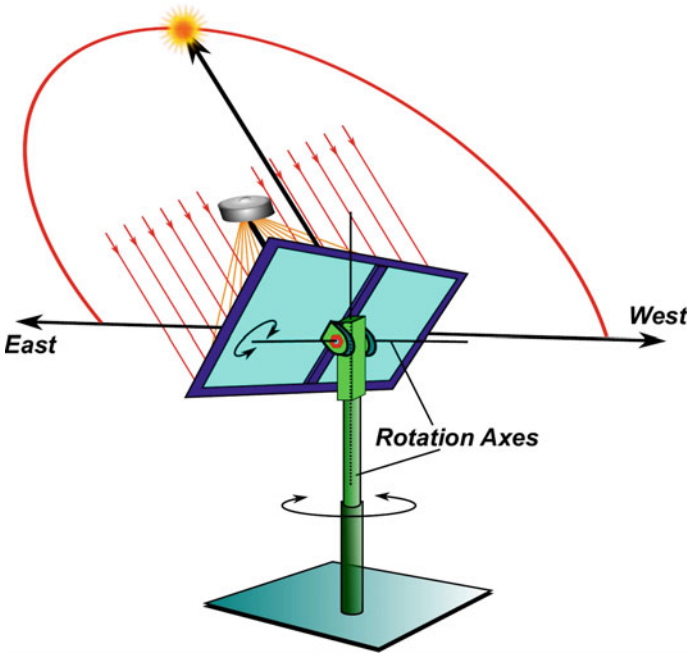

Fig. 8.6 If a Fresnel Reflector System can be constantly adjusted so that it always faces Sun, then the light rays fall always perpendicular to its aperture

$$\begin{aligned} S_j &= W_{j-1} \cdot \cos\beta_{j-1} + W_{j-1} \cdot \sin\beta_{j-1} \cdot \tan\left(90^\circ - \theta_{\mathrm{T,max}} - 2 \cdot \beta_j\right) \\ S_j &= W_{j-1} \cdot \cos\beta_{j-1} + W_{j-1} \cdot \sin\beta_{j-1} \cdot \tan\left(90^\circ - 90^\circ - 2 \cdot \beta_j\right) \\ S_j &= W_{j-1} \cdot \cos\beta_{j-1} + W_{j-1} \cdot \sin\beta_{j-1} \cdot \tan\left(2 \cdot \beta_j\right) \end{aligned} \tag{8.1}$$

Hence, the position, Q_j, of the jth reflective element of both the Linear and the Conical Fresnel Reflector Solar Cookers can be calculated from the position Q_{j-1} of its previous (the $(j-1)$th) reflective element by adding the proper shift distance, S_j, from Eq. 8.1:

$$\begin{aligned} Q_j &= Q_{j-1} + S_j \\ Q_j &= Q_{j-1} + W_{j-1} \cdot \cos\beta_{j-1} + W_{j-1} \cdot \sin\beta_{j-1} \cdot \tan\left(2 \cdot \beta_j\right) \end{aligned} \tag{8.2}$$

However, in the case of Conical Fresnel Reflector Solar Cooker, the distance Q_j denotes the inner radius of the jth Fresnel ring, as we will analyse it later in this chapter.

All Fresnel Reflector Systems are designed so that the light ray coming from the centre of Sun's disc and hitting the centre of the jth reflective element to be reflected to the centre of the receiver. In order for this condition to be accomplished, each

reflective element has to be inclined, in relation to the reflectors' plane, by an angle equal to β_j, its tilt angle, given by the formula (Fig. 8.7) (Eq. 7.51)

$$\beta_j = \frac{\xi_j - \theta_{T,\max}}{2} \tag{8.3}$$

In this equation, the angle ξ_j is the angle formed by the horizontal plane with the line connecting the jth reflector's midpoint with the receiver's midpoint on the transversal plane of the System.

The tilt angle, β_j, of the reflective elements changes its sign exactly below the absorber. However, since this reflector would be always shaded by the absorber, we do not place any reflective element at this position. This reflector would have subscript, j, equal to zero ($j = 0$). The subscripts of the rest reflectors take values in the closed interval $[-n, 1]$ (or $-n \leq j \leq 1$), if they are southern from the 0th reflector and, in the closed interval $[1, n]$ (or $1 \leq j \leq n$), if they are northern from it. In addition, the number, n, of the reflective elements satisfies the condition, $N = 2 \cdot n$, where N is the total number of the reflectors, since there is not any reflector with subscript, j, equal to zero ($j \neq 0$). Moreover, as it has been mentioned in the previous chapter, the introduction of the shift distance, S_j, between consecutive reflective elements leads the System to design constraints. The density of the reflective elements is limited; or else, the number, N, of the reflective elements for the given System area has an upper threshold.

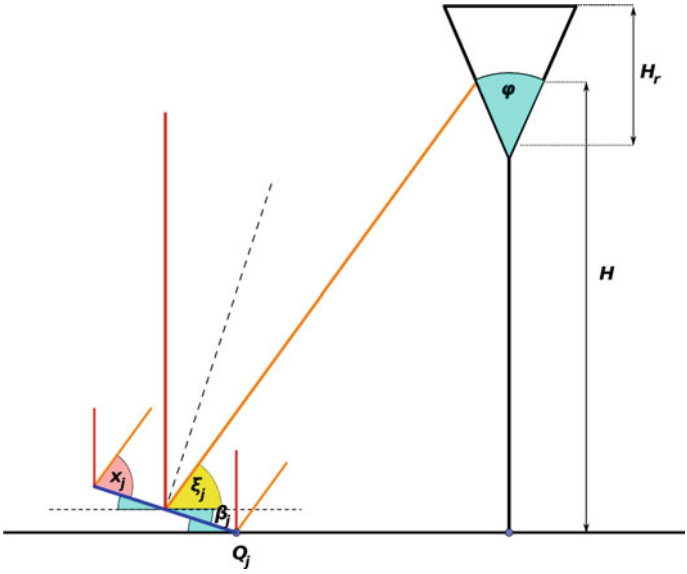

Fig. 8.7 Geometry of the Conical Fresnel Reflector Solar Cooker cross section

In the case the reflective elements are pivoted around their northern edge, their tilt angle, β_j, is given by the following formula, if we set $\theta_{\mathrm{T,max}} = \pi/2$ (valid for reflectors being placed southern from the receiver) (Eq. 7.73)

$$\beta_j = \frac{1}{2}\tan^{-1}\left(\frac{H + \frac{W_j}{2}\cdot\sin\beta_j}{Q_j - \frac{H_r}{2}\cdot\tan\frac{\varphi}{2} + \frac{W_j}{2}\cdot\cos\beta_j}\right) - \frac{\theta_{T,\max}}{2} \Rightarrow$$

$$\beta_j = \frac{1}{2}\tan^{-1}\left(\frac{H + \frac{W_j}{2}\cdot\sin\beta_j}{Q_j - \frac{H_r}{2}\cdot\tan\frac{\varphi}{2} + \frac{W_j}{2}\cdot\cos\beta_j}\right) - \frac{90^\circ}{2} \Rightarrow$$

$$\beta_j = \frac{1}{2}\tan^{-1}\left(\frac{H + \frac{W_j}{2}\cdot\sin\beta_j}{Q_j - \frac{H_r}{2}\cdot\tan\frac{\varphi}{2} + \frac{W_j}{2}\cdot\cos\beta_j}\right) - 45^\circ \tag{8.4}$$

for the Conical Fresnel Reflector Solar Cooker, as we deemed that the System has a triangular absorber, and (Eq. 7.71)

$$\beta_j = \frac{1}{2}\tan^{-1}\left(\frac{H + \frac{W_j}{2}\cdot\sin\beta_j}{Q_j + \frac{W_j}{2}\cdot\cos\beta_j}\right) - 45^\circ \tag{8.5}$$

for the Linear Fresnel Reflector Solar Cooker.

In these equations, H is the height of the central point of the absorber above the origin of the local Cartesian coordinate System.

The tilt angle, β_j, takes negative values as it concerns reflective elements placed southern from the receiver. For the reflectors of the System being placed northern from the receiver, it takes positive values. In other words, it is positive if it is formed anticlockwise; otherwise, it is negative. The main reason originates from the definition of the tilt angle, β_j. It is the acute angle formed by the reflectors' plane and the jth reflector surface measured towards reflector surface. Moreover, in the case of the concentric Conical Fresnel Reflector System, the tilt angle β_j is connected with the bevel angle of the frustum cone formed by of the jth Fresnel reflective ring, as it will be presented later.

On the other hand, the width, W_j, of each reflector for both types of Solar Cookers developed in this chapter has been decided to be varying. Hence, for a receiver with triangular cross section on the System's transversal plane, which has a height equal to H_r and the angle formed by its two sides is equal to φ, the width, W_j, of each reflector is given by the formula

$$W_j = H_r \cdot \frac{\cos\left(\xi_j - \frac{\varphi}{2}\right)}{\cos\frac{\varphi}{2}\cdot\sin x_j} \tag{8.6}$$

where the angle x_j, as illustrated in Fig. 8.6, is given by the formula

$$\begin{aligned} x_j &= \xi_j + |\beta_j| \Rightarrow \\ x_j &= \xi_j - \beta_j \end{aligned} \tag{8.7}$$

In the case of the Linear Fresnel Reflector Solar Cooker where the receiver has circular cross section with radius equal to R_r, the width, W_j, of each reflector is given by the formula (Eq. 7.86)

$$W_j = \frac{2 \cdot R_r}{\sin x_j} \tag{8.8}$$

Substituting Eq. 8.7 into Eq. 8.6 and Eq. 8.8, they take the forms

$$W_j = H_r \cdot \frac{\cos\left(\xi_j - \frac{\varphi}{2}\right)}{\cos\frac{\varphi}{2} \cdot \sin\left(\xi_j - \beta_j\right)} \tag{8.9}$$

$$W_j = \frac{2 \cdot R_r}{\sin\left(\xi_j - \beta_j\right)} \tag{8.10}$$

However, from Eq. 8.3, we have

$$\begin{aligned} \xi_j &= 2 \cdot \beta_j + \theta_{T,\max} \Rightarrow \\ \xi_j &= 2 \cdot \beta_j + \frac{\pi}{2} \end{aligned} \tag{8.11}$$

Substituting Eq. 8.11 into Eq. 8.9 and Eq. 8.10, they become

$$\begin{aligned} W_j &= H_r \cdot \frac{\cos\left(2 \cdot \beta_j + \frac{\pi}{2} - \frac{\varphi}{2}\right)}{\cos\frac{\varphi}{2} \cdot \sin\left(2 \cdot \beta_j + \frac{\pi}{2} - \beta_j\right)} \\ W_j &= H_r \cdot \frac{\cos\left(2 \cdot \beta_j + \frac{\pi}{2} - \frac{\varphi}{2}\right)}{\cos\frac{\varphi}{2} \cdot \sin\left(\beta_j + \frac{\pi}{2}\right)} \end{aligned} \tag{8.12}$$

and

$$\begin{aligned} W_j &= \frac{2 \cdot R_r}{\sin\left(2 \cdot \beta_j + \frac{\pi}{2} - \beta_j\right)} \\ W_j &= \frac{2 \cdot R_r}{\sin\left(\beta_j + \frac{\pi}{2}\right)} \end{aligned} \tag{8.13}$$

Obviously, in the case of concentric Conical Fresnel Reflector Systems, the reflective elements width, W_j, provides the slant height of the conical frustum corresponding to the jth Fresnel ring.

8.3 Design Parameters' Computation

As in the case presented in Sect. 7.5 of Chap. 7, in order to install the reflective elements of these Solar Cookers on the right place and with the right inclination, the set of the corresponding equations have to be resolved and the basic design parameters—the width, W_j, the position or location, Q_j, and the tilt angle, β_j—of the N reflective elements have to be calculated. However, the set of the nonlinear equations 8.2, 8.4 and 8.12 are as follows:

$$Q_j = Q_{j-1} + W_{j-1} \cdot \cos\beta_{j-1} + W_{j-1} \cdot \sin\beta_{j-1} \cdot \tan\left(2 \cdot \beta_j\right) \tag{8.2}$$

$$\beta_j = \frac{1}{2}\tan^{-1}\left(\frac{H + \frac{W_j}{2} \cdot \sin\beta_j}{Q_j - \frac{H_r}{2} \cdot \tan\frac{\varphi}{2} + \frac{W_j}{2} \cdot \cos\beta_j}\right) - 45^\circ \tag{8.4}$$

$$W_j = H_r \cdot \frac{\cos\left(2 \cdot \beta_j + \frac{\pi}{2} - \frac{\varphi}{2}\right)}{\cos\frac{\varphi}{2} \cdot \sin\left(\beta_j + \frac{\pi}{2}\right)} \tag{8.12}$$

for the Conical, and the set of the nonlinear equations 8.2, 8.5 and 8.13

$$Q_j = Q_{j-1} + W_{j-1} \cdot \cos\beta_{j-1} + W_{j-1} \cdot \sin\beta_{j-1} \cdot \tan\left(2 \cdot \beta_j\right) \tag{8.2}$$

$$\beta_j = \frac{1}{2}\tan^{-1}\left(\frac{H + \frac{W_j}{2} \cdot \sin\beta_j}{Q_j + \frac{W_j}{2} \cdot \cos\beta_j}\right) - 45^\circ \tag{8.5}$$

$$W_j = \frac{2 \cdot R_r}{\sin\left(\beta_j + \frac{\pi}{2}\right)} \tag{8.13}$$

for the Linear Fresnel Reflector Solar Cooker, respectively, is not possible to be resolved explicitly, but only approximately, using an appropriate numerical method like this presented in Sect. 7.5 of Chap. 7. In the following paragraphs, only the computation of the parameters of the Conical Fresnel Reflector Solar Cooker will be presented. The case of the Linear Fresnel Reflector Solar Cooker can be treated identically.

The location, Q_1, and the tilt angle, β_1, of the first reflector ($j = 1$) must be calculated taken into account the fact that the absorber will cast a shadow on the plane of the reflective elements, and hence, no reflectors should be placed underneath it. The first reflective element must be placed at an appropriate location, Q_1, so that it can contribute to the solar radiation concentration on the absorber surface. Therefore, it must be at least outside the shadow the absorber casts on the reflectors' plane, and simultaneously, it must have an appropriate tilt angle, β_1.

So, the first reflector must be placed at an appropriate distance from the origin of the local Cartesian coordinate system, at least equal to the receiver's half-width, W_r:

$$Q_1 = \frac{W_r}{2} \tag{8.14}$$

While the angular size of Sun, δ_0, is not taken into account, it does not affect substantially the numerical results (the distance between the reflective elements and the receiver is significantly short). However, if we would place a reflector very close to the shade the receiver casts on the reflectors' plane then it should be almost horizontal, $\beta_j \approx 0$. For this reason, it would be preferable to move the reflector by a proper distance, S_1, away from the position calculated by Eq. 8.14. Otherwise, in the case of the conical reflective elements, the first reflective cone is very difficult to be constructed, and in the case of the linear reflectors, the first reflector is very difficult to be properly inclined. Therefore, the first reflective element is placed at a distance Q_1 given by the formula

$$Q_1 = W_r + S_1 \tag{8.15}$$

A arbitrary, but rational, value for the shift distance, S_1, of the first reflector is equal to three times the half-width, W_r, of the receiver

$$S_1 = 3 \cdot \frac{W_r}{2} \tag{8.16}$$

Hence, the position of the first reflective element is given by the formula

$$\begin{aligned} Q_1 &= \frac{W_r}{2} + S_1 \\ Q_1 &= \frac{W_r}{2} + 3 \cdot \frac{W_r}{2} \\ Q_1 &= 2 \cdot W_r \end{aligned} \tag{8.17}$$

For the Linear Fresnel Reflector Solar Cooker, the first reflective element is placed at a distance equal to $2 \cdot R_r$, $Q_1 = 2 \cdot R_r$.

Moving on to the tilt angle, β_1, of the first reflective element, it can be calculated from Eq. 8.4, after the necessary modification:

$$\beta_1 = \frac{1}{2}\tan^{-1}\left(\frac{H + \frac{W_1}{2} \cdot \sin\beta_1}{Q_1 - \frac{H_r}{2} \cdot \tan\frac{\varphi}{2} + \frac{W_1}{2} \cdot \cos\beta_1}\right) - 45^\circ \tag{8.18}$$

where Q_1 is its location, as it has been calculated from Eq. 8.17, and W_1 is the value of its width, which can be estimated from Eq. 8.12 by setting the angle β_j equal to β_1:

$$W_1 = H_r \cdot \frac{\cos\left(2 \cdot \beta_1 + \frac{\pi}{2} - \frac{\varphi}{2}\right)}{\cos\frac{\varphi}{2} \cdot \sin\left(\beta_1 + \frac{\pi}{2}\right)} \tag{8.19}$$

From Eq. 8.19 (as well as from Eq. 8.12), we can conclude that the reflectors width does not depend directly on its value, as it is the case of the tilt angle, β_1, through Eq. 8.18. Nevertheless, Eqs. 8.18 and 8.19 cannot be solved analytically for β_1 and W_1. The only possibility to calculate their values is to resort in an iterative approximate (numerical) method.

We will apply the same methodology presented in Sect. 7.5 of Chap. 7, starting from an arbitrary, but reasonable, initial value for the desired parameters, β_1 and W_1, and then we will proceed stepwise until the new results do not differ substantially from the previously computed. The reasonable initial values for the tilt angle, β_1, and the width, W_1, for the first reflector are $\beta_1^0 = 0$ and $W_1^0 = \frac{H_r}{\cos\frac{\varphi}{2}}$, respectively.

Essentially, only the tilt angle, β_1, and the width, W_1, of the first reflective element have to be calculated approximately, since its location, Q_1, along with its shift distance, S_1, is explicitly defined by Eq. 8.17. However, in each step, i, of the approximate method only the value of the tilt angle β_1^{i-1}, calculated in the previous step, $(i - 1)$, is increased (or reduced) by a small amount, $\Delta\beta$, (a small angular increment) in the order of 1°:

$$\beta_1'^i = \beta_1^{i-1} + \Delta\beta \tag{8.20}$$

Afterwards, the values of the width, W_1, and the tilt angle, β_1, are recalculated using the expressions

$$W_1^i = H_r \cdot \frac{\cos\left(2 \cdot \beta_1'^i + \frac{\pi}{2} - \frac{\varphi}{2}\right)}{\cos\frac{\varphi}{2} \cdot \sin\left(\beta_1'^i + \frac{\pi}{2}\right)} \tag{8.21}$$

$$\beta_1^i = \frac{1}{2}\tan^{-1}\left(\frac{H + \frac{W_1^i}{2} \cdot \sin\beta_1'^i}{Q_1 - \frac{H_r}{2} \cdot \tan\frac{\varphi}{2} + \frac{W_1^i}{2} \cdot \cos\beta_1'^i}\right) - 45° \tag{8.22}$$

First, we recalculate the new value of the width, W_1, and then the tilt angle, β_1, as the width W_j is independent from its previous value.

This iterative procedure is terminated when the new values differ from the previously calculated in a very small amount, a and b, respectively, the required precision, or else when the following condition is satisfied

$$\left|\beta_1^i - \beta_1^{i-1}\right| \leq a \tag{8.23}$$

$$\left|W_1^i - W_1^{i-1}\right| \leq b \tag{8.24}$$

or

$$\frac{\left|\beta_1^i - \beta_1^{i-1}\right|}{\beta_1^i} \cdot 100 \leq p_a\% \tag{8.25}$$

$$\frac{\left|W_1^i - W_1^{i-1}\right|}{W_1^i} \cdot 100 \leq p_b\% \tag{8.26}$$

where $i = 0, 1, 2, 3, \ldots$ is the step number of the iterative procedure, and p_a and p_b are the required levels of accuracy.

The location, Q_2, the width, W_2, and the tilt angle, β_2, of the second reflective element must be chosen so that the light ray emanating from the centre of the solar disc and striking the midpoint of the reflector to be reflected and directed towards the centre of the absorber. In addition, the solar radiation reflected by the second reflector must not be blocked by the first reflector. Hence, we again have to introduce a space between the first and second reflector, the shift distance S_2. Thus, the location, Q_2, of the second reflective element can be calculated using Eq. 8.2, after introducing the proper modifications (set $j = 2$):

$$Q_2 = Q_1 + W_1 \cdot \cos\beta_1 + W_1 \cdot \sin\beta_1 \cdot \tan(2 \cdot \beta_2) \tag{8.27}$$

In addition, the width, W_2, of the second reflective element and its tilt angle, β_2, are

$$W_2 = H_r \cdot \frac{\cos\left(2 \cdot \beta_2 + \frac{\pi}{2} - \frac{\varphi}{2}\right)}{\cos\frac{\varphi}{2} \cdot \sin\left(\beta_2 + \frac{\pi}{2}\right)} \tag{8.28}$$

$$\beta_2 = \frac{1}{2}\tan^{-1}\left(\frac{H + \frac{W_2}{2} \cdot \sin\beta_2}{Q_2 - \frac{H_r}{2} \cdot \tan\frac{\varphi}{2} + \frac{W_2}{2} \cdot \cos\beta_2}\right) - 45^\circ \tag{8.29}$$

To compute the location, Q_2, the width, W_2, and the tilt angle, β_2, of the second reflective element, we must solve approximately (numerically) the system of the three nonlinear equations Eqs. 8.27, 8.28 and 8.29 using the above-presented iterative procedure. The initial values for the second reflector are $Q_2^0 = Q_1 + W_1$ and $W_2^0 = \frac{H_r}{\cos\frac{\varphi}{2}}$ and $\beta_2^0 = 0$. Their approximate values, Q_2^i, W_2^i and β_2^i, at the i step of the iterative procedure are recalculated from the corresponding values in the previous step, $(i - 1)$, Q_2^{i-1}, W_2^{i-1} and β_2^{i-1}, by increasing (or reducing) the tilt angle β_2^{i-1} by a small amount, $\Delta\beta$, (a small angular increment) in the order of 1°

$$\beta_2'^i = \beta_2^{i-1} + \Delta\beta \tag{8.30}$$

using the expressions

$$Q_2^i = Q_1 + W_1 \cdot \cos\beta_1 + W_1 \cdot \sin\beta_1 \cdot \tan\left(2 \cdot \beta_2'^i\right) \tag{8.31}$$

$$W_2^i = H_r \cdot \frac{\cos\left(2 \cdot \beta_2'^i + \frac{\pi}{2} - \frac{\varphi}{2}\right)}{\cos\frac{\varphi}{2} \cdot \sin\left(\beta_2'^i + \frac{\pi}{2}\right)} \tag{8.32}$$

$$\beta_2^i = \frac{1}{2}\tan^{-1}\left(\frac{H + \frac{W_2^i}{2} \cdot \sin\beta_2'^i}{Q_2^i - \frac{H_r}{2} \cdot \tan\frac{\varphi}{2} + \frac{W_2^i}{2} \cdot \cos\beta_2'^i}\right) - 45^\circ \tag{8.33}$$

This iterative procedure is terminated when the new values differ from the previously calculated in a very small amount, a, b and c, respectively; the required precision, or else when the following condition is satisfied

$$\left|\beta_2^i - \beta_2^{i-1}\right| \le a \tag{8.34}$$

$$\left|W_2^i - W_2^{i-1}\right| \le b \tag{8.35}$$

$$\left|Q_2^i - Q_2^{i-1}\right| \le c \tag{8.36}$$

or

$$\frac{\left|\beta_2^i - \beta_2^{i-1}\right|}{\beta_2^i} \cdot 100 \le p_a\% \tag{8.37}$$

$$\frac{\left|W_2^i - W_2^{i-1}\right|}{W_2^i} \cdot 100 \le p_b\% \tag{8.38}$$

$$\frac{\left|Q_2^i - Q_2^{i-1}\right|}{Q_2^i} \cdot 100 \le p_c\% \tag{8.39}$$

where $i = 0, 1, 2, 3,\ldots$ is the step number of the iterative procedure, and p_a, p_b and p_c are the required levels of accuracy.

Similarly, the position, Q_j, the width, W_j, and the tilt angle, β_j, of the jth reflective element, and consequently of all reflective elements, of the Fresnel Reflector System illustrated in Fig. 8.8, can be calculated by applying the above-presented iterative method in the following equations

$$Q_j^i = Q_{j-1} + W_{j-1} \cdot \cos\beta_{j-1} + W_{j-1} \cdot \sin\beta_{j-1} \cdot \tan\left(2 \cdot \beta_j'^i\right) \tag{8.40}$$

$$W_j^i = H_r \cdot \frac{\cos\left(2 \cdot \beta_j'^i + \frac{\pi}{2} - \frac{\varphi}{2}\right)}{\cos\frac{\varphi}{2} \cdot \sin\left(\beta_j'^i + \frac{\pi}{2}\right)} \tag{8.41}$$

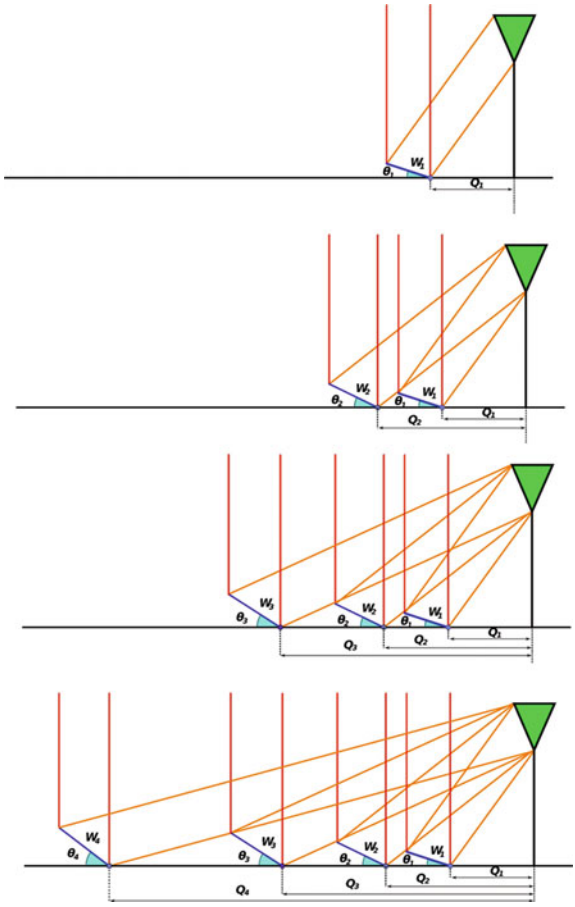

Fig. 8.8 Placement of the reflective elements in the two Fresnel Reflector Solar Cookers can be accomplished only stepwise. First, we calculate the position, Q_1, the width, W_1, and the tilt angle, β_1, of the first reflective element. Next, we proceed to the calculation of the place, Q_2, the width, W_2, and the inclination angle, β_2, of the second reflective element, taking into account the results of the previous step. We keep on until the last reflective element is placed, taking into account the primary reflectors field dimensions. However, due to the inherent symmetry of the illustrated Systems (the sunrays hit always perpendicular on the reflectors' aperture, and, therefore, Sun's maximum transversal angle, $\theta_{T,max}$, is always equal to 90°, the reflective elements are side pivoted with the southern reflectors to be pivoted on their northern longer edge, while the northern reflectors to be pivoted on their southern longer edge), the arrangement of the southern reflective elements is a reflective image of the northern elements in relation to the longitudinal plane of the (linear) System

$$\beta_j^i = \frac{1}{2}\tan^{-1}\left(\frac{H + \frac{W_j^i}{2}\cdot \sin \beta_j'^i}{Q_j^i - \frac{H_r}{2}\cdot \tan\frac{\varphi}{2} + \frac{W_j^i}{2}\cdot \cos \beta_j'^i}\right) - 45^\circ \tag{8.42}$$

where Q_j^i, W_j^i and β_j^i are the approximate values at the i step of the iterative procedure, which are recalculated from the corresponding values in the previous step (i-1), Q_j^{i-1}, W_j^{i-1} and β_j^{i-1}, by increasing (or reducing) the tilt angle β_j^{i-1} by a small amount, $\Delta\beta$ (a small angular increment), in the order of 1°

$$\beta_j'^i = \beta_j^{i-1} + \Delta\beta \tag{8.43}$$

The corresponding initial values are $Q_j^0 = Q_{j-1} + W_{j-1}$ and $W_j^0 = \frac{H_r}{\cos\frac{\varphi}{2}}$ and $\beta_j^0 = 0$, and the termination conditions are described by the expressions

$$\left|\beta_j^i - \beta_j^{i-1}\right| \le a \tag{8.44}$$

$$\left|W_j^i - W_j^{i-1}\right| \le b \tag{8.45}$$

$$\left|Q_j^i - Q_j^{i-1}\right| \le c \tag{8.46}$$

or

$$\frac{\left|\beta_j^i - \beta_j^{i-1}\right|}{\beta_j^i}\cdot 100 \le p_a\% \tag{8.47}$$

$$\frac{\left|W_j^i - W_j^{i-1}\right|}{W_j^i}\cdot 100 \le p_b\% \tag{8.48}$$

$$\frac{\left|Q_j^i - Q_j^{i-1}\right|}{Q_j^i}\cdot 100 \le p_c\% \tag{8.49}$$

where i = 0, 1, 2, 3,…, is the step number of the iterative procedure and p_a, p_b and p_c are the required levels of accuracy, which usually are the same ($p_a = p_b = p_c$) for all reflective element and for all design parameters (position, Q_j, width, W_j, and tilt angle, β_j), or rarely, they are defined separately ($p_a \neq p_b \neq p_c$).

Lastly, the fact that the aperture length, L_a, or diameter, D_a, of the primary reflectors field is finite (along with the height of the position, H, of the receiver above the reflectors plane and the dimensions of its cross section on the System's transversal plane) affects the total number, N, of the reflective elements. As we calculate the width, W_j, the tilt angle, β_j, and the position, Q_j, of each reflector, we must always check if there is sufficient space to include it in the Systems. In other words, we must each time check whether the following condition is satisfied or not:

$$\text{if} \quad 2 \cdot Q_j \leq D_a \text{ or } L_a \quad \begin{matrix} \text{then the } j\text{th reflecting element} \\ \text{can be added in the System} \end{matrix} \tag{8.50}$$

$$\text{else if} \quad 2 \cdot Q_j > D_a \text{ or } L_a \quad \begin{matrix} \text{no space is available for} \\ \text{additional reflecting elements} \end{matrix} \tag{8.51}$$

The construction of the Conical Fresnel Reflector Solar Cooker with a cylindrical vertically positioned receiver is more challenging. Although the design parameters of its reflective elements, the width, W_j, the tilt angle, β_j, and their position, Q_j, are calculated using the above-presented methodology; the reflectors are not plane rectangular strips, but right frustum cones (conical frustum) . A frustum of a cone is a shape formed when a portion of a cone is cut through by a plane parallel to its base. The remaining part between the cutting plane and the base of the cone composes the frustum cone.

The full set of parameters describing the frustum of a right cone are the radius of its base, R, the radius of its top, r, its thickness or height, h, its slant height, hs, and the opening angle, φ, of the corresponding right cone. The opening angle, φ, is equivalent to the double angle formed by the frustum cone height, h, and its slant height, hs (Fig. 8.9). So, the width, W_j, of the jth reflective elements corresponds to the slant height, hs_j, of the jth conical frustum reflective ring, the position, Q_j, corresponds to the radius, r_j, of its smallest base (top), while the tilt angle, β_j, corresponds to the complementary angle of the half opening angle, φ_j, of the corresponding cone ($\beta_j = \pi/2 - \varphi_j/2$).

To construct a conical frustum surface, we must be able to create a flat pattern of it (a development) calculating its geometric parameters. The shape obtained if the conical frustum is cut along its slanted height, hs, can be used to reconstruct it (Fig. 8.9a). This shape is part (a sector) of a circular ring. If we now prolong its sides, we obtain an angular sector of a circular disc (Fig. 8.9b). To construct the frustum, we need to know the two radii R_{in} and R_{out} and the central angle ω of this sector. These parameters are related with the conical frustum parameters through the following relationships (this is basic geometry theory and there is no any need to be further analysed here):

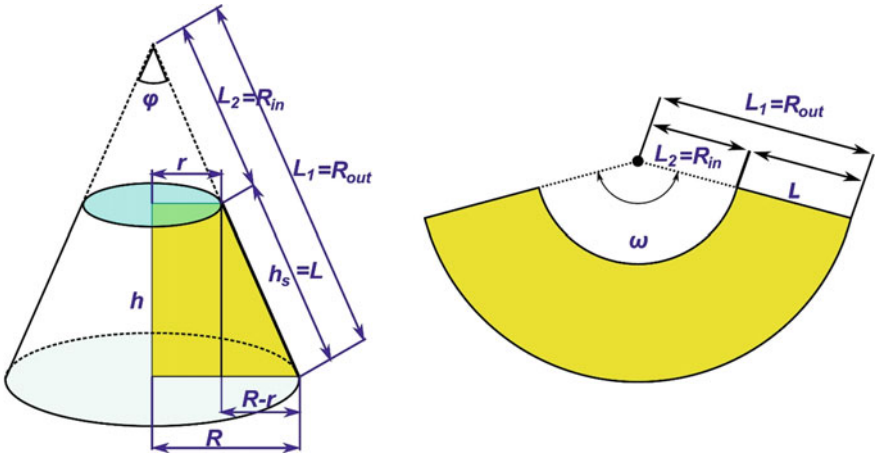

Fig. 8.9 To construct a conical frustum, we must calculate the parameters describing its development in relation to the frustum parameters

$$R_{\text{out}} = \frac{R \cdot \sqrt{h^2 + (R-r)^2}}{R-r} \tag{8.52}$$

$$R_{\text{in}} = R_{\text{out}} - \sqrt{h^2 + (R-r)^2} \tag{8.53}$$

$$\omega = \frac{R}{R_{\text{out}}} \tag{8.54}$$

If we take into account the fact that $r_j = Q_j$, $R_j = Q_j + W_j \cdot \cos\beta_j$, and $h_j = W_j \cdot \sin\beta_j$, we can calculate the parameters, R_{in}, R_{out} and ω, of the development of the conical frustum from the design parameter of the Conical Fresnel reflective elements. Thus, we can create a flat ring that gains a bevel if we remove a section corresponding to an angle equal to $2 \cdot \pi - \omega_j$ and rejoin its two edges. This way we form a conical ring, which is what we need to construct a Conical Fresnel Reflector (Fig. 8.10).

The concentration ratio *CR* of both Linear and Conical Fresnel Reflectors Solar Cooker is defined as the ratio of the effective area of all (*N*) reflective elements, A_e, to the illuminated area of the receiver A_r:

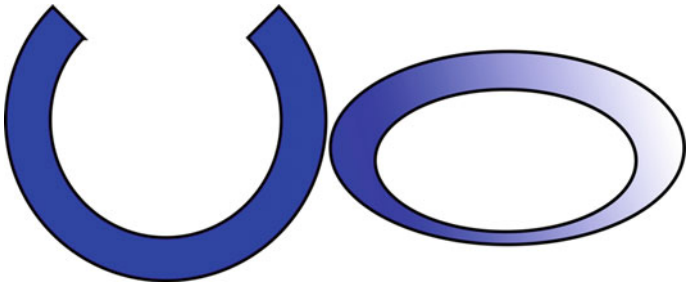

Fig. 8.10 Reflective elements of a Conical Fresnel Reflector Solar Cooker can be constructed from a flat reflective circular ring after removing a proper angular section and rejoining the two edges of the remaining ring

$$CR = \frac{A_e}{A_r} \tag{8.55}$$

In the Conical Fresnel Reflector Solar Cooker, despite the fact that the receiver has been treated as if it was of triangular cross section, in fact it is a vertically positioned cylinder, and the concentrated solar radiation is spread across its side and bottom surface. This area, A_r, is given by the following equation:

$$\begin{aligned} A_r &= H_r \cdot (2 \cdot \pi \cdot R_r) + \pi \cdot R_r^2 \Rightarrow \\ A_r &= H_r \cdot \left(2 \cdot \pi \cdot \frac{W_r}{2}\right) + \pi \cdot \frac{W_r^2}{4} \Rightarrow \\ A_r &= \pi \cdot \left(H_r \cdot W_r + \frac{W_r^2}{4}\right) \end{aligned} \tag{8.56}$$

where W_r is the receiver cross section width, or else its diameter, R_r is its radius, $R_r = W_r/2$, and H_r is its height.

The effective area, $A_{e,j}$, of each reflective element is equal to the area of their projection on the reflector's plane. However, since the reflective elements are conical rings, their effective area is given by the formula:

$$\begin{aligned} A_{e,j} &= \pi \cdot R_j^2 - \pi \cdot r_j^2 \Rightarrow \\ A_{e,j} &= \pi \cdot \left(R_j^2 - r_j^2\right) \Rightarrow \\ A_{e,j} &= \pi \cdot \left[\left(Q_j + W_j \cdot \cos\beta_j\right)^2 - Q_j^2\right] \end{aligned} \tag{8.57}$$

Consequently, the total reflectors' effective area is obtained by summing up the individual effective areas, $A_{e,j}$, for all, N, reflectors:

$$A_e = \sum_{j=1}^{N} \left\{ \pi \cdot \left[\left(Q_j + W_j \cdot \cos \beta_j \right)^2 - Q_j^2 \right] \right\} \Rightarrow$$

$$A_e = \pi \cdot \sum_{j=1}^{N} \left[\left(Q_j + W_j \cdot \cos \beta_j \right)^2 - Q_j^2 \right] \tag{8.58}$$

Hence, the concentration ratio, *CR*, of the Conical Fresnel Reflector Solar Cooker is given by the equation

$$CR = \frac{A_e}{A_r} = \frac{\pi \cdot \sum_{j=1}^{N} \left[\left(Q_j + W_j \cdot \cos \beta_j \right)^2 - Q_j^2 \right]}{\pi \cdot \left(H_r \cdot W_r + \frac{W_r^2}{4} \right)} \Rightarrow$$

$$CR = \frac{A_a}{A_r} = \frac{\sum_{j=1}^{N} \left[\left(Q_j + W_j \cdot \cos \beta_j \right)^2 - Q_j^2 \right]}{H_r \cdot W_r + \frac{W_r^2}{4}} \tag{8.59}$$

On the other hand, in the Linear Fresnel Reflector Solar Cooker, the effective area, $A_{e,j}$, of each reflective element is equal to the area of their projection on the reflectors' plane:

$$A_{a,j} = L_j \cdot W_j \cdot \cos \beta_j \tag{8.60}$$

where L_j is their length.

Consequently, the total reflectors' effective area is obtained by summing up the individual effective areas, $A_{e,j}$, for all reflectors (*N* reflective elements on each side of the System):

$$A_e = 2 \cdot \sum_{j=1}^{N} L_j \cdot W_j \cdot \cos \beta_j \tag{8.61}$$

The real area, A_r, of the illuminated receiver surface is not very easy to be computed, because its surface is cylindrical. However, a rough, but reasonable, approximation is to be considered equal to three quarter (3/4) of its total surface:

$$A_r = \frac{3}{4} \cdot L \cdot 2 \cdot \pi \cdot R_r = \frac{3}{2} \cdot L \cdot \pi \cdot R_r \tag{8.62}$$

where *L* is the receiver length and R_r is its radius.

Hence, the concentration ratio *CR* of the Linear Fresnel Reflector Solar Cooker is given by the equation

$$CR = \frac{A_e}{A_r} = \frac{2 \cdot \sum_{j=1}^{N} L_j \cdot W_j \cdot \cos \beta_j}{\frac{3}{2} \cdot L \cdot \pi \cdot R_r} \tag{8.63}$$

However, since the receiver's and the reflectors' length is the same, $L_j = L$, for all j, Eq. 8.52 takes the form:

$$CR = \frac{A_e}{A_r} = \frac{4 \cdot \sum_{j=1}^{N} W_j \cdot \cos \beta_j}{3 \cdot \pi \cdot R_r} \tag{8.64}$$

8.4 The Solar Cookers' Construction

The above methodology is more or less a theoretical modification and adaptation of this presented in Sect. 7.5 of Chap. 7. In order to be able to calculate the design parameters of these Solar Cookers, we have to define: (a) the receiver dimensions, (b) the height of its position, (c) the size of the primary reflectors field as well as (d) the desired accuracy levels of the calculations.

The size of the illuminated receiver's area (or broadly speaking, the size of the focus) determines how tightly the light will be focused. It also controls the width of the reflective elements (strips, or conical frustum rings). A small area offers higher concentrating power but produces many thinner reflectors (strips or rings). In addition, the receiver position height, or else the System's focal length, affects the reflectors position and tilt angle. Short focal lengths produce reflectors with very large tilt angles, β_j. This leads to more rigid structures. At the same time, the gaps, or shift distances, S_j, between two consecutive reflective elements increase, and the reflective coverage, the part of the primary reflectors' aperture surface that is reflective, drops. On the other hand, long focal lengths increase the coverage but produce reflective elements (strips or rings) with shallow angles. When constructing such Systems we have to take into account the physical properties of the material used to build the reflectors, how flexible it is. Small tilt angles result in less rigid and more difficult to be accurately built structures. The design characteristics of the Fresnel Reflector Solar Cookers developed in this book have been chosen so that the tilt angles of their reflective elements, especially of the rings of the Conical Fresnel Reflector Solar Cooker, to be large enough so that they can be constructed easily without introducing significant errors, as well as produce a sturdy structure.

The receiver in the Linear Fresnel Reflector Solar Cooker is 30.5 cm high, with 11 cm diameter, whereas the height of the receiver in the Conical Fresnel Reflector Solar Cooker is 6 cm, and its diameter is 14 cm. Both are placed at a height (their

Table 8.1 Construction parameter for the two Fresnel Reflector Solar Cookers

Linear Fresnel Reflector Solar Cooker			
Fresnel reflective elements			
Reflector no.	Tilt angle (degrees)	Position (cm)	Width (cm)
1	10	11.0	11.0
2	17	23.0	11.5
3	22	37.0	11.9
4	27	54.0	12.5
Conical Fresnel Reflector Solar Cooker			
Fresnel Reflective Elements			
Reflector no.	Tilt angle (degrees)	Position (cm)	Width (cm)
1	17	28.0	9.5
2	22	39.4	9.8
3	26	52.8	10.0
Construction data of the frustum conical reflective rings			
Reflective ring no.	R_{in} (cm)	R_{out} (cm)	ω (degrees)
1	29.2	38.7	344.6
2	42.4	52.3	334.8
3	58.7	68.7	324.3

centres), H, equal to 45 cm above the reflectors plane. The Conical Fresnel Reflector Solar Cooker cross section is rectangular. However, it can be regarded as triangular receivers, whose sides coincide with the line segments BM and CM, of Fig. 8.6. They can easily be calculated using the Pythagorean theorem and the dimensions of the original shape of the receiver. The levels of accuracy of the calculations have been chosen to be the same for all construction parameters, $p_a = p_b = p_c$, and equal to 0.1%.

Using the aforementioned dimensions of the two receivers and applying the above-presented iterative procedure, we can calculate the construction parameters of these two Fresnel Reflector Solar Cookers (Table 8.1). It must be noted that the Systems' dimensions are 130 cm × 30 cm for the Linear and 120 cm × 120 cm for the Conical Fresnel Reflector Solar Cooker, respectively.

8.4.1 The Linear Fresnel Reflector Solar Cooker

The primary reflectors' field of the Linear Fresnel Reflector Solar Cooker consists of two 65 cm × 33 cm section where 2 × 4 = 8 rectangular plane reflective strips are mounted. Each of these reflective elements is 33 cm long and their widths are presented in Table 8.1. The receiver, the cooking vessel, is mounted on two wooden boards. The whole structure is rotatable around two individual axes,

through a simple supporting System. It allows the inclination adjustment of the entire construction, both the primary reflectors field and the receiver, with respect to the horizon. This way the maximum solar radiation intensity on the reflectors, and hence, the best efficiency of the System is obtained. The reflected sunlight remains always focused onto the receiver, because the light source, Sun, remains always perpendicular to the primary reflectors aperture (Fig. 8.6). The Linear Fresnel Reflector Solar Cooker with the eight reflectors has a reflective coverage equal to 67.5%. If built exactly, the solar radiation at the receiver will be concentrated about 3.4 times. The whole assembly is presented in Fig. 8.11. The primary reflectors' field aperture area is equal to 0.263 m^2, so it can transfer on the average nearly 241 W of solar power to the cooking vessel, for a site at Thessaloniki, Greece (22.920227° latitude and 40.736851° longitude), on the 15th of June at the noon (Standard Time).

8.4.2 The Conical Fresnel Reflector Solar Cooker

The primary reflectors' field of the Conical Fresnel Reflector Solar Cooker consists of a 120 cm × 120 cm board where three frustum conical reflective rings are mounted. The rings have been cut out using the data of Table 8.1. After that, the conical reflective elements have been constructed by joining the edges of the circular rings and placing and mounting them at the right place on the reflectors' board, a flat piece of plywood.

The absorber, the cooking vessel, is supported by a metal rod. The whole structure is rotatable around two individual axes, through a simple supporting System. As in the case of the Linear Fresnel Reflector Solar Cooker, it allows the inclination adjustment of the entire construction, both the primary reflectors field and the receiver, with respect to the horizon. This way the maximum solar radiation intensity on the reflectors and, hence, the best efficiency of the System is obtained. The sunlight reflected from all reflectors remains always focused onto the receiver, because the light source, Sun, remains always perpendicular to the primary reflectors' aperture (Fig. 8.6). The Conical Fresnel Reflector Solar Cooker has three (3) rings that provide a 63.53% reflective coverage. If built exactly, the solar radiation at the receiver will be concentrated 18.3 times. The whole assembly is presented in Fig. 8.12. The primary reflectors' field aperture area is equal to 0.7641 m^2, so it can transfer on the average nearly 701 W of solar power to the cooking vessel, for a site at Thessaloniki, Greece (22.920227° latitude and 40.736851° longitude), on the 15th of June at the noon (Standard Time).

Fig. 8.11 Photograph of the complete Linear Fresnel Reflector Solar Cooker designed and developed in this chapter. It consists of the primary reflectors field, the receiver (the cooking vessel) and the supporting System

Fig. 8.12 Photograph of the complete Conical Fresnel Reflector Solar Cooker designed and developed in this chapter. It consist of the primary reflectors field, the receiver (the cooking vessel) and the supporting System

References

Amal, Herez, Mohamad Ramadana, and Mahmoud Khaleda. 2018. Review on solar cooker systems: Economic and environmental study for different Lebanese scenarios. *Renewable and Sustainable Energy Reviews* 81: 421–432.

Cuce, Erdem, and Pinar Mert Cuce. 2013. A comprehensive review on solar cookers. *Applied Energy* 102: 1399–1421.

Farooqui, Suhail Zaki. 2013. A vacuum tube based improved solar cooker. *Sustainable Energy Technologies and Assessments* 3: 33–39.

Muthusivagami, R.M., R. Velraj, and R. Sethumadhavan. 2010. Solar cookers with and without thermal storage—A review. *Renewable and Sustainable Energy Reviews* 14: 691–701.

Panwara, N.L., S.C. Kaushika, and Surendra Kotharib. 2012. State of the art of solar cooking: An overview. *Renewable and Sustainable Energy Reviews* 16: 3776–3785.

Prasanna, U.R., and L. Umanand. 2011. Optimization and design of energy transport system for solar cooking application. *Applied Energy* 88: 242–251.

Stine, William B. and Michael Geyer. 2001. *Power from The Sun*. Available online at the website http://www.powerfromthesun.net/book.html.

Sunil, Indora, and Tara C. Kandpal. 2018. Institutional cooking with solar energy: A review. *Renewable and Sustainable Energy Reviews* 84: 131–154.

Yettou, F., B. Azoui, A. Malek, A. Gama, and N.L. Panwar. 2014. Solar cooker realizations in actual use: An overview. *Renewable and Sustainable Energy Reviews* 37: 288–306.

Chapter 9
Short Introduction to MATLAB®

This book is designed to support the analysis and the development of Solar Radiation Concentrating Systems that use Linear Fresnel Reflectors to harvest the solar power. Although other environments (e.g., Excel/VBA) or languages (e.g., Fortran 90, C++) could also serve this purpose, MATLAB® offers a unique environment. It combines handy programming features with powerful built-in numerical procedures and graphics handling capabilities. It allows the implementation of both simple and moderately complex algorithms, as well as more sophisticated programs that are able to solve more complicated problems.

However, an introductory Chapter in MATLAB® could only focus on those features of MATLAB® that were useful in solving specific kinds of problems. As a consequence, it cannot be a comprehensive overview of all MATLAB® features and capabilities. For this reason, the primary objective of this chapter is to provide a concrete idea of the main characteristics of this computational environment and how they can be applied to solve engineering and scientific problem. In addition, it is assumed that the reader of this book can comfortably use computers and has at least basic knowledge of computer programming. Further information can be found in related bibliography. For example, Attaway (2009), Chapra (2012), Chapra et al. (2010), Dukkipati (2006), Gilat (2017), Hahn et al. (2010), Hunt et al. (2001), Moore (2012), Nagar (2017), and MATLAB® Language Reference Manuals.

9.1 Introduction

MATLAB® (short for **Mat**rix **Lab**oratory) is a very powerful mathematical and graphical software package that has numerical, graphical and programming capabilities with many built-in tools. It allows the performing of scientific and engineering calculations, the solving of sophisticated problems and the creation and handling of graphical illustrations. It excels at computations involving matrices and provides the user with a convenient environment for developing complex scripts (programs).

S. Karathanasis, *Linear Fresnel Reflector Systems for Solar Radiation Concentration*, https://doi.org/10.1007/978-3-030-05279-9_9

When MATLAB® starts, a window is opened, the MATLAB® desktop, or environment, with many parts, or subwindows, or simply windows. MATLAB® uses three primary windows:

- The Command Window, which is used to enter commands and other statements and expressions.
- The Graphics Window, where plots and graphs are displayed.
- The Edit Window, where M-files (scripts and user defined functions) are created and edited.
- The Current Directory, which displays the folder where files (e.g. M-files or data files) are saved. It shows the default directory, which, however, can be changed.

This is a short description of the default layout of MATLAB® desktop environment, which can be altered satisfying specific problem-solving conditions.

After starting MATLAB®, the Command Window opens with the command prompt ≫ being displayed and waiting for a command. The simplest way for using MATLAB® is by typing directly mathematical expressions, or other commands or statements, at the prompt line of the Command Window. MATLAB® immediately responds with a result. We can use it to do arithmetic as we would do with a calculator. We can add, subtract, multiply, divide and perform many more complex calculations. MATLAB® assigns the result to a variable called *ans* and displays the answer on the Command Window. Nevertheless, the problems that can be solved this way are rather simple. To do more complex calculations, we have to assign values to variables and create expressions with them, which are executed one by one. This is not a so easy task to be done in the Command Window.

9.2 Programming with MATLAB®—Script Files

To solve a problem using a computer, we must implement an appropriate numerical method that repeatedly computes the desired parameters. However, in order to obtain acceptable accuracy, we must use many small steps in this approaching procedure. Although all required commands could be typed in the Command Window and executed when the enter key was pressed at the end of each line, this method could be a potential solution only for simple cases. Using the Command Window of MATLAB® to solve complex problems by typing a long series of commands at the prompt line is far from convenient. In fact, it is difficult, extremely laborious and time-consuming, or even impossible, for extremely complicated situations, since some problems cannot be solved with one line mathematical expression. In addition, the commands typed in the Command Window cannot be saved to be executed again, altered, changed or corrected.

Fortunately, MATLAB® provides an easy way to overcome these difficulties as it contains a powerful programming language. Thus, a much better way of executing a series of interrelated commands with MATLAB® is first to create a file

with a list of these commands: a program, or more correctly, a script. Then the script file must be saved and after that it can be executed in the command line like any other built-in MATLAB® command. This way, the commands contained in the file are executed exactly in the order they are listed, and, in addition, they can be corrected, altered or changed, if needed. Obviously, script files can be edited and executed again and again, provided that any change has being saved first. They are useful for occasions where we want to execute large series of commands more than one time.

In other words, a script is merely a collection of multiple sequential mathematical expressions, statements, MATLAB® command and instructions that are listed in a particular order. They create a code that directs the computer to perform a certain task. Scripts are stored in an ASCII text file. Obviously, scripts can also invoke other scripts. These files are similar to other computer languages (like C or FORTRAN) source code files and can be reused anytime we wish to repeat our calculations. Script files are not exactly computer programs, but without loss of generality, they can be considered as programs. They are one of the two different kinds of the so-called M-files of MATLAB®, the script M-files and the function M-files. The terminology M-file comes from the fact that the extension of these files is ".m", e.g. "SolarAngleCalculation.m". We shall limit our study only to scripts M-files as they suffice to treat the problems arisen from the study of the Systems described in the previous chapters of this book.

Creating good computer programs is a precise but tough task. We have to enter each statement in precisely the right position and with precisely the right way if we want to be able to solve scientific and engineering problems successfully. As a computer program is a sequence of instructions in a particular programming language that accomplishes a task, it must be readable and understandable. A well-written code can be evaluated relatively easy, particularly if the problem to be solved is complicated enough. In addition, it is helpful to decompose large programs into subprograms with fewer lines that solve specific parts of a problem, as they are much easier to be read. Moreover, if changes are necessary to be made, they can more easily be implemented in shorter codes.

Generally speaking, a mathematical model of a problem can be defined as the formulation of the equations that express the features of the physical system, or process, in mathematical terms. The physical quantities to be calculated are referred as dependent variables. They usually depend on other physical or mathematical quantities, the independent variables, through specific relationships, which may contain constants or parameters. The mathematical expression of these relationships ranges from simple algebraic relationships to large complicated sets of differential equations. Unfortunately, an analytical, or closed-form, solution that exactly satisfies the original set of these mathematical expressions cannot always be obtained. In other words, only a few problems can be solved exactly. In most cases, the only alternative is to implement a numerical method which results approximate the exact solution of the problem.

Once a problem has been analysed, the algorithm for its solution has to be translated into a computer program using a programming language. Without a

doubt, the resulting code must be well developed (designed) and well written. However, what makes a computer program well written? The objective in designing a well-written program that works effectively is to be readable and easy to understand and modify when required. There are many benefits to writing organized, well-structured code. They are easier to debug, test, update, share and the resulting program needs shorter time to run. For this reason, the detailed description of the code purpose, the determination of the required inputs data, the choice of the most appropriate method of processing to implement, the resulting outputs and any other special requirements of the problem to be solved must be known beforehand, so that they can be used in designing and creating an effective program.

9.2.1 Structuring Script M-Files

Although many problems require sophisticated programs for their solution, any computational code can be composed using three fundamental kinds of structures that result in clear and easy to follow codes: sequences, selections (decisions) and repetitions (loops). An apropos example is the code used to solve numerically a nonlinear equation. It repeats a sequence of calculations until the error in the answer is smaller than a predefined amount.

The simplest code performs instructions sequentially. The statements are executed line by line, starting from the beginning of the code file and moving down to the end. However, the usefulness of strict sequences of statements is highly limited. For this reason, all computer languages include structures that allow the development of computational algorithms with non-sequential paths. These non-sequential structures include decisions (or selections), that branch the flow based on a decision to be made, and loops (or repetitions), that change the flow by allowing a group of statements to be repeated.

MATLAB® provides several structures that can be used to control the flow of a program. Conditional IF statements and the SWITCH/CASE structure make it possible to skip commands, or to execute specific groups of commands in different situations. In addition, MATLAB® provides two kinds of loops that make it possible to repeat a sequence of commands several times, the FOR loops and the WHILE loops.

Another important feature of a well-written script is to be well documented. This way, not only other people can understand our code, what the script does and how, but also we can understand it whenever we read it, even after long time the code is developed.

One way of documenting a script is to add comments in it that describe the code. It is really worthwhile to include comments, especially in lengthy codes. They are completely ignored by MATLAB® when the script is executed. In MATLAB®, we can put a comment simply by typing the symbol % at the beginning of a line. Anything from the % to the end of that particular line is a comment. In any case, we should add enough comments and references so that even years after the time the

script is written we are able to know exactly what the program does and for what purpose (e.g. to explain the calculations or the results of them).

9.2.2 Creating and Saving Script Files

Script files are created and edited in the MATLAB® Editor Window. This window opens from the Command Window by typing the command EDIT or from the Main Menu by selecting New Script. This action opens a new "Untitled" (sub) window in the Editor Window. To create a new script, we simply type the sequence of commands, or other statements, line by line in this window. Each time we insert a new line, MATLAB® puts a line number on the left of the text. These numbers will be used by MATLAB® to refer to code errors. Nevertheless, as scripts are ordinary text files containing MATLAB® commands, they can also be created or modified in any other text editor. Then, the created code can be copied and pasted in the Editor Window. If we choose a different text editor, we must ensure that the file will be saved as text-ASCII format. In this case, we must also make sure that the extension ".m" is added on the filename. The rules for filenames are the same as for variables' names and will be presented later in this chapter (for instance, script filenames must start only with a letter, and after that there can be letters, digits or the underscore. No space is allowed).

A script file can be executed either directly from the Editor Window by clicking on the Run icon or by typing the file name in the Command Window and then pressing the enter key. However, for a file to can be executed, MATLAB® needs to know where it is saved. It looks for scripts files in certain places. By default, scripts files are saved in the Current Directory. Thus, to run a script, its file must be in the Current Directory (folder), or in another folder on the search path. If we want to save a script file in a different directory, the Current Directory must be changed in that directory.

9.2.3 Interpreting Script Files

It is interesting to know how MATLAB® scripts are executed. High-level programming languages use English-like commands and functions, which, however, the computer cannot understand and execute immediately. Any computer can interpret commands only written in its machine language. Therefore, programs written in high-level programming languages, for example MATALAB® scripts, must first be translated into machine language before the computer can actually execute the sequence of instructions they contain. A compiler is a special program, part of many programming languages environments that translate the instructions written in a high-level language into machine language creating an executable file. This file can be run independently from the original file (the source code).

On the other hand, interpreters are another kind of programs, incorporated in the developing environment of a programming language, that goes through the code line-by-line, executing each command immediately, and then proceed to the next command. MATLAB® is an interpreter and not a compiler as other programming languages. This means that each statement in a script file is translated (interpreted) into a language the computer understands (machine language) and is immediately executed, line by line, or statement by statement. So, MATLAB® script files are interpreted, rather than compiled. Therefore, the correct terminology is that the code written in MATLAB® is a script, and not a program.

9.3 Variables

In any problem, the quantities to be calculated and the quantities they depend on are called variables—dependent and independent variables, respectively—while unchanged quantities are called constants. However, all of them are treated by MATLAB® as variables. Variables are fundamental to programming. They are used in mathematical expression, in decision-making processes or as loop counters. In MATLAB®, a variable is determined by its name, made of a letter, or a combination of letters and digits. Variables are used in mathematical expressions, in functions and in any other MATLAB® statement and command.

A variable is created by assigning directly a value to it, or by the output of a function. In MATLAB®, the sign "=" is used to assigns a value to a variable and, therefore, it is called the assignment operator. The corresponding statement has the form

```
Variable_name = A numerical value, or a computable expression
```

In this statement, the left-hand side of the assignment operator can include only one variable name, while the right-hand side can be a number, a computable mathematical, or logical, expression. They may include numbers and/or other variables that were previously assigned an appropriate value as well as operators. When the script is executed the calculated value (numerical, string or logical) of the expression in the right-hand side is computed and assigned to the variable. Then, the content of the variable, its value, can be displayed, saved, exported to applications outside MATLAB®, or used in other statements, commands and functions in various ways. Similarly, data from files outside MATLAB® can be imported and used in a script by assigning them to a variable.

In most cases, the variables are defined and assigned a value in the script file. However, there are cases where we want to run a script or a part of it with different variable values that must be chosen during the execution process. In these cases, the assignment of a value to a variable can be done in the Command Window using the

input command for creating the variable or assigning a new value to it. The *input* command has the following form:

```
variable_name = input('string with a message that is
          displayed in the Command Window')
```

When the *input* command is executed as the script file runs, a message is displayed in the Command Window, prompting the user to enter a value that will be assigned to the variable. The user types the value and presses the enter key. This assigns the value to the variable.

However, when a script is executed, or a command is typed in the Command Window and then the enter key is pressed, MATLAB® apart from calculating the value of the variable and assigning it to the variable, it also displays the variable and its value in the Command Window. Sometimes this may be irritating. For this reason, we can type a semicolon (;) at the end of a command to prevent MATLAB® from displaying a variable and its value.

In MATLAB®, several assignments, command or other expressions can be typed in the same line, but they must be separated with a comma (spaces can be added after the comma or the semicolon). In these cases, the assignments, the commands or the other expressions are executed from left to right and the variables and their values are always displayed, except for a semicolon is typed instead of the comma.

In MATLAB®, a variable name must comply with several well-defined rules. It must start with a letter and it can consist only of letters, digits and the underscore character. It cannot contain any punctuation characters (e.g., period, comma, semicolon), or space between characters (we can use the underscore instead of it).

Although variable names can be of any length, MATLAB® uses only the first 63 characters of the name and ignores the rest. Therefore, each variable name must be unique at least in the first 63 characters to enable MATLAB® to distinguish variables. In addition, MATLAB® is case-sensitive in variable names. This means that it distinguishes between upper and lowercase letters. Thus, the variable x is different from the variable X, and mirrorlength, Mirrorlength and MirrorLength, are three different variables. Command and function names are also case-sensitive. Hence, since excessive lengthy names may lead to code error, it is a good practice to use capital and lowercase letters, as well as numbers in variable names to distinguish them.

Lastly, MATLAB® reserves a list of keywords for specific purposes, e.g. functions' names. For this reason, it would be advisable to avoid using the name of a built-in function for a variable (i.e., avoid using cos, sin, exp, sqrt, etc.), because, once a built-in function name is used for a user-defined variable name, the function cannot be used. The same applies for all built-in functions and user-created scripts with the same name. When the MATLAB® interpreter comes across a name in a script, it checks first if this name is a variable. Next, it looks in the Current Directory for a script file with this name, and after that, it seeks for a built-in function.

9.3.1 Statements

Essentially, any line we type in a script file is a statement. So, a statement can be an assignment, an array operation or simply an expression of the form:

```
Variable = expression
```

An expression is a formula consisting of variables, numbers, operators and function names. A statement that is too long to fit on one line may be continued to the next line with an ellipsis of at least three dots (…).

Statements on the same line must be separated by commas (output not suppressed) or semicolons (output suppressed). The distinction between MATLAB® statements, commands and functions may be a little diffusing, since all can be part of a script file. However, command, in generally, affects the working environment in some way, for example, the command *clear*. On the other hand, statements are usually associated with programming to solve a problem (mathematical or logical expressions, assignments, decision and loops). Lastly, functions usually return a calculated value, such as sin or cos, or perform some operation on data, such as creating a related plot.

9.3.2 Scalars, Vector and Matrices

Unlike most programming languages, MATLAB® language provides mathematical expressions that involve entire matrices. In fact, all variables in MATLAB®, scalars, vectors and matrices, are arrays, as MATLAB® is written to work with matrices. The official MATLAB® documentation refers to all variables as arrays, whether they are single-valued (scalars) or multi-valued (vectors or matrices). In other words, a scalar is an one-by-one array with one element, a vector is equivalent to what is called a one-dimensional array with one row or one column of elements, and a matrix is a two-dimensional array with elements in rows and columns. Any variable in MATLAB® (scalar, vector or matrix) is defined by assigning to it its values without the need to define its size (the dimension of the corresponding array) before the elements (values) are assigned. When MATLAB® encounters a new variable name, it automatically creates the variable and allocates the appropriate amount of storage. If the variable already exists, MATLAB® changes its contents and, if necessary, allocates new storage.

An array is a collection of values that are represented by a single variable name. As a matrix is a two-dimensional array of values organized in rows and columns, its general form is:

$$\mathbf{a} = \begin{bmatrix} a_{11} & a_{12} & a_{13} & \dots & a_{1n} \\ a_{21} & a_{22} & a_{23} & \dots & a_{2n} \\ & \cdot & & \cdot & \cdot \\ & \cdot & & \cdot & \cdot \\ & \cdot & & \cdot & \cdot \\ a_{m1} & a_{m2} & a_{m3} & \dots & a_{mn} \end{bmatrix} \begin{matrix} \\ \\ \\ \\ \\ \leftarrow \text{Row } 2 \end{matrix} \qquad \begin{matrix} \\ \\ \\ \\ \\ \uparrow \\ \text{Column } 3 \end{matrix}$$

$$= a_{ij}, \begin{cases} i = 1, 2, \dots, m \\ j = 1, 2, \dots, n \end{cases}$$

Matrix **a** has m rows and n columns, so it is an $m \times n$ matrix. Matrices where $m = n$ are called square matrices. The main diagonal of a square matrix is the set of elements a_{ij} for which the row and column indices are the same $i = j$. Sometimes it is called just the diagonal. One special form of square matrices is the identity matrix, which is a diagonal matrix, a matrix with all elements equal to zero except for the main diagonal, where all elements on the diagonal are equal to 1 ($a_{ij} = 1$ for $i = j$ and $a_{ij} = 0$ for $i \neq j$). For example, the 3×3 identity matrix is:

$$\mathbf{I} = \begin{bmatrix} 1 & 0 & 0 \\ 0 & 1 & 0 \\ 0 & 0 & 1 \end{bmatrix}$$

Generally, accepted mathematical notation uses the capital letter I to denote identity matrices. MATLAB® has the built-in function *eye* that can create an $n \times n$ identity matrix, given the value of n: $I_{\mathbf{n}} = eye(n)$.

Any element in a matrix can be plucked out by using the row and column indices, that identify its location, enclosed in brackets: $a_{ij} = \mathbf{a}(i, j)$. The first index, i, always identifies the row number, counted from top to bottom, and the second index, j, always is the column number, counted from left to right. Two matrices, **a** and **b**, are equal only if they have the same dimensions (the same size) and all corresponding elements are equal to each other: $\mathbf{a} = \mathbf{b}$ if $a_{ij} = b_{ij}$ for all i, j.

On the other hand, vectors are a special type of matrices, having only one row (a horizontal set of elements), or one column (a vertical set of elements), or in other words, one of their dimensions (either m or n) is equal to 1. A row vector is a $1 \times n$ matrix, while a column vector is an $m \times 1$ matrix:

$$\text{Row Vector} : \mathbf{a} = \begin{bmatrix} a_1 & a_2 & \dots & a_n \end{bmatrix}, \quad \text{Column Vector} : \mathbf{a} = \begin{bmatrix} a_1 \\ a_2 \\ \cdot \\ \cdot \\ \cdot \\ a_n \end{bmatrix}$$

9.3.3 Creating Vector and Matrices

There are several ways to create a row vector variable. The most direct way is to type its values in square brackets, separated by spaces or commas: $\mathbf{a} = [1\,2\,3\,4]$, or $\mathbf{a} = [1, 2, 3, 4]$. If the values in the vector are regularly spaced, the colon operator (:) can be used to assign these values to the vector. For example, the statement $\mathbf{v} = 1 : 5$ is equivalent to $\mathbf{a} = [1\,2\,3\,4\,5]$, (the elements of the vector **a** are all integers from 1 to 5). In this case, the brackets [ ] are not necessary to define the vector. With the colon operator, a step value (an increment) can also be used separated by another colon, in the form *First Element: step: Last Element*. For example, to create a vector with all elements integers from 1 to 9 in steps of 2 we can type the statement: $\mathbf{a} = 1 : 2 : 9$ ($\mathbf{a} = [1\,3\,5\,7\,9]$). Similarly, the statement $\mathbf{a} = 10 : -1 : 1$ creates a row vector which elements are the integers 10, 9, …, 1, since the increment is negative. If the *First Element*, the *Last Element* and the *step* are such that the value of *Last Element* cannot be obtained by adding an integer number of *step* to *First Element*, then the last element in the vector will be the last number that does not exceed the *Last Element*. If only two numbers (the *First Element* and the *Last Element*) are typed (the spacing is omitted), then the default for the spacing is 1.

Another way to create vectors of equally spaced points is the *linspace* function. It can be used to create a linearly (equally) spaced vector with n values from x to y by typing the statement **a** = *linspace*(x, y, n). If the number of elements n is omitted, then the function *linspace* automatically generates 100 points.

All vectors examined so far are row vectors. One way to create a column vector —that is often needed in mathematics—is by typing its values in square brackets, separated by semicolons: $\mathbf{b} = [1;\ 2;\ 3;\ 4]$. Unfortunately, there is no direct way to use the colon operator described above to get a column vector. However, we can transpose any row vector to get a column vector. So, a column vector can be created using an existing row vector created with anyone of the above methods. In general, the transpose of a matrix is a new matrix in which the rows and columns are interchanged. So, transposing a row vector results in a column vector, and transposing a column vector results in a row vector. MATLAB® has a built-in operator, the apostrophe (’), to transpose a matrix, e.g. if $\mathbf{a} = 1 : 4$, then $\mathbf{b} = \mathbf{a}'$.

A two-dimensional array, also called a matrix, has elements in rows and columns. An $m \times n$ matrix has m rows and n columns and can be created by typing its elements row by row, inside square brackets [ ]. First we type the first row, separating the elements with spaces or commas, and then to type the next row, first we have to type a semicolon (;) or press the enter key.

9.4 Array and Matrix Operations

9.4.1 Array Operations or Element-by-Element Operations

There are several common operations on matrices. Some of them are applied term by term, or element by element, implying that the matrices must be the same size. They are referred to as ***array operations***. These include addition, subtraction and scalar multiplication.

Matrix addition means adding two matrices term by term. In mathematical terms, this is written by $c_{ij} = a_{ij} + b_{ij}$. In most languages, this task would be accomplished using an appropriate loop (a nested FOR loop). However, in MATLAB®, this is accomplished with the operator "+": $\mathbf{c} = \mathbf{a} + \mathbf{b}$. The use of a nested FOR loop is still possible in MATLAB®. Similarly, matrix subtraction means to subtract them term by term, $c_{ij} = a_{ij} - b_{ij}$. This could also be accomplished using a nested FOR loop, as in most languages, but in MATLAB® we can use the "−" operator: $\mathbf{c} = \mathbf{a} - \mathbf{b}$. Scalar multiplication means to multiply every element of a matrix by a scalar (a number). This would also be accomplished using a nested FOR loop as in most languages, but using the "*" operator in MATLAB® is more convenient. Similarly, we can add (or subtract) a scalar to an array, element by element in the same way as above. When a scalar (number) is added to (or subtracted from) an array, the scalar is added to (or subtracted from) all elements of the array.

However, element-by-element multiplication, division or exponentiation of two vectors or matrices is carried out by using special operators (array multiplication, division or exponentiation). They are the corresponding matrix operators with a period (a dot) in front of them: * → .* (element-by-element multiplication, $c_{ij} = a_{ij} \cdot b_{ij}$), / → ./ (element-by element-right division, $c_{ij} = a_{ij}/b_{ij}$), \ → .\ (element-by-element left division, $c_{ij} = a_{ij} \backslash b_{ij}$), and ^ → .^ (element-by-element exponentiation, $c_{ij} = a_{ij}^{b_{ij}}$).

Element-by-element calculations are very useful for calculating the value of multiple dimensional variables without using a (nested) for loop (repetition). This can be done by defining vectors or matrices that contain the values of the independent variables, and then using them in mathematical expressions with element-by-element operators. The computations are carried out creating a new vector, or matrix, in which each element is the corresponding value of the dependent variable.

When the argument (input) of a built-in function in MATLAB® is an array the function is executed on each element of the array (element-by-element operation of the function) and its result (output) is an array in which each element is calculated as if we were entering the corresponding element of the array into the function one by one. For example, if **a** is a vector with ten elements, then, if it is substituted in the function *log*, *log*(**a**), the result is a vector with ten elements in which each one is the natural logarithm of the corresponding element in **a**. Most functions, such as *sqrt*, *abs*, sin, *acos*, *tanh* and *exp*, operate in array fashion.

To recapitulate, MATLAB® has four additional arithmetic operators (.*, ./., .\ and .^), that work on corresponding elements of arrays with equal dimensions. They are sometimes called array, or element-by-element, operations because they are performed element by element. For example if **a** and **b** are two vectors with the same size (dimension) the expression **a**.^**b** means that the *i*th element of the first vector is raised to the power of the *i*th element of the second vector. The period (dot, .) is necessary for the array operations of multiplication, division, and exponentiation because these operations are defined differently for matrices. There they are called matrix operations, as we will see latter. For addition and subtraction, array operations and matrix operations are the same, so we do not need the period to distinguish them. Array operations also apply between a scalar and a non-scalar (vectors or matrices) variable. The multiplication of a matrix **a** by a scalar g is obtained by multiplying every element of **a** by g. Multiplication and division operations between scalars and non-scalars can be written with or without the period. Obviously, the same applies for operations between two scalar variables.

9.4.2 Matrix Operations

Array operations are performed element by element on matrices. However, the real power of MATLAB® is its ability to carry out vector-matrix calculations. Matrix operations are based in matrix algebra and in some cases they are defined differently than array operations. Matrix addition and subtraction are the same as in the equivalent array operations (i.e., element by element), but multiplication is quite different. Matrix multiplication does not mean multiplication term by term; it is not an array operation.

Matrix multiplication is probably the most important matrix operation and it is carried out according to the rules of linear algebra. It is used in solving linear systems of equations, and transformations of coordinate systems, to name only a few. When two matrices **A** and **B** are multiplied, their product is a third matrix **C**. MATLAB® uses a single asterisk (*) to denote matrix multiplication. Therefore, the operation is written as **C** = **A***B.

A matrix **A** can be multiplied by a matrix **B** resulting in a matrix **C**, only if the number of columns of **A** is equal to the number of rows of **B**. In other words, if the matrix **A** has dimensions $m \times n$, the matrix **B** must have dimensions $n \times$ *something else* (=p), or else the inner dimensions must be the same. Then, the resulting matrix **C** will have the same number of rows as **A** and the same number of columns as **B**. It will be an $m \times p$ matrix, (the outer dimensions of matrices **A** and **B**). For example, if **A** is 2×3 matrix and **B** is 3×4 matrix, **C** will be a 2×4 matrix. Taking this into account, we deduce that the product of the multiplication of two square matrices of the same size is another square matrix of the same size.

Each element of the matrix **C**, c_{ij}, is formed by taking the product of the corresponding elements of the *i*th row of matrix **A** with the corresponding elements of the *j*th column of matrix **B**, element-by-element multiplication and summing up the individual products:

$$c_{ij} = \sum_{k=1}^{n} a_{ik} b_{kj}$$

where n is the column dimension of matrix **A** and the row dimension of matrix **B**. Thus, matrices **A** and **B** can be successfully multiplied only if the number of columns in **A** is the same as the number of rows in **B**.

If the dimensions of the matrices are suitable, matrix multiplication is associative $(\mathbf{A} * \mathbf{B}) * \mathbf{C} = \mathbf{A} * (\mathbf{B} * \mathbf{C})$, and distributive $\mathbf{A} * (\mathbf{B} + \mathbf{C}) = \mathbf{A} * \mathbf{B} + \mathbf{A} * \mathbf{C}$ or $(\mathbf{A} + \mathbf{B}) * \mathbf{C} = \mathbf{A} * \mathbf{C} + \mathbf{B} * \mathbf{C}$. However, multiplication is not generally commutative $\mathbf{A} * \mathbf{B} \neq \mathbf{B} * \mathbf{A}$. That means that, the order of matrix multiplication is important.

Since vectors are just special cases of matrices, all matrix operations described earlier (addition, subtraction, scalar multiplication, multiplication, transpose, as it will be presented later) can be applied on vectors as well, as long as the dimensions are correct. In other words, two vectors can be multiplied only if they have the same number of elements, and one is a row vector and the other is a column vector.

The dot product, or inner product or scalar product, of two vectors **x** and **y** is written as $\mathbf{x} \cdot \mathbf{y}$, and is defined as

$$\mathbf{x} \cdot \mathbf{y} = \sum_{i=1}^{n} x_i y_i$$

It is like matrix multiplication when multiplying a row vector **x** by a column vector **y**. Thus, if **x** is a $1 \times n$ matrix, a row vector, **y** should be an $n \times 1$ matrix, a column vector. In this case, the resulting matrix would have the dimension of 1×1, which is a scalar, a one-dimensional matrix. Hence, the multiplication of a row vector by a column vector gives a scalar, the dot, or inner, product of the two vectors. This can be accomplished using the * operator and transposing the second vector, or by using the *dot* function in MATLAB®: **x***y' or *dot*(**x**, **y**).

The cross-product, or outer product, $\mathbf{x} \times \mathbf{y}$, of two vectors **x** and **y** makes sense only if both are vectors in the three-dimensional space, which means that they both must have three elements. It can be calculated using the built-in MATLAB® function *cross*: *cross*(**x**, **y**).

The matrix multiplication also applies when a vector is multiplied by an appropriate matrix. This is the case of linear coordinate transformation. In this case, to multiply a vector by a matrix, the vector must be a row vector.

Another operator in matrix operations is the matrix transpose which interchanges the rows and columns of a matrix: the element a_{ij} of the transpose is equal to the a_{ji} element of the original matrix. The transpose of a matrix $\mathbf{A}$, is written as $\mathbf{A}^{\mathrm{T}}$ and, for example, for a 3×3 matrix and a 2×3 matrix it is

$$\mathbf{A} = \begin{bmatrix} a_{11} & a_{12} & a_{13} \\ a_{21} & a_{22} & a_{23} \\ a_{31} & a_{32} & a_{33} \end{bmatrix} \Rightarrow \mathbf{A}^{\mathrm{T}} = \begin{bmatrix} a_{11} & a_{21} & a_{31} \\ a_{12} & a_{22} & a_{32} \\ a_{12} & a_{23} & a_{33} \end{bmatrix}, \mathbf{A} = \begin{bmatrix} 1 & 2 & 3 \\ 4 & 5 & 6 \end{bmatrix} \Rightarrow \mathbf{A}^{\mathrm{T}} = \begin{bmatrix} 1 & 4 \\ 2 & 5 \\ 3 & 6 \end{bmatrix}$$

In MATLAB®, there is a built-in transpose operator, the apostrophe (’): $\mathbf{A}^{\mathrm{T}} \equiv \mathbf{A}$’.

The transpose operator has a variety of application in matrix algebra. Since it is not as easy to create a column vector as to create a row vector, we can first create a row vector and then the corresponding column vector by transposing the row vector. Obviously, vectors can be transposed from a row vectors to a column vectors and vice versa:

$$\text{If } \mathbf{A} = [\, a_1 \quad a_2 \quad \ldots \quad a_n \,], \quad \text{then } \mathbf{A}^{\mathrm{T}} = \begin{bmatrix} a_1 \\ a_2 \\ \cdot \\ \cdot \\ \cdot \\ a_n \end{bmatrix}$$

The matrix division operation is also associated with the rules of linear algebra. This operation is more complex. It can be explained with the help of the identity matrix and the inverse operation. When the identity matrix, $\mathbf{I}$, multiplies another matrix (or vector), $\mathbf{A}$, that matrix (or vector), $\mathbf{A}$, is unchanged (the multiplication has to be done according to the rules of linear algebra) $\mathbf{A} * \mathbf{I} = \mathbf{I} * \mathbf{A} = \mathbf{A}$. This is equivalent to multiplying a scalar by 1. Similarly, if the result of multiplying a matrix $\mathbf{A}$ by a matrix $\mathbf{B}$ is the identity matrix, then matrix $\mathbf{B}$ is the inverse of matrix $\mathbf{A}$, which is written as $\mathbf{A}^{-1}$, so that $\mathbf{A} * \mathbf{A}^{-1} = \mathbf{A}^{-1} * \mathbf{A} = \mathbf{I}$. Obviously $\mathbf{B}$ is the inverse of $\mathbf{A}$, and $\mathbf{A}$ is the inverse of $\mathbf{B}$. Thus, the multiplication of a matrix $\mathbf{A}$ by the inverse, $\mathbf{B}^{-1}$, of another matrix, $\mathbf{B}$, is analogous to division.

In order to compute the inverse $\mathbf{A}^{-1}$ of a matrix, we can use the MATLAB® built-in function *inv*, or by raising matrix $\mathbf{A}$ to the power of -1: $\mathbf{A}^{-1} \equiv \mathrm{inv}(\mathbf{A}) = \mathbf{A}^{\wedge} - 1$ (the operator ^ we be presented later in this paragraph). However, although matrix multiplication is possible, as long as the inner dimensions of the matrices are the same, matrix division is not always possible. Not every matrix has an inverse. A matrix $\mathbf{A}$ has an inverse, $\mathbf{A}^{-1}$, only if it is square and its determinant (MATLAB® built-in function *det*) is not equal to zero.

The matrix operation $\mathbf{A}^2$ means $\mathbf{A} \times \mathbf{A}$, where $\mathbf{A}$ must be a square matrix. For matrix exponentiation, the operator ^ is used in the statement **A**^2. This is the same as **A***A, matrix multiplication of **A** with itself, different form element-by-element multiplication that is accomplished with the operator .^, e.g. **A**.^2.

The square norm of a vector **a**,

$$\|\mathbf{a}\| = \sqrt{\sum_{i=1}^{n} (x_i)^2}$$

which corresponds to its Euclidean length, can be calculated using the built-in MATLAB® function *norm*: *norm*(**a**,2) or simply *norm*(**a**).

As several operations may be combined in one expression, MATLAB® has strict precedence rules. When parentheses are used, they have the highest precedence. In MATLAB®, there is a difference between parentheses and square brackets. Parentheses are used to alter the precedence of operators and to denote array subscripts, while square brackets are used to create vectors. When operators in the same expression have the same precedence, the operations are carried out from left to right. The mathematical operators (matrix and array operators) and their priority order, from highest to lowest, are: ^ (and .^) (exponentiation), ' (transpose), * (.*), / (./), \ (.\) (multiplication and division, of the same precedence), and + and − (addition and subtraction, of the same precedence).

9.5 Decision-Making Structures

In step-by-step sequential structure of a script, all statements are executed in sequence. However, this is not always desired. Changing the flow of a program entails a decision-making process, so that the computer to be able to decide whether to execute the next command or to skip it and continue with the rest of the code. These decisions are made based on the outcome of logical condition, which compare variables using relational and logical operators. Fortunately, MATLAB® selection statements provide a means to split the program's flow into branches.

There are some basic ways for branching the flow of a program. The most simple is the single decision, IF/THEN structure, allows the execution of a group of statements if a logical condition is true. If it is false, nothing happens and the program moves directly to the next statement following the END of the structure. This structure is fundamental to all computer programming languages and the basis of decision-making. The double decision, IF/THEN/ELSE structure, behaves in the same manner as the single IF structure if the condition is true, but in the case the condition is false, the program executes the part of the code place between the ELSE statement and the END of the structure. Although these simple structures are sufficient for the development of any numerical algorithm, there are also other variants. The IF/THEN/ELSEIF structures, or other combinations of the basic

structures, like nested statements, are frequently used. Lastly, another flow branching method can be implemented by using the SWITCH/CASE structure.

9.5.1 The IF Statement

The IF statement is used when we have to decide whether a statement, or a group of statements, is to be executed or not. Its general form is:

```
if condition
   action
end
```

However, the simplest form of IF statement on a single line is:

```
If condition action end
```

The *condition* is usually a logical expression (relational expression, or Boolean expression), which is either true or false. The *action* is a statement, or a group of statements, that will be executed if the *condition* is true. In fact, the *action* can be any number of statements until the reserved word END. When the IF statement is executed, first the *condition* is evaluated. If the *condition* is true, the *action* is executed, but if it is false, nothing happens.

The *condition* may be a vector or a matrix. In this case, the *condition* is true only if all elements of the vector or the matrix are nonzero. Logical expressions use both relational operators, which relate two expressions of compatible types, and logical operators, which operate on logical operands.

9.5.2 The IF-Else Statement

While the IF statement is used to choose whether an action is executed or not, in order to choose between two actions (two single statements, or two sets of statements) the IF-ELSE statement is used. Its general form is:

```
if condition
   action1
else
   action2
end
```

Again, first, the *condition* is evaluated. If it is true, the first set of statements is executed. Otherwise, if the *condition* is false, the second set of statements is executed. Always, only one of the two *actions* will be executed, which one depends on the value of the *condition*.

The simplest general form of IF-ELSE structure is on one line:

```
if condition statement_1, else statement_2, end
```

In this case, commas (or semicolons) are essential between the various clauses, while the use of the reserved word END is mandatory. Without it, MATLAB® will wait forever.

9.5.3 Nested IF-Else Statements

However, in order to choose among more than just two statements, we can use nested IF-ELSE statements (one inside another), or more than one separate IF statements. The last choice, is not very efficient, as all Boolean expressions must be evaluated, regardless of the outcome of the previously checked IF *conditions* (=all *conditions* are always tested, even if the first one is true). Instead of this, we can use nested IF-ELSE structures so that the procedure ends after an expression is found to be true (=not all conditions are checked).

Its general form is:

```
if condition_1
   action_1
else if condition_2
       action_2
   else if condition_3
 &160;         action_3
      else if condition_4
             action_4
      end % of else No. 3 (action_4)
   end % of else No. 2 (action_3)
end % of else No. 1 (action_3)
```

9.5.4 IF-Else Statements

However, except for this structure, MATLAB® has another method to accomplishing this task, the ELSEIF clause. For example, if there are n choices (where $n > 3$), the following general form could be used:

```
if condition_1
    action_1
elseif condition_2
    action_2
elseif condition_3
    action_3
...
else
    action_n
end
```

The actions of the IF, ELSEIFs, and ELSE clauses are bracketed by the pairs of reserved words IF and ELSEIF, ELSEIF and ELSEIF, ELSEIF and ELSE, and ELSE and END.

So, there are three main ways of accomplishing the choice of an action among more than two actions: (a) using separate IF statements, (b) using nested IF-ELSE statements, and (c) using an IF statement with ELSEIF clauses. The last option is the simplest and the better.

9.5.5 The Switch Statement

Instead of using a nested IF-ELSE, or an IF statement with many ELSEIF clauses, there is another option in MATLAB®, the SWITCH statement. It is used when an expression is tested to see whether it is equal to one of several possible values.

The general form of the SWITCH statement is:

```
switch switch_expression
   case case_value_1
       action_1
   case case_value_2
       action_2
   case case_value_3
       action_3
   ...
   otherwise
       action_n
   end
```

The SWITCH statement starts with the reserved word SWITCH and ends with the reserved word END. The *switch_expression* is compared, in sequence, to the *case values* (*case_value_1, case_value_2,* etc.). If, for example, the value of the *switch_expression* matches *case_value_1*, then *action1* is executed and the switch statement ends. If the value matches *case_value*_3, then *action3* is executed, and, in general, if the value matches *case_value_i*, where *i* is any integer from 1 to *n*, then *action_i* is executed. If the value of the *switch_ expression* does not match any of the case values, the *action_n* after the word OTHERWISE is executed.

9.6 Relational and Logical Operators

A conditional statement is a command that allows MATLAB® to make a decision of whether to execute a group of commands that follow this statement or to skip these commands. A conditional statement compares two values, which may be constants, variables or whole expressions, to find whether the comparison statement is true or false. If the expression is true, a group of commands that follow the statement are executed. If the expression is false, the computer skips this group. The general form of a conditional statement is:

constant1		constant2
variable1	relation(relational operator)	variable2
or expressions1		or expressions2

Relational operators examine a logical statement and produce a result which is true or false according to specific operators. Relational operators are used as arithmetic operators in mathematical expressions in combination with other commands, to make a decision that controls the flow of a computer program. The relational operators are: > greater then, < less than, $\geq$ greater than or equals, $\leq$ less than or equals, == equality, and $\sim=$ inequality. The operator for equality is two consecutive equal signs (==) (with no space between them), not a single equal sign (=), since it is the assignment operator). In all relational operators that consist of two characters, there also is no space between them ($\leq$, $\geq$, $\sim=$).

The aforementioned operators allow the comparison of the values of two variables or expressions (relational operators). However, MATLAB® allows testing of more than one logical condition by employing logical operators on logical or Boolean operands. In MATLAB®, the logical true is represented by the integer 1 and the logical false by the integer 0. Therefore, logical operations could also be performed with 1 and 0, as well as mathematical operations could be performed on the resulting 1 or 0, the outcomes of the logical operators.

The NOT ($\sim$) operator takes a Boolean expression, which is true or false, and give the opposite value. The OR (|) operator has two Boolean expressions as

operands. The result is true if one or both of the operands are true and false only if both of them are false. The AND (&) operator also operates on two Boolean operands. The result of an AND expression is true only if both operands are true and it is false if one or both of them are false. Lastly, in addition to these logical operators, MATLAB® has built-in logical functions that are equivalent to them. These functions are: *and*(A,B) equivalent to A&B, *or*(A,B) equivalent to A|B, and *not*(A) equivalent to ∼ A. MATLAB® has another logical built-in functions: the function *xor*, the exclusive or. It returns true only if one of its arguments is true.

Arithmetic, relational and logical operators can be combined in mathematical expressions. Just as for arithmetic operations, when an expression has a combination of more than two arithmetic, relational and logical operators, the result depends on the order they are carried out, their precedence rules. The priority order for evaluating logical operations, from highest to lowest, is: ∼, & and |. If there are two or more operations that have the same precedence, the expression is executed from left to right. Finally, as with arithmetic operators, parentheses can be used to override the priority order. The order of precedence for all mathematical, relational and logical operators, from highest to lowest, is: parentheses (if nested parentheses exist, inner ones have precedence), exponentiation, logical NOT (∼), multiplication/division, addition/subtraction, relational operators (>, <, ≥, ≤, ==, ∼=, with equal precedence), logical AND(&), and logical OR(|) (with the lowest precedence).

9.7 Statements' Iteration or Statements' Loops

Many problem-solving codes that use numerical methods, as this one described in Chaps. 7 and 8, involve a number of calculations that need to be carried out repeatedly. Usually, the solution of a mathematical problem is obtained by computing successive approximations starting from an initial guess. The statements to accomplish this task are called looping statements, or loops. The action of the loop, the statements to be repeated, is repeated several times consecutively.

There are two basic kinds of loops in programming, the counted loops and the conditional loops. Consequently, there are two different loop statements in MATLAB®, the FOR statement and the WHILE statement.

In a counted loop, the group of statements to be repeated, the loop action, is repeated a specified number of times, which is known beforehand. Since in these cases the number of repetitions must be determined in advance, they are also called determinate repetition. On the other hand, conditional loops repeat a group of statements until a specific condition becomes false. Therefore, the exact number of iterations is unknown, and these iteration procedures are called indeterminate. The FOR statement is used for counted loops and the WHILE statements for conditional loops.

9.7.1 FOR Loops

A FOR loop has the following general form:

```
for loopvariable = range
   action
end
```

where *loopvariable* is the loop variable, *range* is the group of values which the loop variable will take during each iteration (a different value each time), and the *action* of the loop consists of all statements up to the END. The name usually used for the *loopvariable* is *i*, and if more than one loop variables are needed, *j*, *k*, *l*, *m*, *n*, etc. are usually used. However, in MATLAB® both *i* and *j* are internally reserved values for $\sqrt{-1}$. So using them as loop variable names will override that value. However, unless this does not cause any problem, we do not use complex number, it is acceptable to use *i* as a loop variable. On the other hand, although, the *range* of the iteration variable values can be specified using a vector, it easier to specify it using the colon operator. Lastly, if the *action* of the loop includes another loop, the latter is called a nested FOR loop. The first FOR loop is the outer loop and the second loop is the inner loop. Usually, if it concerns array calculations, the outer loop is over the rows, and the inner loop is over the columns.

The most common form of a FOR loop is

```
for index_1 = j:k
    statements
end
```

or

```
for index_2 = j:m:k
    statements
end
```

where *index_1* takes the values j, $j+1, j+2, \ldots, k$, while *index_2* takes the values $j, j+m, j+2\cdot m, \ldots$, such that the last element does not exceed k, if $m > 0$, or it is not less than k if $m < 0$ (m is the step, or increment, j the start and k the finish).

As in the case of IF statements, FOR statements can be typed in a single line:

```
for index = j:k, statements, end
```

or

```
for index = j:m:k, statements, end
```

In this case, the statements must be separated by commas or semicolons.

There are situations where a FOR loop is essential, however, although FOR loops are extremely useful in most other programming languages, in MATLAB® they are not always necessary, especially when dealing with arrays. In MATLAB®, we can replace the code of traditional programming languages that implement loops by matrix operations. This is called vectorizing or vectorization. In most programming languages, when performing an operation on a vector or a matrix, one or two FOR loops are used to carry out the calculations through the entire vector or matrix. However, as MATLAB® is written specifically to work with vectors and matrices, many operations and functions work directly with vectors and matrices.

9.7.2 WHILE Loops

If the required number of iterations is not known, and the statements repetition depends on a condition, then the WHILE statement is used. Its general form is:

```
while condition
   action
end
```

The *action*, which may consist of any number of statements, is executed as long as the *condition* is true. First the *condition* is evaluated and if it is true, the *action* is executed. After that, the *condition* is evaluated again. If it is still true, the *action* is executed again. Hence, in order to avoid an infinite loop the *condition* must somehow become false as the statements contained in *action* are executed. In other words, the value of the *condition* must eventually be changed to false in the body of the loop to terminate it, otherwise the looping will continue indefinitely (indefinite loop). If this happens, we can stop the indefinite executions by pressing the *Ctrl +C* or *Ctrl+Break* keys.

The implementation of most iterative solution methods involves decision loops: the approximation process is repeated until the error of the approximate solution falls below a predefined criterion.

9.8 Displaying and Saving Results

MATLAB® automatically displays on the Command Window results calculated by the execution of an expression or an assignment, or other appropriate command. We also can prevent MATLAB® from displaying this output by typing at the end of the command a semicolon (;). In addition to this automatic display, MATLAB® has several commands that can be used to generate customized displays, as well as

messages that provide information, numerical data, results of calculations, and plots, either in the Command Window, or to save them in a file for further editing and use. In the first case, we can use *cut* and *paste* to capture, save and then edit them, while, a more convenient way of capturing output is by using the appropriate MATLAB® commands and save them immediately in an ASCCI file.

Two ways are frequently used in MATLAB® scripts to generate output, the *disp* command and the *fprintf* command. The *disp* command displays the output on the screen, while the *fprintf* command can be used to display them on the screen or to write them to a file, when it is necessary to save the output. Writing to a file is essential. This way we can save the results of our calculation and use them any time later. The saved data can subsequently be displayed or used in MATLAB® and/or in other applications.

The *fprintf* command is a lower level functions that can be used to write data to a file and also to append new data to it. In addition, it allows to mix strings and numbers on the same line and to completely control the format of the output (e.g., number of decimal places). However, as the exact control of the output format is simpler with the *fprintf* command, we will not deal with *disp* statement anymore and we will focus on the *fprintf* command.

Before data can be written to a file, the file must be open, and we should close it once the writing (or appending) process has been completed. The whole process involves the following three steps:

- Opening of the file
- Writing (or appending) to the file
- Closing the file.

Files are opened with the *fopen* function, which creates a new file or opens an existing file. By default, it opens a file for reading. If another mode (e.g., writing or appending) is desired, a permission string must be is used to specify it.

Writing to a file means writing to it from the beginning. Appending to a file is also writing but starting at the end of the file and not at the beginning (adding data to what is already there). There are many different file types, which use different filename extensions. We will keep it simple and just work with files in the ASCII format, which typically use either the extension *.dat* or *.txt*.

The general form of the *fopen* function is:

```
fid=fopen('filename', 'permission string')
```

```
fid = fopen('filename', 'permission string')
```

The *fopen* function returns the value −1 if the file opening it is not successful, or else an integer value assigned to the variable *fid*, which becomes the file identifier. The latter can be used to refer to the file when calling other file functions. The *filename* is written (including its extension) within single quotes as a string. The *permission* is a code (also written as a string) that tells how the file is opened. Some of the more common permission codes are:

- "*r*": Opens a file for reading (default).
- "*w*": Opens a file for writing. If the file already exists, its content is deleted. If the file does not exist, a new file is created.
- "*a*": The same as "w", except that if the file exists the written data is appended to the end of the file.
- "*r*+": Opens a (does not create) file for reading and writing.
- "*w*+": Opens a file for reading and writing. If the file already exists, its content is deleted. If the file does not exist, a new file is created.
- "*a*+": The same as "w+", except that if the file exists, the written data is appended to the end of the file.

If a permission code is not included in the command, the file opens with the default code "*r*".

Once the file is open, the *fprintf* command can be used to write any output to the file. It is used in exactly the same way as it is used to display output in the Command Window, except for that now the value of the variable *fid* is inserted inside the command indicating the file to write to. The screen is the default output device, so if a file identifier is not specified, the output goes to the screen; otherwise, it goes to the specified file. The default file identifier number is 1 for the screen.

Since the *fprintf* command returns the number of bytes written to the file, it is advisable to use a semicolon after it to suppress the output on the computer screen (on the Command Window).

The *fprintf* command can be used to display several values per line with different formats. The general form of the *fprintf* command is

```
fprintf(fid,`format string',list of variables)
```

The *format string* is typed first. It contains any text to be printed, a message as well as formatting information for the data, placeholders and format specifiers. They control and specify where (placeholders: %) the variables listed are embedded in the format string and how their values will be displayed (specifiers).

MATLAB® starts at the left end of the string and displays the labels until it detects one of the symbols: % or \, recognizing that the following text is a format or control code. The symbol \ tells MATLAB® that the following character is a control code, while the symbol % is a placeholder that signifies the place where the variables' values are to be embedded in the format string. It must not be confused with the same symbol used to designate a comment. To display the % character in the text, we just have to type it twice %%. In addition, to place a single quotation mark in the displayed text, we must type two single quotation marks in the string inside the command (''). The format codes allow us to specify whether numeric values are displayed in integer, decimal or scientific format.

The *control codes* provide a means to perform actions such as skipping to the next line (control character *n*: \n) or adding a tab character (control character *t*: \t). To start a new line with the *fprintf* command, the control character \n must be typed

at the start of the string. When a program has more than one *fprintf* command, the display generated is continuous (the *fprintf* command does not automatically start a new line). This is true even if there are other commands between the *fprintf* commands. If we omit the code \n, MATLAB® after displaying the value of a variable, it continues displaying the next information at the end of the last line and not on the next line as it would typically be desired. Lastly, with the *fprintf* command it is possible to start a new line in the middle of the string by inserting the control code \n before the character that we want start the new line.

With the *fprintf* command, it is possible to insert more than one value (of more than one variable) within the text. This is done by typing % at the places in the text where the values are to be inserted. Then, after the string argument of the command (followed by a comma), the names of the variables are typed in the order they are to be inserted in the text. In general, the *fprintf* command has the form:

```
fprintf(fid, '..text...%g...%g...%f...', variable1,...
variable2, variable3, ...)
```

The most common *specifiers* are: *%d* for integer format, *%f* for decimal (floats) format, and *%e* (or *%E*) for scientific format with lowercase e (or uppercase E). A field width can also be included after the placeholder, %, and before the *specifier* in *fprintf*. This determines how many characters are to be used in printing in total, e.g. *x.y*. The field width and precision (*x.y* in the previous example) are optional. The first number, *x*, is the field width, which specifies the minimum number of digits in the display. The precision is the second number, *y*. It specifies the number of digits to be displayed to the right of the decimal point. If the field width is wider than necessary, blanks are printed, and if more decimal places are specified than necessary, zeros are printed.

The *fprintf* command is vectorized. This means that when a variable that is a vector, or a matrix, is included in the command, the command repeats itself until all elements are displayed. If the variable is a matrix, the data is used column by column. In the case of a vector, the sequence of *format specifiers* is repeated until all elements have been displayed.

Before the script ends, or when the writing of data to the file is complete, we should close the file to save the contained data. The function that closes a file is the *fclose* function, which returns 0 if the file has been closed successfully, or 1 if not. If more than one file is open, we can close each file individually by specifying its file identifier, or all files together by using the string "*all*" instead the file identifiers in the *fclose* function. The general form of the *fclose* function is

```
closeresult = fclose(fid),
```

or

```
closeresult = fclose('all')
```

The created file is saved in the current directory.

9.9 Plotting Results

Graphs are a very useful tool for presenting information and computations results. MATLAB® has many commands that can be used for presenting and visualizing data. We can create quickly and conveniently graphs with different types of plots, such as plots with linear, logarithmic or semi-logarithmic axes, bar and stairs plots, polar plots, three-dimensional contour surfaces and mesh plots, and many more. Two-dimensional (2D) graphs are created with the *plot* command. In its simplest form, it takes only a single vector as argument: *plot*(**y**). As we need data on two axes to create a plot, the elements of the vector **y**, $\mathbf{y}(1), \mathbf{y}(2), \mathbf{y}(3), \ldots$, are plotted against their indexes, the element number (1, 2, 3, …). However, the most common form of *plot* command is *plot*(**x**, **y**), where **x** and **y** are vectors of the same length. They must have the same number of elements. First we have to define the vector variable **x** (e.g. a 1×100 matrix), and then the variable **y**, using appropriate operations. We need to use enough x values to ensure that the resulting graph, drawn by connecting the dots of the points (x_i, y_i), will look smooth. Next we use the *plot* function taking as arguments the vectors **x** and **y**.

The first vector in the *plot* command is used for the horizontal axis, and the second vector for the vertical axis. This plot is a single curve with the **x** values on the abscissa (horizontal axis) and the **y** values on the ordinate (vertical axis). The curve is constructed of straight-line segments that connect the points whose coordinates are defined by the elements of the vectors **x** and **y**. Thus, the coordinates of the ith point are x_i, y_i. Straight-line graphs are drawn by giving the x- and y-coordinates of the start and endpoints in two vectors. Lastly, the *area* function creates a similar plot as the *plot* command, but it shades the area under the curve.

9.9.1 Customizing and Formatting Graphics and Plots Using Commands

When the *plot* command is executed, a figure is created in the Figure Window. If not already open, the Figure Window opens automatically when the *plot* command is executed. This command creates plots that usually need to be formatted in order to have a specific look and to display the right information in addition to the graph itself. By default, a plot is created with a solid thin blue line, and axes are automatically scaled to include the minimum and maximum data points. The plots can be formatted using MATLAB® formatting commands that follow the *plot* command.

In general, we can modify a graph in a number of ways. We can change the title above the graph, add a label on the horizontal axis or change the label on the vertical axis. Also, we can change the horizontal and vertical ranges of the graph axis. The line type (solid, dashed, etc.), colour and thickness (width) can be changed. Line markers, their size, edge and face (i.e., interior) colours, and grid

lines can be added, as text comments. If several graphs would be created in the same plot, containing different data points, a legend could be added to the plot.

We can change the style of a graph by modifying the colour of the line or the point markers of the plot using the *plot* command by adding a string as a third argument for every (*x,y*) pair. The *plot* command has additional, optional arguments that can be used to specify the colour and style of the line and the colour and type of markers, if any are desired. With these options, the plot command has the form:

```
plot(x,y,'line specifiers',Property name',Property Value)
```

where

- **x** and **y** values are vectors containing the *x*- and *y*-coordinates of points on the graph.
- *Line specifiers* are an optional argument, a character string that consists of 1, 2, or 3 characters, that specifies the colour, line-style, and the point markers style. The line colour specifiers are "*y*" for yellow, "m" for magenta, "*c*" for cyan, "*r*" for red, "*g*" for green, "*b*" for blue, "*w*" for white, and "*k*" for black. The point markers type specifiers are "*o*" for a circle, "*x*" for an × -mark, "+" for a plus sign, and "*" for a star. The line style specifiers are "−" for a solid line, ":" for a dotted line, and "−" for a dashed line. If a point style is given but no line style, then the points are plotted but no curve is drawn connecting them. The *line specifiers* are optional. This means that none, one, two, or all three types can be included in the *plot* command as a string. In addition, they can be typed in any order.
- *Property Name* and *Property Value* are optional and can be used to specify the thickness of the line, the size of the marker, and the colours of the marker's edge line and fill. The *Property Name* is typed as a string, followed by a comma and a value for the property, all inside the *plot* command. An example is the property *LineWidth* (its default value is 1, in point units), and another property is *MarkerSize* (its default value is 6, in point units).

To insert labels or text into a plot, we can use the commands *text*, *xlabel*, *ylabel*, *legend* and *title*. These commands take a string as input and various optional arguments that can be used to change the font family and font size of the text. There are many commands for controlling font size, tick labels and fonts, as well as for inserting mathematical equations. The most common plot formatting commands are:

- The *xlabel* and *ylabel* commands place labels next to the axes. They have the form: *xlabel*('*text as string'*), and *ylabel*('*text as string'*).
- The *title* command adds a title to the plot at the top of the figure. It has the form: *title*('*text as string'*).
- The *text* command places a note text in the figure whose first character is positioned at the point with the coordinates *x*, *y* (according to the axes of the figure).

- The *legend* command places a legend on the plot which shows a sample of the line type of each curve that is plotted and places a user specified label beside the line sample. The form of the command is: *legend*('*string1*', '*string2*', …,'*Location*', '*LocationValue*'). The strings are the labels that are placed next to the line sample. Their order corresponds to the order in which the graphs were created. '*Location*', is the property name that specifies where in the figure the legend is to be placed. There are several options available, all inserted as strings ('*LocationValue*'): NE Places the legend at the upper-right corner of the plot (default), while *NW* at the upper-left corner, *SE* at the lower-right corner, and *SW* at the lower-left corner.

The text used in the *xlabel*, *ylabel*, *title*, *text* and *legend* commands can be formatted after these commands have been executed. We can define the font, size, position (superscript, subscript), style (italic, bold, etc.), and colour of the characters, the colour of the background, and many more details of the display. The formatting can be done either by using modifiers inside the string (some of them are: *\bf* (bold fond), *\it* (italic style), *\rm* (normal style)), or *PropertyName* and *PropertyValue* arguments that follow the string. In this case, the *text* command, for example, has the form: *text*(*x*,*y*, '*text as string*', *PropertyName*, *PropertyValue*). The *PropertyName* is typed as a string, and the *PropertyValue* is typed as a number, if the property value is a number, and as a string, if the property value is a word or a letter character.

By default, when the *plot* command is executed MATLAB® finds the maxima and minima of the data and creates the plot axes with limits that are based on these minimum and maximum values. In other word, it automatically scales the axis limits to fit the data. However, in many situations, a graph looks better if the range of the axes extends beyond the range of the data, or both axis have the same scale, e.g. when drawing a circle. To override this, we can use the *axis* command that enables us to specify our own limits: *axis*([*xmin*, *xmax*, *ymin*, *ymax*]). It sets the limits of both *x*- and *y*-axes (*xmin*, *xmax*, *ymin*, and *ymax* are numbers). The axis command also enables us to specify a number of other features of the axis. For example,

- The *axis manual* command disables the automatic limit setting.
- The *axis equal* command sets the same scale for both axes and makes the individual tick mark increments on the *x*-axes and *y*-axes the same length, so that circles always appear round.
- The *axis tight* command sets the axis limits to the range of the data.
- The *axis square* command makes the *x*-axis and *y*-axis the same length.
- The *axis auto/normal* commands enable automatic limit selection again and return the axis scaling to its default automatic mode.
- The *axis on* command makes the axes visible (this is the default).
- The *axis off* command makes the axes invisible, as well as the axis labeling and tick marks.

- The *grid* command toggles grid lines on and off. The statement *grid on* turns the grid lines on (adds grid lines to the plot), and the statement *grid off* turns them back off again (it removes grid lines from the plot).

9.9.2 Multiple Graphs in the Same Plot—on the Same Axes

By default, each time we execute a plotting command, MATLAB® erases the old plot and draws a new one. In many situations, there is a need to make several graphs in the same plot. There are at least three ways of drawing multiple plots on the same set of axes, in the same figure. One is by using the *plot* command with multiple arguments, the second is by using the *hold on* and *hold off* commands, and the third is by using the *line* command.

Using the *plot* command two or more graphs can be created in the same plot by typing pairs of vectors inside the *plot* command. For example, the command *plot* (**x1**, **y1**, **x2**, **y2**, **x3**, **y3**, —) creates in the same plot more than three graphs by plotting the vector pairs (**x1**, **y1**), (**x2**, **y2**), …. These vectors may have different lengths, while the vectors of each pair must be of the same length. However, in this case, the axes may be rescaled if the new data plot fall outside the range of the previous data.

MATLAB® automatically selects a different colour for each pair so that they can be identified. However, it is possible to add line specifiers following each pair. For example the command *plot*(**x1**, **y1**, "−*b*", **x2**, **y2**, "−*r*", **x3**, **y3**, "*g*:") plots **y1** versus **x1** with a solid blue line, **y2** versus **x2** with a dashed red line, and **y3** versus **x3** with a dotted green line.

Using the *hold on* and *hold off* commands we can plot several graphs together. One graph is plotted first with the plot command and then the *hold on* commands is typed in the script. The *hold on* command holds the current plot and keeps all axis properties, if any was done. In other words, this command instructs MATLAB® to retain the old graph and draw any new on top of the old so that additional graphing commands can be added to the existing plot. Additional graphs are added with *plot* commands that are typed next. Each *plot* command creates a graph that is added to the same figure. The *hold off* command stops this process. It returns MATLAB® to the default mode, in which the plot command erases the previous plot and resets the axis properties.

Using the *line* command, additional graphs (lines) can be added to a plot that already exists. Its form is:

```
line(x,y,'PropertyName', Propertyvalue)
```

Although its form is almost the same with the *plot*'s command it does not have *line specifiers*, as line style, colour and marker. They only can be specified with the *Property Name* and *Property Value* features. The properties are optional, and if none are entered MATLAB® uses default values.

The major difference between *plot* and *line* commands is that the *plot* command starts a new plot every time it is executed, while the *line* command adds lines to a plot that already exists. Therefore, to make a plot that has several graphs with the *line* command, a *plot* command is typed first and then *line* commands are typed for additional graphs. Otherwise, if a *line* command is entered before a *plot* command, an error message is displayed.

9.10 Saving Graphs and Plots

Any graph created by MATLAB® and appeared in the figure window can be saved into a file in a specified format. The form of the *print* command used to save graphics to a file is:

```
print('filename.extension','formattype')
```

where *'formattype* is the file format:

- *-dill* for file in Adobe Illustrator format,
- *-djpeg* for file as a JPEG image,
- *-dtiff* for file saved as a compressed TIFF image,
- *-dsvg* for files saved in *svg* format, and
- *-dpng* for files saved in *png* format.

For example, for saving in *tiff* format we must type *print('figure1.tif', '−dtiff')* while for saving in *jpeg* format we must type *print('figure2.jpg', '−djpeg')*.

References

Attaway, Stormy. 2009. *MATLAB®: A practical introduction to programming and problem solving*. Amsterdam: Published by Elsevier Ltd. ISBN 978-0-75-068762-1.

Chapra, Steven C. 2012. *Applied numerical methods with MATLAB® for engineers and scientists*. New York: Published by McGraw-Hill. ISBN 978-0-07-340110-2.

Chapra, Steven C., and Raymond P. Canale. 2010. *Numerical methods for engineers*. New York: Published by McGraw-Hill. ISBN 978-0-07-340106-5.

Dukkipati, Rao V. 2006. *Analysis and design of control systems using MATLAB®*. New Age International (P) Ltd., Publishers, ISBN (13): 978-81-224-2484-3.

Gilat, Amos. 2017. *MATLAB® an introduction with applications*. Wiley & Sons, Inc., New York, ISBN: 978-1-119-25683-0 (PBK).

Hahn, Brian H., and Daniel T. Valentine. 2010. *Essential MATLAB® for engineers and scientists*, 4th ed. Published by Elsevier Ltd., Amsterdam, ISBN: 978-0-12-374883-6.

Hunt, Brian R., Ronald L. Lipsman, Jonathan M. Rosenberg, Kevin R. Coombes, John E. Osborn, and Garrett J. Stuck. 2001. *A guide to MATLAB® for beginners and experienced users*, Cambridge University Press, New York, ISBN-13 978-0-521-80380-9.

Moore, Holly. 2012. *MATLAB® for engineers.* Published by Pearson Education, Inc., ISBN-13: 978-0-13-210325-1.

Nagar Sandeep. 2017. *Introduction to MATLAB® for engineers and scientists: Solutions for numerical computation and modeling*. Copyright © 2017 by Sandeep Nagar, New York, USA, https://doi.org/10.1007/978-1-4842-3189-0, ISBN-13 (pbk): 978-1-4842-3188-3, ISBN-13 (electronic): 978-1-4842-3189-0.

Chapter 10
Applications

The theoretical analysis of a matter may be useful when it comes to the understanding of the physical phenomena governing it. However, we need something more than this if we would like to be able to exploit our theoretical knowledge and develop a successful practical application. We need to perform calculations and to produce some numerical results and some outputs. For this reason, the final chapter of this book contains a number of representative applications of the theory presented in the previous chapters. The main question to solve for nine case studies, along with solution tips and a short answer, is briefly, but adequately, described. Except for these, the computational code developed in MATLAB® script language, the corresponding M-files, is also provided. However, more detailed computational information is included in the supplementary CD that contains the corresponding M-files which include extended code documentation, as well as additional code lines, when necessary.

Electronic supplementary material The online version of this chapter (https://doi.org/10.1007/978-3-030-05279-9_10) contains supplementary material, which is available to authorized users.

S. Karathanasis, *Linear Fresnel Reflector Systems for Solar Radiation Concentration*, https://doi.org/10.1007/978-3-030-05279-9_10

Application 1
Extraterrestrial Solar Radiation. Solar Constant on different days of the year

Topic	Solution Tip	Answer
Calculate the **Solar Constant**, I^0, for the 1st of January and for the 1st of July.	The solar constant, I^0, is modified by the term R_c (Eq. 2.35) taking into account the no-circular (elliptical) motion of Earth around Sun. The term R_c can be approximated by Eq. 2.33a of Chap. 2, making use of Eq. 2.34 and 2.66, too.	The Solar Constant on 1/1/2018 is equal to 1,415 Watt/m^2. The Solar Constant on 1/7/2018 is equal to 1,321 Watt/m^2.

Short Code in MATLAB®

```
% Source Code Filename in the supplementary CD:
% A01_ExtraTerrestrialSolarRadiation.m
clearvars; clc;
Day=1; Month=1; Year=2018; I0=1367;
if rem(Year,4)==0
   K=1;
else K=2;
end
n=fix(275*Month/9)-K*fix((Month+9)/12)+Day-30;
d=2*pi*(n-1)/365.242;
Rc=1.000110+0.034221*cos(d)+0.00128*sin(d)...
    +0.000719*cos(2*d)+0.000077*sin(2*d);
Ic=I0*Rc;
fprintf(1,'The Solar Constant on %d/%d/%d is equal to
%4.0f Watt/m2\n',Month,Day,Year,Ic);
```

Application 2
Extraterrestrial Solar Radiation. Solar Constant Annual Variation

Topic	Solution Tip	Answer
Create a graph presenting the **annual variation of Solar Constant**.	Use the same equations Eq. 2.35 and Eq. 2.33a of Chap. 2, but now the number of the day in the year takes all values from 1 to 365.	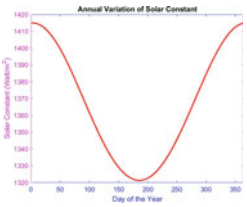

Fig. 10.1 Annual Variation of Solar Constant

Short Code in MATLAB®

```
% Source Code Filename in the supplementary CD:
% A02_ExtraTerrestrialSolarRadiationAnnualVariation.m
clearvars; clc;
I0=1367;
n=linspace(1,365,365);
d=2*pi*(n-1)/365.242;
Rc=1.000110+0.034221*cos(d)+0.00128*sin(d)...
    +0.000719*cos(2*d)+0.000077*sin(2*d);
Ic=I0*Rc;
plot(n,Ic);
print('SolarConstant.tif','-dtiff');
```

Application 3
Local Solar Time

Topic	Solution Tip	Answer
Calculate the **Equation of Time** for Thessaloniki, Greece, located at latitude 40.736851°, and longitude 22.920227°, on the 1st of October. Also calculate for the same date the **local solar time** for 9:00 AM local standard. The Local Standard Time Meridian (LSTM) for Thessaloniki is 30°.	The equation of time can be calculated in minutes by different empirical equation, like Eq. 2.70d of Chap. 2. In addition, Eq. 2.71c and Eq. 2.66 must be used. The local solar time is calculated from the local standard time using Eq. 2.72a of Chap. 2.	The Equation of time on 10/1/2018 is equal to 10.4 min. The Local Solar Time for Thessaloniki, Greece, on 10/1/2018 at Local Standard Time equal to 9:00:00 AM is 9:38:43 AM.

Short Code in MATLAB®

```
% Source Code Filename in the supplementary CD:
% A03_SolarLocalTime.m
clearvars; clc;
Day=1; Month=10; Year=2018;
fl=40.736851; ll=22.920227;% Thessaloniki, Greece
ls=30; tLST=9;
if rem(Year,4)==0
   K=1;
else K=2;
end
*(n-1)/365.242;
Et=0.01719+0.428146*cos(d)-7.352048*sin(d)-...
           3.349758*cos(2*d)-9.362591*sin(2*d);
fprintf(1,'The Equation of time on %d/%d/%d is equal to
%3.1f min\n\n',Month,Day,Year,Et);
Dl=4*(ls-ll)/60;
tLSO=tLST+Dl+Et/60;
tLSTnew=datestr(datenum([0 0 0 tLST 0 0]),14);
tLSOnew=datestr(datenum([0 0 0 tLSO 0 0]),14);
fprintf(1,'The Local Solar Time for Thessaloniki, Greece,
on %d/%d/%d \n',Month,Day,Year);
fprintf(1,'at Local Standard Time equal to ');
fprintf(1,tLSTnew);
fprintf(1,' is ');
fprintf(1,tLSOnew);
fprintf(1,'\n\n');
```

Application 4
Equation of Time. Annual Variation

Topic	Solution Tip	Answer
Create a graph presenting the **annual variation of Equation of Time and its components**	Use the same equations Eq. 2.70d and Eq. 2.71c of Chap. 2, but now the number of the day in the year takes all values from 1 to 365. The different terms of Eq. 2.70d describe the different components of Equation of Time: (obliquity and eccentricity component)	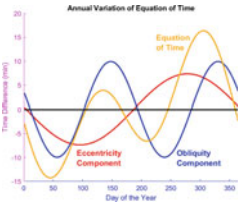 **Fig. 10.2** Annual Variation of Equation of Time

Short Code in MATLAB®

```
% Source Code Filename in the supplementary CD:
% A04_EquationOfTimeVariation.m
clearvars; clc;
n=linspace(1,365,365);
d=2*pi*(n-1)/365.242;
Et1=0.428146*cos(d)-7.352048*sin(d);
Et2=3.349758*cos(2*d)-9.362591*sin(2*d);
Et=0.01719+0.428146*cos(d)-7.352048*sin(d)-...
           3.349758*cos(2*d)-9.362591*sin(2*d);
plot(n,Et1,n,Et2,n,Et);
print('EquationOfTime.tif','-dtiff');
```

Application 5
Solar Coordinates

Topic	Solution Tip	Answer
Calculate the following **Solar Coordinates: solar hour angle, solar declination angle, solar height angle, solar zenith angle, and solar azimuth**, for Thessaloniki, Greece, located at Latitude 40.736851^o, and longitude 22.920227^o, on the 1st of October, at 9:00 AM local standard. The Local Standard Time Meridian (LSTM) for Thessaloniki is 30^o.	After having calculating the Local Solar Time, t he solar hour angle, the solar declination angle, can be calculated by using the Eq.2.74, Eq. 2.64a, Eq. 2.76 and Eq. 2.75 of Cha p. 2, while the solar zenith angle is the complementary angle of the solar height angle.	Solar hour angle: ω= -0.6 hours Solar declination angle: δ= -4.2^o Solar height angle: h=44.2^o Solar zenith angle: θ_z=45.8^o Solar azimuth: A=-13.5^o

Short Code in MATLAB®

```
% Source Code Filename in the supplementary CD:
% A05_SolarCoordinates.m
clearvars; clc;
Day=1; Month=10; Year=2018;
fl=40.736851; ll=22.920227;% Thessaloniki, Greece
ls=30; tLST=12;
```

...(see Application 3)

```
SolarAngle_w=(12-tLSO)*pi/12;
fprintf(1,'Solar hour angle: ω=%3.1f
hours\n',SolarAngle_w*12/pi);
Declin=23.45*sin(2*pi*(284+n)/365)*pi/180;
fprintf(1,'Solar declination angle: δ=%3.1f
degrees\n',Declin*180/pi);
h=asin(cos(Declin)*cos(SolarAngle_w)*cos(fl*pi/180)+sin(D
eclin)*sin(fl*pi/180));
fprintf(1,'Solar height angle: h=%3.1f
degrees\n',h*180/pi);
zenith=90-h*180/pi;
fprintf(1,'Solar zenith angle: θz=%3.1f
degrees\n',zenith);
A=asin(cos(Declin)*sin(SolarAngle_w)/cos(h));
fprintf(1,'Solar azimuth angle: A=%3.1f
degrees\n',A*180/pi);
```

Application 6
Sunrise and Sunset time and Total Sunshine Hours

Topic	Solution Tip	Answer
Calculate the **sunrise and sunset time** and **the total sunshine hours** for a location at Heraclion, on the island of Crete, Greece, (longitude = 25.148254^{o}) on the 9th of September.	The solar hour angles of sunrise and sunset can be computed with the aid of Eq. 2.61 of Chap. 2. They are symmetrical around local noon.	The sunrise time, in Local Solar Time, is 5:52:04 AM The sunset time, in Local Solar Time, is 6:07:55 PM The daytime duration is 12 hours and 15 minutes

Short Code in MATLAB®

```
% Source Code Filename in the supplementary CD:
% A06_SunRise_SunSetTime.m
clearvars; clc;
Month=9; Day=9;Year=2018;
fl=25.148254;
if rem(Year,4)==0, K=1; else K=2; end
n=fix(275*Month/9)-K*fix((Month+9)/12)+Day-30;
d=2*pi*(n-1)/365.242;
Declin=23.45*sin(2*pi*(n-80)/365);
Wss=acos(-tan(Declin*pi/180)*tan(fl*pi/180))*12/pi;
sunrise=12-Wss;
sunrisenew=datestr(datenum([0 0 0 sunrise 0 0]),14);
fprintf(1,'The sunrise time, in Local Solar Time, is');
fprintf(1,sunrisenew);
fprintf(1,'\n\n');
sunset=12+Wss;
sunsetnew=datestr(datenum([0 0 0 sunset 0 0]),14);
fprintf(1,'The sunset time, in Local Solar Time, is');
fprintf(1,sunsetnew);
fprintf(1,'\n\n');
DayDuration=2*Wss;
DayDurationHours=fix(DayDuration);
DayDurationmin=fix((DayDuration-fix(DayDuration))*60);
fprintf(1,'The daytime duration is %2d hours and %2d
minutes\n',DayDurationHours,DayDurationmin);
```

Application 7
Solar Coordinates

Topic	Solution Tip	Answer
Calculate the direct solar irradiance falling on a horizontal surface on Earth, for a site locates in Thessaloniki, Greece, latitude= 40.736851^{o}, longitude= 22.920227^{o}) on the 15th of July, at local noon.	A simple model for computing direct solar irradiance is Eq. 2.77 of Chap. 2. The air mass can be computed from Eq. 2.22a, and the rest parameters using the same equations used in the previous applications.	The direct solar irradiance falling on a horizontal surface is equal to 917 Watt/m^2

Short Code in MATLAB®

```
% Source Code Filename in the supplementary CD:
% A07_SolarRadiationOnEarthSurface.m
clearvars; clc;
Day=15; Month=6; Year=2018;
fl=40.736851; ll=22.920227;
I0=1367; SolarAngle_w=0; %local noon
tb=0.606; b=0.491;
if rem(Year,4)==0 K=1; else K=2; end
n=fix(275*Month/9)-K*fix((Month+9)/12)+Day-30;
d=2*pi*(n-1)/365.242;
Declin=23.45*sin(2*pi*(284+n)/365);
h=asin(cos(Declin*pi/180)*cos(SolarAngle_w*pi/12)*...
     cos(fl*pi/180)+sin(Declin*pi/180)*sin(fl*pi/180));
ZenithAngle=90-h*180/pi;
A=asin(cos(Declin*pi/180)*...
     sin(SolarAngle_w*pi/12)/cos(h));
Rc=1.000110+0.034221*cos(d)+0.00128*sin(d)...
    +0.000719*cos(2*d)+0.000077*sin(2*d);
m=1/(cos(ZenithAngle*pi/180)+0.51*...
     ((93.885-ZenithAngle*pi/180)^-1.1253));
Iearth=I0*Rc*0.7^(m^0.678);
Message1='The direct solar irradiance falling on ';
Message2='a horizontal surface is equal to %4.0f
Watt/m2\n';
Message=strcat(Message1,Message2);
fprintf(1,Message,Iearth);
```

Application 8
Conical Fresnel Reflectors Solar Cooker

Topic	Solution Tip	Answer
Calculate the construction parameters of the Conical Fresnel Reflectors Solar Cooker presented in Chap. 8.	Use the methodology and the equation presented in Chap. 8, as well as the corresponding numerical data (receiver size, position, etc.)	See Table 8.1 of Chap. 8.

Short Code in MATLAB®

```
% Source Code Filename in the supplementary CD:
% A08_ConicalFresnelReflectors_SolarCooker.m

clearvars; clc;
L=60; Wr=14; Hr=6; H=45; Db=pi/180; I0=917;
alfa=0.001; betta=0.001;gamma=0.001;
fi=2*atan(Wr/(2*Hr));
%=========================================================
Q1=2*Wr; b1=0; W1=Hr/cos(fi/2); Accur_b=100; Accur_W=100;
while (Accur_b>alfa)|(Accur_W>betta)
    bnew1=b1+Db;
    Prev_b=b1; Prev_W=W1;
    W1=Hr*cos(2*bnew1+pi/2-
fi/2)/(cos(fi/2)*sin(bnew1+pi/2));
    b1=(1/2)*atan((H+W1*sin(bnew1)/2)/...
        (Q1-Hr*tan(fi/2)/2+W1*cos(bnew1)/2))-pi/4;
    Accur_b=abs(b1-Prev_b)/b1;
    Accur_W=abs(W1-Prev_W)/W1;
end
Apperture=Q1; j=1; Q(1)=Q1; b(1)=b1; W(1)=W1;
fprintf(1,'j=1 b%d=%3.0f degrees, Q%d=%4.1f cm, W%d=%4.1f
cm\n',j,b(j)*180/pi,j,Q(j),j,W(j));
while Apperture<L
    j=j+1;
    b(j)=0; Q(j)=Q(j-1)+W(j-1); W(j)=Hr/cos(fi/2);
    Accur_b=100;
    Accur_W=100;
    Accur_Q=100;
    while
((Accur_b>alfa)|(Accur_W>betta))|(Accur_Q>gamma)
        bnew=b(j)+Db;
        Prev_b=b(j); Prev_W=W(j); Prev_Q=Q(j);
        Q(j)=Q(j-1)+W(j-1)*cos(b(j-1))+W(j-1)*...
             sin(b(j-1))*tan(2*bnew);
        W(j)=Hr*cos(2*bnew+pi/2-...
             fi/2)/(cos(fi/2)*sin(bnew+pi/2));
        b(j)=(1/2)*atan((H+W(j)*sin(bnew)/2)/...
```

```
            (Q(j)-Hr*tan(fi/2)/2+W(j)*...
            cos(bnew)/2))-pi/4;
        Accur_Q=abs(Q(j)-Prev_Q)/Q(j);
        Accur_b=abs(b(j)-Prev_b)/b(j);
        Accur_W=abs(W(j)-Prev_W)/W(j);
    end
    Apperture=Q(j);
    if Apperture<L
       fprintf(1,'j=%d b%d=%3.0f degrees, Q%d=%4.1f cm,
          W%d=%4.1f cm\n',j,j,b(j)*180/pi,j,Q(j),j,W(j));
    end
end
Ar=Hr*Wr+Wr*Wr/4;
Ae=0;
for i=1:j-1
    Ae=Ae+((Q(i)+W(i)*cos(b(i)))*(Q(i)+...
            W(i)*cos(b(i)))-Q(i)*Q(i));
end;
CR=Ae/Ar;
fprintf(1,'\nConcentration Ration of the Conical Cooker,
CR=%g',CR);
I=I0*Ae*pi/10000;
fprintf(1,'\nConcentrated Solar Radiation, I=%g
Watt\n\n',I);
fprintf(1,'\nPrimary reflectors' field aperture area,
Ae=%g m2\n\n',Ae*pi/10000);
r=Q; R=Q+W.*cos(b); h=W.*sin(abs(b));
Rout=(R.*sqrt(h.*h+(R-r).*(R-r))./(R-r);
Rin=Rout-sqrt(h.*h+(R-r).*(R-r));
Omega=360*R./Rout;
for i=1:j-1
    fprintf(1,'j=%d Rin=%4.1f cm, Rout=%4.1f cm,
          φ=%4.1f degrees\n',i,Rin(i),Rout(i),Omega(i))
end;
Cov=Ae/((Q(j-1)+W(j-1)*cos(b(j-1)))*(Q(j-1)+...
          W(j-1)*cos(b(j-1))))*100;
fprintf(1,'\nReflectance Coverage, I=%g%%\n',Cov);
```

Application 9
Linear Fresnel Reflectors Solar Cooker with Cylindrical Receiver

Topic	Solution Tip	Answer
Calculate the construction parameters of the Linear Fresnel Reflectors Solar Cooker presented in Chap. 8.	Use the methodology and the equation presented in Chap. 8, as well as the corresponding numerical data (receiver size, position, etc.)	See Table 8.1 of Chap. 8.

Short Code in MATLAB®

```
% Source Code Filename in the supplementary CD:
% A09_LinearFresnelReflectors_SolarCooker_
% Circular.m

clearvars; clc;
L=60; Rr=5.5; Lr=30; H=45; Db=pi/180; I0=917;
alfa=0.001; betta=0.001;gamma=0.001;
%=================================================
Q1=2*Rr; b1=0; W1=2*Rr; Accur_b=100; Accur_W=100;
while (Accur_b>alfa)|(Accur_W>betta)
    bnew1=b1+Db;
    Prev_b=b1;
    Prev_W=W1;
    W1=2*Rr/sin(b1+pi/2);
    b1=(1/2)*atan((H+W1*sin(bnew1)/2)/...
        (Q1+W1*cos(bnew1)/2))-pi/4;
    Accur_b=abs(b1-Prev_b)/b1;
    Accur_W=abs(W1-Prev_W)/W1;
end
Apperture=Q1; j=1; Q(1)=Q1; b(1)=b1; W(1)=W1;
fprintf(1,'j=1 b%d=%3.0f degrees, Q%d=%4.1f cm, W%d=%4.1f
cm\n',j,b(j)*180/pi,j,Q(j),j,W(j));

while Apperture<L
    j=j+1;
    b(j)=0; Q(j)=Q(j-1)+W(j-1); W(j)=2*Rr;
    Accur_b=100;
    Accur_Q=100;
    while
((Accur_b>alfa)|(Accur_Q>betta))|(Accur_Q>gamma)
        bnew=b(j)+Db;
        Prev_b=b(j); Prev_Q=Q(j);Prev_W=W(j);
        Q(j)=Q(j-1)+W(j-1)*cos(b(j-1))+W(j-1)*...
        sin(b(j-1))*tan(2*bnew);
        W(j)=2*Rr/sin(b(j)+pi/2);
        b(j)=(1/2)*atan((H+W(j)*sin(bnew)/2)/...
             (Q(j)+W(j)*cos(bnew)/2))-pi/4;
```

```
        Accur_Q=abs(Q(j)-Prev_Q)/Q(j);
        Accur_b=abs(b(j)-Prev_b)/b(j);
        Accur_W=abs(W(j)-Prev_W)/W(j);
    end
    Apperture=Q(j);
    if Apperture<L
       fprintf(1,'j=%d b%d=%3.0f degrees, Q%d=%4.1f cm,
       W%d=%4.1f cm\n',j,j,b(j)*180/pi,j,Q(j),j,W(j));
    end
end
Ar=3/2*pi*Rr;
Ae=0;
for i=1:j-1
    Ae=Ae+W(i)*cos(b(i));
end;
Ae=2*Ae;
CR=Ae/Ar;
fprintf(1,'\nConcentration Ration of the Linear Cooker,
CR=%g\n',CR);
I=I0*Ae*Lr/10000;
fprintf(1,'\nConcentrated Solar Radiation, I=%g
Watt\n',I);
fprintf(1,'\nPrimary reflectors' field aperture area,
Ae=%g m2\n\n',Ae*Lr/10000);
Cov=Ae/2/(Q(j-1)+W(j-1)*cos(b(j-1)))*100;
fprintf(1,'\nReflectance Coverage, I=%g%%\n',Cov);
```

Index

A
Airmass/air mass, 25–29, 56–58, 61, 62, 64, 68, 70
Angle of incidence, 31, 74, 77, 78, 81, 82, 86, 88, 89, 105, 107, 109, 169, 189, 190, 192, 198, 204, 209, 212, 238
Array operation, 312, 315, 316
ASCII text file, 307, 309, 327
Atmospheric attenuation effects
  absorption, 19, 21, 22, 77
  scattering, 20–22, 57, 60, 63
    Mie, 20, 21, 172
    non-selective, 20, 21
    Rayleigh, 20, 21, 60, 62, 63
Augustin-Jean Fresnel, 94, 98

B
Black body (blackbody), 15–19
Blocked
  area, 159, 160
  width, 11, 51, 93, 95, 97–100, 102, 103, 105, 121, 123, 124, 129, 142, 147, 149, 150, 160, 161, 164, 167

C
Celestial
  equator, 37–41, 49
  North Pole, 37
Central axis, 88, 141
Commands
  disp, 327
  fclose, 329
  fopen, 327
  fprintf, 327–329
  hold on/off, 333
  input, 311
  line, 333, 334
  plot, 330–334
  print, 334
Command window, 306, 309–311, 326, 328
Compact linear Fresnel reflector systems, 139, 140
Concentrated solar radiation power systems/stations, 2, 3, 7, 22, 26, 35, 39, 49, 55
Concentration ratio, 3, 5, 6, 8, 120–122, 124, 126, 295, 297
Conical frustum, 286, 294, 295, 298
Constant
  Boltzmann's, 16, 17
  Planck's, 16
  solar, 19, 20, 24, 34, 35
  solar constant, 34
  Stefan-Boltzmann, 16, 17
Coordinates, geographic
  latitude, φ, 35–37, 41, 44, 48, 65, 66, 115, 162, 227
  longitude, λ, 35–37, 42, 48, 51, 52, 65, 66
Coordinates, Sun's
  altitude angle, h, 41, 47, 115, 118, 228
  azimuth angle, A, 31 , 42, 55
  declination angle, δ, 340
  ecliptic latitude, β, 40, 41
  ecliptic longitude, l, 42, 43, 51
  elevation angle, h, 37, 38, 116, 128, 142, 169
  height angle, h, 37, 42, 54, 62, 103
  hour angle, ω, 37–40, 42, 44, 45, 48, 50, 52, 54
  right ascension, α, 39–41

S. Karathanasis, *Linear Fresnel Reflector Systems for Solar Radiation Concentration*, https://doi.org/10.1007/978-3-030-05279-9

zenith angle, θ_z, 24–26, 29, 31, 41, 47, 54, 56, 59, 169
Coordinate system
celestial equatorial, 38–40, 44, 49
eclipitic, 39–41, 44, 49
equatorial, 35, 37, 39–41, 44, 45, 48, 51
geographic, 35–37
horizontal, 35, 37, 38, 41–45, 110, 165
terrestrial, 35
Coordinate transformation, 44, 317
Cosine effect, 31, 104, 133, 137, 139, 169–171

D
Diffuse radiation, 20, 22, 141
Diffuse reflection, 78, 79, 81
Direct solar irradiance, 31, 55–57, 60, 62, 64
Direct solar radiation, 13, 21, 22, 25, 30, 35, 41, 48, 55, 56, 59, 61, 63, 68, 97, 105, 109, 120, 122, 127, 131, 133, 139, 141, 169, 171, 270, 277, 280

E
East–West/West–East orientation/oriented system, 7, 112, 116, 117, 170, 226–231, 240, 241, 269, 282
Eccentricity, 32–34, 64
Eccentricity correction factor, 34, 64
Ecliptic, 39–41, 49, 53
Effective aperture area, 121
Efficiency
blocking, 160, 181
factor, 127, 131, 133, 134
optical, 10, 117, 125, 127–129, 133, 137, 161, 162
shading, 158, 181
Electric energy generator, 6, 8
Electric power production, 1, 3
End loss
length, 157, 163, 164, 166–168, 181, 182
ratio, 162, 167, 181
Energy loss
blocking, 129, 130, 132, 137, 146, 160, 161, 181
cosine effect, 139, 169
end loss, 130, 132, 137, 157, 162, 170, 172
shading, 131, 137, 146–148, 151, 157, 158, 161, 162, 181
Energy production, 1, 8, 124
Equation of time, 52–54
Equator, 35, 38–40, 47, 116, 117
Equinox
autumnal, 40
spring, 115
Extraterrestrial irradiance, 27, 32, 57
Extraterrestrial radiation, 32, 35, 57

F
Fermat's principle, 75–77, 79
Focal
lenth, 85, 87, 88, 90, 92–94, 103, 129, 217, 218, 298
plane, 88, 89, 224
point, 9, 85, 87, 88, 91, 93, 95, 98, 99, 244, 247, 248, 280
Function
cross, 317
dot, 317
eye, 313
inv, 318
linspace, 314
norm, 320

G
Gray body, 15
Greenwich Mean Time (GMT), 51

H
Horizon, 25, 28, 32, 35, 37, 115, 118, 128, 300
Hot body, 15

I
Incidence Angle Modifier, 128, 129
Incidence angle, θ, 30, 31, 41, 47, 104, 133
Insolation, 14, 32
Irradiance, 3, 14, 15, 17, 19, 20, 24, 25, 27, 30–34, 41, 48, 55, 56, 60, 64, 112, 127, 169, 225, 228
Irradiation, 14, 128, 186
Iterative approach, 272

L
Law
Beer–Lambert–Bouguer, 23
Kepler's first Law, 33
Kepler's second Law, 33, 49
law of reflection/reflection law, 75, 77–80, 82–87, 89, 107, 159, 164, 165, 196, 198, 199, 205, 238
Planck's Law, 16, 18
Stefan-Boltzmann Law, 16, 18

Wien's displacement Law, 17–19
Leap year, 50, 54
Light ray, 6, 73–79, 81–90, 93, 103, 105, 120, 121, 126, 189, 192, 194, 196–201, 203, 205, 206, 208, 210–213, 215–217, 223, 225, 227, 237, 244, 250, 253, 257, 258, 273, 283, 290
Linear extinction coefficient, 22
Local
longitude, 35, 52
mean time, 51–53
meridian, 35, 37, 38, 51, 53, 226
solar noon, 38
solar time, 38, 48, 50–54, 225
standard time, 48, 51, 52, 54
Longitude correction, 51, 52, 54
Longitudinal plane, 98, 110–112, 115, 129, 132, 227, 271, 282, 292

M
Machine language, 309, 310
Material
translucent, 77
transparent, 77
Medium
homogeneous, 76, 77, 79
inhomogeneous, 76
Meridian, 35–38, 50–52
M-files
function, 306, 307, 337
script, 306–308
Mirror
concave, 5, 84, 85, 87
curved, 7, 78, 83, 84, 89, 137
flat, 4, 5, 8, 79, 82, 83, 223
fresnel, 10, 94
parabolic, 73, 88, 90, 92, 93
plane, 73, 78, 82–84, 96, 192
spherical, 78, 83–89

N
Normal solar radiation, 14
North pole, 35, 37, 44, 45
North–South/South–North orientation/oriented system, 7, 105, 111, 112, 116, 139, 153, 162, 167, 174, 181, 224, 226–229, 267, 269, 270

O
Obliquity angle, 39
Optical
axis, 93, 95, 98
depth, 23–26, 57, 58, 60, 62, 64
efficiency, 10, 125, 127–129
path length, 56, 74, 76, 77

P
Parabola, 88, 90, 92, 93, 103, 217–219, 280
Parabolic
dish, 4–6, 8, 94, 98
trough, 4, 6–11, 93, 94, 96, 98, 103, 105, 106, 119, 123, 125
Paraxial rays, 85, 88
Placeholder, 328, 329
Plane of incidence, 78
Point focusing systems, 4
Point light source, 74, 75, 82–84, 161, 185, 257
Pole, 83–85, 194, 195
Principal axis, 85–90, 93, 192, 194, 195, 205, 215, 216, 280
Programming language, 306, 307, 309, 310, 312, 319, 326
Property, 91–93, 280, 331, 332

R
Radiant
energy, 14, 19
flux, 14, 19
power, 14, 16, 18, 20
Radiation, 1–4, 7, 9, 10, 13–23, 25, 26, 30, 31, 55, 68, 95, 104, 124, 126, 127, 133, 134, 139
Radiation model
empirical, 56
parametric/parameterization, 56, 63
Radius of curvature, 28, 83, 85–87, 144
Ray
optics, 74–76
tracing, 74, 129, 130, 137, 187
Receiver/absorber
aperture area, 120, 121
cavity receivers, 186, 214
circular, 202, 245, 246, 255
horizontal, flat, 226, 244
multiple tubes, 123, 190
one tube, 124, 125
rectangular, 176
reversed V-shaped cavity, 194
semicircular, 177
trapezoidal cavity, 126, 139, 186, 187
trapezoidal-modified cavity, 207
triangular, 186, 244–248, 255, 258, 266, 267, 281, 282, 299
vertical, flat, 258
V-shaped cavity, 186, 187
Receiver energy loss
specular loss, 131, 140, 225
spillage loss, 131, 134

transmissivity loss, 131
Reflection, 20, 73, 74, 77–79, 81–83, 85, 88–90, 103, 107, 113, 119, 125, 127, 141, 204, 206, 208, 238, 239, 257
Refraction/refractive index, index of refraction, 76, 77, 80
Repetitions (loop), 308

S
Secondary reflector/concentrator
arc-shaped, 214
compound parabolic, 125, 126, 186, 187, 207, 217
parabolic, 217
parabolic involute, 186, 187, 207, 220
parabolic wing-like, 126, 186, 187, 207, 219
segmented parabolic, 126, 186, 187, 207, 217–219
semi-circular, 214, 215
Selection (decision), 223, 308, 319
Sequence, 307–309, 319, 323, 329
Shaded
area, 146, 158, 160, 181
length, 146, 149, 157–159
relative shaded area, 158, 181
width, 146, 148–151, 155–157, 161, 175, 179–181
Shading
effect, 11, 131, 135, 138, 145, 146, 158, 159, 161, 172, 175, 177, 181, 228–230, 234
efficiency, 158, 181
loss ratio, 10, 131, 148, 149, 172
Solar cooker
box, 278
conical Fresnel reflectors, 281–285, 287, 294–300, 302
linear Fresnel reflectors solar cooker, 282, 285–288, 297–301
panel, 278
parabolic, 278, 280, 281
Solar radiation, 1–9, 11, 13–15, 18–22, 25, 26, 28, 30–33, 35, 41, 42, 48, 49, 55, 56, 60, 63–65, 73, 75, 88, 95–99, 101, 103–107, 109, 110, 113, 115, 117, 120–122, 124–128, 130–134, 138, 140, 142, 157–165, 169, 185–189, 191–194, 200, 201, 203–205, 208, 210–213, 215, 218, 224–229, 238, 241, 245, 252–259, 270, 278, 280, 282, 290, 300
Solar radiation attenuation, 24
Solar radiation concentrating systems, 4, 7, 13, 93, 109, 126, 130, 162, 277
Solar time true, 41, 50–52
Solar Tower systems, 4, 5, 8
Solstice summer/June, winter/December, 40, 115, 117, 118
Source code, 309
Specifier, 328, 331, 333
Standard longitude, 51
Statements
FOR, 325
IF, 320–322, 325
IF/THEN, 319
IF/THEN/ELSE, 319
SWITCH CASE, 320, 322
WHILE, 326
Sun chart, 116
Sun-Earth/Earth-Sun distance, 32, 34, 35
Sun's
longitudinal angle, 111, 157, 164
size/size of sun, 225, 271, 288
transversal angle, 111, 144, 147, 148, 155, 156, 175, 189, 191–193, 228–231, 237–239, 241, 250, 258, 269, 270, 282
Sun tracking system
active, 106
passive, 105, 106
real-time, 106
System orientation angle, 139

T
Thermal power station, 2
Time zone, 51
Transmission, 22, 32, 77
Transmittance, 63, 64, 67, 68
Transversal plane, 110–112, 121, 129, 144, 164, 169, 200, 229, 237, 252, 254, 256, 257, 282, 285, 294

U
Universal time, 51

V
Variable
dependent, 307, 315
independent, 307, 310, 315
matrix, 312, 315, 316, 329, 330
scalar, 316
vector, 314, 330
Vector-matrix calculations, 316

Vertex, 83–85, 93, 155, 157, 194, 195, 214, 216, 247

W
Wave front
plane, 74, 75, 81
spherical, 74
Wave optics, 74

Z
Zenith, 10, 23–25, 27–29, 37, 41, 42, 47, 54, 56, 59, 68, 110, 151, 284